NBSIR 83-2742

Photonuclear Data - Abstract Sheets 1955 - 1982 Volume VI (Aluminum - Phosphorous)

E. G. Fuller, Henry Gerstenberg

U.S. DEPARTMENT OF COMMERCE
National Bureau of Standards
National Measurement Laboratory
Center for Radiation Research
Gaithersburg, MD 20899

September 1984

U.S. DEPARTMENT OF COMMERCE
NATIONAL BUREAU OF STANDARDS

NBSIR 83-2742

PHOTONUCLEAR DATA - ABSTRACT SHEETS 1955 - 1982 VOLUME VI (ALUMINUM - PHOSPHOROUS)

E. G. Fuller, Henry Gerstenberg

U.S. DEPARTMENT OF COMMERCE
National Bureau of Standards
National Measurement Laboratory
Center for Radiation Research
Gaithersburg, MD 20899

September 1984

U.S. DEPARTMENT OF COMMERCE, Malcolm Baldrige, *Secretary*
NATIONAL BUREAU OF STANDARDS, Ernest Ambler, *Director*

TABLE OF CONTENTS

Photonuclear Data-Abstract Sheets
1955-1982

I. Introduction

As used in connection with this collection of data-abstract sheets, the term photonuclear data is taken to mean any data leading to information on the electromagnetic matrix element between the ground state and excited states of a given nuclide. The most common types of reactions included in this compilation are: (e,e'), (γ,γ), (γ,γ'), (γ,n), (γ,p), etc. as well as ground-state particle capture reactions, e.g. (α,γ_0). Two reactions which fit the matrix element criterion are not included in the compilation because of their rather special nature. These are heavy particle Coulomb excitation and the thermal neutron capture reaction (n,γ_0). While the energy region of particular interest extends from 0 to 150 MeV, papers are indexed which report measurements in the region from 150 MeV to 4 GeV. Most of the experiments listed are concerned with the excitation energy range from 8 to 30 MeV, the region of the photonuclear giant resonance.

The hierarchical grouping of the photonuclear data-abstract sheets within the file is by: 1. Target Element, 2. Target Isotope, and 3. by the Bibliographic Reference Code assigned to the paper from which the data on the sheet were abstracted. In this file, colored pages are used to mark the beginning and end of the sheets for each chemical element. A brief historical sketch of the element is given on the divider sheet marking the start of each section; the information for this sketch was derived from references such as the Encyclopaedia Britannica. In those cases where the sheets for a given element make up a major part of a volume, colored pages are also used to delineate sections pertaining to the individual isotopes of the element. Each of the sections of the file, as delineated by two colored divider sheets, represents a 27 year history of the study of electromagnetic interactions in either a specific nuclide or a specifc element.

The data-abstract sheets are filed under the element and/or isotope in which the ground-state electromagnetic transition takes place. For example, the abstract sheet for a total neutron yield measurement for a naturally occurring copper sample would appear in the elemental section of the copper file. On the other hand, a measurement of the ^{62}Cu 9.73 minute positron activity produced in the same sample by photons with energies below the three-neutron separation energy for ^{65}Cu (28.68 MeV) would be filed with the sheets for ^{63}Cu. Similarly a measurement of the ground-state neutron capture cross section in ^{12}C would be filed under ^{13}C while the corresponding ground-state alpha-particle capture cross section would be filed under ^{16}O.

At the end of this volume there is a master list of the abbreviations that have been used in the index section of the abstract sheets. The listings are those used in the final published index, Photonuclear Data Index, 1973-1981, NBSIR 82-2543, issued in August 1982 by the U. S. Department of Commerce, National Bureau of Standards, Washington, DC 20234. In some cases two notations are entered for the same quantity. The second entry is the abbreviation that was used in one or more of the earlier published editions of the index.

ALUMINUM
Z=13

Aluminum derives its name from the Latin *alumen* -, a naturally occurring aluminous sulfate that was used as an astringent and mordant at least as early as the 5th century B.C. Hans Christian Oersted is credited with having been the first to prepare the metallic aluminum. This he did in 1825 by chemically creating an aluminum amalgam and distilling off the mercury. Oersted's results were published in an obscure Danish journal and made little impact on the scientific community. Friedrich Wohler (1800-1882) improved upon the process and in 1845 he was able to make large droplets of the metal and determine some of its physical properties. The first pure sample was not made until 1854; the French chemist Henri Sainte-Claire Deville (1818-1881) improved Wohler's method and developed it into a successful commercial process until the advent of the cheaper electrolytic method. This process was introduced by Charles Hall of Oberlin College, Ohio, and Paul-Louis-Toussaint Heroult (1803-1914) of France. Both were 22 years old at the time; both independently and almost simultaneously discovered and patented the process. It remains to this day the only method by which aluminum is produced in commercial quantities.

AL
A=25

AL
A=25

Ref. N.H. Gale, N. Tubbs, N. Nath, A.T.G. Ferguson
Phys. Letters 5, 345 (1963)

Elem. Sym.	A	Z
Al	25	13

Method: Van de Graaff; plastic scintillator; pulsed-beam, delayed coincidence technique

Ref. No.: 63 Ga 1 JHH

Reaction	E or ΔE	E_o	Γ	$\int \sigma dE$	Jπ	Notes
$Mg^{24}(p,\gamma)$	0.825	0.450				Lifetime of 0.450 MeV level given in Table I, below.

Table 1

Isomeric level	τ_m (ns)	Reference
Al^{25*} (450 keV)	2.6 ± 0.4	1)
	2.71 ± 0.14	2)
	3.33 ± 0.07	3)
	3.25 ± 0.15	present work
Al^{26*} (418 keV)	1.77 ± 0.07	2)
	1.86 ± 0.09	present work

1) A.T.G. Ferguson, M.A. Grace and J.O. Newton, Nuclear Phys. 17 (1960) 1.
2) S. Gorodetzky et al., Proc. of the Conf. on Electromagnetic Lifetimes and Properties of Nuclear States, Gatlinburg (1962), p. 79.
3) C.L. McClelland and J. Lowe, Proc. of the Conf. on Electromagnetic Lifetimes and Properties of Nuclear States, Gatlinburg (1962), p. 78.

REF. G. C. Morrison, D. H. Youngblood, R. C. Bearse, R. E. Segel
Phys. Rev. 174, 1366 (1968)

ELEM. SYM.	A	Z
Al	25	13

METHOD

REF. NO. 68 Mo 2 HMG

REACTION	RESULT	EXCITATION ENERGY	SOURCE TYPE	SOURCE RANGE	DETECTOR TYPE	DETECTOR RANGE	ANGLE
P,G	LFT	8.0	D	6.0	SCD-I		DST
		(7.916,7.985)		(5.864,5.936)			

G-WIDTH

TABLE I. Partial widths for the various γ-ray transitions from $T=\frac{3}{2}$ to $T=\frac{1}{2}$ states that were observed in the present work. The ratio of the observed width to the single-particle estimate[a] is given under the heading $|M|^2$. Where the $E2$ admixture is not determined, there are three dots in place of the appropriate entry and the transition was assumed to be pure $M1$.

Nucleus	$E_i(T=\frac{3}{2}) \rightarrow E_f(T=\frac{1}{2})$ (MeV)	$J_i^\pi \rightarrow J_f^\pi$	Γ_γ (eV)	$\lvert M_{M1}\rvert^2$	δ^2 $(E2/M1)$	$\lvert M_{E2}\rvert^2$
Al^{26}	7.916 → 0	$\frac{5}{2}^+ \rightarrow \frac{5}{2}^+$	0.82	0.087	0.06	0.4
Al^{26}	7.916 → 0.949	$\frac{5}{2}^+ \rightarrow \frac{3}{2}^+$	0.16	0.025	...	...
Al^{26}	7.916 → 1.610	$\frac{5}{2}^+ \rightarrow \frac{1}{2}^+$	1.02	0.21	...	...
Al^{26}	7.985 → 0	$\frac{3}{2}^+ \rightarrow \frac{5}{2}^+$	1.06[b] 5.76[c]	0.11[b] 0.60[c]	0.045	0.4[b] 2.2[c]
Al^{26}	7.985 → 0.455	$\frac{3}{2}^+ \rightarrow \frac{1}{2}^+$	0.21[b] 1.14[c]	0.025[b] 0.14[c]	...	...
Al^{26}	7.985 → 0.949	$\frac{3}{2}^+ \rightarrow \frac{3}{2}^+$	0.23[b] 1.25[c]	0.030[b] 0.16[c]	...	...
P^{29}	8.374 → 1.277	$\frac{5}{2}^+ \rightarrow \frac{3}{2}^+$	0.16	0.024	...	...
P^{29}	8.374 → 2.027	$\frac{5}{2}^+ \rightarrow \frac{5}{2}^+$	0.42	0.088	...	...
P^{29}	8.374 → 2.425	$\frac{5}{2}^+ \rightarrow \frac{3}{2}^+$	0.22	0.055	...	...

[a] Reference 14.
[b] Derived by use of the value Γ'_{p_0}/Γ from Ref. 10.
[c] Derived by use of the electron scattering data of Ref. 13.

REF.	ELEM. SYM.	A	Z
H. P. Trautvetter, C. Rolfs Nucl. Phys. A242, 519 (1975)	Al	25	13

METHOD	REF. NO.	
	75 Tr 3	egf

REACTION	RESULT	EXCITATION ENERGY	SOURCE		DETECTOR		ANGLE
			TYPE	RANGE	TYPE	RANGE	
P,G	ABX	2- 4	D	0- 2	SCD-D		90

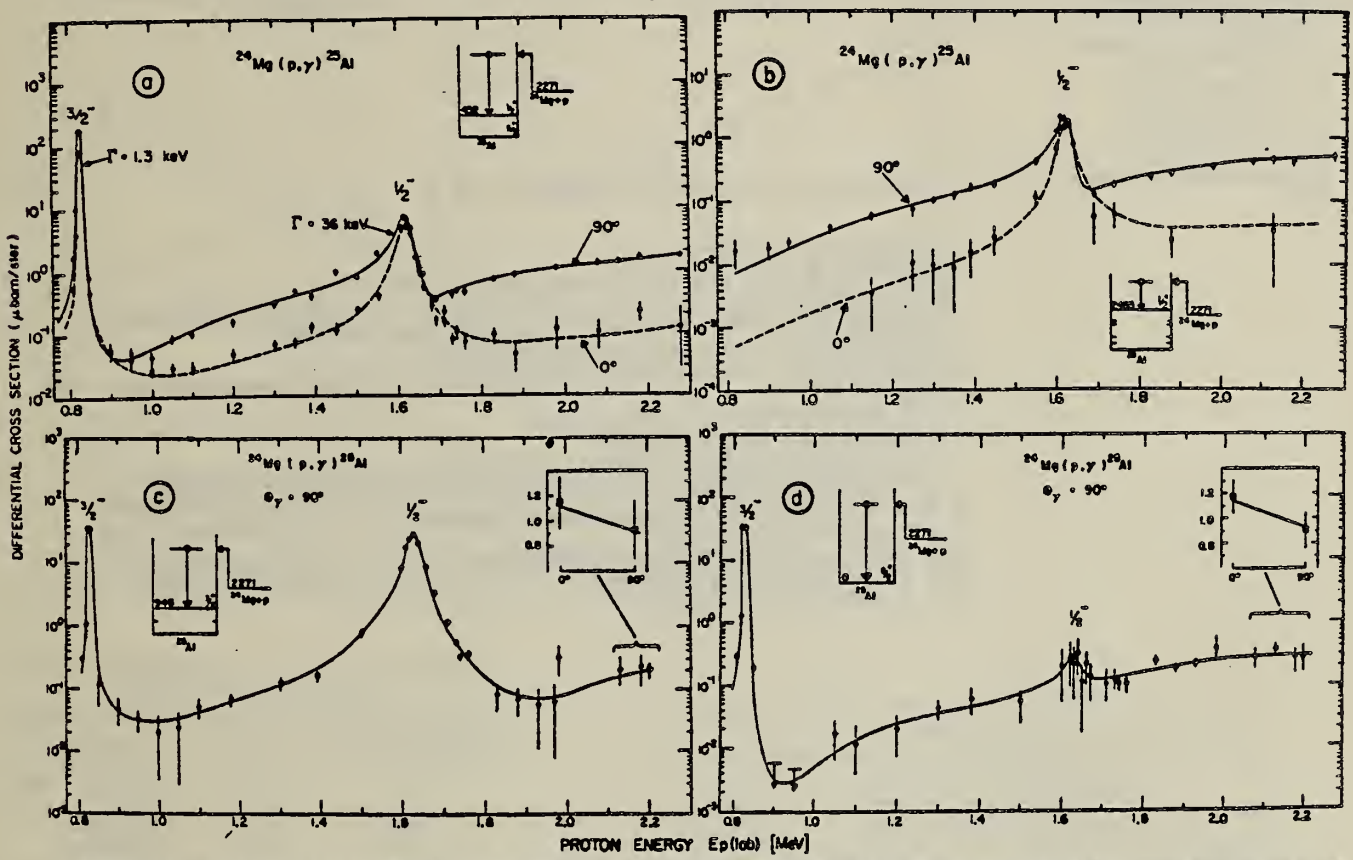

Fig. 4. Excitation functions at $\theta_\gamma = 0°$ and 90° for the transitions to the 452 keV state (a) and 2485 keV state (b). The solid and dashed lines represent best fits to the data (subsects. 3.2 and 3.3). Excitation functions at $\theta_\gamma = 90°$ for the transitions to the ground state and to the 945 keV state are shown in (d) and (c). The solid lines represent the best fits to the data (subsects. 3.4 and 3.5). The insets show the anisotropy of these transitions as observed at $E_p = 2.1$–2.3 MeV and the model predictions for $l_f = 2$ (solid line).

(over)

TABLE 1

Direct capture cross sections for $^{24}Mg(p,\gamma)^{25}Al$ at $E_p = 823$ keV and absolute spectroscopic factors

Transition (keV)	Direct capture $^{24}Mg(p,\gamma)^{25}Al$				Stripping $^{24}Mg(d,n)^{25}Al$		Stripping $^{24}Mg(d,p)^{25}Mg$			Theory[j] (Nilsson model) C^2S		
	σ_{exp} (μb)	σ_{theo}[a]) (μb)	nl_j	C^2S[b])	C^2S[d])	C^2S[e])	C^2S[f])	C^2S[g])	C^2S[h])	$\eta = 2.0$	2.5	3.0
DC → 0	0.008 ± 0.002	0.077	1d	0.10 ± 0.03	0.18	0.58	0.60–0.42	0.26	0.40	0.33	0.33	0.33
DC → 452	0.052 ± 0.011	0.12	2s	0.43 ± 0.09	0.42	0.85	0.50–0.44	0.17	0.76	0.62	0.52	0.44
DC → 945	0.004 ± 0.001	0.035	1d	0.11 ± 0.03	0.14	0.45	0.14–0.32	0.12	0.42	0.13	0.16	0.18
DC → 2485[c])	0.005 + 0.001	0.058	2s	0.08 ± 0.02[i])				0.065	0.18	0.18	0.27	0.35

[a]) Square-well potential with $r_0 = 1.36$ fm [ref. [1])].
[b]) Experimental errors only.
[c]) Bound-state formalism assumed.
[d]) $E_d = 2.3$ MeV [ref. [2])].
[e]) $E_d = 7$–10 MeV [ref. [3])].
[f]) $E_d = 5$–6 MeV [ref. [11])].
[g]) $E_d = 15$ MeV [refs. [12,13])].
[h]) $E_d = 10$ MeV [ref. [4])].
[i]) From the observed proton width [6]) of $\Gamma_p = 11 \pm 2$ meV, a value of $C^2S = 0.05 \pm 0.01$ is deduced at $r_0 = 1.36$ fm.
[j]) Ref. [9]).

1) C. Rolfs, Nucl. Phys. A217 (1973) 29
2) O. Dietsch, D. Wilmore and P. E. Hodgson, Nucl. Phys. A106 (1968) 527
3) S. G. Buccino, D. S. Gemmell, L. L. Lee, Jr., J. P. Schiffer and A. B. Smith, Nucl. Phys. 86 (1966) 353
4) A. Scheib, A. Hofmann, G. Philipp and F. Vogler, Nucl. Phys. A203 (1973) 177
5) P. M. Endt and C. van der Leun, Nucl. Phys. A214 (1973) 1
6) H. P. Trautvetter, Bull. Am. Phys. Soc. 19 (1974) 472; Ph. D. Thesis, Univ. of Toronto (1973), and to be published
7) P. B. Dworkin, Thesis, Univ. of Toronto (1974)
8) M. Piiparinen, Z. Phys. 252 (1972) 206
9) A. E. Litherland, E. B. Paul, G. A. Bartholomew and H. E. Gove, Phys. Rev. 102 (1956) 208; A. E. Litherland, H. McManus, E. B. Paul, D. A. Bromley and H. E. Gove, Can. J. Phys. 36 (1958) 378
10) C. A. Barnes, Nucleosynthesis by charged-particle reactions, vol. 4, ed. M. Baranger and E. Vogt (Plenum, New York, 1971) p. 133
11) A. Gallmann, P. Wagner, G. Frank, D. Wilmore and P. E. Hodgson, Nucl. Phys. 88 (1966) 654
12) B. Čujec, Phys. Rev. 136 (1964) B 1305
13) E. Rost, Phys. Rev. 154 (1967) 994

REF.

D.W.O. Rogers, N. Anyas-Weiss, S.P. Dolan, N.A. Jelley, T.K. Alexander
Can. J. Phys. 55, 206 (1977)

ELEM. SYM.	A	Z
Al	25	13

METHOD

REF. NO.: 77 Ro 1 — hmg

REACTION	RESULT	EXCITATION ENERGY	SOURCE TYPE	SOURCE RANGE	DETECTOR TYPE	DETECTOR RANGE	ANGLE
P,G	LFT	7- 8	D	5, 6	SCD-D		DST

7.90 AND 7.97 MEV STATES

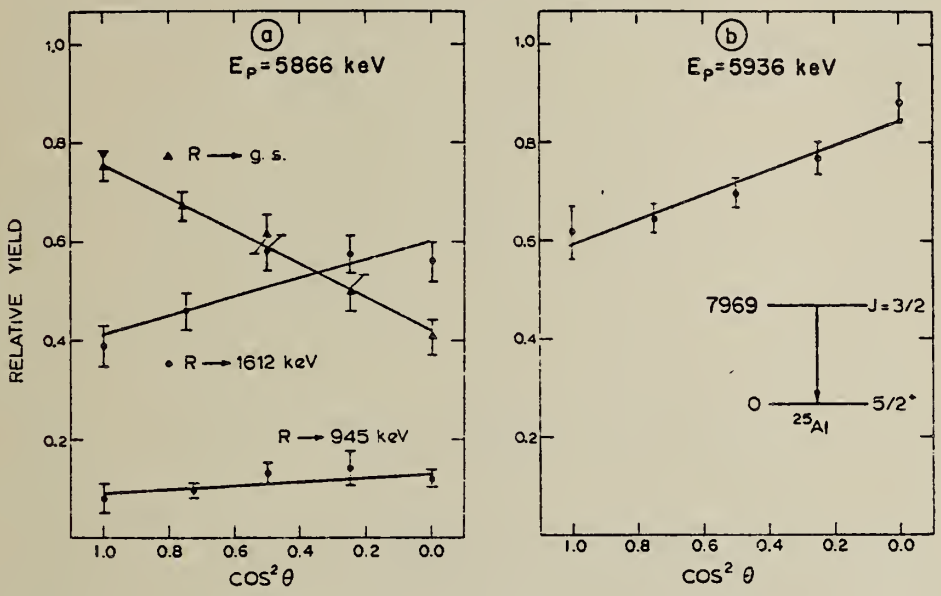

FIG. 2. (*a*) Angular distributions of γ decays from the 7901 keV level. Solid lines are best fits for $J = 5/2$. (*b*) Angular distribution of γ decays from the 7969 keV level. Solid line is best fit for $J = 3/2$.

TABLE 4. Branching ratios from the $T = 3/2$ levels in ^{25}Al compared with previous results

Transition		Present	Morrison *et al.* (1968)
7901	0(5/2⁺)	50 ± 3	41 ± 5
	451(1/2⁺)	<3	—
	945(3/2⁺)	13 ± 2	8 ± 5
	1612(7/2⁺)	37 ± 3	51 ± 7
7969	0(5/2⁺)	100	71 ± 7
	451(1/2⁺)	<5	14 ± 4
	945(3/2⁺)	<5	15 ± 5
	1612(7/2⁺)	<5	—

TABLE 2. Radiative widths and estimates of Γ_γ for the $T = 3/2$ resonances in ^{25}Al

Level (MeV)	$\omega\gamma = \frac{1}{2}(2J+1)\Gamma_{p_0}\Gamma_\gamma/\Gamma$ (eV) Present	Morrison *et al.* (1968)	Γ_γ (eV)[a]
7.90	0.25 ± 0.06	1.0 ± 0.5	0.50 ± 0.13
7.97	0.40 ± 0.09	1.5 ± 0.8	0.40 ± 0.12

[a]Assuming $J = 5/2$ and $3/2$ respectively.

TABLE 3. Mixing ratios and implied transition strengths for the decay of the $T = 3/2$ levels in ^{25}Al and a comparison to shell model calculations

Transition	J_i	χ^2_{min}	δ[a]	$\lvert M\rvert^2$(W.u.) Expt. M1	Expt. E2	Theory[b] M1	Theory[b] E2
7901 → 0(5/2⁺)	5/2	0.9	−0.02 ± 0.03	0.024 ± 0.006	<0.007	0.24	0.26
7901 → 945(3/2⁺)	5/2	1.7	−0.07 ± 0.06	0.009 ± 0.002	<0.02	0.07	0.026
7901 → 1612(7/2⁺)	5/2	8.6	−0.08 ± 0.06	0.035 ± 0.008	<0.1	0.22	0.003
7969 → 0(5/2⁺)	3/2	1.9	−0.11 ± 0.02	0.042 ± 0.012	0.05 ± 0.02	N/A	

[a]Errors are given using the $\chi^2_{min}+1$ rule corresponding to 68% confidence limits (see *e.g.*, Rogers (1975)).
[b]Timmer *et al.* (1976*b*), using their ASDI interaction results.

Morrison, G.C. et al., Phys. Rev. 174, 1366 (1968).
Rogers, D.W.O., Nucl. Instrum. Methods 127, 253 (1975).

A=26

A=26

Ref. D.R. Neher, F.W. Prosser, Jr., R.W. Krone
Nuclear Phys. 31, 231 (1962)

Elem. Sym.	A	Z
Al	26	13

Method: Protron capture; NaI

Ref. No.: 62 Ne 2 | JHH

Reaction	E or ΔE	E_o	Γ	$\int \sigma dE$	Jπ	Notes
$Mg^{25}(p,\gamma)$	0.95-1.80					E_{Po}:
		7.220				0.956 MeV 5% to ground state.
		7.289				1.027 MeV 63% to ground state.
		7.345				1.086 MeV 27% to ground state.
		7.364				1.105 MeV 8% to ground state.
		7.396				1.139 MeV 9% to ground state.
		7.407				1.150 MeV 17% to ground state.
		7.424				1.168 MeV 37% to ground state.
		7.626				1.378 MeV 14% to ground state.
		7.829				1.589 MeV 74% to ground state.
		7.889				1.651 MeV 44% to ground state.
		7.951				1.716 MeV 82% to ground state.

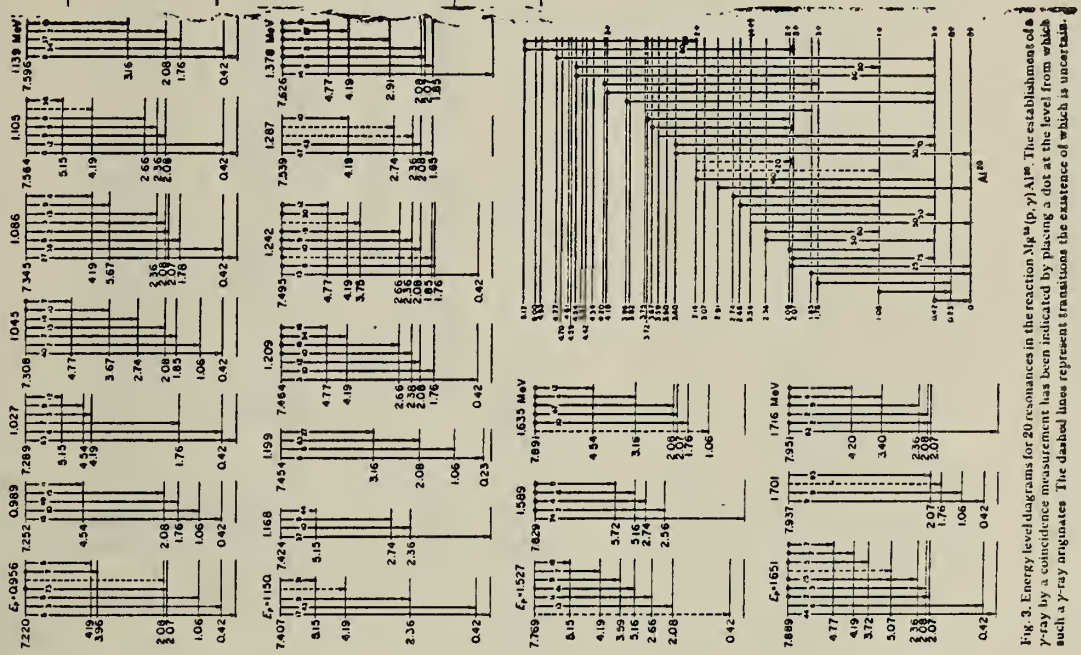

Fig. 3. Energy level diagrams for 20 resonances in the reaction $Mg^{24}(p,\gamma)Al^{25}$. The establishment of a γ-ray by a coincidence measurement has been indicated by placing a dot at the level from which such a γ-ray originates. The dashed lines represent transitions the existence of which is uncertain.

Ref. N.H. Gale, N. Tubbs, N. Nath, A.T.G. Ferguson
Phys. Letters 5, 345 (1963)

Elem. Sym.	A	Z
Al	26	13

Method: Van de Graaff; plastic scintillator; pulsed-beam, delayed coincidence technique

Ref. No.: 63 Ga 1 JHH

Reaction	E or ΔE	E_o	Γ	$\int \sigma dE$	Jπ	Notes
$Mg^{25}(p,\gamma)$	1.00	0.418				Lifetime of 0.418 MeV level given in Table I, below.

Table 1

Isomeric level	τ_m (ns)	Reference
Al^{25*} (450 keV)	2.6 ± 0.4	1)
	2.71 ± 0.14	2)
	3.33 ± 0.07	3)
	3.25 ± 0.15	present work
Al^{26*} (418 keV)	1.77 ± 0.07	2)
	1.86 ± 0.09	present work

1) A.T.G. Ferguson, M.A. Grace and J.O. Newton, Nuclear Phys. 17 (1960) 1.
2) S. Gorodetzky et al., Proc. of the Conf. on Electromagnetic Lifetimes and Properties of Nuclear States, Gatlinburg (1962), p. 79.
3) C.L. McClelland and J. Lowe, Proc. of the Conf. on Electromagnetic Lifetimes and Properties of Nuclear States, Gatlinburg (1962), p. 78.

REF. E.O. De Neijs, M.A. Meyer, J.P.L. Reinecke, D. Reitmann
Nucl. Phys. A230, 490 (1974)

EL.EM. SYM.	A	Z
Al	26	13

METHOD

REF. NO. 74 De 9 egf

REACTION	RESULT	EXCITATION ENERGY	SOURCE		DETECTOR		ANGLE
			TYPE	RANGE	TYPE	RANGE	
P,G	LFT	6- 8	D	0- 2	SCD-D		DST

TABLE 1

Energies and strengths of ^{25}Mg+p resonances for $E_p < 2$ MeV

E_p (keV) present experiment	E_p (keV) ref. [12])	$S=(2J+1)\Gamma_\gamma\Gamma_p/\Gamma^a)$ (eV)	E_p (keV) present experiment	E_p (keV) ref. [12])	$S=(2J+1)\Gamma_x\Gamma_p/\Gamma^a)$ (eV) $x=\gamma$	$x=p_1$	$x=p_2$
316.6±0.7	316.4±0.5	0.2	985.7±0.6	988 ±3	2.6	0.2	
387.4±0.6	390.0±0.5	0.3	1025.2±0.7	1027 ±1	0.8	0.006	
433.0±0.6	435.1±0.7	0.67±0.10 [b])	1042.4±0.7	1043.7±0.6	3.5		
496.1±0.6	496.5±0.6	0.5	1084.3±0.7	1085 ±2	2.3	0.01	
502.1±0.6	501.7±0.8	0.4	1102.6±0.7	1105.9±1.3	0.9	0.006	
514.3±0.6	514.5±0.6	0.3	1137.3±0.7	1137.3±1.0	3.1	0.2	
532.5±0.6	532.8±0.5	0.1	1148.4±0.7	1149 ±2	1.9	0.02	
	535.4±1.0		1164.3±0.7	1165 ±2	0.9	0.02	
568.0±0.7	566.3±0.7	2.0	1183.7±0.7	(1186 ±3)		(10)	
	570.5±1.5		1195.2±0.7	1196.6±0.7	2.0	0.9	
591.9±0.7	591.7±0.4	1.7	1205.4±0.7	1209 ±5	2.4	0.1	
654.9±0.7	655.7±0.8	0.2	1238.2±0.7	1238.3±0.8	3.9	16	
684.6±0.7	684.0±0.8	3.1	1283.8±0.7	1284.8±0.6	3.6	strong	
721.7±0.7	723.9±0.5	1.5	1302.1±0.7		2.2	yes	0.04
736.2±0.7		0.3	1306.5±0.7	1305.4±0.5	4.1	yes	0.2
773.7±0.7	778.1±0.7	1.1	1337.7±0.7	1332	yes		
810.7±0.7	811.9±0.7	1.4	1342.3±0.7	(1341)	yes		
818.1±0.7		0.1	1351.6±0.7	(1354 ±3)		yes	
834.6±0.7		0.3	1370.9±0.7			yes	
879.8±0.6	883.2±0.7	1.7	1375.5±0.7	1376 ±2	strong	yes	
888.0±0.8	890.8±1.5	0.3	1514.7±0.7		yes	yes	yes
895.1±0.8	(903 ±4)	0.4	1525.6±0.7	1531 ±4	1.3	4.1	0.3
927.6±0.6	929.5±0.6	1.8	1568.5±0.7	1573 ±4			strong
952.7±0.6	956 ±2	3.3	1587.5±1.0	1592 ±5	3.2		0.4
968.1±0.8	970 ±2	0.2	1633.6±1.7		2.4		1.7
			1639.1±1.7	1638 ±4		strong	
			1651.1±0.8	1652 ±4	14	5.0	0.3
			1700.5±1.2	1701	10	6.5	4.3
			1716.1±1.4	1713 ±4	17	1.1	0.5

[a]) Present experiment; errors are of the order of 30 %.
[b]) Ref. [14]).

[12] P.M. Endt and C. van der Leun, Nucl. Phys. A105 (1967) 1
[14] G.A.P. Engelbertink and P.M. Endt, Nucl. Phys. 88 (1966) 12

(over)

TABLE

Gamma decay of $^{25}Mg(p,\gamma)^{26}Al$ resonances (the total decay to the triplet at E_x = 2.07 MeV is given)

Resonances			Decay in percentages to E_x (MeV) in ^{26}Al										
E_p [a] (keV)	E_x [b] (keV)	J^π [c]	0 5^+	0.23 0^+ ($T=1$)	0.42 3^+	1.06 1^+	1.76 2^+	1.85 1^+	2.07	2.36 3^+	2.55 3^+	2.66 $(2,3)^+$	other levels E_x (%)
317	6609	2, 3	< 0.4	< 0.5	34	< 0.9	18	< 0.4	7		2		2.91(3), 3.16(13), 3.60(4), 3.750(1), 4.19(18)
387	6677	1, 2, 3	< 0.2	1	8	3	< 0.7	6	21				3.16(7), 4.19(30), 4.55(4), 4.60(18), 5.54(2)
433	6721	3^+, 4	51	< 0.3	30	< 0.3	< 0.2	< 0.5		1	2		4.19(7), 4.60(5), 4.71(4)
496	6782	3	< 0.3	< 0.3	2	< 0.8	15	< 1	23	1			2.91(4), 3.07(10), 3.16(32), 4.19(6), 4.55(7)
502	6788	2	< 0.5	< 0.5	52	< 0.9	16	< 0.4	5				3.16(8), 3.60(1), 3.68(4), 4.19(5), 4.71(9)
514	6799	1, 2, 3	< 0.1	< 0.3	1	3	14	2	16			8	2.91(6), 3.16(26), 3.68(2), 3.72(2), 4.19(4), 4.55(9), 4.60(7)
533	6817	3^+, 4	< 0.9	< 0.3	18	< 0.7	< 0.5	< 1	2 [d]	19	46		3.07(2), 3.40(3), 3.60(3), 3.67(2) 3.96(5)
568	6851	2, 3	< 0.1	< 0.4	35	< 0.9	7		10 [d]		24		2.91(8), 3.07(1), 3.16(2), 3.60(6), 4.35(4), 4.55(2), 4.95(1)
592	6874	2, 3^+	< 0.1	1	30	1	8	2	9		24		2.91(6), 3.07(2), 3.16(3), 3.60(7), 3.72(1), 4.35(4), 4.55(1), 4.95(1)
655	6935	1, 2	< 0.3	8	< 0.4	26	21	< 1	8			3	2.91(3), 3.16(15), 3.750(4), 3.753(1), 5.14(11)
685	6963	2, 3	< 0.5	< 0.2	41	< 0.5	28		2	1	1	4	3.07(1), 3.16(1), 3.60(2), 3.67(1), 3.68(7), 4.19(1), 5.39(5), 5.67(5)
722	6999	1^+, 2, 3	< 0.2	< 0.2	10	< 0.6	2	1	44		5		2.91(2), 3.16(4), 3.60(1), 4.35(1), 4.55(27), 4.60(1), 5.14(2)
736	7013	3	6	< 0.2	5	< 0.7	< 0.5	< 0.4	3	2	1		3.60(1), 3.67(2), 3.96(8), 4.21(1), 4.71(12), 4.77(1), 5.13(31), 5.24(1), 5.73(26)
774	7049	2, 3	< 0.2	< 0.1	5	< 0.2	1	< 0.4	18				3.16(57), 4.71(12), 5.13(7)
811	7084	1	< 0.2	12	< 0.1	< 0.6	0.5	7	51			1	2.74(0.5), 2.91(3), 3.16(2), 3.72(11), 3.750(2), 3.753(1), 4.48(4), 4.94(3), 5.91(2)
818	7091	1, 2, 3^-	< 0.7	2	3	< 3	10	< 2	54				4.55(28), 5.14(3)
835	7107	3, 4	9	< 2	49	< 0.9	< 0.5	< 1	9	9	7		2.91(1), 3.60(2), 3.68(3), 4.43(6), (4.60(3), 4.71(2))
880	7151		< 0.1	< 0.1	1		< 0.1	0.5	5	1.5	2		2.91(1), 3.16(83), 4.55(3), 4.60(1), 5.14(2)
888	7159		< 1	< 1	28		4	< 1	46				(3.16(6)), 3.67(6), 3.68(4), 4.35(1), 4.55(5)
895	7165	2^+, 3, 4	< 0.9	< 0.6	17		< 0.6	< 1	27	12	10		3.07(5), 3.60(6), 3.68(3), 4.60(7), 4.71(9), (5.13(4))
928	7197	1	< 0.2	72	< 2	< 1	< 0.5	< 0.2	23 [d]				3.750(1), 3.753(3), 5.14(1)
953	7221	5	2	< 0.1	< 0.1	< 0.4	< 2	< 0.5	82 [d]				3.40(2), 3.67(9), 4.21(3), 5.24(2)
968	7236	1, 2^+	< 0.3	< 0.4	3	< 1	8	< 0.5				24	2.91(6), 3.07(7), 3.16(37), 3.753(3), 4.19(3), 4.71(9)
986	7252	1^+, 2, 3	< 0.1	< 0.1	6	1	43	< 0.2	5	4			2.74(1), 2.91(7), 3.07(1), 3.16(12), 3.60(4), 3.68(1), 3.750(7), 3.753(1), 4.19(1), 5.69(6)
1025	7290	3^+	58	< 0.3	2	< 0.3	5	< 1					3.68(1), 3.750(5), 4.19(1), 4.60(12), 4.71(4), 5.13(12)
1042	7307	1^+, 2, 3^+	< 0.3	< 0.4	31	6	5	1	10	3	2	6	2.74(6), 2.91(12), 3.07(1), 3.60(9), 3.68(1), 3.72(2), 3.750(3), 4.35(0.5), 5.58(1.5)
1084	7347	3^+, 4, 5^+	18	< 0.3	39	< 0.3	< 0.2	< 0.2		14	4		3.07(2), 3.60(3), 3.67(1), 3.68(4), 4.19(2), 4.60(1), 4.71(2), 5.46(1), 5.69(5), 6.08(4)
1103	7365	3	4	< 0.6	7	< 0.6	< 0.4	< 0.6	4		1		3.60(2), 3.96(2), 4.35(4), 4.71(8), 5.13(68)
1137	7398		< 0.2	< 0.7	37	< 0.3	16	0.5	3	1.5	0.5	7	2.91(4), 3.07(3), 3.16(6), 3.60(5), 3.67(0.5), 3.68(4.5), 3.750(0.5), 4.19(1.5), 4.60(3), 4.77(0.5), 5.46(6)
1148	7409	3^+, 4, 5^+	16	< 0.3	48	< 0.3	< 0.4			9	1		3.07(2), 3.40(1), 3.60(3), 3.67(1), 3.68(3), 4.19(1), 4.71(2), 5.69(7), 6.08(6)
1164	7424	3	32	< 0.4	0.5	< 0.4	1			2		2	2.91(7), 3.40(0.5), 4.60(2), 4.71(3), 5.13(50)
1195	7454	1, 2	< 0.1	2	1	1	< 0.5	2	67 [d]				3.16(26), 3.750(0.5), 5.14(0.5)
1205	7464	2, 3, 4^+	< 0.2	< 0.1	2	< 0.4	6		10	7	9	7	3.16(6), 3.60(1), 3.67(20), 3.68(3), 3.750(1), 4.21(14), 4.60(1), 4.71(3), 4.95(3), [illegible]

REACTION	RESULT	EXCITATION ENERGY	SOURCE TYPE	SOURCE RANGE	DETECTOR TYPE	DETECTOR RANGE	ANGLE

TABLE 2 (continued)

Resonances			Decay in percentages to E_x (MeV) in ^{26}Al									
E_p [a]) (keV)	E_x [b]) (keV)	J^π [c])	0 5^+	0.23 0^+ ($T=1$)	0.42 3^+	1.06 1^+	1.76 2^+	1.85 1^+	2.07	2.36 3^+	2.55 3^+	2.66 $(2,3)^+$	Other levels E_x (%)
1238	7495		< 0.2	< 0.3	8	< 0.3	4	1	8	8	8	6	2.74(1), 3.07(1), 3.16(14), 3.67(13), 3.68(2), 3.750(2), 3.96(3), 4.21(13), 4.60(1), 4.71(1), 4.95(3), 5.13(2), 5.14(1)
1284	7539	1^+ [d])	< 0.4	< 0.5	5	< 1	13	10	19	5		5	2.74(18), 3.72(4), 3.750(4), 4.35(2), 4.62(15)
1302	7557	$1^+, 2, 3^+$			1	1	3	3	23	12	4	1	2.74(3), 2.91(1), 3.16(37), 3.60(6), 4.35(2), 4.60(3)
1307	7561	$1^+, 2, 3^+$		1	3	1	6	6	21	24	11	3	2.74(5), 3.07(1), 3.60(13), 3.96(2), 4.35(3)
1376	7627	$4^+, 5, 6^+$	7	< 0.7	< 0.7		< 0.7	< 1	5				3.40(2), 3.51(6), 3.67(9), 4.21(45), 4.60(1), 4.77(15), 5.24(10)
1526	7771		1	< 0.1	5	1	4	1	7			3	2.74(1), 2.91(1), 3.16(33), 3.72(1), 4.19(11), 4.55(1), 4.60(18), 5.13(5), 5.14(1), 5.54(5), 5.73(1)
1588	7831	3^+	58	< 0.3	3	< 0.4		< 0.6	0.5	2	1	1	3.07(5), 3.16(1), 3.40(0.5), 3.67(1), 3.750(1), 4.19(6), 4.21(1), 4.60(7), 5.13(10), 5.51(1), 5.73(1)
1634	7875		< 0.5		1	< 0.7		< 1	69		1		3.16(5), 3.750(2), 4.19(1), 4.55(8), 4.60(7), 5.14(4), 5.54(2)
1651	7892	4^+ [d])	40	< 0.3	5	< 0.4		< 0.4	3.5	28	1		3.07(6), 3.40(1), 3.67(1), 3.68(1), 3.96(0.5), 4.21(4.5), 4.35(1), 4.77(4), 4.95(3), 5.24(0.5)
1701	7940	$3, 4, 5^+$	< 0.1	< 0.2	5		< 0.5		75	3	6	3	3.68(0.5), 3.750(3), 3.96(2), 4.35(1), 4.77(1), 5.85(0.5)
1716	7955	4^+ [d])	77	< 0.4	1	< 0.6	< 0.3		3	9	0.5		3.16(0.5), 3.40(4), 3.68(0.5), 3.96(1), 5.51(3.5)

[a]) Present experiment.
[b]) Calculated with present values for E_p and $Q = 6305.0 \pm 1.2$ keV.
[c]) Present experiment unless otherwise indicated. See also subsects. 3.6 and 4.1.
[d]) Ref. [12]).
[e]) Decays to the $E_x = 2.0695$ MeV level only.
[f]) Decays to the $E_x = 2.0687$ MeV level only.

(over)

TABLE 5

Angular distribution coefficients

E_γ (keV)	Transition	$A_2 \pm \Delta A_2$ a)	$A_4 \pm \Delta A_4$ a)	E_γ (keV)	Transition	$A_2 \pm \Delta A_2$ a)	$A_4 \pm \Delta A_4$ a)
317	$r \rightarrow 0.42$	-0.43 ± 0.03	0.08 ± 0.05	655	$r \rightarrow 0.23$	-0.31 ± 0.07	0.16 ± 0.12
	$r \rightarrow 1.76$	0.24 ± 0.04	0.03 ± 0.06		$r \rightarrow 1.06$	-0.14 ± 0.06	0.13 ± 0.09
	$r \rightarrow 3.16$	0.11 ± 0.06	-0.19 ± 0.09		$r \rightarrow 1.76$	-0.16 ± 0.03	0.12 ± 0.06
387	$r \rightarrow 0.42$	-0.08 ± 0.06	-0.07 ± 0.10	685	$r \rightarrow 0.42$	-0.25 ± 0.02	0.04 ± 0.04
	$r \rightarrow 1.85$	-0.08 ± 0.06	-0.08 ± 0.09		$r \rightarrow 1.76$	-0.03 ± 0.01	-0.01 ± 0.02
433	$r \rightarrow 0$	-0.22 ± 0.01	0.01 ± 0.02	722	$r \rightarrow 0.42$	0.01 ± 0.02	0.08 ± 0.03
	$r \rightarrow 0.42$	-0.38 ± 0.06	0.05 ± 0.09		$r \rightarrow 2.0695$	-0.14 ± 0.01	0.03 ± 0.01
496	$r \rightarrow 0.42$	-0.07 ± 0.08	0.05 ± 0.12	736	$r \rightarrow 0$	-0.06 ± 0.06	-0.17 ± 0.10
	$r \rightarrow 1.76$	-0.58 ± 0.03	0.17 ± 0.04		$r \rightarrow 0.42$	0.33 ± 0.13	-0.24 ± 0.19
	$r \rightarrow 3.16$	-0.52 ± 0.06	0.07 ± 0.09	774	$r \rightarrow 0.42$	-0.26 ± 0.03	0.08 ± 0.05
502	$r \rightarrow 0.42$	-0.49 ± 0.05	0.08 ± 0.07		$r \rightarrow 3.16$	-0.06 ± 0.03	-0.02 ± 0.04
	$r \rightarrow 1.76$	0.11 ± 0.06	-0.11 ± 0.08	811	$r \rightarrow 0.23$	-0.05 ± 0.02	0.04 ± 0.03
514	$r \rightarrow 1.06$	-0.30 ± 0.07	-0.07 ± 0.11		$r \rightarrow 1.85$	0.14 ± 0.04	-0.08 ± 0.06
	$r \rightarrow 1.76$	-0.10 ± 0.05	0.03 ± 0.08	835	$r \rightarrow 0$	0.01 ± 0.04	0.05 ± 0.07
	$r \rightarrow 1.85$	0.04 ± 0.16	-0.16 ± 0.24		$r \rightarrow 0.42$	-0.28 ± 0.02	0.00 ± 0.03
533	$r \rightarrow 0.42$	-0.19 ± 0.04	0.04 ± 0.06	928	$r \rightarrow 0.23$	-0.09 ± 0.02	-0.04 ± 0.04
	$r \rightarrow 2.36$	-0.14 ± 0.04	-0.02 ± 0.06		$r \rightarrow 2.0695$	0.04 ± 0.02	-0.06 ± 0.03
	$r \rightarrow 2.55$	-0.22 ± 0.05	0.02 ± 0.08	953	$r \rightarrow 0$	0.46 ± 0.02	-0.13 ± 0.03
568	$r \rightarrow 0.42$	-0.11 ± 0.04	-0.02 ± 0.07		$r \rightarrow 2.0687$	-0.26 ± 0.00	0.00 ± 0.00
	$r \rightarrow 1.76$	-0.17 ± 0.03	-0.04 ± 0.05	986	$r \rightarrow 0.42$	0.00 ± 0.03	0.07 ± 0.04
	$r \rightarrow 2.55$	-0.13 ± 0.03	-0.01 ± 0.05		$r \rightarrow 1.76$	-0.39 ± 0.02	0.01 ± 0.03
592	$r \rightarrow 0.42$	-0.07 ± 0.01	-0.01 ± 0.02				
	$r \rightarrow 1.76$	-0.18 ± 0.05	0.06 ± 0.08				
	$r \rightarrow 2.55$	-0.15 ± 0.02	0.12 ± 0.04				

a) Corrected for finite size of the detector.

A=27

A=27

P.S. Baranov, V. I. Goldanskii
Zhur. Eksp. i Teoret. Fiz. 28, 746 (1955)
Soviet Phys. JETP 1, 613 (1955)

A1	27	13

METHOD

REF. NO. 55 Ba 5 EGF

Synchrotron; ion chamber monitor; $^{12}C(n,2n)$ threshold detector

REACTION	RESULT	EXCITATION ENERGY	SOURCE		DETECTOR		ANGLE
			TYPE	RANGE	TYPE	RANGE	
G,XN	ABY	30-200	C	150-250	THR	30-	DST

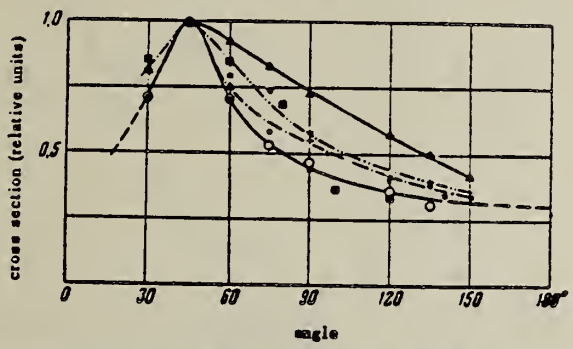

FIG. 2. Angular distribution of photoneutrons with energies higher than 30 mev. ● – C_{250}, + – C_{200}; ▲ – Be_{250}; ○ – Al_{250}; * – Pb_{250}; ■ – data of work[5].

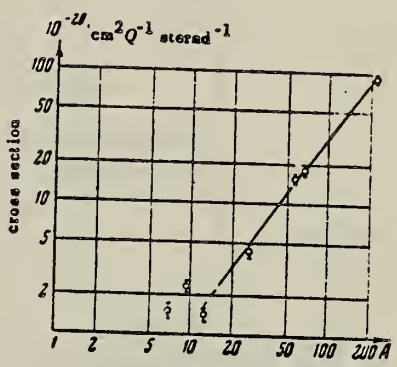

FIG. 4. The dependence of the yield of photoneutrons with energies higher than 30 mev at an angle of 90° (in units $10^{-28} cm^2$ per eff. quant steradian on the mass number A).

Ref.	Elem. Sym.	A	Z
W.R. Dixon Can. J. Phys. 33, 785 (1955)	Al	27	13

Method	Ref. No.	
Synchrotron; neutron angular distribution; scintillator; ion chamber	55 Di 1	NVB

Reaction	E or ΔE	E_0	Γ	$\int \sigma dE$	Jπ	Notes
Al(γ,xn)	70					Curves fitted to a + b $\sin^2\theta$

TABLE II

EXPERIMENTAL VALUES FOR b/a

Target	Correction factor for self-scattering	Corrected b/a
Lead	1.10	-0.08 ± 0.08
Tin	1.08	0.12 ± 0.17
Copper	1.48	0.23 ± 0.15
Iron	1.35	0.09 ± 0.25
Aluminum	1.17	0.36 ± 0.29
Carbon	1.8	1.6 ± 0.8
Beryllium (1)	2.6	1.2 ± 0.4
Beryllium (2)	1.35	

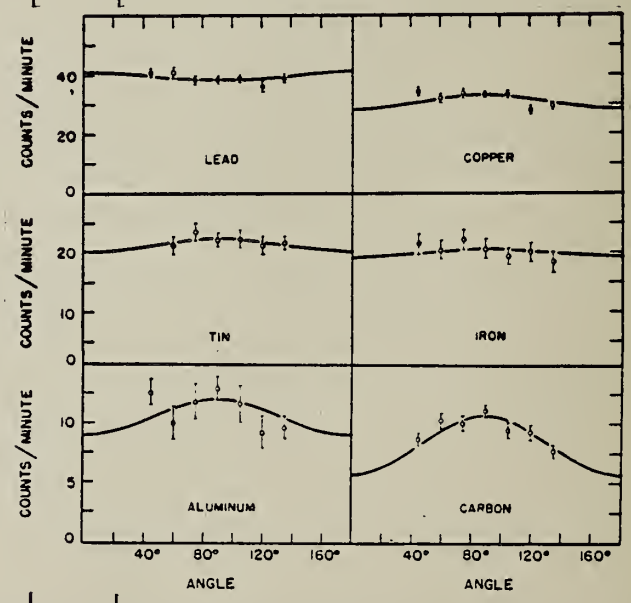

REF.

Sven A. E. Johansson
Phys. Rev. 97, 434-43 (1955)

ELEM. SYM.	A	Z
Al	27	13

METHOD
Synchrotron; ZnS counter; ion chamber

REF. NO. 55 Jo 1 NVB

REACTION	RESULT	EXCITATION ENERGY	SOURCE		DETECTOR		ANGLE
			TYPE	RANGE	TYPE	RANGE	
G,P	RLY	THR - 65	C 65		SCI-D	14 - +	DST
G,N	RLY	15 - 65	C 65		SCI-D	2 - +	DST
G,N	RLY	18 - 65	C 65		SCI-D	5 - +	DST
G,N	RLY	23 - 65	C 65		SCI-D	10 - +	DST

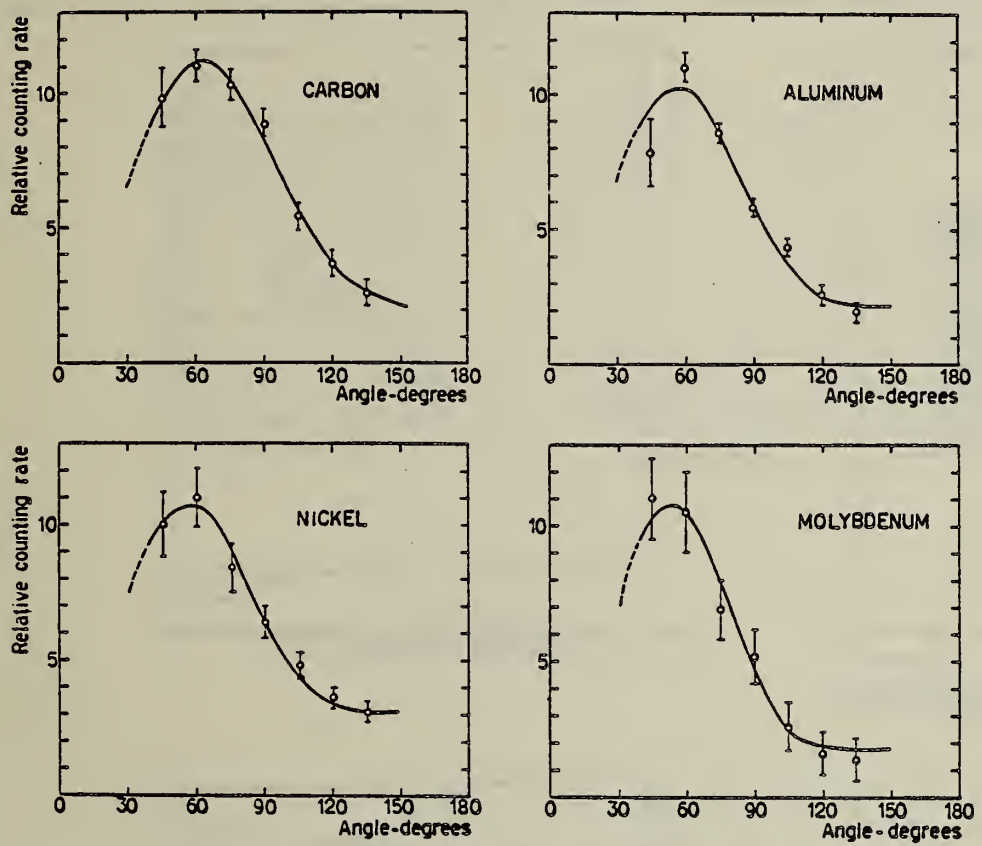

FIG. 5. The angular distributions of protons with an energy above 14 Mev.

(Aluminum)

TABLE I. Target thickness and the constants a and b in the angular distribution curve $a+(\sin\theta+b\sin\theta\cos\theta)^2$.

Element	Target thickness mg/cm²	a	b
Carbon	182	0.32	0.80
Aluminum	274	0.58	1.35
Nickel	352	0.94	1.45
Molybdenum	295	0.62	2.00

(For Protons)

REF.

Sven A. E. Johansson
Phys. Rev. 97, 434-43 (1955)

ELEM. SYM.	A	Z
Al	27	13

METHOD

Synchrotron; ZnS counter; ion chamber

REF. NO. 55 Jo 1 NVB

REACTION	RESULT	EXCITATION ENERGY	SOURCE		DETECTOR		ANGLE
			TYPE	RANGE	TYPE	RANGE	

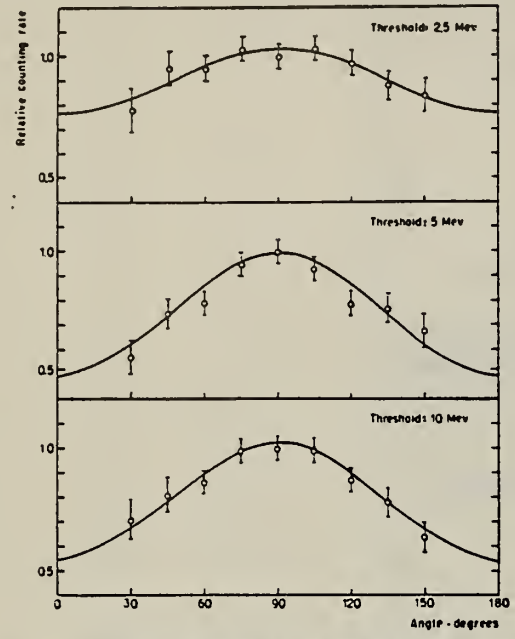

FIG. 7. The angular distributions of the neutrons from aluminum. Counter thresholds at 2.5, 5, and 10 Mev.

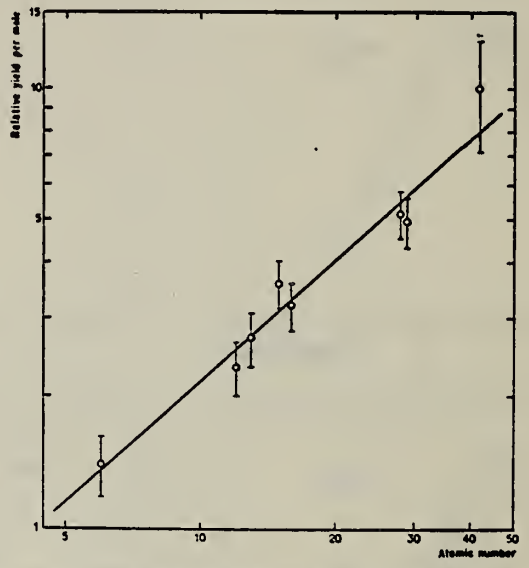

FIG. 10. The relative yield per mole for protons above 14 Mev as a function of the atomic number.

Curves of form $a + b \sin^2\theta$

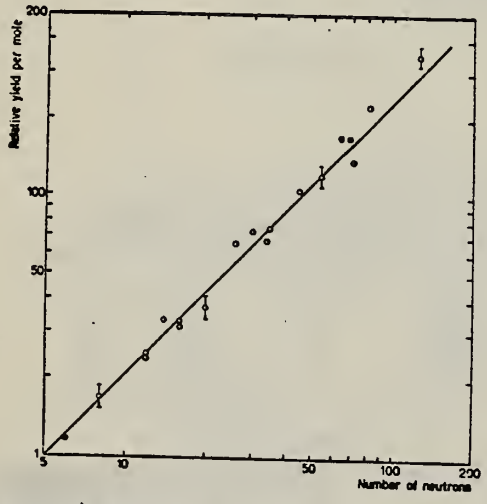

FIG. 11. The relative yield per mole for neutrons above 7.5 Mev as a function of the neutron number.

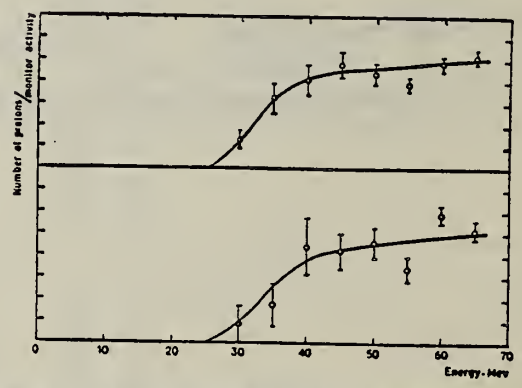

FIG. 12. The ratio between the number of high-energy protons and the activity of the monitor foil as a function of the sychrotron energy. The top curve is for aluminum and the bottom curve is for phosphorus.

U.S. DEPARTMENT OF COMMERCE
NATIONAL BUREAU OF STANDARDS

REF.

D. Reagan
Phys. Rev. 100, 113-120 (1955)

ELEM. SYM.	A	Z
Al	27	13

METHOD

Linac; counted delayed neutrons from N^{17}

REF. NO. 55 Re 1 NVB

REACTION	RESULT	EXCITATION ENERGY	SOURCE		DETECTOR		ANGLE
			TYPE	RANGE	TYPE	RANGE	
G,N17	ABI	THR - 400	C	80-400	ACT-1		4PI

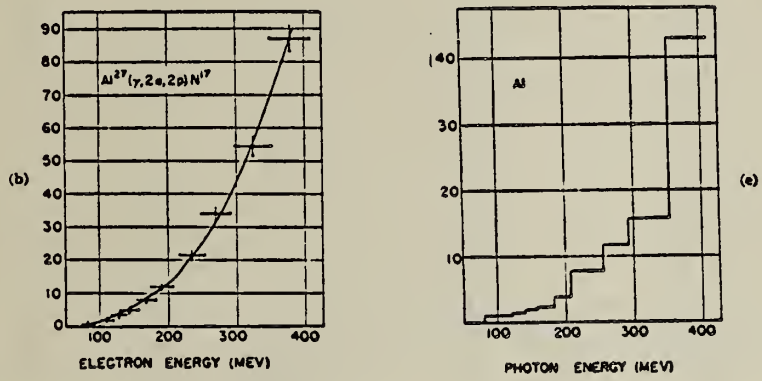

FIG. 5. Graphs a, b, and c show activation points for N^{17} yields in magnesium and aluminum. Graphs d, e, and f are the calculated photon cross sections, from which the solid lines in a, b, and c have been reconstructed. The third cross-section curve is actually the slightly modified result of an early aluminum run, and is included to illustrate the effects of moderate errors in data upon the photon cross section results.

Ref. W.K. Dawson
Can. J. Phys. 34, 1480 (1956)

Elem. Sym.	A	Z
Al	27	13

Method: Synchrotron; proton yield; spectrum; angular distribution; nuclear emulsion; ion chamber

Ref. No.: 56 Da 2 | NVB

Reaction	E or ΔE	E_o	Γ	$\int \sigma dE$	Jπ	Notes
$Al^{27}(\gamma,xp)$	70					Yield = 4.0×10^5 protons (up to 14 MeV)/r-mole ±30% from 70 MeV bremss.

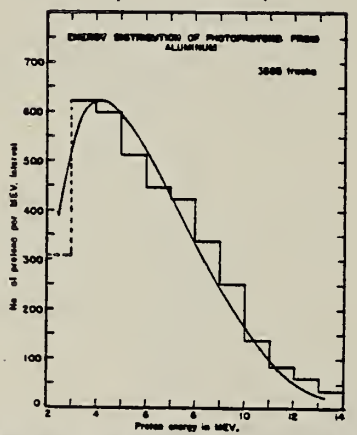

FIG. 2. The smooth curve is the energy distribution calculated assuming compound-nucleus formation only and a constant nuclear temperature of 2.1 Mev. The histogram represents the experimental results.

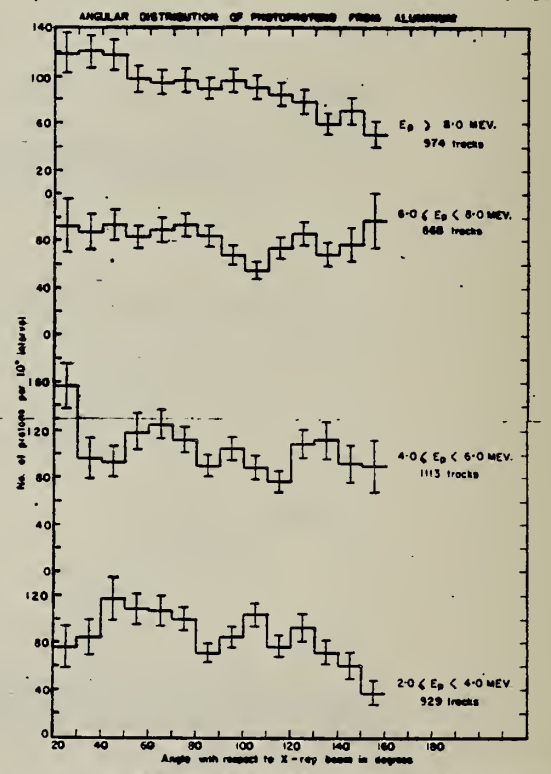

FIG. 6. The angular distributions of photoprotons of various energies from aluminum. Standard deviations are shown.

Ref. E.G. Fuller, E. Hayward
Phys. Rev. 101, 692 (1956)

Elem. Sym.	A	Z
Al	27	13

Method: Betatron; photon scattering; NaI spectrometer

Ref. No.: 56 Fu 1 | NVB

Reaction	E or ΔE	E_o	Γ	$\int \sigma dE$	Jπ	Notes
$Al^{27}(\gamma,\gamma)$	Bremss. 4-40					Detector at 120°. Cross sections given here are 13% too high due to erroneous cos β factor in denominator of Eq. 5. [See Footnote 8 in Phys. Rev. 106, 993 (1957)].

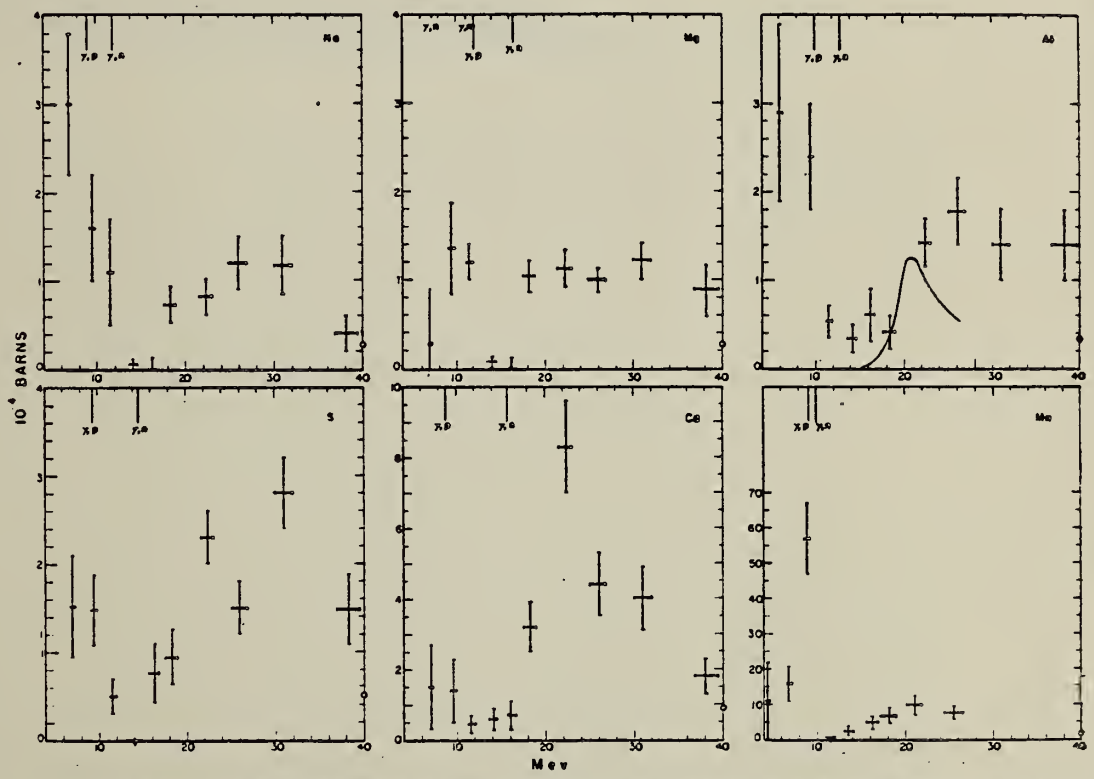

FIG. 4. The elastic scattering cross sections for Na, Mg, Al, S, Ca, and Mn. The indicated spread in energy is the width of the differential discriminator channel, and the standard deviations are based only on the number of counts. The vertical lines at the top represent the particle thresholds for the most important isotopes. The open circles at the extreme right indicate the magnitude of the Thomson cross section for Z free protons scattering coherently. The solid curve superimposed on the Al data is the scattering cross section calculated from the dispersion relation by substituting for $\sigma_a(E)$ in Eq. (6) the sum of the neutron and proton yield[1,18] cross sections.

REF.

F. Heinrich and H. Waffler
Helv. Phys. Acta 29, 232 (1956)

ELEM. SYM.	A	Z
Al	27	13

METHOD

REF. NO. 56 He 1 EGF

REACTION	RESULT	EXCITATION ENERGY	SOURCE		DETECTOR		ANGLE
			TYPE	RANGE	TYPE	RANGE	
G,T	RLY	THR-31	C	31	ACT-I		4PI

Yields relative to (G,N) yields.

Tabelle 1.
Experimentelle und theoretische nukleare Ausbeute der (γ, T)-Prozesse.

Element	$\eta_{exp} \times 10^5$	$\eta_{theor} \times 10^5$
Al	240 ± 14	200
Co	$.6 \pm 1,7$	4
Cu	$4,5 \pm 1,5$	3

REF.

H. Waffler and F. Heinrich
Physica 22, 1146 (1956)

ELEM. SYM.	A	Z
Al	27	13

METHOD

REF. NO.	
56 Wa 1	EGF

REACTION	RESULT	EXCITATION ENERGY	SOURCE		DETECTOR		ANGLE
			TYPE	RANGE	TYPE	RANGE	
G,T	RLY	THR - 31	C	31.	ACT-I		4PI

Detected activity of tritium. Yields are relative to $^{63}Cu(\gamma,n)$.

Reaction	Threshold energy MeV	$\eta_{exp} \times 10^5$	$\eta_{theor} \times 10^5$
Al	18.2 ± 0.2	34 ± 2	31
Co	16.5 ± 0.3	7 ± 2	5
^{63}Cu	16.2 ± 0.3	6 ± 2	4
^{65}Cu	15.1 ± 0.3		
^{107}Ag	13.9 ± 0.6	6.5 ± 1	0.4
^{109}Ag	13.1 ± 0.6		

The table shows the calculated yield ratios (according to statistical theory) as well as the measured relative yield

$$\eta = \int_0^{31\ \mathrm{MeV}} N(E_\gamma)\, \sigma^{(x)}(\gamma,f) E_\gamma\, dE_\gamma \Big/ \int_0^{31\ \mathrm{MeV}} N(E_\gamma)\, \sigma^{(^{63}Cu)}(\gamma,f)\, E_\gamma\, dE_\gamma$$

taking the (γ, n) yield on ^{63}Cu as unity. The good agreement between the experimental

REF.
E. B. Bazhanov, Iu. M. Volkov, A. P. Komar, L. A. Kul'chitskii and V. P. Chizhov
Dokl. Akad. Nauk SSSR 113, 65 (1957)
Soviet Phys. Dokl. 2, 107 (1957)

ELEM. SYM.	A	Z
Al	27	13

METHOD

REF. NO. 57 Ba 2 · EGF

REACTION	RESULT	EXCITATION ENERGY	SOURCE		DETECTOR		ANGLE
			TYPE	RANGE	TYPE	RANGE	
G,XP	SPC	THR - 85	C	85	TEL-D	15-60	DST

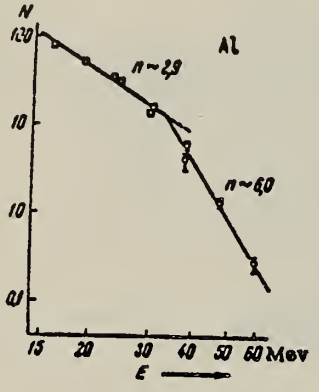

Fig. 2. Energy distribution of photoprotons from Al. The vertical axis gives the number of protons in a 1 Mev interval per monitor unit, in arbitrary units. Only the statistical errors are indicated.

REF.

F. Bobard, G. Boulegue, and P. Chanson
Compt. Rend. 244, 1761 (1957)

ELEM. SYM.	A	Z
Al	27	13

METHOD

REF. NO. 57 Bo 1 EGF

REACTION	RESULT	EXCITATION ENERGY	SOURCE TYPE	SOURCE RANGE	DETECTOR TYPE	DETECTOR RANGE	ANGLE
G,A	SPC	THR - 30	C	31	EMU-D	5-15	
							NO ANG DST DATA

Yield per milligram per roentgen Cu 0.86, Ni 0.99, Al 1.15 for 30.5 MeV bremsstrahlung.

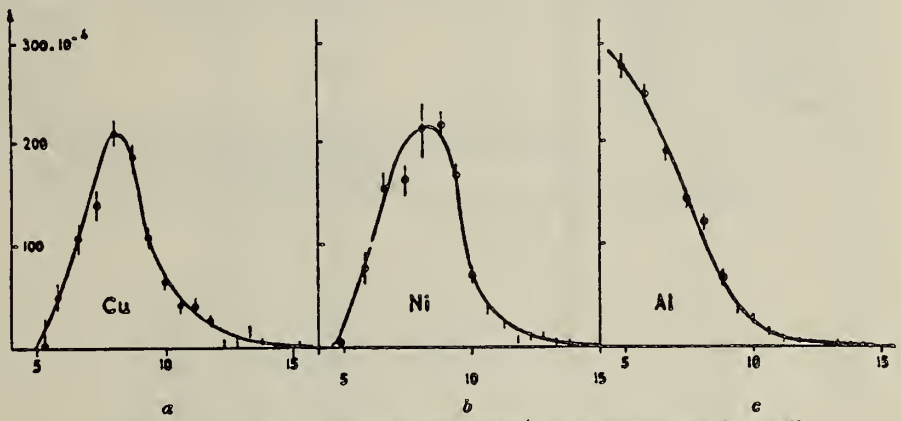

Fig. 2. — Nombre de particules α/mg/stéradian/Röntgen/intervalle de 1 MeV.

Ref. F. Ferrero, L. Gonella, R. Malvano, C. Tribuno, A.O. Hanson — Nuovo Cimento 5, 242 (1957)

Elem. Sym.	A	Z
Al	27	13

Method 31 MeV betatron; neutron yield; angular distribution; threshold detector, $Si^{28}(n,p)Al^{27}$ reaction.

Ref. No. 57 Fe 1 — EGF

Reaction	E or ΔE	E_o	Γ	$\int \sigma dE$	Jπ	Notes
Al(γ,n!)	Bremss. 31					Data not clear but probably normalized at 30 MeV.

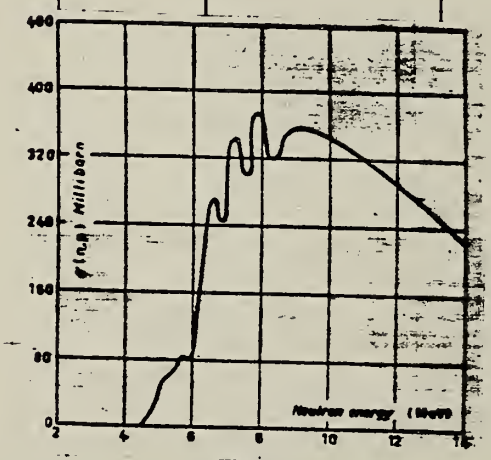

Fig. 1.

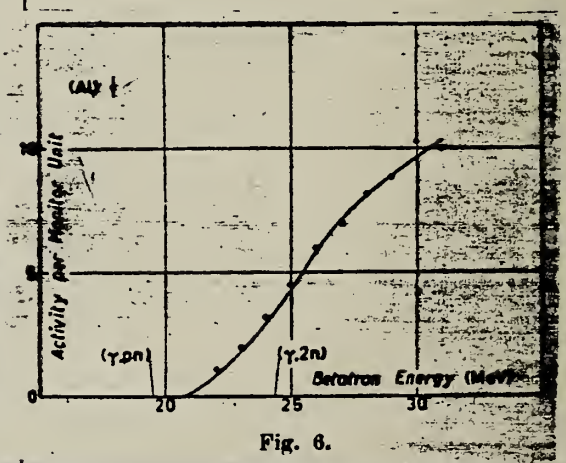

Fig. 6.

Ref. T. Asada, M. Masuda, M. Okumura, J. Okuma
J. Phys. Soc. Japan 13, 1 (1958)

Elem. Sym.	A	Z
Al	27	13

Method: Betatron; angular distribution; scintillator; ionization chamber

Ref. No.: 58 As 1 KH

Reaction	E or ΔE	E_o	Γ	$\int \sigma dE$	Jπ	Notes
$Al^{27}(\gamma,n)$	Bremss. 17					Angular distribution is of form, $a + b \sin^2\theta$ where $b/a = 1.6 \pm 0.8$

Table I. The values of b/a.

Energy	Target nucleus Al	Cu	Pb	Be	Detector
Present (17 Mev)	1.6±0.8	0.17±0.06	0.30±0.11	1.29±0.53	Emmerich[a]
Dixon (70 Mev)	0.36±0.29	0.23±0.15	uniform	1.2±0.4	Hornyak[b]
Halpern (70 Mev)				1.26±0.11	Emmerich[a]
Price (22 Mev)		0.33	0.84	uniform	Al (n, p)[c]
Johanson (65 Mev)	1		0.8	1.5	Hornyak[b]

a) A scintillation detector with a ZnS-paraffin-Lucite light guide.
b) A scintillation detector with a ZnS-Lucite.
c) A fast neutron detector by measuring the beta activity of Al^{27} (n, p) Mg^{27} reaction.

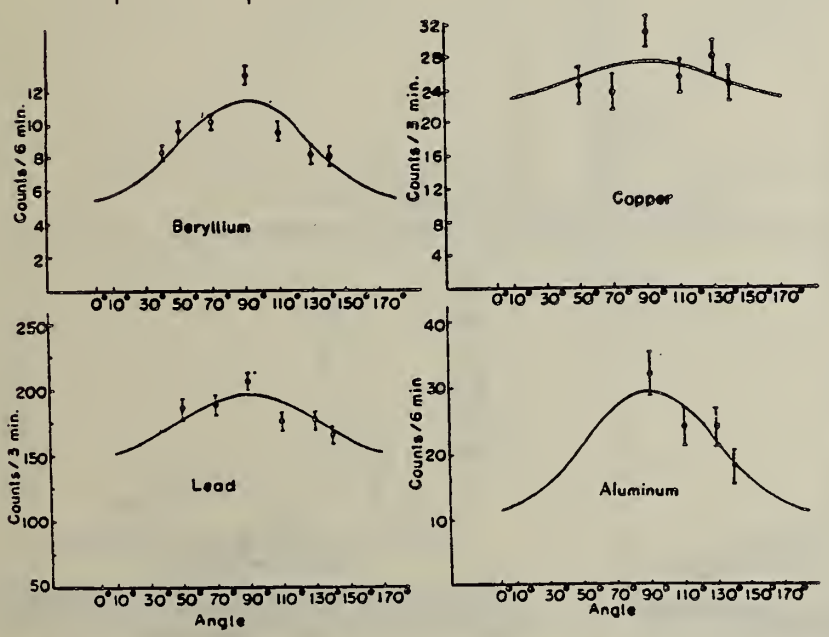

Fig. 6. The angular distributions of photo-neutrons as measured with Emmerich button type scintillation detector.

References:
1) E. D. Courant: Phys. Rev. 82 (1951) 703.
2) S. A. E. Johansson: Phys. Rev. 97 (1955) 434.
3) W. R. Dixon: Can. J. Phys. 33 (1956) 785.
4) G. A. Price: Phys. Rev. 93 (1954) 1268.

Ref. L.B. Aull, W.D. Whitehead Phys. Rev. 110, 1113 (1958)	Elem. Sym.	A	Z
	Al	27	13
Method Activation; Cu standard.	Ref. No. 58 Au 1		EH

Reaction	E or ΔE	E_o	Γ	$\int \sigma dE$	Jπ	Notes 770+
(γ,2p)	20-63	32		28 MeV-mb		E_{th} = 21.4 MeV; σ_{max} = 0.29 mb.

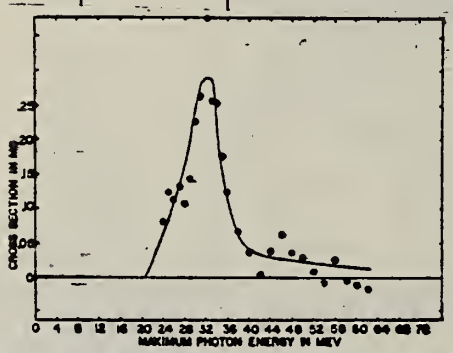

FIG. 3. Cross section for the $Al^{27}(\gamma,2p)Na^{25}$ reaction derived from the smooth yield curve of Fig. 2. The estimated statistical uncertainty in the points is about 30%.

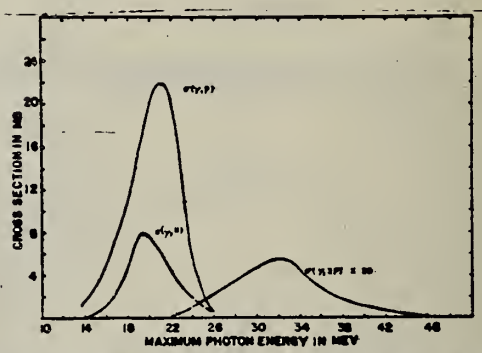

FIG. 4. Cross sections for the $Al^{27}(\gamma,p)Na^{26}$ reaction from Halpern and Mann,[21] for the $Al^{27}(\gamma,n)Al^{26}$ reaction from Katz and Cameron[22] and for $Al^{27}(\gamma,2p)Na^{25}$ from this work.

Reference 22: Katz and Cameron, Phys. Rev. 84, 1115 (1951).

REF.

R. Basile and M. Gusakow
Compt. Rend. 246, 588 (1958)

ELEM. SYM.	A	Z
Al	27	13

METHOD

REF. NO.	
58 Ba 5	EGF

REACTION	RESULT	EXCITATION ENERGY	SOURCE		DETECTOR		ANGLE
			TYPE	RANGE	TYPE	RANGE	
G,XN	RLY	THR - 15	C	12-15	BF3-I		4PI

BREAKS

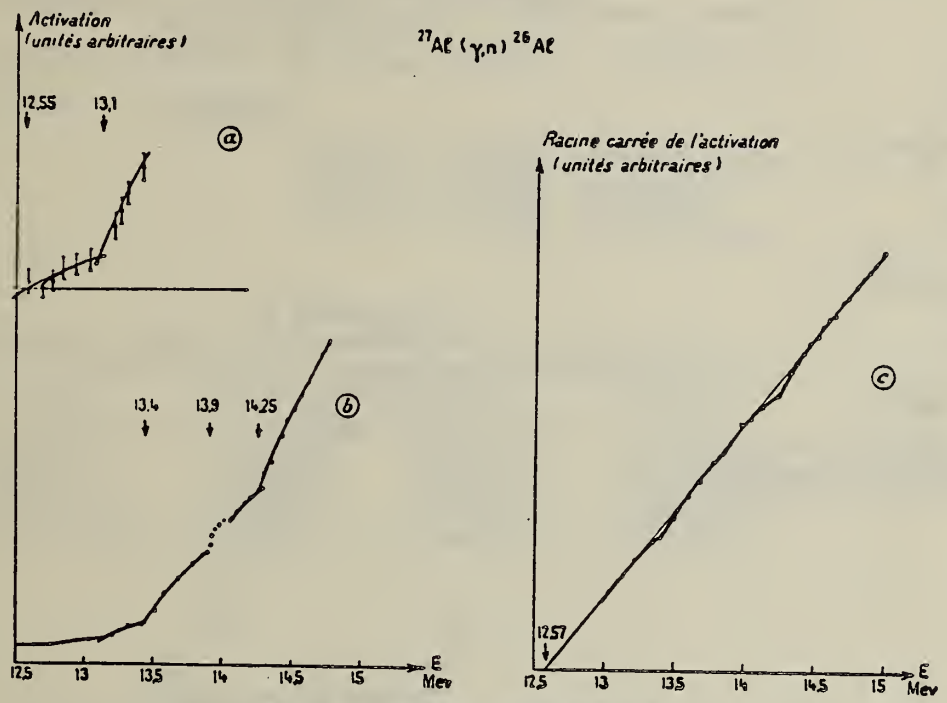

Fig. 2. — Courbe d'activation de l'aluminium.
a, voisinage du seuil; *b*, discontinuités; *c*, racine carrée de l'activation.

REF.

E. B. Bazhanov, Iu. M. Volkov, and L. A. Kul'Chitskii
J. Exptl. Theoret. Phys. (USSR) 35, 322 (1958)
Soviet Phys. JETP 35, 224 (1958)

ELEM. SYM.	A	Z
Al	27	13

METHOD

REF. NO.	
58 Ba 6	EGF

REACTION	RESULT	EXCITATION ENERGY	SOURCE		DETECTOR		ANGLE
			TYPE	RANGE	TYPE	RANGE	
G,XP	SPC	THR - 85	C	85.90	TEL-D	13 - 40	DST

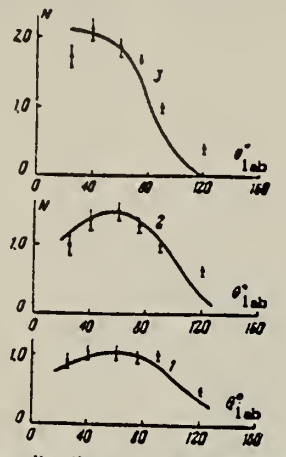

FIG. 3. Angular distributions of photoprotons from Al. The solid curves give the results of calculation. Only statistical errors are shown. 1) E_p = 13.7-17.5; 2) E_p = 17.5-21.5; 3) E_p = 21.5-41.0 Mev.

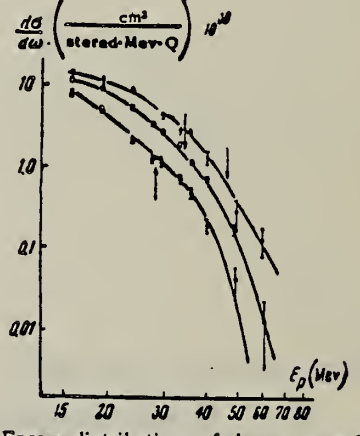

FIG. 5. Energy distributions of photoprotons from Al for various angles, $E_{\gamma max}$ = 90 Mev. Only statistical errors are shown. ● – θ = 30°; ○ – θ = 90°; Δ – θ = 130°.

B.G. Chidley, L. Katz, S. Kowalski
Can. J. Phys. 36, 407 (1958)

ELEM. SYM.	A	Z
Al	27	13

METHOD: Betatron

REF. NO.: 58 Ch 2 NVB

REACTION	RESULT	EXCITATION ENERGY	SOURCE TYPE	SOURCE RANGE	DETECTOR TYPE	DETECTOR RANGE	ANGLE
G,N	RLY	THR	C	THR	BF3-I		4PI

See 58 Ka 1 for cross sections.

THRESHOLD

TABLE I

MEASURED PHOTONEUTRON THRESHOLDS

Reaction	Measured Q value, Mev.	Other Q values, Mev.	Method	Reference
$Al^{27}(\gamma, n)Al^{26}$	12.98±0.08 (12.93±0.08)			
		14.4 ±0.3	Threshold	Becker *et al.* (1947)
		14.0 ±0.1	Threshold	McElhinney *et al.* (1949)
		12.75 ±0.20	Threshold	Sher *et al.* (1951)
		13.06 ±0.06	Mass data	Wapstra (1955)
		12.98 ±0.11	Q^+ value	Laubitz (1955)
			Mass data	Mattauch *et al.* (1956)

TABLE II

COMPARISON OF THRESHOLDS FROM MASS DATA AND FROM PHOTONEUTRON REACTIONS

Reaction	Photoneutron threshold, Mev.	Mass data threshold, Mev.	Difference, Mev.
$Na^{23}(\gamma, n)Na^{22}$	12.47±0.05	12.417±0.014	−0.05±0.05
$Al^{27}(\gamma, n)Al^{26}$	12.96±0.06	13.03 ±0.06	+0.07±0.08
$P^{31}(\gamma, n)P^{30}$	12.48±0.05	12.39 ±0.03	−0.09±0.06
$Co^{59}(\gamma, n)Co^{58}$	10.44±0.05	10.49 ±0.01	+0.05±0.05
$Pr^{141}(\gamma, n)Pr^{140}$	9.46±0.05	9.30 ±0.06	−0.16±0.08

Ref. F. Ferrero, R. Malvano, S. Menardi, O. Terracini
Nuclear Phys. 9, 32 (1958)

Elem. Sym.	A	Z
Al	27	13

Method: Moderation with Rh detectors; activation, Si detector.

Ref. No.: 58 Fe 1 EH

Reaction	E or ΔE	E_o	Γ	$\int \sigma dE$	Jπ	Notes
(γ,n)	~ 13-30	~ 21				Figure 4: Dotted line calculated using Wilkinson theory.
(γ,xn)		~ 18				
(fast n's)		~ 20				

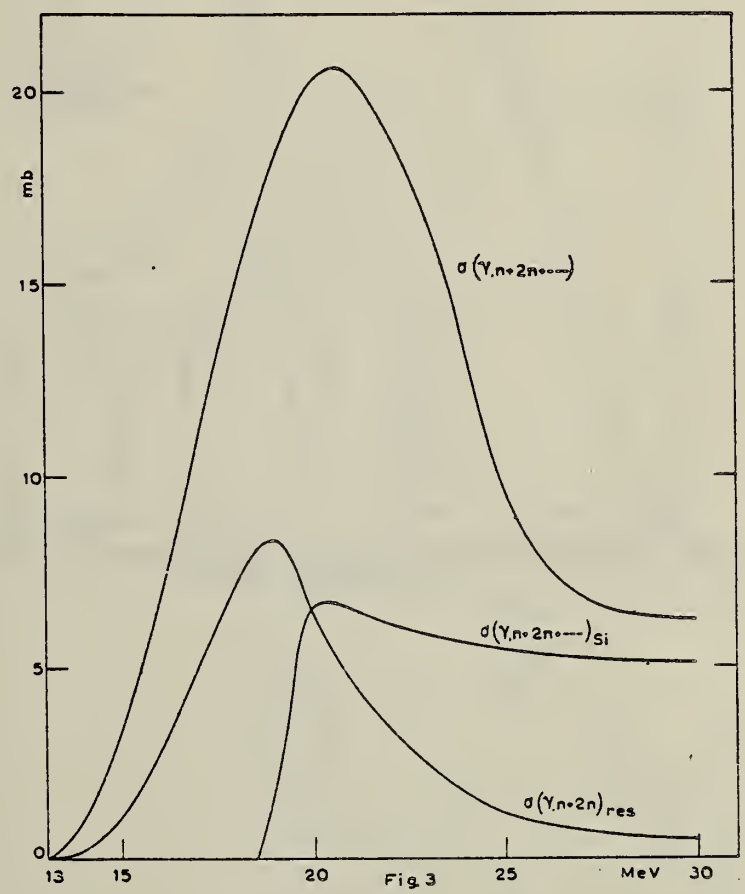

Fig. 3. Cross sections deduced by analyzing the yields of fig. 2.

(OVER)

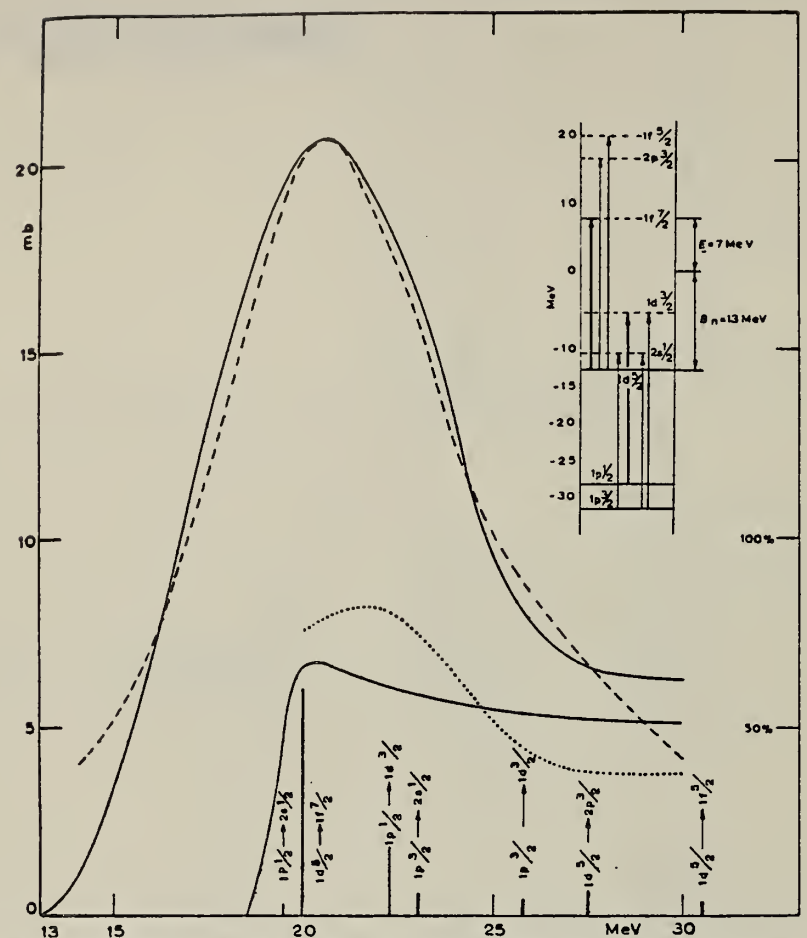

Fig. 4. Comparison between the experimental t.n. and f.n. cross sections and the predictions of the independent particle model.

Ref. M.E. Toms, J.McElhinney
Phys. Rev. 111, 561 (1958)

Elem. Sym.	A	Z
Al	27	13

Method: Betatron; alpha yield; nuclear emulsion

Ref. No.: 58 To 2 | NVB

Reaction	E or ΔE	E_o	Γ	$\int \sigma dE$	Jπ	Notes
$Al^{27}(\gamma,\alpha)$	Bremss. 22					Yield = 1.3×10^{-4} alpha/mole/roentgen

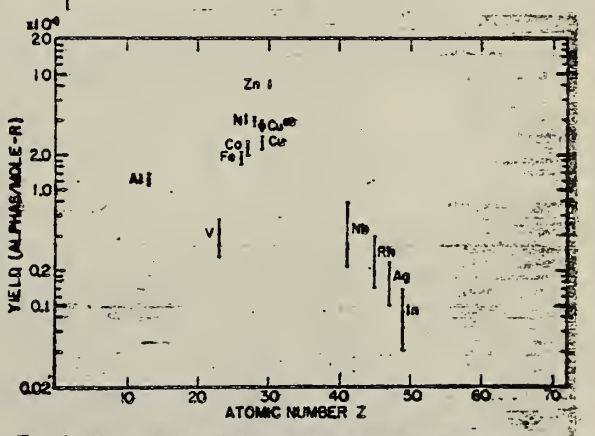

FIG. 8. Photo-alpha yields plotted against atomic numbers for the exposures of the survey.

Ref. B. Ziegler
Z. Physik 152, 566 (1958)

Elem. Sym.	A	Z
Al	27	13

Method: 32 MeV betatron; pair spectrometer; absorption measurement; ionization chamber

Ref. No.: 58 Zi 1 | EH

Reaction	E or ΔE	E_o	Γ	$\int \sigma dE$	Jπ	Notes
Al(μ_t)	Bremss. 30			150±30 MeV-mb		

[7] MONTALBETTI, R., L. KATZ u. J. GOLDEMBERG: Phys. Rev. 91, 659 (1953).
[12] HALPERN, J., u. A.K. MANN: Phys. Rev. 83, 370 (1951).

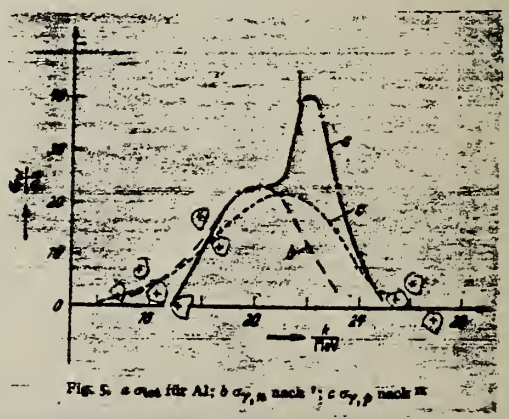

Fig. 5. a σ_{tot} für Al; b $\sigma_{\gamma,n}$ nach [7]; c $\sigma_{\gamma,p}$ nach [12]

Ref.	Elem. Sym.	A	Z
E.S. Kuzmanov Zhur. Eksp. i Teoret. Fiz. 37, 374 (1959) Soviet Phys. JETP 10, 267 (1960)	Al	27	13

Method	Ref. No.	
Bremss.; NaI-CsI telescope	59 Ba 2	JH

Reaction	E or ΔE	E_o	Γ	$\int \sigma dE$	Jπ	Notes
(γ,p)	protons 17.8-52.2MeV					Took difference of yield measured with 2 bremss. spectra 82-89 MeV.

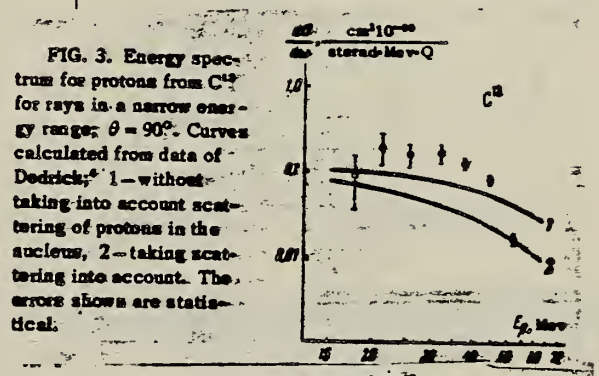

FIG. 3. Energy spectrum for protons from C^{12} for rays in a narrow energy range; $\theta = 90°$. Curves calculated from data of Dedrick;[6] 1—without taking into account scattering of protons in the nucleus, 2—taking scattering into account. The errors shown are statistical.

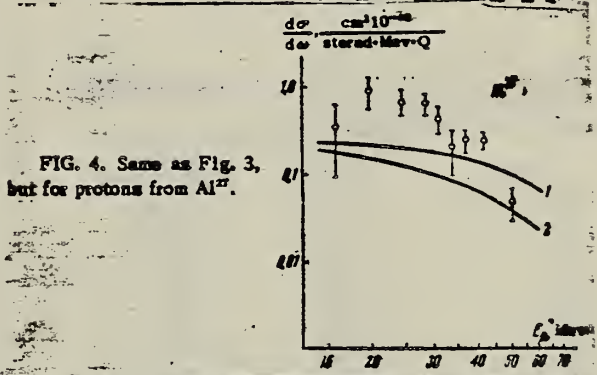

FIG. 4. Same as Fig. 3, but for protons from Al^{27}.

Target	Mean proton energy E_p, Mev	Proton yield, $cm^2 10^{-30}$ / ster·d·Mev·Q: E_γ max = 82 Mev	E_γ max = 89 Mev	Target	Mean proton energy E_p, Mev	Proton yield, $cm^2 10^{-30}$ / ster·d·Mev·Q: E_γ max = 82 Mev	E_γ max = 89 Mev
C^{12}	12.8	6.028±0.040	4.120±0.042	Al^{27}	15.4	18.63 ±0.18	18.98 ±0.19
	21.4	2.841±0.052	3.134±0.055		19.1	11.01 ±0.22	11.90 ±0.24
	28.0	1.862±0.034	2.044±0.036		24.0	5.71 ±0.13	6.38 ±0.16
	31.6	0.961±0.029	1.127±0.030		27.7	4.07 ±0.12	4.70 ±0.12
	37.8	0.442±0.019	0.575±0.021		28.8	2.59 ±0.08	3.01 ±0.11
	44.0	0.113±0.004	0.186±0.008		33.8	1.85 ±0.08	2.06 ±0.08
	50.2	0.000±0.005	0.020±0.002		38.7	0.88 ±0.40	1.06 ±0.05
					44.5	0.423±0.026	0.784±0.034
					49.9	0.078±0.013	0.127±0.016

REF.

W. C. Barber and W. D. George
Phys. Rev. 116, 1551 (1959)

ELEM. SYM.	A	Z
A1	27	13

METHOD

REF. NO.	
59 Ba 3	EGF

REACTION	RESULT	EXCITATION ENERGY	SOURCE		DETECTOR		ANGLE
			TYPE	RANGE	TYPE	RANGE	
E,N	ABY	THR - 36	D	10 - 36	BF3-I		4PI

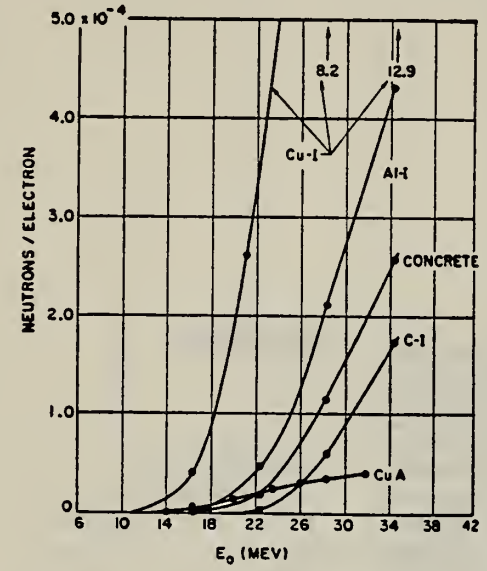

FIG. 5. Yield of neutrons per incident electron as a function of initial electron energy for the low-Z elements. The concrete target is a simple 3:1 sand:cement mixture. The numbers at the top right refer to the Cu-I curve at the indicated energies.

TABLE I. Thicknesses of the targets used in the experiment. with the exception of heavy water, all targets contained isotopes in their naturally-occurring proportions.

Target	Thickness (g/cm²)	Thickness (radiation lengths)
Heavy water	0.698	"thin"
Be	0.589	0.00867
C-I	38.91	0.88
Al-I	24.19	1.00
Cu-A	1.372	0.108
Cu-I	13.26	1.04
Cu-II	26.56	2.08
Cu-III	39.86	3.13
Cu-IV	53.13	4.17
Ta-I	6.21	0.98
Pb-I	5.88	1.01
Pb-II	11.42	1.97
Pb-III	17.30	2.98
Pb-IV	22.89	3.94
Pb-VI	34.42	5.93
U-I	6.17	1.14
U-II	12.42	2.30
U-III	18.61	3.46
Concrete	28.5	1.19

[19] A. I. Berman and K. L. Brown, Phys. Rev. 96, 83 (1954).

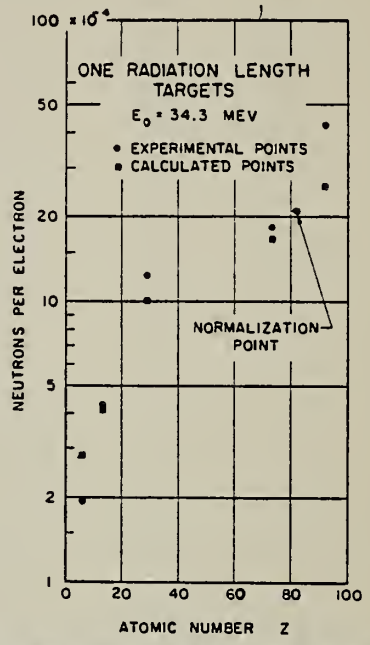

FIG. 14. Experimental and expected yields of neutrons per incident electron for 1-radiation-length targets at 34.3 Mev, as a function of atomic number Z. The experimental yields were obtained by dividing the measured yields from the targets labeled I by the actual target thicknesses listed in Table I. The expected yields were calculated from expression (8).

G. Cortini, C. Milone, T. Papa, R. Rinzivillo
Nuovo Cimento 14, 54 (1959)

Al	27	13

METHOD
Betatron; neutron

REF. NO.
59 Co 3 | EH

REACTION	RESULT	EXCITATION ENERGY	SOURCE		DETECTOR		ANGLE
			TYPE	RANGE	TYPE	RANGE	
G,XN	SPC	15-30	C	24,30	EMU-D	2-15	90

Differences between 24 MeV and 30 MeV (bremss. energies) prove that above 24 MeV n's are emitted mainly by direct effect.

Neutron spectrum measured at 90° to beam.

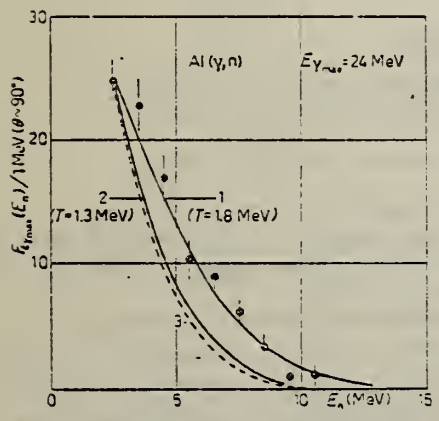

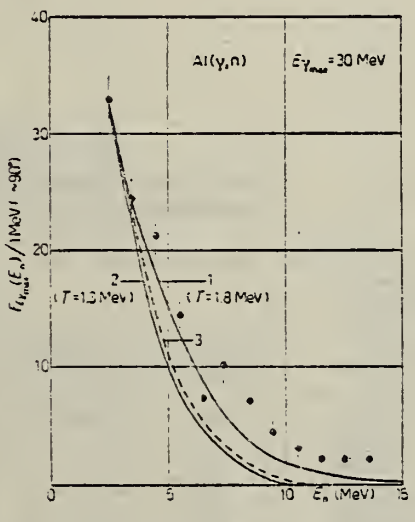

Fig. 1. – Energy spectrum of photoneutrons from Al at $E_{\gamma max}$ 24 MeV (Fig. 1*a*) and $E_{\gamma max} = 30$ MeV (Fig. 1*b*). For the curves see text.

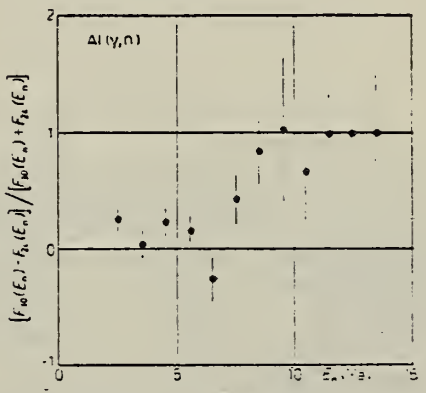

Fig. 2. – The ratio $(F_{30}(E_n) - F_{24}(E_n))/(F_{30}(E_n) + F_{24}(E_n))$ plotted against E_n.

Ref. J. Dular, G. Kernel, M. Kregar, M.V. Mihailović, G. Pregl, M. Rosina, C. Zupancic
Nuclear Phys. 14, 131 (1959)

Elem. Sym.	A	Z
Al	27	13

Method: compton spectrometer; 30 MeV Betatron

Ref. No. 59 Du 1 | EH

Reaction	E or ΔE	E_o	Γ	$\int \sigma dE$	Jπ	Notes 769
(μ_t)	Bremss. 28.9 30.3					

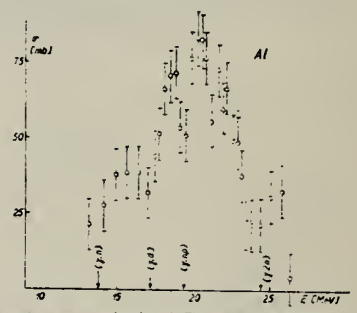

Fig. 4. Nuclear absorption cross section for Al. This figure is essentially the same as in ref. [4] except for an arbitrary shift of the ordinate scale. It differs somewhat from the figure given in ref. [2], which is the result of a preliminary evaluation of the experimental data.

Ref. 4: Mihailović, Pregl, Kernel, and Kregar, Phys. Rev. 114, 1621 (1959)

Ref. 2: Comptes rendus du Congres international de Physique nucléaire (Paris, juillet 1958) 157.

Ref. J. Kockum, N. Starfelt
Nucl. Instruments 5, 37 (1959)

Elem. Sym.	A	Z
Al	27	13

Method: 30 MeV synchrotron; NaI(Tℓ) scintillator spectrometer; photon spectrum

Ref. No.: 59 Ko 1 | EH

Reaction	E or ΔE	E_o	Γ	$\int \sigma dE$	Jπ	Notes
$Al^{27}(\sigma_t)$	Bremss.					
	30.5	21.5	7.8	$\int_{10}^{27}$ = 0.24 MeV-mb		

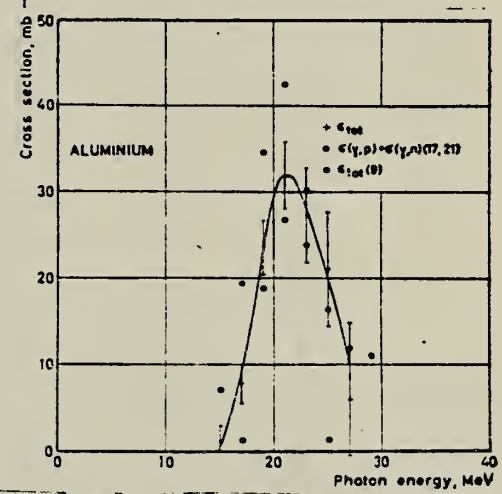

Fig. 4. Experimentally determined photonuclear absorption cross sections (crosses). The open circles show the sum of the (γ,n), and (γ,p) cross sections and the filled squares the (γ,np) + (γ,d) cross section where available[6, 7, 16–18]. The dashed circles give the total photonuclear absorption cross section as measured by Ziegler[9].

TABLE 2

Experimentally determined giant resonance data; peak energy, E_{max}, width at half height, ΔE, and integrated cross section, $\int_{10\,MeV}^{27\,MeV} \sigma dE$, and values of $\int_0^{\infty} \sigma dE$ predicted by the dipole sum rule.

Absorber	E_{max} (MeV)	ΔE (MeV)	$\int_{10\,MeV}^{27\,MeV} \sigma dE$	$\int_0^{\infty} \sigma dE$
Carbon	23	4.6	0.12	0.18
Aluminium	21.5	7.8	0.24	0.40
Sulphur	21	6.6	0.30	0.48
Iron	19.5	9.4	0.76	0.84

[9] B. Ziegler, Z. Physik 152 (1958) 566.

[17] J. Halpern and A. K. Mann, Phys. Rev. 83 (1951) 370.

[18] R. Montalbetti, L. Katz and J. Goldemberg, Phys. Rev. 91 (1953) 659.

[19] L. W. Jones and K. M. Terwilliger, Phys. Rev. 91 (1953) 699.

[20] W. C. Barber, W. D. George and D. D. Reagan, Phys. Rev. 98 (1955) 73.

[21] F. Ferrero, R. Malvano, S. Menardi and G. Torrelessa, Nuclear Physics 9 (1958) 32.

[22] L. Katz and A. S. Penfold, Phys. Rev. 81 (1951) 815.

Ref.	Elem. Sym.	A	Z
L.A. Kul'chitskii, V. Presperin Zhur. Eksp. i Teoret. Fiz. 37, 1524 (1959) Soviet Phys. JETP 10, 1082 (1960)	Al	27	13

Method	Ref. No.	
88 MeV Synchr.; proton recoil telescopes	59 Ku 1	JH

Reaction	E or ΔE	E_o	Γ	$\int \sigma dE$	Jπ	Notes
(γ,n)	Bremss: $E_{\gamma max}$=88Mev; $E_n \geq$ 10 Mev					Angular distribution; results consistent with quasi-deutron model, but some direct resonance abs. may be present.

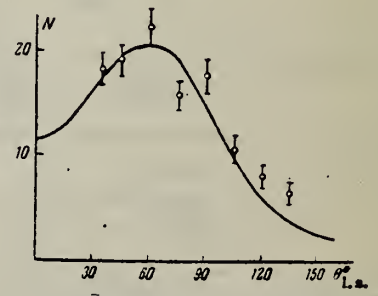

FIG. 6. Angular distribution of photoneutrons from Al^{27}. Solid curve—data calculated in reference 14.

Ref. M.V. Mihalovic, G. Pregel, G. Kernel, M. Kregar
Phys. Rev. 114, 1621 (1959)

Elem. Sym.	A	Z
Al	27	13

Method Comptron spectrometer; Bremsstrahlung

Ref. No. 59 Mi 1 EH

Reaction	E or ΔE	E_o	Γ	$\int \sigma dE$	Jπ	Notes
(μ_t)	Bremss. 30			~ 800 MeV-mb		σ_{max} = 100 ± 10 mb.
		~ 18.5				
		~ 21				
		~ 26				

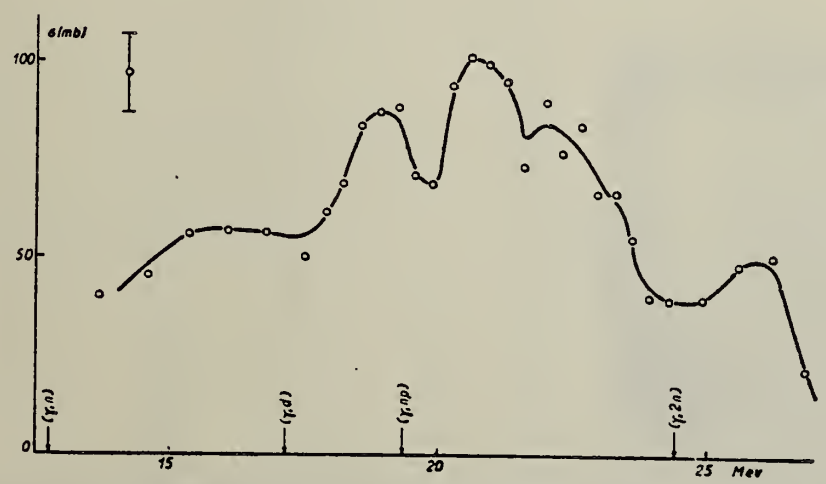

FIG. 2. Total photonuclear cross section in Al.

REF.

P. Paul and U. Stierlin
Nucl. Physics 13, 576 (1959)

ELEM. SYM.	A	Z
Al	27	13

METHOD

REF. NO. 59 Pa 3 EGF

REACTION	RESULT	EXCITATION ENERGY	SOURCE		DETECTOR		ANGLE
			TYPE	RANGE	TYPE	RANGE	
G,G	ABX	17	D	15,18	NAI-D	17	90

Source Li(p,γ) with E_p = 500 keV.

Tabelle 1

Die gemessenen totalen Streuquerschnitte in cm² unter Annahme von E1- und E2-Streuung

Element	eigene Werte	Fuller und Hayward [13])	Stearns [6])
Pb	$(5.6\pm1)\times10^{-27}$	$(4-8)\times10^{-27}$	$(5-9)\times10^{-27}$
Al	$(2\ \pm1)\times10^{-29}$	$(2-6)\times10^{-29}$	
O	$(1\ -5)\times10^{-30}$		
C	$(5.8\pm2)\times10^{-30}$		

Durch die Wahl der Meßgeometrie ergibt sich für eine E1- wie eine E2-Winkelverteilung innerhalb der Fehlergrenzen der numerischen Rechnung der gleiche Wert für den totalen Streuquerschnitt. Die angegebenen Fehler enthalten nur den Fehler in der Bestimmung des primären γ-Flusses und die statistischen Fehler der Streuraten. Zum Vergleich sind die entsprechenden Ergebnisse von Fuller und Hayward [13]) und Stearns [6]) gegenübergestellt. Die angegebenen Werte gehören jeweils zu den Fehlergrenzen.

Ref.	Elem. Sym.	A	Z
[illegible] Phys. Rev. 118, 1295 (1960)	Al	27	13

Method	Ref. No.	
Monoenerg. γ's from $B^3(p,\gamma)Be^8$ reaction, coinc det.; NaI	60 Ca 1	PR

Reaction	E or ΔE	E_o	Γ	$\int \sigma dE$	J π	Notes
μ_s	20.0-20.5					No observed structure. σav. (nuclear) = 37 ± 4.5 mb. Calculated atomic cross-sections subtracted, using Borsellino for triplet.

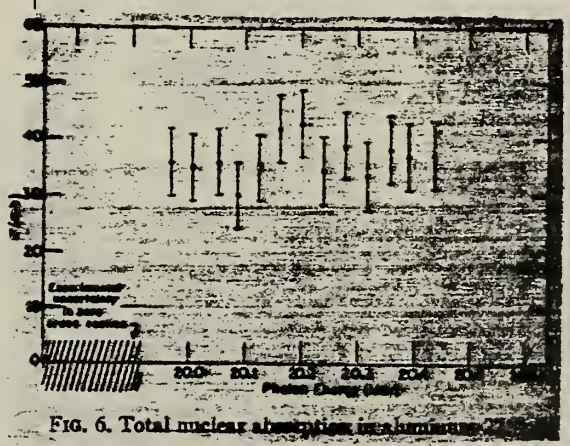

FIG. 6. Total nuclear absorption in aluminum-27.

Ref.	Elem. Sym.	A	Z
V.P. Chizhov Zhur. Eksp. i Teoret. Fiz. 38, 809 (1960) Soviet Phys. JETP 11, 587 (1960)	Al	27	13

Method	Ref. No.	
90 MeV Bremss; scintillator counter telescope	60 Ch 1	JHH

Reaction	E or ΔE	E_o	Γ	$\int \sigma dE$	Jπ	Notes
$Al^{27}(\gamma,p)$	Bremss. 90					Ratio: $\sigma(\gamma,d)/\sigma(\gamma,p)$, $\theta = 90^\circ$
$Al^{27}(\gamma,d)$						Energy range of particles detected: E_p, E_d: 15.5-30 MeV

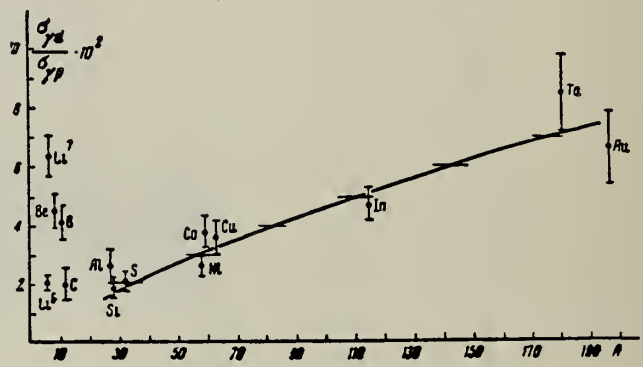

FIG. 3. Ratio of (γ, d) to (γ, p) cross sections for protons and deuterons of energies 15.5–30 Mev as function of atomic weight A. The solid curve shows the dependence given by Eq. (2), arbitrarily normalized.

YIELD DATA TABLE:

It should be noted that the yield of photoprotons of the energy considered rises smoothly with Z for the elements plotted in Fig. 3, and that starting already with Al, no direct proportionality to Z is observed on account of the effect of the Coulomb barrier. For illustration, we give the yields of photoprotons Y(γ, p) per proton in the nucleus for several elements in relative units (the error in these measurements was estimated to be ±10%):

	Li^6	Li^7	Be	C	Al	Cu
$Y(\gamma,p)$ =	1.49	1.57	1.5	1.31	1.00	0.56

FORM NBS-418
(8-1-63)
USCOMM-DC 18556-P63

Ref.	Elem. Sym.	A	Z
R.R. Carlson, A.H. Kunde Phys. Rev. 119, 748 (1960)	Al	27	13

Method	Ref. No.	
Betatron; photon difference; beam passes through one target surrounded by proton (proportional) counters; continues to second target surrounded by BF3-filled neutron counters.	60 Ch 2	JH

Reaction	E or ΔE	E_o	Γ	$\int \sigma dE$	Jπ	Notes
$(\gamma,n)^{152}$	11.7-20.8					$\sigma(E_\gamma = 20\ MeV) = 21\ mb$
$(\gamma,p)^{151}$						$\sigma(E_\gamma = 20\ MeV) = 19.mb$; $\sigma_{av}(12\text{-}20.8M) = 7.6\ mb$
						Ratio $\sigma(\gamma,p)/\sigma(\gamma[n) \sim 5$ times ratio calculated by compound nucleus assumptions (compare reciprocal of curve in Figure 7 with Al^{27} column in Table II)

751+

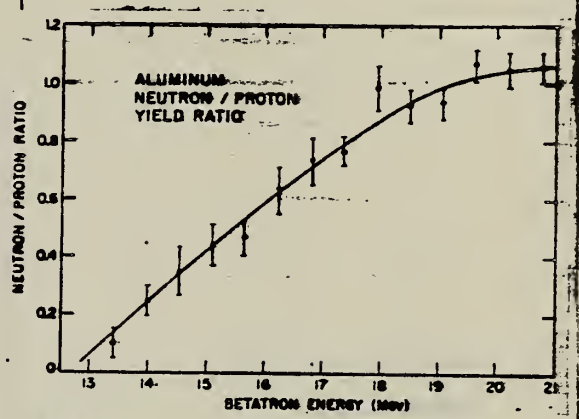

FIG. 7. The photoneutron to photoproton yield ratio for aluminum as a function of betatron energy.

TABLE II. Calculated ratios of photoproton to photoneutron cross sections.

E_γ (Mev)	Al^{27}	Cu^{63}	Cu^{65}	Cu^{nat}
12	...	0.20	...	0.14
13	...	0.16	0.014	0.11
14	0.83	0.16	0.017	0.11
15	0.54	0.16	0.021	0.12
16	0.44	0.18	0.026	0.13
17	0.39	0.19	0.032	0.14
18	0.35	0.22	0.038	0.17
19	0.32	0.24	0.046	0.18
20	0.30	0.26	0.053	0.20
21	0.28	0.29	0.062	0.22
22	0.27	0.29	0.072	0.23

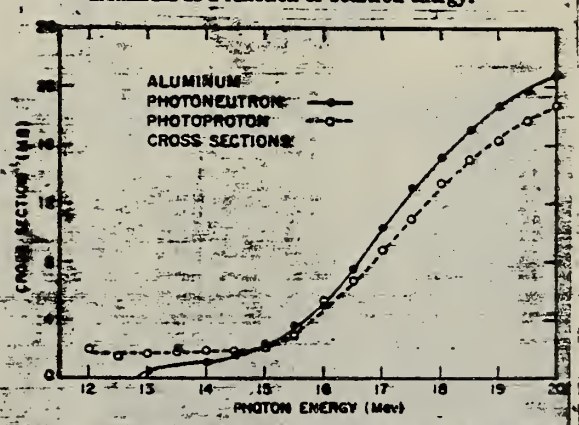

FIG. 9. The photoneutron cross section and the photoproton cross section for aluminum as a function of photon energy.

K. N. Geller, J. Halpern, and E. G. Muirhead
Phys. Rev. 118, 1302-12 (1960)

ELEM. SYM.	A	Z
Al	27	13

METHOD: Betatron; neutron threshold; ion chamber

REF. NO.: 60 Ge 3 NVB

REACTION	RESULT	EXCITATION ENERGY	SOURCE TYPE	SOURCE RANGE	DETECTOR TYPE	DETECTOR RANGE	ANGLE
G,N	NØX	THR	C THR		BF3-I		4 PI

THRESHØLD

TABLE I. Summary and comparison of neutron separation energies inferred from present threshold measurements with values predicted from mass data and reaction energies. All energies are expressed in the center-of-mass system in Mev.

Reaction	No. runs	Present results	Other results	Method	Reference
$Al^{27}(\gamma,n)Al^{26}$	2	13.26 ±0.07 (13.03)	13.06 ±0.06	LSA	c
			13.057±0.011	mass data	d
				$Q(\beta+)$	e
			13.038±0.015	reaction cycle	e
			12.98 ±0.08	threshold	f

[a] A. H. Wapstra, Physica 21, 367 (1955).
[d] T. T. Scolman, K. S. Quisenberry, and A. O. Nier, Phys. Rev. 102, 1076 (1956).
[e] P. M. Van Patter and W. Whaling, Revs. Modern Phys. 26, 402 (1954); 29, 756 (1957).
[f] See reference 4.

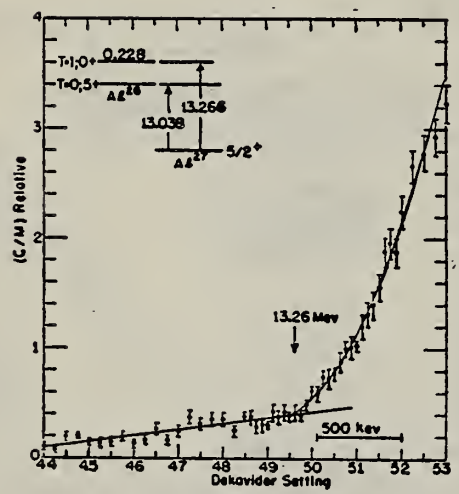

FIG. 5. Neutron yield data for aluminum from 11.8 Mev to 14.2 Mev.

Ref.	Elem. Sym.	A	Z
A.M. Gorbunov, V.P. Denisov, V.A. Kolmkhin Zhur. Eksp. i Teoret. Fiz. 38, 1084 (1960) Soviet Phys. JETP 11, 783 (1960)	Al	27	13

Method	Ref. No.	
260 MeV Synchrotron; activation; 2 ctrs. "photon difference"	60 Ga 2	JETP

Reaction	E or ΔE	E_0	Γ	$\int \sigma dE$	Jπ	Notes
$Al^{27}(\gamma,?)Na^{24}$	30-260			~9 MeV-mb[150] (from graph: E.H.)		Activation probably mostly due to (γ,dp), $(\gamma,2pn)$. (γ,He^3) also possible. Refers to "quasi-neutron mechanism."

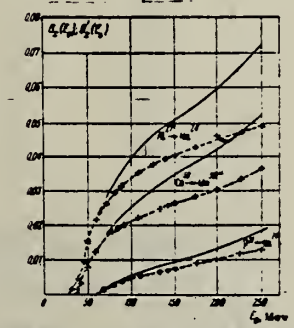

FIG. 1. Active yields of the $Al^{27} \rightarrow Na^{24}$, $Co^{59} \rightarrow Mn^{56}$, and $P^{31} \rightarrow Na^{24}$ reactions as a function of the peak bremsstrahlung energy. The values of $B_\gamma(E_0)$ are given by the continuous curves, of $B_\gamma(E_0)$ – by the dashed curves [the values of $B_\gamma(E_0)$ are given in arbitrary units].

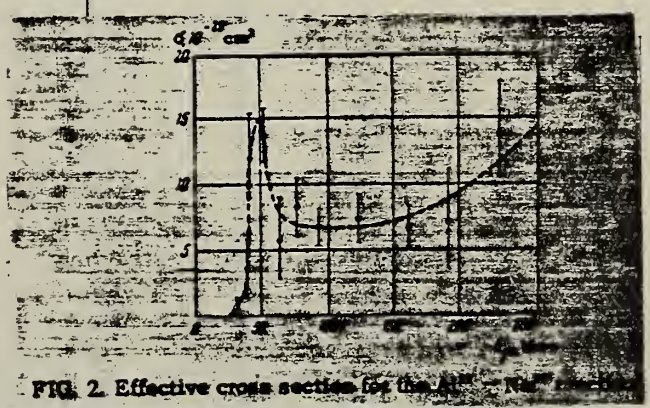

FIG. 2. Effective cross section for the $Al^{27} \rightarrow Na^{24}$ reaction.

Ref.	Elem. Sym.	A	Z
L.A. Kul'chitskii, V. Presperin Zhur. Eksp. i Teoret. Fiz. 39, 1001 (1960); Soviet Phys. JETP 12, 696 (1961)	Al	27	13

Method	Ref. No.	
90 MeV Synchr.; proton recoil counter telescopes	60 Ku 2	JH

Reaction	E or ΔE	E_o	Γ	$\int \sigma dE$	Jπ	Notes
$Al^{27}(\gamma,xn)$	Bremss.; $E_{\gamma max}$=90MeV					Relative yields in table are per nuclear neutron.

Element	Relative neutron yield	Element	Relative neutron yield
Li	1.00±0.05	Cu	0.37±0.02
Be	1.22±0.09	Cd	0.35±0.02
O	0.74±0.05	I	0.39±0.02
Al	0,49±0.03	Bi	0.41±0.03
Ca	0.33±0.02		

Ref. F.R. Metzger, C.P. Swann, V.K. Rasmussen
Nuclear Phys. 16, 568 (1960)

Elem. Sym.	A	Z
Al	27	13

Method Protons from Bartol-ONR generator; (p,p'γ) etc. reactions for γ source; ring scatterer; NaI.

Ref. No. 60 Me 1 JHH

Reaction	E or ΔE	E_o	Γ	$\int \sigma dE$	Jπ	Notes
(γ,γ)	1.01		$3.9 \pm 1.6 \times 10^{-4}$ ev		$3/2^+$	0.98 of total Γ; $W(\theta)=1+(0.02\pm0.13) P_2(\cos\theta)$
	2.21		$2.4 \pm 0.3 \times 10^{-2}$ ev			0.98 of total Γ; $W(\theta) = 1 + (0.23\pm0.03) P_2(\cos\theta)$.

Ref.	Elem. Sym.	A	Z
K. Reibel, A.K. Mann Phys. Rev. 118, 701 (1960)	Al	27	13

Method	Ref. No.	
γ's from $F^{19}(\gamma,\alpha\gamma)$ reaction; protons from Van de Graaff; NaI	60 Re 1	JHH

Reaction	E or ΔE	E_o	Γ	$\int \sigma dE$	Jπ	Notes
$Al^{27}(\gamma,\gamma)$	~ 7					$\langle \bar{\sigma} \rangle$ (E_p = 2.05 MeV) = < 0.008 mb Detector at 90°.

Ref. P.C. Stein, A.C. Odian, A. Wattenberg, R. Weinstein
Phys. Rev. 119, 348 (1960)

Elem. Sym.	A	Z
Al	27	13

Method: 320 MeV synchrotron; proton telescope; neutron counter

Ref. No.: 60 St 1 JHH

Reaction	E or ΔE	$E_\bullet$	Γ	$\int \sigma dE$	$\int \pi$	Notes
$Al^{27}(\gamma, np)$	Bremss. 320					$(\sigma/\sigma_{H^2}) = 4.4 \pm 0.6$ $[\sigma_{H^2} = 63\ \mu b]$ Mean photon energy ~ 262 MeV Proton counter at 76°

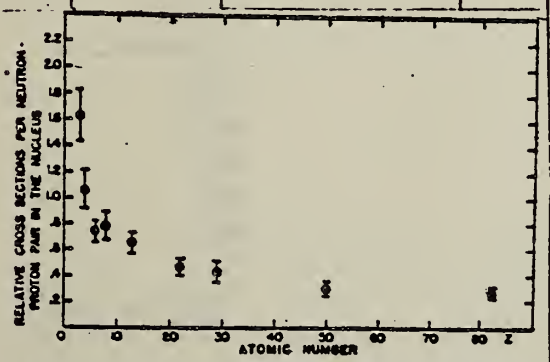

FIG. 2. Relative cross sections per neutron-proton pair in the nucleus versus atomic number. The cross section of the element of interest is divided by the cross section for deuterium and by the factor NZ/A.

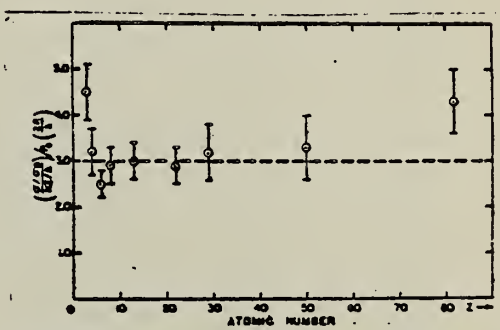

FIG. 3. The relative cross sections per neutron-proton pair corrected for the probability of escape is plotted against atomic number. The probability of escape factor is calculated using $r_0 = 1.30 \times 10^{-13}$ cm and $\lambda = 3.6 \times 10^{-13}$ cm. The probability of escape factor is given in expression (1). The data shown are those of Fig. 2 divided by $P(2R/\lambda)$.

G. Tamas, J. Miller, C.G. Schuhl, C. Tzara
J. Phys. Radium 21, 532 (1960)

ELEM. SYM.	A	Z
Al	27	13

METHOD: Linac; total absorption; magnetic compton spectrometer; ion chamber

REF. NO.: 60 Ta 2 | NVB

REACTION	RESULT	EXCITATION ENERGY	SOURCE TYPE	SOURCE RANGE	DETECTOR TYPE	DETECTOR RANGE	ANGLE
G, MU-T	ABX	7-28	C	28	MAG-D		4PI

467

$$\int_7^{28} \sigma_{nucl.} dE = 580 \pm 100 \text{ MeV-mb}$$

$$\int_7^{28} \frac{\sigma}{E_\gamma} dE = 31 \pm 7 \text{ mb}$$

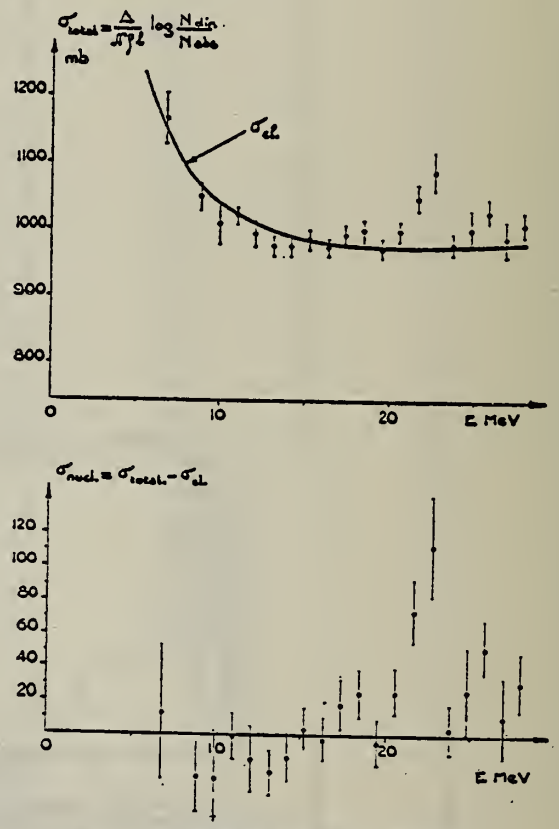

FIG. 5. — Sections efficaces d'absorption de photons pour ^{27}Al.

V. J. Vanhuyse and G. J. Vanpraet
J. Phys. Radium 21, 291 (1960)

A1	27	13

METHOD

REF. NO. 60 Va 1 EGF

REACTION	RESULT	EXCITATION ENERGY	SOURCE		DETECTOR		ANGLE
			TYPE	RANGE	TYPE	RANGE	
G,G	LFT	1	C	3	NAI-D	0-1	120
		(1.01 MeV)		(2.5 MeV)			

$\tau = \left(4.1\ ^{+2.9}_{-1.6}\right) \times 10^{-14}$ sec by self-indication.

REF.

T.G. Walker, W.T. Morton
Proc. Phys. Soc. 75, 4 (1960)

ELEM. SYM.	A	Z
Al	27	13

METHOD: Synchrotron; proton-neutron cross section; radioactivity

REF. NO.: 60 Wa 2 — NVB

REACTION	RESULT	EXCITATION ENERGY	SOURCE TYPE	SOURCE RANGE	DETECTOR TYPE	DETECTOR RANGE	ANGLE
G,F18	ABX	THR-240	C	120-240	ACT-I		4PI
				(120,180,240)			

$\sigma = (0.12 \pm 0.01)\ 10^{-27} cm^2$/equivalent quantum

In Table, data below 120 MeV from other workers; 50 MeV data is that of Barber et al, Phys. Rev. 98, 73 (1955).

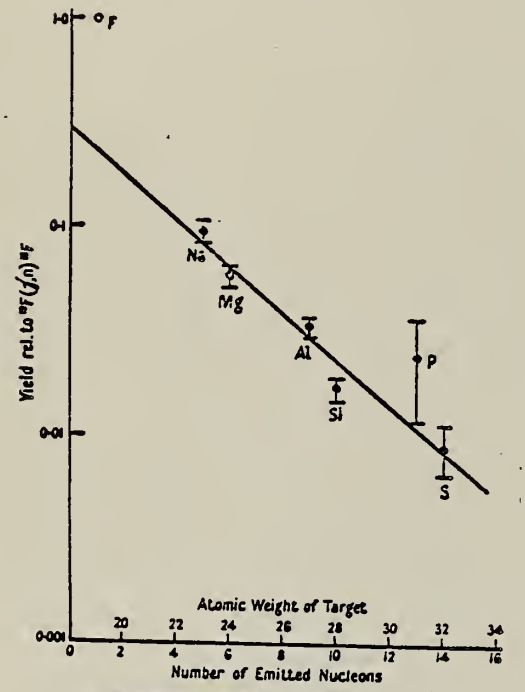

Yields relative to $^{19}F(\gamma, n)^{18}F$ at 240 Mev.

Maximum bremsstrahlung energy (Mev)	Yield of ^{18}F from ^{19}F	^{23}Na	^{27}Al	$^{12}C(\gamma, n)^{11}C$ yield
240	1·83(17)	0·18(9)	0·062(13)	1·62
180	1·78(16)	0·18(16)	0·058(16)	1·50
120	1·6(14)	0·15(14)	0·045(14)	1·34
100	1·5	—	—	1·27
70	1·4	0·11	—	1·15
50	1·22	0·07	—	1·0

Ref. J.M. Wyckoff, H.W. Koch
Phys. Rev. 117, 1261 (1960)

Elem. Sym.	A	Z
Al	27	13

Method 180 MeV Synchrotron; total absorption; NaI

Ref. No. 60 Wy 1 JHH

Reaction	E or ΔE	E_o	Γ	$\int \sigma dE$	Jπ	Notes
$Al^{27}(\sigma_t)$	Bremss. 35-90			0.373±15% ~ 14 (γ, meson thr)		Substraction of σ elecytonic as base-line.

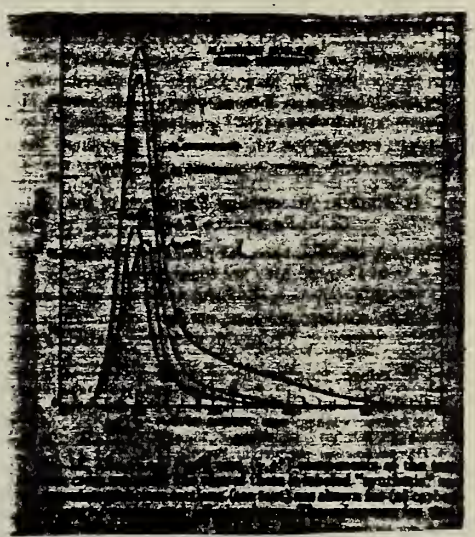

Ref. B. Ziegler
Nuclear Phys. 17, 238 (1960)

Elem. Sym.	A	Z
Al	27	13

Method
32 MeV betatron; magnetic pair spectrometer

Ref. No.
60 Zi 1

JHH

Reaction	E or ΔE	E_o	Γ	$\int \sigma dE$	Jπ	Notes
$Al^{27}(\mu_t)$	Bremss. 10-30					

846

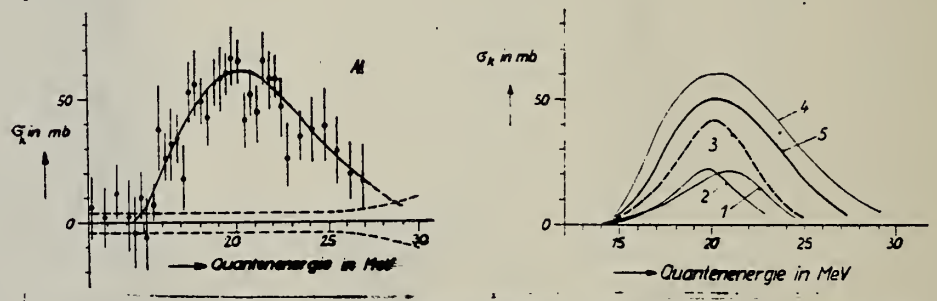

Fig. 8. Kernabsorptionsquerschnitt von Aluminium,
a) berechnet nach (3). Wird an der Summe $(\sigma_p+\sigma_c)$ eine Korrektur von +1·% angebracht, um zwischen 10 und 15 MeV bessere Übereinstimmung zwischen I'_0 und I zu erhalten (s. Fig. 7), so rückt die Nullinie für σ_k um 11 mb nach oben.
b) 1) $\sigma(\gamma, p)$ nach Halpern [30]) *et al.*;
2. $\sigma(\gamma, n)$ nach Montalbetti *et al.* [31]);
3. Summe $\sigma(\gamma, p)+\sigma(\gamma, n)$.
4. Kurve aus 8a;
5. Kurve aus 8a, verschoben um 11 mb.

Ref. J.E.E. Baglin, M.N. Thompson, B.M. Spicer
Nuclear Phys. 22, 207 (1961)

Elem. Sym.	A	Z
Al	27	13

Method: Melbourne 19 MeV synchrotron; 25 r Victoreen ionization chamber; BF_3 neutron counters.

Ref. No.: 61 Ba 1 EGF

Reaction	E or ΔE	E_o	Γ	$\int \sigma dE$	Jπ	Notes
(γ,n)	Bremss. 11.6-18.6 16.25			$\int_{}^{18.5}$ = 28 MeV-mb		

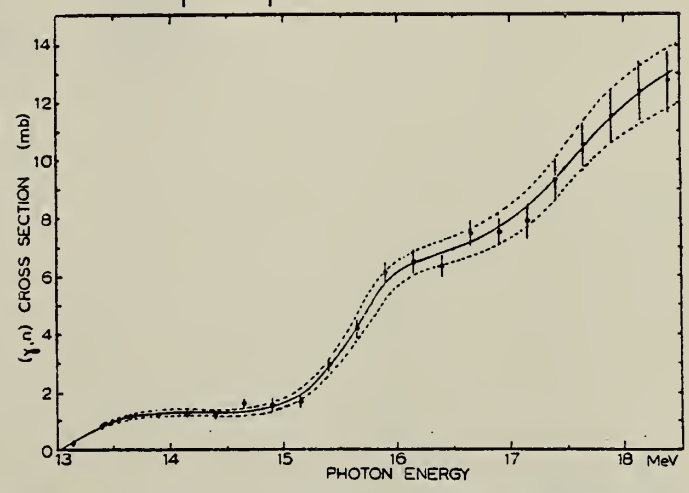

Fig. 2. Cross section for the $Al^{27}(\gamma, n)Al^{26}$ reaction plotted as a function of photon energy. The solid line is the curve of best fit consistent with the experimental points. The dotted lines define an estimated error band (see text).

REF.	ELEM. SYM.	A	Z
A. Bussiere de Nercy J. Phys. Radium 22, 535 (1961) (See 61 Bu 4)	Al	27	13

METHOD	REF. NO.
Betatron; photon scattering; NAI	61 Bu 3 Nvb

REACTION	RESULT	EXCITATION ENERGY	SOURCE		DETECTOR		ANGLE
			TYPE	RANGE	TYPE	RANGE	
G,G	ABX	14-32	C	32	NAI-D		DST

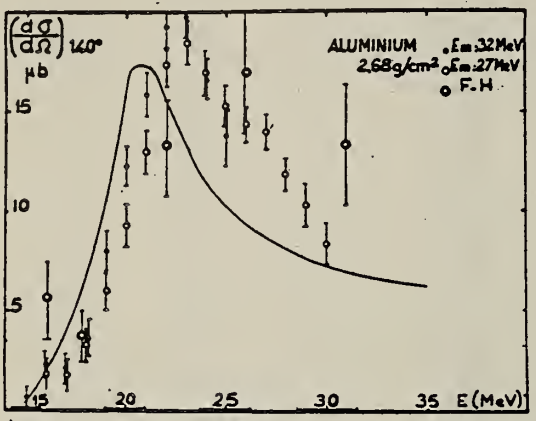

FIG. 3.

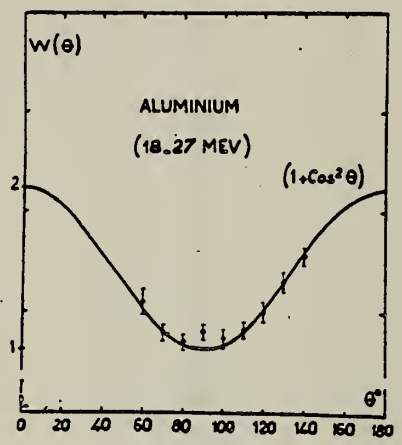

FIG. 5.

REF.

A. Bussiere de Nercy
Ann. Phys. (Paris) Third Series 6, 1379 (1961)

ELEM. SYM.	A	Z
Al	27	13

METHOD

REF. NO.	
61 Bu 4	egf

REACTION	RESULT	EXCITATION ENERGY	SOURCE		DETECTOR		ANGLE
			TYPE	RANGE	TYPE	RANGE	
G,G	ABX	15-30	C	27,32	NAI-D		140

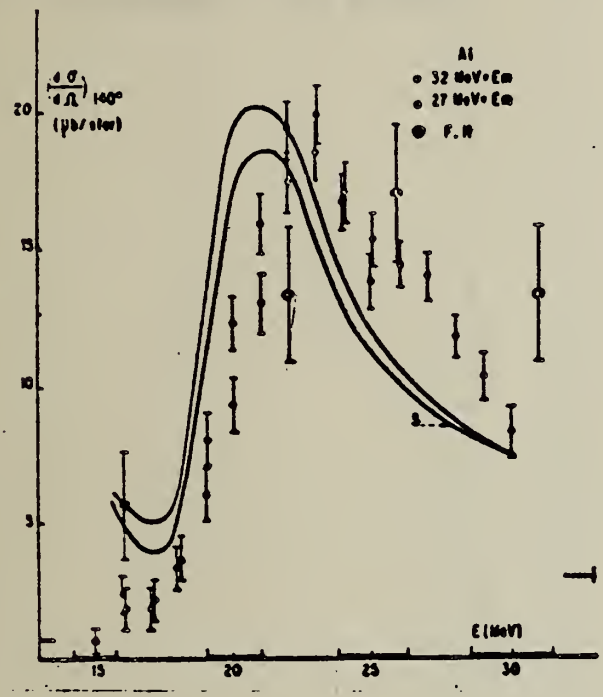

Fig. ... Sec... lisse efficace différentielle de diffusion (γ, γ) à ... pour l'alu... minium.

... courbes en trait plein représentent les sections efficaces pré...

Ref. E.D. Makhnovskii
Zhur. Eksp. i Teoret. Fiz. 41, 1091 (1961)
Soviet Phys. JETP 14, 779 (1962)

Elem. Sym.	A	Z
Al	27	13

Method: Magnetic spectrometer and emulsions

Ref. No.: 61 Ma 1 JHH

Reaction	E or ΔE	E_o	Γ	$\int \sigma dE$	Jπ	Notes
(γ,p) (γ,d) (γ,a)	Bremss.: 35					Yield ratios: $\frac{Y(\gamma,d)}{Y(\gamma,p)} = 0.009 \pm .007$ for particles 2.9 to 10 MeV. $\frac{Y(\gamma,a)}{Y(\gamma,p)} = 0.023 \pm 0.019$ for particles 8.8 to 14 MeV neglecting possible (γ,tr) contribution.

REF.	ELEM. SYM.	A	Z
M. Masuda J. Phys. Soc. 16, 1801 (1961)	Al	27	13

METHOD	REF. NO.	
Betatron; proton angular distribution; ZnS scintillator	61 Ma 2	NVB

REACTION	RESULT	EXCITATION ENERGY	SOURCE		DETECTOR		ANGLE
			TYPE	RANGE	TYPE	RANGE	
G,XP	NΦX	8 - 21	C	21	SCI-I	1 - 10	DST

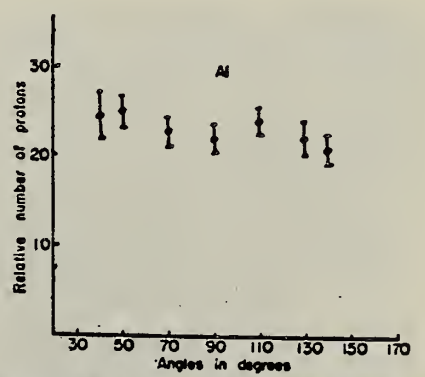

Fig. 5. Angular distribution of photo-protons from aluminum.
Interpreted as isotropic.

Ref. R. Nordhagen
Nuclear Phys. 27, 112 (1961)

Elem. Sym.	A	Z
Al	27	13

Method
See "Notes" below.

Ref. No. 61 No 1 JHH

Reaction	E or ΔE	E_o	Γ	∫σdE	Jπ	Notes
(p,γ)		648 kev	Γ_γ=0.023eV		5/2⁻	E_{γ_o} = 8.9 MeV This tentative spin assignment is an addendum to the results of S.L. Anderson et al [Nuclear Phys. 13, 310, (1959)].

TABLE I

Possible transition strengths of a 8.9 MeV 100 % ground state transition in the decay of the 648 keV resonance

Possible spins	Corresponding Γ_γ	$\|M\|^2$ in W.U.
½	0.035 eV	E1 : $1.1 \cdot 10^{-4}$ M1 : $2.3 \cdot 10^{-2}$
½	0.023 eV	E1 : $7.2 \cdot 10^{-5}$ M1 : $1.5 \cdot 10^{-2}$

Ref. V. Presperin, L.A. Kul'chitskii
Zhur. Eksp. i Teoret. Fiz. 41, 60 (1961)
Soviet Phys. JETP 14, 46 (1962)

Elem. Sym.	A	Z
Al	27	13

Method $Cu^{63}(n,2n)$ threshold detectors; positrons counted; neutron cross section; quantometer

Ref. No. 61 Pr 1 JHH

Reaction	E or ΔE	E_o	Γ	$\int \sigma dE$	Jπ	Notes
$Al^{27}(\gamma,n)$	Bremss. 25-85					In figure, curve 2 is calculated (using Penfold-Leiss) from curve 1, $\sigma(\gamma,n)$ for all $E_n > 11$ MeV; curve 3 is $\sigma(\gamma,n)$ for $E_n > 11$-21 MeV. Yields analyzed in terms of $Cu^{63}(n,2n)Cu^{62}$ cross section and assumed neutron spectrum of form E^{-n}; n = 1.5 (curve 2); n = 2.5 (curve 3).

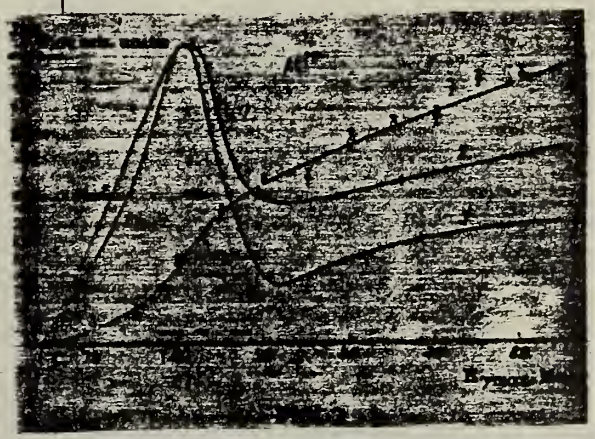

Ref. T. Tohei, M. Sugawara, S. Mori, M. Kimura
J. Phys. Soc. Japan 16, 1657 (1961)

Elem. Sym.	A	Z
Al	27	13

Method 25 MeV betatron; photon scattering; NaI(Tℓ) spectrometer; ion chamber.

Ref. No. 61 To 1 NVB

Reaction	E or ΔE	E_o	Γ	$\int \sigma dE$	Jπ	Notes
$Al^{27}(\gamma,\gamma)$	Bremss. 5-12	8.3				Detector at 120° Table II from J. Phys. Soc. Japan 18, 17-22 (1963)

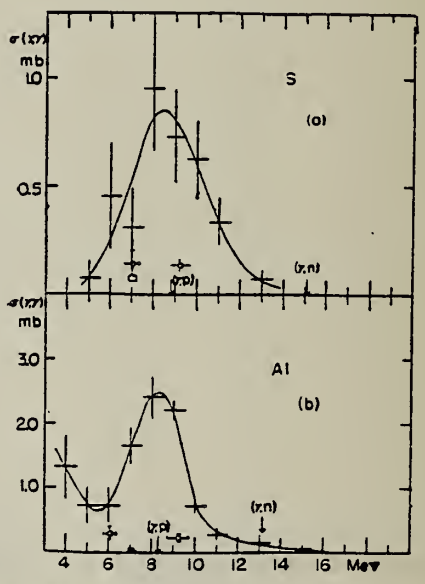

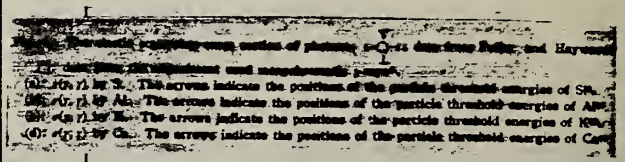

References

1) E. G. Fuller and E. Hayward: Phys. Rev. **101** (1956) 692.

4) K. Reibel and A. K. Mann: Phys. Rev. **118** (1960) 701.

Table II. The correction of the energy scale.

Energy in Ref. 1	should be read
4.0 Mev	3.3 Mev
6.0	5.5
8.0	7.7
10.0	9.9
12.0	12.1
14.0	14.3

Ref. C. Bacchi, L. Meneghetti, S. Vitale
Phys. Letters 3, 89 (1962)

Elem. Sym.	A	Z
Al	27	13

Method: 31 MeV betatron; Si detectors (semi-conductor)

Ref. No.: 62 Be 3 | BG

Reaction	E or ΔE	E_o	Γ	$\int \sigma dE$	Jπ	Notes
$Al^{27}(\gamma,\alpha)$	Bremss. 30					Two counters: one at 60° ± 25° from beam axis and one at 120° ± 25°. Asymmetry spectrum, $A = \frac{N_f - N_b}{N_f + N_b}$ N_f, N_b are number of α's produced in forward and backward direction with energy between E and Δ E. Irregular behavior not wholly due to statistical fluctuations. Forward-backward asymmetry due to interference between E2 and E4; absorption indicates direct photo effect in this energy range.

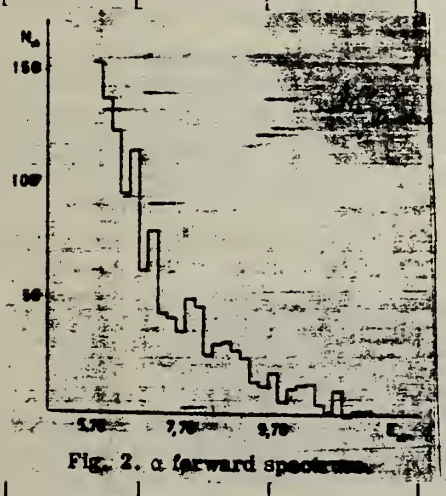

Fig. 2. α forward spectrum.

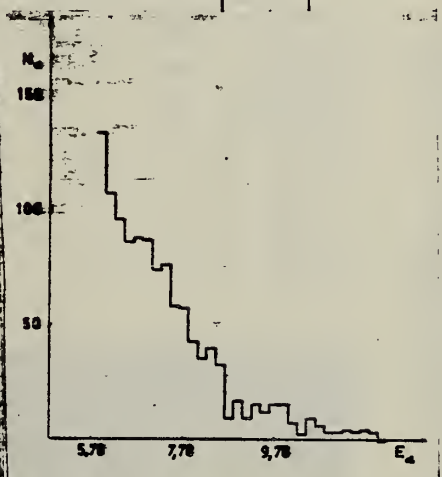

Fig. 3. α Backward spectrum.

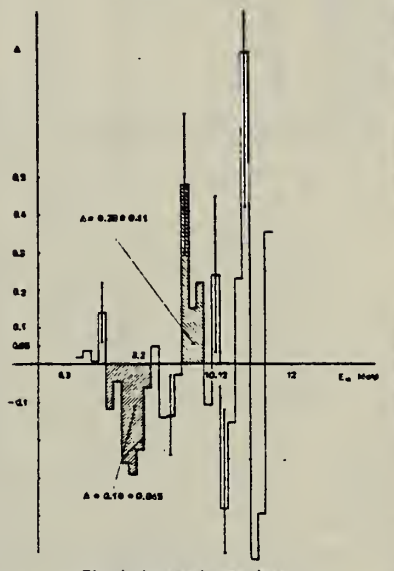

Fig. 4. Asymmetry spectrum

Ref. L.N.Bolen, W.D.Whitehead
Phys.Rev.Letters 9, 458 (1962)

Elem. Sym.	A	Z
Al	27	13

Method
70 MeV synchrotron - BF_3

Ref. No. 62Bo2 — β G

Reaction	E or ΔE	E_o	Γ	∫σdE	Jπ	Notes
(γ,n)	14-30	14.6 16.4 18.1 19.8 21.4	see Table II			801

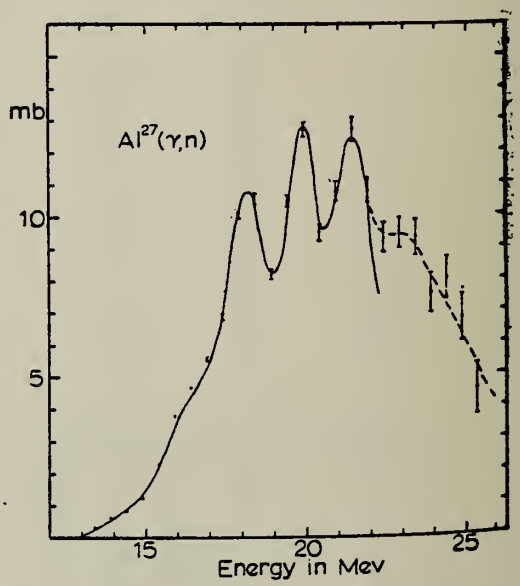

FIG. 2. $Al^{27}(\gamma,n)Al^{26}$ cross section. Data points are the result of this experimental determination. The solid line is the resultant of five Gaussian resonances used to synthesize the cross section.

Table II. The values of the parameters of the Gaussian curves used to synthesize the Al^{27} cross section in Fig. 2. E_m is the energy at which the maximum cross section occurs, σ_m is the maximum cross section, and Γ is the width at half maximum of the Gaussian curve. The experimental values of E_m determined from a total absorption experiment[a] are also given.

E_m (MeV)	σ_m (MeV)	Γ (MeV)	∫σdE (MeV-mb)	E_m[a] (MeV)
14.6	1	1.7	1.77	
16.4	3.6	1.7	6.37	15.8
18.1	10.6	1.7	18.8	18.5
19.8	11.2	1.2	13.9	20.3
21.4	12.5	1.7	22.1	21.8

[a] See reference 21.

Ref. E.C. Booth, K.A. Wright
Nuclear Phys. 35, 472 (1962)

Elem. Sym.	A	Z
Al	27.	13

Method 4 MeV electron Van de Graaff; bremss.; nuclear resonance scattering, ring scatterer; NaI

Ref. No. 62 Bo[redacted] JHH

Reaction	E or ΔE	E_0	Γ	$\int \sigma dE$	Jπ	Notes
$Al^{27}(\gamma,\gamma)$	Bremss. 0 - 4					

TABLE 2
Comparison of mean lifetime measurements

Nucleus	Energy	%	Spins	g	Γ_0/Γ	$W'(\theta)$	$\tau \times 10^{14}$ sec This work	Other	
Li^6	3.56	7	$1^+ - 0$	$\frac{1}{2}$	(1)	1	0.012	0.0072	$^{+0.0018}_{-0.0013}$ [redacted]
								0.0105	± 0.001 [redacted]
B^{11}	2.14	81	$\frac{1}{2}^- - (\frac{1}{2})$	$\frac{1}{2}$	1	1	0.53	0.47	± 0.06 [redacted]
Al^{27}	2.21	100	$\frac{1}{2}^+ - \frac{1}{2}^-$	$\frac{1}{2}$	(1)	1	3.2	2.7	± 0.3 [redacted]
Al^{27}	1.01	100	$\frac{1}{2}^+ - \frac{1}{2}^+$	$\frac{1}{2}$	0.98	1	520	170	± 50 [redacted]
Si^{28}	1.78	92	$0^+ - 2^+$	5	1	0.63	88	73	± 22 [redacted]
S^{32}	2.24	95	$0^+ - 2^+$	5	1	0.63	26	≈16	[redacted]
Mg^{24}	1.37	78.6	$0^+ - 2^+$	5	1	0.63	220	155	± 40 [redacted]
Mg^{25}	1.61	25	$\frac{1}{2}^+ - \frac{1}{2}$	$\frac{1}{2}$	(1)	1	3.6	2.5	$^{+0.6}_{-0.4}$ [redacted]
Cu^{65}	0.963	69	$\frac{1}{2} - \frac{1}{2}$	$\frac{1}{2}$	1	0.92	230	72	± 18 [redacted]
								90	± 15 [redacted]
Cu^{65}	0.67	69	$\frac{1}{2} - \frac{1}{2}$	$\frac{1}{2}$	1	1	100	31	± 3 [redacted]

The factor g equals $(2I+1)(2I_0+1)^{-1}$.

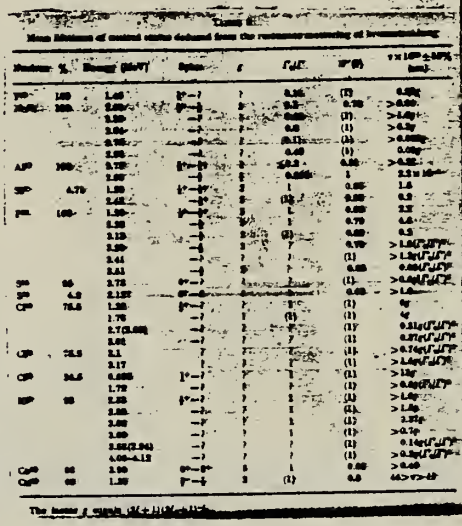

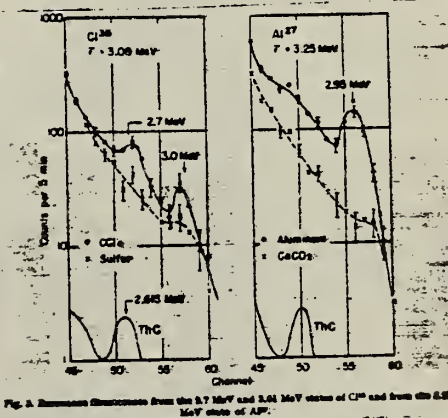

FORM NBS-418
(6-1-63)
USCOMM-DC 18656-P62

U.S. DEPARTMENT OF COMMERCE
NATIONAL BUREAU OF STANDARDS

REF.

E. Braun
Z. Physik 166, 62 (1962)

ELEM. SYM.	A	Z
Al	27	13

METHOD

Van de Graaff; proton spectrum, angular distribution; nuclear emulsion.

REF. NO. 62 Br 3 NVB

REACTION	RESULT	EXCITATION ENERGY	SOURCE		DETECTOR		ANGLE
			TYPE	RANGE	TYPE	RANGE	
G,P	SPC	18	D	18	EMU-D	2-10	DST
		(17.6)		(17.6)			

In Figure 3, $W(\theta) = a + b \sin^2\theta$

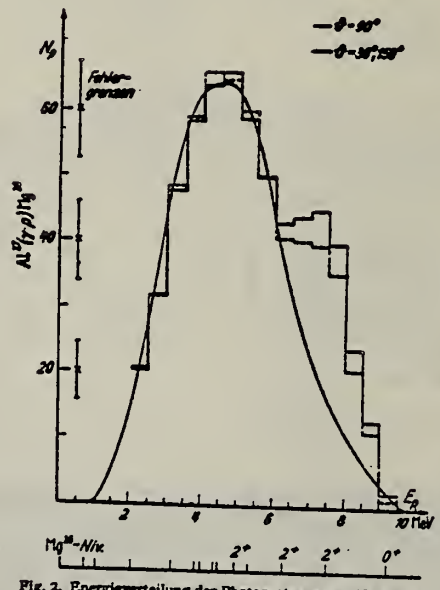

Fig. 2. Energieverteilung der Photoprotonen aus Aluminium. Ausgezogene Kurve: Verteilung nach der statistischen Theorie, Stufenkurven: gemessenes Spektrum für $\theta = 90°$ bzw. Mittelwert der Spektren für $\theta = 30°$, 150°. Darunter: Niveauschema des Restkerns Mg^{26} (von rechts nach links)

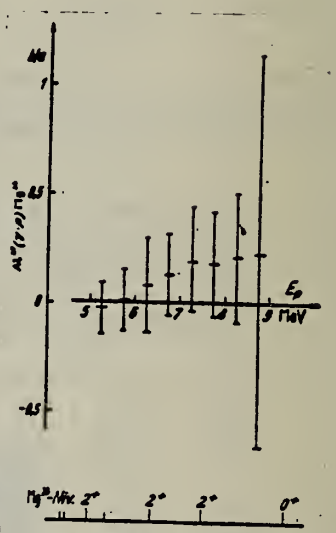

Fig. 3. Anisotropie-Faktor b/a in Abhängigkeit von der Protonenenergie mit statistischem Fehler, darunter Niveaus des Restkerns Mg^{26} (von rechts nach links)

Ref. V.P. Chizhov, A.P, Komar, L.A. Kulchitsky, A.V. Kulikov, E.D. Makhnovsky, Yu.M. Volkov
Nuclear Phys. 34, 562 (1962)

Elem. Sym.	A	Z
Al	27	13

Method: 90 MeV Synchrotron; magnetic spectrometer; emulsions;

Ref. No.: 62 Ch 2 JHH

Reaction	E or ΔE	E_0	Γ	$\int \sigma dE$	Jπ	Notes
	Bremss.					
(γ,d)	35					
(γ,p)						

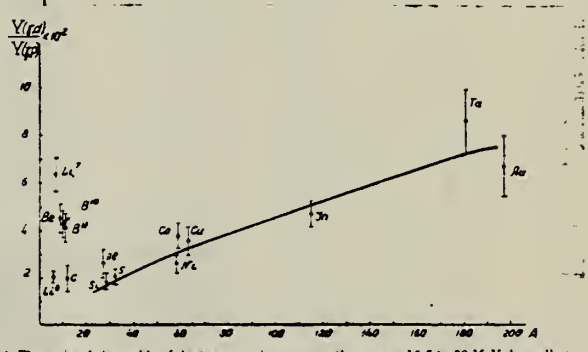

Fig. 4. The ratio of the yields of deuterons and protons with energies 15.5 to 30 MeV depending on the mass number of nuclei A for $E_{\gamma max}$ = 90 MeV. The solid line stands for the normalized dependence (8).

TABLE 1

Experimental data

Elements	$E_{\gamma\ max}$ (MeV)	Particle energy interval (MeV)	$\frac{Y(\gamma, d)}{Y(\gamma, p)}$	θ	Method
Li^6	30	7.5 to 15	0.003 ± 0.008		
	43		0.007 ± 0.005	90°	I
	90		0.097 ± 0.014		
Li^7	25		0.020 ± 0.030		
	43	7.5 to 15	0.056 ± 0.006	90°	I
	90		0.160 ± 0.054		
B^{11}	40	7.5 to 19	0.006 ± 0.002	90°	I
Al^{27}	35	2.9 to 10	0.009 ± 0.007	50° ÷ 120°	II
Ca^{48}	35	3.7 to 10	0.036 ± 0.017	50° ÷ 100°	II
$Cu^{63, 65}$	34	4.5 to 15	0.007 ± 0.003	90°	I
	34	7.5 to 15	0.007 ± 0.003	90°	I
	70	3 to 10	0.05 ± 0.01	20° ÷ 50°	II
	70	4 to 10	0.04 ± 0.01	20° ÷ 50°	II
	90	7 to 19	0.021 ± 0.005	90°	I

I. Scintillation telescope method.
II. Method of deflecting charged particles in magnetic field.

Ref.	Elem. Sym.	A	Z
W. R. Dodge, W. C. Barber Phys. Rev. 127, 1746 (1962)	Al	27	13

Method	Ref. No.	
Magnetic analysis of proton spectron produced by electron bombardment	62Do1	BG

Reaction	E or ΔE	E_o	Γ	$\int \sigma dE$	Jπ	Notes 804
(e,p)	18 24.5 30			$\int_{18.5}^{29} \sigma(\gamma,p)dE_\gamma$ = 94±19% 100% ground state transitions assumed.		Data fit with E= (27/26)E_p + 16 MeV for E_p interval 3.4 - 7 MeV. Beyond 7 MeV E = (27/26)E_p + 14 MeV. K = photon energy. Correspondence between (e,pe') reaction and (γ,p) reaction. Assumed electron has associated with it a virtual photon spectrum. Electron production yields analyzed by use of E1 virtual photon spectrum to obtain σ(γ,p).

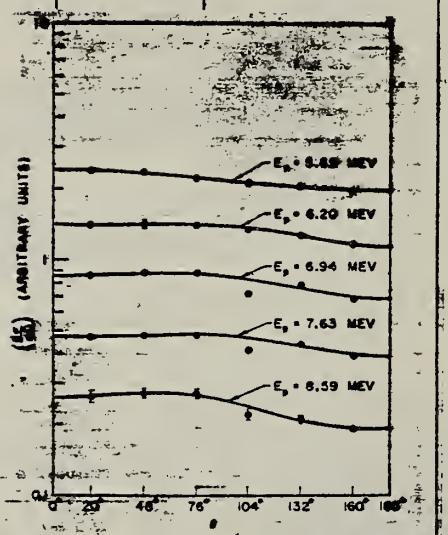

Fig. 25. Aluminum (e,pe') proton angular distributions E_0=24.5 MeV, $\Delta E_p \leq \pm 0.25$ MeV.

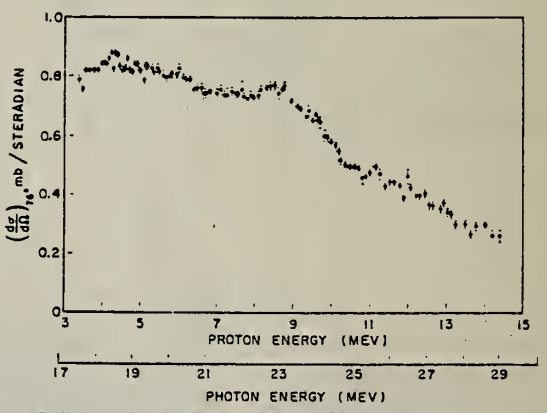

Fig. 26. Aluminum (e,pe') cross section for E_0=30 MeV and θ=76°, assuming k=(27/26)E_p+14 MeV.

Ref. B.T. Lawergren, T.R. Ophel
Phys. Letters 2, 265 (1962)

Elem. Sym.	A	Z
Al	27	13

Method: (source not given); NaI

Ref. No.: 62 La 1 JHH

Reaction	E or ΔE	E_o	Γ	$\int \sigma dE$	Jπ	Notes
$Mg^{26}(p,\gamma)$	2.81	10.98			(5/2)	In the cascade, the level at 2.21 MeV is inferred to have $J^\pi = \frac{7^+}{2}$

Table I
Correlation measurements at the 2.81 MeV resonance of the $Mg^{26}(p,\gamma)$ reaction.

Gamma ray transition (sequence)	Observed distribution
$r \rightarrow 0$	$1+(0.49\pm0.02)\,P_2-(0.08\pm0.02)\,P_4$
$r \rightarrow 1.01$	$1-(0.39\pm0.06)\,P_2$
$r \rightarrow 2.21$	$1+(0.05\pm0.04)\,P_2$
$2.21 \rightarrow 0$	$1+(0.39\pm0.03)\,P_2-(0.03\pm0.03)\,P_4$
$r \rightarrow 2.21 \rightarrow 0$ (Geometry A)	$1-(0.03\pm0.10)\,P_2$
$r \rightarrow 2.21 \rightarrow 0$ (Geometry B)	$1+(0.48\pm0.07)\,P_2$

Ref.	Elem. Sym.	A	Z
N. Mutsuro, K. Kageyama, M. Mishina, T. Nakagawa, E. Tanaka, M. Kimura J. Phys. Soc. Japan 17, 1672 (1962)	Al	27	13

Method	Ref. No.
Betatron; BF_3 counters; Aℓ thin-wall ion chamber monitor	62 Mu 1 NVB

Reaction	E or ΔE	E_o	Γ	$\int \sigma dE$	Jπ	Notes 753
$Al^{27}(\gamma,n)$	Bremss. 12.5-24	13.75 14.75 15.75 17.1 18.25 19.1		$\int_{12.5}^{24}$ = 115 MeV-mb		Results discussed in terms of compound nucleus model and statistical model.

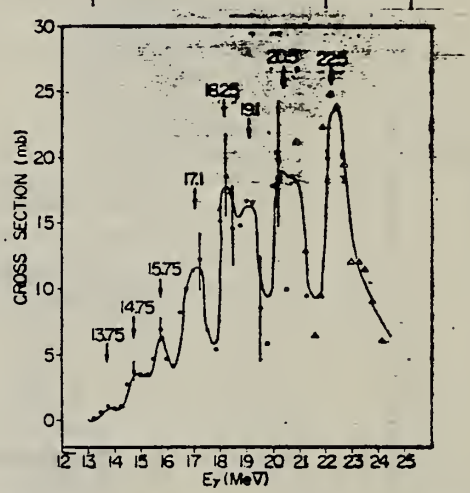

Fig. 1. Cross section curve of $Al^{27}(\gamma, n)$ reaction.

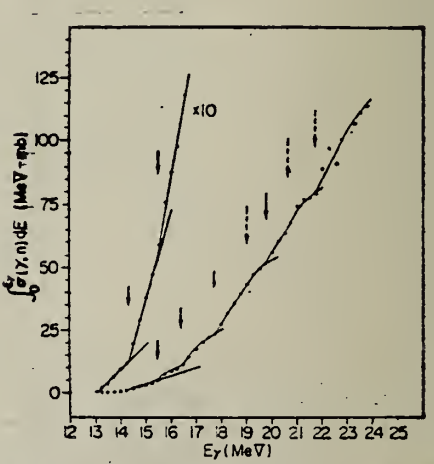

Fig. 2. Running integral of $Al^{27}(\gamma, n)$ reaction.

Ref. T.R. Ophel, B.T. Lawergren
Nuclear Phys. 30, 215 (1962)

Elem. Sym.	A	Z
Al	27	13

Method 1.2 MeV Cockraft-Walton generator; NaI

Ref. No.	
62 Op 1	JHH

Reaction	E or ΔE	E_o	Γ	$\int \sigma dE$	Jπ	Notes
(p,γ)	710-960 kev	9.03 MeV			5/2	E_{γ_o} = 9.03±0.05 MeV For angular distributions, see Table 3. Resonance also at E_{po} = 839 kev, but ground-state transition (E_{γ_o} =9.05 MeV) is ≤ 0.5%.

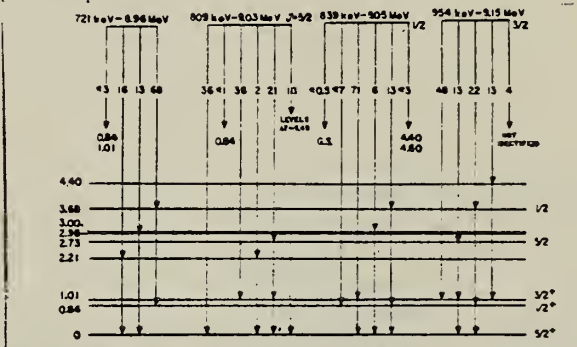

Fig. 8. Summary of the de-excitations of the 721, 809, 839 and 954 keV resonances.

TABLE 3

Gamma rays observed at the 809 keV resonance

Gamma ray energy (MeV)	Interpretation	Calculated energy	Relative intensity	Angular distribution
9.03±0.05	r → 0	9.03	100	$1+(0.26\pm0.02)P_2+(0.03\pm0.03)P_4$
8.04±0.05	r → 0.84	8.19	≤3	
8.04±0.05	r → 1.01	8.02	102	$1-(0.37\pm0.03)P_2+(0.01\pm0.05)P_4$
6.92±0.10	r → 2.21	6.83	5	Small negative anisotropy
6.34±0.05	r → 2.73	6.30	60	$1-(0.32\pm0.06)P_2-(0.13\pm0.10)P_4$
5.41±0.10	Levels at ≈ 5.4 → 0		10	
5.17±0.10	?		≤2.5	
2.25±0.05	2.21 → 0	2.2	17 a)	
1.72±0.03	2.73 → 1.01	1.72	42 a)	
1.01±0.03	1.01 → 0	1.01	100 a)	
0.84±0.03	0.84 → 0	0.84	≤3 a)	

a) Relative intensities at 90°. Intensity scale not related to relative intensities of gamma rays of energies greater than 5 MeV.

FORM NBS-418
(8-1-63)
USCOMM-DC 16856-P63

U.S. DEPARTMENT OF COMMERCE
NATIONAL BUREAU OF STANDARDS

W. Sebaoun
J. Phys. Radium 23, 989 (1962)

Al	27	13

METHOD: proton cross section; CSI; $Cu^{63}(\gamma,n)$ reaction

REF. NO.: 62 Se 2 | NVB

REACTION	RESULT	EXCITATION ENERGY	SOURCE TYPE	SOURCE RANGE	DETECTOR TYPE	DETECTOR RANGE	ANGLE
G,P	ABX	15, 18	D	15, 18	SCI		
		(14.8, 17.6)		(14.8) (17.6)			

σ = (7.2±1.1) mb, assuming σ [$Cu^{63}(\gamma,n)$] = 82±8 mb.

Ref. K. Shoda, T. Ishizuka, K. Shimizu, M. Akashi
J. Phys. Soc. Japan 17, 1536 (1962)

Elem. Sym.	A	Z
Al	27	13

Method: Betatron; proton spectrum, angular distribution; nuclear emulsion

Ref. No.: 62 Sh 8 | NVB

Reaction	E or ΔE	E_0	Γ	$\int \sigma dE$	Jπ	Notes
$Al^{27}(\gamma,p)$	Bremss. 24					

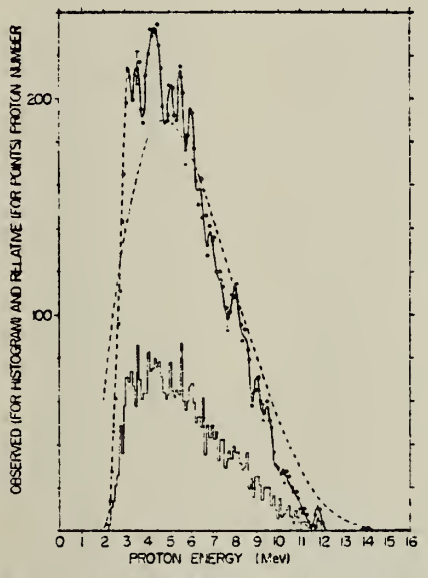

Fig. 1. The energy distribution of photoprotons emitted from Al^{27} (histogram). The solid and broken curve is the smoothed one. The broken-curve is a calculated one using the statistical model with the Weisskopf level density and a classical Coulomb barrier height.

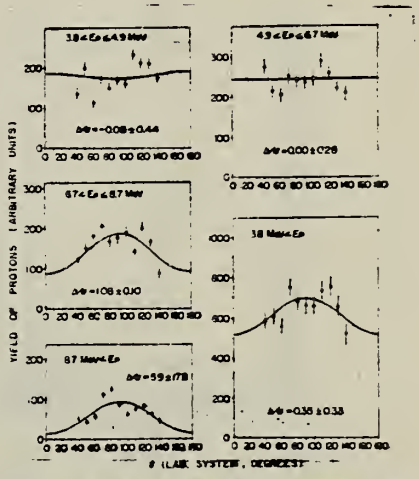

Fig. 2. Angular distributions of photoprotons from Al^{27}. Full lines and values of b/a were obtained by least squares for $a+b\sin^2\theta$.

Ref. K. Shoda, T. Ishizuka, K. Shimizu, M. Akashi
J. Phys. Soc. Japan 17, 407 (1962)

Elem. Sym.	A	Z
Al	27	13

Method: Betatron; proton spectrum; nuclear emulsion

Ref. No.: 62 Sh 10 | NVB

Reaction	E or ΔE	E_o	Γ	$\int \sigma dE$	Jπ	Notes
$Al^{27}(\gamma, p)$	Bremss. 24					Index entry listed as 62 Sh 8. Bibliography listed as 62 Sh 10.

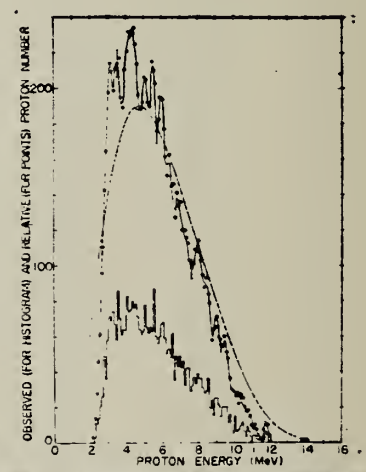

Fig. 1. The photoproton energy distributions from Al^{27}. The solid curve is a smoothed one. The broken curve is a calculated one using the statistical model with the Weisskopf level density $\omega = C \exp[2\sqrt{0.45 E}]$ MeV^{-1} and a classical Coulomb barrier height of 4.49 MeV.

Ref. K. Shoda, K. Abe, T. Ishizuka, N. Kawamura, M. Kimura
J. Phys. Soc. Japan 17, 735 (1962)

Elem. Sym.	A	Z
Al	27	13

Method: 25 MeV betatron; proton yield; scintillator; ion chamber

Ref. No.: 62 Sh 11 NVB

954

Reaction	E or ΔE	E_o	Γ	$\int \sigma dE$	Jπ	Notes
$Al^{27}(\gamma,p)$	Bremss. Thr=24	20	7 MeV	$\int_0^{23}$ = 0.11 MeV-b		σ_{max} = 17.5 mb. 6 detectors at angles: 20°, 55°, 90°, 125°, 160°. Measured all protons above E_o = 1.5MeV

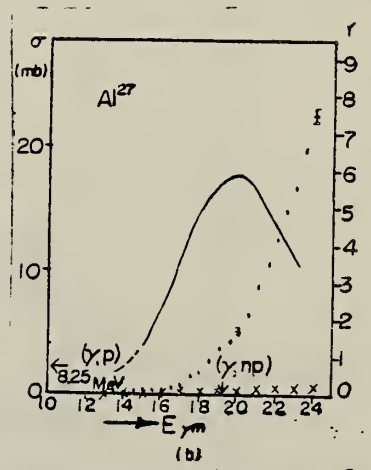

Fig. 8. Photoproton yield and cross section curves for (a)-Mg, (b)-Al, (c)-Si, (d)-S. Arrows in the figures show the threshold energies. The backgrounds observed without targets are shown by x.

FORM NBS-418
(6-1-63)
USCOMM-DC 18556-P63

U.S. DEPARTMENT OF COMMERCE
NATIONAL BUREAU OF STANDARDS

Ref.	Elem. Sym.	A	Z
R.C.Barber, J.Goldemberg, G.A.Peterson, Y.Torizuka Nuclear Phys. 41, 461 (1963); erratum to be published (as of 9/5/63)	Al	27	13

Method	Ref. No.
Linac (Stanford Mark II) - counter telescope	63Bal 28

Reaction	E or ΔE	E_0	Γ	$\int \sigma dE$	Jπ	Notes
(e,e')	41.5		determined see Table II		see Table II	inelastic scattering cross section at 180° $(cm^2/sr)\times10^{-32}$
		4.8		0.10 MeV·mb		0.7±30%
		8.0		0.50		1.9±30%
		10.6		0.23		0.6±40%
		12.8		0.65		1.4±30%

NUCLEAR MAGNETIC TRANSITIONS

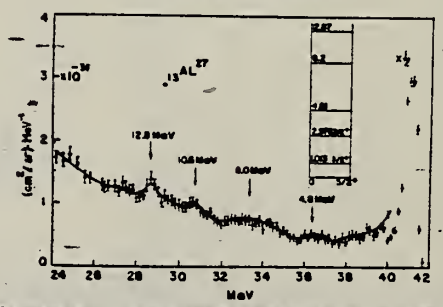

Fig. 13. Spectrum of 41.5 MeV electrons scattered from an Al^{27} target at 180°.

Table 2

Isotope	Energy of level (MeV)	Spin and parity: Ground state	Spin and parity: Excited state	Inelastic electron scattering cross section (cm^2/sr) $\times10^{-32}$: Estimated error (%)	Inelastic electron scattering cross section (cm^2/sr) $\times10^{-32}$: MeV·mb	Radiation width to ground state (eV): This experiment*)	Radiation width to ground state (eV): Weisskopf
$_3Li^6$	3.56	1+	0+	4.0	20	0.42	4.7	0.82
	5.7		0+ 1+ 2+	0.15	50	0.03	0.9 0.3 0.16	3.6
	9.3		0+ 1+ 2+	0.6	30	0.39	13 5 3	16
	14.0		0+ 1+ 2+	0.25	30	0.14	24 6 5	56
	15.6		0+ 1+ 2+	0.25	50	0.17	37.5 12.5 7.5	80
$_3Li^7$	9.6	½-	½- ½- ½-	0.18	30	0.06	3.4 1.7 1.1	16
	10.3		½- ½- ½-	0.78	30	0.30	19.2 9.6 6.4	23
	14.0		½- ½- ½-	0.48	40	0.27	31.2 15.6 10.4	58
$_7N^{14}$	9.3	1+	0+ 1+ 2+	0.92	30	0.30	23.4 7.6 4.6	17
	10.6		0+ 1+ 2+	0.65	30	0.25	24.6 8.2 4.9	25
$_8O^{16}$	19.0	0+	1-	0.45	40	0.41	14.1	145
$_9F^{19}$	7.7	½+	½-	2.0	25	0.56	4.7	9.8
$_{10}Ne^{20}$	≈ 9	0+	1-	3.0	20	0.9	7.1	14.5
	≈13		1+	2.0	20	1.0	16.6	48
$_{11}Na^{23}$	3.0	½+	½-	0.2	30	0.02	0.05	0.43
			½-				0.035	
	4.6		½-	0.5	40	0.07	0.43	1.6
	6.1		½-	1.0	40	0.20	4.4	4.6
	8.0		½-	2.5	30	0.68	12.8	10.8
			½+				8.6	
$_{12}Mg^{24}$	11.0	0+	1-	4.4	20	1.76	21.0	29
	≈14		1+	1.5	30	0.83	15.8	58
$_{13}Al^{27}$	4.8	½+	½-	0.7	30	0.10	1.0	2.1
			½-				0.67	
			½-				0.50	
	8.0		½-	1.9	30	0.30	14.0	10.6
			½-				9.3	
			½-				7.0	
	10.6		½-	0.6	40	0.23	11.5	25
			½-				7.7	
			½-				5.8	
	12.8		½-	1.4	30	0.65	44.5	45
			½-				31.2	
			½-				23.3	
$_{14}Si^{28}$	3.6	1+	½-	0.9	30	0.1	0.29	0.82
			½-				1.1	
	5.6		½-	0.7	30	0.12	0.61	3.6
			½-				0.55	
	8.9		½-	0.7	30	0.22	4.0	14.5
$_{16}S^{32}$	5.7	0+	1-	1.3	30	0.24	0.76	3.6
	8.5		1-	1.7	30	0.31	3.5	12.5
	11.4		1-	2.6	30	1.11	14.2	32
$_{18}A^{40}$		0+	no resonances					
$_{19}K^{39}$		½+	no resonances					
$_{20}Ca^{40}$		0+	no resonances					
$_{40}Zr^{90}$		½-	no resonances					

*) The results in this column were derived in the "long wave approximation".

Ref. S. Costa, F. Ferrero, S. Ferroni, B. Minetti, C. Molino, R. Malvano Phys. Letters 6, 226 (1963)	Elem. Sym.	A	Z
	Al	27	13

Method 100 MeV Synchrotron; 4 π neutron detector; calculated integrated cross sections - fitted with polynomial of degree 7	Ref. No.	
	63 Co 3	EGF

Reaction	E or ΔE	E_o	Γ	$\int \sigma dE$	Jπ	Notes
$Al^{27}(\gamma,xn)$						$\sigma_b = \int \frac{\sigma(E)}{E} dE$ gets $< \bar{\nu}_p \cdot \bar{\nu}_n - \bar{\nu}_n \cdot \bar{\nu}_{n1} >$ $= (Rc^2 - R_p^2 - \frac{3}{\pi^2} \frac{tr\ c}{e^2} \sigma_b \frac{A-1}{A^2}) \times \frac{2}{A-2}$ See "Boron" for plots of this and $\int \sigma dE/60\ NZ/A$.

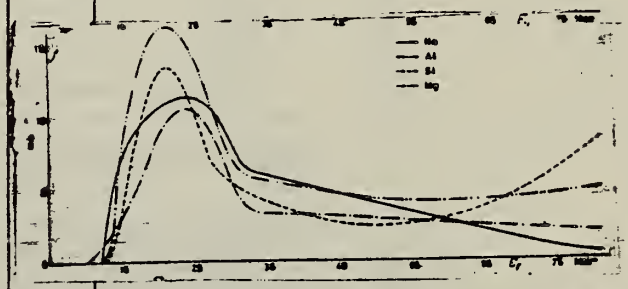

Figure 1: Photoneutron cross sections for several light elements versus γ-ray energy.

Ref. J. Goldemberg, Y. Torizuka, W.C. Barber, J.D. Walecka
Nuclear Phys. 43, 242 (1963)

Elem. Sym.	A	Z
Al	27	13

Method: Linac; electron scattering; magnetic spectrometer

Ref. No.: 63 Go 4 JHH

Reaction	E or ΔE	E_o	Γ	$\int \sigma dE$	Jπ	Notes
$Al^{27}(e^-,e^{-\prime})$	41.4					

TABLE 1

Summary of experimental and theoretical inelastic electron scattering cross sections at 180°

Element	Target	Density (g/cm³)	Thickness (mg/cm²)	Thickness (radiation lengths)	$\left(\frac{d\sigma}{d\Omega}\right)^T_{in} \times \frac{10^{32}\,sr}{cm^2}$ measured	$\left(\frac{d\sigma}{d\Omega}\right)^T_{in} \times \frac{10^{32}\,sr}{cm^2}$ calculated	$\left(\frac{d\sigma}{d\Omega}\right)^T_{in}$ (calc.) / $\left(\frac{d\sigma}{d\Omega}\right)^T_{in}$ (measured) maximum	average	minimum
$_6C^{12}$	C_8H_8 (Styrofoam)	0.033	466	0.0105	3.8±0.8	16.7	5.6	4.4	3.6
$_{13}Al^{27}$	Stack of 0.013 cm foils	2.70	380	0.016	4 ±2	25	12.5	6.2	4.1
Kr_{36}	Gas	0.016	460	0.041	8 ±4	36	9	4.5	3

Ref. C. Milone
Nuclear Phys. 47, 607 (1963)

Elem. Sym.	A	Z
Al	27	13

Method
Betatron; nuclear emulsions

Ref. No.
63 Mi 4 JHH

Reaction	E or ΔE	E_0	Γ	$\int \sigma dE$	Jπ	Notes
$Al^{27}(\gamma,n)$	Bremss.					
	24					
	30					

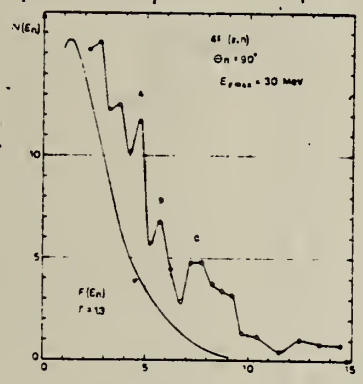

Fig. 2. Neutron energy spectrum for $E_{\gamma max}$ = 30 MeV. The points indicate experimental results (ordinates in arbitrary units). The curve is the calculated evaporation distribution.

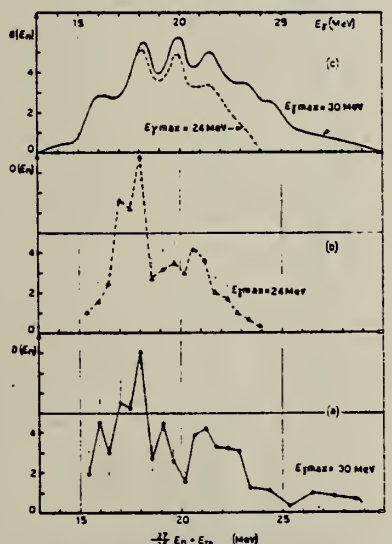

Fig. 4. Contribution of mainly direct emission for $E_{\gamma max}$ = (a) 30 MeV, (b) 24 MeV. (c) The function $G(E_n) = \sigma(\gamma, n)/(E_\gamma \cdot E_{\gamma max})$. See the text. The units are arbitrary.

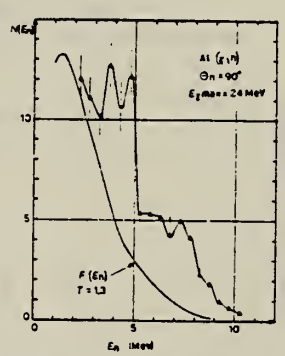

Fig. 3. Neutron energy spectrum for $E_{\gamma max}$ = 24 MeV. Points: experimental results (ordinates in arbitrary units). Curve: calculated evaporation distribution.

TABLE I

Summary of resonances

γ absorption experimental Ref. [11] (MeV)	γ absorption calculated Ref. [4] (MeV)	σ(γ, n) experimental Ref. [2] (MeV)	Neutron spectra present paper (MeV)
15.5	14, 15.5		(16)
18.5	19 several energies	18.2	18 ±0.5
20.3		19.9	19.4±0.5
21	21.5	21.4	21.2±0.5
22.3	22.1	(22.6 hump)	(22.5)
25.5	26		(26.5)

Energies in parenthesis are probable energies.

References

1) G. Cortini, C. Milone, T. Papa and R. Rinzivillo, Nuovo Cim. 14 (1959) 54
2) L. N. Bolen and W. D. Whitehead, Phys. Rev. Lett. 9 (1962) 458
3) L. Rosen, Nucleonics 11 (1953) 38
4) V. F. Weisskopf and D. E. Ewing, Phys. Rev. 76 (1949) 1550
5) H. Feshbach and V. F. Weisskopf, Phys. Rev. 76 (1949) 1550
6) V. Emma, C. Milone, A. Rubbino, S. Jannelli and F. Mezzanares, Nuovo Cim. 22 (1961) 135
7) J. E. E. Baglin, M. N. Thompson and B. M. Spicer, Nuclear Physics 22 (1961) 216
8) H. E. Johns, L. Katz, R. Douglas and R. Haslan, Phys. Rev. 80 (1950) 1062
9) L. Katz and A. G. Cameron, Can. J. Phys. 29 (1951) 518
10) J. H. Carver and K. H. Lokan, Austr. J. Phys. 10 (1957) 312
11) C. Milone, S. Milone Tamburino, R. Rinzivillo, A. Rubbino and C. Tribuno, Nuovo Cim. 7 (1958) 729

FORM NBS-418
(8-1-63)
USCOMM-DC 18556-P63

U.S. DEPARTMENT OF COMMERCE
NATIONAL BUREAU OF STANDARDS

Ref.	Elem. Sym.	A	Z
O.M.M. Mitchell, K.G. McNeill Can. J. Phys. 41, 871 (1963)	Al	27	13

Method	Ref. No.	
Betatron; proton yields, angular distribution; scintillator; ion chamber	63 Mi 5	NVB

Reaction	E or ΔE	E_o	Γ	$\int \sigma dE$	Jπ	Notes
$Al^{27}(\gamma,xp)$	Bremss. 22					Angular distribution: $Y(\theta) = a + b \sin^2\theta (1+p \cos\theta)^2$ where a = 75±10; b = 22±16; p = 0.4±0.5 and b/a = 0.3±0.2. Yield (E_p > 8 MeV): (1.0±0.2) 10^5 protons/mole-r Yield (3.7 < E_p < 14): (6.8±0.7) 10^5

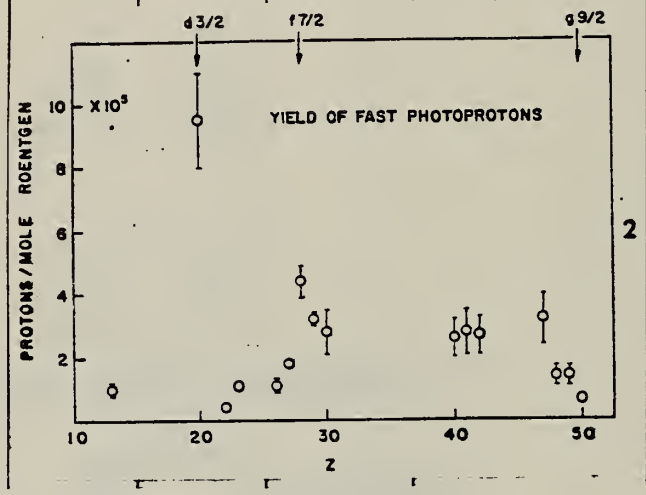

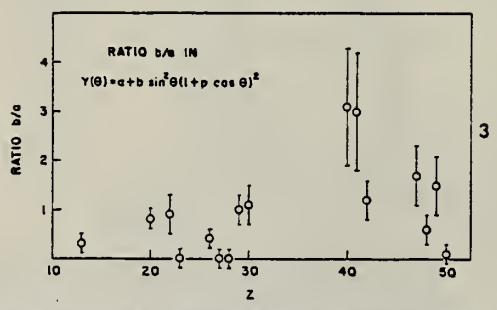

FIG. 2. The yields of fast photoprotons (E_p > 8 Mev) obtained from targets of various elements when irradiated with 22-Mev bremsstrahlung. The target thicknesses range from 351 to 572 mg/cm² (about 8 Mev for protons). The errors noted are statistical.

FIG. 3. The anisotropy coefficient b/a for fast photoprotons (E_p > 8 Mev) from 16 elements. The errors noted are statistical.

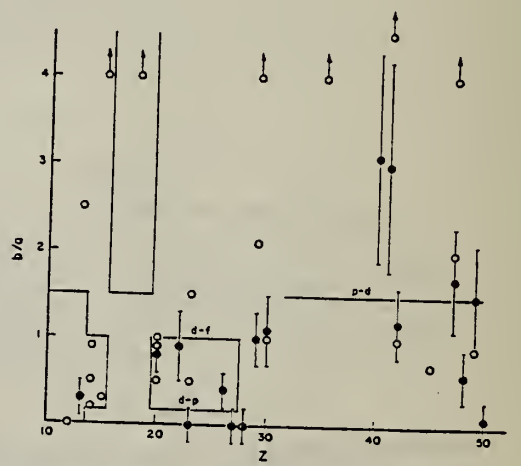

FIG. 4. The values of the fast photoproton anisotropy coefficient b/a found by the present authors (●) and other workers (○) in the region of the periodic table 10 < Z < 50. Arrows indicate off-scale points. The references to the results of other workers are given in Table II. The demarcations are explained in the text.

Ref. M.Odera, N. Yamamuro J.Phys.Soc.Japan 18, 325 (1963)	Elem. Sym.	A	Z
	Al	27	13
Method Synchrotron; foils; emulsions	Ref. No. 630d1		BG

Reaction	E or ΔE	E_o	Γ	$\int \sigma dE$	Jπ	Notes
(γ,p)	bremss. $E_{\gamma max}$ = 22 MeV			3.9 ± 10^5 protons/mole/roentgen		Angular distributions: 2 MeV $\leq E_p \leq$ 4 MeV $E_p \geq$ 6 MeV total Forward peak

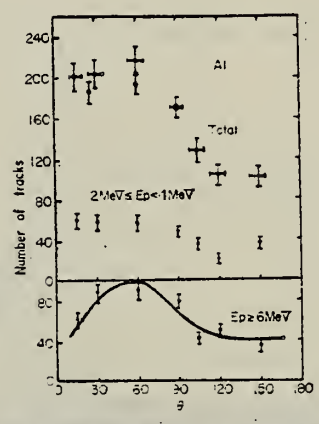

Fig. 2. Angular distribution of photo-protons from Al. Open circles are the results of Hoffman and Cameron.[7] Errors indicated are statistical ones. Solid curve drawn for $E_p \geq 6$ Mev is calculated from

$$I(\theta) = 1 + 0.64 \sin^{10}\theta(1 + 1.5 \cos\theta)^8$$

Ref. V. J. Vanhuyse, G. J. Vanpraet
Nuclear Phys. 45, 602 (1963)

Elem. Sym.	A	Z
Al	27	13

Method: Linac; photon scattering , self-absorption; NaI

Ref. No.: 63 Va 3 | JHH

Reaction	E or ΔE	E_o	Γ	$\int \sigma dE$	Jπ	Notes
$Al^{27}(\gamma,\gamma)$	Bremss. 2.85	2.21	gΓ= 1.8±0.4 eV			$\omega(\theta) = 1+(0.26\pm0.05)P_2(\cos\theta)$

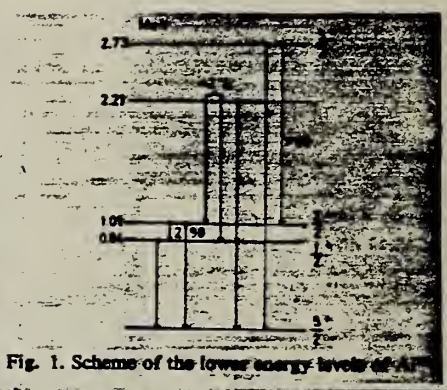

Fig. 1. Scheme of the lower energy levels of Al

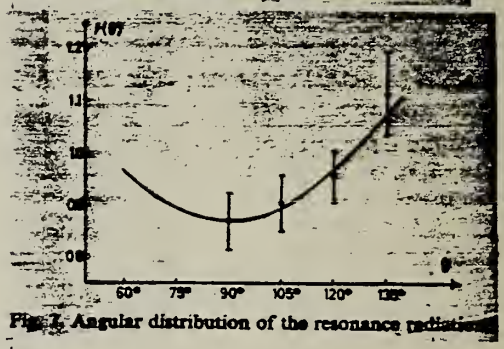

Fig. 2. Angular distribution of the resonance radiation

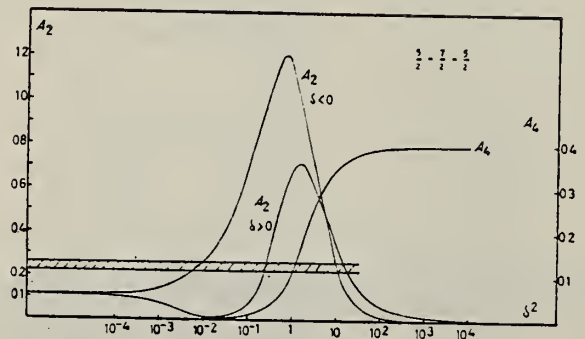

Fig. 4. Theoretical coefficients of the P_2-terms in the angular distribution function $W(\theta) = 1 - A_2 P_2$ (cos θ) for mixed dipole-quadrupole resonance radiation for the spin sequence $\frac{1}{2}-\frac{3}{2}-\frac{1}{2}$.

Ref. V.J. Vanhuyse, G.J. Vanpraet, K.J. Van Camp
Phys. Letters 5, 89 (1963)

Elem. Sym.	A	Z
Al	27	13

Method Linac; self-absorption method; NaI

Ref. No. 63 Va 4 JHH

Reaction	E or ΔE	E_o	Γ	$\int \sigma dE$	Jπ	Notes
$Al^{27}(\gamma,\gamma)$	Bremss. 3.65	2.2 2.98				$\theta_\gamma = 120^\circ$ Electron energy ±2%

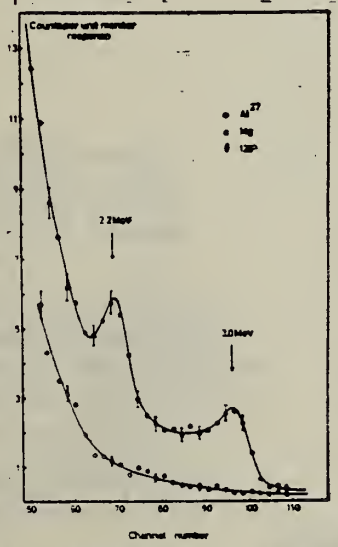

Fig. 1. Pulse-height distribution of photons scattered from an Al scatterer and from a Mg scatterer.

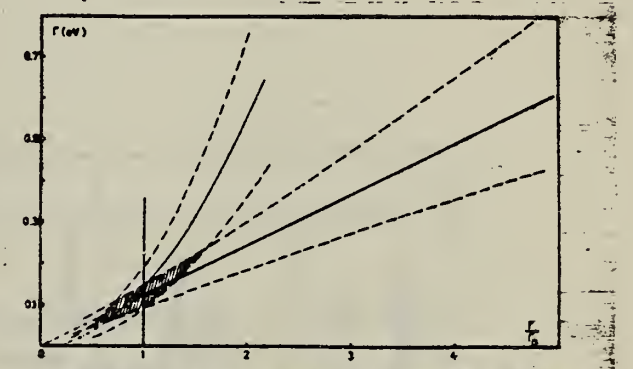

Fig. 2. The level width Γ plotted as a function of the ratio Γ/Γ_0; the dotted lines indicate the probable error band. The parabola results from the experiment of Booth and Wright.

1) E.C. Booth and K.A. Wright, Nuclear Phys. 35 (1962) 472.

REF.

A.K. Val'ter, E.G. Kopanets, A.N. L'vov, A. Stegner, S.P. Tsytko
Izv. Akad. Nauk SSSR 27, 1419 (1963)

ELEM. SYM.	A	Z
Al	27	13

METHOD Van de Graaff; inverse; NaI spectrometer

REF. NO. 63 Va 5 NVB

REACTION	RESULT	EXCITATION ENERGY	SOURCE TYPE	SOURCE RANGE	DETECTOR TYPE	DETECTOR RANGE	ANGLE
P,G	RLY	9-10	D	1-2	NAI-D		DST
				(1.8-2.0)			

SEP ISOTPS

Excitation Energy (MeV)	A*
9.995	- 0.38±0.05
10.087	+ 0.4±0.1
10.160	+ 0.26±0.003

$$^{*}\ A = \frac{W(0^{\circ}) - W(90^{\circ})}{W(90^{\circ})}$$

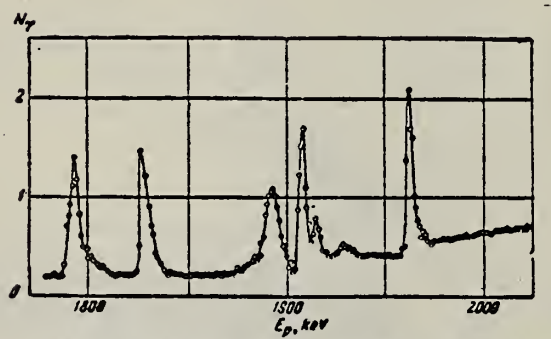

Рис. 1. Функция возбуждения в реакции $Mg^{26}(p, \gamma)\ Al^{27}$ в интервале энергий протонов от 1,78 до 2,0 MeV

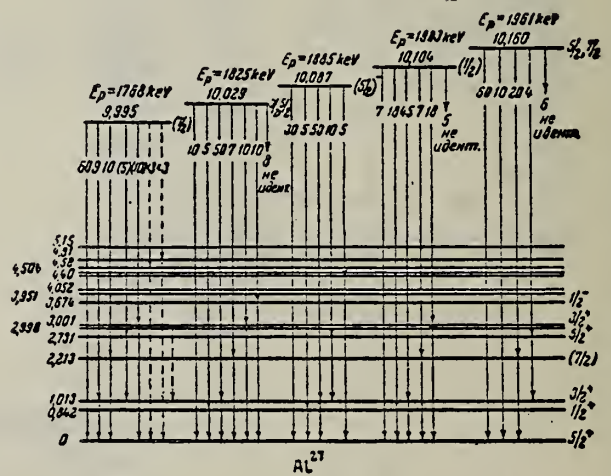

Рис. 7. Схема уровней и пороходов в Al^{27}

REF.

F.R. Allum, T.W. Quirk, and B.M. Spicer
Nucl. Phys. 53, 545 (1964)

ELEM. SYM.	A	Z
Al	27	13

METHOD

REF. NO. 64 Al 5 JOC

REACTION	RESULT	EXCITATION ENERGY	SOURCE		DETECTOR		ANGLE
			TYPE	RANGE	TYPE	RANGE	
G,XN	NØX	THR-34	C	34	THR-I	6-	DST

TABLE I

Summary of present experimental data at 34 MeV bremsstrahlung

Element		$-\frac{a_2}{a_0}$	$\frac{a_1}{a_0}$
$_{4}$Be		0.43±0.02	0.05±0.01
$_{6}$C		0.61±0.04	0.09±0.02
$_{13}$Al		0.39±0.03	0.05±0.01
$_{22}$Ti		0.34±0.02	0.06±0.01
$_{24}$Cr	34 MeV	0.33±0.02	0.02±0.01
	22 MeV	0.13±0.07	−0.02±0.03
$_{29}$Cu		0.36±0.02	0.10±0.01
$_{50}$Sn		0.38±0.02	0.11±0.01
$_{56}$Ba		0.39±0.03	0.11±0.02
$_{73}$Ta	Before installation of iron shielding	0.26±0.04	0.13±0.02
	After installation of iron shielding	0.27±0.02	0.12±0.01
$_{82}$Pb	target diameter 3.0 cm	0.39±0.03	0.15±0.02
	target diameter 1.5 cm	0.40±0.03	0.19±0.02
$_{83}$Bi		0.42±0.03	0.17±0.02

$$Y = a_0 + a_1 \cos\theta + a_2 \cos^2\theta$$

REF.
U. Amaldi, Jr., G. Campos Venuti, G. Cortellessa, C. Fronterotta, A. Reale, P. Salvadori, P. Hillman
Phys. Rev. Letters 13, 341 (1964)

ELEM. SYM.	A	Z
Al	27	13

METHOD
Synchrotron

REF. NO.
64 Am 1

REACTION	RESULT	EXCITATION ENERGY	SOURCE		DETECTOR		ANGLE
			TYPE	RANGE	TYPE	RANGE	
E,E/P	RLX	THR - 150	D	550	MAG-D		51

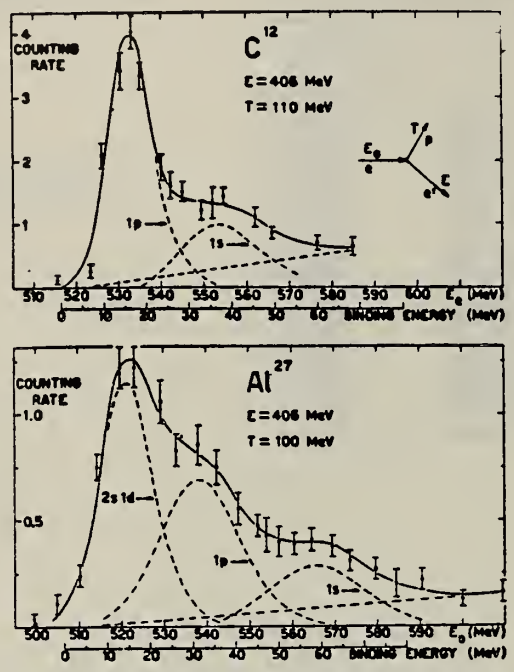

FIG. 2. Electron-proton coincidence counting rate per 10^{11} equivalent quanta at 550 MeV as a function of the incident energy. The dashed lines indicate the contributions of the various shells and the background as explained in the text.

REF. E.C. Booth, B. Chasan and K. A. Wright
Nucl. Phys. 57, 403-420 (1964)

ELEM. SYM.	A	Z
Al	27	13

METHOD
Van de Graaff; resonance fluorescence

REF. NO. 64 Bo 1

NVB

REACTION	RESULT	EXCITATION ENERGY	SOURCE		DETECTOR		ANGLE
			TYPE	RANGE	TYPE	RANGE	
G,G	LFT	1-3	C	1 - 3	NAI-D		100
		(0.5 - 3.0)		(0.5 - 3.0)			

ABI

TABLE 1
Cases of observed resonance fluorescence

Nucleus multipol.	State (MeV)	Spin	Γ_0/Γ	$T(g_W\Gamma_0^2/\Gamma^2)^{-1}$ (sec).	Mean lifetime T BCW (sec)	Mean lifetime T other (sec)	Ref.	Γ_0/Γ_W BCW
Al^{27}	0.00	$\frac{5}{2}^+$						
E1	2.21	$\frac{1}{2}^-$	0.98	absorption	$20\pm3\times10^{-15}$	$18.2\pm2.3\times10^{-15}$	10)	3.6×10^{-3}
				$41\pm13\times10^{-15}$	$27\pm9\times10^{-15}$			
M1	2.98	$\frac{3}{2}^{(+)}$	0.9	absorption	$7.6\pm1.4\times10^{-15}\Gamma_0/\Gamma$	$5.4\pm1.8\times10^{-15}\Gamma_0/\Gamma$	12)	0.16
				$8.5\pm3\times10^{-15}$	$5.7\pm2\times10^{-15}\Gamma_0/\Gamma$			

REF.

K.W. Chen, J.R. Dunning,Jr., J.R. Rees, W. Shlaer, J.K. Walker and R. Wilson
- Phys. Rev. 135, 4B B1030 (1964)

ELEM. SYM.	A	Z
Al	27	13

METHOD

REF. NO.: 64 Ch 1 JOC

REACTION	RESULT	EXCITATION ENERGY	SOURCE TYPE	SOURCE RANGE	DETECTOR TYPE	DETECTOR RANGE	ANGLE
E,P	ABX		D	4 BEV	MAG-D	110-450	DST

TABLE I. Cross sections for production of protons by electr...

Electron target	Energy angle (deg)	4 BeV proton energy (MeV)	$d^2\sigma/d\Omega dE$ 10^{-33} cm^2/sr Me...
H	59.8	374	3.8[a]
Li_6	59.8	448	0.082
Li_6	59.8	368	0.175
Li_6	59.8	332	0.280
C	59.8	374	0.425
Al	59.8	374	1.19
H	63.1	291	7.5[a]
Li_6	63.1	355	0.146
Li_6	63.1	319	0.204
Li_6	63.1	290	0.313
C	63.1	291	1.01
Al	63.1	291	2.42
H	67.1	208	16[a]
Li_6	67.1	226	0.6
Li_6	67.1	206	0.92
C	67.1	209	2.37
Al	67.1	209	6.4
H	72.1	124	46[a]
Li_6	72.1	166	1.20
Li_6	72.1	144	1.53
Li_6	72.1	124	2.46
Li_6	72.1	119	2.80
Li_6	72.1	109	2.90
C	72.1	123	6.6
Al	72.1	124	16.9
Cu	72.1	124	42.3
H	44.8	291	2.9[a]
Li^6	44.8	337	0.16
Li^6	44.8	293	0.29
C	44.8	291	0.76
Al	44.8	291	1.58
H	52.3	208	8.5[a]
Li^6	52.3	200	0.91
C	52.3	208	2.13
Al	52.3	208	4.95
H	61.1	124	25[a]
C	61.1	145	3.95
C	61.1	124	5.75
C	61.1	115	6.43
Al	61.1	145	10.7
Al	61.1	124	16.0

[a] $d\sigma/d\Omega$ in mb/sr; inside a 5.5% momentum interval.

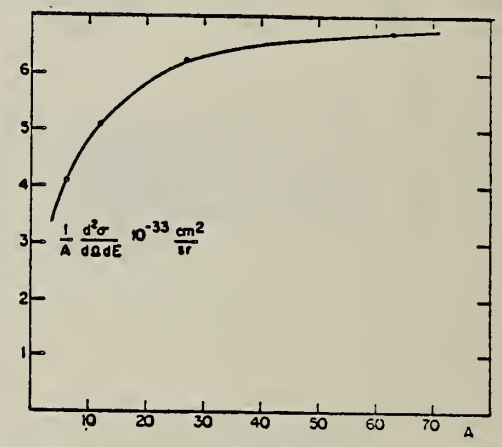

FIG. 4. Cross section, divided by A, as a function of A, for producing protons of 124 MeV from 4-BeV electrons at 72.1°.

REF.	ELEM. SYM.	A	Z
B. S. Dolbilkin, V. A. Zapevalov, V. I. Korin, L. E. Lazareva and F. A. Nikolaev Proc. Paris Conference 1060 (1964)	Al	27	13

METHOD	REF. NO.	
Synchrotron	64 Do 2	JDM

REACTION	RESULT	EXCITATION ENERGY	SOURCE		DETECTOR		ANGLE
			TYPE	RANGE	TYPE	RANGE	
G,MU-T	ABX	9-29	C	250	MGP-D	9-29	4PI

756

$$\int_{9}^{28.5} \sigma dE = 360 \pm 60 \text{ MeV.mb}$$

$h\nu_{max.}$ (MeV)	10.7	12.9	21.4	26.6
$\int \sigma.d(h\nu)$ (MeV·mb)	28	23	280	26

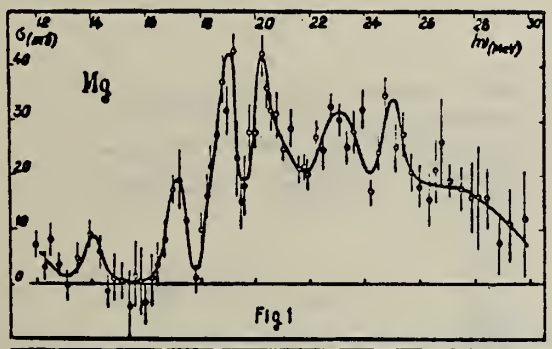

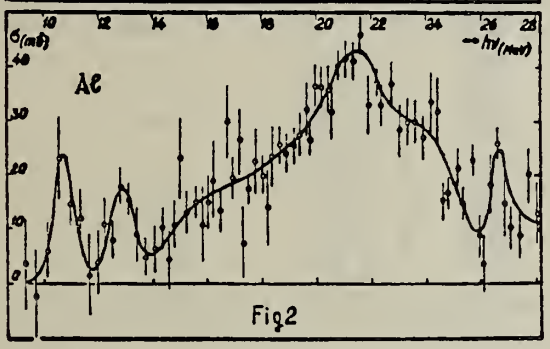

Fig. 1. — Nuclear γ-ray absorption cross-section of Mg(Mg^{24} — 78.6, Mg^{25} — 10.1, Mg^{26} — 11.3 per cent).
The cross sections for Mg in the above figure have to be raised by 2.5 mb.
Fig. 2. — Nuclear γ-rays absorption cross-section of Al^{27}.

REF.

M. Masuda, M. Kondo, S. Takeda, M. Okumura, and J. Ookuma
J. Phys. Soc. Japan 19, 2339 (1964)

ELEM. SYM.	A	Z
Al	27	13

METHOD

REF. NO. 64 Ma 2 — EGF

REACTION	RESULT	EXCITATION ENERGY	SOURCE		DETECTOR		ANGLE
			TYPE	RANGE	TYPE	RANGE	
G,XP	SPC	THR - 20	C	20	SCD-D	3 - 9	

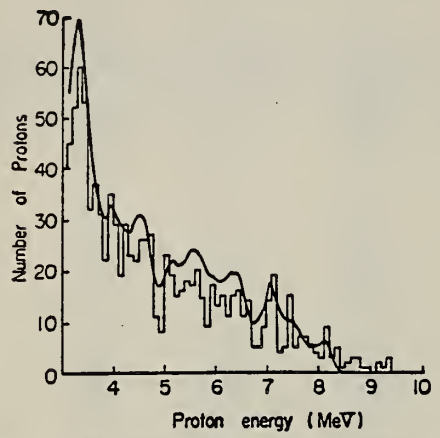

Fig. 1. Energy spectrum of emitted protons from aluminum foil irradiated by 20 MeV bremsstrahlung.

Table I. Resonance energies of excitation for Al(γ, p) in MeV.

Solid State Detector	Nuclear Emulsion[a]	CsI Scintillation[a]
11.8		
12.1		
12.5		12.4
		12.8
13.1	13.1	13.1
13.3		
13.6	13.5	13.6
14.0	13.9	14.0
14.2		
14.5	14.4	14.6
14.7	14.6	
15.0	14.9	
15.2	15.1	15.3
15.7	15.5	
	15.8	
16.0	16.1	
16.3	16.5	16.3
16.8	16.9	16.7
17.0		
17.3	17.3	17.3
17.8	17.9	17.8
18.4	18.2	18.3

REF. Akira Masaike
J. Phys. Soc. Japan 19, 427 (1964)

ELEM. SYM.	A	Z
Al	27	13

METHOD

REF. NO. 64 Ma 4 egf

REACTION	RESULT	EXCITATION ENERGY	SOURCE		DETECTOR		ANGLE
			TYPE	RANGE	TYPE	RANGE	
G,PI+	ABY	150-720	C	150-720	ACT-I		4PI
G,XXX	ABY	150-720	C	150-720	ACT-I		4PI
G,YYY	ABY	150-720	C	150-720	ACT-I		4PI

XXX=NA24 FINAL
YYY=F 18 FINAL

Table I.

	$Al^{27}(\gamma, \pi^+)Mg^{27}$	$Al^{27} \rightarrow Na^{24}$	$Al^{27} \rightarrow F^{18}$	$C^{12} \rightarrow C^{11}$
Integrated Cross Section (200 MeV~400 MeV)	2.2×10^{-26} cm²·MeV	6.2×10^{-26} cm²·MeV	2.4×10^{-26} cm²·MeV	2.0×10^{-25} cm²·MeV

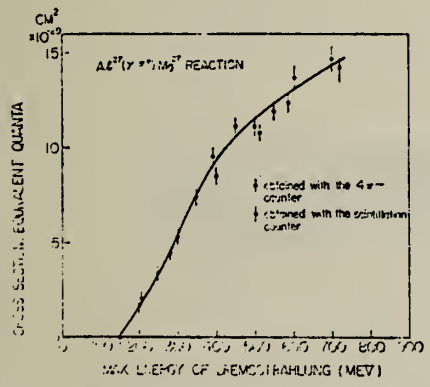

Fig. 4. The yield curve per equivalent quanta for the reaction $Al^{27}(\gamma, \pi^+)Mg^{27}$.

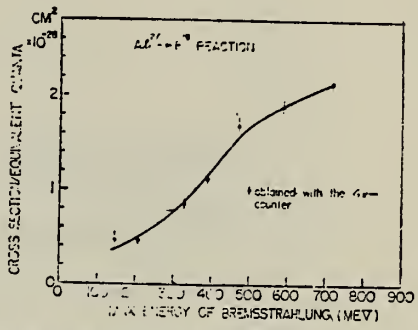

Fig. 6. The yield curve per equivalent quanta for the reaction $Al^{27} \rightarrow F^{18}$.

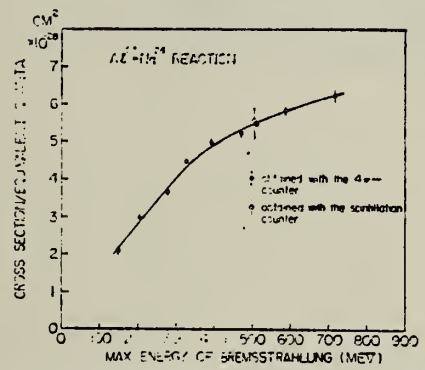

Fig. 5. The yield curve per equivalent quanta for the reaction $Al^{27} \rightarrow Na^{24}$.

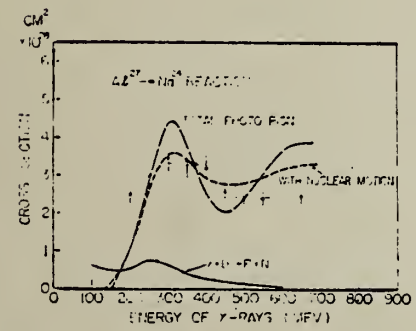

Fig. 9. The excitation curve for the reaction $Al^{27} \rightarrow Na^{24}$ calculated by the photon difference method. The long dashed line shows the total cross section per nucleon for photo-pion production from a nucleon and the solid line shows the cross section for the photo-disintegration of deuteron. The short dashed line shows the effect of nuclear motion in the nucleus.

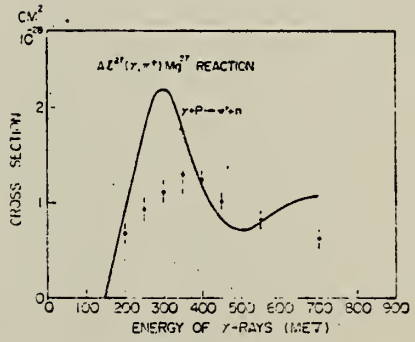

Fig. 10. The excitation curve for the reaction $Al^{27}(\gamma, \pi^+)Mg^{27}$ calculated by the photon difference method. The solid line shows the cross section for the positive pion photo-production from proton.

REF.	ELEM. SYM.	A	Z
F. R. Metzger Proc. Paris Conference 392 (1964)	Al	27	13

METHOD	REF. NO.	
Resonance Scattering $^{15}N(p,\alpha\gamma)^{12}C$	64 Me 2	JDM

REACTION	RESULT	EXCITATION ENERGY	SOURCE		DETECTOR		ANGLE
			TYPE	RANGE	TYPE	RANGE	
G,G	LFT	4	D	4	NAI-D	4	DST

The 4.403 MeV state in ^{27}Al has spin 5/2 and $\Gamma_o = (0.24 \pm 0.03)$eV.

REF.

G. Tessler, W.E. Stephens
Phys. Rev. 135, B129-36 (1964)

ELEM. SYM.	A	Z
Al	27	13

METHOD

Tandem, $T^3(p,\gamma)$

REF. NO. 64 Te 1 NVB

REACTION	RESULT	EXCITATION ENERGY	SOURCE		DETECTOR		ANGLE
			TYPE	RANGE	TYPE	RANGE	
G,MU-T	ABX	20-21	D	20-21	NAI-I		96

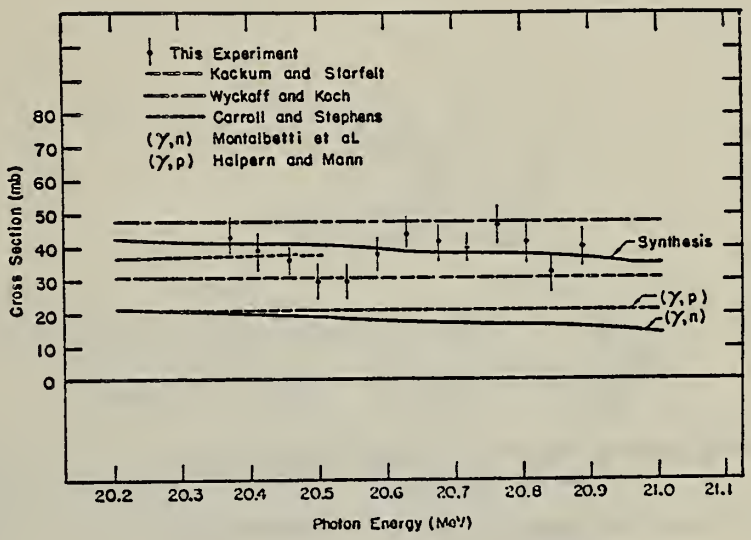

FIG. 11. Nuclear absorption cross section in Al^{27} as a function of photon energy. The results of this experiment are plotted as dots. Other results are shown for comparison.

REF. M. N. Thompson, J. M. Taylor and B.M. Spicer
Proc. Paris Conference 1008 (1964)

ELEM. SYM.	A	Z
Al	27	13

METHOD

REF. NO.	
64 Th 1	JDM

REACTION	RESULT	EXCITATION ENERGY	SOURCE		DETECTOR		ANGLE
			TYPE	RANGE	TYPE	RANGE	
G,N	ABX	15-24	C	15-24	ACT-I		4PI

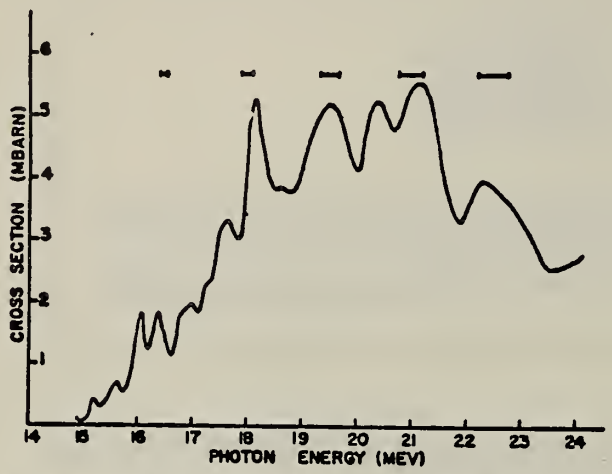

FIG. 1. — Least structure analysis of yield data, in 100 keV intervals from 12.5 MeV upward.

REF.

A.K. Val'ter, E.G. Kopanets, A.N. L'vov, S.P. Tsytko
Izv. Akad. Nauk.SSSR, Ser.Fiz., 28, 271 (1964)

ELEM. SYM.	A	Z
Al	27	13

METHOD

- Van de Graaff; $Mg^{26}(p,\gamma)Al^{27}$ [Page 1 of 2 pages]

REF. NO. 64 Va 1 NVB

REACTION	RESULT	EXCITATION ENERGY	SOURCE TYPE	SOURCE RANGE	DETECTOR TYPE	DETECTOR RANGE	ANGLE
P,G	NØX	10-11	D	2-3	NAI-D		DST
				(2.0-2.3)			

J-PI

Asymmetry
in
Angular
Distribution

Таблица 2

Результаты анализа γ-спектров для различных резонансов

№ п/п	E_p, keV	E_γ, MeV	Предполагаемый γ-переход между уровнями ядра Al^{27}	Расчетная энергия γ-перехода, MeV	Асимметрия в угловом распределении γ-лучей, $A_{эксп}$	Относительная интенсивность γ-лучей
1	2015	9,4±0,1	10,212→0,842	9,370	0,0±0,1	—
		0,84±0,03	0,842→0	0,842	0,0±0,05	
2	2047	10,2±0,1	10,243→0	10,243	—	0,15
		9,3±0,1	10,243→0,842	9,401	0,30±0,07	1,0
		9,3±0,1	10,243→1,013	9,230		
		1,01±0,03	1,013→0	1,013	—0,10±0,7	1,0
		0,84±0,03	0,842→0	0,842	0,00±0,05	0,5
3	2148	9,4±0,1	10,341→0,842	9,499	0,30±0,05	—
		9,4±0,1	10,341→1,013	9,328		
		1,01±0,03	1,013→0	1,013	0,1±0,1	1,0
		0,84±0,03	0,842→0	0,842	—	0,15
4	2183	10,4±0,1	10,3,4→0	10,374	—	0,1
		9,5±0,1	10,374→0,842	9,532	—	1,0
		9,5±0,1	10,374→1,013	9,361	—	
		1,01±0,03	1,013→0	1,013	—0,10±0,07	1,0
		0,84±0,03	0,842→0	0,842	—	0,3
5	2185	10,4±0,1	10,376→0	10,376	—	0,2
		9,5±0,1	10,376→0,842	9,534	—0,3±0,1	1,0
		9,5±0,1	10,376→1,013	9,363		
		1,01±0,03	1,013→0	1,013	—1,0±0,1	1,0
		0,84±0,03	0,842→0	0,842	0,00±0,05	4,0
6	2221	9,4±0,1	10,411→1,013	9,398	—	—
		1,01±0,03	1,013→0	1,013	—	—

REF.

A.K. Val'ter, E.G. Kopanets, A.N. L'vov, S.P. Tsytko
Izv. Akad. Nauk.SSSR, Ser.Fiz., 28, 271 (1964)

ELEM. SYM.	A	Z
Al	27	13

METHOD

• Van de Graaff; $Mg^{26}(p,\gamma)Al^{27}$

[Page 2 of 2 pages]

REF. NO. 64 Va 1 NVB

REACTION	RESULT	EXCITATION ENERGY	SOURCE		DETECTOR		ANGLE
			TYPE	RANGE	TYPE	RANGE	

Level	Proposed J^{π}
10.212 MeV	1/2
10.243	3/2 or 5/2
10.374	3/2 or 5/2
10.376	3/2 or 5/2

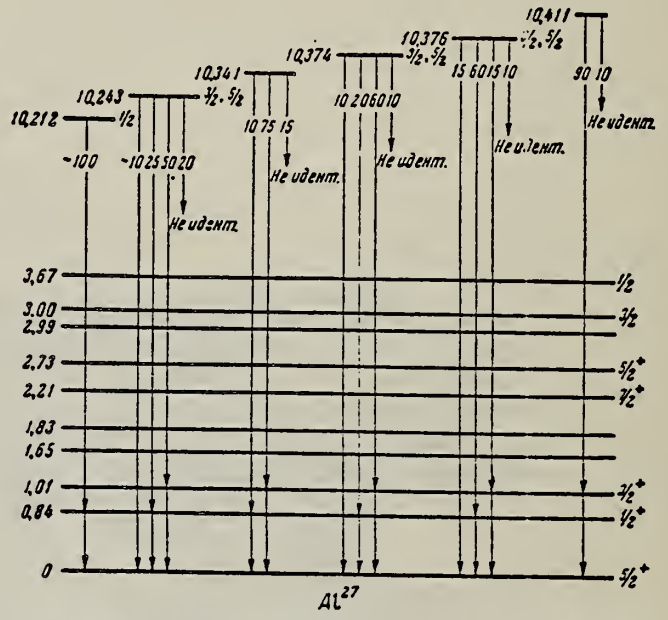

Рис. 3. Схема распада резонансных состояний ядра Al^{27}. Цифры в разрывах стрелок указывают относительные интенсивности γ-переходов

REF.

A.K. Val'ter, E.G. Kopanets, A.N. L'vov, S.P. Tsytko
Izv. Akad. Nauk.SSSR, Ser.Fiz., 28, 268 (1964)

ELEM. SYM.	A	Z
Al	27	13

METHOD

$Mg^{26}(p,\gamma)Al^{27}$

REF. NO. 64 Va 2 NVB

REACTION	RESULT	EXCITATION ENERGY	SOURCE TYPE	SOURCE RANGE	DETECTOR TYPE	DETECTOR RANGE	ANGLE
P,G	NØX	10	D	2	NAI-D		

J-PI

level	Proposed J^{π}
2.2 MeV	$7/2^+$
1.65	< 7/2, perhaps 1/2
1.83	< 7/2, perhaps 3/2

Possibly these levels form a new bond with k = 1/2.

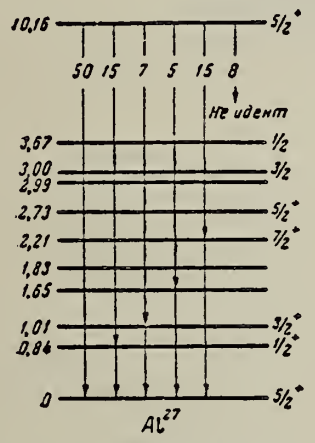

Рис. 3. Схема распада резонансного состояния 10,16 MeV ядра Al^{27}. Цифры в разрывах стрелок указывают относительные интенсивности γ-переходов

REF.

F. I. Havliček and M. Modesto
Energ. Nucl. 12, 77 (1965)

ELEM. SYM.	A	Z
Al	27	13

METHOD

REF. NO.	
65 Ha 2	JOC

REACTION	RESULT	EXCITATION ENERGY	SOURCE		DETECTOR		ANGLE
			TYPE	RANGE	TYPE	RANGE	
G,A	SPC	THR-31	C	31	EMU-D	5-20	4PI

Exp. cut off at 4 MeV.

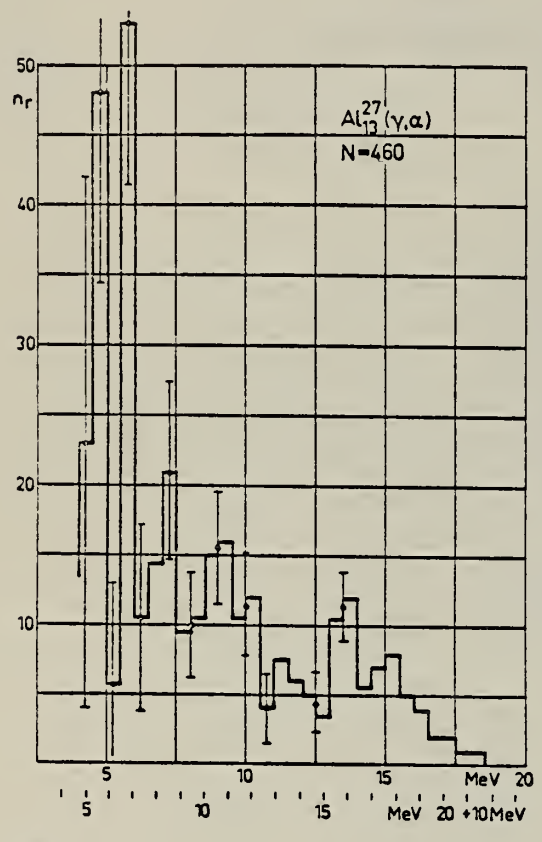

Fig. 3.

N. A. Khan, V. K. Rasmussen
Phys. Rev. 138, B1385 (1965)

Al	27	13

METHOD

Van de Graaff; $Al^{27}(p,p')Al^{27*}(2.98)$ source

REF. NO. 65 Kh 1 NVB

REACTION	RESULT	EXCITATION ENERGY	SOURCE TYPE	SOURCE RANGE	DETECTOR TYPE	DETECTOR RANGE	ANGLE
G,G	LFT	2, 3	D	2,3	NAI-D		DST
		(2.21, 2.98)	(2.21, 2.98)				

2.98 MeV level:

mean life $\tau = (6.6 \pm 0.7) \times 10^{-15}$ sec.
angular distribution $W(\theta) = 1 + (0.06 \pm 0.04)P_2(\cos\theta)$
E2/M1 mixing ratio δ: $-0.36 < \delta < +0.20$

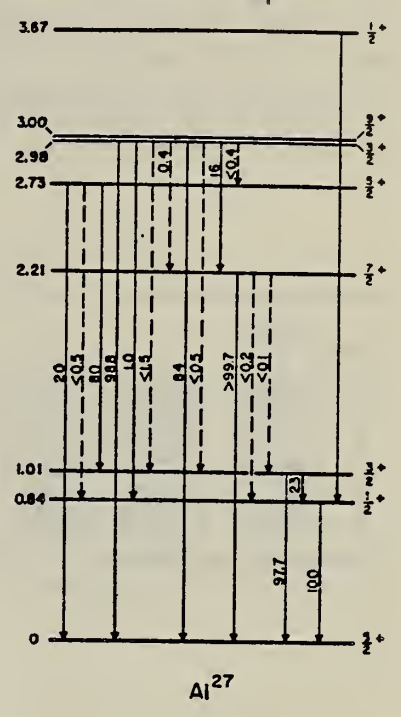

FIG. 1. Decay scheme of the low-lying levels of Al^{27}. The spin assignments and branching ratios up to 2.73 MeV are from Ophel and Lawergren, Ref. 11. For the 2.98- and 3.00-MeV levels they are from Lawergren, Ref. 5. The mode of decay of the 3.68-MeV level shown has been reported only in Ref. 3.

2.21 MeV level:

At $E_p = 5.00$ MeV, $W(\theta) = 1 + (0.37 \pm 0.02)P_2(\cos\theta)$

At $E_p = 4.155$ MeV, $W(\theta) = 1 + (0.21 \pm 0.04)P_2(\cos\theta)$

Difference may be due to a partial linear polarization of the x-ray source.

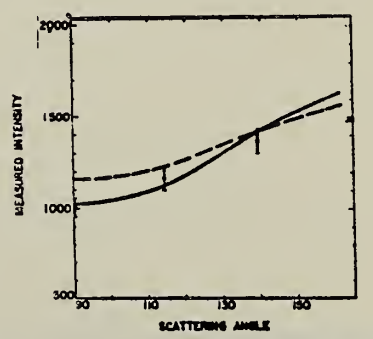

FIG. 6. The angular distribution for resonant scattering of 2.21-MeV radiation at $E_p = 5.00$ MeV. The solid curve is the function $W(\theta) = 1 + 0.37\ P_2(\cos\theta)$, the least-squares fit to the experimental points. This is indistinguishable from $W(\theta) = 1 + 0.23\ P_2(\cos\theta) - 0.053 P_2^3(\cos\theta)$, which includes a polarization term. The broken curve is the distribution $W(\theta) = 1 + 0.23 P_2(\cos\theta)$ obtained at $E_p = 4.115$ MeV by Metzger *et al.* (Ref. 8) and in the present work. The normalization of the two curves at 140° is arbitrary.

REF.

B. MacDonald, J. A. Diaz, S. N. Kaplan, and R. V. Pyle
Phys. Rev. 139, B1253 (1965)

ELEM. SYM.	A	Z
Al	27	13

METHOD

Cyclotron; μ^- capture

REF. NO.: 65 Ma 2 | NVB

REACTION	RESULT	EXCITATION ENERGY	SOURCE TYPE	SOURCE RANGE	DETECTOR TYPE	DETECTOR RANGE	ANGLE
MU-,XN	NØX	10 - 20	D	0	SCI-I		4PI
		[DO NOT PUT IN DATA INDEX]					

Tries to fit data with Fermi gas and Gaussian momentum distributions.

NEUT MULTIPLICITY

TABLE IV. Corrected experimental results.

Target	Average multiplicity, ⟨n⟩	Multiplicity distribution (adjusted to 0.543 efficiency) F_0	F_1	F_2	F_3	F_4	F_5	F_6	F_7
Al	1.262±0.059	0.449±0.027	0.464±0.028	0.052±0.013	0.036±0.007	−0.0023±0.004	−0.001 ±0.004	0.003 ±0.004	
Si	0.864±0.072	0.611±0.042	0.338±0.042	0.045±0.018	−0.002±0.008	0.003 ±0.005	0.002 ±0.003	0.003 ±0.006	
Ca	0.746±0.032	0.633±0.021	0.335±0.022	0.025±0.009	0.004±0.006	0.003 ±0.003			
Fe	1.125±0.041	0.495±0.018	0.416±0.019	0.074±0.011	0.014±0.005	−0.0001±0.003	0.002 ±0.003		
Ag	1.615±0.060	0.360±0.031	0.456±0.023	0.144±0.017	0.031±0.009	0.007 ±0.005	0.002 ±0.004	0.001 ±0.003	
I	1.436±0.056	0.396±0.021	0.474±0.023	0.087±0.018	0.033±0.009	0.007 ±0.005	0.0002±0.004		
Au	1.662±0.044	0.370±0.015	0.425±0.016	0.156±0.012	0.032±0.006	0.014 ±0.004	0.003 ±0.003	0.0003±0.003	
Pb	1.709±0.066	0.324±0.022	0.483±0.025	0.137±0.018	0.045±0.010	0.011 ±0.006			
Ag[a]	1.60 ±0.18	0.389±0.100	0.455±0.075	0.120±0.035	0.030±0.015	0.001 ±0.003	0.009 ±0.006	0.000 ±0.007	0.010±0.007
Pb[a]	1.64 ±0.16	0.348±0.100	0.479±0.057	0.137±0.027	0.018±0.012	0.010 ±0.003	0.003 ±0.004	0.003 ±0.002	0.002±0.002

[a] Results of Kaplan, Moyer, and Pyle (Ref. 1).

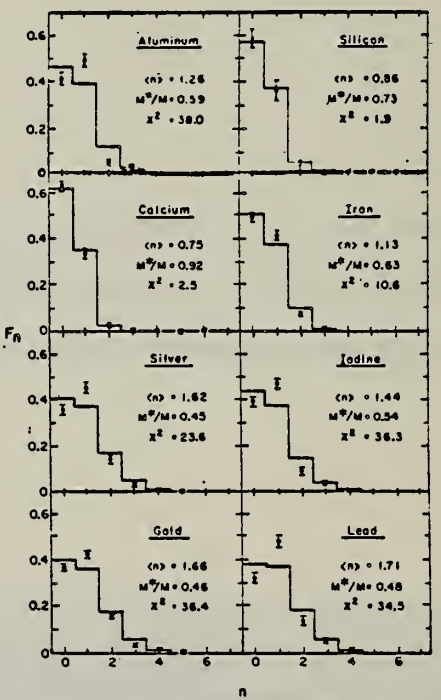

FIG. 11. Comparison of the observed neutron multiplicities with histograms calculated by using the Gaussian momentum distribution, $\alpha^2/2M = 20$ MeV.

REF.

F. R. Metzger
Phys. Rev. 139, B1464 (1965)

DECOM. SYM.		
A1	27	13

METHOD

$N^{;5}(p,\alpha)C^*$ source

REF. NO. 65 Me 3 NVB

REACTION	RESULT	EXCITATION ENERGY	SOURCE		DETECTOR		ANGLE
			TYPE	RANGE	TYPE	RANGE	
G,G	LFT	4	D	4	NAI-D		DST
		(4.403)		(4.403)			

J

Mean life $\tau = 1.57 \times 10^{-15}$ sec., using J = 5/2.

(width $\Gamma = (0.42 \pm 0.06)$ eV

Angular distribution $W(\theta) = 1 + (0.30 \pm 0.05)\ P_2(\cos\theta) + A_4 P_4(\cos\theta)$, $A_4 < 0.07$.

J = 5/2 ±, or 7/2 +, probably 5/2 ±.

REF.

M.N. Thompson, J.M. Taylor, B.M. Spicer and J.E.E. Baglin
Nuclear Phys. 64, 486 (1965)

ELEM. SYM.	A	Z
Al	27	13

METHOD

Betatron; NBS chamber monitor

REF. NO. [Page 1 of 2] 65 Th 2 EGF

REACTION	RESULT	EXCITATION ENERGY	SOURCE		DETECTOR		ANGLE
			TYPE	RANGE	TYPE	RANGE	
G,N	ABX	13 - 24	C	13-25	ACT-I		4PI

THRESHOLD 76

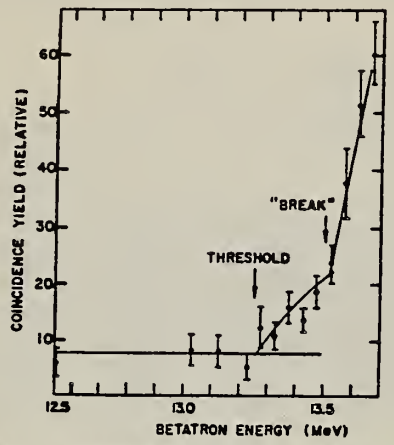

Fig. 1. The threshold for the $Al^{27}(\gamma, n)Al^{26m}$ reaction.

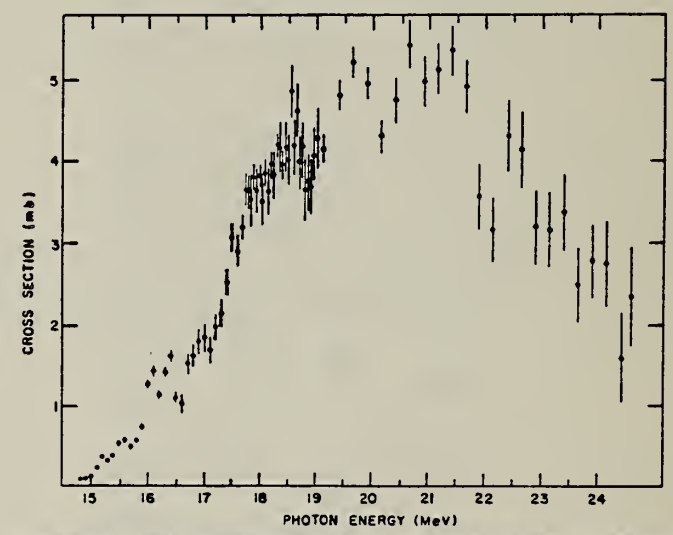

Fig. 2. Cross section points calculated from the yield data using the method of Penfold and Leiss, as described in the text.

REACTION	RESULT	EXCITATION ENERGY	SOURCE TYPE	SOURCE RANGE	DETECTOR TYPE	DETECTOR RANGE	ANGLE

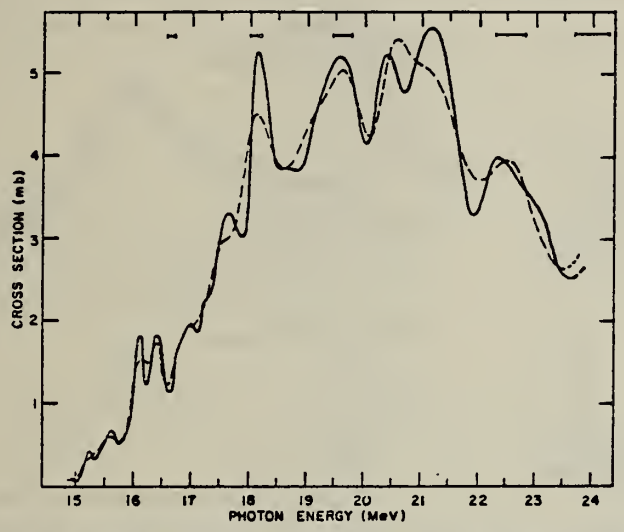

Fig. 3. The cross section, as given by the least-structure analysis of the yield data, in 100 keV intervals from 12.5 MeV upward, and, on the second curve, from 12.55 MeV upward. The width of the resolution function is indicated at a number of energies along the top of the figure.

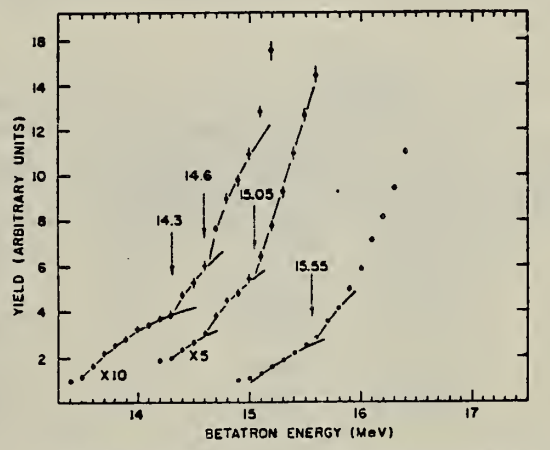

Fig. 4. The yield of coincidence counts plotted as a function of betatron energy, showing "breaks" at the energies indicated.

REF. A. K. Val'ter, E. G. Kopanets and S. P. Tsytko
Izv. Akad. Nauk. SSSR Ser. Fiz. 29, 803 (1965)
Bull. Acad. Sci. USSR (Phys. Sci.) 29, 806 (1965)

ELEM. SYM.	A	Z
Al	27	13

METHOD

REF. NO. 65 Va 5 JDM

REACTION	RESULT	EXCITATION ENERGY	SOURCE		DETECTOR		ANGLE
			TYPE	RANGE	TYPE	RANGE	
P,G	SPC	10	D	2	NAI-D	1 - 10	DST

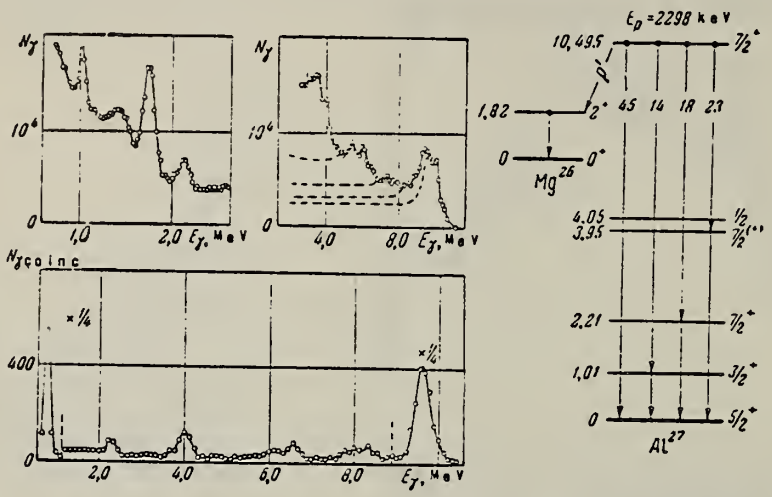

Fig.1. Gamma-ray spectra recorded by means of the one-crystal and two-crystal spectrometers and decay scheme for the 10.495 MeV state of Al^{27}. Above - the soft (for $\theta = 0^\circ$) and the hard (for $\theta = 90^\circ$) parts of the spectra measured by means of the one-crystal γ spectrometer. Below - γ-ray spectrum measured by means of the two-crystal summing spectrometer (coincidence spectrum).

Results of analysis of the spectra

E_γ, MeV	Assumed transition in the Al^{27} diagram	Calculated transition energy, MeV	Asymmetry in angular distrib., A_{exp}	Relative γ-ray intensity
10,50±0,07	10,495→0	10,495	−0,42±0,07	1,00
9,50±0,07	10,495→1,013	9,482	—	0,30
8,35±0,07	10,495→2,213	8,282	—	0,35
6,55±0,07	10,495→3,951	6,544	−0,12±0,07	0,50
4,00±0,07	3,951→0	3,951	0,84±0,07	0,50
2,21±0,03	2,213→0	2,213	0,87±0,15	0,25
1,82±0,03	—	—	0,55±0,15	1,00
1,01±0,03	1,013→0	1,013	0,42±0,15	0,20

REF.

J.M. Wyckoff, B. Ziegler, H.W. Koch, and R. Uhlig
Phys. Rev. 137, B576-94 (1965)

A1	27	13

METHOD

Synchrotron; ion chamber monitor

REF. NO. 65 Wy 1 NVB

REACTION	RESULT	EXCITATION ENERGY	SOURCE TYPE	SOURCE RANGE	DETECTOR TYPE	DETECTOR RANGE	ANGLE
G,MU-T	ABX	10-70	C	90	SCI-D		4PI

454

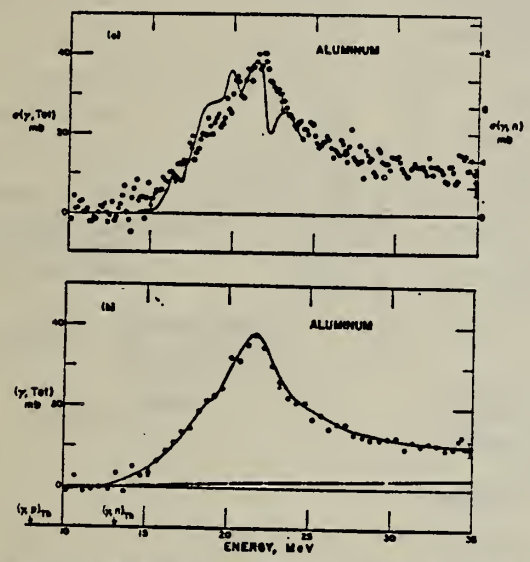

FIG. 15. Aluminum total photonuclear cross section. The solid line on (a) represents the $\sigma(\gamma,n)$ data of Spicer (Ref. 28) shifted up in energy by 250 keV using the right-hand ordinate scale.

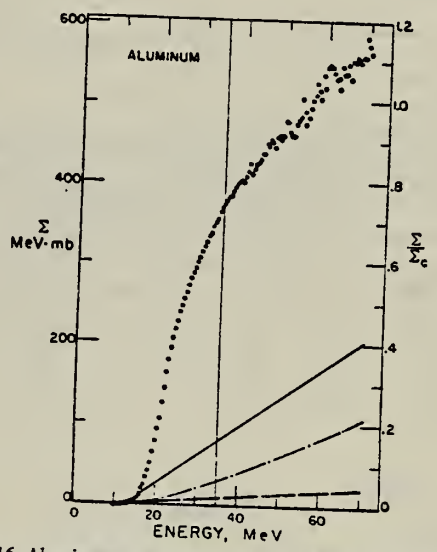

FIG. 16. Aluminum total photonuclear cross section integrated over energy. The solid line represents the baseline uncertainty due to statistical considerations. The dashed line represents the correction actually applied to normalize the photonuclear cross section to zero at 12.5 MeV. The dot-dashed line is the corrected baseline resulting from introduction of radiative corrections.

REF. G. Bishop, S. Costa, S. Ferroni, R. Malvano and G. Ricco
Nuovo Cimento, 42B, 158 (1966)

ELEM. SYM.	A	Z
Al	27	13

METHOD

Linac; S.E.M. Monitor; NBS Ionization Chamber

REF. NO.	
66 Bi 1	JDM

REACTION	RESULT	EXCITATION ENERGY	SOURCE TYPE	SOURCE RANGE	DETECTOR TYPE	DETECTOR RANGE	ANGLE
G,N	ABX	20 - 200	C	20 - 200	BF3-I		4PI

TABLE I. – *In this Table are given the cross-sections measured in millibarn averaged over the energy ranges indicated in column* 1. The contributions from the internal (*I*) and external (*E*) counters add together to give the total (*T*) cross-section.

		^{12}C	^{27}Al	S
Thres. ÷ 40 MeV	*T*	3.66	10.15	7.15
	E	0.38	0.80	0.70
	I	3.28	9.35	6.45
(40 ÷ 80) MeV	*T*	2.52	7.80	6.78
	E	0.94	1.35	1.48
	I	1.58	6.45	5.30
(80 ÷ 120) MeV	*T*	2.55	7.70	6.12
	E	1.13	1.87	2.37
	I	1.42	5.83	3.73
(120 ÷ 160) MeV	*T*	2.80	9.18	6.58
	E	1.36	3.00	3.66
	I	1.44	6.18	2.92
(160 ÷ 200) MeV	*T*	3.18	13.40	12
	E	1.48	5.25	3.60
	I	1.70	8.15	8.6

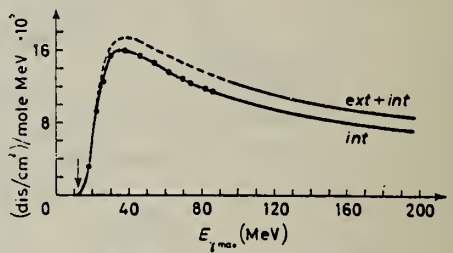

Fig. 4. – Aluminium yield.

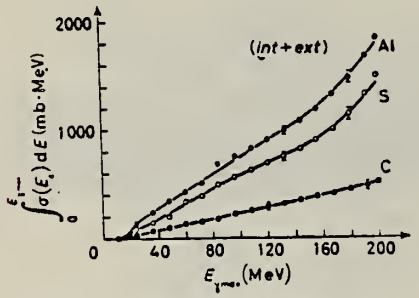

Fig. 9. – Total neutron integral cross-sections.

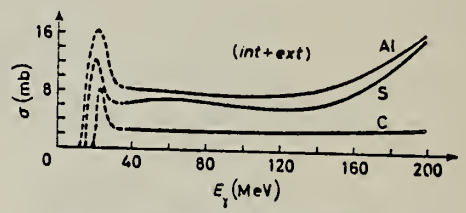

Fig. 10. – Total neutron differential cross-sections.

REF. G. Bishop, S. Costa, S. Ferroni, R. Malvano and G. Ricco
Nuovo Cimento, 42B, 158 (1966)

ELEM. SYM.	A	Z
Al	27	13

METHOD

Linac; S.E.M. Monitor; NBS Ionization Chamber [Page 2 of 2]

REF. NO. 66 Bi 1 JDM

DETECTOR TYPE	DETECTOR RANGE	ANGLE

TABLE II. – *In this table the data from Table I are treated, as discussed in the text to give cross-sections corresponding to photoneutrons in the approximate energy ranges* (0÷15) MeV *and above* 15 MeV. Thus the result *a*) corresponds to the relation $a = I - 0.4E$, and *b*) corresponds to $b = 1.4 \cdot E$.

		^{12}C	^{27}Al	S
Thres.÷ 40 MeV	*a*)	3.13	9.03	6.17
	b)	0.53	1.12	0.98
(40÷ 80) MeV	*a*)	1.20	5.91	4.71
	b)	1.32	1.89	2.07
(80÷120) MeV	*a*)	0.97	5.08	3.35
	b)	1.58	2.62	3.35
(120÷160) MeV	*a*)	0.90	4.98	1.46
	b)	1.90	4.20	5.12
(160÷200) MeV	*a*)	1.11	6.05	6.95
	b)	2.07	7.35	5.05

a) $= I - 0.4E$. I = int. counter.
b) $= E \cdot 1.4$, E = ext. counter.

TABLE IV. – *The total absorption cross-section for γ-rays is calculated by dividing the total neutron production cross-section by the neutron multiplicity.* The result is given in the first column under each element and, for comparison, in the second column the value of *b* is inserted from Table II.

	^{12}C		^{27}Al		S	
(40÷ 80) MeV	2.2	1.3	6.0	1.9	5.2	2.1
(80÷120) MeV	1.8	1.6	4.7	2.6	3.7	3.4
(120÷160) MeV	1.8	1.9	4.6	4.2	3.4	5.1
(160÷200) MeV	1.7	2.1	5.7	7.4	5.1	5.1

TABLE V.

E	$\sigma(Al)/\sigma(C)$	NZ/A
40	3.1	
70	2.75	
100	2.52	2.25
130	2.64	
160	3.15	

TABLE VI.

	σ_{interp} [14] 0÷35	σ_{interp} 35÷140	σ_{interp}	σ_{int} [16]	σ_{int} (B.L.)
1	2	3	4	5	6
C	144	220	364 ± 40	373	252
Al	344	590	934 ± 100	840	567
S	466	382	848 ± 90	990	670

REF.		ELEM. SYM.	A	Z
	F. W. K. Firk Proc. Gatlinburg Conference 352 (1966)	Al	27	13
METHOD		REF. NO.		
		66 Fi 2		hmg

REACTION	RESULT	EXCITATION ENERGY	SOURCE		DETECTOR		ANGLE
			TYPE	RANGE	TYPE	RANGE	
G,XN	SPC	THR-65	C	65	TOF-D	5-40	90

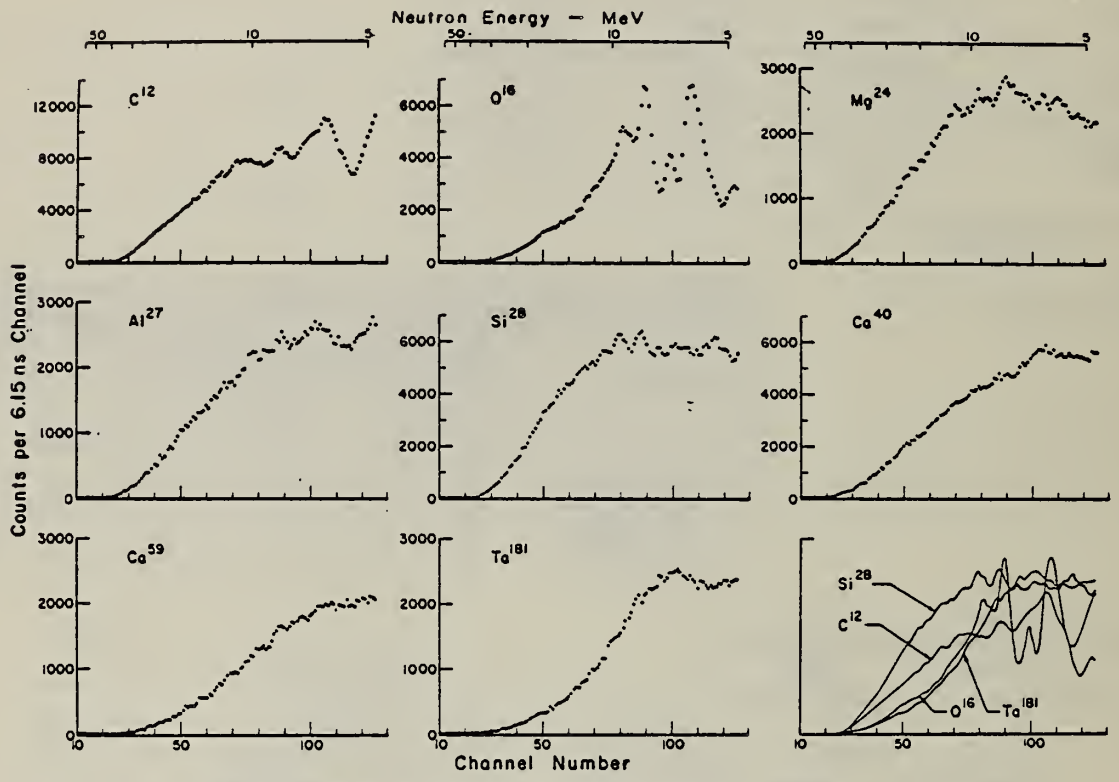

Fig. 1. Observed photoneutron time-of-flight spectra of C, O, Mg, Si, Ca, Co, V, and Ta.

REF.

S.C. Fultz, J.T. Caldwell, B.L. Berman, R.L. Bramblett, and R.R. Harvey
Phys. Rev. 143, B790 (1966)

ELEM. SYM.	A	Z
Al	27	13

METHOD

Nearly monochromatic x-rays from positron annihilation

REF. NO. 66 Fu 1 JDM

REACTION	RESULT	EXCITATION ENERGY	SOURCE		DETECTOR		ANGLE
			TYPE	RANGE	TYPE	RANGE	
G,N	ABX	13 - 37	D	13 - 37	BF3-I		4PI
G,2N	ABX	25 - 37	D	25 - 37	BF3-I		4PI

^{27}Al emits neutrons mostly by direct interactions.

115+
116

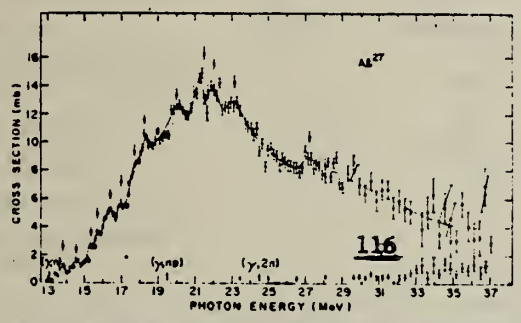

FIG. 5. Photoneutron-cross-section data for aluminum. The upper data and curve represent the photoneutron yield cross section $[\sigma(\gamma,n)+\sigma(\gamma,np)+2\sigma(\gamma,2n)]$ for Al^{27}. The lower data and curve represent the cross section for the reaction $Al^{27}(\gamma,2n)Al^{25}$.

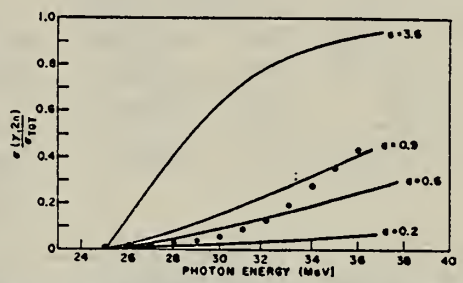

FIG. 6. Data points are values of $\sigma(\gamma,2n)/\sigma_{tot}$ for Al^{27} (where σ_{tot} denotes the total cross section for photon absorption) at various incident photon energies. The curves are calculated values for this ratio corresponding to values of the level-density parameter a=3.6 (top curve), 0.9, 0.6, and 0.2 MeV^{-1} (bottom curve).

(G,N) #115
(G,2N) #116
(G,SN) #516
(G,N+NP) #517

TABLE IV. Energy levels observed in Al^{27} (MeV).

Present work $(\gamma,n)+(\gamma,np)$	Thompson *et al.* (γ,n)	Bolen and Whitehead $(\gamma,n)+(\gamma,np)$	Masuda *et al.* (γ,p)	Theory[a]
13.8			13.6	
	14.2		14.0, 14.2	
14.5	14.5	14.6	14.5, 14.7	14.3
15.4	15.2		15.0, 15.2	15.5
15.7	15.6		15.7	15.7
	16.1		16.0	
16.4	16.4	16.4	16.3, 16.8	16.4, 16.6
17.0	17.0		17.0, 17.3	17.0, 17.2
17.7	17.6		17.8	
18.2	18.1	18.1	18.4	18.1, 18.3, 18.4
	19.6			19.4, 19.6, 19.7
20.0	20.5	19.8		20.0, 20.1, 20.2
21.5	21.2	21.4		21.0
22.0	22.4			
23.1				
27.2				

[a] All theoretical values are given in Ref. 29.

[29] M.N. Thompson, J.M. Taylor, B.M. Spicer, and J.E.E. Baglin, Nucl.Phys. 64, 486 (1965).

REF.

J.H. Hough and W.L. Mouton
Nucl. Phys. 76, 248 (1966)

ELEM. SYM.	A	Z
Al	27	13

METHOD

1.4 MeV Linac; self-absorption

REF. NO. 66 Ho 2 JDM

REACTION	RESULT	EXCITATION ENERGY	SOURCE		DETECTOR		ANGLE
			TYPE	RANGE	TYPE	RANGE	
G,G	LFT	1	C	1	NAI-D	0 - 1	117

TABLE 1
Mean lifetimes

Nucleus	State (MeV)	Spin	Mean lifetime (psec) (Hough and Mouton)	Mean lifetime (psec) (Other workers)	Ref.
^{27}Al	1.01	$\frac{1}{2}$	$0.5^{+0.5}_{-0.2}$	5.2 ± 1.7	[6]
				$0.041^{+0.029}_{-0.016}$	[2]
				$1.7^{+1.2}_{-0.5}$	[8]
^{31}P	1.26	$\frac{1}{2}$	$0.73^{+0.19}_{-0.12}$	0.46 ± 0.23	[6]
				0.22 ± 0.07	[6]
				$0.96^{+0.50}_{-0.21}$	[1]
				$0.72^{+0.13}_{-0.10}$	[7]
^{35}Cl	1.22	$\frac{1}{2}$	$0.13^{+0.03}_{-0.02}$	0.30 ± 0.10	[6]

REF.

H. Hoffmann, B. Prowe and H. Ullrich
Nuclear Phys. 85, 631 (1966)

ELEM. SYM.	A	Z
Al	27	13

METHOD

Betatron

REF. NO. 66 Ho 3 JDM

REACTION	RESULT	EXCITATION ENERGY	SOURCE		DETECTOR		ANGLE
			TYPE	RANGE	TYPE	RANGE	
G,A	SPC	THR-31	C	31	SCD-D	2-13	130

TABLE 1

Experimental data and results

Element	Mg	Al	S	Ni	Cu	Zn	Error (%)
target thickness (mg/cm²)	0.81	1.54	0.80	2.50	2.68	3.00	5 a)
dose (r)	6190	25400	23200	3880	5840	4220	10
yield absolute (10^6/mole · r) for $E_m > 3.16$ MeV	0.61	0.93	1.46	1.65	0.92	2.42	11 a)
yield relative to Ni	0.36	0.56	0.88	1	0.55	1.43	5 a)
$Y_{\gamma,\alpha}/Y_{\gamma,tot}$(%)	9.6	11.4	12.4	7.0	3.2	b)	
nuclear temp. θ (MeV)	1.43	1.48	1.46	1.04		0.91	10
level density parameter a (MeV^{-1})	5.1	4.8	4.9	8.6		10.8	10

a) For S, the error of the target thickness has been 10 %, of the absolute yield 14 % and of the relative yield 10 %.
b) For Zn $\sigma_{\gamma,tot}$ is not known.

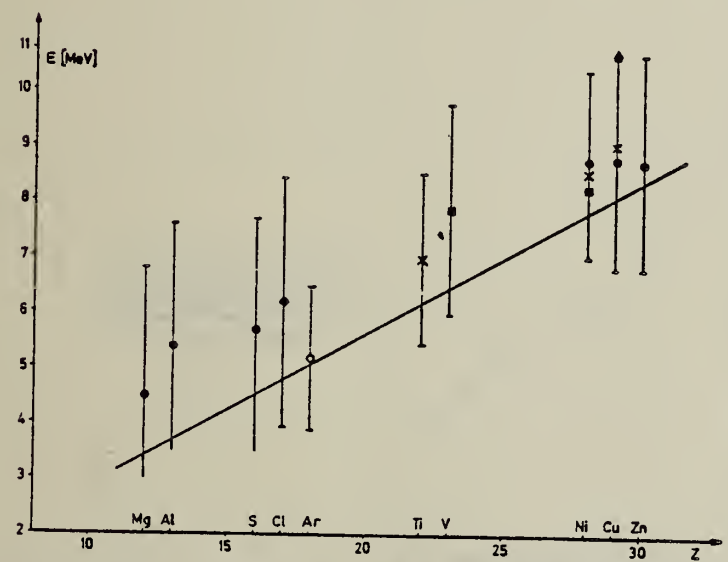

Fig. 4. Position of the peaks in different photoalpha spectra plotted against Z of the target nuclei. × : Scheer *et al*[10]), ■ : Kregar and Povh[9]). ▲ : Meneghetti and Vitale[8]), ◆ : Erdös *et al*[1]), ○ : Komar *et al*[7]), ● : this work. The signs show the position of the maximum, the bars give the widhs at half maximum. The curve shows the height of the Coulomb barrier.

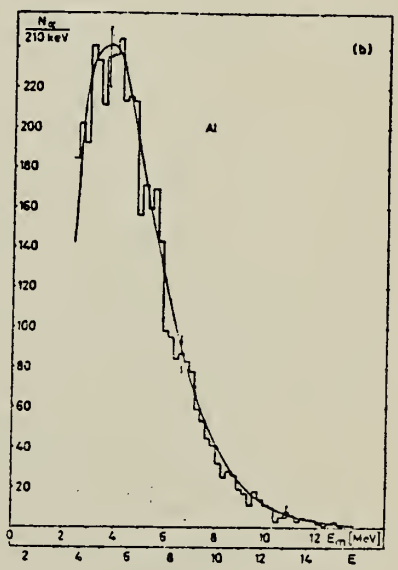

Fig. 3 (b)

REF.	ELEM. SYM.	A	Z
H. Lichtblau and B.M. Spicer Aust. J. Phys. 19, 297 (1966)	Al	27	13

METHOD	REF. NO.	
35 MeV Betatron; NBS ionization chamber	66 Li 1	JDM

REACTION	RESULT	EXCITATION ENERGY	SOURCE		DETECTOR		ANGLE
			TYPE	RANGE	TYPE	RANGE	
G,P	SPC	THR - 32	C	32	SCI-D	1 - 20	90

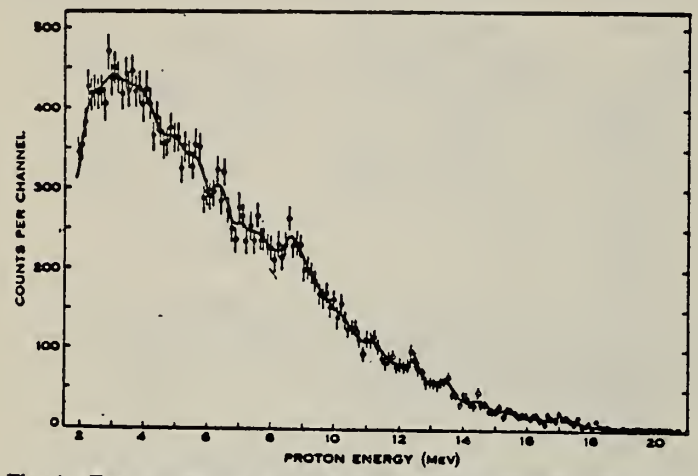

Fig. 4.—Energy spectrum of photoprotons from aluminium, with bremsstrahlung end-point energy 32 MeV.

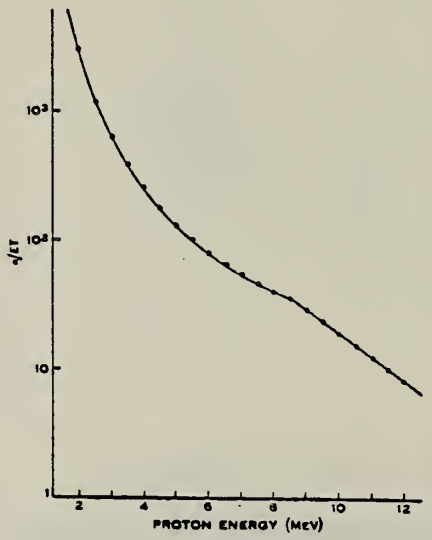

Fig. 5.—Log–linear plot of n/ET versus proton energy E, constructed from the data of Figure 4.

REF.

C. Van der Leun and N. C. Burhoven Jaspers
Nuclear Phys. 88, 235 (1966)

ELEM. SYM.	A	Z
Al	27	13

METHOD

Doppler recoil

REF. NO. 66 Va 4 JDM

REACTION	RESULT	EXCITATION ENERGY	SOURCE		DETECTOR		ANGLE
			TYPE	RANGE	TYPE	RANGE	
G,G	ABI	10	D	10	NAI-D	0-10	80

Used $^{26}Mg(p,\gamma)$ with E_p = 1966 keV.

$(2J+1)\Gamma_p\Gamma_\gamma/\Gamma$ = 5.6±1.8 eV $\quad \Gamma_\gamma$ = 1.0±0.3 eV

Γ_p = 22 ± 5 eV

REF.

R. Wendling and R. Kosiek
Z. fur Physik 192, 502 (1966)

ELEM. SYM.	A	Z
Al	27	13

METHOD

REF. NO. 66 We 2 EGF

REACTION	RESULT	EXCITATION ENERGY	SOURCE		DETECTOR		ANGLE
			TYPE	RANGE	TYPE	RANGE	
G,A	ABX	10-33	C	33	SCD-D	4-16	90
				(32.5)			

Tabelle

Element	Dicke (mg/cm²)	Gesamtauflösung (keV)	Gesamtzahl gemessener α-Teilchen	Ausbeute (μb/MeV · ster)	Ausbeute $\frac{10^4 N\alpha}{\text{Mol} \cdot r}$	$E_{\gamma\,max}$ (exp) (MeV)	$E_{\gamma\,min}$ (MeV)
Al	2,35	770	14600	1,3 ±0,2	3,5 ±0,6	(≈3,5)	3,5
Ar	200 Torr	480	5200	3,0 ±0,5	8,3 ±1,3	5,2	3,5
Se	3,72	790	12200	0,28±0,04	0,76±0,12	9,2	4,5
Ag	3,12	670	3150	0,12±0,02	0,33±0,05	11,8	6,5

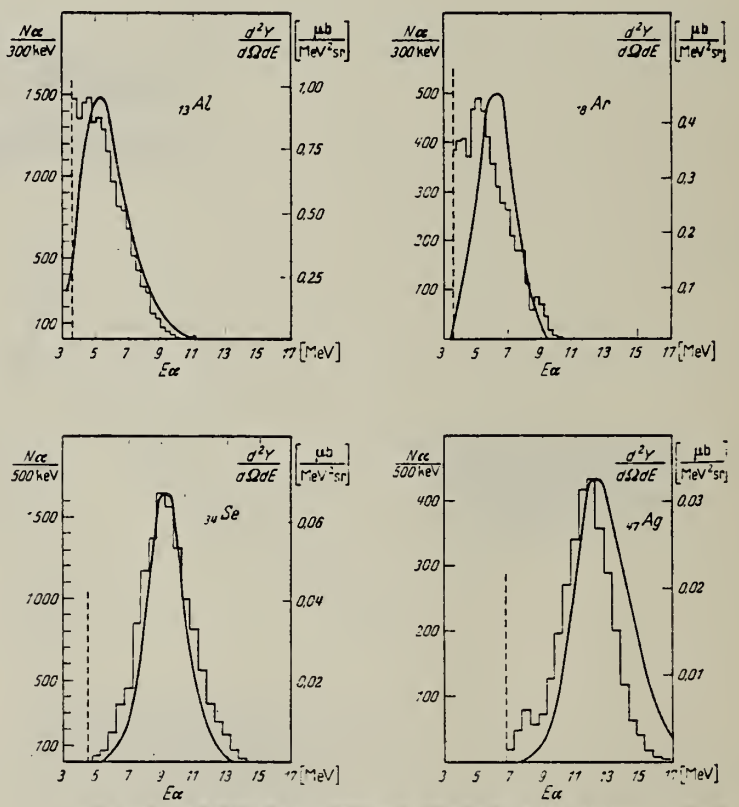

Fig. 1. a Histogramm: Gemessene Energieverteilung und differentielle Ausbeute der Photo-α-Teilchen.
b Kurve: Berechnetes Spektrum. Nähere Angaben im Text

REF. Yu. P. Antuf'ev, I. I. Miroshnichenko, V. I. Noga, and P. V. Sorokin
Yad. Fiz. 6, 431 (1967)
Sov. J. Nucl. Phys. 6, 312 (1968)

ELEM. SYM.	A	Z
Al	27	13

METHOD

REF. NO.	
67 An 1	HMG

REACTION	RESULT	EXCITATION ENERGY	SOURCE		DETECTOR		ANGLE
			TYPE	RANGE	TYPE	RANGE	
G,N2P	RLX	THR-999	C	THR-999	ACT-I		4PI

999= 1.25 GEV

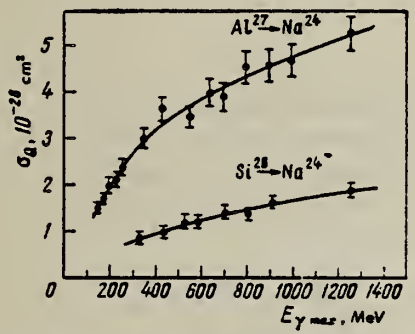

Fig. 2. Cross section σ_Q of the reactions $Al^{27} \rightarrow Na^{24}$ and $Si^{28} \rightarrow Na^{24}$ per equivalent γ quantum as a function of the maximum bremsstrahlung energy.

G. P. Antropov, I. E. Mitrofanov, V. S. Russkikh
Izv. Akad. Nauk SSR Fiz. 31, 336 (1967)
Bull. Acad. Sci. USSR 31, 320 (1967)

Al	27	13

METHOD

REF. NO. 67 An 2 egf

REACTION	RESULT	EXCITATION ENERGY	SOURCE		DETECTOR		ANGLE
			TYPE	RANGE	TYPE	RANGE	
G,XN	ABX	THR-26	C	13-26	BF3-I		4PI

551

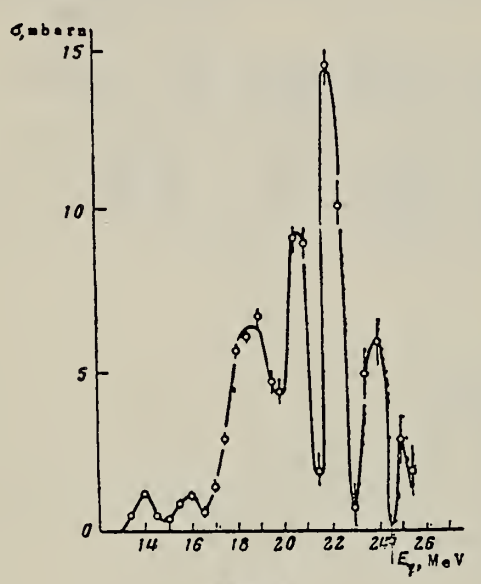

Fig.3

Fig.3. Total cross section $[\sigma_{(\gamma,n)} + 2\sigma_{(\gamma,2n)} + \ldots]$ for the (γ,n) reaction on ^{27}Al.

REF.	ELEM. SYM.	A	Z
H. M. Gerstenberg and E. G. Fuller NBS Tech. Note 416, June 1967	Al	27	13

METHOD	REF. NO.
	67 Ge 2 HMG

REACTION	RESULT	EXCITATION ENERGY	SOURCE		DETECTOR		ANGLE
			TYPE	RANGE	TYPE	RANGE	
G,N	ABY	THR-27	C	22,27	BF3-I		4PI

Table 7. Comparison of neutron yields. Yields are given in units of (neutron cm^2/MeV nucleus)$\times 10^{-28}$. The estimated uncertainties in Y and Y_c are of the order of 6% and 10%, respectively.

Element	E_o	$Y(E_o)$	Y_c				Y_c/Y				Ref.
			UCRL	Saclay	Va.	NBS(Old)	UCRL Exp	Saclay Exp	Va. Exp	NBS(Old) Exp	
Pb	27	103	86				0.83				26,30
	22	111	92	116			0.83	1.05			
Au	27	89	97				1.09				24,30,
	22	92	98	88		115	1.07	0.96		1.25	38
Ta	27	81	82	77			1.01	0.95			27,30,
	22	85	79	80		113	0.93	0.94		1.33	38
Ho	27	67	75				1.12				27,31,
	22	69	77	82		103	1.12	1.19		1.49	39
Ag	27	36									
	22	34.8									
Cu	27	14.4	13.2				0.92				28,30
	22	12.6	11.5	12.4			0.91	0.98			
Co	27	12.7	12.1				0.95				29,34
	22	10.6	9.9		13.5		0.94		1.27		
Ca	27	1.69		1.13	1.01			0.67	0.60		32,35
P	27	2.35			1.76				0.75		36
Al	27	1.92	1.62		1.38		0.84		0.72		25,37
O^{16}	27	0.54	0.42	0.48	0.42		0.78	0.89			16,32, 37
C	27	0.50	0.35	0.33	0.46		0.70	0.66			25,32, 33

(OVER)

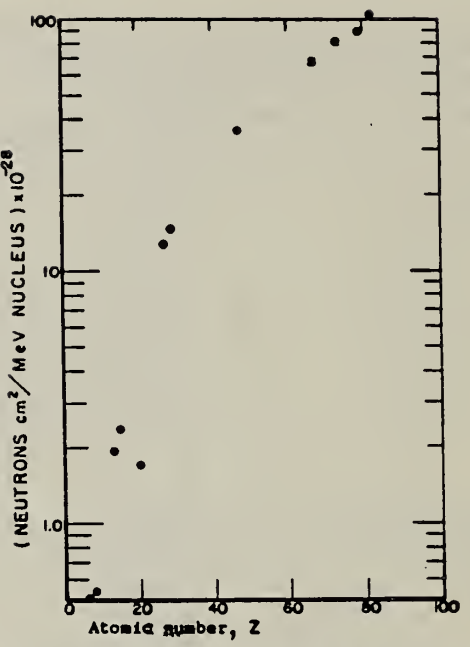

Fig. 31. Absolute neutron yield as a function of atomic number. The neutron yield from calcium (Z = 20) is particularly low in comparison with the other elements because its (γ,n) threshold is high compared to the mean energy of the giant resonance.

REF. R. M. Lombard and G. R. Bishop
Nucl. Phys. A101, 601 (1967)

ELEM. SYM.	A	Z
Al	27	13

METHOD

REF. NO. 67 Lo 2

EGF

REACTION	RESULT	EXCITATION ENERGY	SOURCE		DETECTOR		ANGLE
			TYPE	RANGE	TYPE	RANGE	
E,E/	FMF	0-3	D	90-190	MAG-D	85-190	DST

Level (MeV)	B(E2 ↑) (e^2fm^4)	B(M1)(e^2fm^2)
.84 + 1.01	50±6	$1.5\pm0.8\times10^{-2}$
2.21	86±10	
2.73	20±10	
3.00 (2.98+3.00?)	90±10	

TABLE 2

The cross sections measured for the scattering of electrons of various incident energies through various angles by the nucleus ^{27}Al

Incident energy (MeV)	Scattering angle θ	Momentum transfer q (fm^{-1})	Elastic cross section ($\mu b \cdot sr^{-1}$)	Inelastic cross section (10^{-7} $fm^2 \cdot sr^{-1}$) 0.84 MeV+1.01 MeV	2.21 MeV	2.73 MeV	3 MeV
99.04	60	0.510	484 ±50				
150.312	44	0.570	541 ±54	3200 ±2300	3730 ±1500	416 ±30	
79.78	90	0.570	96 ±10	453 ± 232	839 ± 330		415 ± 290
99.29	70	0.576	169 ±16				
89.47	100	0.693	21.8 ± 2				
180.28	45	0.698	183 ±30	2740 ± 930	3620 ±1370	910 ±70	2870 ±1150
151.91	60	0.769	49.9 ± 4.9				
99.58	100	0.771	12.7 ± 1				
180.24	55	0.842	33.6 ± 6	450 ± 156	1310 ± 300		874 ±260
149.10	70	0.865	12.8 ± 1.3				
111.94	100	0.867	5.4 ± 0.5				
119.84	105	0.961	1.79 ± 0.18				
179.33	65	0.978	5.75 ± 0.60	254 ± 99	408 ± 84	126 ±63	460 ± 110
149.84	90	1.071	0.64 ± 0.12				
119.58	135	1.115	0.067 ± 0.007	10 ± 2.2	19.4± 3	3.35± 2.3	20 ± 8
181.88	75	1.119	0.92 ± 0.030	88.4 ± 18	165 ± 33		175 ± 26
190.157	75	1.169	0.67 ± 0.2	67.6 ± 32	128.4± 30	25.4±18	114 ± 28
128.61	135	1.199	0.019 ± 0.004				
179.887	85	1.227	0.109 ± 0.011	36.2 ± 10			
190.238	80	1.235	0.253 ± 0.09	37.9 ± 6.4	67.5± 24	17.7 ±13.6	59.7 ± 12.6
178.92	90	1.277	0.043 ± 0.006				
179.75	95	1.338	0.031 ± 0.005	8.5 ± 4.9	14.9± 3	4.1 ± 0.3	
150.06	135	1.39	0.0069± 0.0016				
179.83	105	1.439	0.027 ± 0.005	2.41± 0.85	5.6± 2.4		
158.66	135	1.477	0.0079± 0.0016				
190.16	110	1.571	0.0175± 0.0035				
170.44	135	1.587	0.0054± 0.001	1.99± 1.73	2.1± 0.8		1.57± 0.30

(Over)

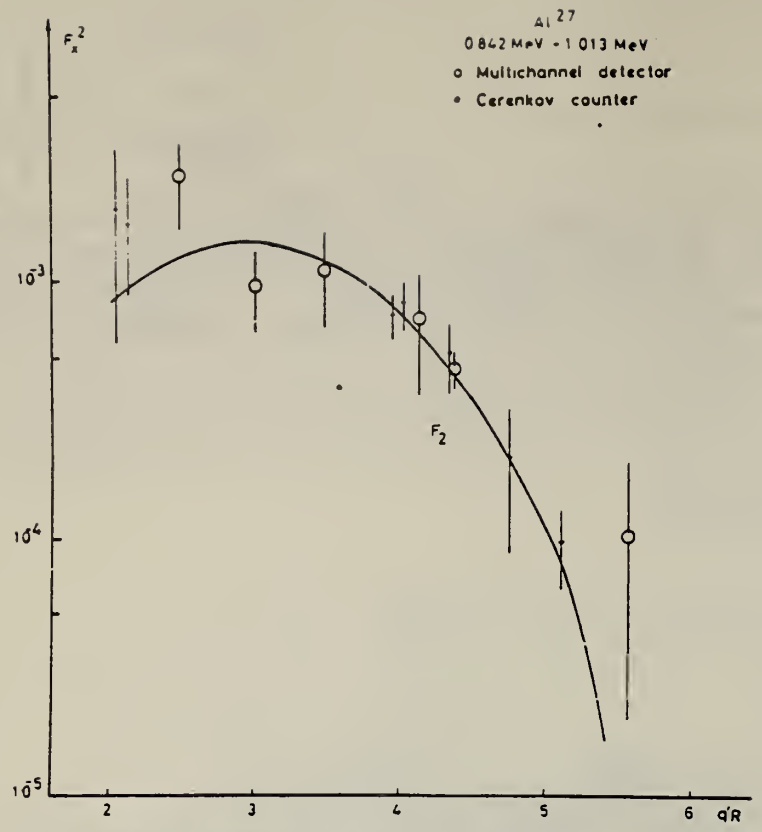

Fig. 7. The experimental form factors obtained for the levels at 0.84 MeV and 1.01 MeV. The full line represents the expression $F_2 = j_2^2(qR)\exp(-q^2g^2)$ multiplied by the normalizing factor $\beta_2 = (2.78 \pm 0.33) \cdot 10^{-3}$.

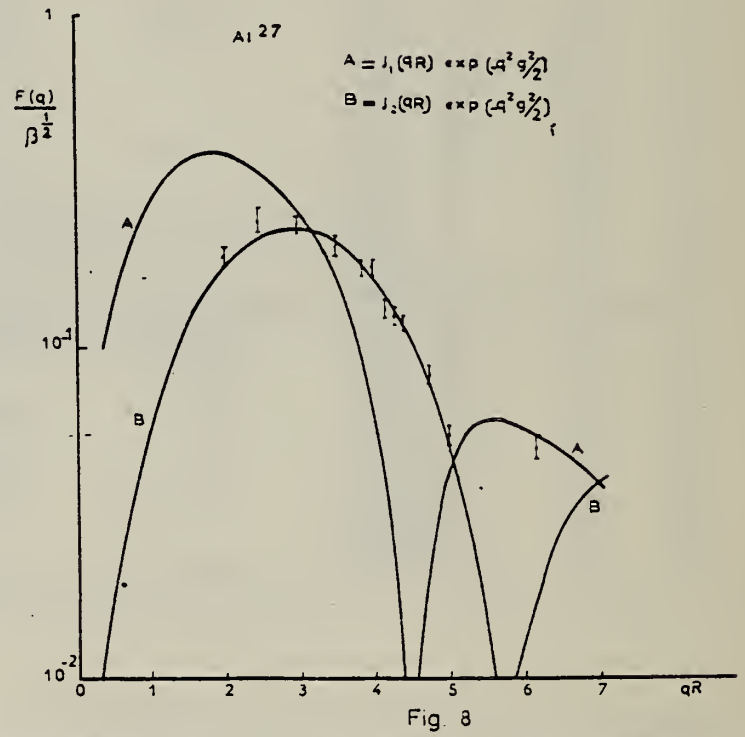

Fig. 8

Fig. 8. The inelastic form factor for scattering from the 2.21 MeV level compared with the functions $B = j_2(qR)\exp(-\frac{1}{2}q^2g^2)$ and $A = j_1(qR)\exp(-\frac{1}{2}q^2g^2)$.

REF. R. M. Lombard and G. R. Bishop
Nucl. Phys. A101, 601 (1967)

ELEM. SYM.	A	Z
Al	27	13

METHOD

[Page 3 of 4]

REF. NO. 67 Lo 2 EGF

REACTION	RESULT	EXCITATION ENERGY	SOURCE		DETECTOR		ANGLE
			TYPE	RANGE	TYPE	RANGE	

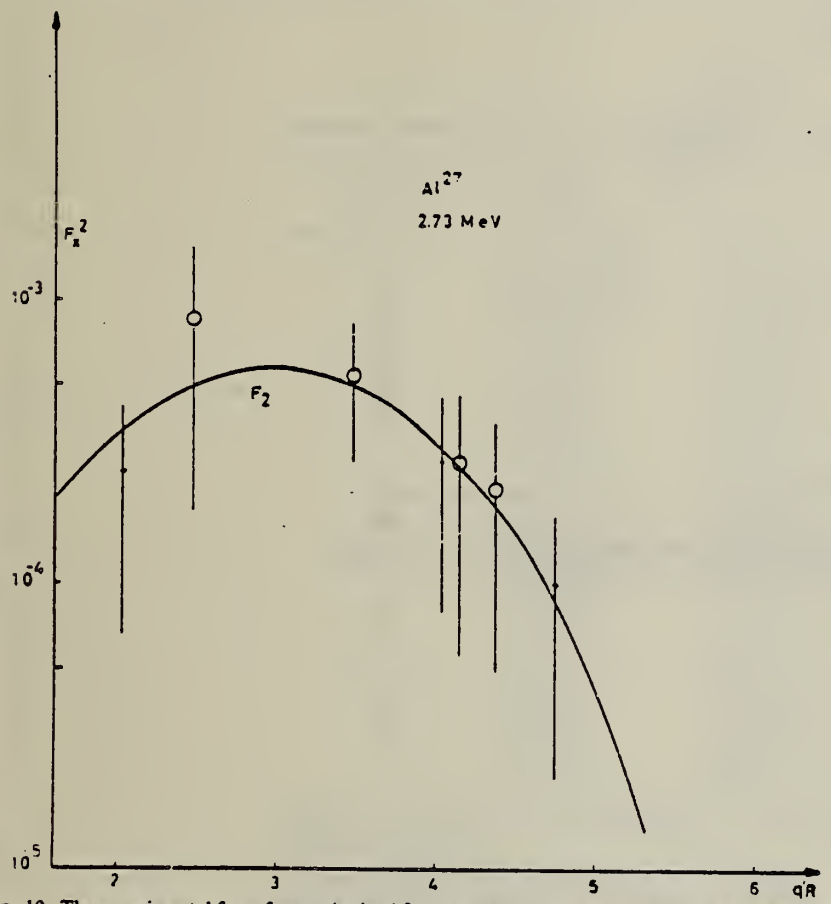

Fig. 10. The experimental form factor obtained for the level at 2.73 MeV. The full line represents F_2 multiplied by $\beta_2 = (1.11 \pm 0.55) \cdot 10^{-2}$.

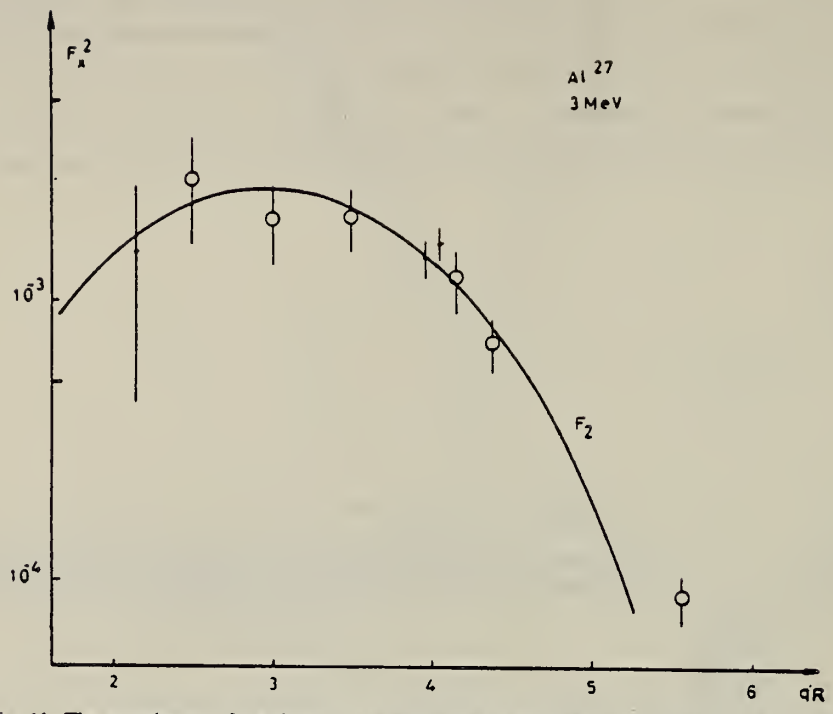

Fig. 11. The experimental form factor obtained for the peak observed at 3 MeV. The full line represents the expression F_2 multiplied by $\beta_2 = (5.01 \pm 0.56) \cdot 10^{-2}$.

REF. D. M. Sheppard and C. Van Der Leun
Nucl. Phys. A100, 333 (1967)

ELEM. SYM.	A	Z
Al	27	13

METHOD

REF. NO. 67 Sh 2 EGF

REACTION	RESULT	EXCITATION ENERGY	SOURCE		DETECTOR		ANGLE
			TYPE	RANGE	TYPE	RANGE	
P,G	LFT	8-11	D	0-3	SCD-D	0-10	DST

TABLE 1

Angular distribution coefficients a_2 and a_4 of gamma rays de-exciting resonance levels in the reaction $^{26}Mg(p,\gamma)^{27}Al$

E_p [a]) (keV)	Transition [b])	a_2 [c])	a_4 [c])
292	8.55→0.84	−0.01 ±0.08	+0.06 ±0.09
338	8.60→0.84	−0.74 ±0.06	+0.04 ±0.07
454	8.71→(0.84+1.01)	+0.002±0.005	−0.002±0.006
479	8.73→0	−0.19 ±0.02	−0.04 ±0.03
501	8.75→0	+0.43 ±0.03	−0.02 ±0.03
522	8.77→0	+0.59 ±0.12	−0.05 ±0.12
650	8.90→0	+0.12 ±0.02	−0.01 ±0.02
1249	9.48→0	−0.27 ±0.01	+0.04 ±0.02
	9.48→2.21	+0.47 ±0.03	+0.02 ±0.03
1409	9.63→0	+0.01 ±0.01	−0.01 ±0.01
1548	9.76→0	+0.66 ±0.01	−0.02 ±0.02
1609	9.82→0	+0.12 ±0.06	+0.01 ±0.06
	9.82→1.01	+0.17 ±0.01	+0.00 ±0.01
1733	9.94→0	+0.08 ±0.04	−0.03 ±0.05
	9.94→3.00	−0.20 ±0.03	−0.01 ±0.04
1785	9.99→0	−0.34 ±0.02	−0.02 ±0.02
	9.99→4.81	−0.29 ±0.01	−0.01 ±0.01
1965	10.16→0	+0.20 ±0.01	−0.04 ±0.01
2141	10.33→0.84	+0.46 ±0.09	−0.16 ±0.09
2220	10.41→0	+0.67 ±0.02	−0.06 ±0.02
2293	10.48→0	−0.37 ±0.01	−0.03 ±0.01
	10.48→6.48	+0.45 ±0.04	−0.02 ±0.05
2323	10.51→0	−0.25 ±0.01	+0.01 ±0.01

[a]) Resonance energies from ref. [1]), corrected for the new recommended value [44]) of the $^{27}Al(p,\gamma)^{28}Si$ calibration resonance.
[b]) Excitation energies of the initial and final states (in MeV).
[c]) After correction for eccentricity, background and random coincidences, but without solid angle attenuation correction.

(Over)

TABLE 4

Quadrupole/dipole amplitude mixing ratios of primary gamma rays de-exciting ^{27}Al resonances

E_p (keV)	Transition (E_x in MeV)	$J_i^\pi \rightarrow J_f^\pi$	Mixing ratio
338	8.60→0.84	$\frac{3}{2}^- \rightarrow \frac{1}{2}^+$	$+0.10 \pm 0.03$
	8.60→2.98	$\frac{3}{2}^- \rightarrow \frac{3}{2}^+$	$+0.02 \pm 0.03$
501	8.75→0	$\frac{5}{2} \rightarrow \frac{5}{2}^+$	$+0.00 \pm 0.03$ (or -1.3 ± 0.3)
522	8.77→0	$\frac{3}{2} \rightarrow \frac{5}{2}^+$	-0.18 ± 0.18 (or -0.9 ± 0.4)
650	8.90→0	$\frac{5}{2} \rightarrow \frac{5}{2}^+$	$+0.29 \pm 0.08$
	8.90→1.01	$\frac{5}{2} \rightarrow \frac{3}{2}^+$	$+0.06 \pm 0.07$
	8.90→2.98	$\frac{5}{2} \rightarrow \frac{3}{2}^+$	$+0.00 \pm 0.01$
1249	9.47→0	$\frac{7}{2} \rightarrow \frac{5}{2}^+$	-0.07 ± 0.02
	9.47→2.21	$\frac{7}{2} \rightarrow \frac{7}{2}^+$	$+0.04 \pm 0.02$
1548	9.76→0	$\frac{5}{2}^+ \rightarrow \frac{5}{2}^+$	-0.16 ± 0.02
	9.76→2.21	$\frac{5}{2}^+ \rightarrow \frac{7}{2}^+$	$+0.06 \pm 0.02$
1609	9.82→0	$\frac{3}{2}^+ \rightarrow \frac{5}{2}^+$	$+0.21 \pm 0.06$ (or $+2.2 \pm 0.3$)
	9.82→1.01	$\frac{3}{2}^+ \rightarrow \frac{3}{2}^+$	$+0.14 \pm 0.01$ (or -8.9 ± 0.3)
	9.82→2.73	$\frac{3}{2}^+ \rightarrow \frac{5}{2}^+$	-0.13 ± 0.03
1733	9.94→0	$\frac{7}{2} \rightarrow \frac{5}{2}^+$	-0.20 ± 0.02
	9.94→3.00	$\frac{7}{2} \rightarrow \frac{9}{2}^+$	-0.02 ± 0.01
1785	9.99→0	$\frac{7}{2}^- \rightarrow \frac{5}{2}^+$	$+0.00 \pm 0.02$
	9.99→4.81	$\frac{7}{2}^- \rightarrow \frac{5}{2}$	-0.02 ± 0.02
1965	10.16→0	$\frac{5}{2}^+ \rightarrow \frac{5}{2}^+$	$+0.23 \pm 0.01$
	10.16→2.21	$\frac{5}{2}^+ \rightarrow \frac{7}{2}^+$	$+0.12 \pm 0.01$
2141	10.33→0.84	$\frac{3}{2} \rightarrow \frac{1}{2}^+$	-0.55 ± 0.07 (or $+50 \pm 20$)
	10.33→2.98	$\frac{3}{2} \rightarrow \frac{3}{2}^+$	$+0.02 \pm 0.02$ (or -4.3 ± 0.3)
2220	10.41→0	$\frac{5}{2}^+ \rightarrow \frac{5}{2}^+$	-0.39 ± 0.07
	10.41→2.98	$\frac{5}{2}^+ \rightarrow \frac{3}{2}^+$	-0.03 ± 0.02
2293	10.48→0	$\frac{7}{2}^- \rightarrow \frac{5}{2}^+$	$+0.03 \pm 0.01$
	10.48→6.48	$\frac{7}{2}^- \rightarrow (\frac{7}{2})$	$+0.01 \pm 0.03$
2323	10.51→0	$\frac{7}{2}^- \rightarrow \frac{5}{2}^+$	-0.04 ± 0.01
	10.51→2.21	$\frac{7}{2}^- \rightarrow \frac{7}{2}^+$	$+0.06 \pm 0.04$
	10.51→3.00	$\frac{7}{2}^- \rightarrow \frac{9}{2}^+$	$+0.00 \pm 0.02$
2574	10.75→2.21	$\frac{9}{2} \rightarrow \frac{7}{2}^+$	$+0.10 \pm 0.04$
	10.75→3.00	$\frac{9}{2} \rightarrow \frac{9}{2}^+$	$+0.05 \pm 0.07$

REACTION	RESULT	EXCITATION ENERGY	SOURCE		DETECTOR		ANGLE
			TYPE	RANGE	TYPE	RANGE	

TABLE 5

Quadrupole/dipole amplitude mixing ratios of gamma transitions between bound states of ^{27}Al

Transition (E_x in MeV)	$J_1^\pi \to J_f^\pi$	Resonance investigated (E_p in keV)	Mixing ratio	Average
1.01→0	$\frac{1}{2}^+ \to \frac{5}{2}^+$	650	+0.40±0.08	+0.37±0.03
		1380	+0.39±0.05	
		1609	+0.33±0.05	
1.01→0.84	$\frac{3}{2}^+ \to \frac{1}{2}^+$	338	−0.05±0.06 [a])	
2.21→0	$\frac{7}{2}^+ \to \frac{5}{2}^+$	1249	−0.42±0.02	−0.40±0.01
		1548	−0.41±0.04	
		1965	−0.40±0.02	
		2323	−0.36±0.03	
		2574	−0.40±0.02	
2.73→0	$\frac{5}{2}^+ \to \frac{5}{2}^+$	1609	−0.09±0.03	
2.73→1.01	$\frac{5}{2}^+ \to \frac{3}{2}^+$	1609	−0.09±0.03	
2.98→0	$\frac{3}{2}^+ \to \frac{5}{2}^+$	338	−0.04±0.05	+0.01±0.01
		650	+0.08±0.09	
		2141	+0.02±0.02	
		2220	+0.00±0.02	
3.00→0	$\frac{9}{2}^+ \to \frac{5}{2}^+$	1733	∞	
		2323	∞	
		2574	∞	
3.00→2.21	$\frac{9}{2}^+ \to \frac{7}{2}^+$	1733	−0.00±0.03	
4.81→0	$\frac{9}{2}^- \to \frac{5}{2}^+$	1785	+0.29±0.03 (or 2.7±1.0)	
4.81→1.01	$\frac{9}{2}^- \to \frac{3}{2}^+$	1785	+0.06±0.02	
4.81→2.21	$\frac{9}{2}^- \to \frac{7}{2}^+$	1785	+0.05±0.02 (or 5.5±1.0)	

[a]) See subsect. 4.2.2.

TABLE 6

Transition strengths of gamma rays de-exciting ^{26}Mg(p, γ)^{27}Al resonance levels

Transition (E_x in MeV)	$J_1^\pi \to J_f^\pi$	Γ_γ [a]) (meV)	$\lvert M\rvert^2 \times 10^3$			
			E1	M1	E2	M2
9.76→0	$\frac{3}{2}^+ \to \frac{5}{2}^+$	100		5	7	
9.76→2.21	$\frac{3}{2}^+ \to \frac{7}{2}^+$	135		15	5	
9.82→2.73	$\frac{3}{2}^+ \to \frac{5}{2}^+$	130		17	30	
9.99→0	$\frac{7}{2}^- \to \frac{5}{2}^+$	280	0.45			
10.16→0	$\frac{5}{2}^+ \to \frac{5}{2}^+$	620		25	70	
10.16→2.21	$\frac{5}{2}^+ \to \frac{7}{2}^+$	190		18	20	
10.41→0	$\frac{5}{2}^+ \to \frac{5}{2}^+$	130		5	35	
10.41→2.98	$\frac{5}{2}^+ \to \frac{3}{2}^+$	150		17	(2)	
10.48→0	$\frac{7}{2}^- \to \frac{5}{2}^+$	1000 [b])	1.7			50
10.51→0	$\frac{7}{2}^- \to \frac{5}{2}^+$	530 [b])	0.75			45
10.51→2.21	$\frac{7}{2}^- \to \frac{7}{2}^+$	230 [b])	0.65			150
10.51→3.00	$\frac{7}{2}^- \to \frac{9}{2}^+$	150	0.60			

[a]) Calculated using the resonance strength of ref. [1]) (as corrected in refs. [39, 40])) and the branching ratios of ref. [2]).

[b]) For resonance strengths, see sect. 5.3.

TABLE 7

Strengths of gamma transitions between bound states of ^{27}Al

Transition (E_x in MeV)	$J_i^\pi \to J_f^\pi$	Γ_γ [a] (meV)	$\lvert M\rvert^2$(M1) ($\times 10^2$)	$\lvert M\rvert^2$(E2)
0.84→0	$\frac{1}{2}^+ \to \frac{5}{2}^+$	0.02 [b]		13
1.01→0	$\frac{3}{2}^+ \to \frac{5}{2}^+$	0.3 [c]	12	9
1.01→0.84	$\frac{3}{2}^+ \to \frac{1}{2}^+$	0.01	100	
2.21→0	$\frac{7}{2}^+ \to \frac{5}{2}^+$	17 [d]	65	11
2.73→0	$\frac{1}{2}^+ \to \frac{5}{2}^+$	15 [e]	35	0.2
2.73→1.01	$\frac{1}{2}^+ \to \frac{3}{2}^+$	45 [e]	430	6
2.98→0	$\frac{3}{2}^+ \to \frac{5}{2}^+$	110 [f]	200	< 0.05
3.00→0	$\frac{3}{2}^+ \to \frac{5}{2}^+$	6 [g]		6
3.00→2.21	$\frac{3}{2}^+ \to \frac{7}{2}^+$	0.6 [g]	60	< 0.5

[a]) Widths based on the averages of the lifetimes reported in the literature (for a few typical references, see below) and the branchings reported in this article.
[b]) Ref. [17]).
[c]) Ref. [18]).
[d]) Ref. [22]).
[e]) Ref. [22]); the lifetime reported in ref. [47]), however, leads to widths that are about a factor of 25 lower than the values listed here.
[f]) Refs. [21,22]).
[g]) Refs. [46,47]).

REF. C. Van der Leun, D. M. Sheppard and P. M. Endt
Nucl. Phys. A100, 316 (1967)

ELEM. SYM.	A	Z
Al	27	13

METHOD

REF. NO. 67 Va 1 EGF

REACTION	RESULT	EXCITATION ENERGY	SOURCE		DETECTOR		ANGLE
			TYPE	RANGE	TYPE	RANGE	
P,G	NOX	8-11	D	0-3	SCD-D	0-10	

Note: See Sheppard and Van der Leun, NP A100, 333 (1967) for analysis of angular distribution.

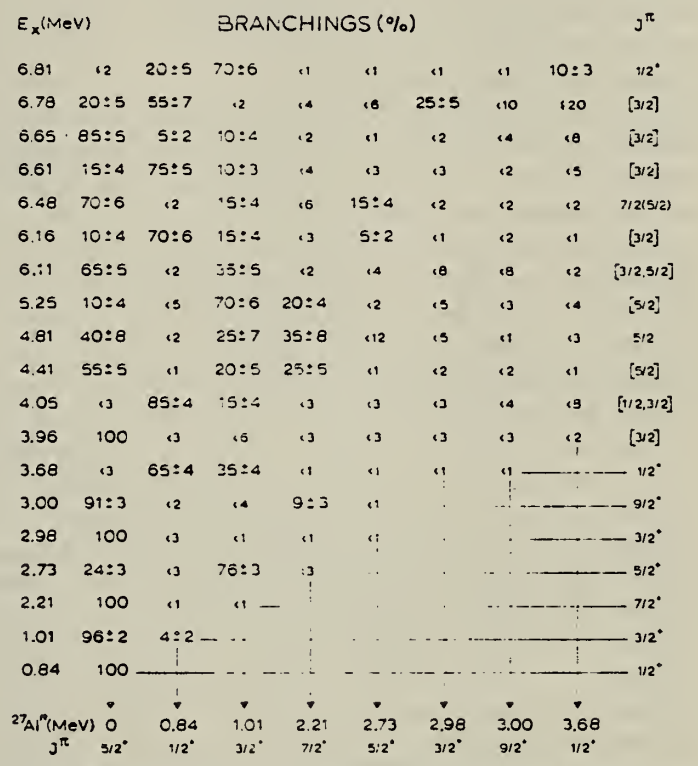

Fig. 6. Branching ratios of bound states of ^{27}Al deduced from gamma-ray spectra measured at thirty ^{26}Mg(p, γ)^{27}Al resonances. For spins, see paper II. Ground-state transitions were observed from the levels at E_x = 4.58, 5.16, 5.43, 5.55, 5.75, 6.08, 6.28, 6.47, 6.82, 7.00 and 7.29 MeV. The levels at E_x = 7.00, 723 and 7.47 MeV decay at least partly through ^{27}Al* = 2.21 MeV.

REF.	ELEM. SYM.	A	Z
C. Van der Leun, D. M. Sheppard and P. M. Endt Nucl. Phys. A100, 316 (1967)	Al	27	13

METHOD	REF. NO.	
[Page 2 of 2]	67 Va 1	EGF

REACTION	RESULT	EXCITATION ENERGY	SOURCE		DETECTOR		ANGLE
			TYPE	RANGE	TYPE	RANGE	

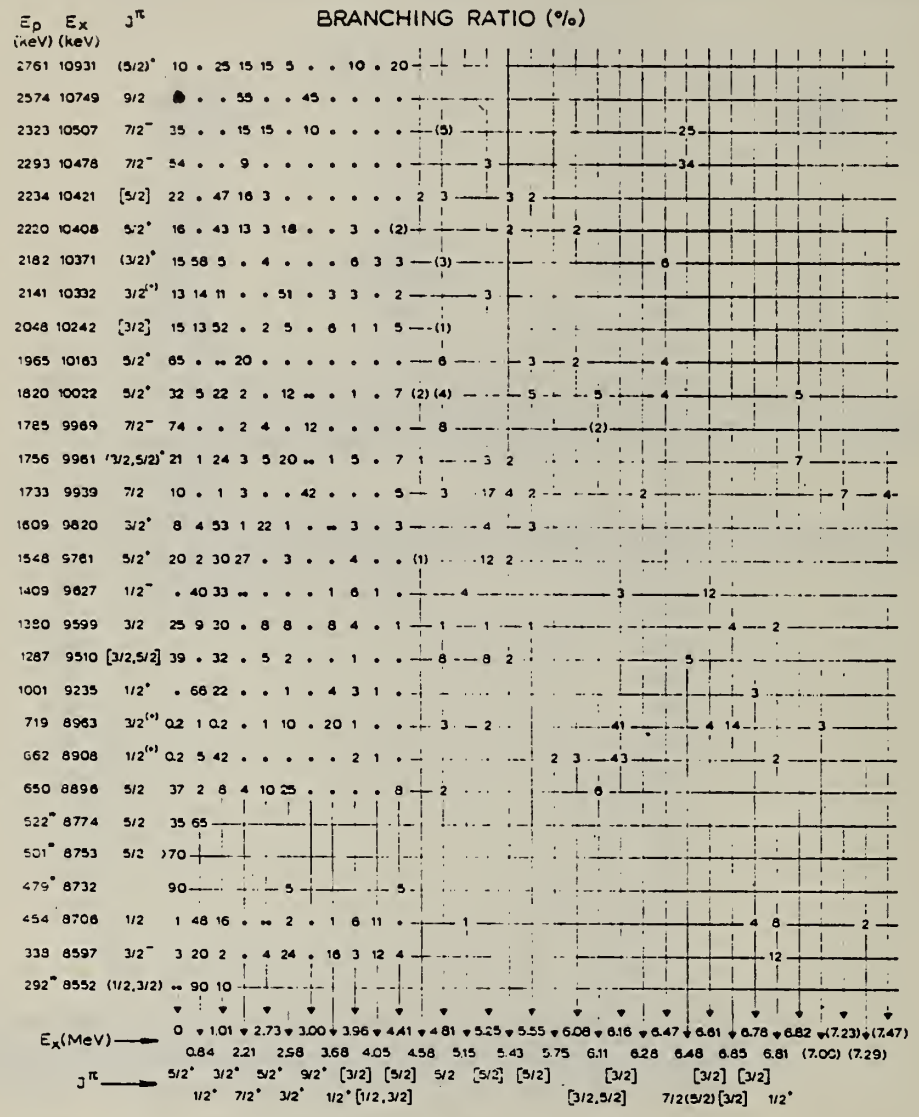

Fig. 4. Branching ratios of resonance levels in the reaction $^{26}Mg(p,\gamma)^{27}Al$. Typical errors range from 50 % for weak (≤ 3 %) γ-rays to about 10 % for γ rays with intensities of ≈ 50 %. Upper limits for the intensities of unobserved transitions are indicated by one dot (< 1 %) or two dots (< 2 %). For a discussion of the level spins, see paper II.

REF.

K. Abe, N. Kawamura and N. Mutsuro
J. Phys. Soc. Japan 25, 1724 (1968)

ELEM. SYM.	A	Z
Al	27	13

METHOD

REF. NO. 68 Ab 3 egf

REACTION	RESULT	EXCITATION ENERGY	SOURCE		DETECTOR		ANGLE
			TYPE	RANGE	TYPE	RANGE	
G,XP	SPC	THR-27	C	22,27	SCD-D	3-15	90
				(21.6,26,6)			

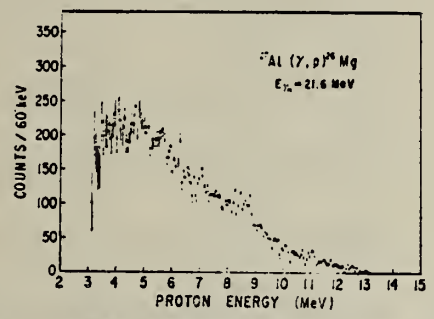

Fig. 1. Energy spectrum of photoprotons from aluminium at 90°, with bremsstrahlung end-point energy 21.6 MeV.

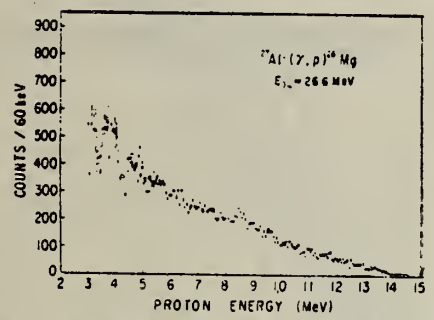

Fig. 2. Energy spectrum of photoprotons from aluminium at 90°, with bremsstrahlung end-point energy 26.6 MeV.

REF.

B. C. Cook, D. W. Anderson, T. J. Englert
Phys. Letters 26B, 341 (1968)

ELEM. SYM.	A	Z
Al	27	13

METHOD

REF. NO. 68 Co 1 HMG

REACTION	RESULT	EXCITATION ENERGY	SOURCE		DETECTOR		ANGLE
			TYPE	RANGE	TYPE	RANGE	
G,N	RLX	THR- 65	C	13-65	ACT-I		4PI

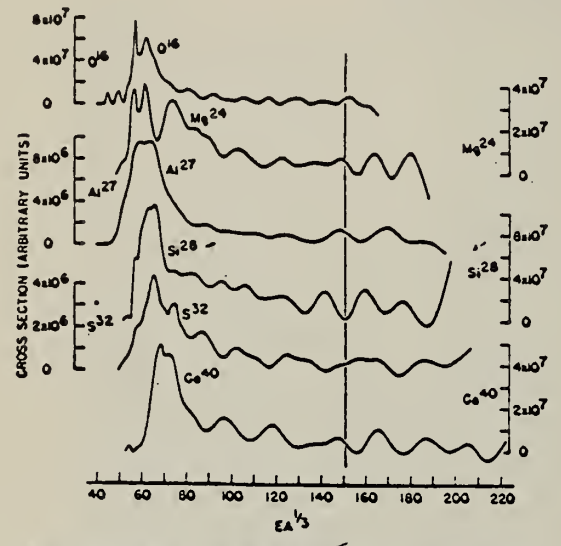

Fig. 1. Cross section for elements in the s-d shell as a function of $EA^{1/3}$. The vertical line is only an aid to the eye. Universal curves expected for the hydrodynamical model are not evident.

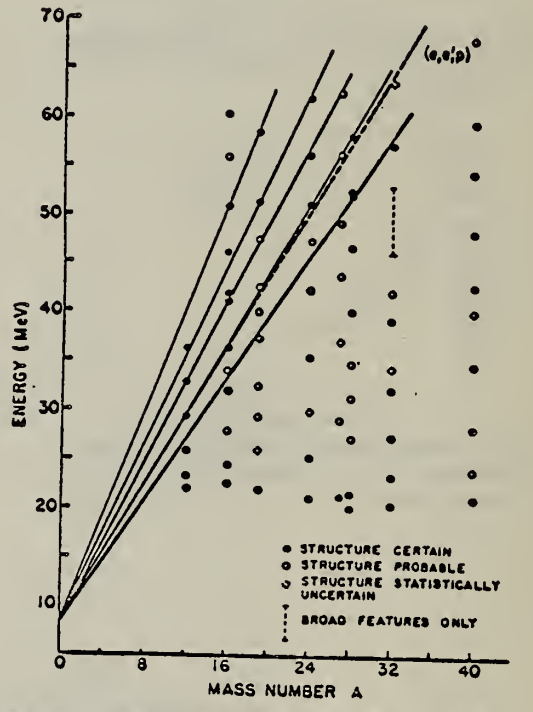

Fig. 2. A dependence of structure. A qualitative estimate for the statistical validity for structure is also indicated. The solid straight lines have the form mA + + 8 MeV while the dashed line represents the position of the 1s level as determined from (e,e'p) experiments.

REF. N. N. Kaushal, E. J. Winhold, P. F. Yergin, H. A. Medicus and R. H. Augustson
Phys. Rev. 175, 1330 (1968)

ELEM. SYM.	A	Z
Al	27	13

METHOD

REF. NO. 68 Ka 1

HMG

[Page 1 of 2]

REACTION	RESULT	EXCITATION ENERGY	SOURCE		DETECTOR		ANGLE
			TYPE	RANGE	TYPE	RANGE	
G,N	ABX	50-85	C	55,85	TOF-D	10-85	67
							(67.5)

NEUT ENGY SPEC

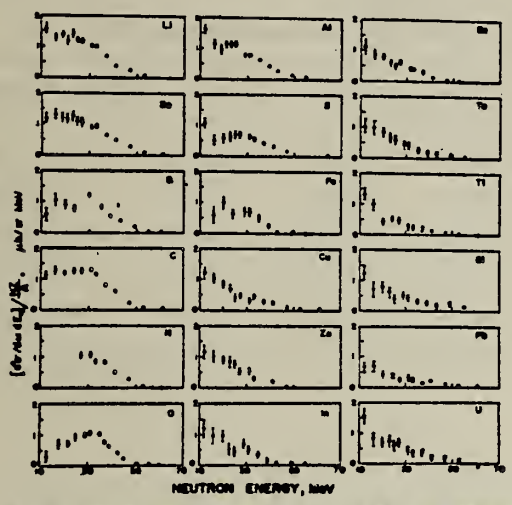

FIG. 6. Observed neutron spectra due to 55–85-MeV difference photon spectra. The effective cross sections have been divided by NZ/A.

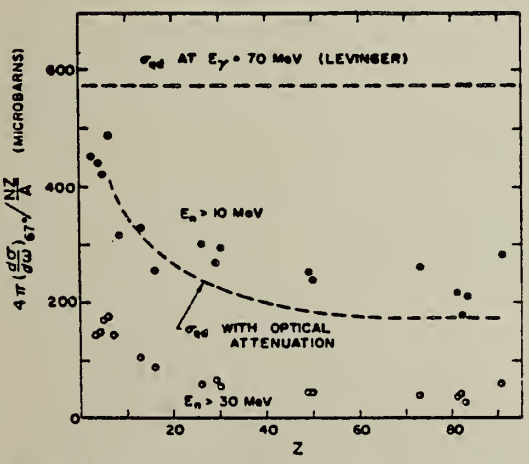

FIG. 7. Effective cross sections for production of fast neutrons with energies greater than 10 MeV (solid circles) and 30 MeV (open circles) by the 55–85-MeV photon difference spectrum. The dashed curves are modified quasideuteron model predictions as discussed in the text.

TABLE I. Comparison of present cross-section values in mb for production of high-energy photoneutrons by 55–85-MeV photons with measured cross sections $\sigma(\gamma,Tn)$, also in mb, for total photoneutron production. The present cross-section values are uncertain by 8 to 10% because of counting statistics and normalization errors; in addition all values depend on an absolute normalization in terms of the deuteron photodisintegration cross section, which is known to about 10% at these energies.

Target	$4\pi(d\sigma/d\omega)_{\pi^0}$ (E_n>10 MeV) [Present experiment]	$\sigma(\gamma,Tn)$ Jones and Terwilliger[a]	$\sigma(\gamma,Tn)$ Costa *et al.*[b]	Other results
Li	0.75		1.0	
Be	1.0	2.7	2.3	2.3[c]
B	1.0		1.4	
C	1.5	1.3	1.4	2.4[d]
O	1.3		1.6	
Al	2.8	5.5	4.6	8[d]
S	2.1		4.4	6.5[d]
Fe	4.2	16	12	
Cu	4.3	20	19	
Zn	4.4		15	
In	7.4			
Sn	7.0			
Ta	10.7	95		
Tl	10.7			
Pb	8.3	100		
Bi	13			
U	16	65		

[a] Average cross sections between 55 and 85 MeV, as read from Figs. 4 and 5 of Ref. 4.
[b] $\int_{\pi}^{\infty}\sigma_{qd}dE - \int_{\pi}^{\infty}\sigma_{qd}dE/50$, as taken from Fig. 4 of Ref. 5 and Table I of Ref. 6.
[c] S. Costa, L. Pasqualini, G. Piragino, and L. Roasio, Nuovo Cimento 42, 306 (1966).
[d] G. Bishop, S. Costa, S. Ferroni, R. Malvano, and G. Ricco, Nuovo Cimento 42, 148 (1966).

REF. N. N. Kaushal, E. J. Winhold, P. F. Yergin, H. A. Medicus and R. H. Augustson
Phys. Rev. 175, 1330 (1968)

ELEM. SYM.	A	Z
Al	27	13

METHOD

REF. NO. 68 Ka 1 HMG

REACTION	RESULT	EXCITATION ENERGY	SOURCE		DETECTOR		ANGLE
			TYPE	RANGE	TYPE	RANGE	

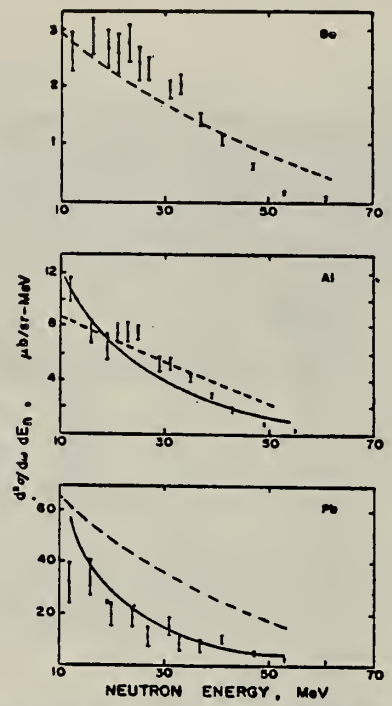

FIG. 8. Neutron energy spectra for beryllium, aluminum, and lead. The dashed curves are Dedrick's quasideuteron model calculations of the primary neutron spectra, arbitrarily multiplied by 1.15. For aluminum and lead these have been modified by estimates of the effects of secondary interactions on the outgoing neutrons, as discussed in the text, to produce the solid curves.

REF.

R. A. Meyer, W. B. Walters, J. P. Hummel
Nucl. Phys. A122, 606 (1968)

ELEM. SYM.	A	Z
Al	27	13

METHOD

REF. NO. 68 Me 4 egf

REACTION	RESULT	EXCITATION ENERGY	SOURCE		DETECTOR		ANGLE
			TYPE	RANGE	TYPE	RANGE	
G,2PN	ABX	THR-300	C	20-300	ACT-I		4PI

311

TABLE 1

Summary of integrated cross sections $\int_0^{E_{max}} \sigma dE$(MeV · mb) for the reactions studied

Reaction/E_{max}(MeV)	65	105	145	215	295
$^{16}O(\gamma, 2n)^{14}O$	0.42±0.02	0.57±0.04	0.56±0.05	0.63±0.09	1.29±0.16
$^{19}F(\gamma, 2pn)^{16}N$	3.7 ±0.2	5.0 ±0.3	6.1 ±0.5	8.4 ±1.0	13.6 ±1.5
$^{27}Al(\gamma, 2pn)^{24}Na$	8.3 ±0.3	13.3 ±0.7	17.1 ±1.2	24.1 ±2.3	31.2 ±3.3 [a]
$^{51}V(\gamma, \alpha)^{47}Sc$	12.3 ±1.7	20.2 ±3.5	32.5 ±2.6	68.4 ±3.8	112 ±14
$^{51}V(\gamma, \alpha 3n)^{44}Sc$	0.7 ±0.2	6.0 ±0.9	12.2 ±1.3	34.1 ±4.1	91 ±11

[a]) E_{max} = 275 MeV.

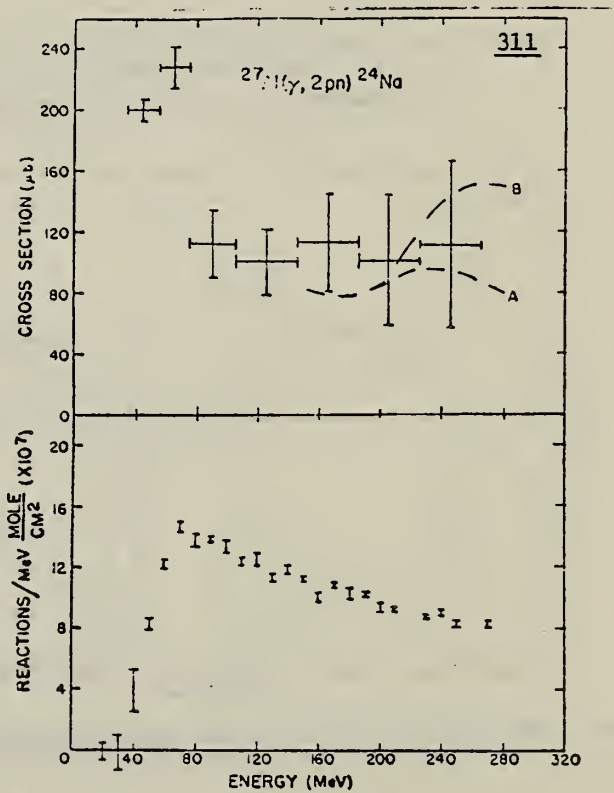

Fig. 3. Yields and cross sections for the $^{27}Al(\gamma, 2pn)^{24}Na$ reaction. The zero yield value at 20 MeV was obtained from an irradiation using the University of Illinois 22 MeV betatron. The dashed lines have the same significance as in fig. 1.

The dashed lines show the cross sections expected for quasi-deuteron processes (curve A) and the sum of the cross sections expected for quasi-deuteron and pion emission processes (curve B).

REF. G. Nydahl and B. Forkman
Nucl. Phys. B7, 97 (1968)

ELEM. SYM.	A	Z
Al	27	13

METHOD

REF. NO. 68 Ny 1 egf

REACTION	RESULT	EXCITATION ENERGY	SOURCE		DETECTOR		ANGLE
			TYPE	RANGE	TYPE	RANGE	
G,PI+	ABX	140-700	C	140-700	ACT-I		4PI

MG-27 ACT

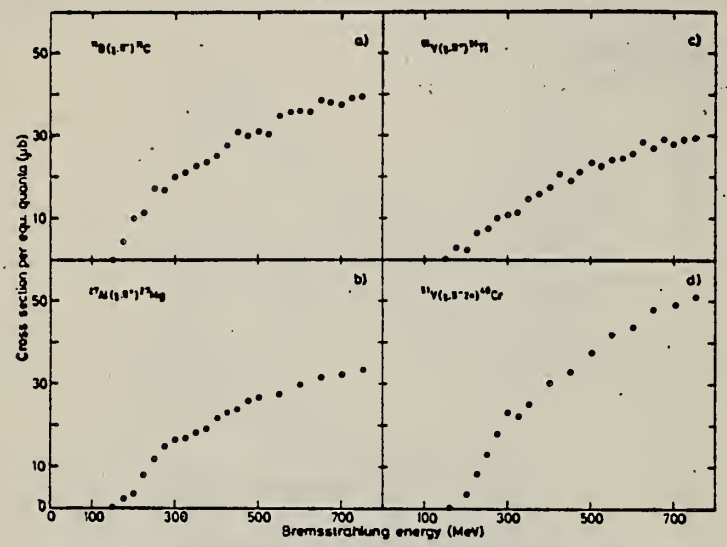

Fig. 3. Absolute yields for the measured reactions.

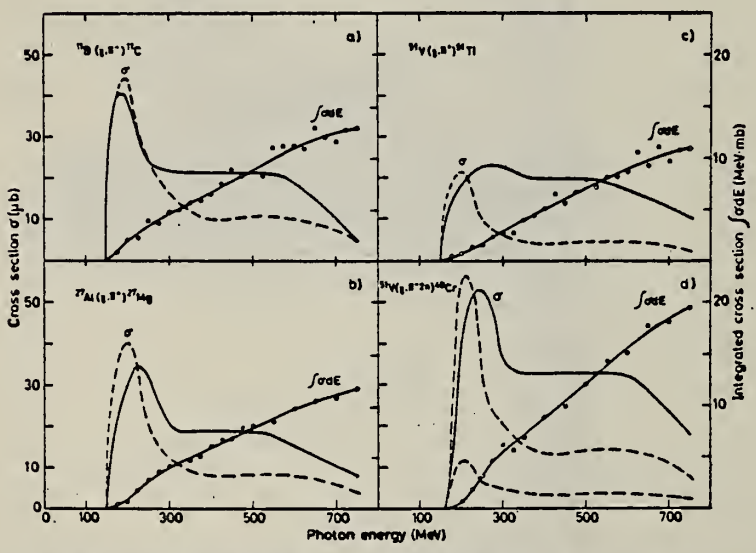

Fig. 4. Experimentally determined true and integrated cross sections. Theoretical calculations of the cross sections are marked with dashed lines.

REF. S. W. Robinson, C. P. Swann, V. K. Rasmussen
Phys. Rev. 174, 1320 (1968)

ELEM. SYM.	A	Z
Al	27	13

METHOD

REF. NO.	
68 Ro 1	HMG

REACTION	RESULT	EXCITATION ENERGY	SOURCE		DETECTOR		ANGLE
			TYPE	RANGE	TYPE	RANGE	
G,G	LFT	3.0	C	3	NAI-I		
		(3.0,2.98,2.21)					

SELF-ABSORPTION

Energy(MeV)	Γ_o/Γ	Γ (MeV)
3.00	0.87	6.1 ± 1.2
2.98	~ 1.0	$125. \begin{smallmatrix} + 14 \\ - 13 \end{smallmatrix}$
2.21	~ 1.0	$17.6 \begin{smallmatrix} + 2.9 \\ - 3.3 \end{smallmatrix}$

Note - Analysis based on single scattered photon spectrum measured with 30-cc Ge(Li) detector.

D. W. Anderson, A. J. Bureau, B. C. Cook, T. J. Englert
Phys. Rev. 183, 978 (1969)

ELEM. SYM.	A	Z
Al	27	13

METHOD

REF. NO. 69 An 3 hmg

REACTION	RESULT	EXCITATION ENERGY	SOURCE TYPE	SOURCE RANGE	DETECTOR TYPE	DETECTOR RANGE	ANGLE
G,N	RLX	13-65	C	13-65	ACT-I		4PI

Data normalized to measurements previously reported.

360

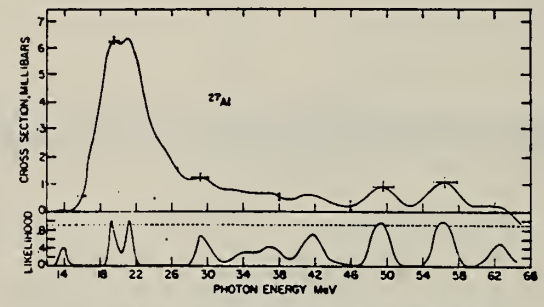

FIG. 4. The least-structure cross-section solution, $\sigma=\sigma_n+0.9\sigma_{2n}$, for aluminum. Vertical bars indicate errors in cross section. The experimental timing was such that the contribution due to the reaction $Al^{27}(\gamma, 2n)Al^{25}$ was depressed relative to the contribution due to the $Al^{27}(\gamma, n)Al^{26g}$ reaction. A likelihood estimate of the statistical certainty of the indicated structure is also shown.

[13] A. S. Penfold and J. E. Leiss, Phys. Rev. 114, 1332 (1959).

TABLE I. Peak energies for the cross-section maxima of Figs. 4 and 5. All maxima with greater than 70% likelihood as computed from the cross-section errors[a] are shown. Maxima with less than 90% likelihood are doubtful.

Al^{27} Energy (MeV)	Likelihood	Si^{28} Energy (MeV)	Likelihood
(41.6±1.0)	0.72	(27.1±0.5)	0:90
49.4±0.8	0.96	(31.4±0.4)	0.88
56.3±0.9	0.98	(3.47±0.6)	0.86
		(40.1±0.9)	0.89
		(46.4±0.8)	1.00
		52.2±0.8	1.00
		58.2±1.0	0.98

[a] B. C. Cook (to be published).

S. Costa, L. Ferrero, L. Pasqualini, C. Manfredotti
Lettere al Nuovo Cimento 2, 318 (1969)

ELEM. SYM.	A	Z
Al	27	13

METHOD

REF. NO.: 69 Co 2 | egf

REACTION	RESULT	EXCITATION ENERGY	SOURCE		DETECTOR		ANGLE
			TYPE	RANGE	TYPE	RANGE	
G,XN	ABX	15-35	D	15-35	BF3-I		4PI

536

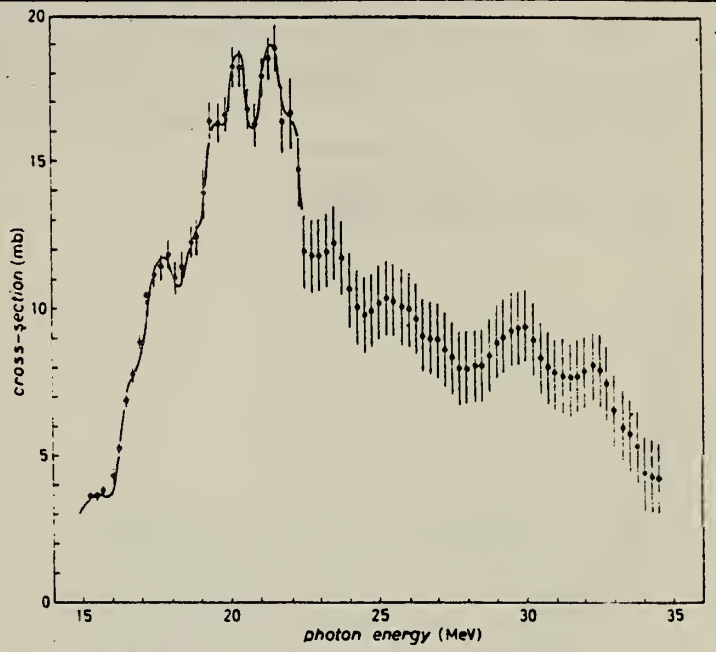

Fig. 1. – Photoneutron cross-section for ^{27}Al. The solid line represents a fit obtained with eight Lorentz curves.

TABLE I. – *Energy levels observed in* ^{27}Al.

(γ, Tn) (a)				(γ, n) + (γ, np) (b)		(γ, n) (c)		(γ, n) + (γ, np) (d)	
E_m (MeV)	Γ (MeV)	σ_t (mb)	σ_m (mb)	E_m (MeV)	σ_m (mb)	E_m (MeV)	σ_m (mb)	E_m (MeV)	σ_m (mb)
				13.8	1.2				
				14.5	1.5				
15.3	1.2	3.4	3.7	15.4	2.5	15.2	1.3		
						16.1	6.0		
16.5	0.5	2.2	7.6	16.4	5.2	16.4	6.0	16.4	4.2
				17.0	5.7	17.0	6.3		
17.7	1.7	11.8	11.8	17.7	8.5	17.6	10.7		
				18.2	11.0	18.1	17.3	18.1	10.6
18.7	0.4	3.4	12.5						
19.5	0.8	14	16.4			19.6	17.3		
				20.0	12.9			19.8	12.6
20.3	0.6	12	18.7			20.5	17.3		
21.4	1.2	19	19.1	21.5	14.8	21.2	18.3	21.4	12.2
				22.0	13.8				
22.3	0.6	10	16.6			22.4	13.3		

(a) Present work: E_m is the energy at which the maximum cross-section occurs, Γ and σ_t are the width at half maximum and the maximum of the Lorentz curve, σ_m is the experimental cross-section at E_m.
(b) See ref. (3).
(c) See ref. (2).
(d) See ref. (1).

(1) L. N. BOLEN and W. D. WHITEHEAD: *Phys. Rev. Lett.*, 9, 158 (1962).
(2) M. N. THOMSON, J. M. TAYLOR, B. M. SPICER and J. E. BAGLIN: *Nucl. Phys.*, 64, 486 (1965).
(3) S. C. FULTZ, J. T. CALDWELL, B. L. BERMAN, R. L. BRAMBLETT and R. R. HARVEY: *Phys. Rev.*, 143, 790 (1966).

REF.

S. Costa, L. Ferrero, R. Garfagnini, G. Piragino and A. Zanini
Lettere al Nuovo Cimento 2, 336 (1969)

Al	27	13

METHOD

REF. NO. 69 Co 4 hmg

REACTION	RESULT	EXCITATION ENERGY	SOURCE		DETECTOR		ANGLE
			TYPE	RANGE	TYPE	RANGE	
G,P	ABY	8-85	C	85	CCH-D	4-21	180

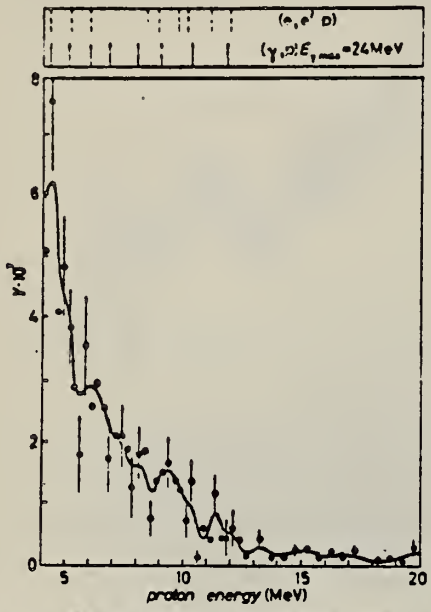

Fig. 1. – Energy spectrum and absolute yield (protons/MeV sr(cm²/MeV mol)) of photoprotons from ^{27}Al at 180° of 0.6 sr solid angle, produced with an $E_{\gamma max}$ = = 85 MeV bremsstrahlung spectrum. In the upper part the location of the proton groups found in our experiment and in ref. (**) is indicated.

REF.

C. B. Fulmer, I. R. Williams, K. S. Toth, G. F. Dell
Phys. Rev. 188, 1752 (1969)

ELEM. SYM.	A	Z
Al	27	13

METHOD

REF. NO. 69 Fu 2 hmg

REACTION	RESULT	EXCITATION ENERGY	SOURCE		DETECTOR		ANGLE
			TYPE	RANGE	TYPE	RANGE	
G,SPL	RLY	THR-999	D	999	ACT-I		DST
		(THR- 3 GEV)		(3 GEV)			

Relative thick target yield as a function of target thickness. 999 = 3 GEV

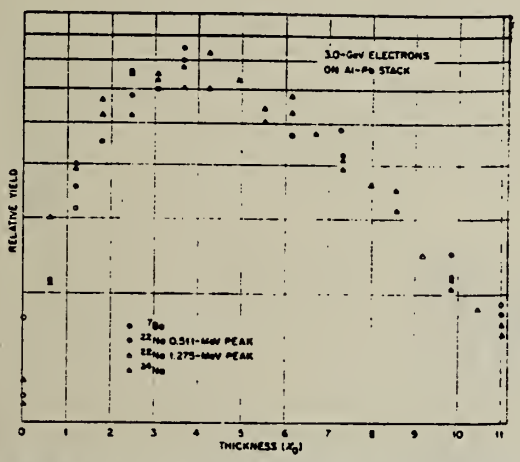

FIG. 5. Relative yields of ^{7}Be, ^{22}Na, and ^{24}Na produced in aluminum foils in a thick lead target bombarded with 3.0-GeV electrons. The data for the various nuclides are normalized at the peaks of the yield curves.

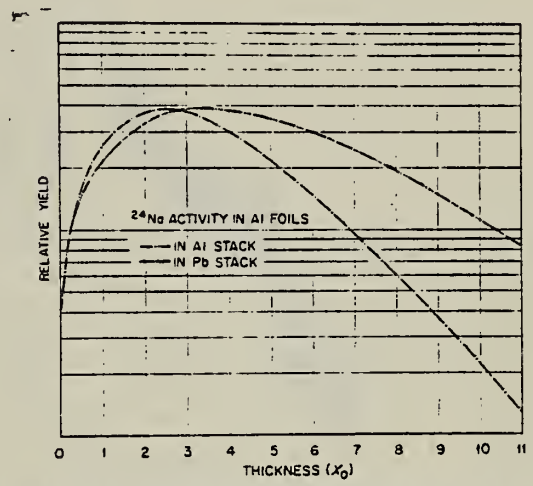

FIG. 6. Relative yields of ^{24}Na produced in thick targets bombarded with 3.0-GeV electrons.

	Punched	Checked w/PO
[illegible] Ctrl DATA	3/22	✓
[illegible] REFERENCE	3/22	✓

REF.	ELEM. SYM.	A	Z
B.S. Ishkhanov, I.M. Kapitonov, E.V. Lazutin, I.M. Piskarev and V.G. Shevchenko Izv. Akad. Nauk. Fiz. 33, 1742 (1969) Bull. Acad. Sci. USSR-Phys. 33, 1594 (1969)	Al	27	13

METHOD	REF. NO.	
	69 Is 3	hmg

REACTION	RESULT	EXCITATION ENERGY	SOURCE		DETECTOR		ANGLE
			TYPE	RANGE	TYPE	RANGE	
G,XN	ABX	13-30	C	5-30	BF3-I		4PI

453

$\int_{13}^{30} \sigma dE = 185 \pm 20$ MeV mb

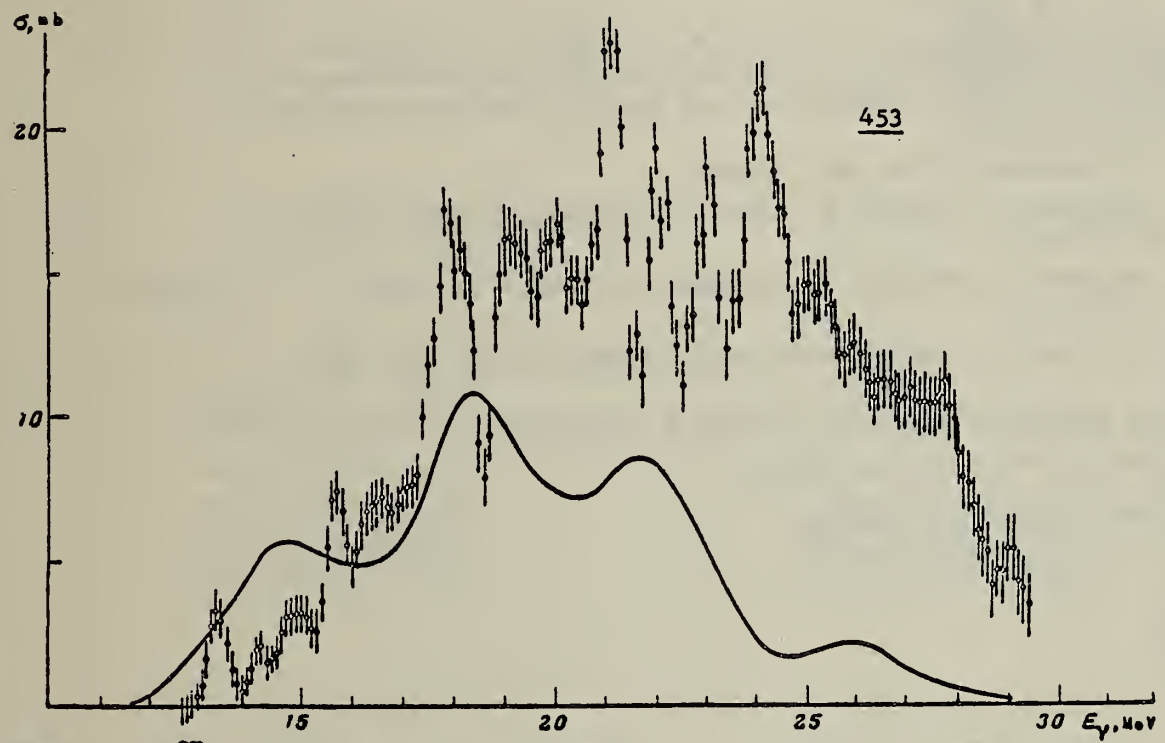

Fig.1. The $^{27}Al(\gamma,n)$ cross section. The calculated curve is from Ref. 13.

(over)

Positions (MeV) of Resonances in $^{27}Al(\gamma,n)$ and $^{31}P(\gamma,n)$

Aluminum					Phosphorous		
Our work	Ref.4	Ref.9	Ref.10	Ref.7	Our work	Ref.6	Ref.8
13,3		—	—		12,8		
	13,8			13,7	13,7		13,3
14,1		14,2					
	14,5	14,5	14,6		14,3		
14,9				14,7			
	15,4	15,2			14,8	14,75	14,6
15,6	15,7	15,6		15,75	15,4	15,75	
		16,1			16,2		15,8
16,5	16,4	16,4	16,4				17,1
	17,0	17,0		17,1	17,7	17,25	17,5
18,0	17,7	17,6					
	18,2	18,1	18,1	18,25	18,4	18,25	
19,1				19,1	19,3	19,25	19,0
		19,6					
20,0	20,0		19,8		20,5	20,25	20,3
		20,5			21,3	21,25	
21,1		21,2	21,4		22,0		
	21,5					22,75	
22,0	22,0				23,6		
		22,4			24,6	24,25	
23,0	23,1						
24,1					27,5		
25,0							
27,8	27,2						

[4] A.N. Tikhonov, V.G. Shevchenko, V.Ya. Galkin, B.I. Goryachev, P.N. Zaikin, B.S. Ishkhanov & I.M. Kapitonov, Program and Abstracts for the Eighteenth Annual Conference on Nuclear Spectroscopy and Nuclear Structure, Riga, M.-L., 1968, p. 268.

[6] L.N. Bolen & W.D. Whitehead, Ibid. 132, 5 (1965).

[7] N. Mutsuro, K. Kageyama, M. Mishina, E. Tanaka & M. Kimura, J. Phys. Soc. Japan 17, 1673 (1962).

[8] N. Mutsuro, K. Kageyama, M. Mishina, T. Nakagawa, E. Tanaka & M. Kimura, Ibid. 17, 1672 (1962).

[9] M.N. Thompson, J.M. Taylor, B.M. Spicer & J.E.E. Baglin, Nuclear Phys. 64, 486 (1965).

[10] L.N. Bolen & W.D. Whitehead, Phys. Rev. Letters 9, 458 (1962).

[13] J.E.E. Baglin, Nuclear Phys. 22, 216 (1961).

V. I. Noga, Yu. N. Ranyuk, and P. V. Sorokin
Yad. Fiz. 9, 1152 (1969)
Sov. J. Nucl. Phys. 9, 673 (1969)

Al	27	13

METHOD

REF. NO. 69 No 1 egf

REACTION	RESULT	EXCITATION ENERGY	SOURCE		DETECTOR		ANGLE
			TYPE	RANGE	TYPE	RANGE	
G,NA24	ABY	31-999	C	100-999	ACT-I		4PI

999 = 1.2 GEV

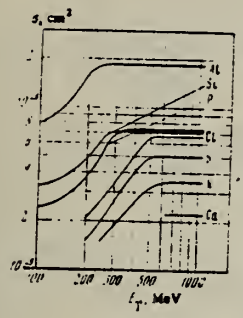

FIG. 2. Cross sections as a function of γ-ray energy.

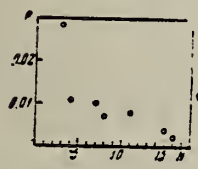

FIG. 3. Dependence of P on number of nucleons which have left the nucleus.

Table I

Reaction	Nucleons emitted	Threshold,* MeV	Target	Distribution of isotopes, %
$Al^{27} \rightarrow Na^{24}$	2p, α	31	Al	100
$Si^{28} \rightarrow Na^{24}$	3p, α	43	Si	92.27
$P^{31} \rightarrow Na^{24}$	4p, 3n	60	P	100
$S^{32} \rightarrow Na^{24}$	5p, 3n	78	S	95.02
$Cl^{35} \rightarrow Na^{24}$	6p, 5n	101	NH_4Cl	75.5
$K^{39} \rightarrow Na^{24}$	8p, 7n	140	K_2CO_3	93.08
$Ca^{40} \rightarrow Na^{24}$	9p, 7n	148	CaO	96.97

*The threshold was calculated as the binding energy of the emitted nucleons.

Table II. Cross sections for reactions in the saturation region

Reaction	$\int \sigma_0 dE_\gamma$, 10^{-28} cm^2	Reaction	$\int \sigma_0 dE_\gamma$, 10^{-28} cm^2
$Al^{27} \rightarrow Na^{24}$	185±20	$Cl^{35} \rightarrow Na^{24}$	68±7
$Si^{28} \rightarrow Na^{24}$	72±8	$K^{39} \rightarrow Na^{24}$	35±5
$P^{31} \rightarrow Na^{24}$	71±8	$Ca^{40} \rightarrow Na^{24}$	22±5
$S^{32} \rightarrow Na^{24}$	52±6		

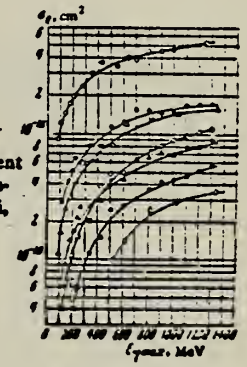

FIG. 1. Cross section σ_0 per equivalent photon as a function of maximum bremsstrahlung energy. Points: O – Al, ● – Si, Δ – P, ▲ – S, □ – Cl, ■ – K, ◇ – Ca.

According to the photomesonic mechanism, the cross section for the reaction can be written in the form

$$\sigma = \sigma_0 AP. \quad (1)$$

Here σ_0 is the total cross section for interaction of the photon with a free nucleon with inclusion of the nucleon motion in the nucleus (σ_0, as has been shown by Roos and Peterson,[6] depends only weakly on photon energy for $E_\gamma > 300$ MeV); A is the number of nucleons in the nucleus, and P is the probability that the reaction will proceed by a given channel.

REF. V. V. Verbinski and W. R. Burrus
Phys. Rev. 177, 1671 (1969)

ELEM. SYM.	A	Z
Al	27	13

METHOD

REF. NO.	
69 Ve 1	hmg

REACTION	RESULT	EXCITATION ENERGY	SOURCE		DETECTOR		ANGLE
			TYPE	RANGE	TYPE	RANGE	
G,XN	SPC	THR-33	C	33	TOF-D	0-14	DST

TABLE II. (γ,n) reactions induced by 33-MeV end-point thin-target bremsstrahlung.

Target	E_γ giant resonance peak (MeV)	θ	T* (MeV)	Thresholds (γ,n)	(γ,pn)	(γ,2n)
^{27}Al	~22	55°	3.07 ± 0.1	13.1	19.4	24.4
		93°	3.07 ± 0.1			
^{nat}Pb	~13	90°	1.50 ± 0.1	8.0	14.8	14.8
		141°	1.43 ± 0.1			
^{206}Pb	~13	90°	1.52 ± 0.1	7.4	14.8	14.1
		141°	1.52 ± 0.1			
^{209}Bi	~13	90°	1.66 ± 0.1	7.4	11.1	14.3
		141°	1.47 ± 0.1			

* From plot of $\ln[\phi(E)/\sigma_c E^{3/2}]$ versus E.

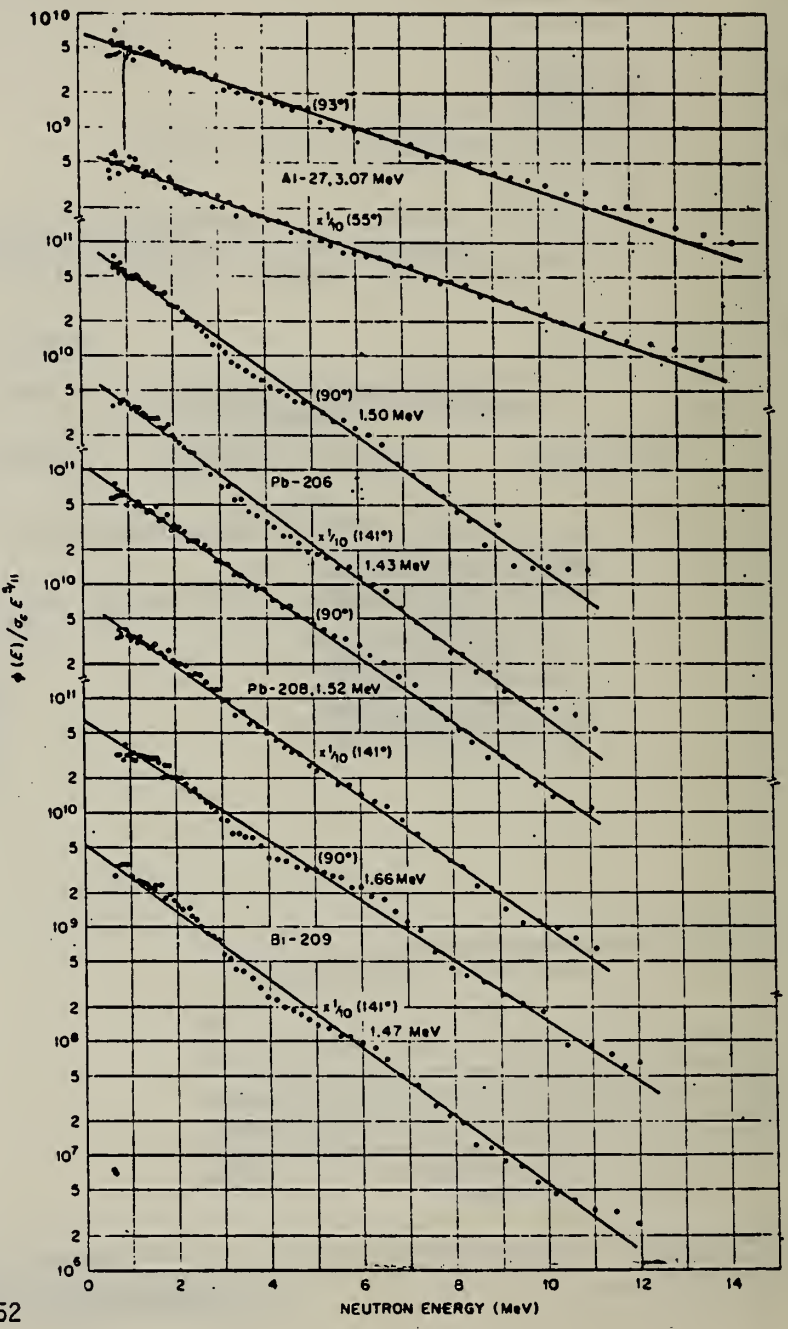

FIG. 7. Evaporation-analysis plots of neutron spectra from (γ,n) reactions. The logarithmic plots of $\phi(E)/(\sigma_c E^{3/2})$ show moderately good straight-line fits. Values of T, the magnitude of the reciprocal slope, are shown. In some cases, T is slightly higher at 90° than at 141°, indicating that a weak component of direct emissions is present. These are preferentially emitted at 90°, the direction of the electromagnetic field.

REF. Yu. P. Antuf'ev, V. L. Agranovich, V. G. Ganenko, V. S. Kuz'menko, I. I. Miroshnichenko, and P. V. Sorokin
Yad. Fiz. 12, 1143 (1970); Sov. J. Nucl. Phys. 12, 627 (1971)

ELEM. SYM.	A	Z
Al	27	13

METHOD

REF. NO. 70 An 5 hmg

REACTION	RESULT	EXCITATION ENERGY	SOURCE		DETECTOR		ANGLE
			TYPE	RANGE	TYPE	RANGE	
E,P	RLY	88-999	C	999	TEL-D	80-265	DST

999 = 1140 MEV

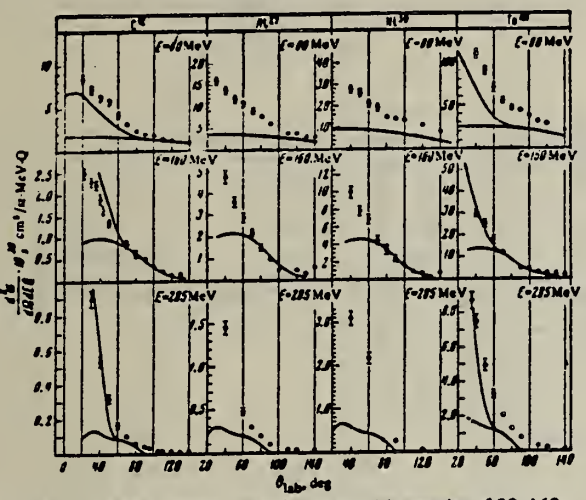

FIG. 1. Angular distributions of protons with energies of 80, 160, and 285 MeV produced from C^{12}, Al^{27}, Ni^{59}, and Ta^{181} nuclei by photons with maximum energy 1140 MeV. Only the statistical errors are shown.

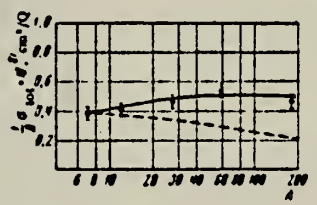

FIG. 3

FIG. 3. Total cross section for proton production per nucleon. $E_{\gamma\,max}$ = 1140 MeV. Dashed curve—theory from ref. 11.

[11] K. S. Kölbig and B. Margolis, Nucl. Phys. B6, 85 (1968).

S. Costa, L. Ferrero, G. Garfagnini, L. Pasqualini, G. Piragino and A. Zanini
Nuovo Cimento 72A, 517 (1970)

Al	27	13

METHOD

REF. NO. 70 Co 2 egf

REACTION	RESULT	EXCITATION ENERGY	SOURCE		DETECTOR		ANGLE
			TYPE	RANGE	TYPE	RANGE	
G,P	RLY	8-34	C	-85	TEL-D	6-20	DST

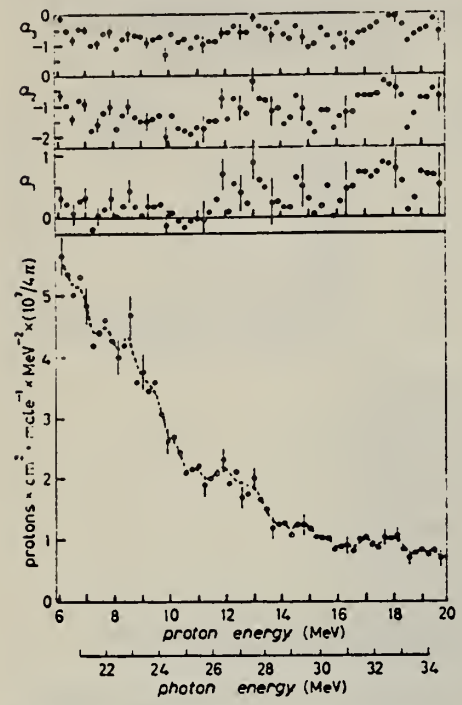

Fig. 1. – Integrated yield of photoprotons from ^{27}Al (bottom) and Legendre expansion coefficients a_1, a_2, a_3 (top), as a function of proton energy. The photon energy scale is drawn according to ref. ([20]).

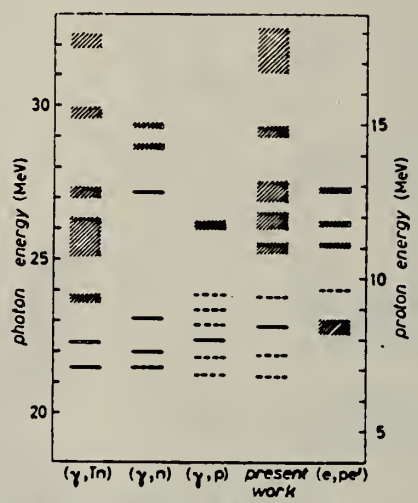

Fig. 2. – Comparison among the structures observed in ^{27}Al photodisintegration: *a*) (γ, Tn) total neutron cross-section (ref. ([28])), *b*) (γ, n) cross-section (ref. ([29])), *c*) photoproton spectrum (ref. ([20])), *d*) photoproton spectrum, present work, *e*) photoprotons spectrum, virtual photons (ref. ([19])).

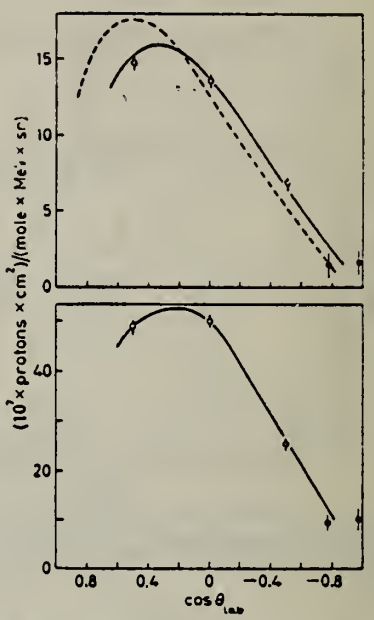

Fig. 3. – Quasi-deuteron model, dotted line, and one-particle direct-interaction, solid line, angular distributions (calculated as described in the text) fitting the experimental data for $6 < E_p < 20$ MeV (bottom) and $12 < E_p < 20$ MeV (top). The open circles represent solid-state detector measurements, the dots are data obtained with the diffusion cloud chamber.

[19] K. Shoda, T. Ishizuka, K. Shimizu and M. Akashi: Journ. Phys. Soc. Japan 17, 1536 (1962).

[20] W. R. Dodge and W. C. Barber: Phys. Rev. 127, 1746 (1962).

[28] S. Costa, L. Ferrero, L. Pasqualini and C. Manfredotti: Lett. Nuovo Cimento 2, 318 (1969).

[29] S. C. Fultz, J. T. Caldwell, B. L. Berman, R. L. Bramblett and R. R. Harvey: Phys. Rev. 143, 790 (1966).

REF. L. A. Currie and R. H. Rodriguez-Pasques
Nucl. Phys. A157, 49 (1970)

ELEM. SYM.	A	Z
Al	27	13

METHOD

REF. NO. 70 Cu 1 egf

REACTION	RESULT	EXCITATION ENERGY	SOURCE		DETECTOR		ANGLE
			TYPE	RANGE	TYPE	RANGE	
G,T	ABY	THR-90	C	90	ACT-I		4PI

TABLE 4

Bremsstrahlung-weighted and integrated (γ, t) cross sections (90 MeV)

	^{27}Al	Zn	Sn	^{209}Bi
σ_{-1}(mb)	0.072	0.007_4	0.065	0.007_3
σ_0(MeV · mb)	4.0	0.4_2	3.8	0.4_1

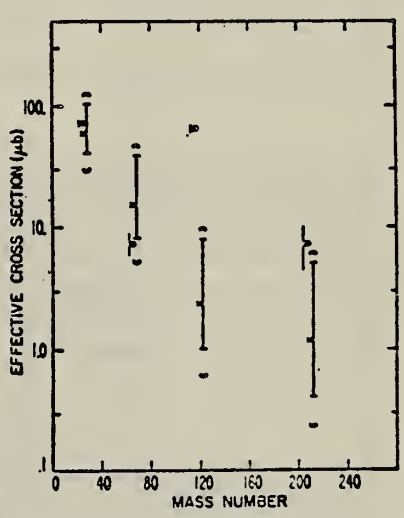

Fig. 3. Experimental (o) and statistical model (x) absolute phototriton yields (90 MeV). Yields, expressed in terms of "effective cross sections" (μb), are plotted versus mass number. Limits for the experimental yields represent ± one standard deviation; those for the calculated yields correspond to limiting values for the level density parameter (—) and for the photon absorption cross section (⊃).

	Punched	Checked w/PO
IBM Card DATA	6/9/71	✓
IBM Card REFERENCE	"	✓

REF. C. B. Fulmer, K. S. Toth, I. R. Williams, T. H. Handley, G. F. Dell, E. L. Callis, T. M. Jenkins, and J. M. Wyckoff
Phys. Rev. C2, 1371 (1970)

ELEM. SYM.	A	Z
Al	27	13

METHOD

REF. NO. 70 Fu 1 hmg

REACTION	RESULT	EXCITATION ENERGY	SOURCE TYPE	SOURCE RANGE	DETECTOR TYPE	DETECTOR RANGE	ANGLE
E,F	RLY	999	D	999	ACT-D		4PI

Evidence of a fissionlike process for nuclides with a mass < 35.

999 = 1.5-16.0 GEV

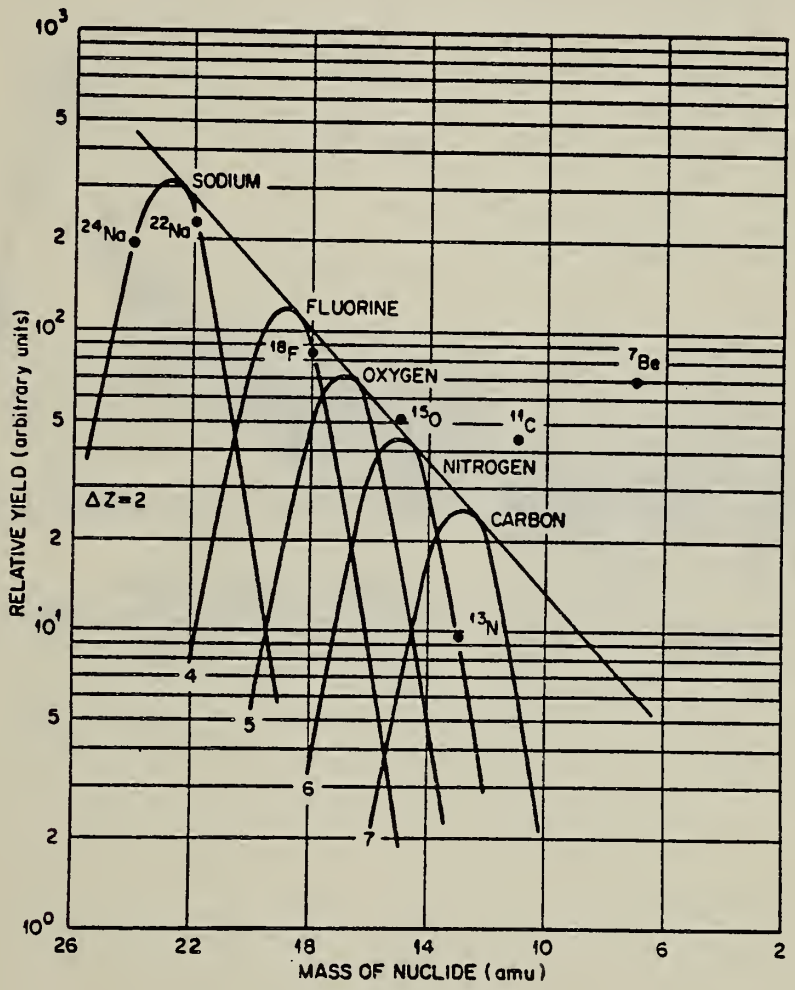

FIG. 4. Yields of radionuclides observed in a thin aluminum target bombarded with 16.0-GeV electrons versus mass of nuclides.

[over]

TABLE I. Ratio of yields of nuclides used to determine values of K. ^{44}Sc yields include 4.0-h ^{44}Sc and 2.4-day ^{44}Sc^{m}, which for the 1.5-, 3.0-, and 5.0-GeV data were assumed to be twice the yield of ^{44}Sc^{m}.

Energy (GeV)	Target	Nuclides	Ratio of yields (experimental)	$\Delta Z_1 - \Delta Z_2$	K
1.5	iron	^{51}Cr/^{44}Sc	6.2	3	1.86
3.0	iron	^{51}Cr/^{44}Sc	8.4	3	2.03
5.0	iron	^{51}Cr/^{44}Sc	5.95	3	1.82
16	iron	^{51}Cr/^{44}Sc	4.0	3	1.59
16	aluminum	^{22}Na/^{18}F	2.7	2	1.64
0.32	arsenic		(Halpern *et al.*)[a]		2.3

[a] See Ref. 19. I. Halpern, R. J. Debs, J. T. Eisinger, A. W. Fairhall, and H. G. Richter, Phys. Rev. 97, 1327 (1955).

REF.

J. Ahrens, H. Borchert, H.B. Eppler, H. Gimm, H. Gundrum, P. Riehn, G. Sita Ram, A. Zieger, and B. Ziegler
Elba-71, Tagungsbericht Elektronen Beschleuniger Arbeits Gruppen (Sept. 1971) Justus Liebig-Universitat Giessen.

ELEM. SYM.	A	Z
Al	27	13

METHOD

REF. NO. 71 Ah 1 hmg

REACTION	RESULT	EXCITATION ENERGY	SOURCE		DETECTOR		ANGLE
			TYPE	RANGE	TYPE	RANGE	
G,MU-T	ABX	THR-150	C	10-150	MGC-D		4PI

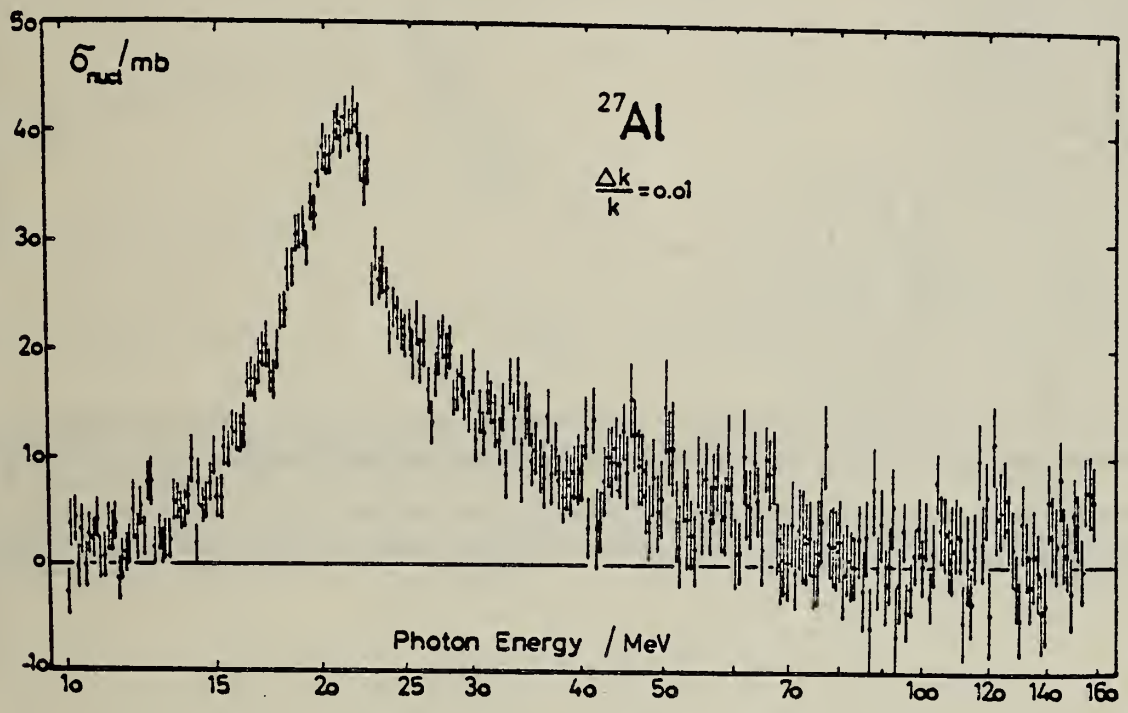

fig. 6

REF. Yu. P. Antuf ev, V.I. Agranovich, V.B. Ganenko, V.S. Kuz menko, I.I. Miroshnichenko, and P.V. Sorokin
Yad. Fiz. 14, 898 (1971)
Sov. J. Nucl. Phys. 14, 502 (1972)

ELEM. SYM.	A	Z
Al	27	13

METHOD

REF. NO.	
71 An 2	hmg

REACTION	RESULT	EXCITATION ENERGY	SOURCE		DETECTOR		ANGLE
			TYPE	RANGE	TYPE	RANGE	
G,XD	ABX	107-999	C	999	MAG-D		DST

999= 1.14 GEV

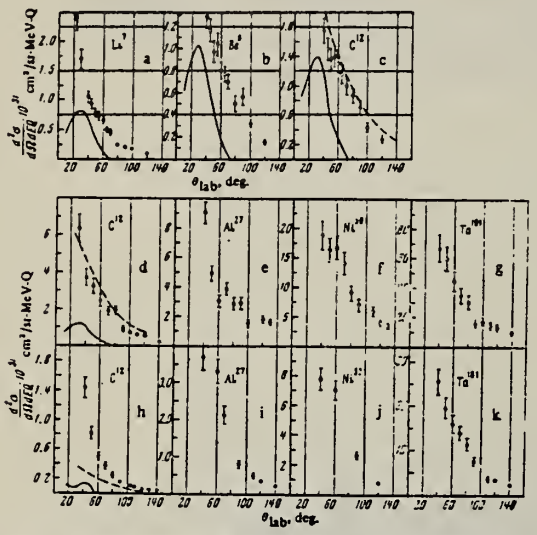

FIG. 1. Angular distributions of deuterons in (γ, d) reactions in nuclei for E_0 = 620 MeV (a–c) and E_0 = 1140 MeV (d–k). The statistical errors are shown. a–g–angular distributions of deuterons with energies of 90 MeV, h–k–with energy 160 MeV.

EF.

S. Costa, L. Ferrero, L. Pasqualini, and E. Mancini
Lettere al Nuovo Cimento 2, 665 (1971)

ELEM. SYM.	A	Z
Al	27	13

ETHOD

REF. NO.	
71 Co 2	egf

REACTION	RESULT	EXCITATION ENERGY	SOURCE		DETECTOR		ANGLE
			TYPE	RANGE	TYPE	RANGE	
G,XN	ABI	36-64	C	10-64	BF3-I		4PI

FAST N YIELD

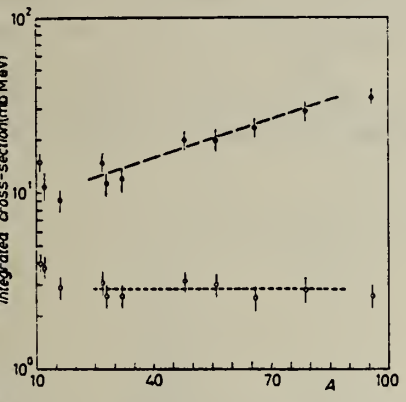

ig. 2.

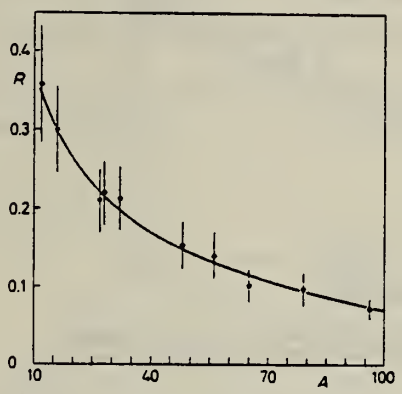

Fig. 3.

ig 2. – Experimental photoneutron cross-sections integrated over photon energy between 36 and 4 MeV and divided by NZ/A are plotted as a function of the mass number. Black dots are total cross-ections not corrected for neutron multiplicity; open circles represent fast neutron cross-sections (see ext). The dashed lines are drawn only to guide the eye.

ig. 3. – The ratio between « fast » and total photoneutron integrated cross-sections as a function of he mass number A. The solid line represents a fit of the ratios calculated for some nuclei by taking nto account the theoretical neutron energy spectra given by GABRIEL and ALSMILLER (4) and the effi-iencies of our detector (see Fig. 1).

REF.	ELEM. SYM.	A	Z
V. DiNapoli, A.M. Lacerenza, F. Salvetti, H.G. de Carvalho, J. Benuzzi Martins Lettere al Nuovo Cimento 1, 835 (1971)	Al	27	13

METHOD	REF. NO.	
	71 Di 3	egf

REACTION	RESULT	EXCITATION ENERGY	SOURCE		DETECTOR		ANGLE
			TYPE	RANGE	TYPE	RANGE	
G,NA22	ABY	THR-999	C	300-999	ACT-I		4PI
G,NA24	ABY	THR-999	C	300-999	ACT-I		4PI

999 = 1 GEV

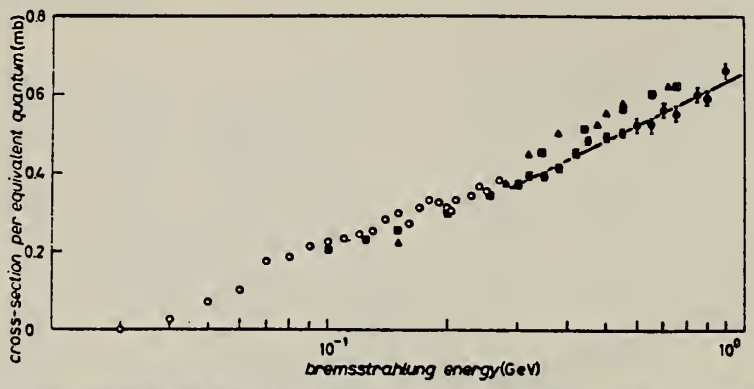

Fig. 1. – Cross-section data for the ^{27}Al(γ, 2p n)^{24}Na reaction: open circles, MEYER *et al.* (6); triangles, MASAIKE (7); squares, FRIBERG and FORKMAN (8); filled circles, present work. The straight line is a least-squares fit of the latter values.

[6] R.A. Meyer, W.B. Walters, J.P. Hummel: Nucl. Phys. 122A, 606 (1968).

[7] A. Masaike: Journ. Phys. Soc. Japan, 19, 427 (1964).

[8] B. Friberg and B. Forkman: Annual Report 1969, University of Lund, Lund Institute of Technology (Jan.70).

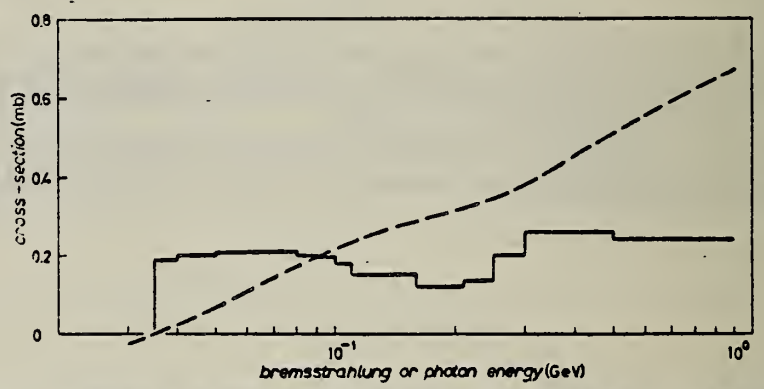

Fig. 2. – The smooth curve (dashed line) is a polynomial fit of the data reported in Fig. 1. The histogram (full line) represents the σ_e values obtained from the curve by means of the photon-difference method.

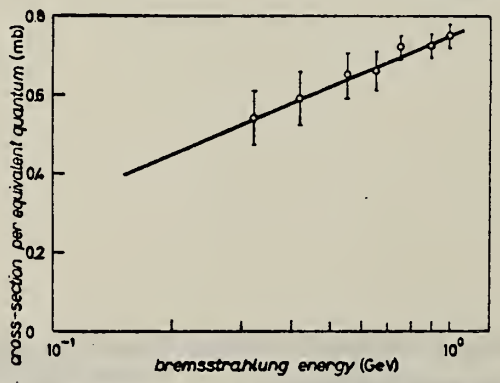

Fig. 3. – Cross-section values for the ^{27}Al(γ, 2p 3n)^{22}Na reaction. The straight line is a least-squares fit of these values.

REF. V. Di Napoli, D. Margadonna, F. Salvetti, H.G. De Carvalho, J.B. Martins
Nucl. Inst. Meth. 93, 77 (1971)

ELEM. SYM.	A	Z
Al	27	13

METHOD

REF. NO. 71 Di 5 hg

REACTION	RESULT	EXCITATION ENERGY	SOURCE		DETECTOR		ANGLE
			TYPE	RANGE	TYPE	RANGE	
G,NA24	ABY	23-999	C	300-999	ACT-I		4PI

The use of the $^{19}F(\gamma,n)^{18}F$, $^{27}Al(\gamma,x)^{24}Na$, $^{197}Au(\gamma,n)^{196}Au$, and $^{12}C(\gamma,x)^{7}Be$ reactions as absolute monitors for high-energy, high-intensity bremsstrahlung beams is discussed. The cross sections per equivalent quantum and the absolute cross sections, in the energy range 300-1000 MeV, are reported for these reactions. $^{19}F(\gamma,n)^{18}F$, $^{27}Al(\gamma,x)^{24}Na$, and $^{12}C(\gamma,x)^{7}Be$ reactions are proposed as very simple and suitable systems for monitoring purposes.

999 = 1 GEV

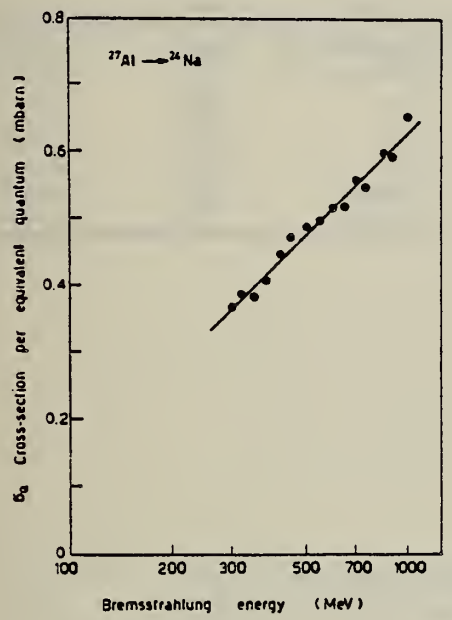

Fig. 2. $^{27}Al \rightarrow ^{24}Na$ reaction cross sections per e.q. The straight line is a least-squares fit of the experimental values.

TABLE 2

Energy (MeV)	σ_Q(mb) $^{19}F \rightarrow ^{18}F$	$^{27}Al \rightarrow ^{24}Na$	$^{197}Au \rightarrow ^{196}Au$ [a]	$^{12}C \rightarrow ^{7}Be$ [a]
260			270±14	
300	5.90±0.20	0.37±0.01	258±13	0.37±0.01
320		0.39±0.01		
350	5.90±0.20	0.39±0.01		0.38±0.01
380	5.95±0.20	0.41±0.01		
400				0.42±0.01
420		0.45±0.01		
450	5.95±0.20	0.48±0.01	249±12	0.44±0.02
500	6.65±0.20	0.49±0.01		
550	6.65±0.20	0.50±0.02		0.47±0.02
600	6.80±0.20	0.52±0.02		
650		0.52±0.02	266±13	0.47±0.02
700	7.20±0.30	0.56±0.02		
750		0.55±0.02		
850	7.60±0.30	0.60±0.02	246±12	0.49±0.03
900		0.59±0.02		
1000	7.10±0.30	0.66±0.02	249±12	0.51±0.03

[a] The values given in the last two columns are, in most cases, an average of two or more measurements (see figs. 3 and 4).

REF. C. B. Fulmer, K. S. Toth, I. R. Williams, and G. F. Dell
Phys. Rev. C4, 2123 (1971)

ELEM. SYM.	A	Z
Al	27	13

METHOD

REF. NO. 71 Fu 4 hmg

REACTION	RESULT	EXCITATION ENERGY	SOURCE TYPE	SOURCE RANGE	DETECTOR TYPE	DETECTOR RANGE	ANGLE
G,SPL	RLX	THR-999	D	999	ACT-I		4PI
		(5 GEV)		(5 GEV)			

Measurement of F values (the ratio of photodisintegration to electrodisintegration cross sections).

999 = 5 GEV

TABLE I. Experimentally measured *F* values for several nuclides produced in targets bombarded with 5-GeV electrons.

Target	Nuclide	*F*
Aluminum	^{24}Na	2.4 ± 0.4
Aluminum	^{7}Be	3.3 ± 0.5
Iron	^{52}Mn	2.0 ± 0.3
Iron	^{48}Cr	2.0 ± 0.2
Iron	^{44m}Sc	2.4 ± 0.4
Iron	^{24}Na	3.2 ± 0.4
Tantalum	^{175}Hf	2.0 ± 0.3
Tantalum	^{177}Lu	1.9 ± 0.4

REF. I.A. Grishaev, A.N. Krinitsyn, N.I. Lapin, V.I. Nikiforov, G.D. Pugachev, and B.I. Shramenko
Yad. Fiz. 14, 35 (1971)
Sov. J. Nucl. Phys. 14, 20 (1972)

ELEM. SYM.	A	Z
Al	27	13

METHOD

REF. NO. 71 Gr 2 hmg

REACTION	RESULT	EXCITATION ENERGY	SOURCE		DETECTOR		ANGLE
			TYPE	RANGE	TYPE	RANGE	
G,PI+	ABY	150-560		560	EMU-D		DST
G,PI-	ABY	150-560		560	EMU-D		DST

PI-/PI+ YIELD RATIO

Cross section for photoproduction of π^- and π^+ mesons for E_0 = 560 MeV

10^{-33} cm^2/sr·MeV·equiv-quant

Nucleus	θ = 60°: Data of ref. 1, T = 33 MeV π^+	θ = 60°: Our data, T = 40 MeV π^+	θ = 60°: Our data, T = 40 MeV π^-	θ = 120°: Our data, T = 40 MeV π^+	θ = 120°: Our data, T = 40 MeV π^-	θ = 120°: Our data, T = 60 MeV π^+	θ = 120°: Our data, T = 60 MeV π^-
C	21.4±0.8	20.6±1.5	26.2±2	27.6±2.1	36.8±2.8	21.8±2.1	26.8±2.6
Al	42.4±1.0	38.5±3	47.8±4	57±4	76±5.4	40.2±3.5	52±4.7
Cu	78.8±1.6	71.8±5.6	98±6.6	109±7.5	152±10.6	81.5±8.6	93.5±10.7
Pb				206±18.5	369±27	170±19	250±26.5

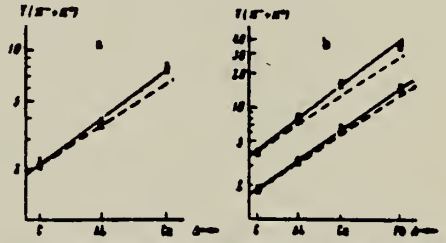

FIG. 1. Total yield of charged mesons as a function of atomic weight. The solid straight line is the experimental dependence, and the dashed straight line is the $A^{2/3}$ law. a – ϑ = 60°, T = 40 MeV; b – ϑ = 120°. Points: O – T = 40 MeV, Δ – T = 65 MeV.

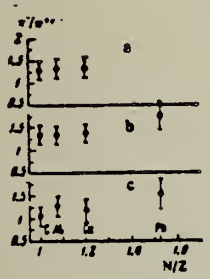

FIG. 3. π^-/π^+ yield ratio as a function of N/Z. a – ϑ = 60°, T = 40 MeV; b – ϑ = 120°, T = 40 MeV; c – ϑ = 120°, T = 65 MeV.

REF. G. J. Kumbartzki, Ung Kim and Ch. K. Kwan
Nucl. Phys. A160, 237 (1971)

ELEM. SYM.	A	Z
Al	27	13

METHOD

REF. NO. 71 Ku 2 egf

REACTION	RESULT	EXCITATION ENERGY	SOURCE		DETECTOR		ANGLE
			TYPE	RANGE	TYPE	RANGE	
G,SPL	ABY	THR-999	C	800-999	ACT-I		4PI

$\sigma_q(A,Z) = K\exp[PA-R(A-SZ+TZ^2)^2]$, cross section per equivalent quantum. 999 = 2.1 GEV

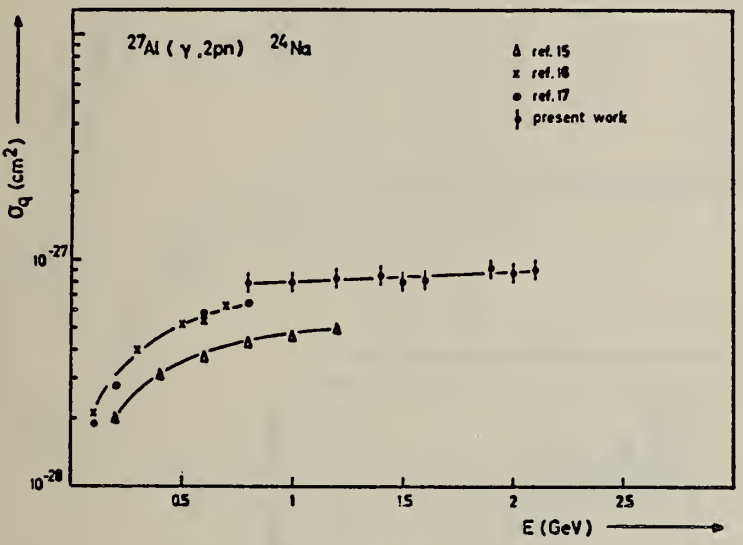

Fig. 2. Yields of the reaction $^{27}Al(\gamma, 2pn)^{24}Na$.

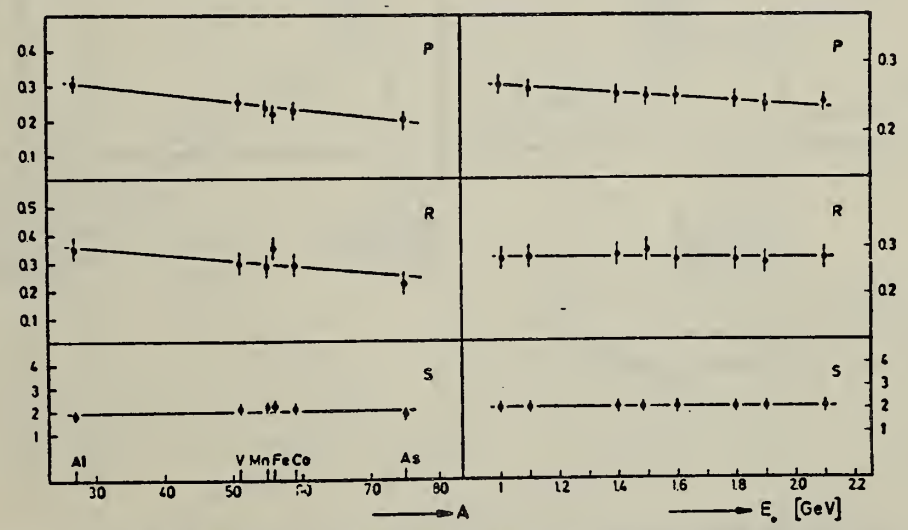

Fig. 6. Behaviour of the parameters *P*, *R* and *S* as functions of *A* and E_0.

[over]

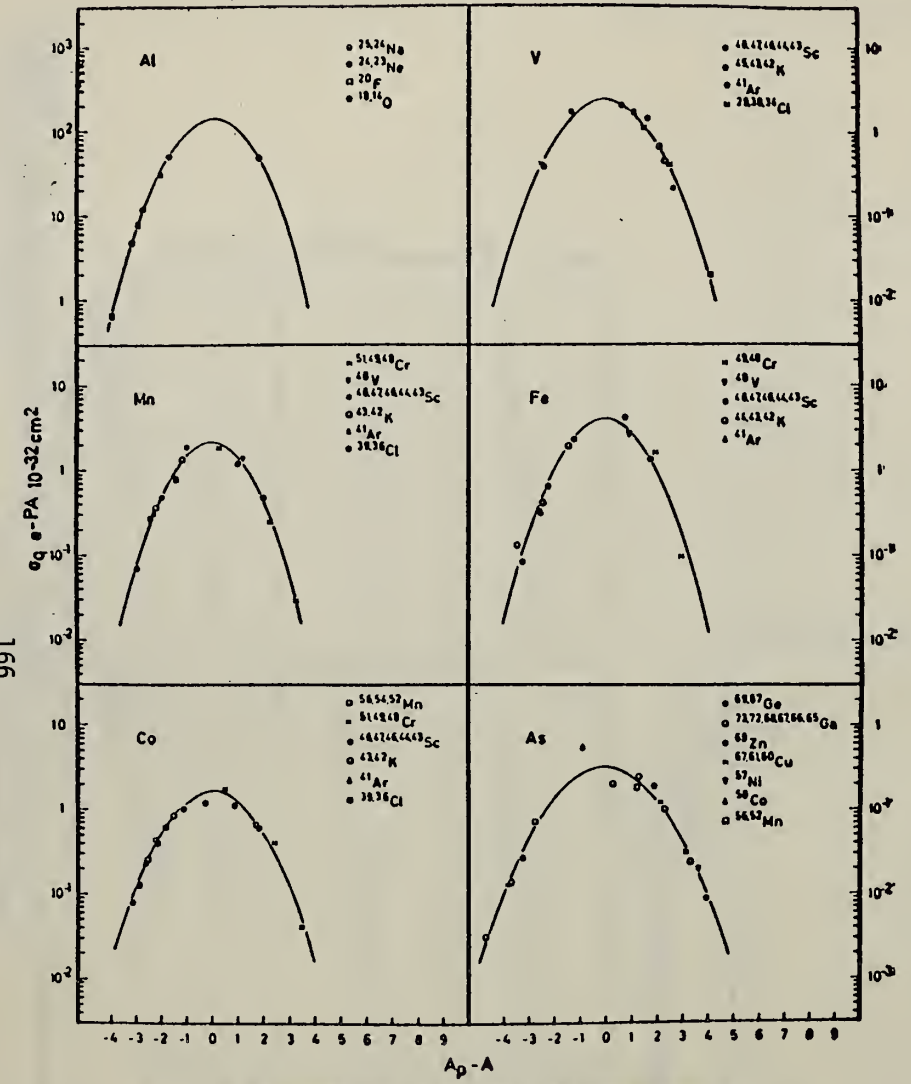

Fig. 4. Yield distributions from various targets with bremsstrahlung of 1.5 GeV.

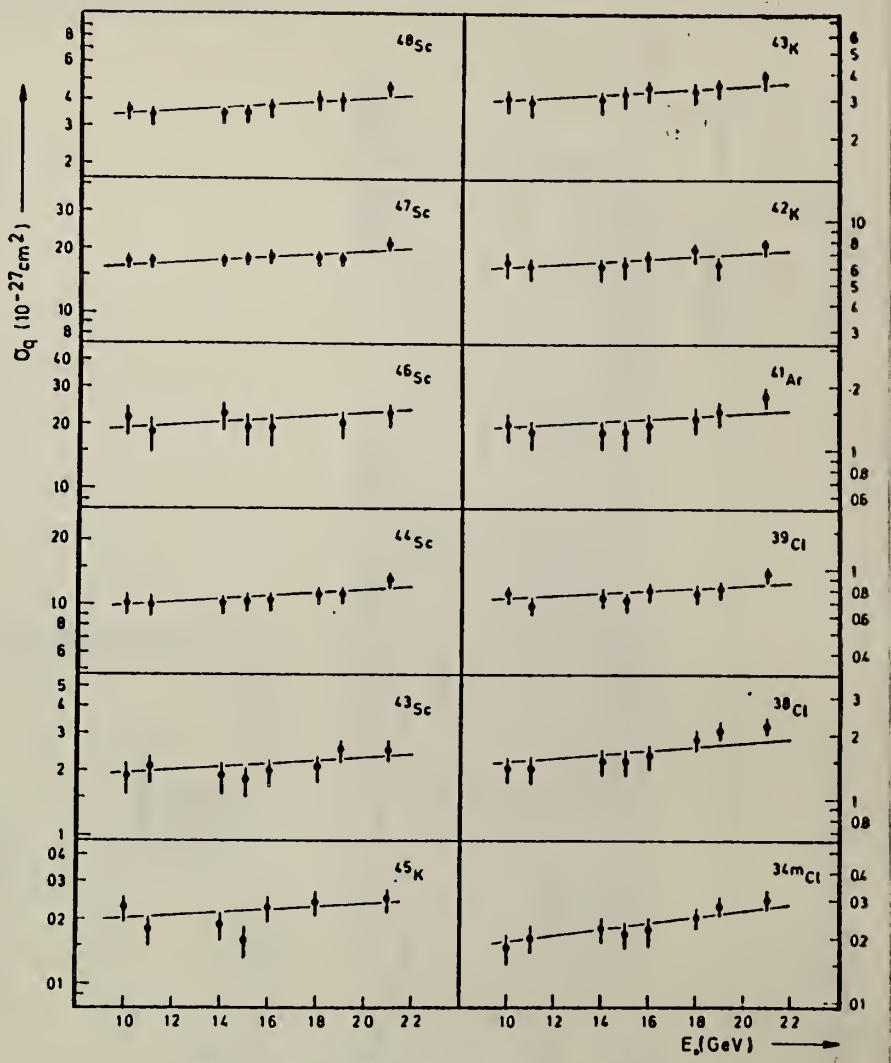

Fig. 5. Yields of spallation products using vanadium targets.

REF.

Tatsuya Saito
Bull. Chem. Soc. Japan 44, 1800 (1971)

ELEM. SYM.	A	Z
Al	27	13

METHOD

REF. NO.	
71 Sa 2	egf

REACTION	RESULT	EXCITATION ENERGY	SOURCE		DETECTOR		ANGLE
			TYPE	RANGE	TYPE	RANGE	
G,NA24	ABX	THR-250	C	20-250	ACT-I		4PI

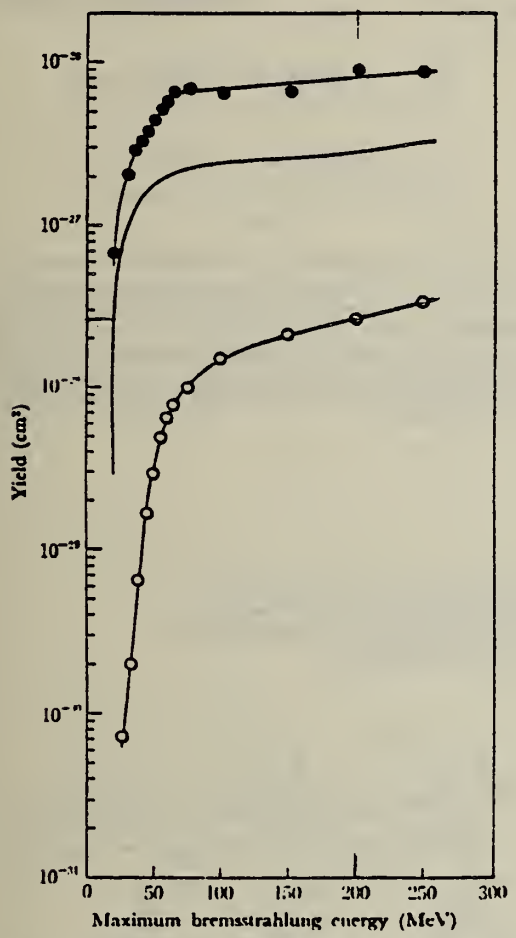

Fig. 3. The yield curves for the reactions $^{25}Mg(\gamma,p)^{24}Na$, $^{27}Al \rightarrow ^{24}Na$, and $^{12}C(\gamma,n)^{11}C$ as a monitor.
●: $^{25}Mg(\gamma,p)^{24}Na$, ○: $^{27}Al \rightarrow ^{24}Na$, ——: $^{12}C(\gamma,n)^{11}C$

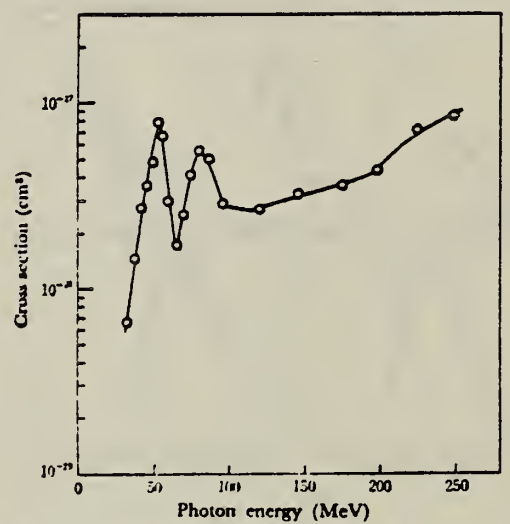

Fig. 6. The excitation function for the reaction $^{27}Al \rightarrow ^{24}Na$.

REF.	ELEM. SYM.	A	Z
V. G. Vlasenko, N. G. Afanas'ev, V. A. Gol'dshtein, S. V. Dementii, and E. L. Kuplennikov Yad. Fiz. 13, 259 (1971); Sov. J. Nucl. Phys. 13, 144 (1971)	Al	27	13

METHOD	REF. NO.	
	71 V1 1	hmg

REACTION	RESULT	EXCITATION ENERGY	SOURCE		DETECTOR		ANGLE
			TYPE	RANGE	TYPE	RANGE	
E,E/	FMF	0-300	D	592- 999	MAG-D		DST

999 = 1143

QUASIELASTIC SCTNG

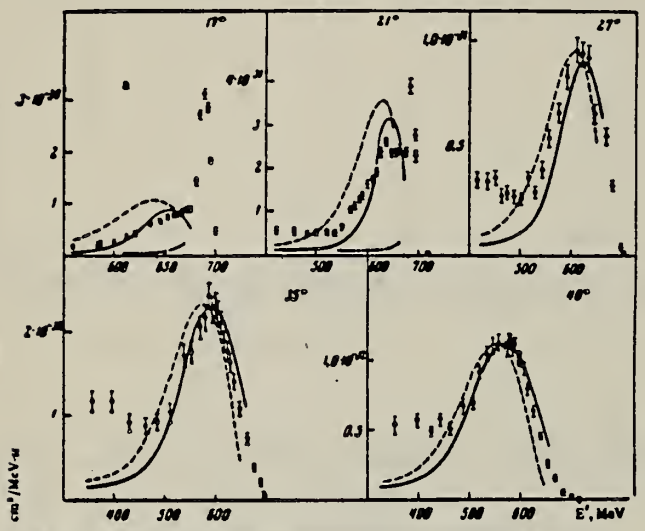

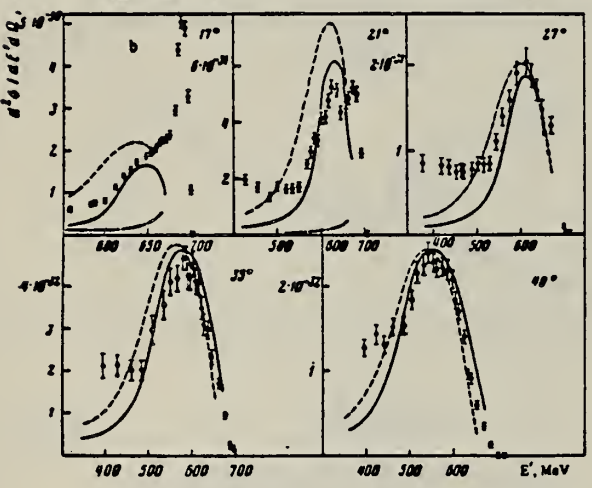

FIG. 1. Cross sections for scattering of 690-MeV electrons by B^{11} (a) and Al^{27} (b) at angles 17, 21, 27, 35, and 40°, as a function of scattered-electron energy. The dashed and solid curves have been calculated from Eqs. (1), (2), (4) and (1), (3), (4), respectively.

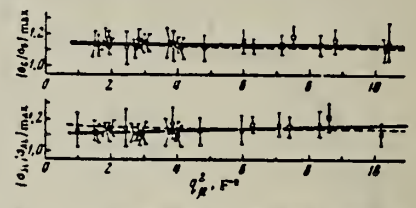

FIG. 2. Ratios of cross sections for scattering of electrons, $\sigma_{C^{12}}/\sigma_{B^{11}}$ and $\sigma_{58^\circ}/\sigma_{Al^{27}}$ at the maximum of the continuum, as a function of squared momentum transfer. The solid lines are the result of fitting a linear function to the experimental points, and the dashed lines correspond to calculations using Eq. (5) for the cross section. The following designations are used for the experimental ratios at the various initial electron energies: ●–592 MeV, O–690 MeV, Δ–802 MeV, □–969 MeV, X- 1143 Mev.

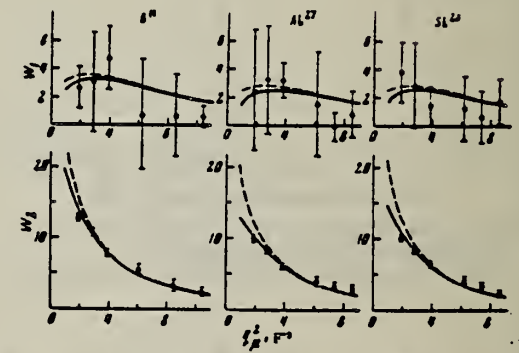

FIG. 3. Inelastic electromagnetic form factors of B^{11}, Al^{27}, and Si^{28}, measured in the region of the continum. The dashed curves are the result of a calculation based on Eqs. (2), (7), and (8), and the solid curves based on Eqs. (3), (7), and (8).

Nucleus	Quasielastic electron scattering						Elastic electron scattering	
	Pauli principle not taken into account			Pauli principle taken into account				
	p_0, MeV/c	$\frac{x^2}{N-1}$	$\langle r_Z^2\rangle^{1/2}$, F	p_0, MeV/c	$\frac{x^2}{N-1}$	$\langle r_Z^2\rangle^{1/2}$, F	$\langle r_Z^2\rangle^{1/2}$, F	p_0, MeV/c
B^{11}	150±5	1,6	2,07±0,07	155±5	1,5	2,01±0,07	2,42±0,12 [10]	125±6
Al^{27}	145±4	1,4	2,39±0,07	149±4	1,2	2,33±0,07	2,96±0,09 [11]	114±3

REF.

H. J. Von Eyss, H. Schier, and B. Schoch
Elba-71, Tagungsbericht Elektronen Beschleuniger Arbeits Gruppen
(Sept. 1971) Justus Liebig-Universitat Giessen. p.391

ELEM. SYM.	A	Z
Al	27	13

METHOD

REF. NO.	
71 Vo 1	hmg

REACTION	RESULT	EXCITATION ENERGY	SOURCE		DETECTOR		ANGLE
			TYPE	RANGE	TYPE	RANGE	
E,N	ABX	THR-266	C	150-266	TOF-D		90

See over for figure.

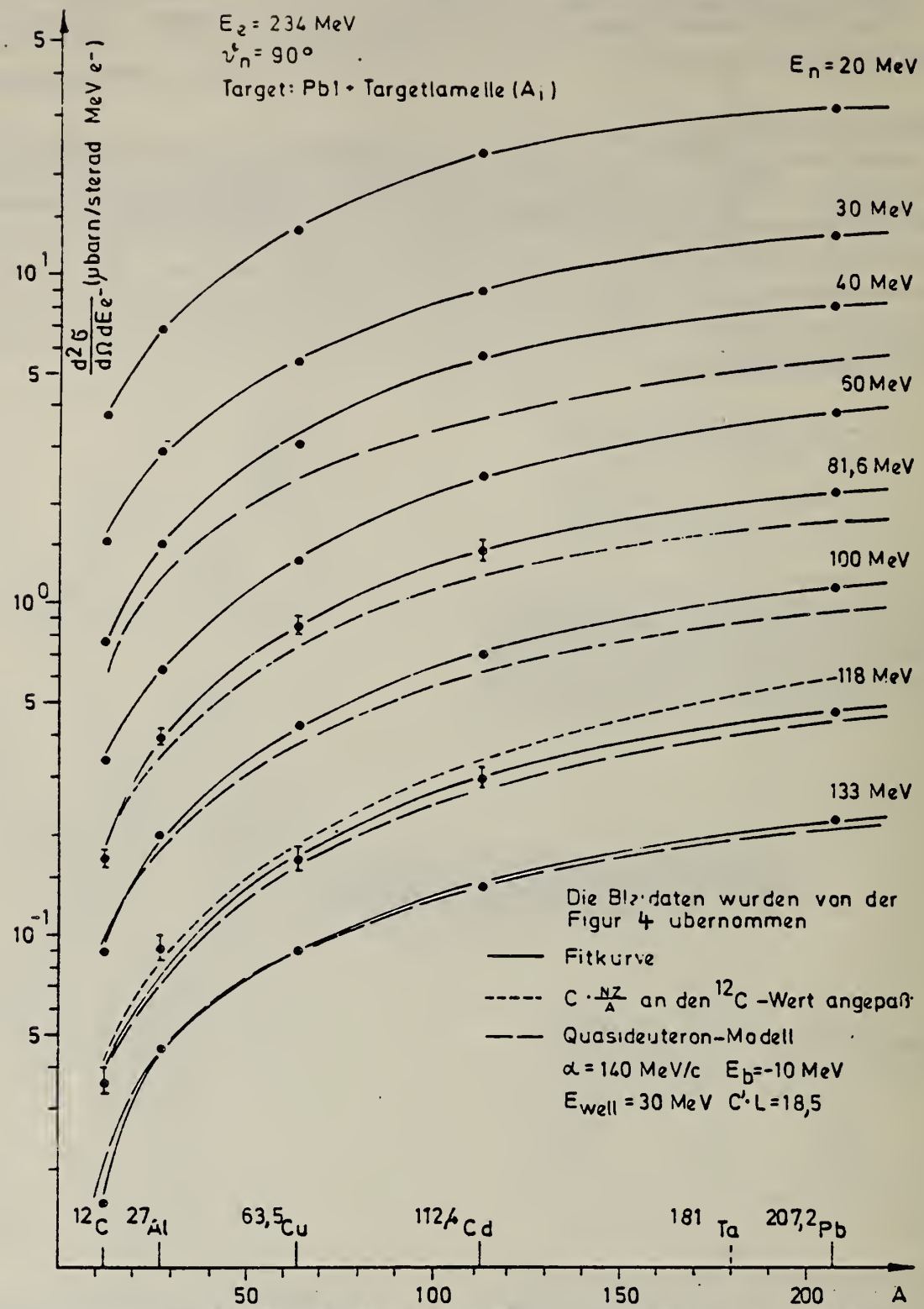

Figur 3: Differentieller Neutronenproduktions-Wirkungsquerschnitt als Funktion der Massenzahl A für einige Neutronenenergien

REF. J. Ahrens, H. Borchert, H. B. Eppler, H. Gimm, H. Gundrum, P. Riehn, G. Sita Ram, A. Zieger, M. Kroning, B. Ziegler
Proc. International Conference on Nuclear Structure Studies Using Electron Scattering and Photoreaction, Sendai, Japan p. 213 (1972)

ELEM. SYM.	A	Z
Al	27	13

METHOD

REF. NO. 72 Ah 7 egf

REACTION	RESULT	EXCITATION ENERGY	SOURCE		DETECTOR		ANGLE
			TYPE	RANGE	TYPE	RANGE	
G,MUT	ABX	10-140	C	140	MGC-D		4PI

595

Fig. 9. Total nuclear cross-sections for Al.

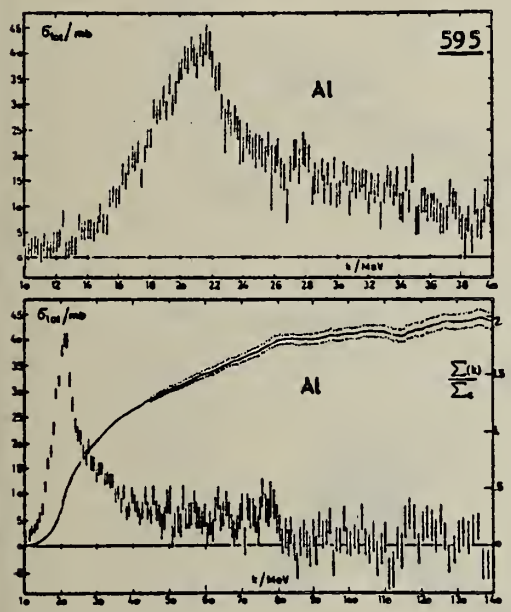

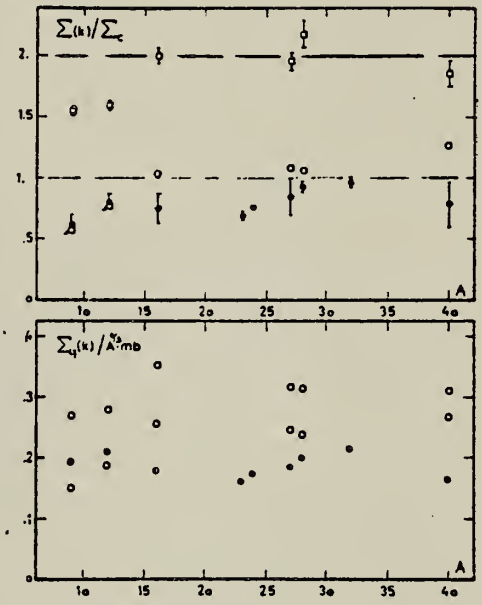

$\Sigma_c = 60\frac{NZ}{A}$, $\Sigma(k) = \int_{k_0}^{k}\delta(k)\,dk$, $\Sigma_1(k) = \int_{k_0}^{k}\delta(k)\frac{dk}{k}$

● NBS k=35 MeV, ○ k=35 MeV, ◎ k=140 MeV

Fig.11 Integrated cross-sections

REF. G. Andersson, I. Blomqvist, B. Forkman, G. G. Jonsson, A. Jarund, I. Kroon, K. Lindgren and B. Schroder
Nucl. Phys. A197, 44 (1972)

ELEM. SYM.	A	Z
Al	27	13

METHOD

REF. NO. 72 An 8 egf

REACTION	RESULT	EXCITATION ENERGY	SOURCE TYPE	SOURCE RANGE	DETECTOR TYPE	DETECTOR RANGE	ANGLE
G,PI+	ABX	1- 7	C	1- 7	ACT-I		4PI
G,2PN	ABX	1- 7	C	1- 7	ACT-I		4PI

ENERGIES GEV

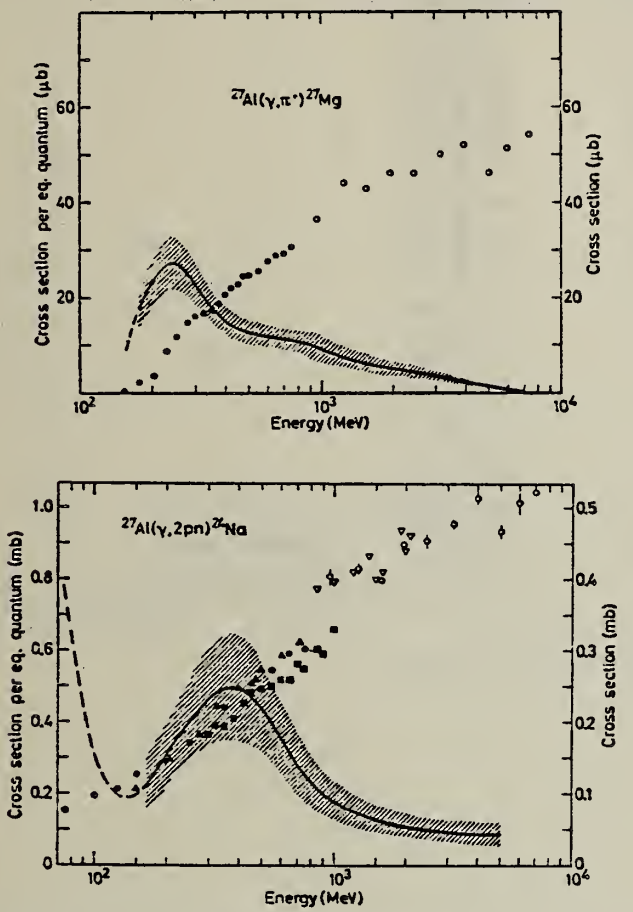

Fig. 16. Yield and cross section for the ^{27}Al(γ,π⁺)^{27}Mg and ^{27}Al(γ, 2pn)^{24}Na reactions: ○ this work, ● data from refs. [11, 27]), ▲ data from ref. [28]), ■ data from ref. [29]) and ▽ data from ref. [4]).

[4] G. Kumbartzki et al., Nucl. Phys. A160 (1971) 237.

[11] I. Blomqvist et al., Nucl. Phys. A162 (1971) 193.

[27] B. Friberg, Lund, private comm.

[28] A. Masaike, J. Phys. Soc. Jap. 19 (1964) 427.

[29] V. di Napoli et al., Nucl. Instr. 93 (1971) 77.

(over)

TABLE 6

Partial reaction cross sections relative to the total photoabsorption cross section, σ/σ_{tot} (in %)

Reaction	0.3 GeV	1.0 GeV	5.0 GeV
$^{12}C(\gamma, n)$	10 ± 5	6.8± 3.4	0 ± 5
$^{27}Al(\gamma, \pi^+)$	0.2± 0.1	0.1± 0.1	0.04± 0.02
$(\gamma, 2pn)$	1.7± 0.9	1.5± 0.8	1.7 ± 0.6
$^{127}I(\gamma, 3n)$	1.6± 0.8	0 ± 3	5.5 ± 2.8
$(\gamma, 6n)$	0.9± 0.5	1.2± 0.6	1.5 ± 0.8
$(\gamma, 7n)$	0.9± 0.5	0.5± 0.3	0.1 ± 0.1
$(\gamma, 8n)$	0.7± 0.4	0.6± 0.3	0.4 ± 0.2
$(\gamma, 9n)$	0.3± 0.2	0.2± 0.1	0.5 ± 0.3
$\Sigma(\gamma, xn)$	4.4± 2.2	2.6± 1.3	7.8 ± 3.9
$(\gamma, p5n)$	1.7± 0.9	1.7± 0.9	0.9 ± 0.5
$(\gamma, p7n)$	1.9± 1.0	2.1± 1.1	0.9 ± 0.5
$(\gamma, p9n)$	1.6± 0.8	1.6± 0.8	1.3 ± 0.7
$\Sigma(\gamma, pxn)$	5.2± 2.6	5.4± 2.7	3.1 ± 1.6
$(\gamma, 2p3n)$	0.6± 0.3	0.3± 0.2	0.3 ± 0.2
$(\gamma, 2p5n)$	0.5± 0.3	0.6± 0.3	0.8 ± 0.4
$(\gamma, 2p7n)$	1.3± 0.7	1.0± 0.5	0.4 ± 0.2
$(\gamma, 2p9n)$	1.1± 0.6	1.7± 0.9	2.4 ± 1.2
$(\gamma, 2p10n)$	2.7± 1.4	1.9± 1.0	5.0 ± 2.5
$\Sigma(\gamma, 2pxn)$	6.3± 3.2	5.6± 2.8	8.8 ± 4.4
$(\gamma, 4p12n)$	1.5± 0.8	2.4± 1.2	2.0 ± 1.0
$(\gamma, 4p14n)$	0.8± 0.4	1.9± 1.0	2.5 ± 1.3
$(\gamma, 4p15n)$	0.4± 0.2	0.6± 0.3	1.5 ± 0.8
$\Sigma(\gamma, 4pxn)$	2.7± 1.4	4.9± 2.5	6.0 ± 3.0
$(\gamma, 6p17n)$		0.5± 0.3	1.5 ± 0.8
$(\gamma, 6p18n)$	0.1± 0.1	0.2± 0.1	0.1 ± 0.1
$\Sigma(\gamma, 6pxn)$	0.1± 0.1	0.7± 0.4	1.6 ± 0.8
$(\gamma, 8p18n)$		0.8± 0.4	2.5 ± 1.3
$\Sigma(\gamma, ypxn)$	19 ±10	20 ±10	30 ±15
$^{197}Au(\gamma, 3n)$	0.9± 0.5	2.2± 1.1	1.5 ± 0.8
$(\gamma, 7n)$	0.8± 0.4	1.3± 0.7	2.4 ± 1.2
$(\gamma, 9n)$	0.8± 0.4	0.6± 0.3	0.3 ± 0.2
$(\gamma, 11n)$	0.4± 0.2	0.9± 0.5	0.5 ± 0.3
$\Sigma(\gamma, xn)$	2.9± 1.5	5.1± 2.6	4.6 ± 2.3
$Au(\gamma, f)$	1.5± 0.4	2.7± 0.7	6.9 ± 2.0
$Pb(\gamma, f)$	3.1± 0.8	6.9± 1.7	17 ± 5

REF. D. Hiramatsu, T. Kamae, H. Muramatsu, K. Nakamura, N. Izutsu, and Y. Watase
PICNS-72, p.429 Sendai (see 73Hi5)

ELEM. SYM.	A	Z
Al	27	13

METHOD

REF. NO.	
72 Hi 8	hvm

REACTION	RESULT	EXCITATION ENERGY	SOURCE		DETECTOR		ANGLE
			TYPE	RANGE	TYPE	RANGE	
E,E/P	NOX	G* 60	D	700	MAG-D		DST

*SEP ENERGY RANGE

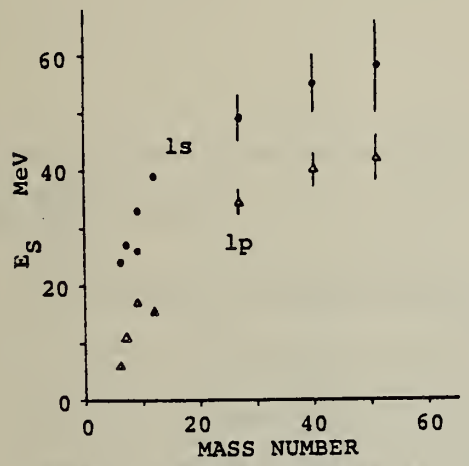

Fig. 6. The separation energy of 1s and 1p states as a function of the mass number.

REF. V.P. Kovalev, V.P. Kharits, V.V. Gordeev, V.I. Isaev (USSR)
Atomnaya Energiya 32, 496 (1972)

ELEM. SYM.	A	Z
Al	27	13

METHOD

REF. NO. 72 Ko 8 hmg

REACTION	RESULT	EXCITATION ENERGY	SOURCE		DETECTOR		ANGLE
			TYPE	RANGE	TYPE	RANGE	
G,N	NOX	13- 22	C	22	THR-I		DST

Мишень	Энергия электронов, *Мэв*	Детектор	Угол, *град*							B/A
			30	50	70	90	110	130	150	
Al	22,5	$P^{31}(n,p)$	1,05±0,08	1,03±0,08	0,97±0,08	1,0±0,08	0,98±0,08	1,02±0,08	1,04±0,08	Изотропно
	22,5	$Al^{27}(n,p)$	0,90±0,15	0,95±0,15	1,02±0,15	1,00±0,14	0,96±0,13	1,07±0,13	1,01±0,13	»
Ti	22,5	$P^{31}(n,p)$	1,04±0,07	0,96±0,07	1,03±0,07	1,00±0,07	0,98±0,07	1,05±0,07	1,03±0,07	»
	22,5	$Al^{27}(n,p)$	1,06±0,13	0,94±0,13	1,04±0,12	1,00±0,12	0,95±0,11	0,98±0,11	1,02±0,10	»
Cu	12,8	$P^{31}(n,p)$	0,97±0,10	1,04±0,10	1,02±0,10	1,00±0,10	1,01±0,10	0,99±0,10	0,96±0,10	»
	17,0	$P^{31}(n,p)$	1,03±0,07	0,97±0,07	1,00±0,07	1,00±0,07	1,06±0,07	0,95±0,07	0,88±0,07	»
	22,5	$P^{31}(n,p)$	0,87±0,05	0,94±0,05	0,97±0,05	1,00±0,05	0,99±0,05	0,93±0,05	0,91±0,05	0,18±0,04
	22,5	$Al^{27}(n,p)$	0,75±0,09	0,86±0,07	0,93±0,06	1,00±0,05	1,02±0,05	0,94±0,04	0,90±0,04	0,28±0,06
Mo	22,5	$P^{31}(n,p)$	0,90±0,05	0,93±0,05	0,98±0,05	1,00±0,05	0,99±0,05	0,92±0,05	0,84±0,05	0,21±0,04
	22,5	$Al^{27}(n,p)$	0,80±0,08	0,95±0,08	0,95±0,07	1,00±0,06	0,94±0,05	0,83±0,04	0,72±0,04	0,44±0,08
	22,5	$Al^{27}(n,\alpha)$	0,72±0,08	0,84±0,08	0,89±0,08	1,00±0,08	0,95±0,08	0,87±0,08	0,63±0,08	0,78±0,18
W	22,5	$P^{31}(n,p)$	0,85±0,04	0,90±0,04	0,98±0,04	1,00±0,04	0,98±0,04	0,92±0,04	0,087±0,04	0,25±0,04
	22,5	$Al^{27}(n,p)$	0,78±0,06	0,84±0,06	0,89±0,05	1,00±0,05	0,97±0,04	0,86±0,04	0,75±0,04	0,54±0,06
Pb	22,5	$P^{31}(n,p)$	0,79±0,04	0,85±0,04	0,96±0,04	1,00±0,04	0,98±0,04	0,88±0,04	0,84±0,04	0,36±0,05
	22,5	$Al^{27}(n,p)$	0,70±0,09	0,81±0,08	0,94±0,07	1,00±0,06	0,94±0,06	0,80±0,05	0,69±0,05	0,69±0,12

(over)

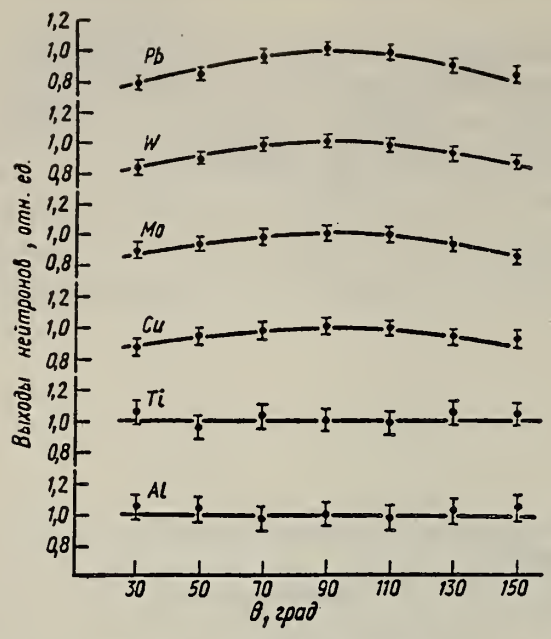

Угловые распределения быстрых фотонейтронов из Al, Ti, Cu, Mg, W, Pb, облучаемых электронами с энергией 22,5 *Мэв*. Детектор $I^{\mu 1}$ (n, γ) Si^{31}.

REF.

V.I. Noga, Yu. N. Ranyuk, P.V. Sorokin, V.A. Tkachenko
Yad. Fiz. 14, 904 (1971)
Sov. J. Nucl. Phys. 14, 506 (1972)

ELEM. SYM.	A	Z
Al	27	13

METHOD

REF. NO. 72 No 3 hmg

REACTION	RESULT	EXCITATION ENERGY	SOURCE		DETECTOR		ANGLE
			TYPE	RANGE	TYPE	RANGE	
G,PI+ *	ABX	150-999	C	150-999	ACT-I		4PI
E,PI+ **	RLY	150-999	C	150-999	ACT-I		4PI

* 999=1.2 GEV
** 999=1.2 GEV RLY TO G

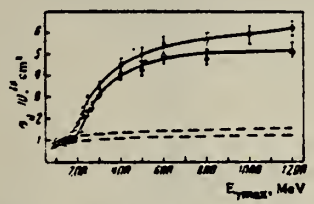

FIG. 2. Yields of C^{11} and Mg^{27} activities from B^{11} and Al^{27} targets. Points: O–$B^{11}(\gamma, \pi^-)C^{11}$; Δ–$Al^{27}(\gamma, \pi^+)Mg^{27}$. The dashed curves are the corresponding background activities.

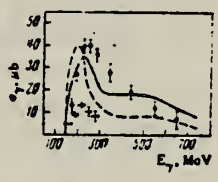

FIG. 4

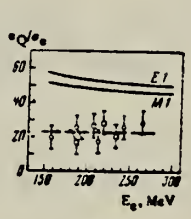

FIG. 5

FIG. 4. Cross section per real photon $\sigma_\gamma(E_\gamma)$ for the reaction $Al^{27}(\gamma, \pi^+)Mg^{27}$. Curves: dashed–theory [5], solid–experimental data [5]. Points ●–experimental data of the present work, points with error bars–experimental data of Walters and Hummel. [7]

FIG. 5. The ratio σ_Q/σ_e as a function of electron energy. Solid curves–theoretical results; points–values obtained experimentally for the reactions:

$$O - B^{11}\left(\begin{matrix}\gamma, \pi^- \\ e, e'\pi^-\end{matrix}\right)C^{11};\ \square - Al^{27}\left(\begin{matrix}\gamma, \pi^+ \\ e, e'\pi^+\end{matrix}\right)Mg^{27}$$

[5] G. Nydahl et al., Nucl. Phys. B7, 97 (1968).
[7] W. B. Walters et al., Phys. Rev. 143, 833 (1966).

REF. Y. Oda, M. Kondo, and H. Hirabayashi
J. Phys. Soc. Japan 32, 869 (1972)

EL EM. SYM.	A	Z
Al	27	13

METHOD

REF. NO. 72 Od 1 egf

REACTION	RESULT	EXCITATION ENERGY	SOURCE TYPE	SOURCE RANGE	DETECTOR TYPE	DETECTOR RANGE	ANGLE
P,G	ABY	9- 11	D	1- 4	NAI-D		DST

758

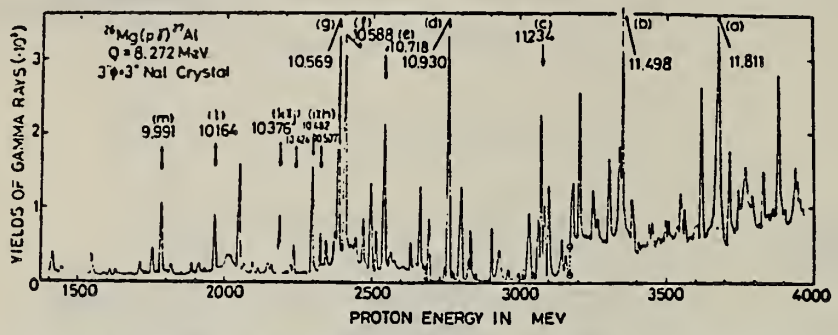

Fig. 6. Excitation functions of the ^{26}Mg$(p,\gamma)^{27}$Al reactions. The data with low backgrounds in the region of $2.7 \lesssim E_p \lesssim 3.17$ MeV are that revised with the new machine in the text.

Table II. Strong resonances in ^{26}Mg$(p,\gamma)^{27}$Al reactions.

Symbol	E_p(keV)	E_x(MeV)	Main decay* 0	1	2	3	Strength** (eV)	J_π
a	3675	11.811	0		2	3		
	3620	11.758			2			
b	3350	11.498	0					
c	3075	11.234	0	1	2			
d	2760	10.930	0		2	3	2	(5/2)+
e	2540	10.718		1	2			
f	2405	10.588	0	1				
g	2385	10.569	0	1	2			
h	2323	10.507	0			3	4	7/2−
i	2293	10.482	0			3	8	7/2−
j	2232	10.424	0		2	3	1	(5/2)
k	2185	10.377	0	1	2		2	(3/2)+
l	1965	10.165	0			3	4	5/2+
m	1785	9.991	0			3	2	7/2−

* ^{26}Mg state number

** $(2J+1)\cdot\frac{\Gamma(p_0)\cdot\Gamma(\gamma_0)}{\Gamma}$

REF.

N. Shikazono and Y. Kawarasaki
Nucl. Phys. A188, 461 (1972)

ELEM. SYM.	A	Z
Al	27	13

METHOD

REF. NO.: 72 Sh 2 egf

REACTION	RESULT	EXCITATION ENERGY	SOURCE		DETECTOR		ANGLE
			TYPE	RANGE	TYPE	RANGE	
G,G/	SPC	0-14	C	14	SCD-D		87

TABLE 3

Gamma-rays resulting from the photon bombardment of an Al target

E_γ (MeV)	Observed peak	Relative intensity	Transition
3.96	D, S, F	32 ±6	3.96 → 0
4.41	D, F	9 ±3	4.41 → 0
6.47	D, S	8.2±0.8	7.49 → 1.01
6.58	D	2.8±0.8	7.59 → 1.01
6.65	D, S, F	8.3±0.8	6.65 → 0
6.83	D	5.9±0.7	6.83 → 0
7.42	D, (S), F	6.9±0.7	7.42 → 0
7.49	D, S	3.9±0.7	7.49 → 0
7.59	D	2.8±0.6	7.59 → 0
7.68	D, S	9.4±0.7	8.70 → 1.01
8.04	D, S, F	6.9±0.7	8.04 → 0
8.45	D, (S)	5.3±0.6	8.45 → 0
8.70	D, (F)	4.4±0.6	8.70 → 0
9.60	D	1.0±0.4	9.60 → 0
9.84	D	1.1±0.4	9.84 → 0
9.97	D	2.2±0.5	9.97 → 0

[8] P.M. Endt et al. Nucl. Phys. A105, (1967)1.

[8] P.M. Endt et al. Nucl. Phys. A105 (1967) 1.

[54] W. Bohne et al. Nucl. Phys. A131 (1969) 273.

[55] C. van der Leun et al. Nucl. Phys. A10C (1967) 316.

TABLE 7

Excitation energies and ground state transition widths obtained from the $^{27}Al(\gamma,\gamma')^{27}Al$ reaction

Excitation energy (keV) present work	Excitation energy (keV) previous work	J^π	$\Gamma_{\gamma 0}/\Gamma_\gamma$ [a]	$(2J+1)\Gamma_{\gamma 0}$ (eV) [b] present work	$(2J+1)\Gamma_{\gamma 0}$ (eV) [b] previous work
3955±6	3955.9±1.3 [a]	$(\frac{3}{2})^+$ [d]	1.0	2.1±0.5	
4409±5	4409 ±2 [c]	$(\frac{3}{2})^+$ [d]	0.55 [c]		1.44±0.18 [a]
6654±5	6653 ±3 [c]	$(\frac{3}{2})$ [f]	0.85±0.05 [f]	3.2±0.4	
6826±5	6831 ±2 [c]		1.0	2.4±0.4	
7419±6			1.0	4.0±0.6	
7486±6		$(\frac{1}{2}, \frac{3}{2})$	0.32±0.04	8±2	
7591±6			0.50±0.08	3.4±0.9	
8042±6			1.0	6.0±1.0	
8447±8			1.0	6.0±1.0 [g]	
8696±8		$(\frac{1}{2}, \frac{3}{2})$	0.32±0.03	20 ±4 [g]	
9604±8	9599 [c]	$(\frac{3}{2})$ [c]	0.25 [c]	8 ±3 [h]	
9842±8	9838 [c]		1.0	2.7±1.0 [h]	
9966±8	9961 [c]	$(\frac{1}{2}, \frac{3}{2})^+$ [c]	0.21 [c]	25 ±6 [h]	

[a] The branchings are obtained from the relative intensities observed at the scattering angle of 87°. The effect of the angular distribution of the γ-rays is not taken into account.

[b] The error for $(2J+1)\Gamma_{\gamma 0}$ only includes the statistical error. An estimate of the uncertainty associated with the shape of the incident bremsstrahlung is not included.

[c] Ref. [8]).

[d] Ref. [54]).

[e] Ref. [8]); this value was used for the normalization of $^{27}Al(\gamma,\gamma')^{27}Al$ intensities in the present work.

[f] Ref. [55]).

[g] The value given is not the $(2J+1)\Gamma_{\gamma 0}$ but the $(2J+1)\Gamma_{\gamma 0}\Gamma_\gamma/\Gamma$ value.

[h] The value of $(2J+1)\Gamma_\gamma\Gamma_p/\Gamma$ from ref. [8]) has been used to estimate the value of $(2J+1)\Gamma_{\gamma 0}$.

	Punched	Checked w/PS
IBM Card DATA	8/72	9/72
IBM Card REFERENCE	8/72	9/72

REF. J. Ahrens, H.B. Eppler, H. Gimm, H. Gundrum, M. Kroning, P. Riehn, G. SitaRam, A. Zieger, and B. Ziegler
PICNS-73, Vol.I, p.23 Asilomar

ELEM. SYM.	A	Z
Al	27	13

METHOD

REF. NO. 73 Ah 4 hmg

REACTION	RESULT	EXCITATION ENERGY	SOURCE		DETECTOR		ANGLE
			TYPE	RANGE	TYPE	RANGE	
G,MU-T	ABX	10-140	C	140	MGC-D		4PI

Statistics may have been improved over those of 72Ah7.

See figure on other side.

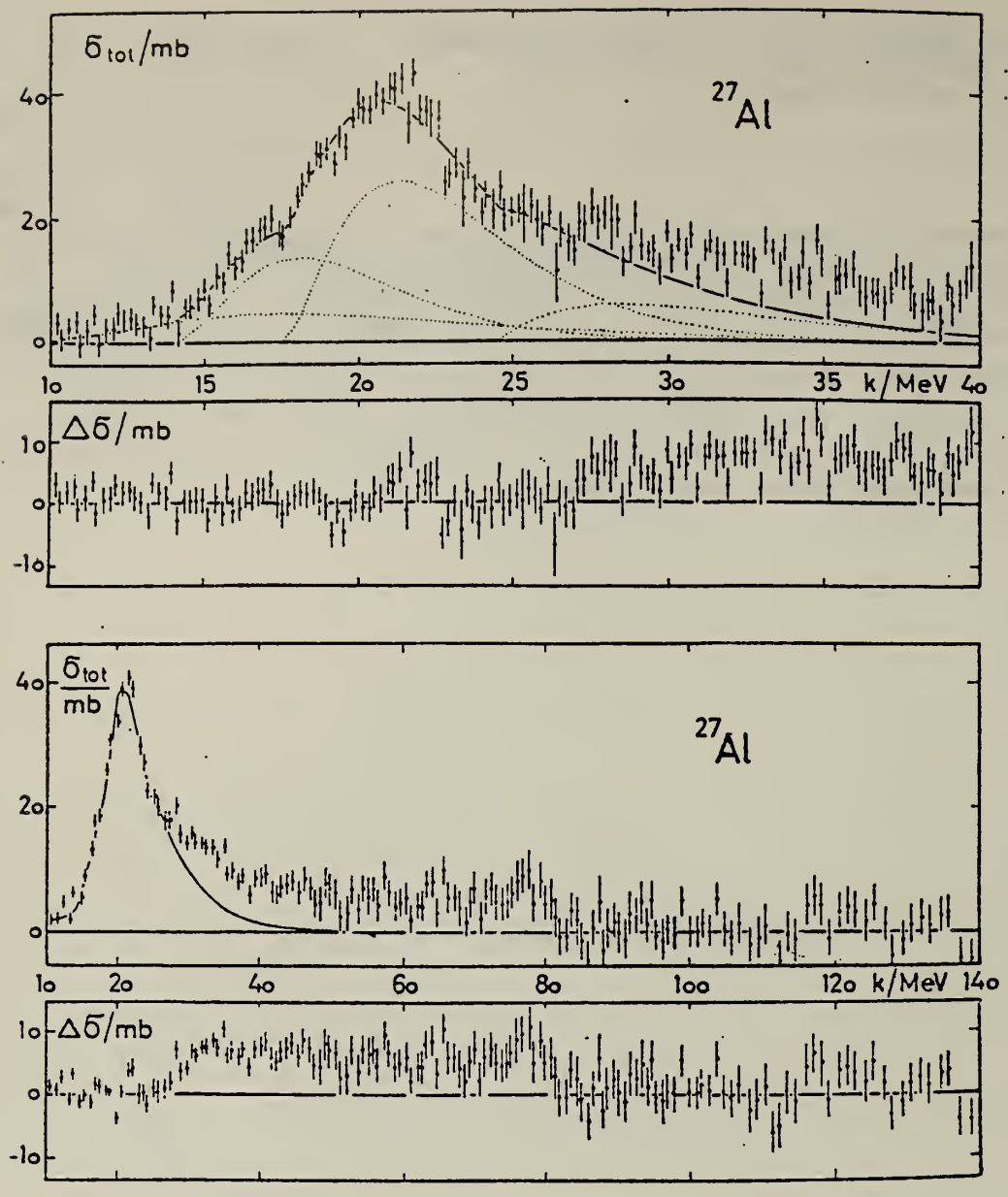

Fig. 6. Same as Fig. 2 for Al.

REF. R. Bergere, H. Beil, P. Carlos, A. Lepretre, A. Veyssiere
PICNS-73, Vol. I, p. 525 Asilomar

ELEM. SYM.	A	Z
Al	27	13

METHOD

REF. NO. 73 Be 10 hmg

REACTION	RESULT	EXCITATION ENERGY	SOURCE		DETECTOR		ANGLE
			TYPE	RANGE	TYPE	RANGE	
G,N	ABX	13- 30	D	13- 30	BF3-I		4PI

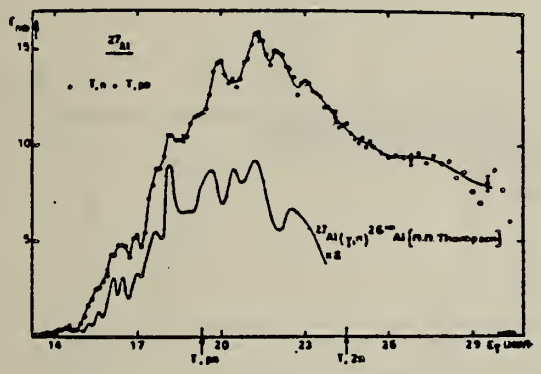

Fig 2 $^{27}Al[\sigma(\gamma,n) + \sigma(\gamma,pn)]$ compared with $^{27}Al(\gamma,n)^{26}Al^{m}$ cross sections measured by Thomson.[5]

[5] M.N. Thompson et al., Nucl. Phys. 64, 486 (1965)

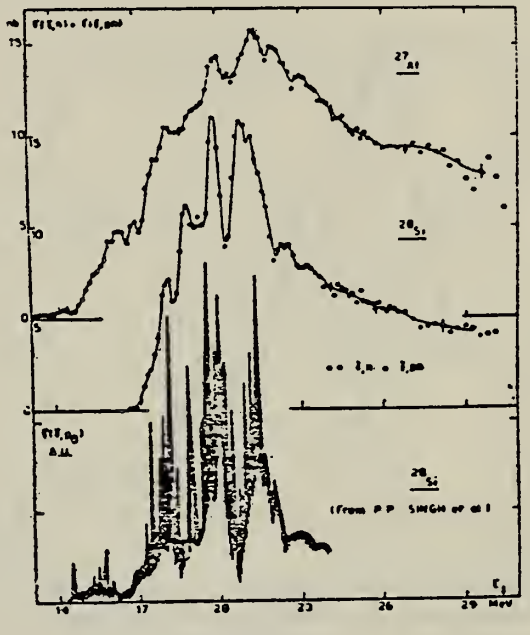

Fig. 3 ^{28}Si and ^{27}Al $[(\gamma,n) + (\gamma,pn)]$ cross-sections compared to $^{27}Al(p,\gamma_0)^{28}Si$ measured by Singh.[6]

[6] P.P. Singh et al., Nucl. Phys. 65, 577 (1965)

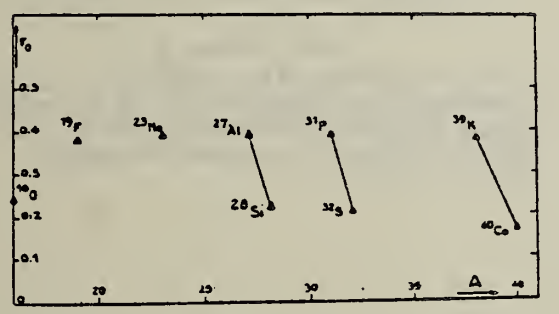

Fig. 13 Integrated photoneutron cross-sections for s-d shell nuclei.

REF. V. di Napoli, F. Salvetti, M.L. Terranova, H.G. de Carvalho, and J.B. Martins
Phys. Rev. C8, 206 (1973)

ELEM. SYM.	A	Z
Al	27	13

METHOD

REF. NO. 73 Di 4 hmg

REACTION	RESULT	EXCITATION ENERGY	SOURCE		DETECTOR		ANGLE
			TYPE	RANGE	TYPE	RANGE	
G,SPL	ABY	THR-999	C	999	ACT-I		4PI

999 = 1 GEV

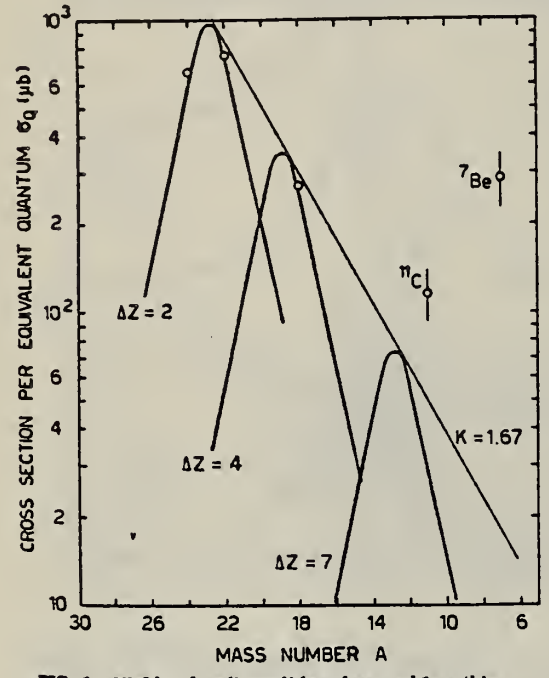

FIG. 1. Yields of radionuclides observed in a thin aluminium target irradiated with 1-GeV bremsstrahlung versus the mass number. ΔZ is the difference between the atomic number of the target nucleus ($Z = 13$) and the atomic number of the produced radionuclide.

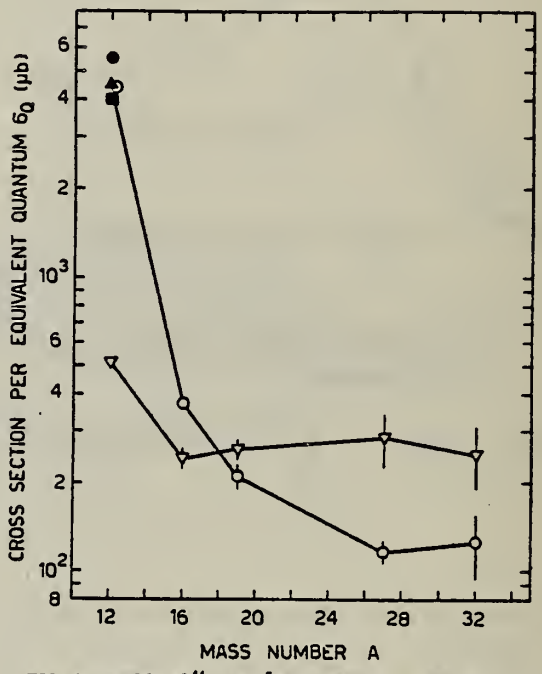

FIG. 3. Yields of ^{11}C and ^{7}Be versus the mass number of the target nucleus. Filled circle: ^{11}C, Ref. 16. Filled triangle: ^{11}C, Ref. 17. Filled square: ^{11}C, Ref. 8. Open circles: ^{11}C, present work. Reversed open triangles: ^{7}Be, present work.

[8] G. Anderson et al., Nucl. Phys. A197, 44 (1972).

[16] V. di Napoli et al., Nuovo Cimento 55B, 95 (1968).

[17] A. Masaike, J. Phys. Soc. Japan 19, 427 (1964).

REF.

V. diNapoli, A.M. Lacerenza, F. Salvetti, S.M. Terenzi, H.G. deCarvalho and J.B. Martins
J. Inorg. Nucl. Chem. 35, 1419 (1973)

ELEM. SYM.	A	Z
Al	27	13

METHOD

REF. NO.: 73 Di 12 egf

REACTION	RESULT	EXCITATION ENERGY	SOURCE TYPE	SOURCE RANGE	DETECTOR TYPE	DETECTOR RANGE	ANGLE
G,F18	ABY	THR-999	C	300-999	ACT-I		4PI

999= 1 GEV

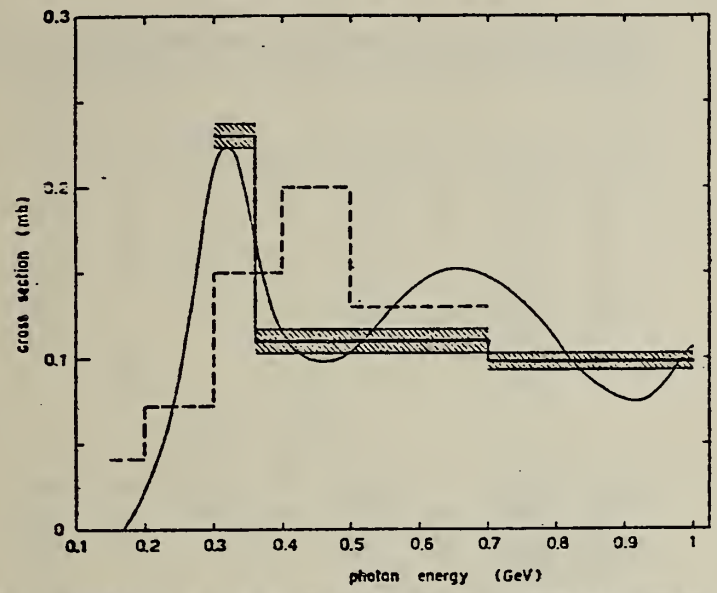

Fig. 4. Average absolute cross-section $\bar{\sigma}_k$ vs photon energy. Dashed line: Masaike[10]. Full line with dashed areas: present work (the dashed areas represent the error which affects $\bar{\sigma}_\omega$). The smoothed curve (full line) represents the trend of the cross-section for both single and double pion photoproduction[11, 13].

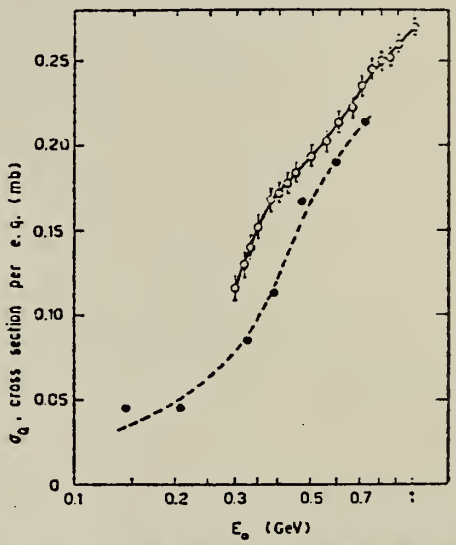

Fig. 3. Cross-section per equivalent quantum vs the natural log of the bremsstrahlung maximum energy. Full circles and dashed line: Masaike[10]. Open circles and full line: present work.

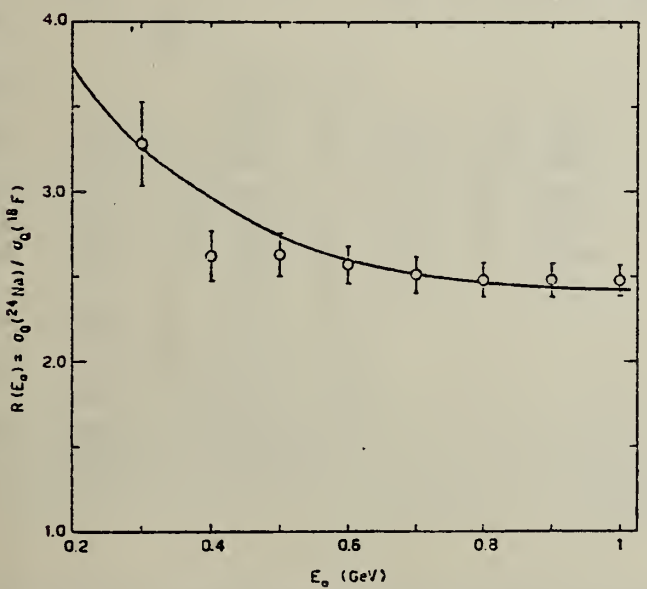

Fig. 5. $R(E_0)$ vs the bremsstrahlung maximum energy. Experimental points were fitted by the least-squares method by polynomials of the form $\Sigma_{i=0}^{n} a_i E_0^i$; the highest power of E_0 was determined from observation of the χ^2 probability of the fit for different values of i.

[10] A. Masaike, J. phys. Soc. Japan 19, 427 (1964)

[11] J.T. Beale, S.D. Ecklund, R.L. Walker, CALT-68, 108 (1968).

[13] C.E. Roos and V.Z. Peterson, Phys. Rev. 124, 1610 (1961).

REF. P. Dougan and W. Stiefler
Z. Physik 265, 1 (1973)

ELEM. SYM.	A	Z
Al	27	13

METHOD

REF. NO. 73 Do 9 egf

REACTION	RESULT	EXCITATION ENERGY	SOURCE TYPE	SOURCE RANGE	DETECTOR TYPE	DETECTOR RANGE	ANGLE
G,XP	ABY	88-400	C	400	TEL-D		DST

Table 6. Aluminium. Bremsstrahlung endpoint energy: 400 MeV. Differential cross-sections in microbarns/sterrad · MeV · eq. quantum. Quoted errors: statistical in percent

Energy	Angle							
	22	30	40	50	60	74	90	110
82.2	6.81 2.3	6.03 2.0	5.17 1.9	4.32 1.7	3.51 1.8	2.81 2.0	2.18 1.9	1.74 2.2
100.1	5.76 2.8	4.53 2.5	3.79 2.4	3.27 2.2	2.59 2.3	1.99 2.6	1.52 2.5	1.12 3.0
104.9	4.71 2.7				2.28 2.7	1.83 2.1	1.43 2.0	0.966 3.1
106.9		4.22 2.5						
110.6			3.15 2.4	2.44 2.2				
117.1	4.09 4.4	3.26 4.2	2.71 4.1	2.24 4.0	1.87 4.1	1.47 4.3	0.932 4.3	0.708 4.7
127.6	3.33 4.1				1.67 3.3	1.23 2.7	0.866 2.8	0.586 4.1
129.4		2.64 3.4						
132.8			2.09 3.1	1.74 2.7				
148.9	2.11 6.7				1.05 4.2	0.798 3.5	0.469 3.9	0.278 6.2
150.5		1.76 4.2						
153.4			1.37 3.9	1.08 3.6				
169.8	1.53 6.9	1.36 2.6	1.09 4.6	0.971 2.8	0.784 2.8	0.512 3.3	0.282 5.7	
186.8	1.16 7.8	0.976 3.2	0.865 5.5	0.643 3.6	0.512 3.7	0.285 4.7	0.168 7.8	
203.7	0.829 9.5	0.710 3.7	0.612 6.5	0.443 4.3	0.296 4.8	0.174 6.0	0.0654 12.4	
222.4	0.568 5.7	0.557 5.1	0.421 5.1	0.346 6.5				
238.8	0.451 6.6	0.400 5.3	0.290 6.4	0.236 7.9				
255.1	0.331 7.6	0.234 9.1	0.161 8.5	0.137 10.3				

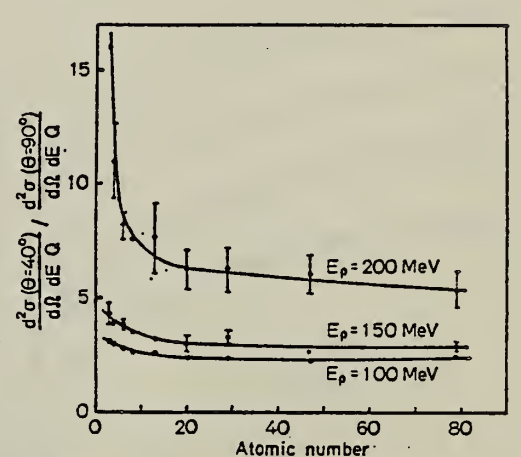

Fig. 6. The ratios of the experimental cross-sections at 40 and 90 degrees for selected proton energies as a function of atomic number

(over)

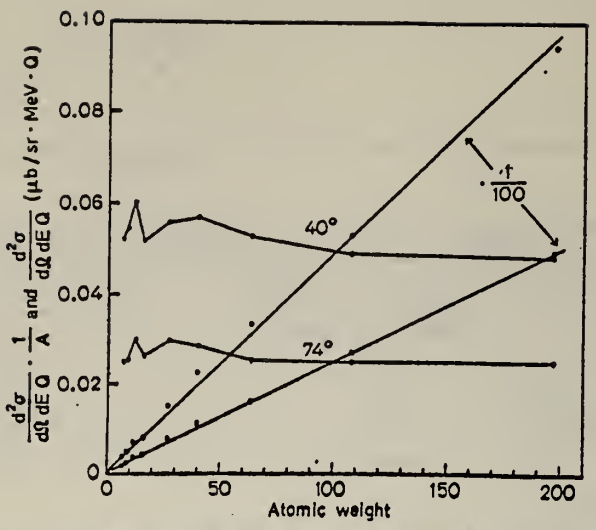

Fig. 9. In this figure, the straight lines show the experimental cross-sections at 40° and 74° for $E_p = 150$ MeV. The other curves are the same cross-sections divided by atomic weight

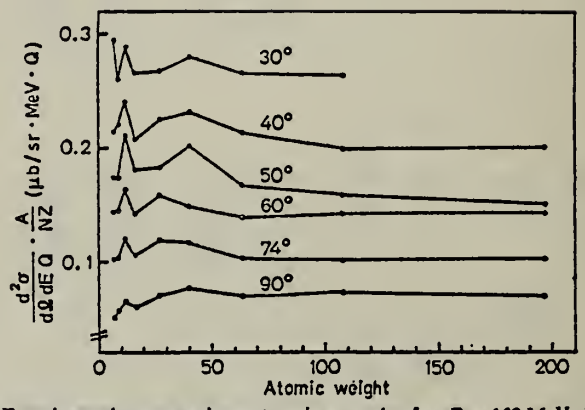

Fig. 8. Experimental cross-sections at various angles for $E_p = 150$ MeV divided by NZ/A plotted as a function of atomic weight

REF. H. J. von Eyss and G. Lührs
Z. Physik 262, 393 (1973)

ELEM. SYM.	A	Z
Al	27	13

METHOD

REF. NO. 73 By 3 egf

REACTION	RESULT	EXCITATION ENERGY	SOURCE		DETECTOR		ANGLE
			TYPE	RANGE	TYPE	RANGE	
G,XN	SPC	THR-234	C	234	TOF-D		90

NEUTS E ABV 12 MEV

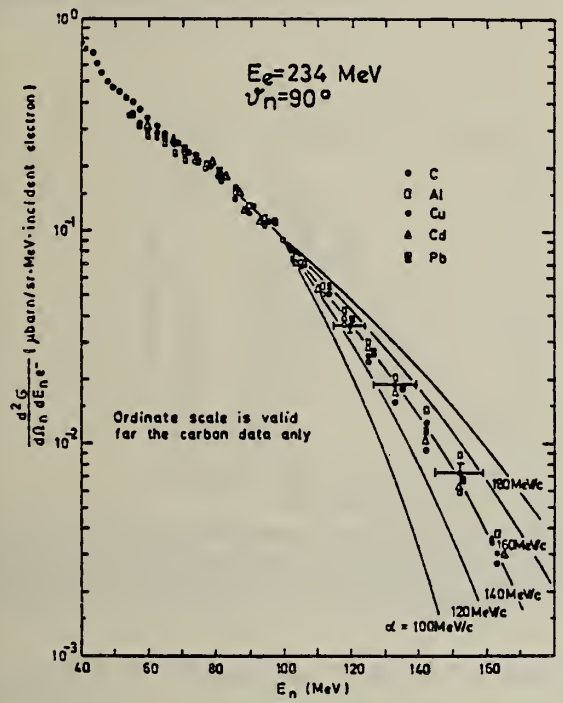

Fig. 8. Comparison of the shape of the high-energy part of the photoneutron spectra from C, Al, Cu, Cd and Pb. These measurements were performed with the same γ-shower spectrum, produced in a 0.3 cm thick lead sheet (see Fig. 2b). All spectra were fitted to the value for carbon at E_n=100 MeV. The values predicted by a quasi-deuteron model (solid lines), which are also fitted at E_n=100 MeV, were calculated with the parameters (defined in the text): E_b=−10 MeV, E_{well}=30 MeV and $C'L$=19.0 for different impulse parameters α=100, 120, 140, 160 and 180 MeV/c

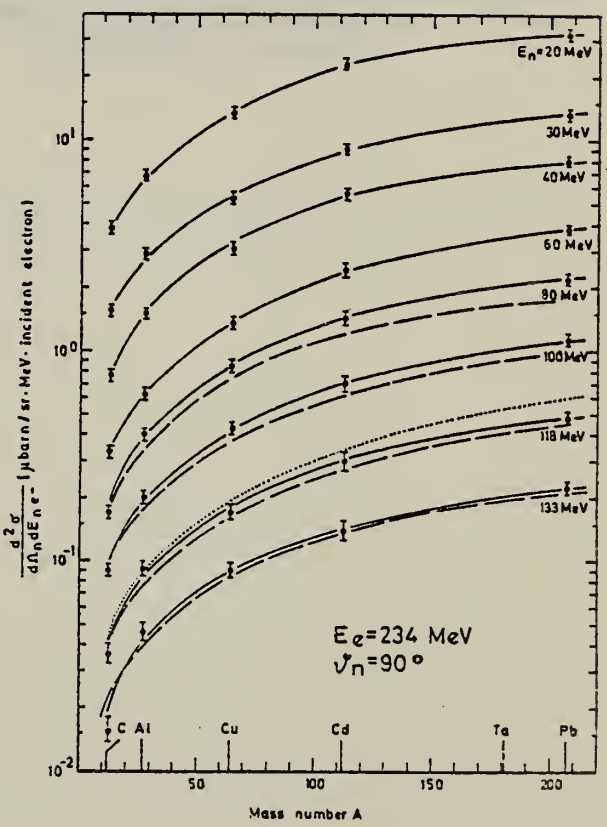

Fig. 9. Dependence of the production cross section on the mass number A with the neutron energy as parameter, measured at E_e=234 MeV. The γ-quanta were produced in a 0.3 cm thick lead sheet (see Fig. 2b) in front of the target of mass number A. The solid lines are fit curves through the measured values. The dashed lines are values calculated using a quasi-deuteron model with the parameters (defined in the text): E_b=−10 MeV, E_{well}=30 MeV, α=140 MeV/c and $C'L$=19.0. The dotted curve represents the dependence NZ/A, fitted at A=12. The error bars correspond to the statistical error

(over)

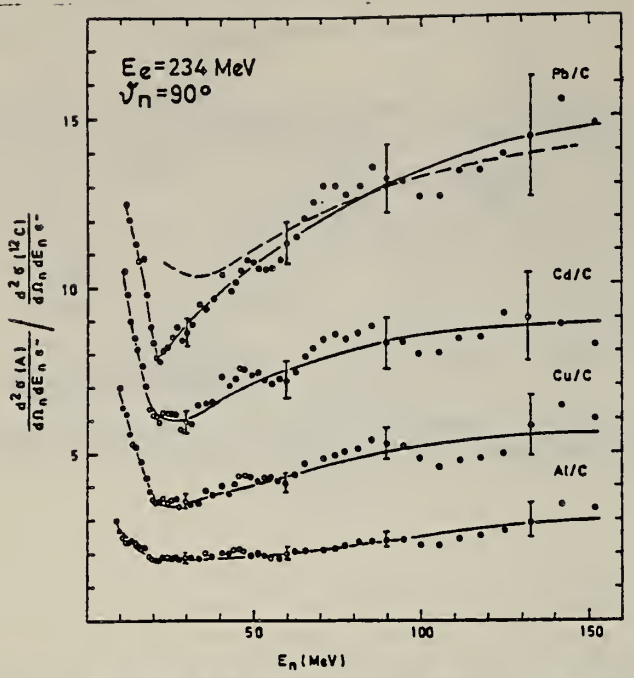

Fig. 10. Neutron yield from targets of mass number A relative to carbon, measured at $E_e = 234$ MeV. The target arrangement is that of Fig. 2b. The solid lines are fit curves through the experimental values. The dashed curve shows the energy dependence of the ratio of the nuclear absorption factors $f_a(\mathrm{Pb})/f_a(\mathrm{C})$, taken from Fig. 6. The error bars correspond to the statistical error

REF. B. Friberg, I. Blomqvist, and B. Forkman
Z. Physik 262, 255 (1973)

ELEM. SYM.	A	Z
Al	27	13

METHOD

REF. NO. 73 Fr 7 egf

REACTION	RESULT	EXCITATION ENERGY	SOURCE		DETECTOR		ANGLE
			TYPE	RANGE	TYPE	RANGE	
G,PI+	ABX	150-800	G	250-800	ACT-I		4PI

Measured range of Mg-27 recoils. MG-27 ACT

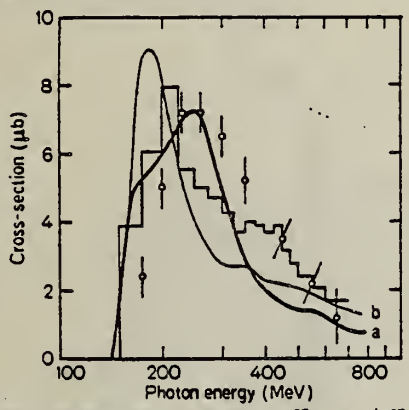

Fig. 5. The calculated cross-sections for the reaction $^{27}Al(\gamma, \pi^+)^{27}Mg$ from this work (curve *a*) compared with the calculations in [2] (curve *b*) and the experimental cross-sections from [2] (histogram) and [3] (open circles). Calculated cross-sections refer to one available nucleon, experimental data are normalized with the factor 5.4 from [2]

2 Blomqvist, I., Nydahl, G., Forkman, B.: Nucl. Phys. A162, 193 (1971).

REF. A. Järund, B. Friberg, and B. Forkman
Z. Physik 262, 15 (1973)

ELEM. SYM.	A	Z
Al	27	13

METHOD

REF. NO. 73 Ja 3 egf

REACTION	RESULT	EXCITATION ENERGY	SOURCE TYPE	SOURCE RANGE	DETECTOR TYPE	DETECTOR RANGE	ANGLE
G,NA24	ABY	THR-999	C	100-999	ACT-I		4PI

999=1 GEV

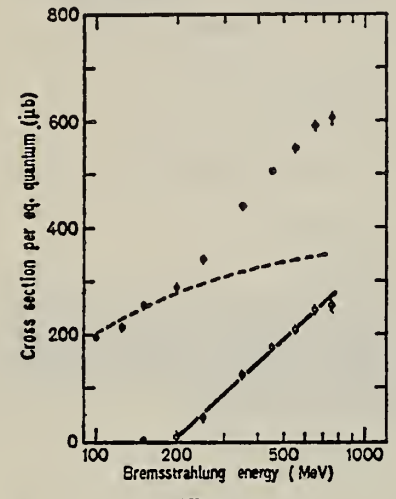

Fig. 1

Fig. 1. The determined yield for the reaction $^{27}Al \rightarrow {}^{24}Na$ (filled circles). Dashed line represents the yield arising from low energy processes, open circles give the difference between the determined yield and the yield from low energy processes. Solid line gives the least-squares fit for the $\bar{\sigma}$ determination

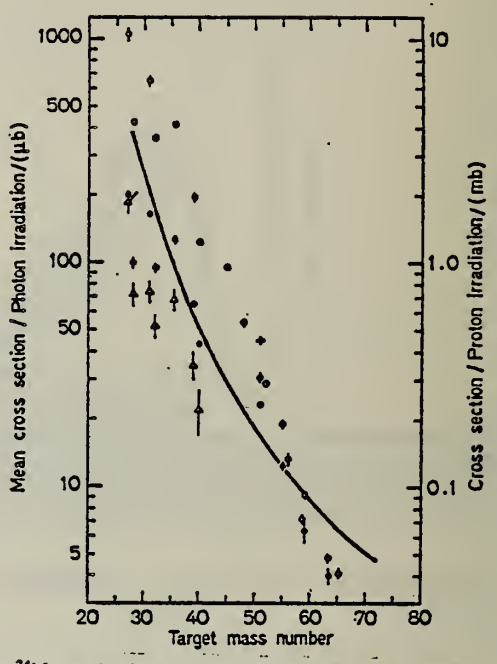

Fig. 7. Mean cross sections for ^{24}Na production as a function of target mass number. Present work filled circles. Noga *et al.* [3] open triangles, Kumbartzki *et al.* [13] cross and Korteling *et al.* [1] 400 MeV protons open circles. The solid line gives the mean cross sections calculated by Jonsson *et al.* [17]

[1] Korteling, R.G. et al., J. Inorg. Nucl. Chem. 29, 2863 (1967).

[3] Noga, V.I. et al., Sov. J. Nucl. Phys. 9, 637 (1969).

[13] Kumbartzki, G. et al., Nucl. Phys. A176, 23 (1971).

[17] Jonsson, G.G. et al., LUNP7212, Oct. 1972, to be published in Physica Scripta.

REF.

T. Saito
J. Phys. Soc. Japan 35, 1 (1973)

A1	27	13

METHOD

REF. NO. 73 Sa 14 egf

REACTION	RESULT	EXCITATION ENERGY	SOURCE		DETECTOR		ANGLE
			TYPE	RANGE	TYPE	RANGE	
G,G	LFT	3	C	5	NAI-D		120

Self-absorption measurements 3=2.98

The bremsstrahlung beam from a 5 MeV electron linear accelerator was used to excite and study low-lying levels in ^{6}Li, ^{11}B and ^{27}Al. A self-absorption method was used to find the widths Γ of these levels. The following level widths are obtained: $\Gamma=(6.5^{+2.4}_{-1.7})$ eV for the 3.56 MeV level in ^{6}Li; $\Gamma=(0.23\pm0.09)$ eV for the 2.12 MeV level, and $\Gamma=(0.53\pm0.21)$ eV for the 4.44 MeV level in ^{11}B. For the 2.98 MeV level in ^{27}Al, the level width is found to be $\Gamma=(0.10\pm0.04)$ eV assuming that the lower energy member of the doublet at 3 MeV is excited.

REF. P. David, J. Debrus, F. Lubke, H. Mommsen, R. Schoenmackers, and G. Stein
Nucl. Phys. A221, 145 (1974)

ELEM. SYM.	A	Z
Al	27	13

METHOD

REF. NO. 74 Da 2 egf

REACTION	RESULT	EXCITATION ENERGY	SOURCE		DETECTOR		ANGLE
			TYPE	RANGE	TYPE	RANGE	
G,P	ABY	12-450	C	450	TEL-D		90
G,T	ABY	23-450	C	450	TEL-D		90
G,HE*	ABY	34-450	C	450	TEL-D		90
G,A	ABY	20-450	C	450	TEL-D		90

*HE=HE3

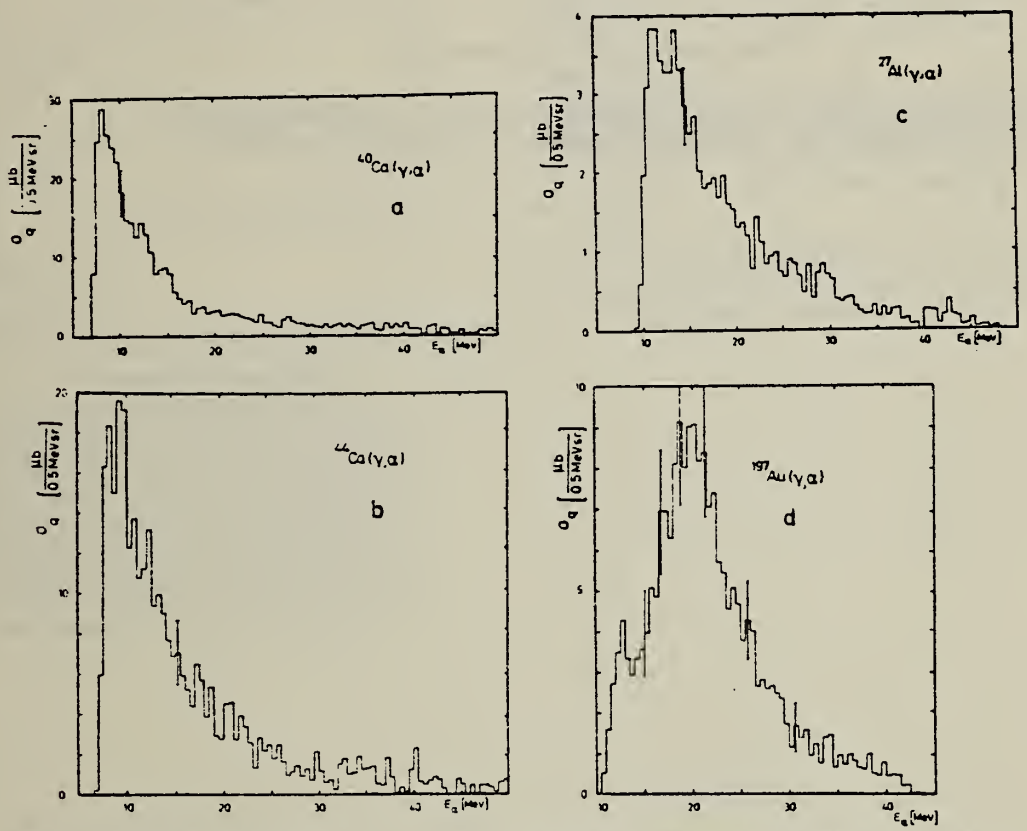

Fig. 4. Characteristic measured spectra of p, t, ^{3}He and ^{4}He from the target nuclei ^{27}Al, ^{40,44}Ca, ^{nat}Ag, ^{197}Au.

(over)

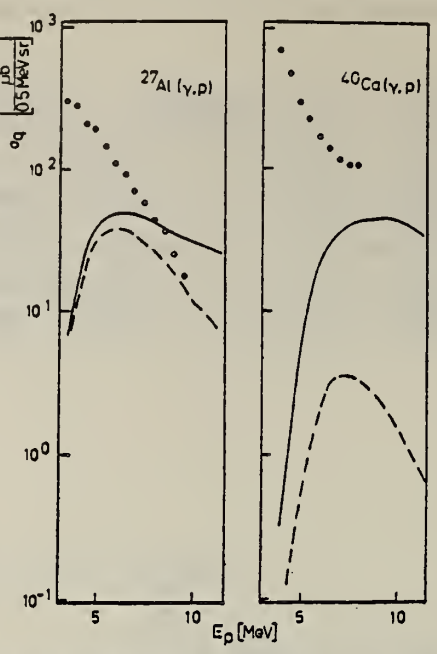

Fig. 6. Experimental data with statistical model calculations for the reactions $^{27}Al(\gamma, p)$ and $^{40}Ca(\gamma, p)$. Broken line for $E_\gamma^{max} = 50$ MeV (calculation). Full line for $E_\gamma^{max} = 450$ MeV (fit).

REF.

V. DiNapoli and M.L. Terranova
J. Inorg. Nucl. Chem. 36, 3633 (1974)

ELEM. SYM.	A	Z
Al	27	13

METHOD

REF. NO. 74 Di 7 egf

REACTION	RESULT	EXCITATION ENERGY	SOURCE TYPE	SOURCE RANGE	DETECTOR TYPE	DETECTOR RANGE	ANGLE
G,3P3N	ABY	THR* 1	C	300* 1	ACT-I		4PI

1 = 1 GEV

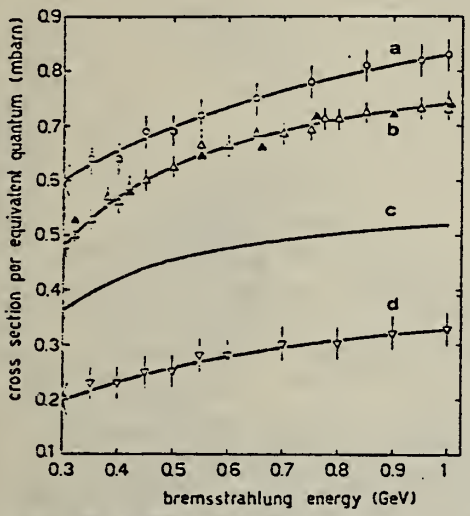

Fig. 1. Cross section per equivalent quantum σ_Q vs the bremsstrahlung maximum energy. Curve a is an eye-fit of the present work values (open circles) for the reaction ^{23}Na(γ, 2p 3n)^{18}F. Curve b is an eye-fit of the present work values (open triangles) and the values taken from Ref. [2] (filled triangles) for the reaction ^{27}Al(γ, 2p 3n)^{22}Na. Curve c is the best-fit of the present work values and values taken from Refs. [18, 20–22] for the reaction ^{12}C(γ, 2p 3n)^{7}Be; for the sake of simplicity, experimental points have not been reported. Curve d is an eye-fit of the present work values (reversed open triangles) for the reaction ^{16}O(γ, 2p 3n)^{11}C.

[2] V. di Napoli, A.M. Lacerenza, F. Salvetti, H.G. de Carvalho, and J.B. Martins, Nuovo Cimento Lettere 1, 835 (1971).

[18] V. di Napoli, D. Margadonna, F. Salvetti, H.G. de Carvalho, and J.B. Martins, Nucl.Inst. Meth. 93, 77 (1971).

[20] V. di Napoli, F. Dobici, O. Forina, F. Salvetti and H.G. de Carvalho, Lett. Nuovo Cimento 55B, 95 (1968).

[21] V. di Napoli, Nucl.Inst. Meth. 69, 155 (1969).

[22] V.I.Noga, Yu.N. Ranyuk, P.V. Sorokin, and V.A. Tkachenko, Ukrainian J. Phys. 16, 1850 (1971) in Russian.

REF.

V.I. Noga, Yu.N. Ranyuk, and P.V. Sorokin
Yad. Fiz. 19, 945 (1974)
Sov. J. Nucl. Phys. 19, 484 (1974)

ELEM. SYM.	A	Z
Al	27	13

METHOD

REF. NO.	
74 No 2	hmg

REACTION	RESULT	EXCITATION ENERGY	SOURCE		DETECTOR		ANGLE
			TYPE	RANGE	TYPE	RANGE	
G,N2P	RLX	THR-999	C	300*999	ACT-I		4PI
E,N2P	RLX	THR-999	C	300*999	ACT-I		4PI

*999=1.2GEV, E/G

The induced-activity method has been used to study the ratio of the cross sections for photo- and electrodisintegration of nuclei for the reactions $^{27}Al \rightarrow {}^{24}Na$ and $^{63,65}Cu \rightarrow {}^{58}Co$ in the energy interval 300–1200 MeV. The results of the measurements are compared with calculations with various assumptions regarding the spectra of virtual and real photons.

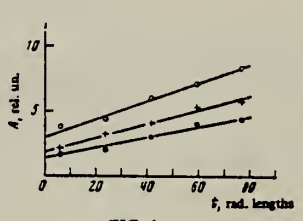

FIG. 1

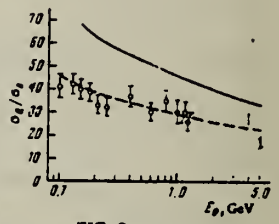

FIG. 2

FIG. 1. Target activity as a function of radiator thickness. Points: ○–E_0 = 800 Mev, +–1170 MeV, ●–600 MeV.

FIG. 2. The ratio σ_Q/σ_e as a function of electron energy E_0. Points: ○–$^{27}Al \rightarrow {}^{24}Na$; ●–$^{63,65}Cu \rightarrow {}^{58}Co$. The thin vertical line shows the data of ref. 4, and the heavy vertical line with end bars shows the data of ref. 5. The curves are theoretical.

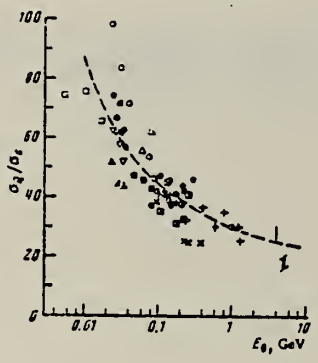

FIG. 4. The ratio σ_Q/σ_e as a function of E_0 for various reactions. Points: +–$^{27}Al \rightarrow {}^{24}Na$; ●–$^{63,65}Cu \rightarrow {}^{58}Co$. These points represent the data of the present work and of ref. 3. The other designations are given in ref. 9.

[3] V.I. Noga et al., Ukr. Fiz. Zh. 13, 2003 (1968).

[4] F.D.S. Butement, H.M.A. Karim, U.V. Myint, and M.B. Zaman, J. Inorg. Nucl. Chem. 33, 2791 (1971).

[5] C.B. Fulmer, K.S. Toth, I.R. Williams, and G.F. Dell, Phys.Rev. C4, 2123 (1971).

[9] G.G. Jonsson and K. Lindgren, Physica Scripta 7, 49 (1973).

REF. H. Tsubota, N. Kawamura, S. Oikawa, and K. Shoda
J. Phys. Soc. Jap. 37, 17 (1974)

EL EM. SYM.	A	Z
Al	27	13

METHOD

REF. NO. 74 Ts 4 egf

REACTION	RESULT	EXCITATION ENERGY	SOURCE TYPE	SOURCE RANGE	DETECTOR TYPE	DETECTOR RANGE	ANGLE
E,P	ABX	8- 26	D	16- 26	MAG-D		90

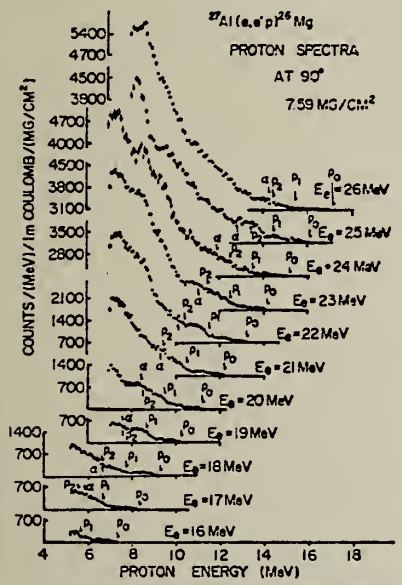

Fig. 1. The proton energy spectra for ^{27}Al(e, e'p) ^{26}Mg reaction at 90° with a thick target (7.59 mg/cm^2). The arrows in the each spectrum indicate the maximum energies for p_0-, p_1- and p_2- protons and photoalphas.

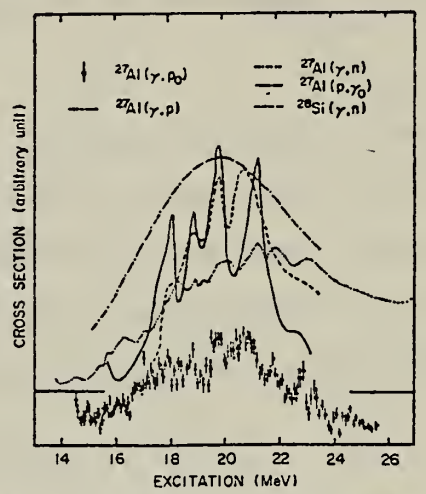

Fig. 6. A comparison of the structures for the ^{27}Al(γ, p_0)^{26}Mg, ^{27}Al(γ, p)^{26}Mg (ref. 15), ^{27}Al(γ, n)^{26}Al (ref. 14), ^{27}Al(p, γ_0)^{28}Si (ref. 2) and ^{28}Si(γ, n)^{27}Si (ref. 16) reactions. The (p, γ_0) cross section is that smoothed by using an averaging interval of 600 keV.

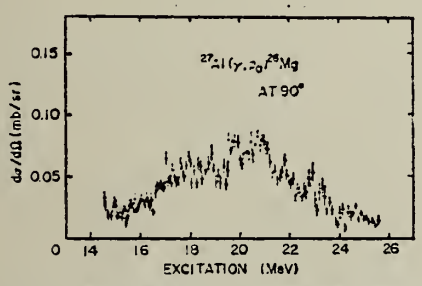

Fig. 4. The differential cross section for ^{27}Al(γ, p_0)^{26}Mg reaction at 90° which was extracted from proton energy spectra of a thick target.

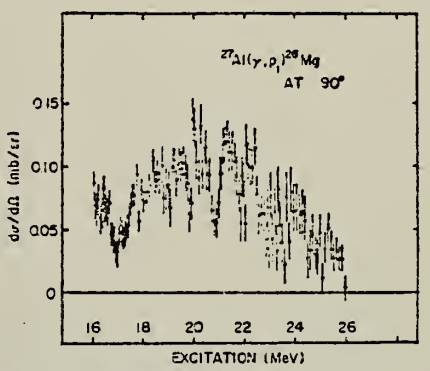

Fig. 5. The differential cross section for the ^{27}Al(γ, p_1)^{26}Mg reaction at 90°.

(over)

Table I. The integrated differential cross sections (MeV-mb/sr) at 90°.

	$\int \frac{d\sigma(\gamma, p_0)}{d\Omega} dE$ *	$\int \frac{d\sigma(\gamma, p_1)}{d\Omega} dE$ *	$\int \frac{d\sigma(\gamma, p)}{d\Omega} dE$ *	R **
^{27}Al	$0.45 \pm 0.06^{25.5}_{14.5}$ a)	$0.92 \pm 0.21^{26.0}_{16.1}$ a)	7.69^{23}_{0} b)	0.05
^{28}Si	$4.68^{23.2}_{0}$ c)		11.15^{23}_{0} b)	0.42

* The subscripts and superscripts in the value of this column give the limits of integration in MeV.

** R is defined as $R = \int \frac{d\sigma(\gamma, p_0)}{d\Omega} dE \Big/ \int \frac{d\sigma(\gamma, p)}{d\Omega} dE$.

a) Present data.

b) Deduced from the (γ, p) cross section by ref. 15 assuming an isotropic angular distribution.

c) Calculated from the data of ref. 2.

2 P.P. Singh et al., Phys. Rev. Lett. 13,

2 P.P. Singh et al., Nucl. Phsy. 65, 577 (1965).

14 S.C. Fultz et al., Phys. Rev. 143, 790 (1966).

15 K. Shoda et al., J.Phys.Soc.Jap. 17, 735 (1962).

16 J.T. Caldwell et al., Phys. Lett. 6, 213 (1963).

REF.

A. Veyssiere, H. Beil, R. Bergere, P. Carlos, A. Lepretre, and A. De Miniac
Nucl. Phys. A227, 513 (1974)

ELEM. SYM.	A	Z
Al	27	13

METHOD

REF. NO. 74 Ve 1 egf

REACTION	RESULT	EXCITATION ENERGY	SOURCE		DETECTOR		ANGLE
			TYPE	RANGE	TYPE	RANGE	
G,N *	ABX	13- 31	D	13- 31	BF3-I		4PI
G,2N **	ABX	24- 31	D	24- 31	BF3-I		4PI

* 886+
** 887

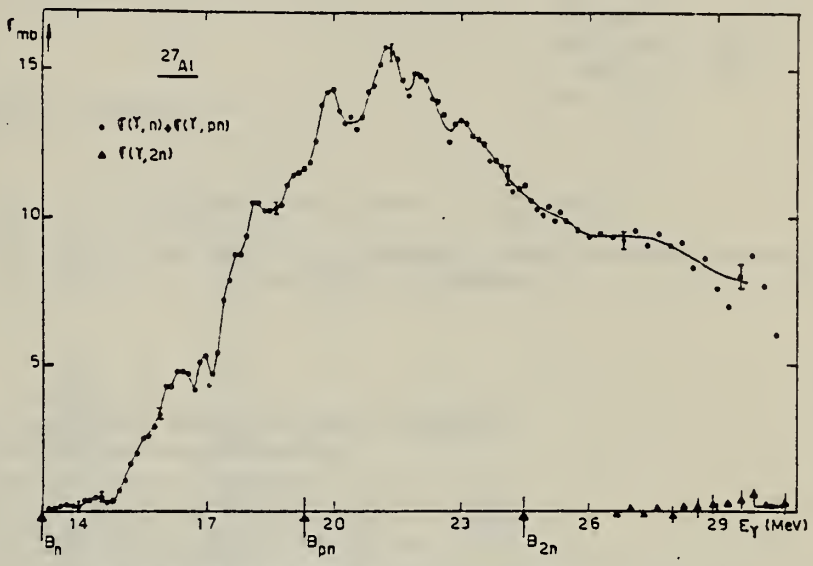

Fig. 6. Photoneutron cross sections $[\sigma(\gamma, n)+\sigma(\gamma, pn)]$ and $\sigma(\gamma, 2n)$ of ^{27}Al.

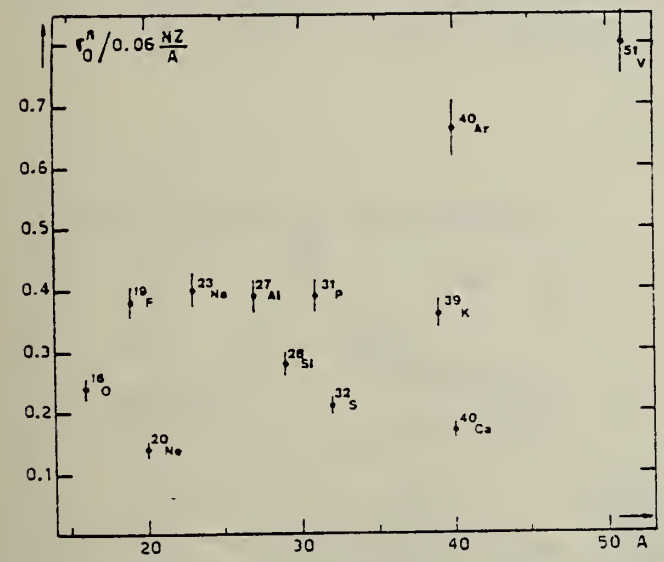

Fig. 22. Ratio of experimental integrated photoneutron cross section σ_0^n over the Thomas, Reiche and Kuhn sum rule $[0.06\ NZ/A]$. Numerical values and upper integration limits E_M are taken from table 3. Also $\Delta\sigma_0^n = \pm 7\%$ for all nuclei.

(over)

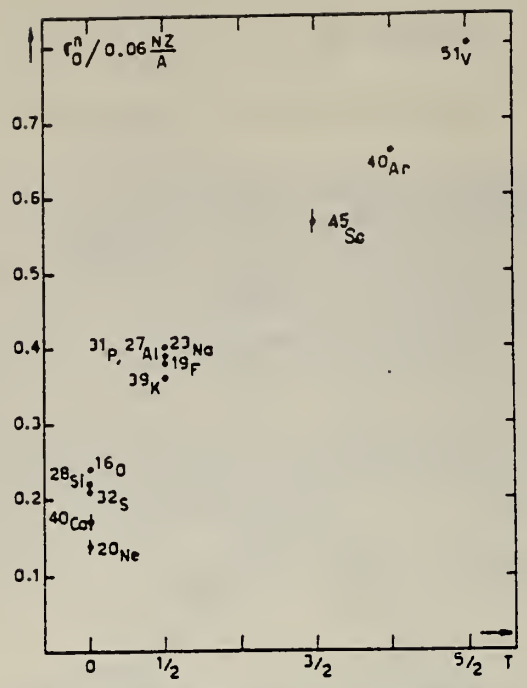

Fig. 24. The $[\sigma_0^n/(0.06\,NZ/A)]$ ratio as a function of isospin T. Possible overall errors of $\pm 7\%$ are to be applied to all nuclei shown.

TABLE 3

Experimental integrated photoneutron cross sections $\sigma_0^n = \int_0^{E_M} \sigma_{T_n}(E)\mathrm{d}E$ compared with the classical sum rule [0.06 NZ/A] of Thomas, Reich and Kuhn

	$T=0$					$T=\frac{1}{2}$					$T=\frac{3}{2}$	$T=2$	$T=\frac{5}{2}$
Nucleus	^{16}O	^{20}Ne	^{28}Si	^{32}S	^{40}Ca	^{19}F	^{23}Na	^{27}Al	^{31}P	^{39}K	^{45}Sc	^{40}Ar	^{51}V
σ_0^n (MeV · mb)	58 ±4	42 ±3	94 ±7	98 ±7	100 ±7	108 ±7	137 ±9	158 ±10	182 ±12	210 ±14	383 ±25	393 ±28	602 ±42
$\sigma_0^n/(0.06NZ/A)$	0.24	0.14	0.22	0.21	0.17	0.38	0.40	0.39	0.39	0.36	0.57	0.66	0.6
E_{x1} (MeV)	30	26.7	30	30	29.5	29	30	30	29	30	28.1	26.7	28

REF. J. Ahrens, H. Borchert, K.H. Czock, H.B. Eppler, H. Gimm, H. Gundrum, M. Kroning, P. Riehn, G. Sita Ram, A. Zieger, and B. Ziegler
Nucl. Phys. A251, 479 (1975)

ELEM. SYM.	A	Z
Al	27	13

METHOD

REF. NO. 75 Ah 3 egf

REACTION	RESULT	EXCITATION ENERGY	SOURCE		DETECTOR		ANGLE
			TYPE	RANGE	TYPE	RANGE	
G,MU-T	ABX	10-160	C	140-275	MGC-D		4PI

928+

TABLE 2

The moments of the experimental nuclear cross section distributions integrated from 10 MeV to the energy E, and their statistical errors

	E (MeV)	Σ_{-2} (mb/MeV)	±(%)	Σ_{-1} (mb)	±(%)	Σ_0 (mb·MeV)	±(%)	Σ_{+1} (b·MeV²)	±(%)	Σ_{+2} (b·MeV³)	±(%)
Li	100	0.196	1.1	4.64	1.0	143	1.7	5.82	3.1	305	5
	140	0.197	1.1	4.79	1.0	161	1.9	8.03	3.4	577	5
	210	0.198	1.1	5.03	1.0	206	2.0	16.60	3.7	2220	5
Be	100	0.192	2.5	5.19	1.5	173	2.0	7.11	3.4	362	5
	140	0.194	2.5	5.33	1.5	189	2.1	9.09	3.6	600	6
	210	0.195	2.5	5.58	1.5	236	2.1	17.80	3.5	2240	5
C	100	0.313	1.7	8.81	1.1	291	1.6	12.00	2.9	630	4
	140	0.316	1.7	9.18	1.2	334	2.2	17.10	5	1250	7
O	100	0.580	1.6	14.50	1.3	432	2.0	16.00	4	748	8
	140	0.585	1.6	15.10	1.3	508	2.5	25.20	5	1880	8
Al	100	1.10	1.8	25.70	1.5	739	2.6	27.9	5	1400	8
	140	1.11	1.8	26.3	1.7	807	3.9	36.4	9	2450	16
Ca	100	2.22	1.2	45.5	1.5	1120	3.6	34.9	9	1430	18
	140	2.23	1.2	46.8	1.7	1290	4.6	56.6	11	3710	19

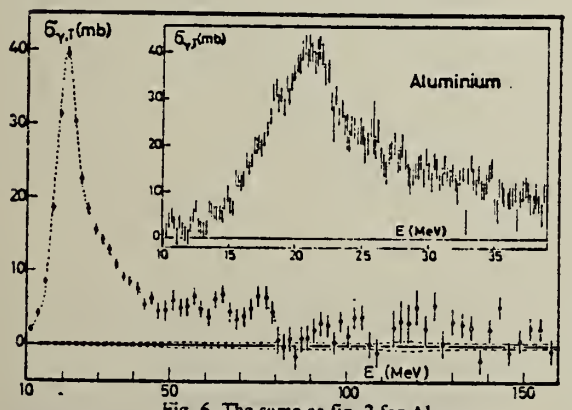

Fig. 6. The same as fig. 2 for Al.

Fig. 2. Total photonuclear cross section for natural Li. The error bars indicate one standard deviation of counting statistics from the main spectrometer. The dashed lines along the abscissa indicate the uncertainty due to counting statistics in the normalizing spectrometer. Oscillations of the base line within this area are possible, the period of these oscillations, however, must not be smaller than 10% in photon energy. The dashed and dotted lines through the cross section values have been drawn to guide the eye.

REF.

V. di Napoli, G. Rosa, F. Salvetti, M. L. Terranova,
H. G. de Carvalho, J. B. Martins, O. A. P. Tavares
J. Inorg. Nucl. Chem. 37, 1101 (1975)

ELEM. SYM.	A	Z
Al	27	13

METHOD

REF. NO. 75 Di 4 egf

REACTION	RESULT	EXCITATION ENERGY	SOURCE		DETECTOR		ANGLE
			TYPE	RANGE	TYPE	RANGE	
G,F18	ABY	THR-999	C	300-999	ACT-I		4PI
G,NA22	ABY	THR-999	C	300-999	ACT-I		4PI
G,NA24	ABY	THR-999	C	300-999	ACT-I		4PI

999 = 1 GEV

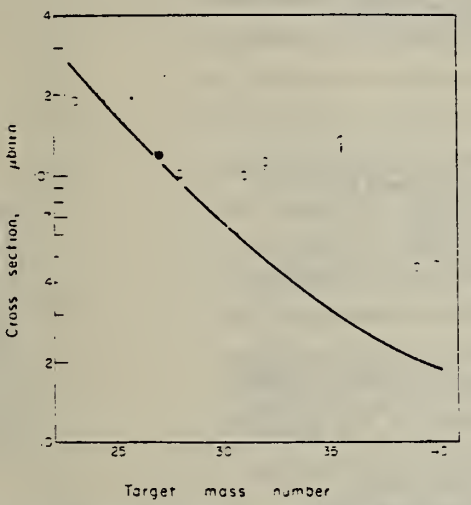

Fig. 2. Mean absolute cross section of ^{18}F photoproduction vs the target mass number. Open triangle: energy range 0·15–0·72 GeV, Ref. [18]. Filled circle: energy range 0·3–1 GeV, Ref. [3]. Open circles: present work. The curve has been calculated by means of Eqn (1).

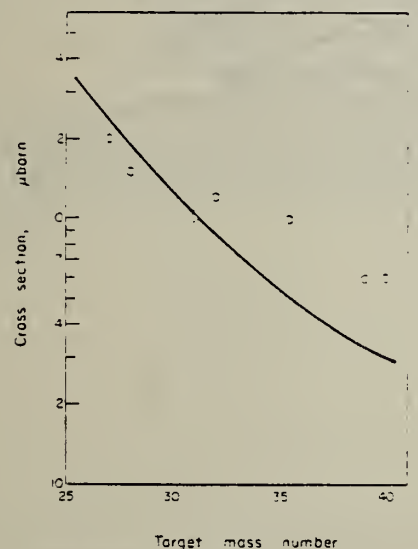

Fig. 3. Mean absolute cross section of ^{22}Na photoproduction vs the target mass number. The curve has been calculated by means of Eqn (1).

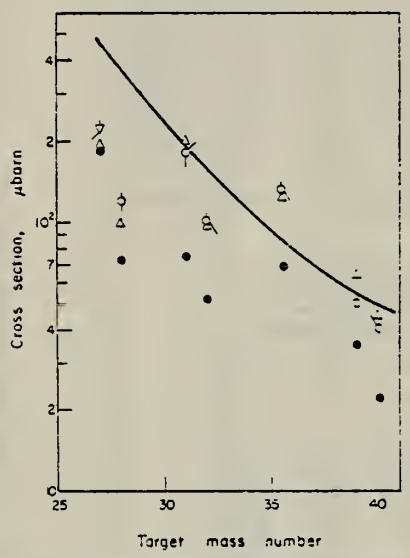

Fig. 4. Mean absolute cross section of ^{24}Na photoproduction vs the target mass number. Filled circles: energy range 0·1–1 GeV, Ref. [20]. Reversed open triangle: energy range 0·3–1 GeV, Ref. [8]. Open triangles: energy range 0·25–1 GeV, Ref. [19]. Open circles: present work. The curve has been calculated by means of Eqn (1).

Table 2. Cross-section per equivalent quantum $\sigma_Q(\mu b)$ of photoproduction of ^{18}F

Target nucleus	Bremsstrahlung maximum energy E_0(GeV)				
	0·30	0·40	0·55	0·75	1·00
^{23}Na	590 ± 30	640 ± 30	720 ± 30	780 ± 30	830 ± 30
^{27}Al*	116 ± 7	172 ± 6	202 ± 6	245 ± 5	270 ± 5
^{28}Si	80 ± 10	110 ± 10	145 ± 10	170 ± 10	200 ± 10
^{31}P	60 ± 10	90 ± 10	130 ± 10	150 ± 10	180 ± 10
^{32}S	55 ± 10	90 ± 10	125 ± 10	160 ± 10	190 ± 10
$^{35,37}Cl$	185 ± 20	230 ± 20	270 ± 20	310 ± 20	350 ± 20
^{39}K	35 ± 5	50 ± 5	65 ± 5	75 ± 5	90 ± 5
^{40}Ca	5 ± 2	20 ± 3	35 ± 5	45 ± 5	60 ± 5

*The results for ^{27}Al have already been published (see [3]) and are reported for comparison.

(over)

Table 3. Cross-section per equivalent quantum $\sigma_Q(\mu b)$ of photoproduction of ^{22}Na

Target nucleus	Bremsstrahlung maximum energy E_0 (GeV)				
	0·30	0·40	0·55	0·75	1·00
^{27}Al	490 ± 20	560 ± 20	667 ± 20	690 ± 20	745 ± 20
^{28}Si	290 ± 20	330 ± 20	380 ± 20	430 ± 20	470 ± 20
^{31}P	230 ± 20	250 ± 20	290 ± 20	330 ± 20	350 ± 20
^{32}S	206 ± 10	240 ± 10	280 ± 10	320 ± 10	350 ± 10
$^{35,37}Cl$	230 ± 10	260 ± 10	290 ± 10	320 ± 10	350 ± 10
^{39}K	30 ± 3	50 ± 5	65 ± 5	80 ± 5	100 ± 5
^{40}Ca	5 ± 2	20 ± 3	45 ± 5	60 ± 5	60 ± 5

Table 4. Cross-section per equivalent quantum $\sigma_Q(\mu b)$ of photoproduction of ^{24}Na

Target nucleus	Bremsstrahlung maximum energy E_0 (GeV)				
	0·30	0·40	0·55	0·75	1·00
$^{27}Al^*$	370 ± 10	440 ± 10	500 ± 20	550 ± 20	660 ± 20
^{28}Si	100 ± 10	140 ± 10	160 ± 10	210 ± 10	240 ± 10
^{31}P	100 ± 20	160 ± 20	200 ± 20	270 ± 20	310 ± 20
^{32}S	120 ± 10	160 ± 10	180 ± 10	210 ± 10	240 ± 10
$^{35,37}Cl$	65 ± 10	100 ± 10	140 ± 10	190 ± 10	220 ± 10
^{39}K	20 ± 5	35 ± 5	55 ± 5	65 ± 5	80 ± 5
^{40}Ca	12 ± 3	25 ± 5	35 ± 5	50 ± 5	60 ± 5

*The results for ^{27}Al have already been published (see [8]) and are reported for comparison.

Table 5. Mean absolute cross-section $\bar{\sigma}_A(\mu b)$ in the energy range 0·3–1 GeV

Target nucleus	Produced radionuclide		
	^{18}F	^{22}Na	^{24}Na
^{22}Na	190 ± 30		
$^{27}Al^*$	120 ± 10	200 ± 20	220 ± 20
^{28}Si	100 ± 10	150 ± 20	120 ± 10
^{31}P	100 ± 10	100 ± 20	180 ± 20
^{32}S	110 ± 10	120 ± 10	100 ± 10
$^{35,37}Cl$	135 ± 20	100 ± 10	130 ± 10
^{39}K	45 ± 5	60 ± 5	50 ± 5
^{40}Ca	46 ± 5	60 ± 5	40 ± 5

*The results for the photoproduction of ^{18}F and ^{24}Na from ^{27}Al have already been published (Ref. [3] and [8]. respectively).

2. V. di Napoli and M. L. Terranova, *J. inorg. nucl. Chem.* 36, 3633 (1974).
3. V. di Napoli, A. M. Lacerenza, F. Salvetti, S. M. Terenzi, H. G. de Carvalho and J. B. Martins, *J. inorg. nucl. Chem.* 35, 1419 (1973).
4. C. M. Lederer, J. M. Hollander and I. Perlman, *Table of Isotopes.* 6th Edn Wiley, New York (1967).
5. R. G. Korteling and A. A. Caretto, Jr., *J. inorg. nucl. Chem.* 29, 2863 (1967).
6. R. G. Korteling and A. A. Caretto, Jr., *Phys. Rev.* C1, 193 (1970).
7. R. G. Korteling and A. A. Caretto, Jr., *Phys. Rev.* C1, 1960 (1970).
8. V. di Napoli, A. M. Lacerenza, F. Salvetti, H. G. de Carvalho and J. B. Martins, *Lett. Nuovo Cimento* 1, 835 (1971).
9. I. Halpern, R. J. Debs, J. T. Eisinger, A. W. Fairhall and H. G. Richter, *Phys. Rev.* 97, 1327 (1955).
10. C. B. Fulmer, K. S. Toth, I. R. Williams, T. H. Handley, C. F. Dell, E. L. Callis, T. M. Jenkins and J. M. Wyckoff, *Phys. Rev.* C2, 1371 (1970).
11. G. J. Kumbartzki, U. Kim and C. K. Kwan, *Nucl Phys.* A160, 237 (1970).
12. G. J. Kumbartzki and U. Kim, *Nucl. Phys.* A176, 23 (1971).
13. K. Lindgren and G. G. Jonsson, *Nucl. Phys.* A197, 71 (1972).
14. C. E. Roos and V. Z. Peterson, *Phys. Rev.* 124, 1610 (1961).
15. T. A. Gabriel and R. G. Alsmiller, Jr., *Phys. Rev.* 182, 1035 (1969).
16. G. G. Jonsson and K. Lindgren, *Phys. Scr.* 7, 49 (1973).
17. G. Rudstam, *Z. Naturf.* 21a, 1027 (1966).
18. A. Masaike, *J. phys. Soc. Japan* 19, 427 (1964).
19. A. Jārund, B. Friberg and B. Forkman, Private communication to G. G. Jonsson and K. Lindgren, quoted in Ref. [16]; see also A. Jārund, B. Friberg and B. Forkman, University of Lund Report No. LUNP-7303, 1973 (unpublished).
20. V. I. Noga, Yu. N. Ranyuk and P. V. Sorokin, *Yad. Fiz.* 9, 1152 (1969) (transl.: *Sov. J. Nucl. Phys.* 9, 673 (1969)).
21. T. Methasiri and S. A. E. Johansson, *Nucl. Phys.* A167, 97 (1971).
22. J. R. Nix and E. Sassi, *Nucl. Phys.* 81, 61 (1966).
23. W. D. Myers and W. J. Swiatecki, *Nucl. Phys.* 81, 1 (1966).

REF.

B. Johnsson, A. Jarund, B. Forkman
Z. Physik A273, 97 (1975)

ELEM. SYM.	A	Z
Al	27	13

METHOD

REF. NO.	
75 Jo 4	egf

REACTION	RESULT	EXCITATION ENERGY	SOURCE		DETECTOR		ANGLE
			TYPE	RANGE	TYPE	RANGE	
G,2PN	ABY	31-965	C	95-965	ACT-I		4PI

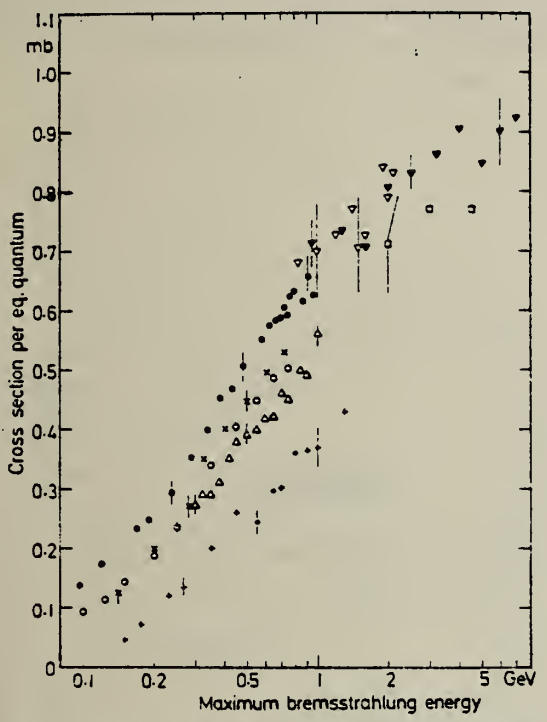

Fig. 1. A survey of the yields of $^{27}Al(\gamma, 2pn)^{24}Na$: ● is the present work. ○ Ref. 5, × Ref. 6, △ Ref. 7, + Ref. 8, ▼ Ref. 3, ▽ Ref. 4 and □ Ref. 9. The bars of the present work and of Refs. 3, 4 and 9 show the standard deviations of the total errors, while these of Refs. 5–7 give the statistical errors. The error bars of Ref. 8 are taken from a figure in the Ref.

Table 1. The absolutely-measured yield per Eq. quantum (mb) with their errors (non-systematical) and the ratio of the absolute to the relative yields

Energy (MeV)	q (mb)	Error (mb)	Ratio $\sigma_{q_{abs}}/\sigma_{q_{rel}}$
95	0.237	±0.017	0.95
120	0.273	0.013	1.04
170	0.333	0.012	0.96
195	0.347	0.014	1.15
240	0.395	0.010	1.00
290	0.454	0.010	1.00
340	0.501	0.004	1.02
385	0.555	0.010	1.04
435	0.568	0.014	0.94
480	0.606	0.008	1.00
580	0.650	0.009	1.03
625	0.675	0.004	1.04
675	0.685	0.010	1.02
700	0.690	0.010	1.02
725	0.705	0.011	1.09
750	0.691	0.010	1.11
770	0.725	0.012	1.02
795	0.731	0.014	0.99
870	0.714	0.013	1.15
915	0.757	0.016	1.06
965	0.726	0.014	0.97
		Mean value	1.03

References

1. Johnsson, B., Järund, A., Forkman, B.: LUNP 7418, December 1974
2. Hyltén, G.: Nucl. Phys. A 158, 225 (1970)
3. Andersson, G., Blomqvist, I., Forkman, B., Jonsson, G.G., Järund, A., Kroon, I., Lindgren, K., Schröder, B., Tesch, K.: Nucl. Phys. A 197, 44 (1972)
4. Kumbartzki, G., Kim, U., Kwan, Ch.K.: Nucl. Phys. A 160, 237 (1971)
5. Järund, A., Friberg, B., Forkman, B.: Z. Physik 262, 15 (1973)
6. Masaike, A.: J. Phys. Soc. Japan 19, 427 (1964)
7. Napoli, N. di, Lacerenza, A.M., Salvetti, F., Carvalho, H.G. de, Benuzzi-Martins, J.: Lett. Nuovo Cimento 1, 835 (1971)
8. Antuf'ev, Yu. P., Miroshnichenko, L.I., Noga, V.I., Sorokin, P.V.: Sov. J. Nucl. Phys. 6, 312 (1968)
9. Vartapetyan, G.A., Danagulyan, A.S., Demëkhina, N.A., Khudaverdyan, A.G.: Sov. J. Nucl. Phys. 17, 685 (1973)

REF. I. Blomqvist, P. Janecek, G.G. Jonsson, R. Peterson, H. Dinter and K. Tesch
Z. Physik A278, 83 (1976)

ELEM. SYM.	A	Z
Al	27	13

METHOD

REF. NO. 76 B1 12 egf

REACTION	RESULT	EXCITATION ENERGY	SOURCE TYPE	SOURCE RANGE	DETECTOR TYPE	DETECTOR RANGE	ANGLE
G,SPL	ABY	THR - 580	C	130-580	ACT-I		4PI
E,SPL	ABY	THR - 580	C	130-580	ACT-I		4PI

Cross sections for some electro- and photoinduced spallation reactions on ^{27}Al and ^{51}V have been measured in the energy region 130-580 MeV with the activation method. The cross sections per photon are compared to Monte-Carlo calculations based on a cascade-evaporation model. The electrodisintegration cross sections are compared to calculations based on the Dalitz formalism for virtual photon spectra.

GIVES YLD RATIO G/E

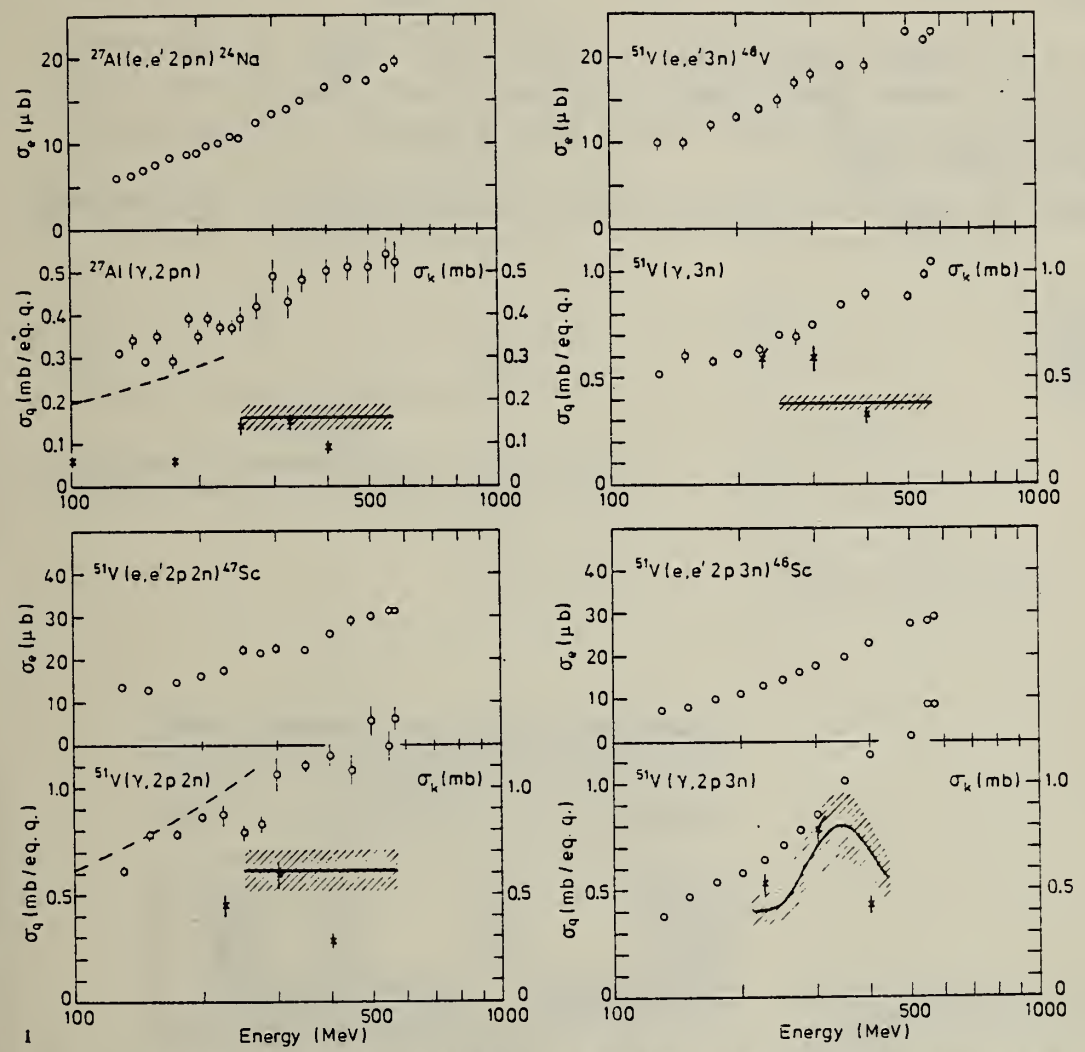

Figs. 1 and 2. Experimental cross sections σ_q and σ_e versus energy for different reactions on ^{27}Al and ^{51}V. The cross sections σ_k deduced from σ_q are given by the solid drawn curves, the hatched areas showing the uncertainty. Dashed curves show σ_q calculated from the low-energy data in Reference 11. Crosses give σ_k calculated with Monte-Carlo method

11 Meyer, R.A., Walters, W.B., Hummel, J.P.: Nucl. Phys. A122, 606 (1968)

(over)

(REV. 7-1-64)
USCOMM-NBS-DC

U.S. DEPARTMENT OF COMMERCE
NATIONAL BUREAU OF STANDARDS

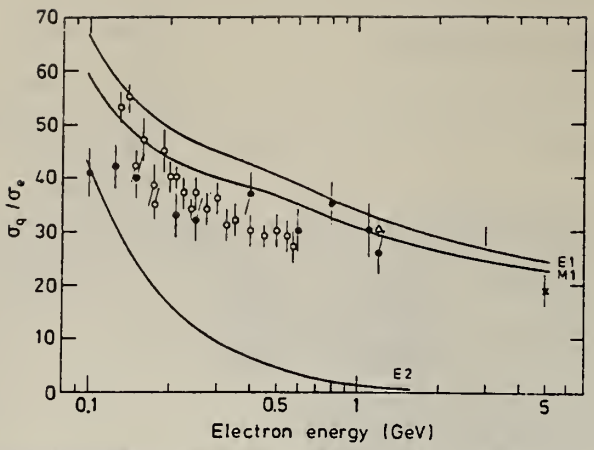

Fig. 4. The ratio σ_q/σ_e versus electron energy for the reaction $^{27}Al\left(\overset{\gamma}{e'}, e', 2pn\right)^{24}Na$. o present work, ● Reference 4, △ Reference 6, ¦ Reference 18, ǂ Reference 19. Solid curves give calculated cross-section ratios

[4] Noga, V.I., Ranyuk, Yu.N., Sorokin, P.V.: Sov. J. Nucl. Phys. 19, 484 (1974)

[6] Noga, V.I., Ranyuk, Yu.N., Sorokin, P.V.: Sov. J. Nucl. Phys. 21, 243 (1975)

[18] Butement, F.D.S., Karim, H.M.A., Myint, U.V., Zaman, M.B.: J. Inorg. Nucl. Chem. 33, 2791 (1971)

[19] Fulmer, C.B., Toth, K.S., Williams, I.R., Dell, G.F.: Phys. Rev. C4, 2123 (1971)

REF. A. S. Danagulyan, N. A. Demekhina
Yad. Fiz. 24, 681 (1976)
Sov. J. Nucl. Phys. 24, 355 (1976)

ELEM. SYM.	A	Z
Al	27	13

METHOD

REF. NO. 76 Da 4 hmg

REACTION	RESULT	EXCITATION ENERGY	SOURCE		DETECTOR		ANGLE
			TYPE	RANGE	TYPE	RANGE	
G,NA24	ABX	THR* 5	C	2* 5	ACT-I		4PI

*ENERGY,GEV

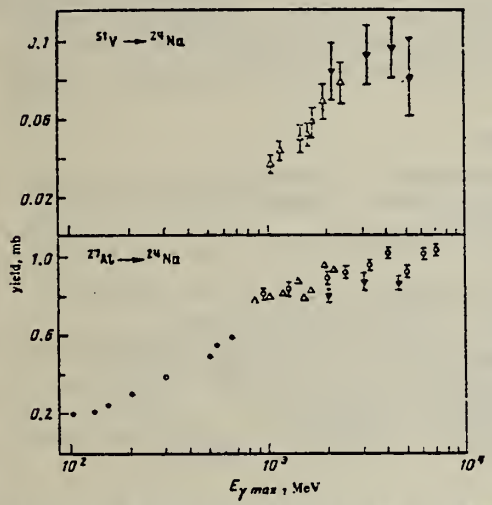

FIG. 1. Yields of the reactions. Points: ▼—present work, ●—Ref. 10, △—Ref. 3, ○—Ref. 9.

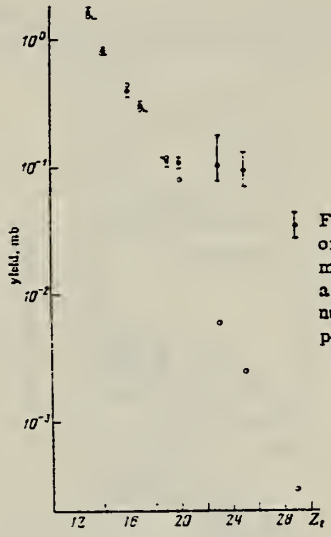

FIG. 2. Yield values and theoretical values according to the modified Rudstam formula as a function of the target charge number Z_t. Points: ●—experiment, ○—theory.

TABLE I. Experimental yields and reaction cross sections obtained in the measurements at the Erevan electron accelerator.

Target nucleus	Reacuon yield, mb $E_{\gamma\ max}$, GeV					Reaction cross section, mb
	2	3	4	4.5	5	
^{27}Al	0.81±0.09	0.87		0.87		0.07215±0.0348
^{28}Si	0.27±0.02	0.28		0.29		0.0287±0.013
^{32}S	0.24±0.02	0.22		0.27		0.0323±0.0155
Cl	0.28±0.03	0.30		0.28		–
^{39}K	0.1±0.01	0.125		0.15		0.06±0.0288
^{40}Ca	0.086±0.01	0.09		0.115		0.035±0.0168
^{51}V	0.085±0.02	0.094±0.02	0.095±0.02		0.082±0.025	0.019
^{55}Mn	0.079±0.02	0.075±0.02	0.087±0.017		0.088±0.015	0.01076±0.0056
Cu	0.029±0.006	0.037±0.007	0.036±0.007		0.034±0.007	0.00547±0.0026

Note. The reaction cross sections have been calculated in the $1/E$ approximation of the bremsstrahlung spectrum.

[3] G. Kumbartzki et al., Nucl. Phys. A176, 23 (1971).

[9] G. Andersson et al., Nucl. Phys. A197, 44 (1972).

[10] I. Blomqvist et al., Nucl. Phys. A162, 193 (1971).

REF. B. Johnsson, A. Jarund and B. Forkman
Z. Physik A276, 410 (1976)

ELEM. SYM.	A	Z
Al	27	13

METHOD

REF. NO. 76 Jo 1 egf

REACTION	RESULT	EXCITATION ENERGY	SOURCE		DETECTOR		ANGLE
			TYPE	RANGE	TYPE	RANGE	
G,2PN	ABX	31-965	C	90-965	ACT-I		4PI

ERRATUM 75Jo4

The present Figure 1 replaces the earlier published one, in which the ordinate scale was displaced 0.1 unit upwards.

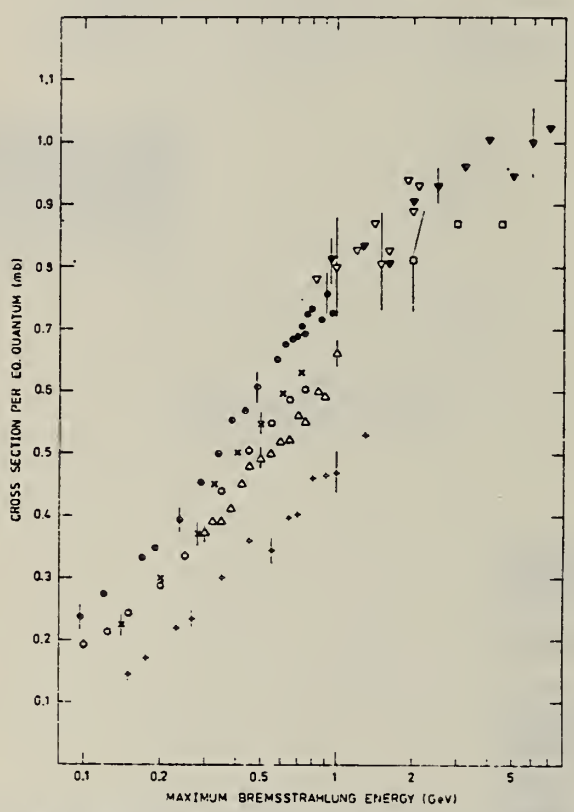

Fig. 1. A survey of the yields of $^{27}Al(\gamma, 2pn)^{24}Na$: ● is the present work, ○ Reference 5, × Reference 6, △ Reference 7, + Reference 8, ▼ Reference 3, ▽ Reference 4 and □ Reference 9. The bars of the present work and of References 3, 4 and 9 show the standard deviations of the total errors, while these of References 5–7 give the statistical errors. The error bars of Reference 8 are taken from a figure in the Reference

References

3. Andersson, G., Blomqvist, I., Forkman, B., Jonsson, G. G., Järund, A., Kroon, I., Lindgren, K., Schrøder, B., Tesch, K.: Nucl. Phys. A197, 44 (1972)
4. Kumbartzki, G., Kim, U., Kwan, Ch. K.: Nucl. Phys. A160, 237 (1971)
5. Järund, A., Friberg, B., Forkman, B.: Z. Physik 262, 15 (1973)
6. Masaike, A.: J. Phys. Soc. Japan 19, 427 (1964)
7. Napoli, N. di, Lecerenza, A. M., Salvetti, F., Carvalho, H. G. de, Benuzzi-Martins, J.: Lett. Nuovo Cimento 1, 835 (1971)
8. Antufév, Yu. P., Miroshnichenko, I. I., Noga, V. I., Sorokin, P. V.: Sov. J. Nucl. Phys. 6, 312 (1968)
9. Vartapetyan, G. A., Danagulyan, A. S., Demëkhina, N. A., Khudaverdyan, A. G.: Sov. J. Nucl. Phys. 17, 635 (1973)

B. Johnsson
A. Järund
Prof. Dr. B. Forkman
Department of Physics
University of Lund
Sölvegatan 14
S-223 62 Lund, Sweden

REF. K. Nakamura, S. Hiramatsu, T. Kamae, H. Muramatsu, N. Izutsu, Y. Watase
Nucl. Phys. A271, 221 (1976)

ELEM. SYM.	A	Z
Al	27	13

METHOD

REF. NO. 76 Na 3 egf

REACTION	RESULT	EXCITATION ENERGY	SOURCE		DETECTOR		ANGLE
			TYPE	RANGE	TYPE	RANGE	
E,E/P	SPC	0*130	D	700	MAG-D		DST

Abstract: Information on proton hole states has been obtained for ^{27}Al, ^{40}Ca and ^{51}V through the (e, e'p) reaction. Lower-lying hole states have been identified. For ^{40}Ca an extensive analysis has been performed to study the structure of the 1s hole state. For ^{27}Al and ^{51}V, the properties of the 1s hole states have also been determined. The separation energies of the 1p and 1s states seem to be constant (40 and 60 MeV, respectively) for $A > 30$.

*SEPARATION ENERGY

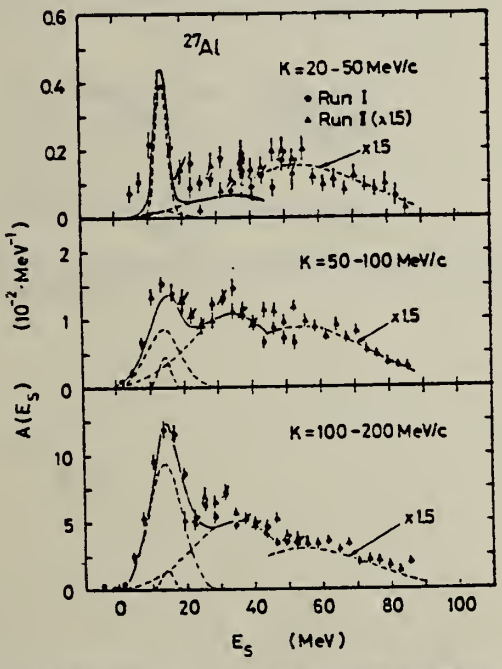

Fig 4a. Proton separation energy spectra for ^{27}Al. The solid curves are the result of the PWIA fit. The contributions from each proton state are shown by the dashed curves.

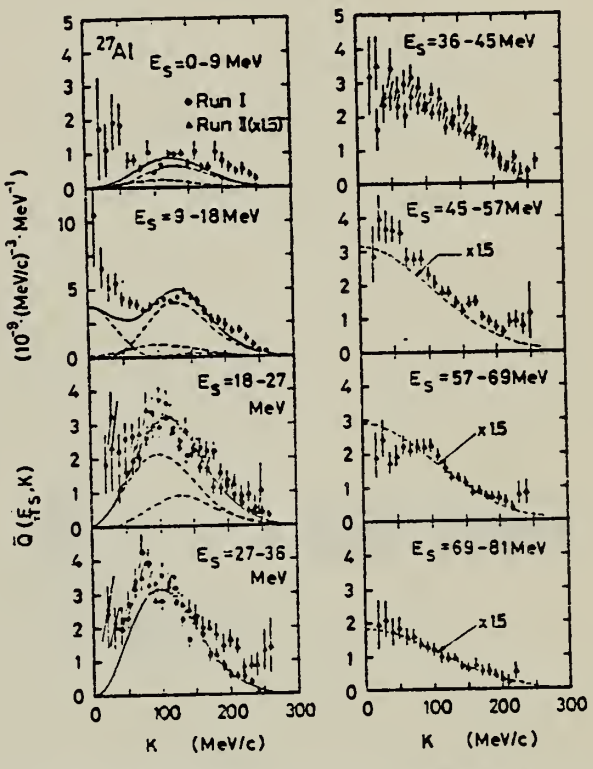

Fig. 4b. Recoil momentum distributions for ^{27}Al. The curves are as in fig. 4a.

(over)

TABLE 6

Results of the PWIA analysis

Nucleus	α	Z'_α	Peak energy (MeV)	Width (FWHM) [a] (MeV)	Oscillator const (MeV/c)
^{27}Al	2s	0.12±0.01	14.3±0.2	4± 3	82±4
	1d	1.6 ±0.1	14.0±0.6	12± 2	91±1
	1p	2.4 ±0.2	34 ±1	31± 3	100±1
	1s [b]		57 ±3	31± 9	148±4
^{40}Ca	$1d_{3/2}$	1.1 ±0.3	10.9±0.7	9± 1	76±4
	2s	0.9 ±0.1	14.4±0.3	13± 1	83±3
	$1d_{5/2}$	1.5 ±0.3	19.0±1.1	10± 1	93±4
	1p	1.8 ±0.4	35 ±1	21± 3	85±3
	1s [b]		59 ±3	34±10	144±6
^{51}V	1f	0.4 ±0.1	10.3±1.1	5± 3	115±8
	2s	0.3 ±0.1	15.1±0.2	5± 2	99±5
	1d	1.7 ±0.3	19.5±0.5	19± 2	94±6
	1p	1.1 ±0.1	40 ±1	25± 4	91±4
	1s [b]		60 ±3	36±11	143±4

The errors are statistical only except for those assigned to the peak energies and widths for the 1s states.

[a] The experimental energy resolution (≈ 7 MeV) is not unfolded.

[b] Parameters were determined from the fit to the data of run II.

REF.	ELEM. SYM.	A	Z
V.G. Vlasenko, V.A. Gol'dshtein, A.V. Mitrofanova, V.I. Noga, Yu.N. Ranuuk, V.I. Startsev, P.V. Sorokin, Yu.N. Telegin Yad. Fiz. 23, 504 (1976) Sov. J. Nucl. Phys. 23, 265 (1976)	Al	27	13

METHOD	REF. NO.	
	76 V1 1	hmg

REACTION	RESULT	EXCITATION ENERGY	SOURCE		DETECTOR		ANGLE
			TYPE	RANGE	TYPE	RANGE	
E,E/	ABX	100-500	D	812-999	MAG-D		14

999=1.396 GEV

Inelastic electron scattering has been used to measure the total hadronic cross sections for absorption of photons with energy 150-500 MeV by nuclei of C, Al, Ni, Mo, and W. The results obtained are compared with calculations carried out in the impulse approximation.

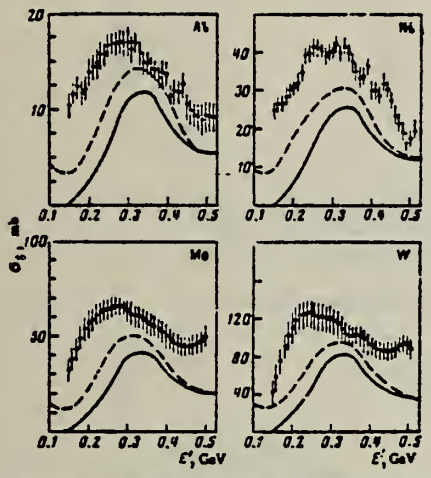

FIG. 5. Total hadronic cross sections for absorption of photons by nuclei.

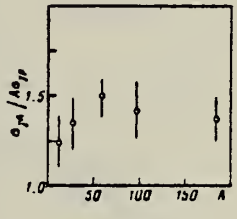

FIG. 6. The ratio $\sigma_{\gamma A}/A\sigma_{\gamma p}$ as a function of A for $k=0.32$ GeV.

REF. Y. Watase, S. Homma and T. Kitagaki
J. Phys. Soc. Japan 40, 1531 (1976)

EL EM. SYM.	A	Z
Al	27	13

METHOD

REF. NO. 76 Wa 3 egf

REACTION	RESULT	EXCITATION ENERGY	SOURCE		DETECTOR		ANGLE
			TYPE	RANGE	TYPE	RANGE	
G,PI+	ABY	140-250	C	250	MAG-D		90
G,PI-	ABY	140-250	C	250	MAG-D		90

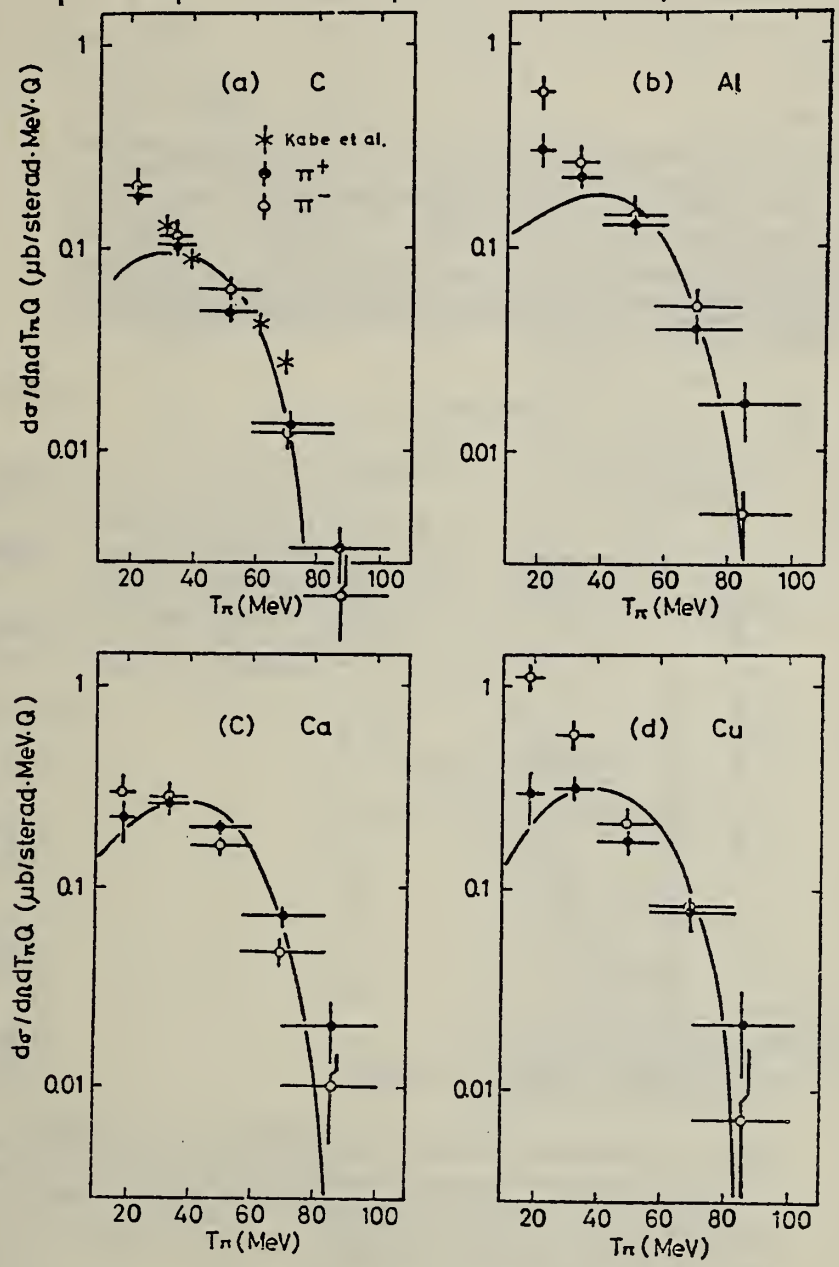

Fig. 2. The energy spectra of photoproduced $\pi^{\pm}$ from C, Al, Ca, and Cu at 90° in the laboratory system by 250-MeV bremsstrahlung. The data of Ca are normalized to 0.26 μb sterad^{-1} MeV$^{-1}\Omega^{-1}$ for π^{+} at 35 MeV. The solid curves are the calculated spectra of π^{+} by a theoretical model.

over

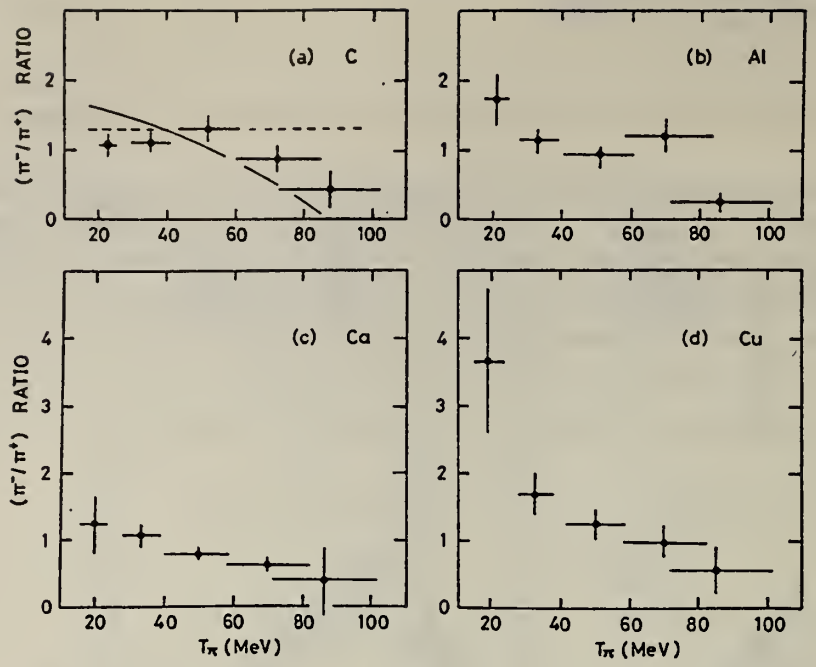

Fig. 3. The π^-/π^+ ratio as a function of the kinetic energy of pions produced from C, Al, Ca, and Cu by 250-MeV bremsstrahlung. The solid curve in (a) is the calculated energy spectrum of π^-/π^+ ratio including the Coulomb potential for C. The dashed curve is the ratio calculated neglecting the Coulomb potential.

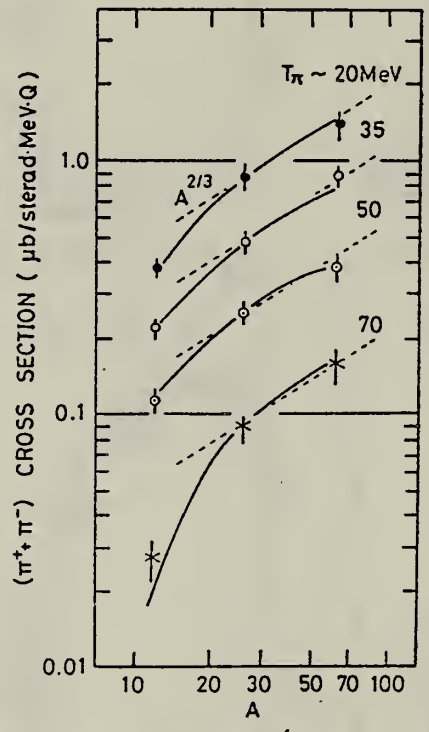

Fig. 4. The A-dependence of the $(\pi^+ + \pi^-)$ cross sections at the pion kinetic energies of ~20 MeV, ~35 MeV, ~50 MeV and ~70 MeV. The solid curves show the relative A-dependence obtained from the theoretical calculation. The dashed lines show $A^{2/3}$ dependence only for guiding eyes.

REF. K.V. Alanakyan, M.Dzh. Amaryan, R.A. Demirchyan, K.Sh. Egiyan, M.S. Ogandzhanyan, & Yu.G. Sharabyan
Yad. Fiz. 25, 545 (March 1977)
Sov. J. Nucl. Phys. 25, 292 (March 1977)

ELEM. SYM.	A	Z
27	Al .	13

METHOD

REF. NO. 77 Al 9 hmg

REACTION	RESULT	EXCITATION ENERGY	SOURCE TYPE	SOURCE RANGE	DETECTOR TYPE	DETECTOR RANGE	ANGLE
G,P	ABX	72-999	C	2 *5 (4-5)	TEL-D	---	DST

COMMENTS: $f \sim \exp(-Bp^2)$

$$B = \frac{E}{p^4(d^2\sigma/d\Omega dpQ)}$$

*E,GEV, 999=4.5 GEV

The A^n-dependence and momentum spectra of photoprotons in the nuclei ^{12}C, ^{27}Al, ^{63}Cu, ^{118}Sn, and ^{208}Pb have been studied experimentally for maximum bremsstrahlung energies of 2.0, 3.0, and 4.5 GeV. The A-dependence shows that the proton photoproduction mechanism for $E_\gamma > 400$ MeV is identical for the entire kinetic-energy region 65–280 MeV and the angle region 45–150° for the secondary protons studied. The dependence of the exponent n on the transverse momentum $p_\perp$ is in good agreement with the same dependence for protons produced in nuclei by primary protons. In the momentum spectra of the invariant cross section $f = (E/p^2)(d^3\sigma/d\Omega dpQ) \sim \exp(-Bp^2)$ it is observed that the parameter B does not depend on the incident-photon energy and on the target nucleus, but depends on the proton-detection angle.

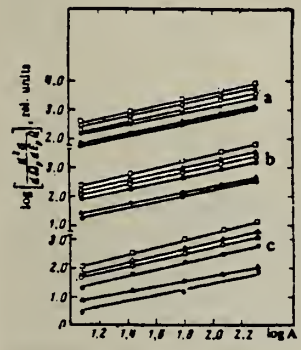

FIG. 1. Differential cross section for proton photoproduction as a function of atomic number A of the nucleus at E_0 = 2 GeV. The lines a correspond to ϑ_p = 60°, b to 90; and c to 150°. Points: □—E_p = 64, Δ—80, ○—101, ■—137, ▲—209, and ●—280 MeV.

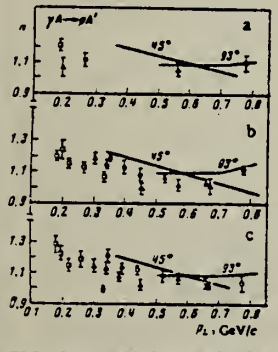

FIG. 2. Dependence of the exponent n in the A^n dependence of the cross section for the reaction $\gamma A \to pA'$ as a function of proton transverse momentum: a—E_0 = 2.0 GeV, b—E_0 = 3.0 GeV, c—E_0 = 4.5 GeV. The points for a and b: Δ—ϑ_p = 60°, ○—90°, □—150°; for c: Δ—ϑ_p = 46°, ○—86°, □—136°. The curves show the dependence of n on $p_\perp$ for the reaction $A(p,p')A'$ taken from Ref. 9.

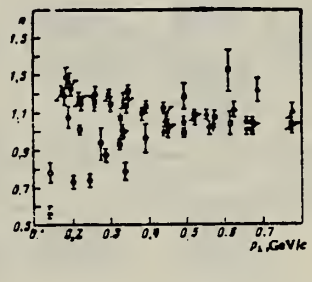

FIG. 3. The same as Fig. 2. Experimental points: ▲—E_0 = 0.13, ○—0.25, ▲—0.4, □—1.2, □—2.0, ×—3.0, and ●—4.5 GeV.

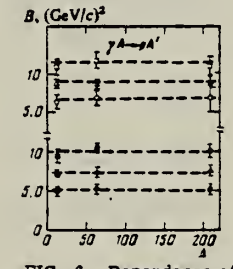

FIG. 6. Dependence of the parameter B from the relation $f \sim \exp(-Bp^2)$ on the atomic number of the target nucleus. The solid points refer to E_0 = 2.0 GeV, and the hollow points to E_0 = 3.0 GeV; the points ● and ○ are for ϑ_p = 60°, ▲ and Δ are for 90°, and ■ and □ are for 150°.

(OVER)

TABLE I. Differential cross section $d^2\sigma/d\Omega dTQ$ of the reaction $\gamma A \to pA'$ in μb/MeV-sr.

A	E_γ, GeV	θ_p, deg	ε_p, MeV					
			64	80	101	137	209	279
^{12}C	2	60	3.720±0.056	2.630±0.032	1.907±0.057	1.423±0.038	0.725±0.220	0.429±0.016
		90	2.274±0.045	1.587±0.047	1.130±0.039	0.763±0.022	0.256±0.008	0.117±0.007
		150	1.152±0.032	0.690±0.014	0.505±0.026	0.218±0.007	0.071±0.005	0.021±0.002
	3	60	4.240±0.100	3.424±0.063	1.960±0.043	1.629±0.046	0.653±0.024	0.452±0.019
		90	2.440±0.056	2.031±0.040	1.145±0.029	0.807±0.028	0.243±0.009	0.088±0.005
		150	1.380±0.042	0.877±0.029	0.438±0.016	0.300±0.010	0.057±0.003	–
	4,5	60	8.460±0.127	6.014±0.120	4.083±0.109	3.253±0.097	1.513±0.046	–
		90	5.920±0.107	3.750±0.086	2.502±0.084	1.718±0.052	0.603±0.018	–
		150	3.127±0.078	1.797±0.035	1.189±0.060	0.644±0.019	0.164±0.011	–
^{27}Al	3	60	9.980±0.239	7.492±0.131	4.160±0.092	3.527±0.100	1.568±0.058	0.925±0.037
		90	6.090±0.130	4.845±0.107	2.688±0.076	1.995±0.065	0.596±0.021	0.239±0.013
		150	3.750±0.103	2.943±0.081	1.234±0.042	0.747±0.025	0.136±0.008	–
	4,5	46	–	9.510±0.250	–	–	–	1.320±0.720
		86	–	6.200±0.095	–	–	–	0.248±0.020
		136	–	3.380±0.050	–	–	–	–
^{63}Cu	2	60	23.500±0.329	15.170±0.299	10.931±0.289	8.163±0.240	3.939±0.110	2.115±0.084
		90	16.721±0.268	9.757±0.231	6.856±0.082	4.411±0.134	1.424±0.042	0.743±0.037
		150	10.592±0.212	5.217±0.103	3.362±0,165	1.807±0.050	0.342±0.021	0.115±0.011
	3	60	26.180±0.790	20.580±0.340	10.200±0.191	8.594±0.246	3.869±0.140	1.681±0.064
		90	17.800±0.320	13.601±0.280	7.316±0.100	5.245±0.172	1.403±0.048	0.678±0.032
		150	11.640±0.271	7.834±0.205	3.388±0.107	2.287±0.075	0.368±0.017	0.097±0.008
	4,5	46	–	27.000±0.750	–	–	–	3.550±0.180
		86	–	17.401±0.250	–	–	–	0.785±0.060
		136	–	9.750±0.150	–	–	–	–
^{116}Sn	2	60	45.601±0.538	30.050±0.593	19.970±0.587	13.102±0.380	7.137±0.210	–
		90	32.550±0.553	18.890±0.486	13.840±0.428	8.297±0.320	2.588±0.078	–
		150	19.571±0.391	10.289±0.203	6.548±0.321	3.032±0.090	0.585±0.041	–

A	E_γ, GeV	θ_p, deg	ε_p, MeV					
			64	80	101	137	209	279
^{116}Sn	3	60	55.070±1.270	39.920±0.680	17.800±0.430	16.550±0.490	7.028±0.038	3.873±0.140
		90	36.600±0.720	28.280±0.550	14.370±0.400	9.544±0.328	2.664±0.099	1.187±0.055
		150	22.500±0.560	14.590±0.350	6.251±0.210	4.103±0.150	0.664±0.033	–
	4,5	46	–	53.900±1.400	–	–	–	5.640±0.320
		86	–	32.200±0.51	–	–	–	1.420±0.114
		136	–	18.250±0.290	–	–	–	0.230±0.038
^{208}Pb	2	60	80.000±1.280	56.850±1.120	35.200±1.030	23.930±0.720	13.440±0.400	7.745±0.310
		90	60.990±0.970	34.080±0.800	23.690±0.720	14.220±0.480	4.522±0.135	2.453±0.120
		150	36.890±0.730	18.980±0.370	10.638±0.520	5.794±0.168	1.102±0.077	0.531±0.035
	3	60	100.740±2.130	76.030±1.200	28.00±0.870	28.000±0.820	12.810±0.450	7.092±0.250
		90	71.350±1.270	48.320±0.900	24.760±0.650	16.420±0.520	4.580±0.170	2.244±0.120
		150	42.090±0.970	27.240±0.680	12.150±0.42	7.294±0.250	1.220±0.054	0.589±0.039
	4,5	46	–	85.000±0.350	–	–	–	11.600±0.540
		86	–	58.780±0.920	–	–	–	3.050±0.214
		136	–	29.600±0.430	–	–	–	0.485±0.084

				80	119	166	231	281
^{12}C	4,5	46		5.210±0.280	3.670±0.086	2.530±0.064	1.190±0.046	0.785±0.042
		86		2.460±0.080	1.350±0.052	0.845±0.037	0.363±0.019	0.105±0.007
		136		1.330±0.029	0.427±0.029	0.196±0.015	0,045±0,005	0,018±0.002

REF. V.M. Asaturyan, E.O. Grigoryan, G.A. Vartapetyan, A.S. Danagulyan, N.A. Demëkhina & A.G. Khudaverdyan
Sov. J. Nucl. Phys. 25, 601 (1977)
Yad. Fiz. 25, 1133 (1977)

ELEM. SYM.	A	Z
27	Al	13

METHOD

REF. NO. 77 As 10 hmg

REACTION	RESULT	EXCITATION ENERGY	SOURCE TYPE	SOURCE RANGE	DETECTOR TYPE	DETECTOR RANGE	ANGLE
G,Be7 G,Cl1	ABY	THR*5	C	2*5	SCD-D		UKN
G,N13 G,F18				(4.5)			
G,Na22 G,Na24							

Photonuclear reactions in the targets ^{27}Al, ^{28}Si, ^{31}P, ^{32}S, and ^{40}Ca have been studied for maximum bremsstrahlung energies of 2, 2.4, 3, and 4.5 GeV. The yields of the residual nuclei ^{7}Be, ^{11}C, ^{13}N, ^{18}F, ^{22}Na, and ^{24}Na were measured by means of a germanium-lithium semiconductor detector with a sensitive volume of 30 cm^3. In discussion of the results we took into account the contribution of the low energy part of the bremsstrahlung spectrum. Comparison of the measured yields with estimates calculated by Rudstam's formula permitted us to conclude that there is a difference in the mechanism of formation of the light fragments ^{7}Be, ^{11}C, and ^{13}N from that of the other residual nuclei ^{18}F, ^{22}Na, and ^{24}Na.

*GEV 5=4.5 GEV

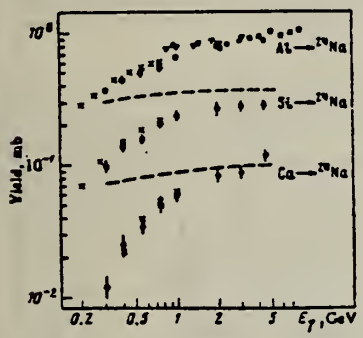

FIG. 1. Yields of the isotope ^{24}Na from targets of Al, Si, and Ca. ×—Data of Ref. 4, ○—data of Ref. 2, ▽—data of Ref. 6, □—data of Ref. 10, ●—data of the present work. The dashed lines show the contributions of the low energy part of the bremsstrahlung spectrum to the yields of the reactions Al—^{24}Na, Si—^{24}Na according to the data of Ref. 4 and the results of the calculations of the present work.

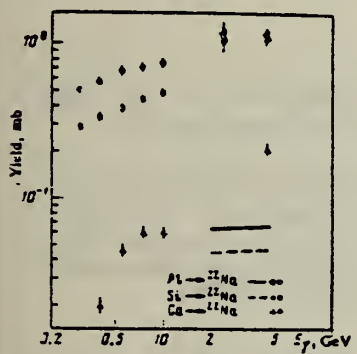

FIG. 2. Yields of ^{22}Na from targets of Al, Si, and Ca. The hollow symbols show the data of Ref. 2, and the solid symbols the data of the present work. The lines indicate the results of the calculations of the present work, which determine the contribution of the low-energy part of the bremsstrahlung spectrum to the yields of the reactions Al—^{22}Na and Si—^{22}Na for 2 GeV $\leq E_{\gamma_{max}} \leq$ 4.5 GeV.

TABLE II.

Residual nucleus	Reaction yields, mb/Q: $K_{\gamma max}$ = 1 GeV (γ, η)	2 GeV	2.4 GeV	3 GeV	4.5 GeV	Normalized yields	$\sigma_{\gamma np}/\sigma_{\gamma 1 bosor}$
Al target							
^{24}Na	0.66±0.02	0.81	0.81	0.87	0.87	0.98	0.58
^{22}Na	0.743±0.02		1.02±0.15		1.07±0.1	0.868	0.98
^{18}F	0.27±0.005	0.38±0.02		0.4±0.02	0.38±0.01	0.298	1.6
^{13}N		0.021±0.004		0.025±0.005	0.022±0.004	0.0127	2.54
^{11}C	0.117±0.013	0.104±0.013		0.12±0.02	0.107±0.013	0.091	3.3·10^3
^{7}Be	0.29±0.03		0.37±0.08		0.3±0.03	0.256	1.58·10^3
Si target							
^{24}Na	0.24±0.01	0.274±0.025	0.27±0.02	0.28±0.02	0.29±0.02	0.34	0.43
^{22}Na	0.47±0.02		1.22±0.2		1.22±0.1	1.17	2.39
^{18}F	0.2±0.04	0.36±0.03		0.39±0.02	0.39±0.02	0.38	2.69
^{13}N		0.033±0.01		0.037±0.01	0.039±0.01	0.0247	7.28
^{11}C		0.108±0.02		0.115±0.028	0.124±0.027	0.107	7.2·10^3
^{7}Be			0.168±0.05		0.32±0.04	0.291	6.2·10^3
P target							
^{24}Na	0.31±0.02				0.35±0.03	0.426	0.72
^{22}Na	0.33±0.02				0.35±0.06	0.421	2.03
^{7}Be					0.33±0.08	0.299	8.81·10^3
S target							
^{24}Na	0.24±0.01	0.23±0.02	0.25±0.02	0.24±0.02	0.27±0.02	0.417	1.1
^{22}Na	0.53±0.01				0.61±0.08	0.588	3.88
^{18}F	0.19±0.01	0.28±0.01		0.25±0.01	0.27±0.01	0.284	4.73
^{13}N		0.047±0.03		0.063±0.03	0.06±0.025	0.064	2.66·10^3
^{11}C	0.122±0.013	0.163±0.038		0.142±0.028	0.15±0.03	0.138	1.23·10^3
^{7}Be	0.25±0.06		0.38±0.06		0.34±0.04	0.314	1·10^3
Cl target							
^{24}Na	0.22±0.01	0.28±0.03		0.3±0.03	0.28±0.03	0.297	1.8
^{18}F	0.35±0.02	0.21±0.01				0.18	7.82
K target							
^{24}Na	0.08±0.005	0.1±0.01		0.125±0.012	0.15±0.015	0.16	2
^{18}F	0.09±0.005	0.11±0.05				0.1	7.58
Ca target							
^{24}Na	0.06±0.005	0.086±0.01		0.09±0.01	0.12±0.012	0.117	2.2
^{22}Na	0.06±0.005				0.21±0.02	0.21	6.37
^{7}Be					0.245±0.025	0.23	1.5·10^3

Data for Cl and K targets previously published in Reference 11.

[11]G. A. Vartapetyan *et al.*, Yad. Fiz. 17, 685 (1973) [Sov. J. Nucl. Phys. 17, 350 (1973)].

REF. I. Blomqvist, P. Janecek, G. G. Jonsson, H. Dinter, K. Tesch, N. Freed, P. Ostrander
Phys. Rev. C15, 988 (1977)

ELEM. SYM.	A	Z
Al	27	13

METHOD

REF. NO. 77 B1 2 hmg

REACTION	RESULT	EXCITATION ENERGY	SOURCE		DETECTOR		ANGLE
			TYPE	RANGE	TYPE	RANGE	
G,PI+	ABX	150-577	D	131-577	ACT-I		4PI
E,PI+	ABY	150-577	D	131-577	ACT-I		4PI

Cross sections for electroproduction and photoproduction of charged pions on ^{27}Al and ^{51}V have been measured in the energy region 130–580 MeV by use of the activation method. Special care has been taken to subtract out background yields. Photoproduction cross sections have been calculated from the region just above threshold to the tail of the (3,3) resonance. π-nucleus final state interactions are taken into account through optical potentials. Calculated photoproduction cross sections are decomposed into multipoles which are used to derive relative bremsstrahlung-induced to electron-induced yields. The pronounced effect of final state interactions is pointed out and discussed.

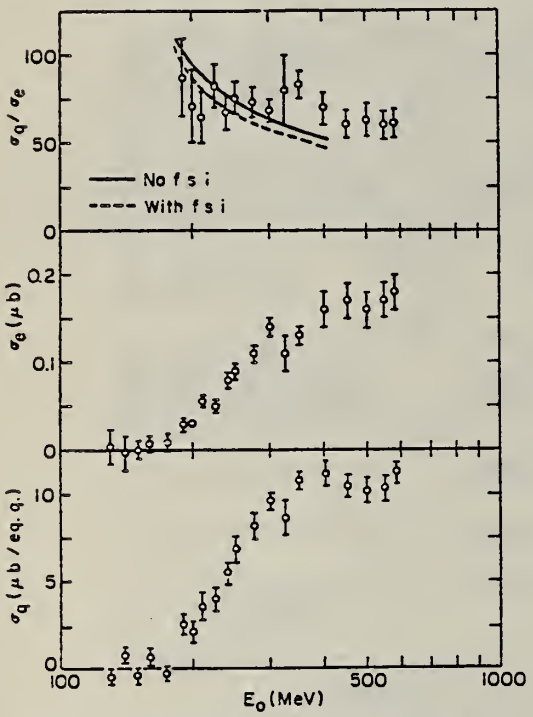

FIG. 3. Bremsstrahlung cross section per equivalent quantum σ_q and electron cross section σ_e and ratio σ_q/σ_e as a function of electron energy for the reactions ^{27}Al$(\gamma,\pi^+)^{27}$Mg and ^{27}Al$(e,e'\pi^+)^{27}$Mg. See text for theoretical curves.

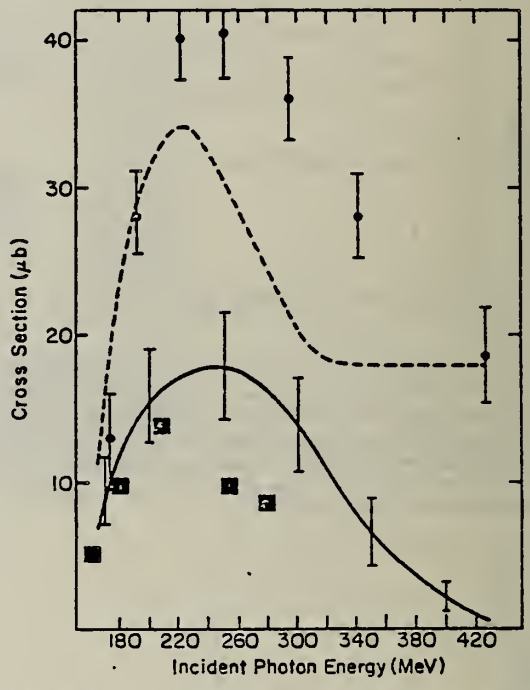

FIG. 6. Experimental cross sections per photon for the reaction ^{27}Al$(\gamma,\pi^+)^{27}$Mg. The solid curve with error bars is the result of the present work. Circles with error bars are the data of Ref. 17. The dashed curve is the work of Ref. 13. The full squares are the work of Ref. 12. Reaction threshold is 142 MeV.

12 W.B. Walters et al., Phys. Rev. 143, 833 (1966).
13 G. Nydahl et al., Nucl. Phys. B7, 97 (1968).
17 V.I. Noga et al., Yad. Fiz. 14, 904 (1971); Sov. J. Nucl. Phys. 14, 506 (1972).

REF. L.W. Fagg, W.L. Bendel, R.A. Lindgren, and E.C. Jones, Jr. Phys. Rev. C 16, 923 (1977)

ELEM. SYM.	A	Z
Al	27	13

METHOD

REF. NO. 77 Fa 4 hmg

REACTION	RESULT	EXCITATION ENERGY	SOURCE		DETECTOR		ANGLE
			TYPE	RANGE	TYPE	RANGE	
E,E/	ABX	2-13	D	37-61	MAG-D		180

A survey of electromagnetic transitions excited in ^{27}Al by 180° inelastic electron scattering has been made at incident energies of 37, 51, and 61 MeV. Transitions to levels at 2.23, 2.98, 4.42, 8.74, and 11.69 MeV are dominantly $M1$ with some possible $E2$ contributions. Tentative $M1$ assignments are given transitions at 7.57 and 8.05 MeV, but the possibility of their being $E1$ cannot be excluded. Transitions to levels at 10.68 and 12.30 MeV are probably $M1$ but with considerable $E2$ admixture. A transition at 6.50 MeV is also probably $M1$, but both $E1$ and $E2$ are possible alternative assignments. Model-dependent radiative widths $\Gamma_0(M1)$ for the $M1$ transitions are given based on an analysis of the data using simple but representative harmonic-oscillator wave functions to calculate cross sections.

10 LEVELS

TABLE I. Values of cross sections for excitation of the nuclear transitions studied at the three incident energies of 37.3, 50.9, and 60.5 MeV.

Excitation energy (MeV)	Cross section (nb/sr) 37.3 MeV	50.9 MeV	60.5 MeV
2.23	3.40±0.95	2.19±0.44	1.74±0.42
2.98	2.97±1.01	1.79±0.39	1.06±0.29
4.42	2.69±1.16	2.10±0.46	1.36±0.37
6.50	4.29±1.33	2.43±0.49	2.00±0.50
7.57	6.61±1.65	3.66±0.66	1.43±0.53
8.05	4.00±1.08	1.67±0.48	1.22±0.54
8.74	4.49±1.03	2.52±0.55	2.51±1.26
10.68	2.53±0.96	2.53±0.62	2.72±0.68
11.69	4.90±1.22	3.29±0.72	2.34±0.72
12.30	3.98±1.00	3.54±0.88	2.78±0.97

TABLE II. Tentative multipolarities and ground-state transitions widths for states in ^{27}Al electroexcited at 180°.

Excitation energy (MeV)	J^π, T	Multipolarity	Γ_0 (eV) This work	Other techniques
2.23	$\frac{5}{2}^+, \frac{1}{2}$ [a]	$M1(E2)$	$(3.2\pm1.2)\times10^{-2}$	$(17\pm9)\times10^{-2}$ [b] 1.9×10^{-2} $(1.22\pm0.12)\times10^{-2}$ 1.4×10^{-2}
2.98	$\frac{3}{2}^+, \frac{1}{2}$ [a]	$M1(E2)$	0.12 ± 0.04	0.12 [c]
4.42	$\frac{3}{2}^+, \frac{1}{2}$ [a]	$M1(E2)$	0.25 ± 0.13	0.24 ± 0.03 [d]
6.50	e	$M1(E1,E2)$	$(1.2\pm0.5)w$ [f]	
7.57	e	$M1(E1)$	$(2.3\pm1.0)w$ [f]	
8.05	e	$M1(E1)$	$(1.7\pm0.9)w$ [f]	
8.74	e	$M1(E2)$	$(3.4\pm1.7)w$ [f]	
10.68	e	$M1(E2)$		
11.69	e	$M1(E2)$	$(8.8\pm2.8)w$ [f]	
12.30	e	$M1(E2)$		

[a] Spin assignments are taken from Ref. 11.
[b] In descending order, Refs. 2, 12, 13, and 11.
[c] Reference 11.
[d] Reference 17.
[e] $J=\frac{3}{2}, \frac{5}{2}$, or $\frac{7}{2}$.
[f] $w=(2J_0+1)/(2J+1)$, where J_0 and J are the ground and excited state spins, respectively.

[2] R.M. Lombard and G.R. Bishop, Nucl. Phys. A101, 601 (1967)
[11] P.M. Endt and C. Van der Leun, Nucl. Phys. A214, 1 (1973)
[12] V.K. Rasmussen, F.R. Metzger, and C.P. Swan, Phys. Rev. 123, 1386 (1961)
[13] V.J. Vanhuyse and G.J. Vanpraet, Nucl. Phys. 45, 602 (1963)
[17] F.R. Metzger, Phys. Rev. 139, B1464 (1965)

(over)

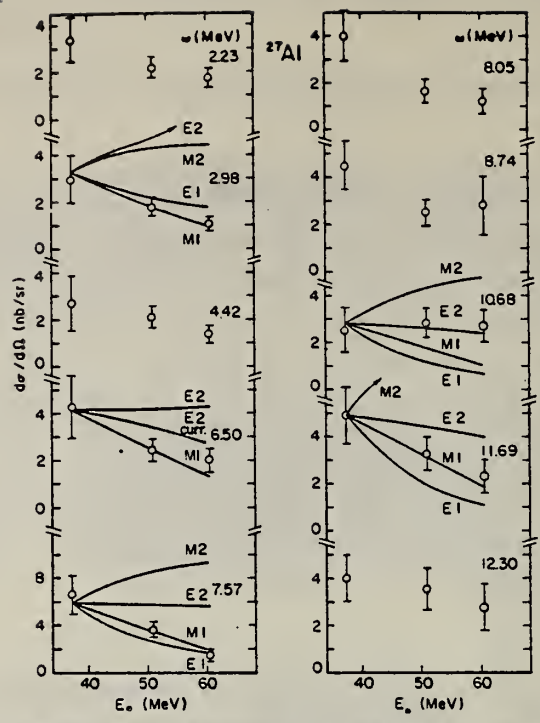

FIG. 2. Plots of experimental cross section vs incident energy for the transitions observed. In selected cases comparison has been made with cross section curves calculated from the generalized Helm model for four different multipolarities. Shown with the 6.5-MeV plot is a comparison with only the $E2$, $E2$ current, and $M1$ Helm curves. The model parameters used were: $\rho_1 = \bar{\rho}_1 = 1.16$ fm^{-3}, $\gamma_1 = 1$, $g = \bar{g} = 0.77$, with $\beta_1 = 1$ for the electric transitions and $\beta_1 = 0$ for the magnetic transitions (see Ref. 7).

[7] M. Rosen, R. Raphael, and H. Überall, Phys. Rev. 163, 927 (1967)

REF.

V.S. Kuz'menko, A.V. Mitrofanova, V.I. Noga, Yu.N. Ranyuk, P.V. Sorokin, Yu.N. Telegin, I. Blomqvist, G.G. Jonsson, and N. Freed
Phys. Rev. C 16, 1513 (1977)

ELEM. SYM.	A	Z
Al	27	13

METHOD

REF. NO. 77 Ku 3 hmg

REACTION	RESULT	EXCITATION ENERGY	SOURCE TYPE	SOURCE RANGE	DETECTOR TYPE	DETECTOR RANGE	ANGLE
G,PI+	ABX	150-999	C	600-999	ACT-I		4PI

Cross sections for photoproduction and electroproduction of π^+ on ^{27}Al and ^{51}V leading to bound states in the daughter nuclei have been measured at Kharkov in the energy range 600–1200 MeV by use of the activation method. Careful comparison is made to other recent results obtained at intermediate and high energies. Agreement is found between the present data and results of earlier work carried out at Lund and DESY. Discrepancies between photoproduction data taken at different laboratories are attributed to differences between methods of background subtraction. Relative bremsstrahlung-induced to electron-induced yield ratios are compared with predictions based on the Dalitz-Yennie formalism for virtual-photon spectra.

999=1.2 GeV

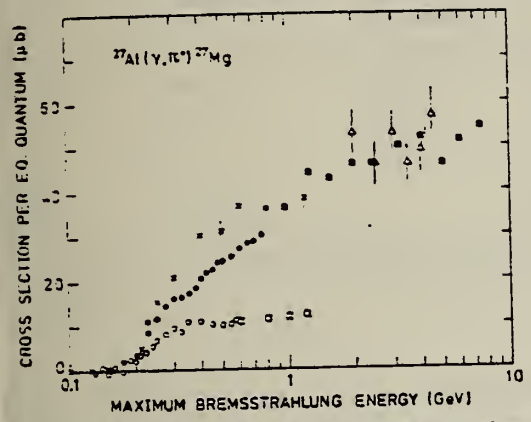

FIG. 2. Bremsstrahlung cross section per equivalent quantum, σ_q, as a function of bremsstrahlung end-point energy for the reaction ^{27}Al(γ, π⁺)^{27}Mg. □, present work; ○, Ref. 2; ●, Ref. 10; ×, Ref. 11; ■, Ref. 12; △, Ref. 14.

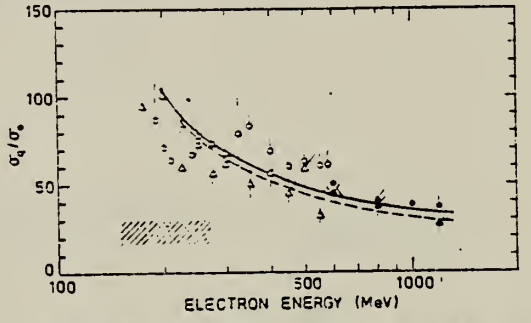

FIG. 6. The cross section ratio σ_q/σ_e versus electron energy. ^{27}Al→^{27}Mg: ●, present work; ○, Ref. 2; hatched region, Ref. 11. ^{51}V→^{51}Ti: ▲, present work; △, Ref. 2. The solid and dashed curves are calculated results assuming *E*1 and *M*1 transitions, respectively.

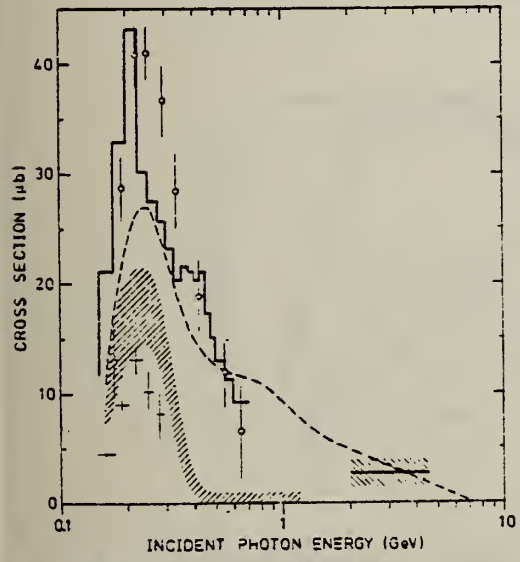

FIG. 4. Experimental cross sections per photon, σ_k, vs photon energy for the reaction ^{27}Al(γ, π⁺)^{27}Mg. The hatched area between threshold and 1.2 GeV represents the present results with the uncertainties indicated. + Ref. 8; ○, Ref. 11; histogram, Ref. 13; dashed curve, Ref. 12; hatched region between 2 and 4.5 GeV, Ref. 14.

[2] I. Blomqvist, P. Janecek, G.G. Jonsson, H. Dinter K. Tesch, N. Freed, and P. Ostrander, Phys. Rev. C 15, 988 (1977); DESY Report No. 76/51 (unpublished)

[8] W.B. Walters and J.P. Hummel, Phys. Rev. 143, 833 (1966)

[10] I. Blomqvist, G. Nydahl, and B. Forkman, Nucl. Phys. A162, 193 (1971)

[11] V.I. Noga, Yu. Ranyuk, P.V. Sorokin, and V.A. Tkachenko, Yad. Fiz. 14, 904 (1971) [Sov. J. Nucl. Phys. 14, 506 (1972)]

[12] G. Andersson, I. Blomqvist, B. Forkman, G.G. Jonsson, A. Jarund, I. Kroon, K. Lindgren, B. Schroder, and K. Tesch, Nucl. Phys. A197, 44 (1972)

[13] B. Freberg, I. Blomqvist, and B. Forkman, Z. Physik 262, 255 (1973)

[14] A.S. Danagulian and N.A. Demiokhina, Fisika 8, 321 (1973) (in Russian)

REF. R.P. Singhal, A. Johnston, W.A. Gillespie and E.W. Lees
Nucl. Phys. A279, 29 (1977)

ELEM. SYM.	A	Z
Al	27	13

METHOD

REF. NO. 77 Si 4 egf

REACTION	RESULT	EXCITATION ENERGY	SOURCE TYPE	SOURCE RANGE	DETECTOR TYPE	DETECTOR RANGE	ANGLE
E,E/		2- 3	D	62-112	MAG-D		DST

3 LEVELS

TABLE 3

Summary of the results of the analysis for the 2.21 and 3.00 MeV states in ^{27}Al

	2.21 MeV, $\frac{7}{2}^+$		2.00 MeV, $\frac{5}{2}^+$	
	present data	other measurements	present data	other measurements
B(E2) ($e^2 \cdot fm^4$)	104±4	90±11 [a] 75±8 [b] 97±12 [c]	55 ±3	60±7 [b]
c_{tr} (fm)	2.43		1.92	
t_{tr} (fm)	2.69		2.67	
R_{tr} (fm)	4.59±0.09		4.35±0.12	

[a]) Ref. [18]).
[b]) Ref. [1]).
[c]) For $\delta = -0.48 \pm 0.02$ (see text).

[1] P.M. Endt and C. van der Leun, Nucl. Phys. A214 1 (1973)

[18] P.R. Gardner, A.M. Baxter, R.A.I. Bell, L.E. Carlson, D.C. Kean, T.R. Ophel and R.H. Spear, Austral. J. Phys. 26, 739 (1973)

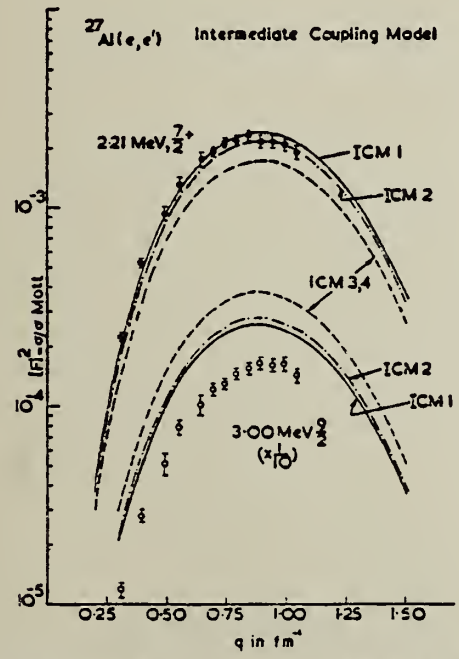

Fig. 4. The PWBA form factors for the 2.21 and 3.00 MeV levels in ^{27}Al. The various curves are the C2 contributions calculated within the framework of the intermediate-coupling model [4]). The C4 contribution to these form factors is small and is omitted from this plot.

(OVER)

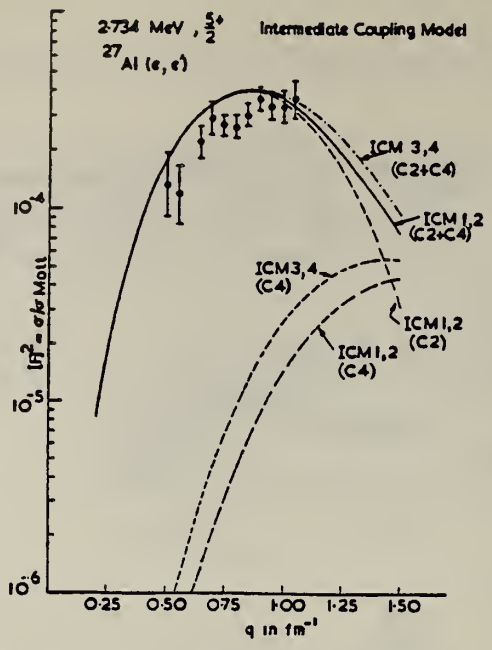

Fig. 5. PWBA form factor for the 2.734 MeV, $\frac{5}{2}^+$ level in ^{27}Al. The C2 and C4 contributions to the form factors were calculated within the framework of the intermediate-coupling model. Results for ICM1 and ICM2 are so similar that they cannot be shown separately. Similarly ICM3, ICM4 are shown as one curve.

REF. S. V. Dementii, V. I. Ogurtsov, N. G. Afanas'ev
Yad. Fiz. 28, 865 (1978)
Sov. J. Nucl. Phys. 28, 443 (1978)

ELEM. SYM.	A	Z
Al	27	13

METHOD

REF. NO. 78Dell hg

REACTION	RESULT	EXCITATION ENERGY	SOURCE		DETECTOR		ANGLE
			TYPE	RANGE	TYPE	RANGE	
E,E/	ABX	50-230	D	1*2	MAG-D		DST
				(799-1178)			

Measurements were made of quasielastic scattering of electrons in the (e, e') reaction by the nuclei ^{9}Be, ^{12}C, ^{14}N, ^{16}O, and ^{27}Al. An experimental estimate is obtained of the effective mass of an intranuclear nucleon. At excitation energies up to 80 MeV, a ratio $M^*/M \approx 0.6$ is obtained, corresponding to a linear potential $V(E) = V_0 + 0.4E$ and in good agreement with the data on proton scattering by nuclei [C. M. and F. G. Perey, Atomic Data and Nuclear Tables 13, 294 (1974)]. At excitation energies above 120 MeV the nucleon effective mass turned out to be close to that of the free nucleon, $M^*/M = 0.9$.

*GEV, QUASIELASTIC

PACS numbers: 25.30.Cg, 27.20.+n, 27.30.+t

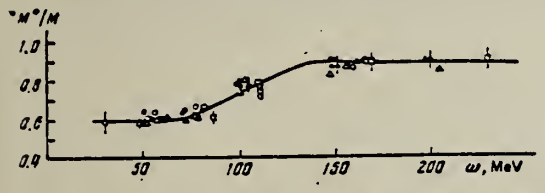

FIG. 4. Reduction coefficient M^*/M as a function of energy transfer: ●—^{9}Be, ▲—^{12}C, ○—^{14}N, △—^{16}O, □—^{27}Al. The curve has been drawn through the experimental points by hand.

REF. S. Di Liberto, F. Meddi, G. Romano, G. Rosa and C. Sgarbi
Nucl. Phys. A296, 519 (1978)

ELEM. SYM.	A	Z
Al	27	13

METHOD

REF. NO. 78 Di 3 rs

REACTION	RESULT	EXCITATION ENERGY	SOURCE		DETECTOR		ANGLE
			TYPE	RANGE	TYPE	RANGE	
E,LI	RLY	THR-800	D	800	TRK-D		DST
E,8LI	RLY	THR-800	D	800	TRK-D		DST
E,7BE	RLY	THR-800	D	800	TRK-D		DST
E,9BE	RLY	THR-800	D	800	TRK-D		DST
E,10B	RLY	THR-800	D	800	TRK-D		DST
E,12C	RLY	THR-800	D	800	TRK-D		DST

Abstract: The disintegration of aluminium nuclei by 800 MeV electrons is studied using plastic detectors. Angular and energy distributions of emitted Li, Be and B isotopes are presented. The compatibility of the results with a two-stage process (cascade and evaporation) is studied with the aid of a Monte Carlo calculation.

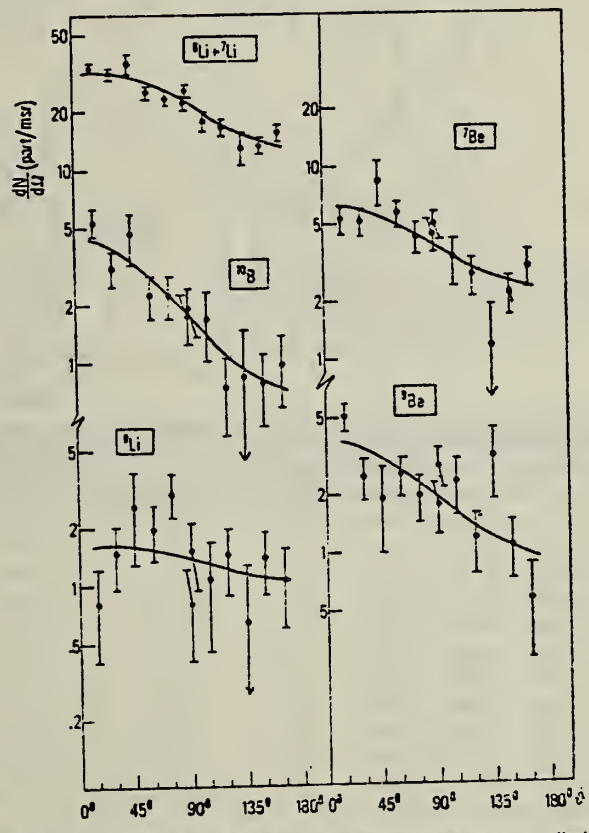

Fig. 4. Angular distributions of most of the detected fragments within the energy limits quoted in table 1. The lines, normalized to the experimental data, are the results of a Monte Carlo calculation (see text).

over

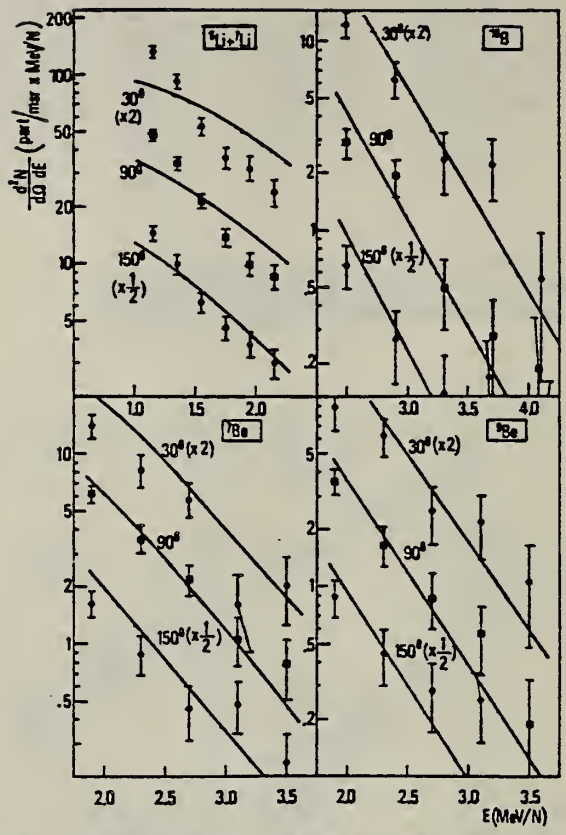

Fig. 5. Energy spectra of the fragments $^{6}Li + ^{7}Li$, ^{7}Be, ^{9}Be and ^{10}B at mean emission angles of 30°, 90° and 150° to the beam in the lab system. The lines are the result of a Monte Carlo calculation (see text) and are normalized to the experimental data at 90° only. The data and curves at 30° have been raised by a factor of two, those at 150° have been lowered by a factor of two.

REF. V. Di Napoli, J. B. Martins, G. Rosa, F. Salvetti, O. A. P. Tavares, M. L. Terranova and H. G. De Carvalho
J. Inorg. Nucl. Chem. 40, 1619 (1978)

ELEM. SYM.	A	Z
Al	27	13

METHOD

REF. NO.	
78 Di 10	hg

REACTION	RESULT	EXCITATION ENERGY	SOURCE		DETECTOR		ANGLE
			TYPE	RANGE	TYPE	RANGE	
G,C11	ABY	33(33.53)-999	C	300-999	ACT-I		4PI
G,Be7	ABY	17(17.27)-999	C	300-999	ACT-I		4PI

Abstract—Mean cross sections for the photoproduction of ^{7}Be and ^{11}C from ^{19}F, ^{27}Al, ^{28}Si and ^{32}S targets, ^{7}Be from ^{10,11}B, and ^{11}C from ^{14}N and ^{16}O targets have been measured using bremsstrahlung beams in the energy range 0.3–1.0 GeV. The results have been compared with previous measurements and an excellent agreement has been found. In most cases, the values obtained turned out to be much larger than those expected from a simple spallation mechanism. A fragmentation and/or a fission-like process has been suggested in explaining the mechanism of such reactions.

999= 1 GEV

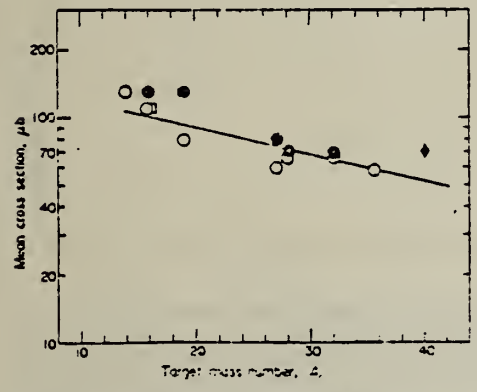

Fig. 1. Mean cross sections per photon, $\bar{\sigma}_\gamma$, of ^{11}C photoproduction vs the target mass number A_t. Experimental data are taken from: ●, Ref. [9]; □, Ref. [13]; ◆, Ref. [2]; ○, present work. The straight line is a least squares fit of the experimental points.

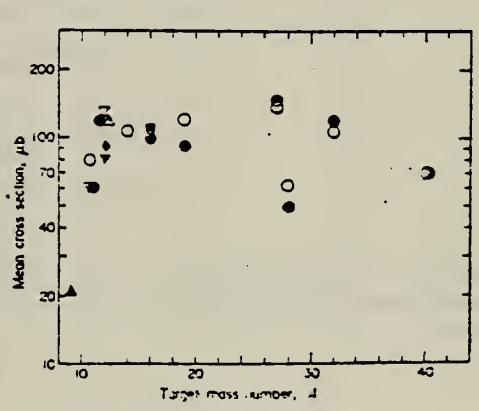

Fig. 2. The same as in Fig. 1 for ^{7}Be photoproduction. Experimental data are taken from: ▲, Refs. [6,7]; ▽, Ref. [8]; ❍, Ref. [9]; △, Ref. [10]; ◆, Ref. [11]; ▼, Ref. [12]; □, Ref. [13]; ■, Ref. [14]; ◇, Ref. [2]; ○, present work.

Table 1. Cross sections per equivalent quantum of ^{11}C photoproduction

E_0 (GeV)	Cross Section, σ_Q (μb)						
	^{14}N	^{16}O	^{19}F	^{27}Al	^{28}Si	^{32}S	^{35,37}Cl
0.30	520±30	200±20	110±20	28±10	35±10	45±10	30±10
0.32	520±30	210±20	120±20	30±10	42±10	50±10	30±10
0.35	530±30	230±20	125±20	38±10	45±10	60±10	40±10
0.40	530±30	230±20	130±20	42±10	52±10	65±10	50±10
0.48	550±30	255±20	150±20	60±10	70±10	80±10	60±10
0.55	570±30	260±20	160±20	60±10	78±10	85±10	60±10
0.65	600±30	290±20	180±20	70±10	85±10	98±10	75±10
0.75	620±30	300±20	180±20	79±10	95±10	110±10	85±10
0.90	650±30	320±20	190±20	90±10	110±10	120±10	95±10
1.00	680±30	330±20	210±20	100±10	115±10	125±10	100±10

Table 2. Cross sections per equivalent quantum of ^{7}Be photoproduction

E_0 (GeV)	Cross Section, σ_Q (μb)						
	^{10,11}B	^{14}N	^{16}O	^{19}F	^{27}Al	^{28}Si	^{32}S
0.30	150±20	200±20	113±20	152±20	40±20	20±20	50±20
0.32	160±20	200±20	120±20	150±20	45±20	30±20	54±20
0.35	160±20	210±20	130±20	159±20	42±20	30±20	60±20
0.40	175±20	226±20	145±20	170±20	98±20	20±20	70±20
0.48	190±20	245±20	163±20	186±20	100±20	50±20	140±20
0.55	200±20	260±20	187±20	200±20	93±20	48±20	90±20
0.65	220±20	280±20	197±20	214±20	140±20	68±20	130±20
0.75	225±20	300±20	215±20	227±20	180±20	70±20	130±20
0.90	240±20	318±20	230±20	245±20	166±20	88±20	165±20
1.00	250±20	330±20	242±20	260±20	200±20	97±20	190±20

(OVER)

Table 3. Comparison between experimentally determined and calculated cross sections of ^{7}Be and ^{11}C photoproduction and indication of the dominant reaction channels

Target Nucleus	Product Nucleus	Nominal Nucleon Loss, ΔA	$\Delta A/A_t$ (x100)	$\bar{\sigma}_{exp}$ (*) (μb)	$\bar{\sigma}_{CDM0}$ (**) (μb)	$\frac{\bar{\sigma}_{exp}}{\bar{\sigma}_{CDM0}}$	Apparent Threshold (Exp.) E_{th} (MeV)	Possible Mechanism of Production
$^{10,11}B$	^{7}Be	(3)	(30).36	67	28	2	≤ 50	Spallation
^{12}C	^{7}Be	5	42	110	20	5	≤ 50	Spallation
^{14}N	^{7}Be	7	50	108	12	9	≤ 50	Fission Spallation
^{14}N	^{11}C	3	21	130	60	2	≤ 50	Spallation
^{16}O	^{7}Be	9	56	107	8	13	$50<E_{th}<200$	Fission Fragmentation
^{16}O	^{11}C	5	31	117	33	3	≤ 50	Spallation
^{19}F	^{7}Be	12	63	106	5	21	$50<E_{th}<200$	Fission Fragmentation
^{19}F	^{11}C	8	42	105	16	7	$50<E_{th}<200$	Fission Fragmentation Spallation
^{27}Al	^{7}Be	20	74	142	2	71	> 200	Fragmentation
^{27}Al	^{11}C	16	59	70	5	14	$50<E_{th}<200$	Fission Fragmentation
^{28}Si	^{7}Be	21	75	56	2	28	> 200	Fragmentation
^{28}Si	^{11}C	17	61	68	4	17	$50<E_{th}<200$	Fission Fragmentation
^{32}S	^{7}Be	25	78	114	2	57	> 200	Fragmentation
^{32}S	^{11}C	21	66	68	3	23	$50<E_{th}<200$	Fission Fragmentation
$^{35,37}Cl$	^{11}C	24.(26)	60.(70)	59	3	20	$50<E_{th}<200$	Fission Fragmentation
^{40}Ca	^{7}Be	33	83	70	1	70	> 200	Fragmentation
^{40}Ca	^{11}C	29	73	70	2	35	> 200	Fragmentation

(*) Mean values of the different measurements (see Figs. 1 and 2).

(**) Calculated values according to Ref. [9].

REF. D.J.S. Findlay, D.J. Gibson, R.O. Owens, J.L. Matthews
Phys. Lett. 79B, 356 (1978)

ELEM. SYM.	A	Z
Al	27	13

METHOD

REF. NO. 78 Fi 7

REACTION	RESULT	EXCITATION ENERGY	SOURCE		DETECTOR		ANGLE
			TYPE	RANGE	TYPE	RANGE	
G,P	NOX	45-85	C	60-100	MAG -D		DST

Experimental data on the (γ, p) reaction at $E_\gamma = 60-100$ MeV for targets in the range $A = 7-93$ are compared with predictions based on a single-particle knock-out mechanism using shell model wavefunctions. The results show that this mechanism is more important than has generally been believed

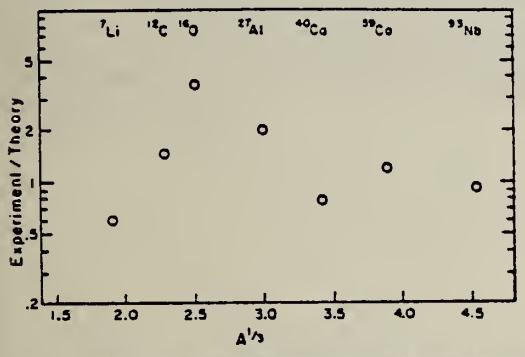

Fig. 2. The ratio of the measured photoproton emission populating low-lying states to the single-particle direct knock-out predictions is shown as a function of nuclear mass A for 80 MeV bremsstrahlung. Errors in the ratio, due to uncertainties in our calculations, are estimated to be a factor of ≈ 1.5. Errors in the experimental data are negligible.

REF. K. Masumoto, T. Kato, N. Suzuki
Nucl. Inst. Meth. 157, 567 (1978)

ELEM. SYM.	A	Z
Al	27	13

METHOD

REF. NO.: 78 Ma 10 hg

REACTION	RESULT	EXCITATION ENERGY	SOURCE		DETECTOR		ANGLE
			TYPE	RANGE	TYPE	RANGE	
G,AN	ABY	22-68	C	30-68	ACT -I		4PI
G,NA24	ABY	24-68	C	30-68	ACT -I		4PI

Analysis is made of reactions interfering with photon activation analysis procedures.

The activation yield curves have been presented for a number of photonuclear reactions in the energy range from 30 to 68 MeV, in order to evaluate quantitatively the interferences due to competing reactions in multielement photon activation analysis. The general features of the yields as functions of both target mass number and excitation energy were elucidated from the data obtained, discussion being given on the results in terms of the reaction mechanism.

Simultaneous neutron activation due to appreciable neutron production from the converter and surrounding materials has also been studied, and, finally, the magnitudes of interferences in real multielement analysis were given in the form of their energy dependences.

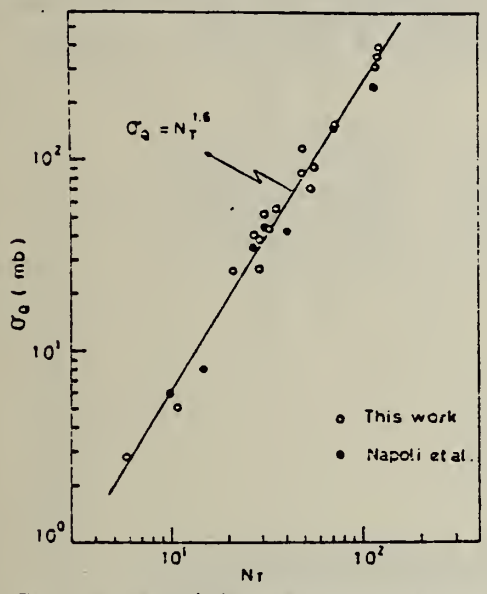

Fig. 2. Yield per equivalent quanta versus target neutron number.

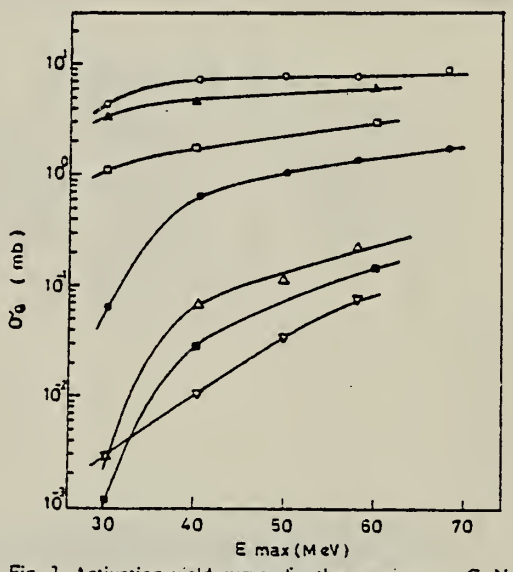

Fig. 3. Activation yield curves for the reactions on C, Na, Mg and Al.
□ $^{12}C(\gamma, n)^{11}C$, ■ $^{12}C(\gamma, \pi n)^{7}Be$, ▲ $^{23}Na(\gamma, n)^{22}Na$,
○ $^{25}Mg(\gamma, p)^{24}Na$, ● $^{24}Mg(\gamma, pn)^{22}Na$, △ $^{27}Al(\gamma, \pi n)^{22}Na$,
▽ $^{27}Al \rightarrow {}^{24}Na$.

(over)

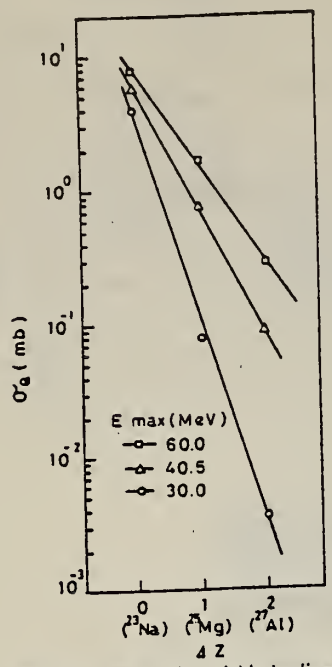

Fig. 12. The reaction yields leading to ^{22}Na as a function of difference in atomic number between target and product nuclides.

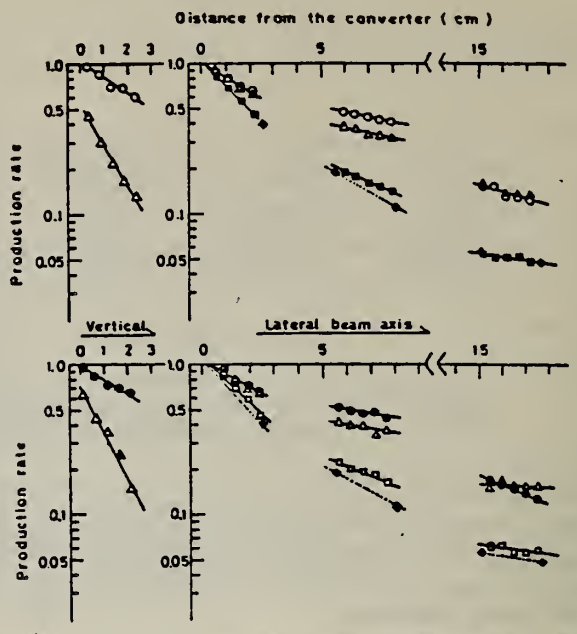

Fig. 13. Production rates of the neutron reactions and the photonuclear reactions as a function of distance from the converter in vertical and lateral directions.
○ $^{55}Mn(n, \gamma)^{56}Mn$, ● $^{23}Na(n, \gamma)^{24}Na$, △ $^{27}Al(n, \alpha)^{24}Na$,
■ $^{55}Mn(\gamma, n)^{54}Mn$, □ $^{23}Na(\gamma, n)^{22}Na$, ◆ $^{65}Cu(\gamma, n)^{64}Cu$.

REF. J.W. Maas, A.J.C.D. Holvast, A. Baghus, H.J.M. Aarts, P.M. Endt, Nucl. Phys. A301, 237 (1978)

ELEM. SYM.	A	Z
Al	27	13

METHOD

REF. NO. 78 Ma 11 hg

REACTION	RESULT	EXCITATION ENERGY	SOURCE TYPE	SOURCE RANGE	DETECTOR TYPE	DETECTOR RANGE	ANGLE
P,G	NOX	0-10	D	0-1	SCD-D		DST
		(.84-9.22)		(.338-.981)			

Abstract: Measurements of the γ-ray decay and angular distributions at eight low-energy (E_p < 1 MeV) ^{26}Mg(p, γ)^{27}Al resonances lead to the spin and parity assignments $J^\pi = \frac{1}{2}^+, \frac{1}{2}^-, \frac{3}{2}^-, \frac{3}{2}^+, \frac{5}{2}^+, \frac{5}{2}^-, \frac{7}{2}^-$ and $\frac{9}{2}^-$ for the bound states at E_x = 3.96, 4.05, 5.16, 5.25, 5.44, 6.16, 6.99, 7.23 and 7.48 MeV, respectively. For other levels, spin and parity limitations are set. Also reported are precise excitation energies, branching and mixing ratios, and lifetime limits. For the resonances additional information is given on energies, strengths and widths. The reaction Q-value is Q = 8271.0±0.5 keV. The level scheme of ^{27}Al, complemented with these new data, is compared with the results from recent shell-model calculations.

J-PI, STRENGTHS

E NUCLEAR REACTIONS ^{26}Mg(p, γ), E = 338, 454, 700–1000 keV; measured $\sigma(E_p)$, $\sigma(E_\gamma, 0)$, $E_\gamma(0)$; deduced Q. ^{27}Al deduced levels, E_p, γ-branchings, J, π, δ, τ_m, Γ. Enriched target.

TABLE 5

Angular distribution coefficients and mixing ratios of primary ^{26}Mg(p, γ)^{27}Al transitions

$E_{x1} \rightarrow E_{xf}$ (MeV)	J_f^π	J_1^π	A_2 [c]	A_4 [c]	δ [b]
8.60 → 0.84	$\frac{1}{2}^-$	$\frac{1}{2}^+$	−0.726±0.004		0.155±0.011 [a]
2.74		$\frac{3}{2}^+$	−0.04 ±0.03		0.05 ±0.02
2.98		$\frac{3}{2}^+$	0.394±0.007		0.004±0.005 [a]
3.68		$\frac{1}{2}^+$	−0.453±0.017		−0.022±0.011 [a]
4.05		$\frac{1}{2}^-$	−0.571±0.008		−0.045±0.006 or 1.56±0.02
6.81		$\frac{1}{2}^+$	−0.490±0.004		−0.004±0.003 [a]
8.96 → 0.84	$\frac{1}{2}^-$	$\frac{1}{2}^+$	−0.05 ±0.05		−0.25 ±0.04 or 3.5 ±0.6
2.98		$\frac{3}{2}^+$	0.36 ±0.07		0.01 ±0.04 [a]
3.68		$\frac{1}{2}^+$	−0.449±0.011		−0.033±0.016 [a]
5.25		$\frac{1}{2}^+$	−0.21 ±0.04		−0.09 ±0.04 [a]
6.16		$\frac{3}{2}^-$	0.608±0.015		−0.130±0.010 or −2.49±0.07
6.61		$(\frac{1}{2}, \frac{3}{2})^-$	−0.14 ±0.11		
6.65		$\frac{1}{2}^-$	−0.171±0.019		0.058±0.016
9.050 → 0	$\frac{1}{2}^-$	$\frac{1}{2}^+$	−0.091±0.018	0.05 ±0.02	−0.140±0.009
2.21		$\frac{3}{2}^+$	0.43 ±0.03	−0.07 ±0.03	0.08 ±0.03
2.74		$\frac{3}{2}^+$	−0.337±0.008		0.010±0.004
4.41		$\frac{1}{2}^+$	−0.411±0.010	0.055±0.013	0.021±0.004
4.58		$\frac{3}{2}^+$	0.41 ±0.03		0.07 ±0.04
5.25		$\frac{3}{2}^+$	−0.367±0.014	0.062±0.018	0.006±0.006
5.44		$\frac{1}{2}^-$	−0.45 ±0.09		0.05 ±0.05
6.65		$\frac{3}{2}^-$	−0.05 ±0.03		−0.148±0.015
7.23		$\frac{3}{2}^-$	−0.430±0.016		−0.169±0.011 or −8.6 ±1.0
7.48		$\frac{3}{2}^-$	0.48 ±0.04		−0.06 ±0.05 or −0.81±0.08
9.051 → 0	$\frac{1}{2}^+$	$\frac{1}{2}^+$	0.396±0.016		0.041±0.017
1.01		$\frac{1}{2}^+$	−0.439±0.018	0.08 ±0.03	0.002±0.013
2.98		$\frac{3}{2}^+$	0.09 ±0.10		−0.28 ±0.05
3.96		$\frac{3}{2}^+$	−0.99 ±0.03		0.35 ±0.03 or 1.04±0.06
5.55		$(\frac{1}{2}^+, \frac{3}{2})$	0.35 ±0.06		
9.19 → 0	$\frac{1}{2}^-$	$\frac{1}{2}^+$	−0.19 ±0.03		−0.07 ±0.03 or 7.0 ±1.3
0.84		$\frac{3}{2}^+$	−0.84 ±0.02		0.26 ±0.04 or 1.02±0.07
1.01		$\frac{1}{2}^+$	0.455±0.014		−0.086±0.015 or −2.80±0.16
2.74		$\frac{3}{2}^+$	0.04 ±0.02		0.106±0.014
2.98		$\frac{3}{2}^+$	0.39 ±0.04		0.05 ±0.02 or −4.8 ±0.6
3.68		$\frac{1}{2}^+$	−0.50 ±0.02		−0.023±0.017 or 1.83±0.08
5.55		$(\frac{1}{2}^+, \frac{3}{2})$	−0.07 ±0.04		
5.75		$\frac{1}{2}^+$	−0.39 ±0.03		−0.055±0.013 or 1.98±0.08
5.83		$(\frac{1}{2}^-, \frac{3}{2}^+)$	0.39 ±0.04		
9.22 → 0	$\frac{1}{2}^-$	$\frac{1}{2}^+$	−0.329±0.012		−0.189±0.011 [a]
2.74		$\frac{3}{2}^+$	−0.091±0.013		0.007±0.011
2.98		$\frac{3}{2}^+$	0.388±0.019		0.009±0.013 [a]
3.96		$\frac{3}{2}^+$	0.31 ±0.06		0.09 ±0.04 [a]
5.75		$\frac{3}{2}^+$	−0.59 ±0.04		0.03 ±0.02 [a]
6.16		$\frac{3}{2}^-$	0.27 ±0.06		−0.01 ±0.04 or −3.7 ±0.6
6.65		$\frac{1}{2}^-$	0.05 ±0.03		0.12 ±0.02

[a] A higher δ-value has been excluded on transition strength considerations.
[b] Sign convention of Rose and Brink [18].
[c] All values have been corrected for solid-angle attenuation.

(over)

TABLE 2

Gamma decay from $^{26}Mg(p,\gamma)^{27}Al$ resonances

From / To E_x (MeV)	E_p (keV) E_x (MeV) $J^\pi; T$ [a]	338 8.60 $\frac{1}{2}^-$	454 8.71 $\frac{1}{2}$	718 8.96 $\frac{1}{2}^-$	809 9.050 $\frac{1}{2}^-$	810 9.051 $\frac{1}{2}^+$	840 9.08 $\frac{1}{2}^+$	954 9.19 $\frac{1}{2}$	981 9.22 $\frac{1}{2}^-$
0	$\frac{5}{2}^+$	2.5 ±0.2	1.15±0.09	0.27±0.06	21.1 ±1.1	41 ±2	0.65±0.06	1.62±0.10	32.6 ±1.7
0.84	$\frac{3}{2}^+$	20.3 ±1.4	47.0 ±1.8	0.90±0.08		1.08±0.14	11.6 ±0.7	4.9 ±0.3	1.21±0.11
1.01	$\frac{1}{2}^+$	4.4 ±1.2	16.1 ±0.9	0.11±0.08		39 ±2	64.2 ±1.8	32.0 ±1.6	0.86±0.08
2.21	$\frac{7}{2}^+$				4.8 ±0.3	2.5 ±0.2			
2.74	$\frac{5}{2}^+$	4.6 ±0.4		1.0 ±0.3	39.4 ±1.8	7.4 ±0.5	0.28±0.11	11.1 ±0.6	25.0 ±1.3
2.98	$\frac{3}{2}^+$	20.8 ±1.4	1.90±0.13	8.7 ±0.5		2.07±0.18	5.6 ±0.5	3.9 ±0.2	17.2 ±0.9
3.00	$\frac{9}{2}^+$				0.7 ±0.2				
3.68	$\frac{1}{2}^+$	14.5 ±0.8	1.37±0.10	23.5 ±1.4			12.5 ±0.8	15.0 ±0.8	0.91±0.09
3.96	$\frac{3}{2}^+$	3.2 ±0.3	6.0 ±0.4	1.0 ±0.3		1.74±0.10	0.67±0.06	2.00±0.14	2.82±0.17
4.05	$\frac{1}{2}^-$	10.5 ±0.7	10.8 ±0.6				1.26±0.09	0.62±0.07	1.43±0.18
4.41	$\frac{5}{2}^+$	3.2 ±0.3			13.9 ±0.7	1.68±0.15			0.50±0.09
4.58	$\frac{7}{2}^+$				2.11±0.18				
4.81	$\frac{5}{2}^{(+)}$	0.52±0.06		1.5 ±0.3				0.94±0.10	0.7 ±0.2
5.16	$\frac{3}{2}^-$		1.04±0.09	2.4 ±0.6				0.68±0.09	0.75±0.08
5.25	$\frac{3}{2}^+$	1.9 ±0.6		2.8 ±0.2	4.9 ±0.3	1.74±0.11		1.12±0.09	
5.42	$(\frac{1}{2}-\frac{9}{2})$				1.0 ±0.2				
5.43	$(\frac{3}{2}^+-\frac{11}{2}^-)$				0.3 ±0.2				
5.44	$\frac{5}{2}$			1.72±0.13	5.4 ±0.5			1.04±0.10	1.67±0.14
5.55	$(\frac{1}{2}^+, \frac{3}{2})$			1.7 ±0.2	0.34±0.04	0.98±0.08		4.5 ±0.6	0.42±0.13
5.75	$\frac{1}{2}^+$			0.9 ±0.3			1.08±0.11	8.9 ±0.6	1.3 ±0.2
5.83	$(\frac{1}{2}^-, \frac{3}{2}^+)$			1.6 ±0.5	0.54±0.12	0.13±0.03	0.77±0.06	8.3 ±0.5	0.96±0.15
5.96	$\frac{7}{2}$					0.32±0.07			
6.08	$(\frac{1}{2}-\frac{3}{2}^+)$	0.55±0.04					0.93±0.12		0.21±0.03
6.12	$(\frac{3}{2}^--\frac{7}{2}^-)$				0.29±0.03			0.75±0.16	1.13±0.10
6.16	$\frac{1}{2}^-$	0.52±0.04		29.0 ±1.8				0.92±0.16	2.84±0.18
6.29	$\frac{7}{2}$				0.25±0.02	0.09±0.02			
6.48	$\frac{7}{2}^-$				0.89±0.06				
6.61	$(\frac{1}{2}, \frac{3}{2})^-$	1.17±0.07	0.77±0.13	3.1 ±0.2				1.4 ±0.3	
6.65	$\frac{3}{2}^-$	0.39±0.03		13.0 ±0.7	1.17±0.09			0.31±0.07	6.4 ±0.4
6.776	$(\frac{1}{2}, \frac{3}{2})^+$		5.4 ±0.3				0.46±0.05		
6.81	$\frac{1}{2}^+; T = \frac{1}{2}$	10.7 ±0.6	7.9 ±0.4	3.5 ±0.3					
6.99	$\frac{1}{2}^-$	0.25±0.03		3.3 ±0.5	0.17±0.03	0.27±0.05			
7.23	$\frac{9}{2}^-$				1.81±0.10				
7.28	$\leqq \frac{5}{2}$		0.57±0.06						0.14±0.02
7.48	$\frac{7}{2}$				0.93±0.05				
8.18	$(\frac{1}{2}, \frac{3}{2})^-$								0.95±0.07

[a]) For notation see table 7.

Σ 100. 100.

REF. J.W. Maas, A.J.C.D. Holvast, A. Baghus, H.J.M. Aarts, P.M. Endt, Nucl. Phys. A301, 237 (1978)

ELEM. SYM.	A	Z
Al	27	13

METHOD

REF. NO. 78 Ma 11 hg

REACTION	RESULT	EXCITATION ENERGY	SOURCE TYPE	SOURCE RANGE	DETECTOR TYPE	DETECTOR RANGE	ANGLE
P,G	NOX	0-10	D	0-1	SCD-D		DST
		(.84-9.22)		(.338-.981)			

J-PI, STRENGTHS

TABLE 6

Angular distribution coefficients and mixing ratios of transitions between bound states in ^{27}Al

$E_{xi} \rightarrow E_{xf}$ (MeV)	J_i^π	J_f^π	E_γ (keV)	A_2 [c]	A_4 [c]	δ [b]	δ_{III} [d]
2.74 → 0	$\frac{1}{2}^+$	$\frac{1}{2}^+$	338	0.34 ±0.06		−0.06 ±0.09	
			954	0.53 ±0.07		−0.32 $\pm^{0.20}_{0.80}$	
			981	0.48 ±0.04		−0.20 ±0.07	
						av = −0.18 ±0.06 [e]	[e]
1.01		$\frac{1}{2}^+$	338	−0.081±0.016		−0.132±0.015 [e]	
			954	−0.12 ±0.09		−0.10 ±0.07 [e]	
			981	−0.101±0.019		−0.124±0.012 [e]	
						av = −0.126±0.009	−0.11±0.02
2.98 → 0	$\frac{3}{2}^+$	$\frac{1}{2}^+$	810	−0.15 ±0.03		−0.05 ±0.07 [e]	0.01±0.01
3.96 → 0	$\frac{3}{2}^+$	$\frac{1}{2}^+$	981	−0.026±0.020		−0.04 ±0.16	
						or 6 $\pm^{56}_{3}$	
4.41 → 0	$\frac{3}{2}^+$	$\frac{1}{2}^+$	809	0.376±0.019		0.033±0.020	−0.11±0.06
1.01		$\frac{3}{2}^+$		−0.36 ±0.05		0.00 ±0.03	0.09±0.08
4.58 → 0	$\frac{7}{2}^+$	$\frac{1}{2}^+$	809	0.04 ±0.05		−0.21 ±0.04	−0.24±0.05
						or 16 $\pm^{8}_{\cdot}$	
2.74		$\frac{3}{2}^+$		−0.22 $\pm^{\cdot}_{}$0.10		−0.04 ±0.06	
						or 4.5 ±1.4	
5.16 → 0	$\frac{1}{2}^-$	$\frac{1}{2}^+$	718	−0.18 ±0.07			
			981	−0.19 ±0.12			
5.25 → 1.01	$\frac{3}{2}^+$	$\frac{1}{2}^+$	809	−0.44 ±0.04	0.14±0.05	0.04 ±0.02	−0.14±0.03
2.21		$\frac{3}{2}^+$		−0.06 ±0.05		0.08 ±0.04	
						or 5.3 ±1.2	
5.44 → 0	$\frac{1}{2}$	$\frac{1}{2}^+$	809	0.53 ±0.04		−0.18 $\pm^{0.12}_{0.04}$	
						or −0.92 ±0.14	
2.74		$\frac{3}{2}^+$		0.51 ±0.18	−0.63±0.15	−0.05 ±0.09	
						or −1.7 ±0.3	
2.98		$\frac{1}{2}^+$		0.3 ±0.2		−0.30 ±0.20	
						or −10 $\pm^{7}_{27}$	
6.16 → 0.84	$\frac{1}{2}^-$	$\frac{1}{2}^+$	718	−0.091±0.013		−0.02 ±0.04 [e]	
6.65 → 0	$\frac{1}{2}^-$	$\frac{1}{2}^+$	718	0.37 ±0.03		−0.06 ±0.04 [e]	
			809	0.31 ±0.09		0.08 ±0.09 [e]	
			981	0.30 ±0.03		−0.04 ±0.05 [e]	
						av = −0.04 ±0.04	
7.23 → 2.21	$\frac{5}{2}^-$	$\frac{3}{2}^+$	809	−0.36 ±0.06		0.13 ±0.13	0.05±0.03 [f]
						or 3.5 ±1.0	
3.00		$\frac{5}{2}^+$		0.7 ±0.3		0.4 ±0.7	−0.06±0.15 [f]
7.48 → 0	$\frac{7}{2}$	$\frac{1}{2}^+$	809	−0.18 ±0.14		−0.06 ±0.11 [g]	

[a]) A higher δ-value has been excluded on transition strength considerations.
[b]) Sign convention of Rose and Brink [18]).
[c]) Corrected for solid angle attenuation.
[d]) From ref. [13]), if not indicated otherwise.
[e]) Several different values, see text.
[f]) Ref. [22]).
[g]) The present work yields a second solution, $\delta = -1.11 \pm 0.12$, which is excluded by the γ-ray polarization measurements of refs. [24, 25]).

REF. A. G. Flowers, D. Branford, J. C. McGeorge, A. C. Shotter, P. Thorley, C. H. Zimmerman, R. O. Owens, J. S. Pringle
Phys. Rev. Lett. 43, 323 (1979)

ELEM. SYM.	A	Z
Al	27	13

METHOD

REF. NO. 79F12 hg

REACTION	RESULT	EXCITATION ENERGY	SOURCE		DETECTOR		ANGLE
			TYPE	RANGE	TYPE	RANGE	
E,A	SPC	UKN	D	120	MAG-D		30

This paper presents energy spectra of α particles emitted following the bombardment of ^{27}Al, ^{nat}Ni, ^{92}Mo, ^{94}Mo, and ^{197}Au with 120-MeV electrons, together with α-particle angular distributions from ^{197}Au and ^{nat}Ni for $E_\alpha = 30$ and 50 MeV. The data are compared with preequilibrium exciton-model and statistical-model calculations. It is concluded that few-step processes are dominant in the production of α particles with energies above 20 MeV.

PREEQUILIB A EMISS

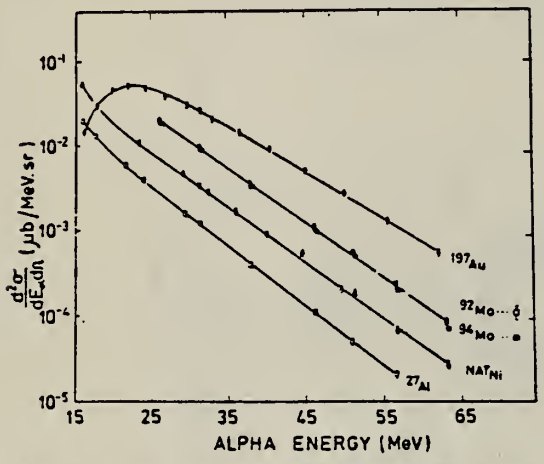

FIG. 1. α-particle energy spectra at $\theta_\alpha = 30°$, for $E_e = 120$ MeV. Errors shown are the sum of statistical and systematic contributions. The solid lines are a guide to the eye.

TABLE I. Temperatures corresponding to the preequilibrium component of the (e,α) reaction, derived from energy spectra at $\theta_\alpha = 30°$ for $E_e = 120$ MeV.

Target	Temperature[a] (MeV)
^{27}Al	5.3
^{nat}Ni	5.5
^{68}Zn	5.4
^{92}Mo	5.6
^{94}Mo	5.4
^{197}Au	6.1

[a]Error is ± 0.2 MeV.

REF. S. Hartwig, F. H. Heimlich, G. Huber, E. Rössle, J. Bleckwenn, M. Köbberling, J. Moritz, K. H. Schmidt, D. Wegener, D. Zeller, P. David, H. Mommsen
Phys. Lett. 82B, 297 (1979)

ELEM. SYM.	A	Z
Al	27	13

METHOD

REF. NO.	
79Ha2	hg

REACTION	RESULT	EXCITATION ENERGY	SOURCE		DETECTOR		ANGLE
			TYPE	RANGE	TYPE	RANGE	
E,E/	RLX	1*4	D	3,7	MAG-D		9
		(.95-3.28)		(3.08,7.)			

*GEV, RLX E+/E-

The ratio $R = \sigma^+/\sigma^-$ of the cross sections for inelastic positron and electron scattering on ^{12}C and ^{27}Al has been measured for four momentum transfers 0.08 $(GeV/c)^2 \leq q^2 \leq 0.45$ $(GeV/c)^2$ of the virtual photon and invariant masses 0.95 GeV $\leq W \leq$ 3.3 GeV of the hadronic system. The mean value of the ratio is $R = (1.005 \pm 0.027)$. No q^2, respectively, W dependence of the ratio is observed.

Table 2
Ratio $R = \sigma_+/\sigma_-$ for inelastic lepton scattering on ^{27}Al. The variables are defined in table 1. All errors include the systematic error contributions given in the text.

$E_1 = 3.08$ GeV, $\theta_e = 9°$				$E_1 = 7$ GeV, $\theta_e = 9°$			
W (GeV)	q^2 $((GeV/c)^2)$	R	$Re(A_2/A_1)$	W (GeV)	q^2 $((GeV/c)^2$	R	$Re(A_2/A_1)$
0.960	0.223	0.935 ± 0.04	(−1.6 ± 1.0)%	3.080	0.381	0.947 ± 0.055	(−1.33 ± 1.38)%
1.240	0.199	1.038 ± 0.044	(0.95 ± 1.1)%	3.125	0.357	1.089 ± 0.063	(2.2 ± 1.6)%
1.405	0.182	1.071 ± 0.051	(1.8 ± 1.3)%	3.165	0.336	0.964 ± 0.068	(−0.9 ± 1.7)%
1.490	0.172	1.032 ± 0.047	(0.8 ± 1.2)%	3.205	0.315	0.965 ± 0.068	(−0.9 ± 1.7)%
1.570	0.163	1.005 ± 0.045	(0.1 ± 1.1)%	3.245	0.293	0.995 ± 0.058	(−0.1 ± 1.45)%
1.645	0.154	1.029 ± 0.046	(0.7 ± 1.15)%	3.285	0.271	1.040 ± 0.074	(1.0 ± 1.85)%
1.720	0.144	1.011 ± 0.048	(0.3 ± 1.2)%				
1.790	0.134	1.000 ± 0.051	(0.0 ± 1.3)%			0.997 ± 0.035	(−0.1 ± 0.9)%
1.855	0.125	1.023 ± 0.047	(0.6 ± 1.2)%				
1.920	0.115	1.107 ± 0.050	(2.7 ± 1.25)%				
1.980	0.106	1.028 ± 0.049	(0.7 ± 1.2)%				
2.040	0.097	1.114 ± 0.054	(2.85 ± 1.35)%				
2.100	0.087	1.054 ± 0.052	(1.35 ± 1.3)%				
2.150	0.079	1.063 ± 0.053	(1.6 ± 1.3)%				
		1.008 ± 0.040	(0.2 ± 1.0)%				

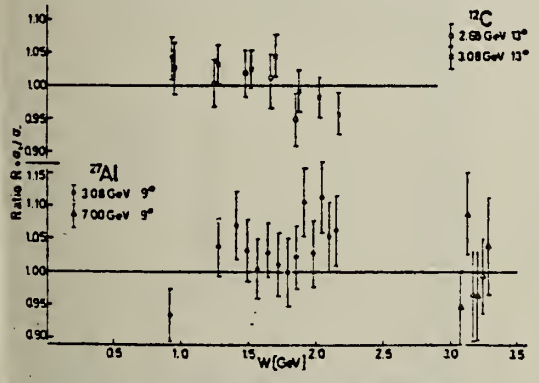

Fig. 1. Ratio $R = \sigma_+/\sigma_-$ of inelastic positron and electron scattering on ^{12}C and ^{27}Al as a function of the invariant mass W of the excited hadronic system, calculated for a free target nucleon.

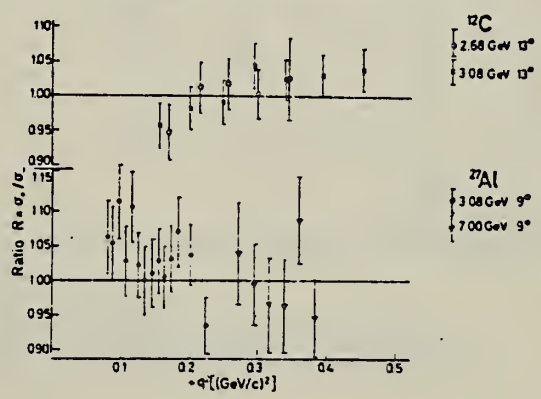

Fig. 2. Ratio $R = \sigma_+/\sigma_-$ of inelastic positron and electron scattering on ^{12}C and ^{27}Al as a function of the four-momentum transfer q^2 of the virtual photon.

REF. R.S. Hicks, A. Hotta, J.B. Flanz, H. deVries
Phys. Rev. C21, 2177 (1980)

ELEM. SYM.	A	Z
Al	27	13

METHOD

REF. NO. 80 Hi 2 hg

REACTION	RESULT	EXCITATION ENERGY	SOURCE		DETECTOR		ANGLE
			TYPE	RANGE	TYPE	RANGE	
E,E/	ABX	4-8	D	70-340	MAG-D		DST

Inelastic electron scattering form factors were measured for the low-lying odd-parity states of ^{27}Al over a momentum transfer range of 0.57 to 2.41 fm^{-1}. Reduced ground-state transition probabilities were deduced for states at 4.055 MeV(1/2$^-$), 5.156 MeV(3/2$^-$), 6.159 MeV(3/2$^-$), 6.477 MeV(7/2$^-$), 6.605 MeV(1/2$^-$ or 3/2$^-$), 6.651 MeV(5/2$^-$), 6.993 MeV(3/2$^-$), and 7.228 MeV(9/2$^-$). In addition, the results support odd-parity assignments for the 5.827 MeV(3/2$^-$ or 5/2$^+$) and 7.477 MeV(7/2) levels. Attempts have been made to interpret the results in terms of the weak-coupling and strong-coupling models. The measurements confirm the apparent high concentration of 1*p*-shell proton hole strength in the 4.055 MeV,1/2$^-$ and 5.156 MeV,3/2$^-$ states. To satisfactorily account for the observed properties of these two levels using the weak-coupling model requires an anomalously small value of 1.35 MeV for the spin-orbit splitting of the 1*p* shell. The structure of levels in the 6 to 7.5 MeV region is shown to be based on the excitation of 1*d*-shell nucleons into the 1*f* shell.

10 LEVELS BEL,J-PI

[NUCLEAR REACTIONS ^{27}Al(e,e'), E=70–340 MeV; measured $\sigma(E;\theta)$, DWBA analysis. π=−1 levels, deduced $B(\Lambda),\delta$. Strong-coupling model, weak-coupling model.]

TABLE I. Transition probabilities for excitations from ground state of ^{27}Al, deduced from harmonic oscillator model fits.

E_x[a] (MeV)	$2J^\pi$	$B(C1\uparrow)$ (e^2fm^2)	$B(C3\uparrow)$ (e^2fm^6)	$B(C5\uparrow)$ (e^2fm^{10})	$B(M2\uparrow)$ (e^2fm^4)
4.055	1^-		60 ± 25		0.034 ± 0.011
5.156	3^-	0.041 ± 0.011	41 ± 17		
5.827	$(3^-,5^+)$		5.5 ± 2		
6.159	3^-		207 ± 44		
6.477	7^-		217 ± 32	(8.0 ± 3.0)×10^4	
6.605	$(1,3)^-$		86 ± 21		
6.651	5^-		367 ± 55	(2.3 ± 1.1)×10^4	
6.993	3^-		<15		
7.228	9^-		604 ± 91	(1.7 ± 1.2)×10^4	
7.477	7		281 ± 42	(3.3 ± 2.0)×10^4	

[a] Excitation energies and spin assignments taken from Ref. 4.

TABLE II. Comparison of experimental excitation energies and transition probabilities with predictions of weak- and strong-coupling models.

		Experiment		Weak coupling		Strong coupling
$2J^\pi$	L	E_x[a] (MeV)	$B(CL\uparrow)$ (e^2fm^{2L})	E_x (MeV)	$B(CL\uparrow)$ (e^2fm^{2L})	$B(CL\uparrow)$ (e^2fm^{2L})
1^+	2	0.843	13.5 ± 1.0[b]	0.62	37	
3^+	2	1.013	27 ± 2[b]	1.11	43	
7^+	2	2.211	95 ± 10[b]	2.27	65	
5^+	2	2.734	8 ± 3[b,d]	1.89	29	
9^+	2	3.001	57 ± 3[b]	2.30	129	
1^-	3	4.055	60 ± 25	4.06[c]	69	
3^-	3	5.156	41 ± 17	5.16[c]	39	
3^-	3	5.827[e]	5.5 ± 2	5.96	12.8	
5^-	3			6.01	4.2	
1^-	3	6.605[e]	86 ± 21	6.52	74	55
3^-	3	6.159	207 ± 44	6.20	156 } 251	207[c]
3^-	3	6.993	<15 ± 47	7.55	95	
5^-	3	6.651	367 ± 55	6.09	398	367[c]
5^-	3			7.73	200	
7^-	3	6.477	217 ± 32 } 498	6.32	898 } 1049	232
7^-	3	7.477[e]	281 ± 42 } ±53	7.87	151	
9^-	3	7.228	604 ± 91	6.92	1282 } 1286	90
9^-	3			8.20	4	
11^-	3			7.83	446	12
11^-	3			9.12	405	

[a] Reference 4.
[b] References 4, 9, 34.
[c] Parameter fitted specifically to measured value.
[d] Assuming C0 excitation strength can be neglected.
[e] Observed state has uncertain spin-parity assignment.

(over)

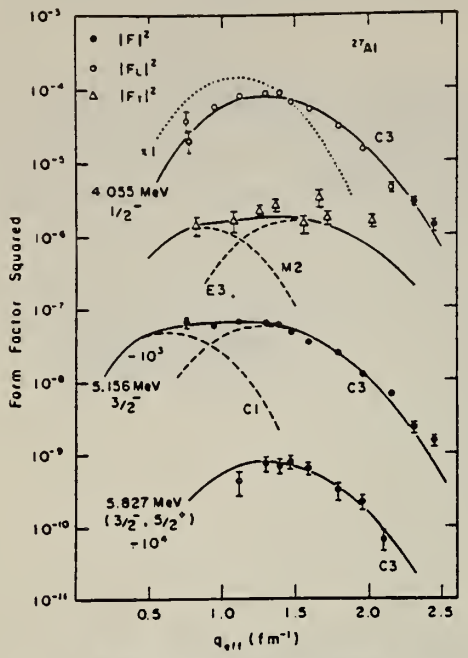

FIG. 5. Inelastic form factors measured for $1p$-hole states in ^{27}Al, and comparison with best-fit theoretical curves. The calculated longitudinal form factors were obtained in the distorted-wave Born approximation using the single-particle, harmonic oscillator model with b = 1.85 fm. The q dependence of the data differs markedly from that expected for the $C3$ multipole of a $1d \rightarrow 1f$ transition, which is represented by a dotted curve at the top of the figure.

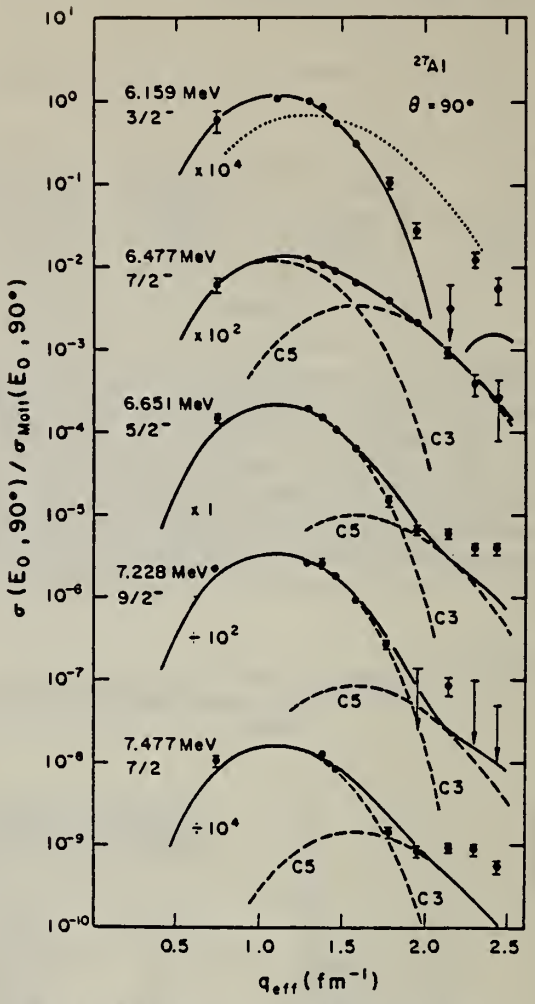

FIG. 6. Measured (e, e') form factors for ^{27}Al odd-parity states characterized, in large part, by the excitation of a $1d$-shell nucleon into the $1f$ shell. For comparison, the q dependence expected for a $C3$ excitation to a $1p$-hole state is shown by the dotted line at the top of the figure. The best-fit DWBA curves were calculated using the single-particle harmonic oscillator model with b = 1.94 fm. Transverse components were assumed to be small and are excluded from the calculated curves.

REF. V.M. Khvastunov, N.G. Afanas'ev, Yu.V. Vladimirov, G.A. Savitskii, V.F. Borzhkovskii, V.G. Vlasov, I.I. Zalyubovskii, N.G. Stervoedov, A.N. Frolov
Sov. J. Nucl. Phys. 32, 152 (1980)
Yad. Fiz. 32, 297 (1980)

ELEM. SYM.	A	Z
Al	27	13

METHOD

REF. NO. 80 Kh 3 hg

REACTION	RESULT	EXCITATION ENERGY	SOURCE		DETECTOR		ANGLE
			TYPE	RANGE	TYPE	RANGE	
E,P	ABX	8-100	D	100	MAG-D		DST
E,D	ABX	21-100	D	100	MAG-D		DST
E,T	ABX	18-100	D	100	MAG-D		DST
E,HE3	ABX	23-100	D	100	MAG-D		20
E,A	ABX	10-100	D	100	MAG-D		DST

Measurements of the charged-particle yield in the electrodisintegration of ^{27}Al have been carried out in the linear electron accelerator at our institute. Positively charged particles emitted from the target were analyzed in momentum by a magnetic spectrometer in the focal plane of which were located 10 surface-barrier silicon detectors. This arrangement permitted separation of particles according to the value of Z^2/A, where Z and A are the charge and atomic weight of the particle, respectively. The technique permitted simultaneous detection of five groups of particles: p, d, t, ^{3}He, and ^{4}He. Protons and α-particles, which have identical Z^2/A, were separated by appropriate choice of the bias voltages on the detectors.[1] An example of this separation is shown in Fig. 1 for particles emitted at an angle $\theta = 20°$.

Yield measurements were made at four angles $\theta = 20$, 55, 90, and 110° for an initial electron energy 100 MeV. The differential cross sections obtained for protons, deuterons, tritons, and α particles as a function of the

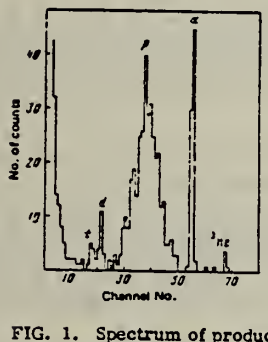

FIG. 1. Spectrum of products of electrodisintegration of ^{27}Al at an angle $\theta = 20°$.

[1])Khar'kov State University.

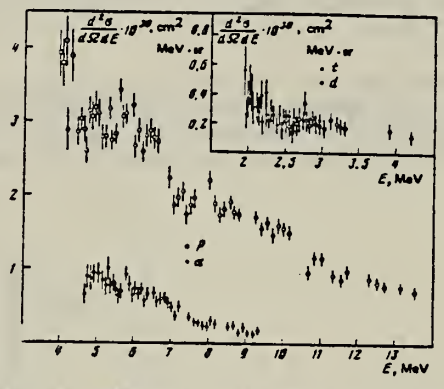

FIG. 2. Differential cross sections for production of p, d, t, and α in electrodisintegration of ^{27}Al. $E_0 = 100$ MeV, $\theta = 55°$. The errors are only statistical.

kinetic energy of the detected particles (Fig. 2) show that the α-particle yield is comparable with the proton yield. In the kinetic-energy region 7–8 MeV the ratio of the cross sections for protons and α particles as a function of angle is isotropic and amounts to 4.8 ± 0.5. The ratio of the triton and α-particle cross sections at 55° is 0.3 ± 0.1. This value agrees with the data of Adler *et al.*,[2] who reported the yield ratio ($t/^4$He) obtained with γ rays at an initial energy 500 MeV.

[1]V. F. Borzhkovskiĭ *et al.*, in: Voprosy atomnoĭ nauki i tekhniki, seriya Obshchaya i yadernaya fizika (Problems of Atomic Science and Technology, General and Nuclear Physics Series), No. 5(5), Khar'kov, 1978, p. 36.
[2]J.-O. Adler *et al.*, Intern. Conf. on Nucl. Phys. with Electromagnetic Interaction, Abstracts of Contributed Papers, Mainz, 5–9 June, 1979, West Germany, p. 4.1.

Translated by Clark S. Robinson

REF. N.K. Sherman, C.K. Ross, K.H. Lokan
Phys. Rev. C21, 2328 (1980)

ELEM. SYM.	A	Z
Al	27	13

METHOD

REF. NO. 80 Sh 10 egf

REACTION	RESULT	EXCITATION ENERGY	SOURCE		DETECTOR		ANGLE
			TYPE	RANGE	TYPE	RANGE	
G,MUT	ABX	3-30	C	42	TOF-D		4PI

D(G,N) SPECTROMETER

Photon absorption by Al, Ta, and Bi between 3 and 30 MeV was measured using as a photon spectrometer a photoneutron time-of-flight detector and a liquid deuterium target. The atomic cross sections of Ta and Bi at the lowest energies (and of Al at higher energies) agree with calculated values appearing in published tabulations but exceed them at 25 MeV by about 2% in Ta and 3% in Bi. Calculations by others using empirical Coulomb corrections and improved screening corrections to the cross section for pair production by the nucleus agree with experiment to within $(0.5 \pm 0.4)\%$. Best experimental values of the combined correction for Bi are given.

[NUCLEAR REACTIONS ^{27}Al, ^{181}Ta, ^{209}Bi; measured total photon absorption $\sigma_\gamma(E)$; observed GDR; deduced electron pair production $\sigma_K(E)$; $E = 3.0$ to 30.0 MeV; resolution 500 keV; deduced experimental values for Bi of the combined Coulomb and screening correction; ^{2}H(γ,n) LD$_2$/TOF spectrometer.]

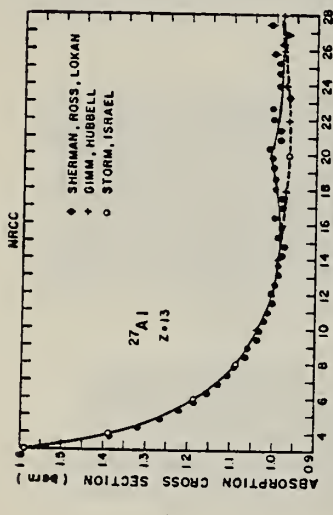

FIG. 3. The measured Al absorption cross section (solid circles) compared to the new (Ref. 6) (crosses) and old (Ref. 5) (open circles) theory. The excess above 15 MeV is photonuclear.

TABLE V. Values σ_A and σ_B of the Al absorption cross section obtained from different data sets A and B for photon energies ω below the photonuclear giant resonance. Data set A was accumulated in about one-quarter the time required for data set B, at an average counting rate about 4% higher. The difference $\delta_{AB}\sigma$ between the two measurements is listed, as are σ_{AB}(Al) obtained by statistically weighting both data sets, σ_{calc} interpolated from a table[a] of calculated values, and $\delta\sigma$ the difference between σ_{calc} and the experimental values σ_{exp}(Al) obtained from σ_{AB}(Al) by correcting for in-scattering and air displacement.

ω (MeV)	σ_A (b)	σ_B (b)	$\delta_{AB}\sigma$ (mb)	σ_{AB}(Al) (b)	σ_{exp}(Al) (b)	σ_{calc}(Al) (b)	$\delta\sigma$ (mb)
3.873	1.398 ± 0.0075	1.385 ± 0.007	+13	1.388 ± 0.007	1.391	1.418	27
4.327	1.338 ± 0.0075	1.323 ± 0.0035	+15	1.326 ± 0.004	1.329	1.354	25
4.830	1.272 ± 0.005	1.272 ± 0.0025	0	1.272 ± 0.003	1.274	1.293	19
5.333	1.233 ± 0.004	1.226 ± 0.002	+7	1.228 ± 0.002	1.230	1.244	14
5.837	1.187 ± 0.0035	1.186 ± 0.002	+1	1.186 ± 0.002	1.188	1.202	14
6.348	1.150 ± 0.0035	1.154 ± 0.002	−4	1.153 ± 0.002	1.155	1.167	12
6.870	1.126 ± 0.0035	1.130 ± 0.002	−4	1.129 ± 0.002	1.131	1.139	8
7.404	1.106 ± 0.004	1.107 ± 0.002	−1	1.107 ± 0.002	1.109	1.115	6
7.936	1.085 ± 0.004	1.089 ± 0.002	−4	1.088 ± 0.002	1.090	1.097	7
8.382	1.068 ± 0.0045	1.067 ± 0.002	+1	1.067 ± 0.002	1.069	1.079	10
8.936	1.059 ± 0.0045	1.058 ± 0.0025	+1	1.058 ± 0.002	1.060	1.062	2
9.476	1.045 ± 0.005	1.038 ± 0.0025	+7	1.040 ± 0.002	1.042	1.051	9
9.992	1.036 ± 0.005	1.035 ± 0.003	+1	1.035 ± 0.003	1.037	1.040	3
10.514	1.022 ± 0.005	1.023 ± 0.0025	−1	1.023 ± 0.003	1.025	1.029	4
11.039	1.019 ± 0.0055	1.015 ± 0.003	+4	1.016 ± 0.003	1.018	1.018	0
11.557	1.008 ± 0.006	1.004 ± 0.003	+4	1.005 ± 0.003	1.007	1.009	2
12.088	0.985 ± 0.008	1.003 ± 0.003	−18	0.999 ± 0.003	1.001	1.001	0
12.629	0.995 ± 0.0065	0.995 ± 0.0035	0	0.995 ± 0.004	0.997	0.995	−2

[a] J. Hubbell, H. Gimm, and I. Øverbø (private communication).

REF. J. Arends, J. Eyink, A. Hegerath, K.G. Hilger, B. Mecking, G. Nöldeke, H. Rost
Phys. Lett. 98B, 423 (1981)

ELEM. SYM.	A	Z
Al	27	13

METHOD

REF. NO. 81 Ar 1 hg

REACTION	RESULT	EXCITATION ENERGY	SOURCE		DETECTOR		ANGLE
			TYPE	RANGE	TYPE	RANGE	
G,MU-T	ABX	215-386	D	215-386	TOF-D		4PI

DATA ALSO IN 81AR3

Double differential cross sections for the photo-emission of protons and charged pion production were investigated for a number of target nuclei (He, Be, C, O, Al, Ti, Cu, Sn, Pb) in the photon energy range k = (215–386) MeV. On the basis of these experimental results the total hadronic cross section was determined.

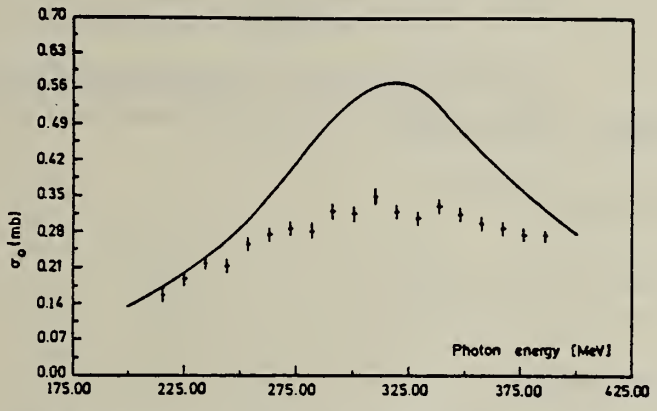

Fig. 7. Parameter σ_0 as a function of photon energy (data points) compared to the mean cross section for a free nucleon (solid line).

The total hadronic cross sections for all measured elements can be parametrized in the form

$$\sigma(k, A) = \sigma_0(k) \cdot A^x ,$$

A being the atomic number, with a constant exponent $x = 1.1$. The photon energy dependence of σ_0 is shown in fig. 7. Compared to the mean cross section for a free nucleon (the solid line in fig. 7) the excitation of the Δ-resonance is suppressed. Such a suppression is expected in the Δ-hole model [11].

REF. J. Arends, J. Eyink, A. Hegerath, K.G. Hilger, B. Mecking, G. Nöldeke, H. Rost
Nucl. Phys. A358, 367c (1981)

ELEM. SYM.	A	Z
Al	27	13

METHOD

REF. NO. 81 Ar 3 | hg

REACTION	RESULT	EXCITATION ENERGY	SOURCE TYPE	SOURCE RANGE	DETECTOR TYPE	DETECTOR RANGE	ANGLE
G,MU-T	ABX	215-386	D	215-386	TOF-D		4PI

Abstract: Double differential cross sections for the photoemission of protons and charged pion photoproduction were investigated for a number of target nuclei (He, Be, C, O, Al, Ti, Cu, Sn, Pb) using the tagged bremsstrahlung beam at the Bonn 500 MeV-Synchrotron in the photon range k = (215-386)MeV. On the basis of these experimental results the total hadronic cross section was determined.

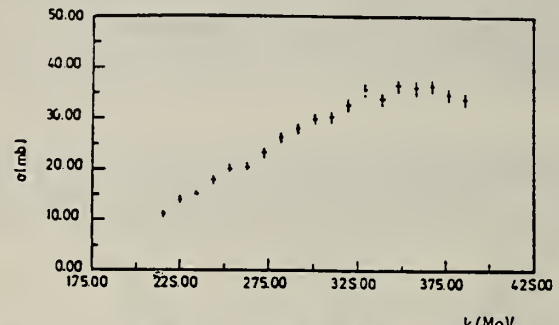

Fig. 2. Cross section for the process: $\gamma + Pb \rightarrow p + X$. The proton threshold is 58 MeV.

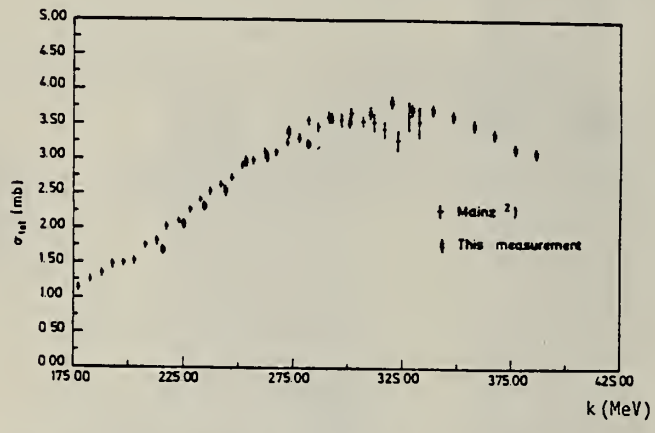

Fig. 3. Total hadronic cross section for Be. The data are compared to the cross section taken from ref.[2]).

The photon energy dependence of the total cross sections for heavier nuclei are similar to the Be results. The complete data set can be parametrized in the form

$$\sigma(k,A) = \sigma_0(k) \cdot A^x.$$

The exponent is constant x = 1.1. The photon energy dependence of σ_0 is shown in fig. 4. Compared to the mean cross section for a free nucleon, the excitation of the Δ-resonance is suppressed.

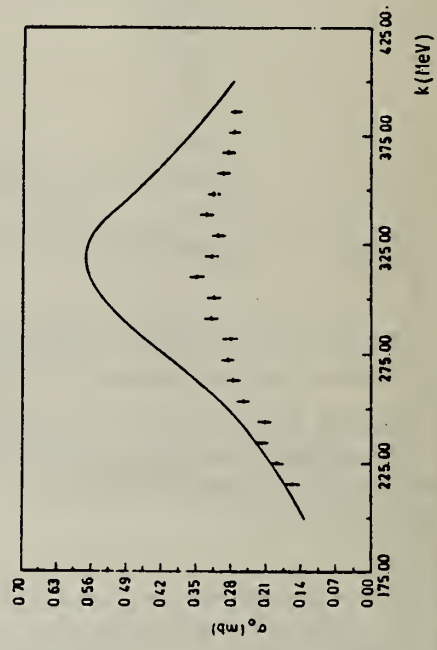

Fig. 4. Parameter σ_0 compared to the cross section for a free nucleon (full line).

REF.

Y. Cauchois, H. Ben Abdelaziz, R. Khérouf, C. Schloesing-Möller
J. Phys. G7, 1539 (1981)

ELEM. SYM.	A	Z
Al	27	13

METHOD

REF. NO.	
81 Ca 2	hg

REACTION	RESULT	EXCITATION ENERGY	SOURCE		DETECTOR		ANGLE
			TYPE	RANGE	TYPE	RANGE	
G,G	LFT	1	C	0 - 2	SCD-D		
		(1.014)					

1.014 MeV

Abstract. Lifetimes of 49 excited states below 1.65 MeV have been measured in ^{24}Mg, ^{27}Al, ^{48}Ti, ^{58}Ni, ^{59}Co, ^{61,62}Ni, ^{63,65}Cu, ^{64,66,68}Zn, ^{75}As, ^{103}Rh, ^{113,115}In, ^{116,118,120}Sn and ^{121,123}Sb by means of nuclear resonance fluorescence experiments. The levels are excited by bremsstrahlung x-ray photons. The self-absorption technique applied to suitable cases provides nuclear absorption cross sections, widths and lifetimes from which the x-ray spectral distributions are also obtained. Scattering experiments are performed for all other cases in order to obtain widths and lifetimes from these x-ray photon curves. The Compton effect in the sample is taken into account. Self-absorption provides $g\Gamma_0$ from which Γ is deduced using adopted J^π and Γ_0/Γ values; scattering provides $u = g(\Gamma_0^2/\Gamma)W(\theta)$ from which Γ is also deduced with J, Γ_0/Γ and mixing ratios taken from the literature. Thanks to simultaneous determination of the x-ray spectra all the lifetimes as given by our programs with their statistical errors form an unusually coherent set of values.

NUCLEAR REACTIONS (γ, γ), bremsstrahlung excitation; natural isotopes; ^{24}Mg, ^{27}Al, ^{48}Ti, ^{58}Ni, ^{59}Co, ^{61,62}Ni, ^{63,65}Cu, ^{64,66,68}Zn, ^{75}As, ^{103}Rh, ^{113,115}In, ^{116,118,120}Sn and ^{121,123}Sb; $E \simeq 0.5$–1.65 MeV; measured $g\Gamma_0$ or $g(\Gamma_0^2/\Gamma)W(\theta)$; deduced $T_{1/2}$.

(OVER)

Tableau 3. Résultats des mesures des niveaux étudiés par diffusion.

Table 3. Results obtained using the diffusion method.

Isotope	Energie (keV)	J^π	J_0^π	Γ_0/Γ	δ	$u=g(\Gamma_0^2/\Gamma)W(\theta)$ (meV)	τ (ps) ce travail	$\tau_{réf}$ (ps)	Références†
^{24}Mg	1368,59(4)	2^+	0^+	1	E2	1,08(13)	1,76(21)	1,98(4)	Endt et van der Leun (1978)
^{27}Al	1014,45(3)	$\frac{1}{2}^+$	$\frac{1}{2}^+$	0,971	+0,351(12)	0,186(13)	2,20(16)	2,12(8)	Endt et van der Leun (1978)
^{46}Ti	983,512(3)	2^+	0^+	1	E2	0,282(23)	6,74(55)	6,1(13)	Been (1978)
^{58}Ni	1454,45(15)	2^+	0^+	1	E2	2,11(26)	0,90(11)	0,92(3)	Kocher et Auble (1976)
^{59}Co	1099,224(25)	$\frac{3}{2}^-$	$\frac{7}{2}^-$	1	(E2)	0,069(8)	4,79(55)	3,17(58)	Kim (1976)
^{59}Co	1458,8(3)	$\frac{5}{2}^-$	$\frac{7}{2}^-$	0,91	(E2)	0,68(8)	1,17(14)	1,52(16)	Kim (1976)
^{59}Co	1480,9(3)	$\frac{5}{2}^-$	$\frac{7}{2}^-$	0,8	$<0,35^a$	1,23(15)	0,254(31)	0,31(3)	Kim (1976)
^{61}Ni	1185,7(6)	$\frac{3}{2}^-$	$\frac{3}{2}^-$	0,77(8)[i]	|0,14|	1,88(49)	0,21(5)	0,16(3)	Andreev *et al* (1974)
^{62}Ni	1172,91(9)	2^+	0^+	1	E2	0,88(17)	2,15(42)	2,09(3)	Halbert (1979a)
^{63}Cu	1327,00(7)	$\frac{7}{2}^-$	$\frac{3}{2}^-$	0,84	(E2)	1,04(14)	0,84(11)	0,88(4)	Auble (1979b)
^{63}Cu	1412,05(4)	$\frac{5}{2}^-$	$\frac{3}{2}^-$	0,72	$+0,61\{^{+9}_{-8}\}$	0,260(38)	1,90(28)	1,61(3)	Auble (1979b)
^{64}Zn	991,54(7)	2^+	0^+	1	E2	0,640(54)	2,97(25)	2,60(13)	Halbert (1979b)
^{65}Cu	1481,83(5)	$\frac{7}{2}^-$	$\frac{3}{2}^-$	0,85	(E2)	1,13(19)	0,79(13)	0,49(5)	Auble (1975a)
^{66}Zn	1039,37(6)	2^+	0^+	1	E2	0,70(6)	2,71(23)	2,25(15)	Auble (1975b)
^{68}Zn	1077,38(5)	2^+	0^+	1	E2	0,70(6)	2,71(23)	2,34(23)	Lewis (1975)
^{75}As	572,5(10)	$\frac{5}{2}^-$	$\frac{3}{2}^-$	1[d]	0,39[b]	0,236(26)	4,14(46)	3,5(9)	Horen et Lewis (1975)
^{75}As	823,0(10)	$\frac{7}{2}^-$	$\frac{3}{2}^-$	0,86[d]	(E2)	0,214(22)	4,27(43)	3,5(3)	Robinson *et al* (1967)
^{75}As	865,5(10)	$\frac{5}{2}^+$	$\frac{3}{2}^-$	0,83[d]	—[c]	0,78(6)	0,863(68)	0,60(12)	Celliers *et al* (1977)
^{75}As	1076,0(10)	$\frac{5}{2}^-$	$\frac{3}{2}^-$	0,94[d]	0,38[d]	1,97(13)	0,287(19)	0,32(7)	Celliers *et al* (1977)
^{75}As	1128,5(10)	$\frac{1}{2}^+$	$\frac{3}{2}^-$	1	E1[d]	0,224(24)	1,47(16)	—	
^{75}As	1349,0(10)	$\frac{3}{2}^-$	$\frac{3}{2}^-$	0,67[d]	0,20[d]	1,61(29)	0,180(32)	0,12(3)	Wilson (1970)
^{75}As	1370,0(10)	$\frac{3}{2}^-$	$\frac{3}{2}^-$	0,47[d]	0,47[d]	0,64(13)	0,218(44)	—	
^{103}Rh	803,1(2)	$\frac{1}{2}^-$	$\frac{1}{2}^-$	0,70	M1	1,85(16)	0,174(15)	—	Harmatz (1979)
^{103}Rh	1277,0(2)	$\frac{3}{2}^-$	$\frac{1}{2}^-$	0,75	−0,62(30)[e]	0,81(9)	0,87(10)	1,3(9)	Harmatz (1979)
^{113}In	1177(1)	$\frac{11}{2}^+$	$\frac{9}{2}^+$	1	+0,5(2)	9,1(8)	0,086(8)	0,10(6)	Tuttle *et al* (1976)
^{113}In	1510(1)	$\frac{7}{2}^+$	$\frac{9}{2}^+$	0,935	$-0,5\{^{+1}_{-2}\}$	6,4(9)	0,071(10)	$0,11\{^{+4}_{-3}\}$	Tuttle *et al* (1976)
^{115}In	1077,7(10)	$\frac{5}{2}^+$	$\frac{9}{2}^+$	0,81[j]	(E2)	0,159(24)	1,61(24)	1,23(7)	Tuttle *et al* (1976)
^{115}In	1290,59(3)	$\frac{11}{2}^+$	$\frac{9}{2}^+$	0,98[j]	(E2)	1,31(11)	0,66(6)	0,55(4)	Tuttle *et al* (1976)
^{115}In	1448,78(3)	$\frac{7}{2}^+$	$\frac{9}{2}^+$	0,86	−8[f]	0,90(11)	0,50(6)	0,52(20)	Tuttle *et al* (1976)
^{115}In	1486,1(1)	$\frac{9}{2}^+$	$\frac{9}{2}^+$	0,787	−0,8[f]	0,63(9)	0,63(9)	0,4(3)	Tuttle *et al* (1976)
^{115}In	1497,2(4)	$(\frac{5}{2}^+)$	$\frac{9}{2}^+$	< 1	(E2)	1,33(16)	< 0,30(4)	—	
^{115}In	1607,8(15)	$(\frac{5}{2}^+)$	$\frac{9}{2}^+$	⩽ 1	(E2)	1,54(24)	⩽ 0,26(4)	—	
^{116}Sn	1293,54(2)	2^+	0^+	1	E2	3,58(37)	0,53(6)	0,522(14)	Carlson *et al* (1975)
^{118}Sn	1229,64(4)	2^+	0^+	1	E2	2,75(28)	0,69(7)	0,67(2)	Carlson *et al* (1976)
^{120}Sn	1171,6(2)	2^+	0^+	1	E2	1,83(16)	1,04(9)	0,91(2)	Kocher (1976)
^{121}Sb	1023,5(10)	$\frac{7}{2}^+$	$\frac{5}{2}^+$	1	|0,57|[g]	3,69(34)	0,228(21)	0,20(7)[h]	Tamura *et al* (1979)
^{121}Sb	1105,5(10)	$\frac{9}{2}^+$	$\frac{7}{2}^+$	0,4	—	0,47(4)	0,42(4)	—	
^{121}Sb	1142,5(10)	$\frac{9}{2}^+$	$\frac{5}{2}^+$	0,6	(E2)	0,85(8)	0,449(40)	0,41(8)[h]	Booth *et al* (1973)
^{121}Sb	1384,0(10)	$\frac{11}{2}^+$	$\frac{5}{2}^+$	1	|0,45|[g]	4,7(5)	0,092(10)	0,088(14)[h]	Booth *et al* (1973)
^{123}Sb	1029,5(10)	$\frac{9}{2}^-$	$\frac{7}{2}^-$	1	|0,57|[g]	2,96(27)	0,272(25)	0,26(4)[h]	Booth *et al* (1973)
^{123}Sb	1086,5(10)	$\frac{9}{2}^+$	$\frac{7}{2}^+$	1	$\|\delta\| > 1,26^g$	1,06(9)	0,67(6)	0,72(15)[h]	Booth *et al* (1973)

† Références pour les colonnes 3, 4, 5, 6 et 9 de chaque ligne, sauf indication appelée au bas de ce tableau. Pour les autres données se reporter au texte.

Remarque. Pour calculer δ^2 quand nous ne disposons que de $B(E2)$, pour un mélange (E2) + (M1), nous déduisons $g\Gamma_0(E2) \propto B(E2)E_\gamma^5$; en admettant $W(\theta)=1$ et connaissant Γ_0/Γ, notre détermination de u donne une première approximation de $g\Gamma_0$ d'où une valeur de $\delta^2=(g\Gamma_0(E2))/(g\Gamma_0-g\Gamma_0(E2))$ qui permet d'améliorer $W(\theta)$ et $g\Gamma_0$ de proche en proche.

[a] Swann (1971); [b] Robinson *et al* (1967); [c] $W(\theta)=0.99$ calculé d'après la formule de Celliers *et al* (1977); [d] Abbondanno *et al* (1978); [e] Sayer *et al* (1972); [f] Tuttle *et al* (1976); [g] d'après $B(E2)$ de Barnes *et al* (1966); [h] calculé d'après Booth *et al* (1973); [i] Williams *et al* (1975); [j] Dietrich *et al* (1970).

REF. B.S. Dol'inskii, R.L. Kondrat'ev, N.N. Kostin, V.P. Lisin, V.N. Ponomarev, A.L. Polonskii
Bull. Acad. Sci. 45,166 (1981)
Izv. Akad. Nauk SSSR 45, 188 (1981)

ELEM. SYM.	A	Z
Al	27	13

METHOD

REF. NO. 81 Do 3 hg

REACTION	RESULT	EXCITATION ENERGY	SOURCE TYPE	SOURCE RANGE	DETECTOR TYPE	DETECTOR RANGE	ANGLE
E,E/	ABX	2,3	D	28 - 75	MAG-D		DST

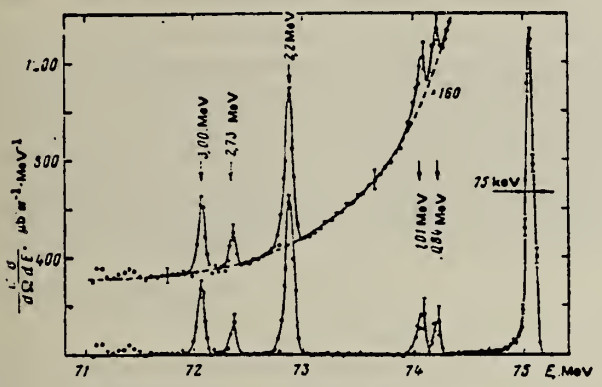

Fig. 1. Spectrum of electrons scattered by the ^{27}Al nucleus at E_0 = 75.31 MeV, θ = 90°. The upper part of the figure shows the inelastic-scattering spectrum against the background of a radiation tail; the lower part shows the spectrum after subtraction of the tail.

LEVELS 2.21, 3.0 MEV

Table 2

Data on Inelastic Scattering of Electrons by ^{27}Al

E_0, MeV	θ, deg	q_{el}, fm^{-1}	E_{yp} = 2.21 MeV $S_{II}\cdot 10^3 / S_{1s}\cdot K$	σ_1, μb·sr^{-1}	error, %	E_{yp} = 3.04 MeV $S_{II}\cdot 10^3 / S_{el}\cdot K$	σ_1, μb·sr^{-1}	error, %
75.31	90	0.539	3.63	0.415	6	1.88	0.215	8
55.24	110	0.453	1.96	0.206	7	0.97	0.102	9
53.86	90	0.386	0.85	0.338	6	0.415	0.165	8
37.35	110	0.310	0.33	0.119	30	—	—	—
28.7	110	0.238	0.096	0.070	45	—	—	—

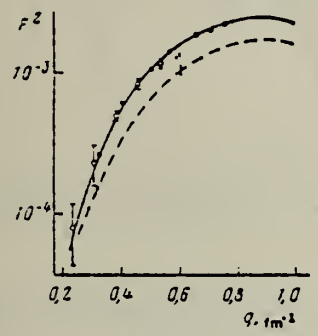

Fig. 3

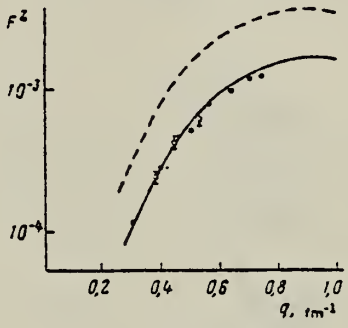

Fig. 4

Fig. 3. Form factor of inelastic scattering of electrons for the 2.21 MeV, $7/2^{+-}$ state of ^{27}Al. The open circles represent the present experiment; the filled circles represent the result of [3]. The solid curve corresponds to calculation according to the shell model [16]; the dashed curve corresponds to calculation according to the intermediate-coupling model [3,17].

Fig. 4. Form factor of inelastic scattering of electrons for the 3.00 MeV, 9/2+ level of ^{27}Al. The open circles represent the present experiment; the filled circles represent the results of [3]. The solid curve corresponds to calculation according to the shell model [16]; the dashed curve corresponds to calculation according to the intermediate-coupling model [3,17].

REF. B.S. Ishkhanov, I.M. Kapitonov, V.I. Shvedunov, A.V. Shumakov
Yad. Fiz. 33, 865 (1981)
Sov. J. Nucl. 33, 453 (1981)

ELEM. SYM.	A	Z
Al	27	13

METHOD

REF. NO. 81 Is 4 egf

REACTION	RESULT	EXCITATION ENERGY	SOURCE		DETECTOR		ANGLE
			TYPE	RANGE	TYPE	RANGE	
G,PØ	ABX	13-29	C	17-30	TEL-D		90
G,PL							

Photoproton spectra have been obtained from the ^{27}Al nucleus at 14 bremsstrahlung maximum energies E_γ^{max} in the range 17.0–29.7 MeV. From the spectra we have calculated the partial cross sections for the photoproton reaction with formation of the final nucleus in the ground state, the first two excited states, and in groups of states with centers of gravity at 4.4, 6.6, 8.5, 11.0, and 13.0 MeV. The sum of the partial cross sections exhausts the total cross section of the (γ,p) reaction. Analysis of the experimental results was carried out simultaneously for the nuclei ^{27}Al, ^{26}Mg, and ^{28}Si with use of data on pickup reactions. The role of nucleons of different shells and the fraction of excitations of the $1p\,1h$ type in the ^{27}Al giant dipole resonance are estimated. The influence of the structure of the ground state of nuclei of the $1d$-$2s$ shell on the properties of the giant resonance is discussed.

PACS numbers: 25.20. + y, 27.30. + t, 24.30.Cz

L=1,2,"5",17,39 (G,PL)

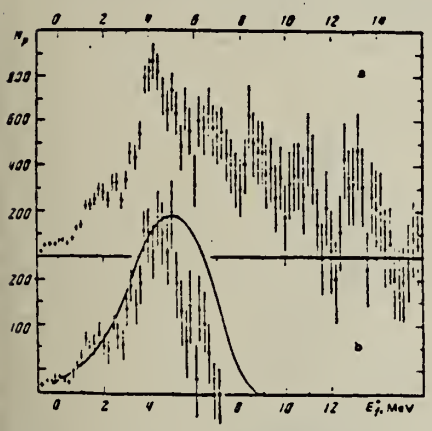

FIG. 2. Combined difference proton spectra from ^{27}Al: a—in the excitation energy region 17–29 MeV; b—in the excitation energy region 17–18.7 MeV.

TABLE I. Energies of states, energy resolution in partial cross sections, and their integrated values.

	E_f^*, MeV							
	0	1.8	3.0	4.4	6.6	8.5	11.0	13.0
ΔE, MeV	0.3–0.1	0.6	0.6	0.6	1.2	1.2	2.0	2.0
$\int \frac{d\sigma}{d\Omega} E\,dE$, MeV · mb/sr	0.8	2.2	1.9	5.0	2.5	2.0	1.3	1.0

[1]B. S. Ishkhanov *et al.*, Izv. AN SSSR, seriya fiz. 33, 1742 (1969) [Bull. USSR Acad. Sci., Phys. Ser.].

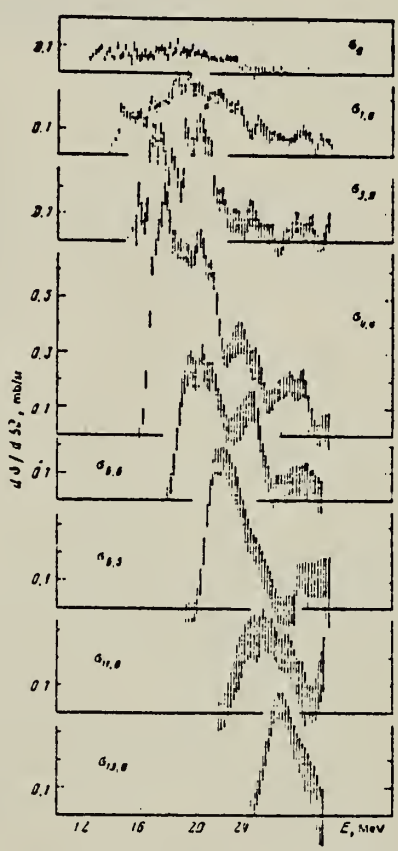

FIG. 3. Partial cross sections for the reaction ^{27}Al$(\gamma,p)^{26}$Mg with formation of the final nucleus in various states.

(OVER)

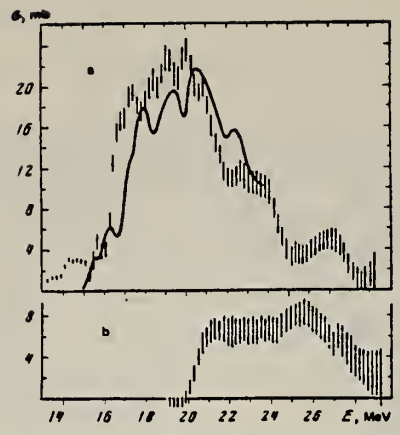

FIG. 4. Cross section for the (γ,p) reaction in ^{27}Al determined by transitions of nucleons from the shells $1d$-$2s$ (a) and $1p$ (b). The solid curve is $\sigma_{\gamma,n}\times 4$.[19]

REF. P.J.P. Ryan, M.N. Thompson, K. Shoda, T. Tanaka
Nucl. Phys. A371, 318 (1981)

ELEM. SYM.	A	Z
Al	27	13

METHOD

REF. NO. 81 Ry 2 hg

REACTION	RESULT	EXCITATION ENERGY	SOURCE		DETECTOR		ANGLE
			TYPE	RANGE	TYPE	RANGE	
E,P	ABX	8-28	D	14-28	MAG-D		90

VIRT PHOTON THEOR

Abstract: Photoproton spectra from ^{27}Al were measured from 14.8 to 27.6 MeV excitation energy in 400 keV steps. From these, high resolution photoproton cross sections to low-lying states of the residual ^{26}Mg nucleus were deduced. The large integrated cross sections to these states justify the interpretation of the de-excitation γ-ray measurements which consistently indicate strong population of low-lying residual states following photodisintegration. Further, the results are discussed with reference to the particle-hole model. By examination of the microscopic configurations of the possible GDR states an explanation is proposed for the differences in the cross sections to various residual states. Finally, the results are compared with spectroscopic factors determined from pickup reactions on ^{27}Al.

E NUCLEAR REACTIONS ^{27}Al(e, p), E = 14.8-27.6 MeV; measured proton energy spectra at θ = 90°. Deduced $\sigma(\gamma, p)$ to different ^{26}Mg states, mechanism. Magnetic spectrometer, isotopically pure target.

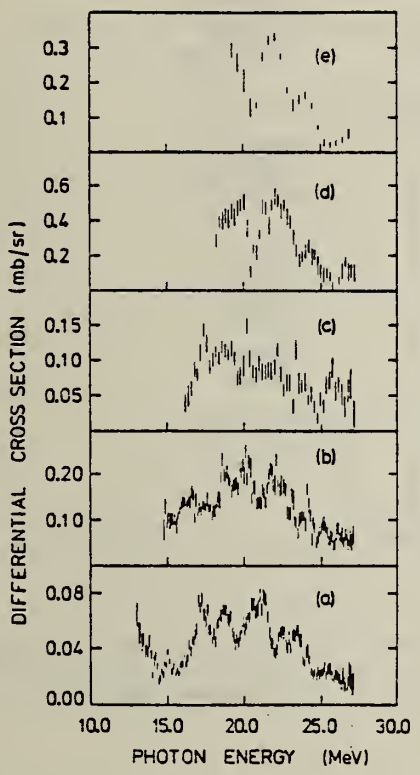

Fig. 3. Differential cross sections at 90° for the reaction ^{27}Al(γ, p_1): (a) ^{27}Al(γ, p_0), (b) ^{27}Al(γ, p_1), (c) ^{27}Al(γ, p_2), (d) ^{27}Al(γ, $p_{..3...}$) and (e) ^{27}Al(γ, $p_{..4...}$).

(OVER)

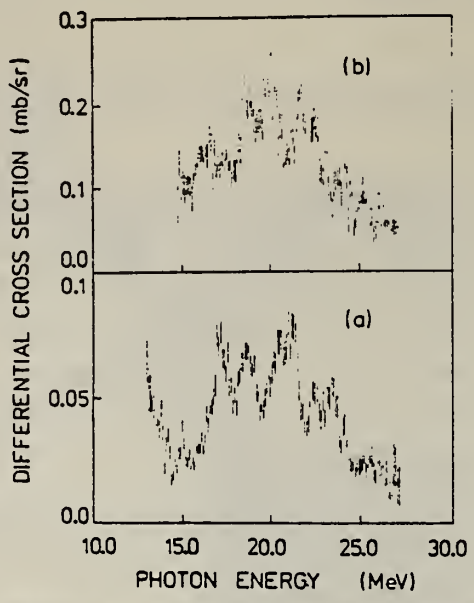

Fig. 4. Differential cross sections at 90° to the ground and first excited states: (a) ^{27}Al(γ, p_0) and (b) ^{27}Al(γ, p_1).

TABLE 1

Results and comparison with previous measurements

Residual state in ^{26}Mg [from ref. [13])] (MeV)	$\int_{14.8}^{27.6} \frac{d\sigma}{d\Omega}(\gamma, p)dE$ (at 90°) (MeV · mb/sr) [a])	$\int_{16}^{26} \frac{d\sigma}{d\Omega}(\gamma, p)dE$ (at 90°) (MeV · mb/sr) [b])	$\int_{16}^{24} \frac{d\sigma}{d\Omega}(\gamma, p_{\gamma'})dE$ (at 150°) (MeV · mb/sr) [c])
0, 0$^+$	0.60 ± 0.06	0.45 ± 0.06	
1.809, 2$^+$	1.61 ± 0 17	0.92 ± 0.2	2.00 ± 0.5
2.938, 2$^+$	0.9 ± 0.2		0.74 ± 0.15
3.588, 0$^+$	[e])		(0.32 ± 0.1) [d])
3.941, 3$^+$	[e])		
4.318, 4$^+$	2.7 ± 0.6		1.5 ± 0.2
4.332, 2$^+$			< 0.25
4.350, 3$^+$			0.5 ± 0.2
4.834, 2$^+$	1.4 ± 0.5		0.63 ± 0.15
4.900, 4$^+$			< 0.2
4.972, 0$^+$			

[a]) Present results.
[b]) Results of Tsubota *et al.* [16]).
[c]) Results of Thomson from a de-excitation gamma-ray measurement [12]).
[d]) This assignment is uncertain [12]).
[e]) These states were assumed to be unpopulated in the present analysis (see text).

REF. P.J.P. Ryan, M.N. Thompson, K. Shoda, M. Hirooka
Nucl. Phys. A389, 29 (1982)

ELEM. SYM.	A	Z
Al	27	13

METHOD

REF. NO. 82 Ry 3 egf

REACTION	RESULT	EXCITATION ENERGY	SOURCE TYPE	SOURCE RANGE	DETECTOR TYPE	DETECTOR RANGE	ANGLE
E,PL	ABX	15-25	D	17-26	MAG-D		DST

Abstract: The angular distributions of the $^{27}Al(\gamma, p_0)$ and $^{27}Al(\gamma, p_1)$ reactions were measured over the GDR energy region. Both reactions exhibit considerable anisotropy indicating the effects of multipole interference. From the behaviour of the fitted Legendre polynomial coefficients the principal 1p-1h configurations in the $^{27}Al(\gamma, p_0)$ reaction were investigated and an approximate cross section for the E2 component deduced using justifiable assumptions. The angular distribution of the $^{27}Al(\gamma, p_1)$ reaction is qualitatively similar to that of the $^{27}Al(\gamma, p_0)$ reaction. However if only a single intermediate configuration is involved it appears that the first excited state (2^+) of ^{26}Mg is likely to be populated by $p_{3/2}$ proton emission whereas the ground state (0^+) is populated predominantly by $f_{7/2}$ proton emission from the ^{27}Al GDR.

E NUCLEAR REACTIONS $^{27}Al(e,p)$, E = 16.8–25.6 MeV; measured $\sigma(E,\theta)$, derived $\sigma(\gamma, p_i, \theta)$. ^{27}Al deduced GDR configurations, E2 decay characteristics.

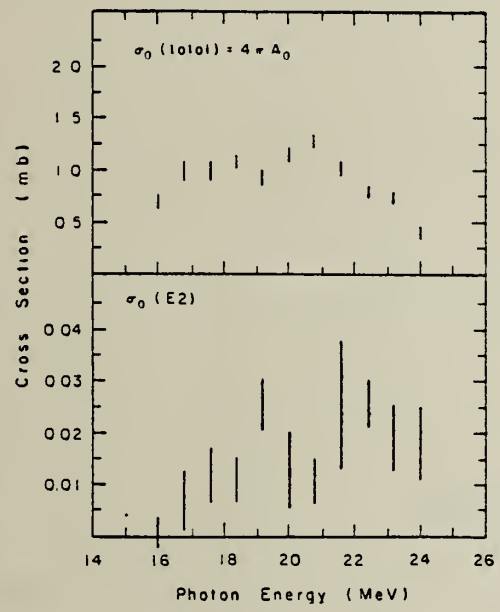

Fig. 7. The small E2 component of the $^{27}Al(\gamma, p_0)$ cross-section calculated from eq. (7) (see text) is plotted in the lower half of the diagram while the total cross section, given by $4\pi A_0$, is plotted in the upper half for comparison.

L=Ø,1, VIR PHOT

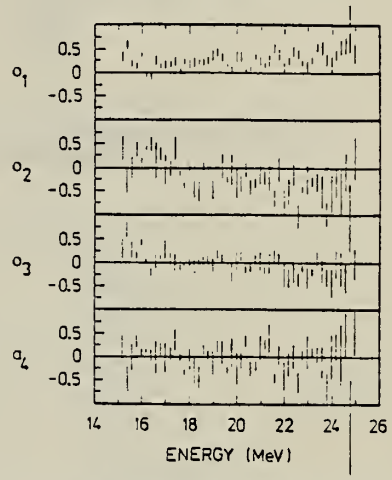

Fig. 5. The Legendre polynomial coefficients a_1, a_2, a_3, a_4 obtained from fits to the measured angular distributions of the $^{27}Al(\gamma, p_0)$ cross section.

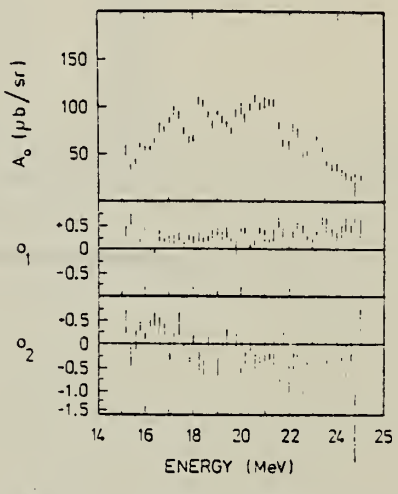

Fig. 6. The Legendre polynomial coefficients A_0, a_1 and a_2 as a function of energy for the $^{27}Al(\gamma, p_0)$ reaction.

(OVER)

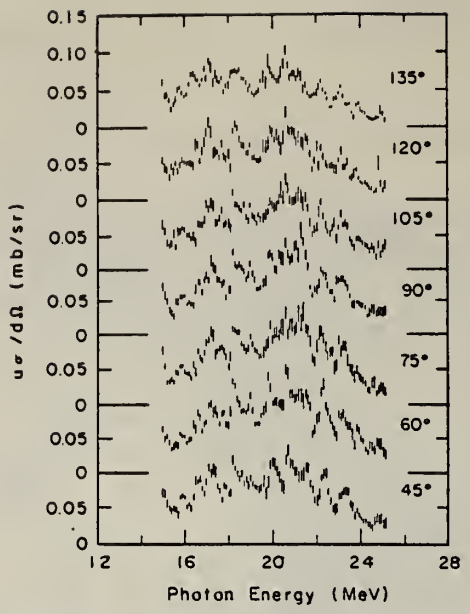

Fig. 1. The $^{27}Al(\gamma, p_0)$ differential cross sections measured in 15° steps from 45° to 135°. The angle at which each cross section is measured is superposed.

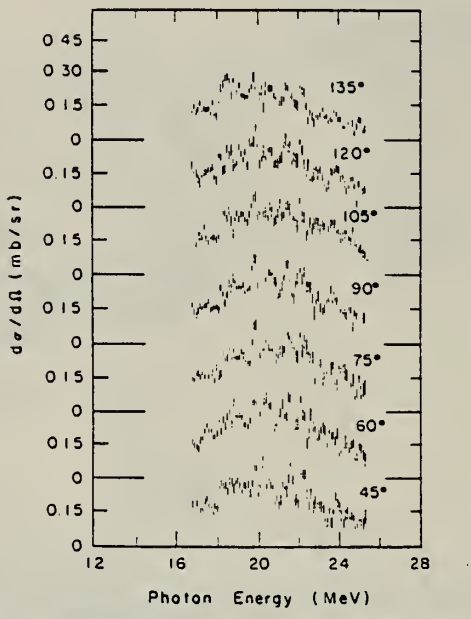

Fig. 2. The $^{27}Al(\gamma, p_1)$ differential cross sections measured at the 7 angles under study.

A=28

A=28

Ref.	Elem. Sym.	A	Z
F.Cvelbar, A.Hudoklin, M.V.Milhailovic, M.Najzer, V.Ramsak Phys.Letters 3, 364 (1963)	Al	28	13

Method	Ref. No.	
telescope scintillation pair spectrometer	63Cv1	BG

Reaction	E or ΔE	E_o	Γ	$\int \sigma dE$	Jπ	Notes
$Al^{27}(n,\gamma)Al^{28}$	$E_{n_{in}}$ = 14 MeV $E_{\gamma_{out}}$ = 12 - 22					Cross section integrated over γ ray energies > 14 MeV = .26±.05 MeV

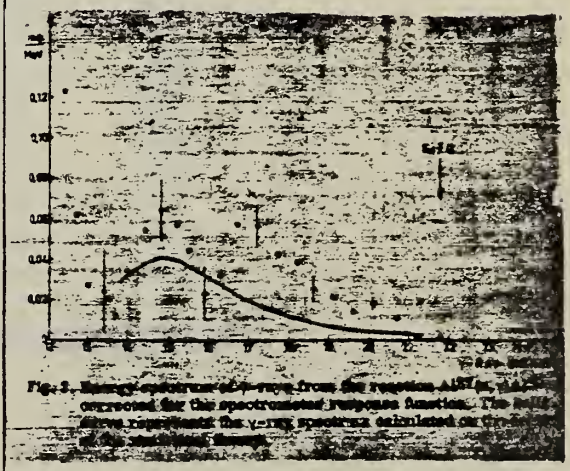

Fig. 3. Energy spectrum of γ-rays from the reaction Al²⁷(n, γ)Al²⁸ corrected for the spectrometer response function. The full drawn curve represents the γ-ray spectrum calculated on the basis of the statistical theory.

REF. I. Bergqvist, J. A. Biggerstaff, J. H. Gibbons, W. M. Good
Phys. Rev. 158, 1049 (1967)

ELEM. SYM.	A	Z
Al	28	13

METHOD

REF. NO. 67 Be 7 egf

REACTION	RESULT	EXCITATION ENERGY	SOURCE TYPE	SOURCE RANGE	DETECTOR TYPE	DETECTOR RANGE	ANGLE
N,G	LFT	7-8	D	0-1	NAI-D	0-7	90

SOURCE 35,89 KEV

TABLE VI. Gamma rays from $^{27}Al(n,\gamma)^{28}Al$; $E_R = 35$ keV, $J^\pi = (3)^+$.

E_γ (MeV)	I_γ (per 100 captures)	Assignment	$J_i^\pi \rightarrow J_f$	Γ_{γ_f} (meV)	$1000\|M\|^2$
7.77	60±5	$C \rightarrow 0$, $C \rightarrow 0.03$	$(3^+) \rightarrow 3^+, 2^+$	540	55
6.74	4±2	$C \rightarrow 0.97, 1.02$	$(3)^+ \rightarrow (0,2)^+, (2,3)^+$	36	6
6.11	10±2	$C \rightarrow 1.63$	$(3)^+ \rightarrow (2,3)^+$	90	19
5.4	4±2	$(C \rightarrow 2.28)$	$[(3)^+ \rightarrow (\leq 5)^+]$	(36)	(11)
4.78	4±2	$4.77 \rightarrow 0$	$(\leq 4)^- \rightarrow 3^+$		
(4.4)[a]	(3)				
4.2	3	$(C \rightarrow 3.59)$	$[(3)^+ \rightarrow (\leq 4)^-]$	(27)	(0.6)
3.9[b]	5	$(C \rightarrow 3.88 \rightarrow 0)$	$[(3)^+ \rightarrow (\leq 4)^- \rightarrow 3^+]$	(22)	(0.6)
3.55	4	$(3.59 \rightarrow 0)$	$[(\leq 4)^- \rightarrow 3^+]$		
3.1[b]	4	$(C \rightarrow 4.77)$	$[(3)^+ \rightarrow (\leq 4)^-]$	(36)	(2)
2.9	3				
2.6	4±2	$(2.59 \rightarrow 0)$	$[(\leq 5)^+ \rightarrow 3^+]$		
2.2	(9)	$2.21 \rightarrow 0$, $(H(n,\gamma)D)$	$(\leq 5)^+ \rightarrow 3^+$		
(2.0)	(3)				
1.63	20±5	$1.63 \rightarrow 0$ (0.03)	$(2,3)^+ \rightarrow 3^+$		
1.35	6±2	$1.37 \rightarrow 0.03$	$1^+ \rightarrow 2^+$		
0.98	12±3	$1.02 \rightarrow 0.03$,	$(2,3)^+ \rightarrow 2^+$		
		$(0.97 \rightarrow 0)$	$[(0,2)^+ \rightarrow 3]^+$		

[a] Parentheses imply marginal credibility. [b] Unresolved structure.

TABLE VII. Gamma rays from $^{27}Al(n,\gamma)^{28}Al$; $E_R = 89$ keV, $J^\pi = 3^+$.

E_γ (MeV)	I_γ (per 100 captures)	Assignment	$J_i^\pi \rightarrow J_f^\pi$	Γ_{γ_f} (meV)	$1000\|M\|^2$
7.80	15±2	$C \rightarrow 0, 0.03$	$3^+ \rightarrow 3^+, 2^+$	90	9
6.81	11±3	$C \rightarrow 0.97, 1.02$	$3^+ \rightarrow (0,2)^+, (2,3)^+$	66	11
(6.4)[a]	(5)	$(C \rightarrow 1.38)$[a]			
5.60	14±3	$(C \rightarrow 2.15, 2.21, 2.28)$	$3^+ \rightarrow (\leq 5)^+$	84	
5.18[b]	12±3	$(C \rightarrow 2.67)$	$3^+ \rightarrow (\leq 5)^+$	12	
4.80	11±3	$(C \rightarrow 2.99, 3.01)$			
4.30	14±3	$(C \rightarrow 3.46, 3.54)$			
(3.9)	(7)	$(C \rightarrow 3.88 \rightarrow 0)$			
3.55	20±4	$C \rightarrow 4.24$; $3.54 \rightarrow 0, 0.03$			
3.1	13±4	$3.10 \rightarrow 0, 0.03$			
2.65	12±4	$2.67 \rightarrow 0, 0.03$			
2.25	26±5	$2.28 \rightarrow 0.03$; $2.21 \rightarrow 0$			
1.66	30±5	$1.63 \rightarrow 0$			

[a] Parentheses imply marginal credibility. [b] Unresolved structure.

SILICON
Z=14

The name silicon was derived from *silic-*, the bare syllables of the Latin word silex meaning "flint". Before 1787 chemists thought that the compound of silicon, silica, was an element. It was then that Lavoisier speculated that silica was an oxide of an unknown element. In 1817 Berzelius decomposed iron silicite in such a way that the presence of another metal was indicated. Finally, in 1824, he showed that this metal was derived from silica and he succeeded in preparing the amorphous form of it. The crystalline form was first prepared by Sainte-Claire Deville in 1854 by electrolysis of impure sodium chloride containing about 10% silicon in the melt. Shiny platelets of silicon were obtained when he dissolved the aluminum.

Si

Si

Ref. V. Emma, C. Milone, A. Rubbino
Il Nuovo Cimento 9, 343 (1958)

Elem. Sym.	A	Z
Si		14

Method: emulsion; Bremss.

Ref. No.: 58 Em 1 | EH

Reaction	E or ΔE	E_o	Γ	$\int \sigma dE$	Jπ	Notes
(γ,p)	Bremss. 30			0.23MeV-mb (using C as standard)		Angular distributions for proton energy groups > 7, > 5.5, and < 3.5 MeV. Forward peaking for protons > 5 MeV.

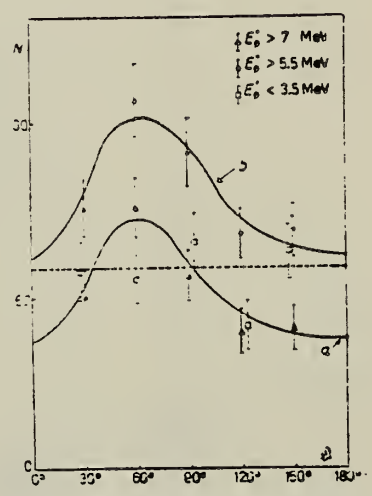

Fig. 1. – Angular distribution of photoprotons from Si. N = number of photoprotons observed with energy E'_p for constant solid angle, and 30° ϑ-interval (arbitrary units). Standard deviations are included.

Ref. J. Dular, G. Kernel, M. Kregar, M.V. Mihailović, G. Pregl, M. Rosina, C. Zupančič
Nuclear Phys. 14, 131 (1959)

Elem. Sym.	A	Z
Si		14

Method: Compton spectrometer; 30 MeV Betatron

Ref. No.: 59 Du 1 | EH

Reaction	E or ΔE	E_o	Γ	$\int \sigma dE$	Jπ	Notes
(μ_t)	Bremss. 30.3 28.9					

829

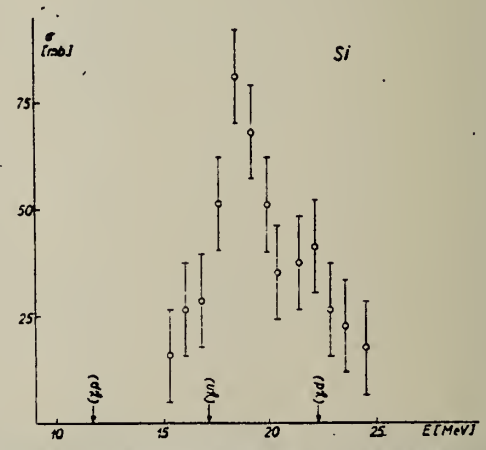

Fig. 5. Nuclear absorption cross section for Si.

Ref. V. P. Chizkov
Zhur. Eksp. i Teoret. Fiz. 38, 809 (1960)
Soviet Phys. JETP 11, 587 (1960)

Elem. Sym.	A
Si	14

Method: 90 MeV Bremsstrahlung; scintillator counter telescope

Ref. No.: 60 Ch 1

Reaction	E or ΔE	E_0	Γ	$\int \sigma dE$	Jπ	Notes
Si (γ, p)						Energy Range of particles detected:
Si (γ, d)						E_d - 15.5-30 MeV
Si (γ, t)						E_p - 15.5-30 MeV
						E_t - 17-30 MeV
						Ratios:
						$\sigma(\gamma,d)/\sigma(\gamma,p)$ } at $\theta = 90^\circ$
						$\sigma(\gamma,t)/\sigma(\gamma,d)$

TABLE I

Element	$100N_t/N_d$	Element	$100N_t/N_d$	Element	$100N_t/N_d$	Element	$100N_t/N_d$
Li^6	30±3	B	39±8	Ni	10±4	In	5±2.5
Li^7	22.5±2.5	Si	10±4	Co	2.5±2	Ta	10±4
Be	13±2.6	S	8±4	Cu	2.2±2	Au	3±3

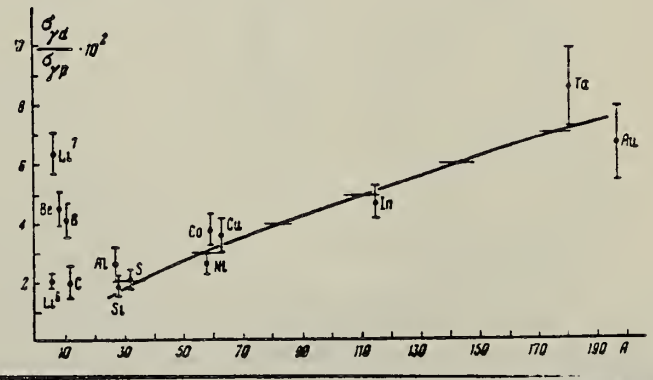

FIG. 3. Ratio of (γ, d) to (γ, p) cross sections for protons and deuterons of energies 15.5–30 Mev as function of atomic weight A. The solid curve shows the dependence given by Eq. (2), arbitrarily normalized.

Ref. K. Reibel, A.K. Mann
Phys. Rev. 118, 701 (1960)

Elem. Sym.	A	Z
Si		14

Method: γ's from $F^{19}(\gamma,\alpha\gamma)$ reaction; protons from Van de Graaff; NaI

Ref. No.: 60 Re 1 JHH

Reaction	E or ΔE	E_o	Γ	$\int \sigma dE$	Jπ	Notes
Si(γ,γ)	~ 7					$\langle \bar{\sigma} \rangle (E_p = 2.05$ MeV) = < 0.057 mb Detector at 90°.

Ref. K. Shoda, K. Kobayashi, S. Siina, K. Abe, M. Kimura
J. Phys. Soc. Japan 16, 1031 (1961)

Elem. Sym.	A	Z
Si		14

Method 24 MeV Bremss; emulsions; proton spectrum

Ref. No. 61 Sh 1 EH

Reaction	E or ΔE	E_o	Γ	$\int \sigma dE$	Jπ	Notes
$Si^{28}(\gamma,p)$	Bremss. 24					

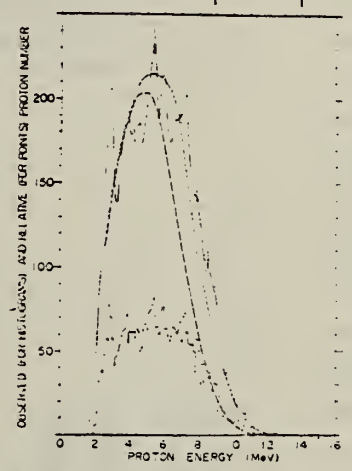

Fig. 1. The energy spectrum of photoprotons from Si. The solid line is a smoothed curve. The broken line and the dotted one are calculated curves of the statistical model with the level densities $\omega = C\exp[2\sqrt{0.45E}]\,\mathrm{MeV}^{-1}$ and $\omega = C\exp[E/2.0]\,\mathrm{MeV}^{-1}$, respectively.

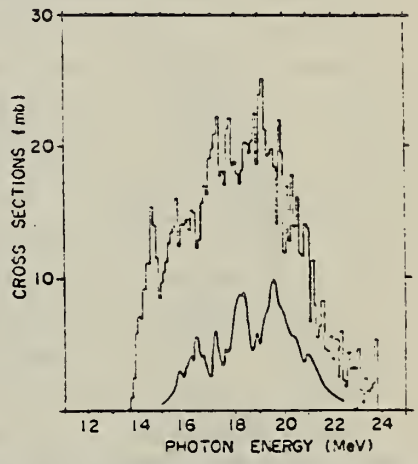

Fig. 2. The comparison of cross section of $Si^{28}(\gamma, p)Al^{27}$ (histogram) and that from $Al^{27}(p,\gamma)Si^{28}$ (solid line).

Ref. K. Shoda, S. Shiina, K. Kobayashi, K. Abe, M. Kimura
J. Phys. Soc. Japan 16, 1807 (1961)

Elem. Sym.	A	Z
Si		14

Method: 24 MeV betatron; proton spectrum; angular distribution; nuclear emulsion; r - chamber

Ref. No.: 61 Sh 4 NVB

Reaction	E or ΔE	E_o	Γ	$\int \sigma dE$	Jπ	Notes
Si(γ,xp)	Bremss. 24					Yield = 2.9 x 10^5 protons/mole-r

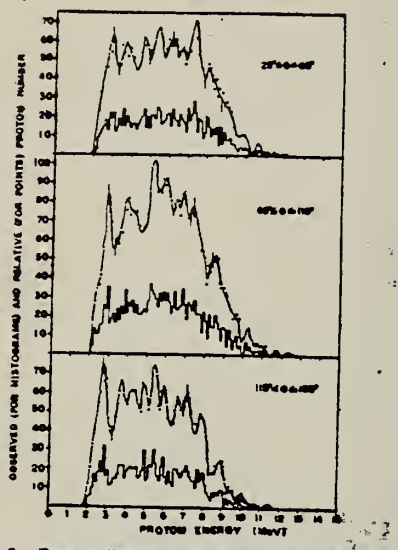

Fig. 2. Energy distributions of protons from Si²⁸ for three directional groups. The smoothed results are shown by the points.

Table II. Angular distributions calculated by least squares for $a+b\sin^2\theta$.

Element	Proton energy (MeV)	Augular distributions
Si²⁹	1.8—3.3	$1-(0.50\pm0.39)\sin^2\theta$
	3.3—4.7	$1-(0.09\pm0.44)\sin^2\theta$
	4.7—6.3	$1+(0.01\pm0.40)\sin^2\theta$
	6.3—7.7	$1+(0.06\pm0.49)\sin^2\theta$
	larger than 7.7	$1-(0.48\pm0.73)\sin^2\theta$
	Total	$1-(0.05\pm0.20)\sin^2\theta$
P³¹	2.7—4.5	$1+(0.85\pm0.42)\sin^2\theta$
	4.5—6.0	$1+(0.35\pm0.34)\sin^2\theta$
	6.0—8.5	$1-(1.31\pm0.59)\sin^2\theta$
	larger than 8.5	$-(0.08\pm0.18)-\sin^2\theta$
	Total	$1+(1.10\pm0.27)\sin^2\theta$

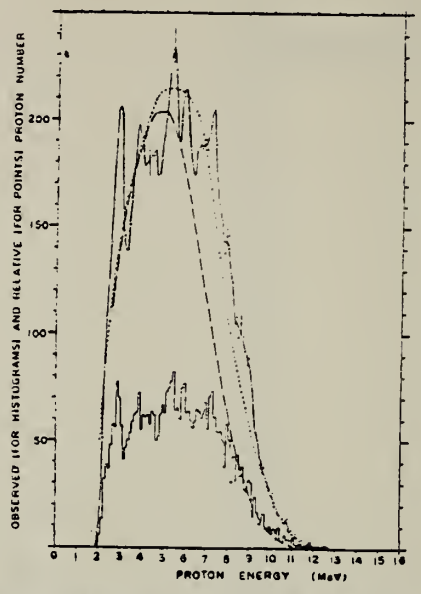

Fig. 3. Energy distribution of total observed protons and calculated distributions by the statistical theory from Si²⁸.
Full line: Observed spectrum smoothed out by the method of Ferreira and Valoshek.
Broken line: Calculated spectrum using $\omega = C\exp[2\sqrt{0.45E}]$ MeV⁻¹
Dotted line: Calculated spectrum using $\omega = C\exp[E/2.8]$ MeV⁻¹
Each curve is normalized to best fit to experimental points.

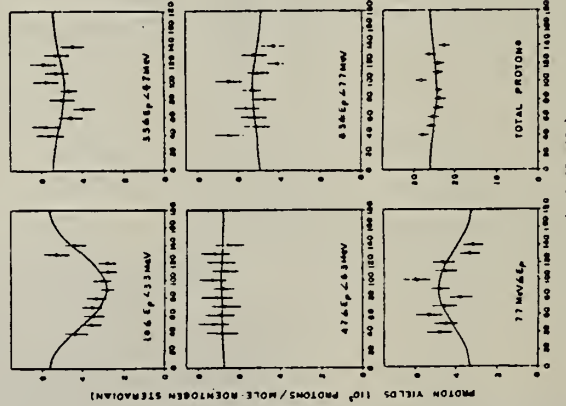

Fig. 4. Angular distributions of protons from Si²⁹. Full lines are obtained by least squares.

K. Shoda, K. Kobayashi, S. Siina, K. Abe. M. Kimura
J. Phys. Soc. Japan 16, 1031 (1961)

ELEM.		
Si		14

METHOD
Betatron; proton cross section, spectrum; nuclear emulsion

REF. NO.
61 Sh 5 NVB

REACTION	RESULT	EXCITATION ENERGY	SOURCE		DETECTOR		ANGLE
			TYPE	RANGE	TYPE	RANGE	
G,XP	SPC	14-24	C	24	EMU-D	2 - 12	UKN

327

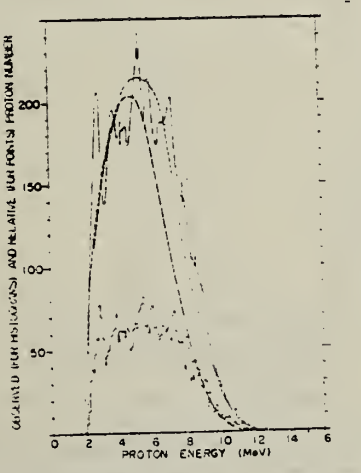

Fig. 1. The energy spectrum of photoprotons from Si. The solid line is a smoothed curve. The broken line and the dotted one are calculated curves of the statistical model with the level densities $\omega = C\exp[2\sqrt{0.45E}]\,\mathrm{MeV}^{-1}$ and $\omega = C\exp[E/2.8]\,\mathrm{MeV}^{-1}$, respectively.

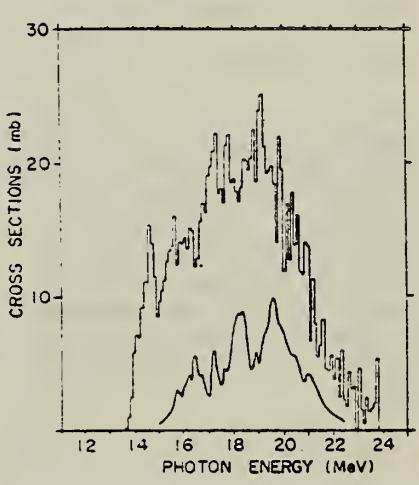

Fig. 2. The comparison of cross section of $Si^{28}(\gamma, p)Al^{27}$ (histogram) and that from $Al^{27}(p, \gamma)Si^{28}$ (solid line).

Ref. M. Sugawara
J. Phys. Soc. Japan 16, 1857 (1961)

Elem. Sym.	A	Z
Si		14

Method 25 MeV betatron; photon scattering; NaI(Tℓ) spectrometer; ion chamber

Ref. No. 61 Su 1 | NVB

Reaction	E or ΔE	E_o	Γ	$\int \sigma dE$	Jπ	Notes
Si(γ,γ)	Bremss.					Detector at 120°.
	6-13	11.3	8.3±2.5eV		1^+	

Figure 2 Caption:
The spectra of the scattered photons from the Mg scatterer. The solid line is the spectra measured without the Mg absorber and the broken line with the absorber. They are all normalized to the unit charge of the ionization chamber.

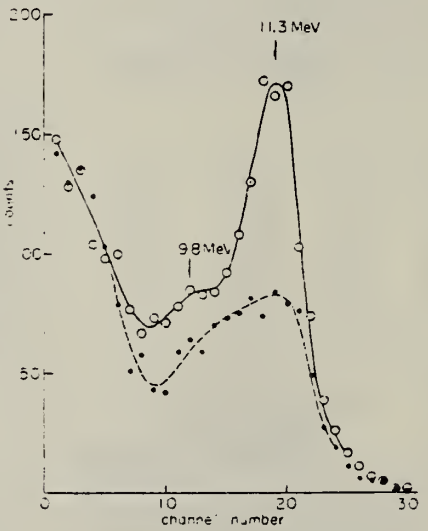

Fig. 3. The same as Fig. 2 with Si scatterer and absorber.

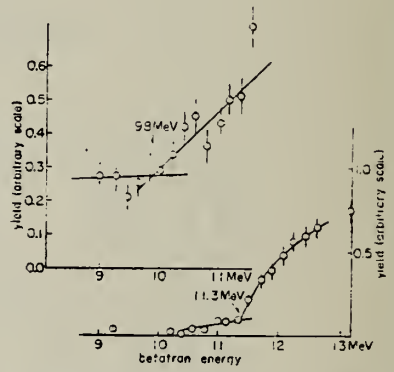

Fig. 5. The excitation curve of Si. The upper curve was obtained by the counts of 1st to 14th channel and the lower curve by the counts of 16th to 24th.

Ref. T. Tohei, M. Sugawara, S. Mori, M. Kimura
J. Phys. Soc. Japan 16, 1657 (1961)

Elem. Sym.	A	Z
Si		14

Method: 25 MeV betatron; photon scattering; NaI(Tℓ) spectrometer

Ref. No.: 61 To 1 | NVB

Reaction	E or ΔE	E_o	Γ	$\int \sigma dE$	Jπ	Notes
Si(γ,γ)	Bremss. 5-12	12.0				Detector at 120°

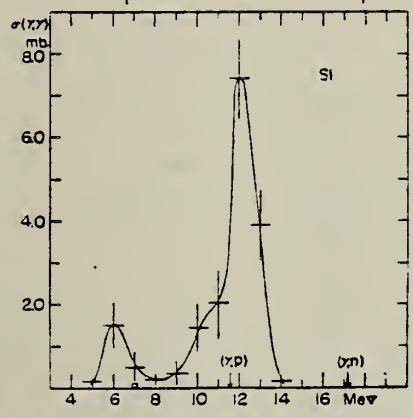

Fig. 5. The elastic scattering cross section of photons by Si. The arrows of (γ, p) or (γ, n) indicate the positions of the particle threshold energies of Si^{28}. □: data from the experiment of the monochromatic γ-rays[4].

References

1) E. G. Fuller and E. Hayward: Phys. Rev. **101** (1956) 692.
2) see E. Segre: *Experimental Nuclear Physics*, vol. 1, p. 346.
3) J. S. Levin and D. J. Hughes: Phys. Rev. **101** (1956) 1328.
4) K. Reibel and A. K. Mann: Phys. Rev. **118** (1960) 701.

Table II. The correction of the energy scale.

Energy in Ref. 1	should be read
4.0 Mev	3.3 Mev
6.0	5.5
8.0	7.7
10.0	9.9
12.0	12.1
14.0	14.3

[Table II from J. Phys. Soc. Japan 18 17-22 (1963)]

Ref. P.G. Bizzeti, A.M. Bizzeti-Sona, M. Bocciolini, G. Di Caporiacco, M. Mandò
Nuovo Cimento 26, 1412 (1962)

Elem. Sym.	A	Z
Si		14

Method Van de Graaff; γ's from $Li^7(p,\gamma)$ reaction; solid state (silicon junction) detector

Ref. No. 62 Bi 1 JHH

Reaction	E or ΔE	E_o	Γ	$\int \sigma dE$	Jπ	Notes
$Si^{28}(\gamma,p)$	17.6					E_p spectra in Figure 1, with E_α peaks included.
$Si^{28}(\gamma,\alpha)$	ΔE = 100 keV					Si detector irradiated giving 4π detector.
						σ fluctuations studied.

TABLE I.

Values of relative intensity of the various peaks with respect to p_0 (*)

θ	cos θ	Energy shift (keV)	$(p_1 - p_2/p_3)$	p_1/p_0	p_2/p_0	α_0/p_0
0°	−1.00	−67.8	0.70 ± 0.06	0.53 ± 0.05	0.17 ± 0.03	0.17 ± 0.02
41° 30′	−0.75	−50.8	1.04 ± 0.06	0.77 ± 0.05	0.27 ± 0.03	0.16 ± 0.02
60°	−0.50	−33.9	1.44 ± 0.08	0.90 ± 0.05	0.54 ± 0.03	0.15 ± 0.02
75° 30′	−0.25	−16.9	1.73 ± 0.10	0.87 ± 0.06	0.86 ± 0.06	0.17 ± 0.02
90°	0	0	1.41 ± 0.08	0.71 ± 0.05	0.70 ± 0.05	0.15 ± 0.02
104° 30′	−0.25	−16.9	0.84 ± 0.04	0.38 ± 0.03	0.46 ± 0.03	0.06 ± 0.01
120°	−0.50	−33.9	0.84 ± 0.05	0.43 ± 0.03	0.41 ± 0.03	< 0.03

(*) Errors shown are only statistical errors; maximum uncertainties of other origin (background evaluation, separation of neighbouring peaks, wall effects, etc.) are estimated to range from 1% to 7% for lower and higher values respectively. In addition a possible uncertainty in the geometrical conditions (estimated to be less than 1°) may introduce a systematic error in the value of the energy shift which ranges from 1.5 keV at 0° to 3.5 keV at 90°. The energy-spread for every single point, however, is determined essentially by the width of the resonance as ±6 keV. The ratios shown were evaluated through an objective criterion suitable chosen for the best separation of the peaks; as a result, the values may be expected to differ somewhat from the cross-section ratios for transitions to the corresponding final levels. They are, however, proportional to them through a factor which is about 1 and does not depend on energy.

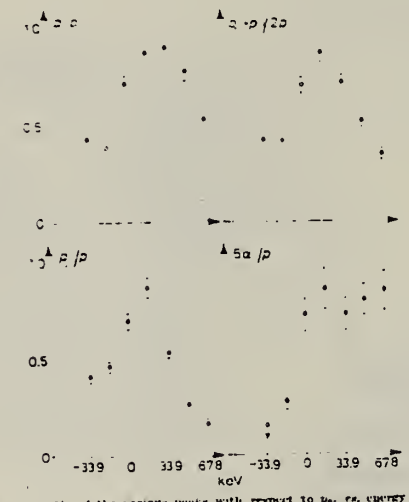

Fig. 2. – Intensity ratio of the various peaks with respect to p_0 vs. energy shift of incident γ radiation.

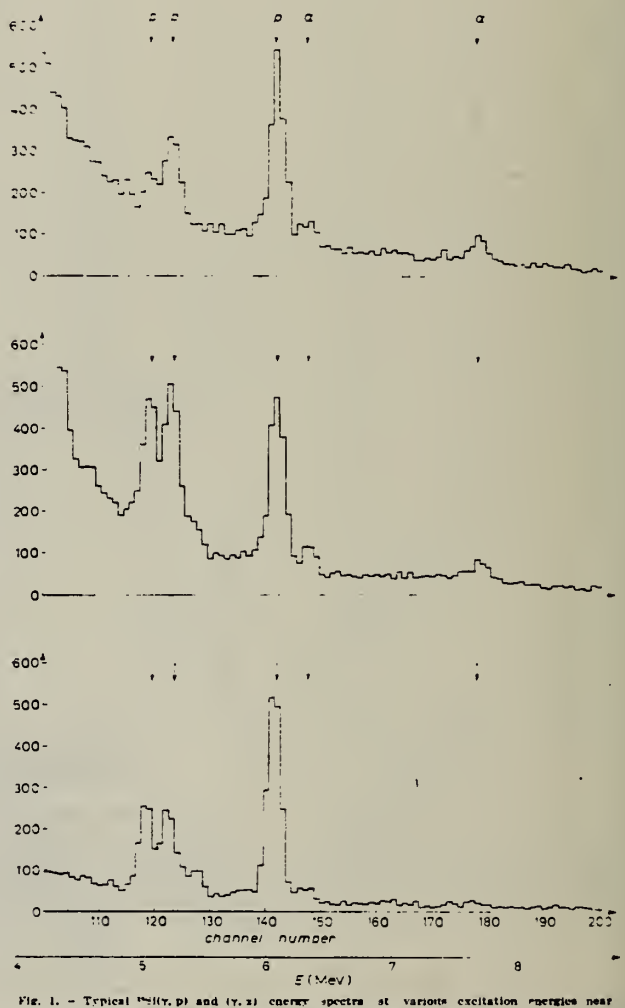

Fig. 1. – Typical $^{28}Si(\gamma,p)$ and (γ,α) energy spectra at various excitation energies near 17.64 MeV. The energy shifts ΔE of incident γ-rays are, from the top, +67.8, +16.9 and −33.9 keV, respectively. Note shifted energy-zero.

Ref. F.D. Seward
Phys. Rev. 125, 335 (1962)

Elem. Sym.	A	Z
Si		14

Method
Linac; NaI; detector at 90°.

Ref. No. 62 Se 1 JHH

Reaction	E or ΔE	E_o	Γ	$\int \sigma dE$	Jπ	Notes
Si(γ,γ)	Bremss. 16	11.4				11.4 MeV assumed to be resonance scattering by level in Si^{28}. 9.6 MeV gamma from transition to first excited state of Si^{28}. Based on assumed spins and angular distributions ratio of 9.6 MeV gammas to 11.4 MeV gammas = 0.19±0.04; de Nercy [J. Phys. Rad. 22, 119 (1961)] gave 0.6.

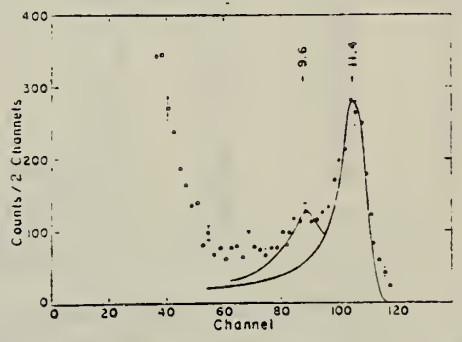

FIG. 8. Pulse-height spectrum for γ rays scattered from a Si sample. Sample-out background has been subtracted. Solid lines are KS response functions for 9.6- and 11.4-Mev γ rays.

Ref. K. Shoda, K. Abe, T. Ishizuka, N. Kawamura, M. Kimura
J. Phys. Soc. Japan 17, 735 (1962)

Elem. Sym.	A	Z
Si		14

Method: 25 MeV betatron; proton yield; scintillator; ion chamber

Ref. No.: 62 Sh 11 | NVB

Reaction	E or ΔE	E_o	Γ	$\int \sigma dE$	Jπ	Notes
Si(γ,p)	Bremss. Thr-24	18.7	4 MeV	$\int_0^{23}$ = 0.14 MeV-b		σ_{max} = 31.4 mb. 6 Detectors at angles: 20° 55° 90° (2) 125° 160° Measured all protons above E_o = 1.5 MeV

8.22

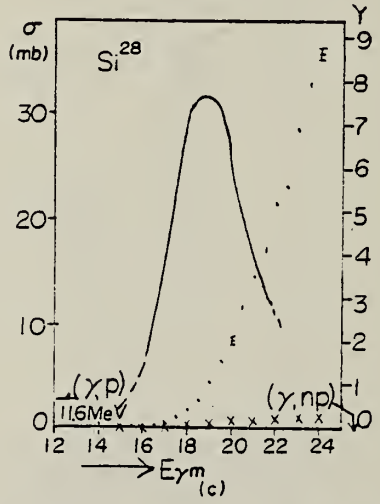

Fig. 5. Photoproton yield and cross section curves for (a)-Mg, (b)-Al[27], (c)-Si[28], (d)-S[32]. Arrows in the figures show the threshold energies. The backgrounds obseryed without targets are shown by ×.

Ref. L.N. Bolen, W.D. Whitehead
Phys. Rev. 132, 2251 (1963)

Elem. Sym.	A	Z
Si		14

Method: Synchrotron; neutron yield; BF_3 counters; NBS chamber monitor

Ref. No.: 63 Bo 1 JHH

Reaction	E or ΔE	E_o	Γ	$\int \sigma dE$	Jπ	Notes 825+
Si(γ,n)	Bremss. 10-30			$\int_{th}^{28}$ = 80 MeV-mb		For "E_o" and "σ(mb)", see Table III, below.

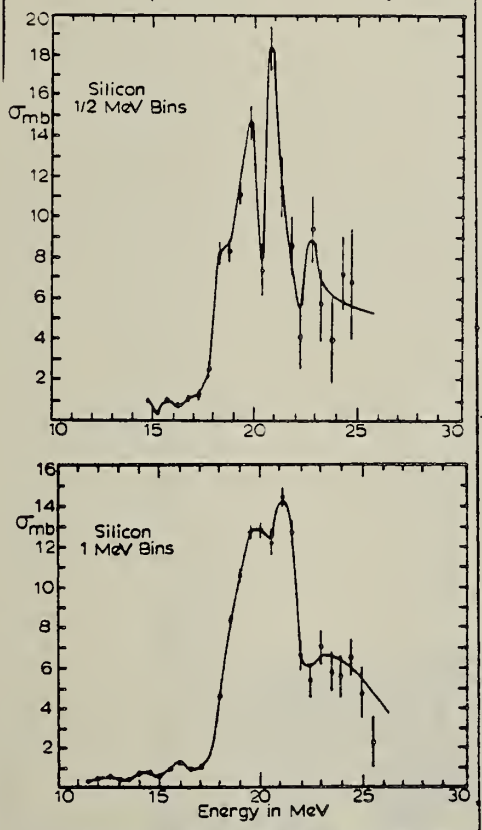

FIG. 2. Si(γ,n) cross section unfolded using ½-MeV bins (top curve) and 1-MeV bins (lower curve).

TABLE III. Summary of data from this experiment giving energy positions of levels found in our cross sections and corresponding data from other experiments.

Element	University of Virginia E(MeV)	σ(mb)	Gove[a] E(MeV)	Kimura[b] E(MeV)
Si	16.0	1.2		
	18.5	8.4	18	
	19.75	14.7	18.9	18.9
	20.75	18.4	20	20.0
	22.75	9.4	21.4	21.4
	24.25	7.1		

	University of Virginia E(MeV)	σ(mb)	Mutsuro[c] E(MeV)	σ(mb)
			13.5	6
P	14.75	3.9	14.6	8
	15.75	5.6	15.8	14
	17.25	9.2	(17)	(17)
	18.25	10.2	17.5	21
	19.25	11.5	19.0	22
	20.25	13.6	20.3	22
	21.25	16.4		
	22.75	19.5		
	24.25	13.2		

	University of Virginia E(MeV)	σ(mb)	Mutsuro[c] E(MeV)	σ(mb)
S	16	1.7	15.7	7
	17.5	6.0	16.8	10
	18.25	9.0	17.9	20
	19.75	13.4	18.75	11
	21.25	12.5	19.7	16
	22.75	11.3		
	24.0	9.0		

[a] See Ref. 19.
[b] See Ref. 28.
[c] See Ref. 5.

[5] N. Mutsuro, K. Kageyama, M. Mishina, E. Tanaka, and M. Kimura, J. Phys. Soc. Japan 17, 1673 (1962).
[19] H. E. Gove, A. E. Litherland, and E. Batchelor, Nucl. Phys. 26, 480 (1961).
[28] M. Kimura, K. Shoda, N. Mutsuro, T. Tohei, K. Sato, K. Kuroda, K. Kuriyama, and T. Akiba, J. Phys. Soc. Japan 15, 1128 (1960).

TABLE II. Integrated cross-section values obtained from the (γ,n) cross sections of elements measured in this laboratory.[a]

Element	Limits of integration threshold to	$\int \sigma dE$ MeV-mb	Dipole sum rule $X=0$ MeV-mb	% of DSR exhausted by (γ,n)
O	31 MeV	46	240	19
Mg	29	84	360	23
Al	28	97.5	405	24
Si	28	80	420	19
P	28	127	465	27
S	28	81	480	17
Ca	28	74	600	12
N	25	60	210	29
	50	116		55
Ar	25	392	600	65
	50	598		100
Li	25	39	105	37
	50	93		89

[a] See Refs. 1, 12, and 13.

[1] L. N. Bolen and W. D. Whitehead, Phys. Rev. Letters 9, 458 (1962).
[12] R. W. Fast, P. A. Flournoy, R. S. Tickle, and W. D. Whitehead, Phys. Rev. 118, 535 (1960).
[13] K. Min, L. N. Bolen, and W. D. Whitehead, Phys. Rev. 132, 749 (1963).

Ref.	Elem. Sym.	A	Z
J.T. Caldwell, R.R. Harvey, R.L. Bramblett, S.C. Fultz Phys. Letters 6, 213 (1963)	Si		14

Method	Ref. No.	
Monochromatic photons (annihilation-in-flight)	63 Ca 1	EGF

Reaction	E or ΔE	E_o	Γ	$\int \sigma dE$	Jπ	Notes
						7.2
(γ,n)	15-30			$\int_0^{31}$ 68.8		Inaction in Table 3 represents fraction of experimentally observed $\int\sigma$ to 31 MeV.

Table 3
Energy levels and fractional dipole strengths of Si^{28}.

(γ,n) Energy (MeV)	Γ (MeV)	σ (mb)	Fraction of Dipole Strength	(p,γ) Energy (MeV)
18.1	0.68	3	0.05±0.02	18.1
18.6	0.47	2.7	0.03±0.02	18.5
19.0	0.68	5	0.08±0.03	19.0
19.8	0.68	8	0.12±0.04	20.0
20.9	1.55	9.5	0.34±0.07	21.3

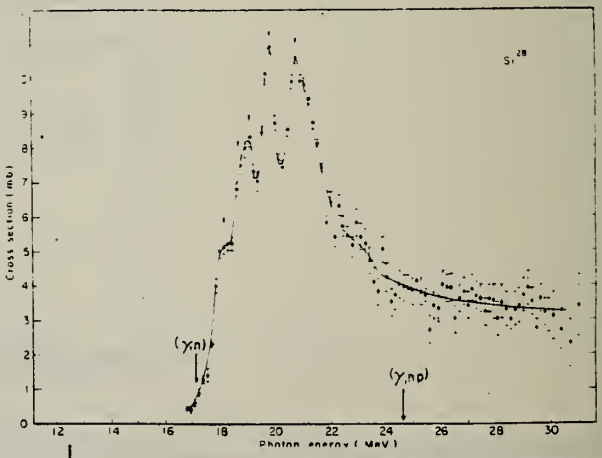

Ref.	S. Costa, F. Ferraro, S. Ferroni, B. Minetti, C. Molino R. Malvano Phys. Letters 6, 226 (1963)	Elem. Sym.	A	Z
		Si		14

Method	100 MeV Synchrotron; 4 π neutron detector; calculated integrated cross sections - fitted with polynomial of degree η	Ref. No.	
		63 Co 3	RCF

Reaction	E or ΔE	E_o	Γ	$\int \sigma dE$	$J\pi$	Notes 788
(γ, xn)						$\sigma_b = \int \frac{\sigma(E)}{E} dE$ gets $\langle \bar{\nu}_p \cdot \bar{\nu}_n - \bar{\nu}_n \cdot \bar{\nu}_{n1} \rangle$ $= (R_s^2 - R_p^2 - \frac{3}{\pi^2} \frac{\pi r_0}{e^2} \sigma_b \frac{A-1}{A^2}) \times \frac{2}{A-2}$ See "Boron" for plots of this and $\int \sigma dE/60$ NZ/A.

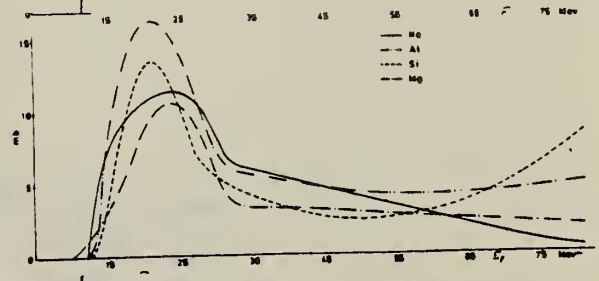

Figure 1: Photoneutron cross sections for several light elements versus γ-ray energy.

K. Sato
J. Phys. Soc. Japan 18, 1353 (1963)

Si		14

METHOD
Betatron; neutron cross sections; BF_3 counters; ion chamber

REF. NO. 63 Sa 1 | NVB

REACTION	RESULT	EXCITATION ENERGY	SOURCE TYPE	SOURCE RANGE	DETECTOR TYPE	DETECTOR RANGE	ANGLE
G,N	ABX	10 - 24	C	10-24	BF3 - I		4 PI
							826

a,b in Table I refer to two Lorentz shaped peaks in the split giant resonance.

Quadrupole moment $Q_{\bar{0}} = 0.3 \times 10^{-24}$ cm^2, based on Danos' theory.

$Q_o = 0.12 \times 10^{-24}$ cm^2

Table I. Resonance Parameters

	Na^{23}	Si^{28}
E_a	16.5 Mev	18.75 Mev
σ_a	6.8 mb	11.0 mb
Γ_a	4.0 Mev	2.0 Mev
E_b	21.0 Mev	20.75 Mev
σ_b	10.5 mb	13.0 mb
Γ_b	4.0 Mev	2.6 Mev

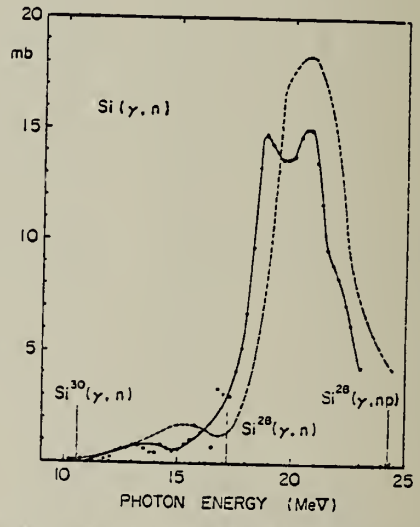

Fig. 3. The (γ, n) cross sections for Si.
Solid line: present data obtained from the yield curve for the summation of the 7 runs.
Dotted line: data of Katz et al[9].
The arrows in the figure show the threshold energies.

9) L. Katz, R. N. H. Haslam, J. Goldemberg and J. G. V. Taylor: Can. J. Phys. 32 (1954) 580.

REF.

J. Goldemberg, W.C. Barber, F.H. Lewis, Jr., J.W. Walecka
Phys. Rev. 134, B1022 (1964)

ELEM. SYM.	A	Z
Si		14

METHOD: Linac

REF. NO.: 64 Go 3 | NVB

REACTION	RESULT	EXCITATION ENERGY	SOURCE TYPE	SOURCE RANGE	DETECTOR TYPE	DETECTOR RANGE	ANGLE
E,E/	ABX	12	D	40-70	MAG-D		180

FMF

TABLE I. Data on $M1$ transitions.

	q MeV/c	Cross section[a]	Reference	$\lvert\langle J_f\rvert\rvert T_1^{\max}(q)\rvert\rvert J_i\rangle\rvert^2$ $(1/q^2)$ (10^{-3})	$\lvert\langle J_f\rvert\rvert T_1^{\max}(q)\rvert\rvert J_i\rangle\rvert^2$ $[10^{-6}(\text{MeV}/c)^{-2}]$
		15.1-MeV level in C^{12}			
Photons	15.1	(2.05±0.27)	8	0.044	(0.19 ±0.025)
Electrons	68	(2.0 ±0.3)	this work	0.55	(0.12 ±0.018)
Electrons (160°)	68	(2.6 $\pm_{0.40}^{0.57}$)	5	0.69	(0.15 $\pm_{0.022}^{0.032}$)
Electrons	93	(2.0 ±0.3)	this work	0.87	(0.10 ±0.015)
Electrons	125	(1.5 ±0.25)	this work	1.10	(0.07 ±0.012)
		3.56-MeV level in Li^6			
Photons	3.56	(0.92$\pm_{0.18}^{0.20}$)	b	0.014	(1.10 $\pm_{0.18}^{0.24}$)
Electrons	76	(3.0 ±0.45)	this work	2.0	(0.38 ±0.057)
Electrons	106	(1.55±0.23)	this work	2.1	(0.19 ±0.028)
Electrons	136	(0.90±0.14)	this work	2.0	(0.11 ±0.017)
		11.6-MeV level in Si^{28}			
Photons	11.6	(9.8 ±2.6)	c	0.016	(1.2 ±0.32)
Electrons	71.5	(3.5 ±1.4)	d	0.92	(0.18 ±0.07)
Electrons	88.4	(3.0 ±0.75)	this work	1.2	(0.15 ±0.038)
Electrons	129.4	(1.8 ±0.45)	this work	1.5	(0.09 ±0.022)
		11-MeV level in Mg^{24}			
Photons	11	(13.1 ±3.8)	c	0.02	(1.7 ±0.50)
Electrons	83	(4.4 ±0.88)	6	1.5	(0.22 ±0.044)
Electrons	97	(3.5 ±0.70)	this work	1.6	(0.1 ±0.034)
Electrons	129	(1.8 ±0.36)	this work	1.3	(0.081±0.016)

[a] In units of 10^{-27} MeV-cm^2 for photons and 10^{-28} cm^2/sr for electrons.
[b] L. Cohen and R. A. Tobin, Nucl. Phys. 14, 243 (1960).
[c] A. B. de Nercy, Ann. Phys. (Paris) 6, 1379 (1961).
[d] R. D. Edge and G. A. Peterson, Phys. Rev. 128, 2750 (1962).

REF.

K.H. Lokan, G.R. Hogg, P.H. Cannington and R.J.J. Stewart
Phys. Letters 11, 73 (1964)

ELEM. SYM.	A	Z
Si		14

METHOD

Betatron; carbon filter; SCD target

REF. NO. 64 Lo 2 JOC

REACTION	RESULT	EXCITATION ENERGY	SOURCE		DETECTOR		ANGLE
			TYPE	RANGE	TYPE	RANGE	
G,XP	SPC	THR-21	C	21	SCD-D	2-10	4PI

SCD TARGET

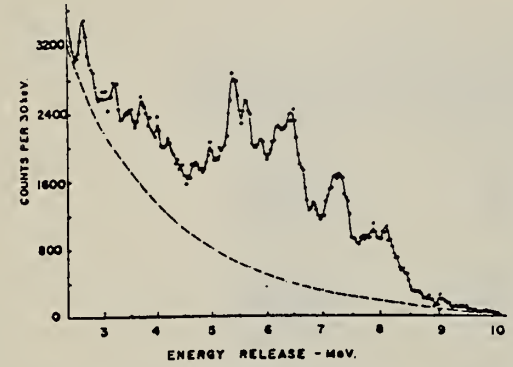

Fig. 1. The observed energy spectrum from the reaction $Si^{28}(\gamma,p)Al^{27}$ when irradiated with bremsstrahlung of maximum energy 21.2 MeV. The dotted curve is the assumed background.

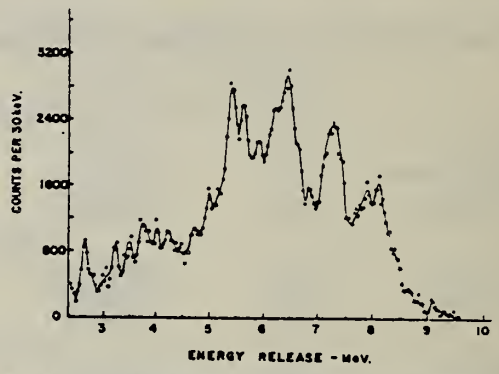

Fig. 2. The energy spectrum corrected for background and escape losses.

"Assuming isotropic angular distribution."

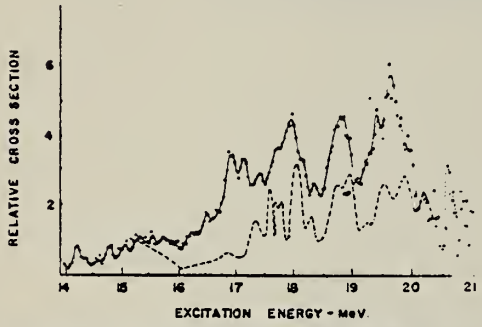

Fig. 3. Relative cross section for the reaction $Si^{28}(\gamma,p)Al^{27}$. The dotted curve represents the cross section for the inverse reaction [2] $Al^{27}(p,\gamma_0)Si^{28}$.

"Assuming ground state transitions."

REF.

S. Matsumoto, H. Yamashita, T. Kamae, Y. Nogami
Phys. Letters 12, 49 (1964)

ELEM. SYM.	A	Z
Si		14

METHOD

SCD targets, $Li^7(p,\gamma_o)$ and $T(p,\gamma_o)$ sources

REF. NO. 64 Ma 1 JOC

REACTION	RESULT	EXCITATION ENERGY	SOURCE		DETECTOR		ANGLE
			TYPE	RANGE	TYPE	RANGE	
G,P	ABX	17-22	D	17 - 22	SCD-D		4 PI
		(17.5 - 22.3)					
G,A	ABX	17-22	D	17 - 22	SCD-D		4 PI
		(17.5 - 22.3)					

BRANCHING RATIOS

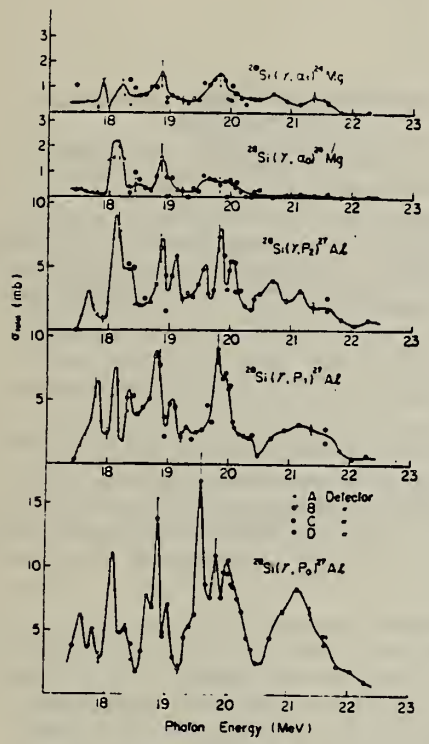

Fig. 3. The cross sections for the $Si^{28}(\gamma,p)Al^{27}$ and the $Si^{28}(\gamma,\alpha)Mg^{24}$ reactions.

REF.

H. Ullrich
Phys. Letters 12, 114 (1964)

ELEM. SYM.	A	Z
Si		14

METHOD

Betatron; beam hardened with graphite; SCD target [Page 1 of 2]

REF. NO.	
64 U1 1	JOC

REACTION	RESULT	EXCITATION ENERGY	SOURCE		DETECTOR		ANGLE
			TYPE	RANGE	TYPE	RANGE	
G,P	SPC	14-20	C	17-20	SCD-D	1-9	4PI
						(1.5 - 9)	
G,A	SPC	14-20	C	17-20	SCD-D		4PI

SCD TARGET

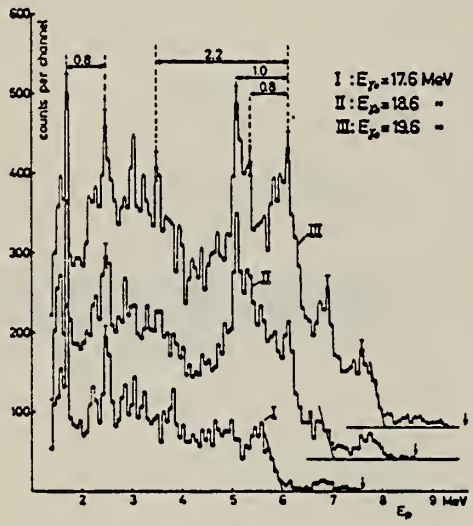

Fig. 1

Fig. 1 shows 3 measured spectra for different end point energies. For each spectrum the highest possible alpha energy is indicated by an arrow, the straight line 1.6 MeV below, indicates the end of the proton distribution. The measured points in the region in between must be attributed to alpha particles **. As the number of observed particles at the proton limits rises considerably, and since the alpha yields in general are small, below these limits the measured distributions should be mainly due to protons.

The observed proton peaks in the spectra clearly indicate the presence of narrow resonances in the excited silicon nucleus. As from each excited state proton transitions to several discrete state in the residual nucleus are possible, identification of the peaks is only possible from a series of measurements. As for instance the proton peaks at 6.2, 5.4, 5.2 and 4.0 MeV are present in curve III and II but not in curve I of fig. 1, they all must be attributed to a resonance between 18.6 and 17.6 MeV excitation energy. Thus the peak at 6.2 MeV must be due to ground state transitions since adding the Q-value of 11.6 MeV one obtains the right excitation energy. The other peaks are associated with transitions into excited states of the residual nucleus. Indeed, the distances between these peaks correspond well to the excitation energies of the first three excited states in Al^{27} with 0.8, 1.0 and 2.2 MeV.

Branching ratios for the transitions mentioned here are given in the table. These values have been derived from the difference of curve II and I. The errors are due to statistical uncertainties. At the high energy limit the proton (and alpha) spectra contain only contributions from ground state transitions. Thus together with the knowledge of the bremsstrahlung spectrum, cross section curves for reactions leading to the ground state can be derived within a certain energy range for each spectrum.

REACTION	RESULT	EXCITATION ENERGY	SOURCE		DETECTOR		ANGLE
			TYPE	RANGE	TYPE	RANGE	

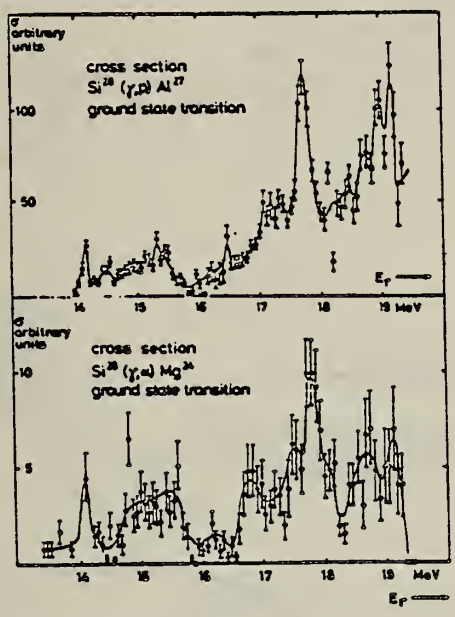

Fig. 2

Table 1
Branching ratio for the 17.8 MeV resonance.

Transition	Branching ratio relative to p_0
p_0	1.0
p_1	1.2 ± 0.6
p_2	1.5 ± 0.8
p_3	0.75 ± 0.4
o	0.08 ± 0.04

REF.

H. Ullrich
Z. Physik 177, 514-28 (1964)

ELEM. SYM.	A	Z
Si		14

METHOD

Betatron; ion chamber

REF. NO. 64 U1 2 NVB

REACTION	RESULT	EXCITATION ENERGY	SOURCE		DETECTOR		ANGLE
			TYPE	RANGE	TYPE	RANGE	
G,XP	SPC	THR-30	C	15-30	SCD-D	2-18	4PI

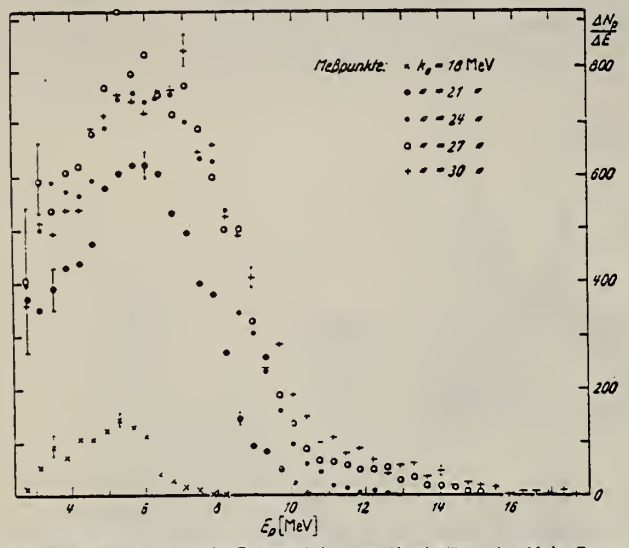

Fig. 3. Korrigierte Energieverteilung der Protonen bei 150 cm Absorberlänge. Anzahl der Protonen ΔN_p pro Energieintervall ΔE = 360 keV, aufgetragen über der Protonenenergie. Die verschieden bezeichneten Meßpunkte wurden bei Bestrahlungen mit verschiedenen Grenzenergien k_0 gewonnen

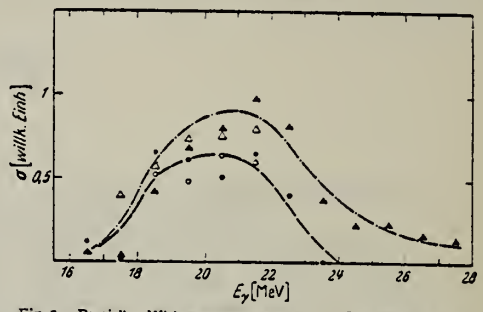

Fig. 7. Partielle Wirkungsquerschnitte für Übergänge in den Grundzustand (—·—·—) und Übergänge in die beiden ersten angeregten Niveaus (·····) des Folgekerns, aufgetragen über der Quantenenergie. (Die Meßpunkte beider Kurven wurden im gleichen Ordinatenmaßstab aufgetragen, der auch mit dem Ordinatenmaßstab der Fig. 5 übereinstimmt.) Meßpunkte: ▲ $\sigma(k, 0)$, aus der Tabelle; ● $\sigma(k, 1)$, aus der Tabelle; ▲ Grundzustandsübergänge, aus Differenzspektren (vgl. Fig. 6); ○ Übergänge in die beiden ersten angeregten Niveaus, aus Differenzspektren

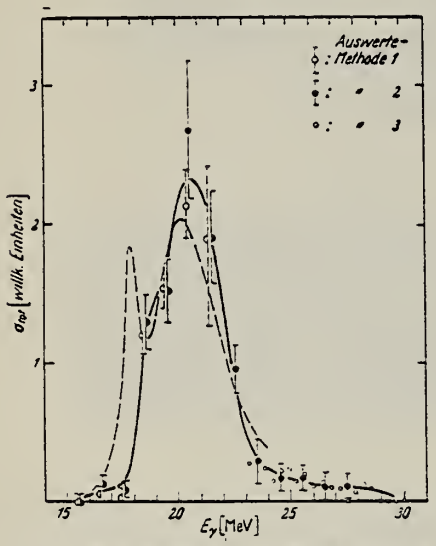

Fig. 5. Totaler Wirkungsquerschnitt der Reaktion $Si^{28}(\gamma, p)$ Al^{27} als Funktion der Quantenenergie. Die verschieden bezeichneten Punkte beziehen sich auf die im Text erläuterten verschiedenen Auswertemethoden. Die ausgezogene Kurve stellt den aufgrund der Meßpunkte wahrscheinlichsten Wirkungsquerschnittsverlauf dar. Die gestrichelte Kurve ist der nach der Methode des detaillierten Gleichgewichts aus Messungen der Umkehrreaktion $Al^{27}(p, \gamma_0)$ Si^{28} abgeleitete Wirkungsquerschnittsverlauf [10], wobei nur Übergänge in den Grundzustand von Si^{28} gemessen worden waren

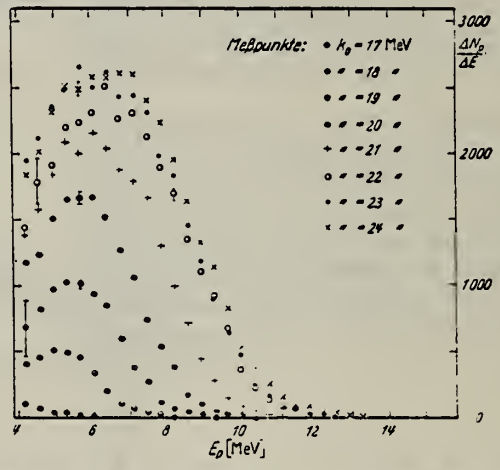

Fig. 4. Korrigierte Energieverteilung der Protonen bei 75 cm Absorberlänge. Anzahl der Protonen ΔN_p pro Energieintervall ΔE = 360 keV, aufgetragen über der Protonenenergie. Die verschieden bezeichneten Meßpunkte wurden bei Bestrahlungen mit verschiedenen Grenzenergien k_0 gewonnen

REF. H. Ullrich
Proc. Paris Conf. 1038 (1964)

ELEM. SYM.	A	Z
Si		14

METHOD

32 MeV Betatron

REF. NO. 64 U1 3 JDM

REACTION	RESULT	EXCITATION ENERGY	SOURCE		DETECTOR		ANGLE
			TYPE	RANGE	TYPE	RANGE	
G,P	SPC	13-23	C	24	SCD-D	1-11	4PI

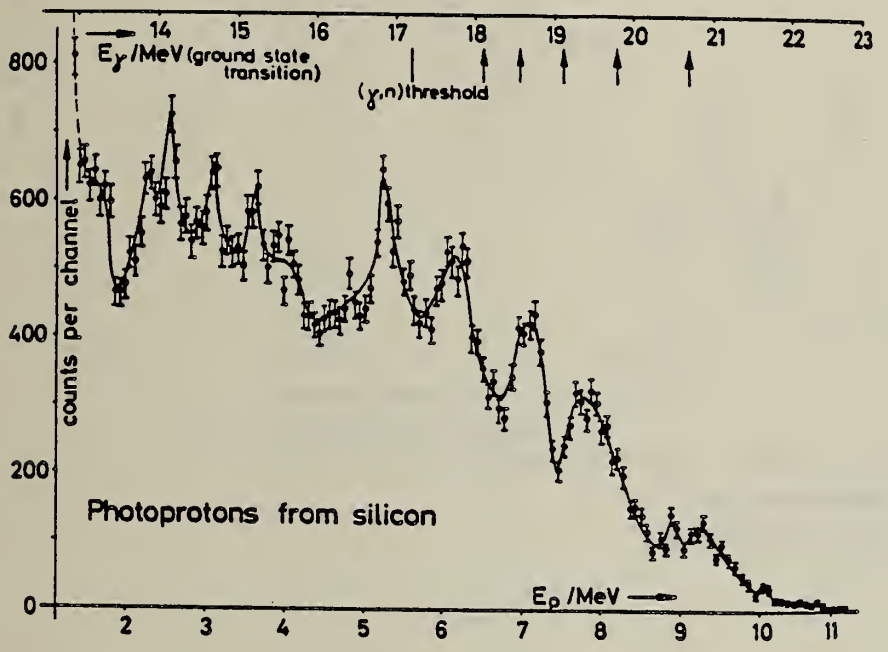

REF.

P. H. Cannington, R. J. J. Stewart, G. R. Hogg, K. H. Lokan and D. G. Sargood
Nuclear Phys. 72, 23 (1965)

ELEM. SYM.	A	Z
Si		14

METHOD

[Page 1 of 2]

REF. NO. 65 Ca 2 EGF

REACTION	RESULT	EXCITATION ENERGY	SOURCE		DETECTOR		ANGLE
			TYPE	RANGE	TYPE	RANGE	
G,P 760	ABX	THR - 23	C	16-23	SCD-D	3-12	4PI
G,A 765	ABX	THR - 23	C	16-23	SCD-D	3-12	4PI

Absolute σ based on $^{63}Cu(\gamma,n)^{62}Cu$ of Berman and Brown. 760+

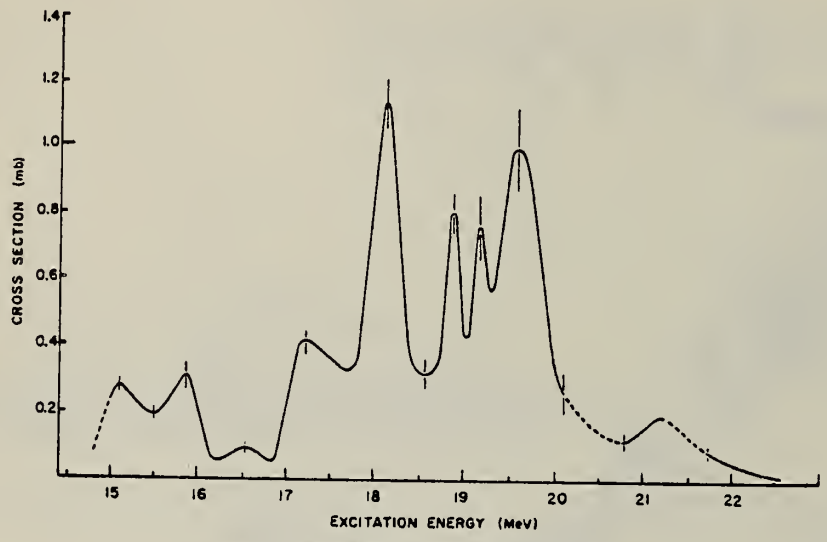

Fig. 2. The $^{28}Si(\gamma,\alpha_0)^{24}Mg$ cross section.

TABLE 1
Proton branching ratios

Energy (MeV)	$\frac{p_1+p_2}{p_0}$
17.6	0.30±0.05
18.0	1.00±0.16
18.9	0.80±0.10
19.7	0.80±0.06
20.7	1.60±0.40
21.5	0.70±0.10

REF.

P. H. Cannington, R. J. J. Stewart, G. R. Hogg, K. H. Lokan and D. G. Sargood
Nuclear Phys. 72, 23 (1965)

ELEM. SYM.	A	Z
Si		14

METHOD

[Page 2 of 2]

REF. NO. 65 Ca 2

EGF

REACTION	RESULT	EXCITATION ENERGY	SOURCE		DETECTOR		ANGLE
			TYPE	RANGE	TYPE	RANGE	

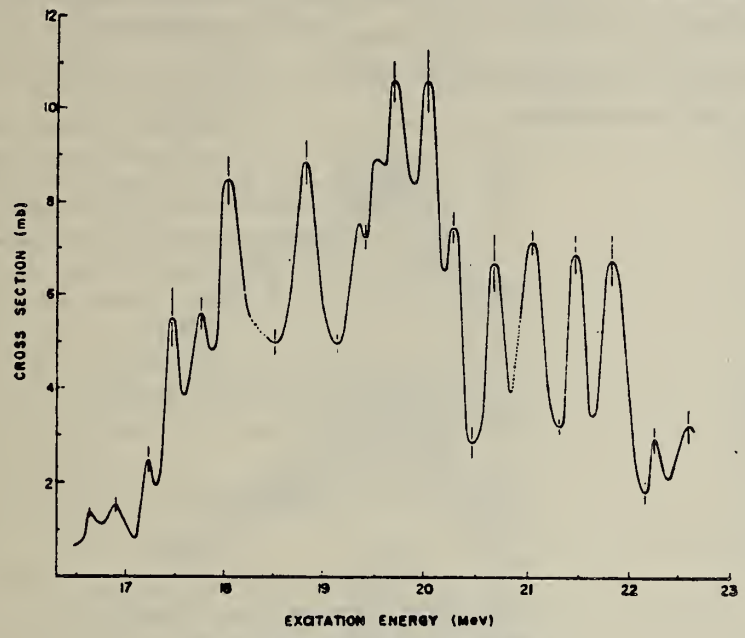

Fig. 4. The $^{28}Si(\gamma, p_0)^{27}Al$ cross section.

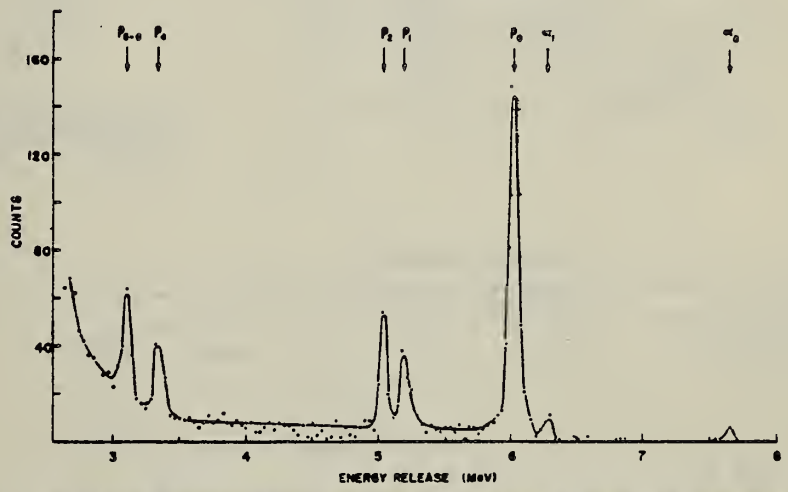

Fig. 5. The observed photoparticle spectrum from the irradiation of silicon with mono-energetic 17.6 MeV photons.

REF.

B. I. Goryachev, B. S. Ishkhanov, I. M. Kapitonov, V. G. Shevchenko, and B. A. Yur'ev
J. Nucl. Phys. (U.S.S.R.) 1, 1005 (1965)
Soviet J. of Nucl. Phys. 1, 716 (1965)

ELEM. SYM.	A	Z
Si		14

METHOD

Betatron, thin wall ion chamber

REF. NO.	
65 Go 1	JOC

REACTION	RESULT	EXCITATION ENERGY	SOURCE		DETECTOR		ANGLE
			TYPE	RANGE	TYPE	RANGE	
G,P	SPC	THR - 27	C	23-27	SCD-D	3-11	90
						(2.7 - 10.7)	

Peaks at E_p = 6.4, 7.3, (7.8), 8.2, 9.7

(corrected for energy loss and recoil)

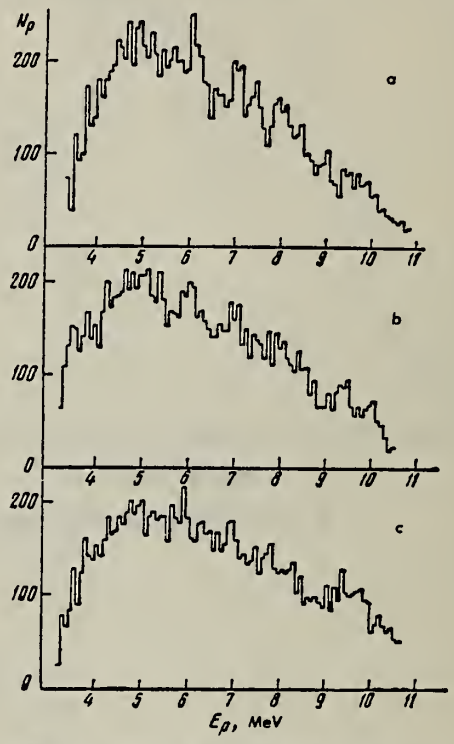

Fig. 2. Energy spectra of photoprotons from the reaction $Si^{28}(\gamma,p)Al^{27}$: $a - E_{\gamma max} = 23$ MeV, $b - E_{\gamma max} = 25$ MeV, $c - E_{\gamma max} = 27$ MeV.

Energies of Levels E^*, MeV

Experiment								Theory
(γ,p) reaction, energy spectra			$\sigma(\gamma,p)$	$\sigma(p,\gamma_0)$		$\sigma(\gamma,n)$		
	[*]	[1]	[4]	[5]	[6]	[7]	[8]	[9]
18.0	18.0	17.9	18.1	18.0	—	—	18.1	—
—	—	—	—	—	—	18.5	18.6	—
18.9	18.9	18.7	18.8	18.9	18.9	—	19.0	18.8
19.8	19.7	19.6	19.9	19.8	20.0	19.75	19.8	19.9
21.3	—	—	21.2	21.2	21.4	20.75	20.9	21.6

*The first column gives the data of the present work.

REF.

F. I. Havliček and M. Modesto
Energ. Nucl. 12, 77 (1965)

ELEM. SYM.	A	Z
Si		14

METHOD

REF. NO.	
65 Ha 2	JOC

REACTION	RESULT	EXCITATION ENERGY	SOURCE		DETECTOR		ANGLE
			TYPE	RANGE	TYPE	RANGE	
G,A	SPC	THR-31	C	31	EMU-D	5-20	DST

TABLE 3

ANGULAR ENERGY DISTRIBUTION FOR THE GAMMA-ALPHA REACTIONS WITH SILICON UP TO 31 MeV. THE DATA ARE CORRECTED FOR THE RELATIVE BACKGROUND

cosΘ	−1	−0.8	−0.6	−0.4	−0.2	0	0.2	0.4	0.6	0.8	1.0
MeV	1	2									
5		1						1	2	3	
	2	1							2	5	
6	2	1	2							2	
	5	1	2					2	2	4	
7	8	4									
		1	2					4	10	3	
8	3	3	3				2	5	9	6	
	10	2	4					5	4	5	
9	2	3	1				1	6	5	3	
	1	5	2				3	6	4	2	
10	5	1	3	2			4	2	5	4	
	5	1	3	2			4	2	3	3	
11	4	4	3				1	1	2	1	
	3	4	13				1	2	3	1	
12	5	4	2	1			4	1	3	3	
	3	2	1	3	1	2	2	2		7	
13	2	7		2		1	1	1		1	
	2	1		2							
14	2	1		3	1		1	1	1	1	
				1	2		2				
15					2	4			1	1	
16				2		4					
						1					
17					1	2					
18				1		2					
						1					
19				1		2					
				1		1					

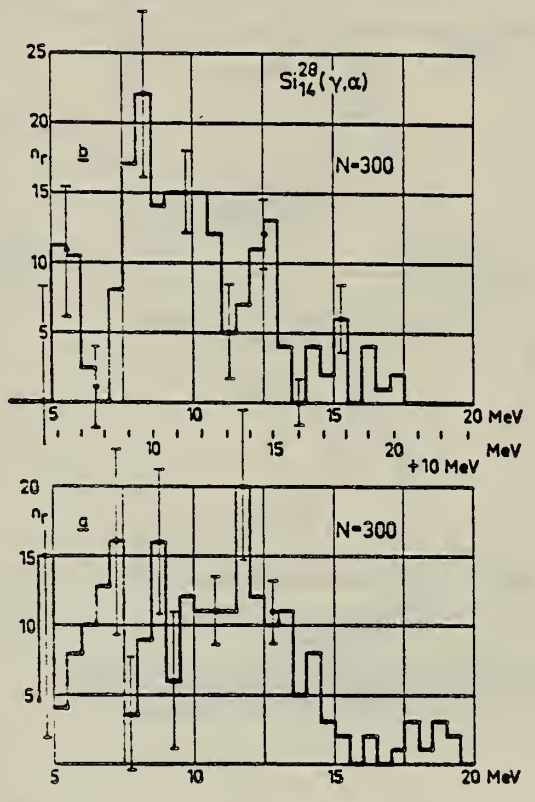

Fig. 6.

REF.

J.M. Wyckoff, B. Ziegler, H.W. Koch, and R. Uhlig
Phys. Rev. 137, B576-94 (1965)

ELEM. SYM.	A	Z
Si		14

METHOD

Synchrotron; ion chamber monitor

REF. NO.

65 Wy 1

NVB

REACTION	RESULT	EXCITATION ENERGY	SOURCE		DETECTOR		ANGLE
			TYPE	RANGE	TYPE	RANGE	
G,MU-T	ABX	10 - 35	C	90	SCI-D		4PI

61+

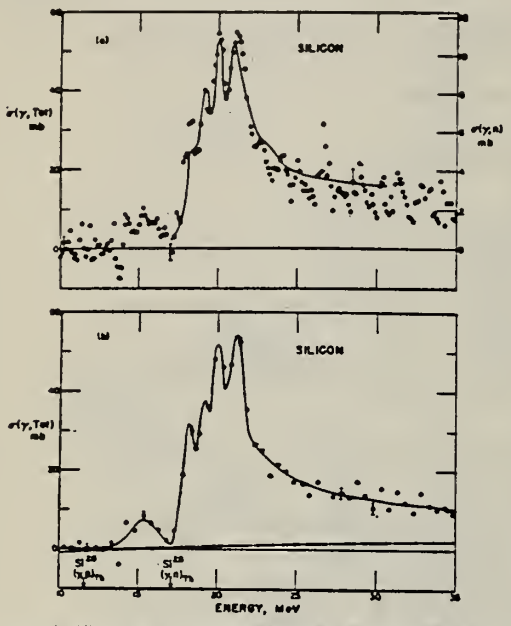

FIG. 17. Silicon total photonuclear cross section. The solid line on (a) represents the $\sigma(\gamma,n)$ data from the Livermore group shifted up in energy by 250 keV using the right-hand ordinate scale.

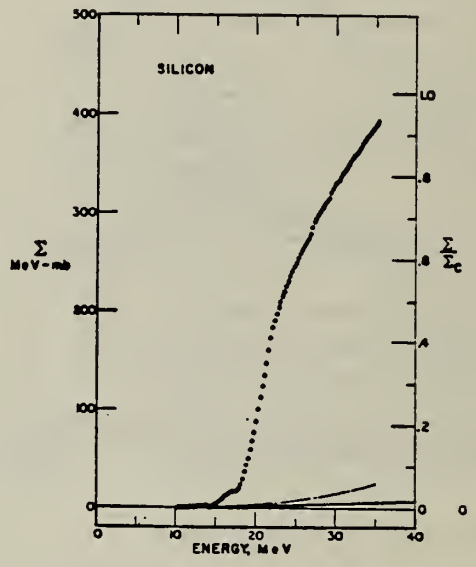

FIG. 18. Silicon total photonuclear cross section integrated over energy.

REF. H. Artus
Z. Physik 189, 355 (1966)

ELEM. SYM.	A	Z
Si		14

METHOD

REF. NO. 66 Ar 1 egf

REACTION	RESULT	EXCITATION ENERGY	SOURCE		DETECTOR		ANGLE
			TYPE	RANGE	TYPE	RANGE	
G,X	RLY	THR- 52	C	52	ACT-I		4PI

X=MG-28,NA-24

4.3. Die $Si^{30}(\gamma, 2p)Mg^{28}$-Reaktion. Die Ausbeute dieses Prozesses relativ zu $C^{12}(\gamma, n)C^{11}$ wurde zu:

$$Y_{28}/Y_{11}=(1{,}6\pm 0{,}3)\cdot 10^{-2} \quad \text{bei} \quad E_m=51{,}4\,\text{MeV}$$

bestimmt. Der Fehler von etwa 20% ist durch die in der Probe gleichfalls erzeugte Na^{24}-Störaktivität bedingt. Das Ausbeuteverhältnis an Na^{24} zu Mg^{28} aus natürlichem Silizium beträgt $(3{,}8\pm 0{,}8)$ bei $E_m=51{,}4$ MeV.

REF. F. W. K. Firk
Proc. Gatlinburg Conference 352 (1966)

ELEM. SYM.	A	Z
Si		14

METHOD

REF. NO. 66.Fi 2 hmg

REACTION	RESULT	EXCITATION ENERGY	SOURCE		DETECTOR		ANGLE
			TYPE	RANGE	TYPE	RANGE	
G,XN	SPC	THR-60	C	60	TOF-D	5-40	90

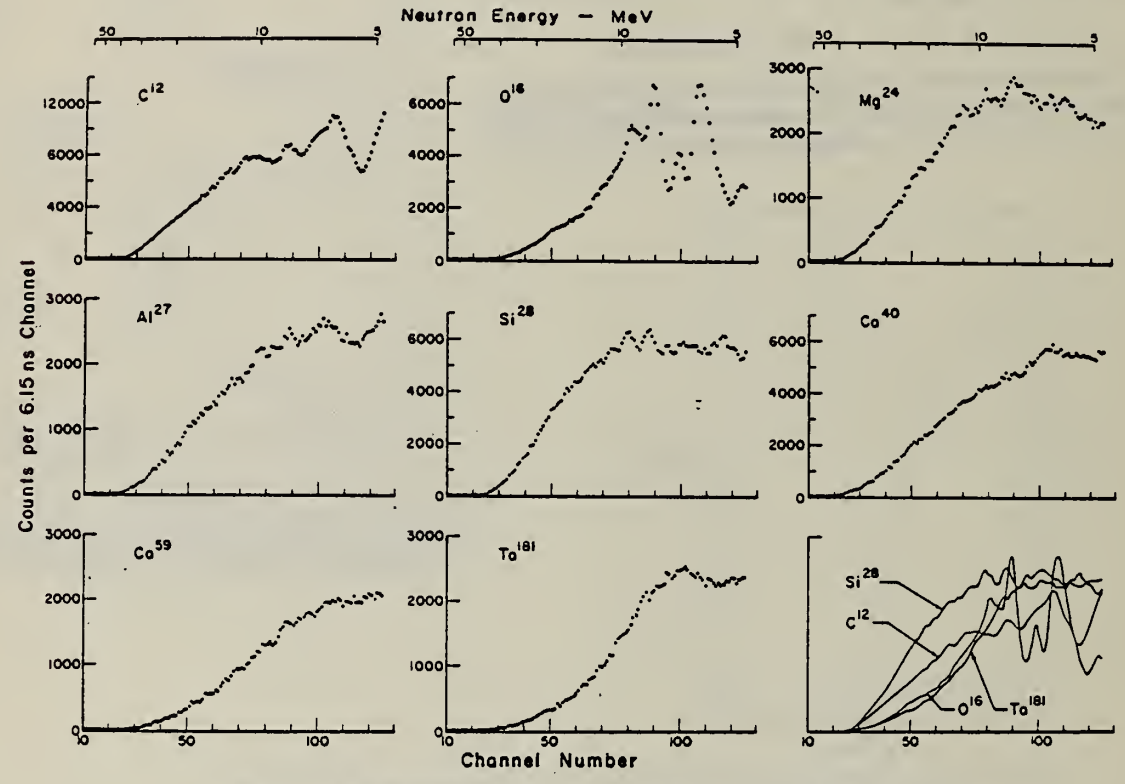

Fig. 1. Observed photoneutron time-of-flight spectra of C, O, Mg, Si, Ca, Co, V, and Ta.

REF. B. I. Goryachev, B. S. Ishkhanov, V. G. Shevchenko, B. A. Yur'ev
ZhETF Pis'ma 4, No. 11, 491 (1966)
JETP Letters 4, 11, 330 (1966)

ELEM. SYM.	A	Z
Si		14

METHOD

REF. NO. 66 Go 3 EGF

REACTION	RESULT	EXCITATION ENERGY	SOURCE		DETECTOR		ANGLE
			TYPE	RANGE	TYPE	RANGE	
G,XN	ABX	17-30	C	17-30	BF3-I		4PI

74

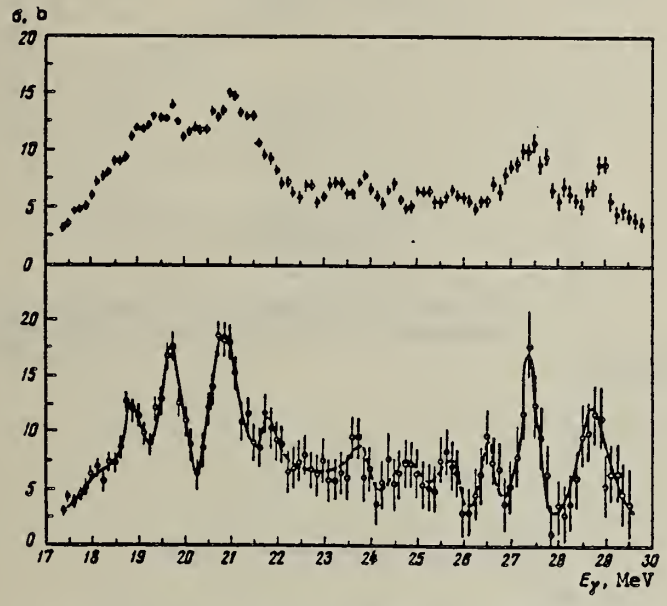

Cross section of the reaction $Si^{28}(\gamma, n)$, measured every 125 keV: a) counted in steps $\Delta E = 1$ MeV, b) counted in steps $\Delta E = 0.5$ MeV.

REF.
H. Lichtblau and B.M. Spicer
Aust. J. Phys. 19, 297 (1966)

ELEM. SYM.	A	Z
Si		14

METHOD
35 MeV Betatron; NBS ionization chamber

REF. NO.
66 Li 1 JDM

REACTION	RESULT	EXCITATION ENERGY	SOURCE		DETECTOR		ANGLE
			TYPE	RANGE	TYPE	RANGE	
G,P	SPC	THR - 32	C	21,32	SCI-D	1 - 19	90

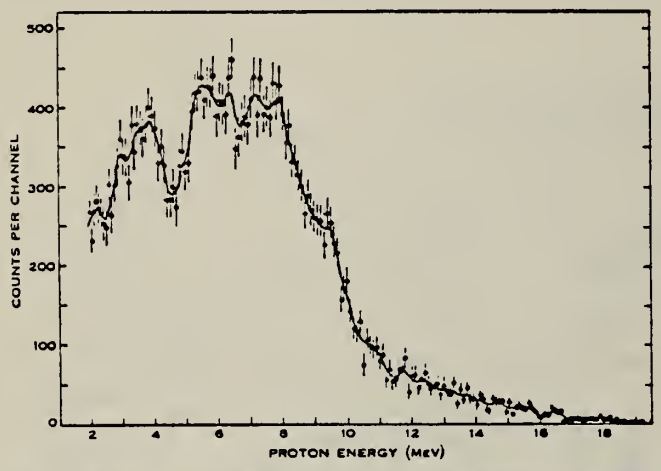

Fig. 7.—Energy spectrum of photoprotons from silicon, with bremsstrahlung end-point energy 32 MeV.

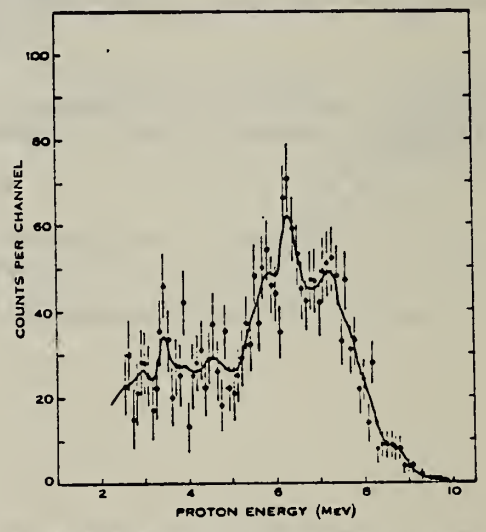

Fig. 8.—Energy spectrum of photoprotons from silicon, with bremsstrahlung end-point energy 21·2 MeV.

REF. Yu. P. Antuf'ev, I. I. Miroshnichenko, V. I. Noga, and P. V. Sorokin
Yad. Fiz. 6, 431 (1967)
Sov. J. Nucl. Phys. 6, 312 (1968)

ELEM. SYM.	A	Z
Si		14

METHOD

REF. NO.	
67 An 1	HMG

REACTION	RESULT	EXCITATION ENERGY	SOURCE		DETECTOR		ANGLE
			TYPE	RANGE	TYPE	RANGE	
G,XXX	RLX	THR-999	C	THR-999	ACT-I		4PI

XXX=NA24

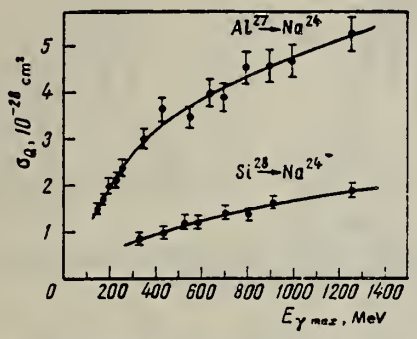

Fig. 2. Cross section σ_a of the reactions $Al^{27} \rightarrow Na^{24}$ and $Si^{28} \rightarrow Na^{24}$ per equivalent γ quantum as a function of the maximum bremsstrahlung energy.

REF.

B. I. Goryachev, B. S. Ishkhanov, I. M. Kapitonov,
Zh. M. Seliverstova, V. G. Shevchenko, and B. A. Yur'ev
J. Nucl. Phys. (USSR) 4, 505 (1966)
Soviet J. Nucl. Phys. 4, 359 (1967)

ELEM. SYM.	A	Z
Si		14

METHOD

REF. NO.	
67 Go 1	JOC

REACTION	RESULT	EXCITATION ENERGY	SOURCE		DETECTOR		ANGLE
			TYPE	RANGE	TYPE	RANGE	
G,P 854+	ABX	THR-29	C	11-29	SCD-D	1-	4PI

854+

$\sigma_{int}(28.5) = 330 \pm 70$ MeV-mb

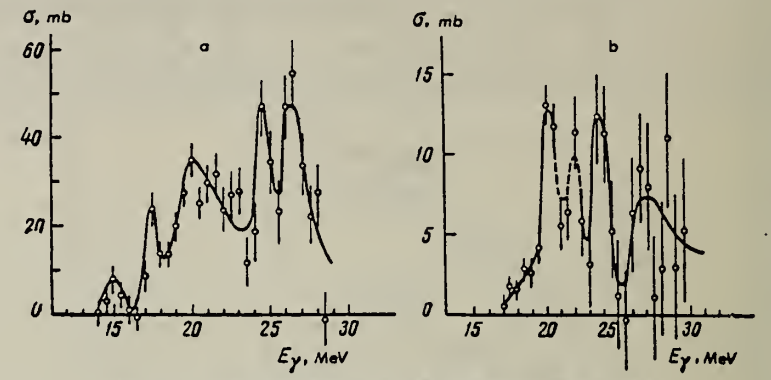

Fig. 1. Cross section for the reaction $Si^{29}(\gamma, p)$ for protons, a—with $E_p \geq 1$ MeV; b—with $E_p \geq 6.5$ MeV.

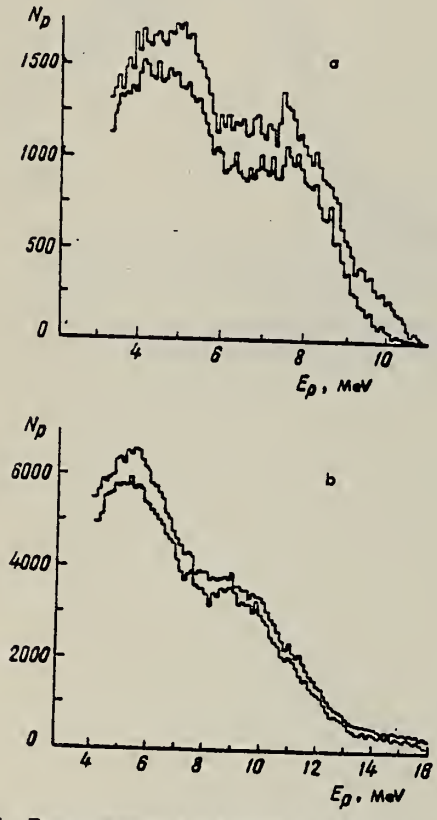

Fig. 3. Energy spectra of photoprotons for $E_{\gamma max}$ = : a—21, 22 MeV; b—26, 27 MeV.

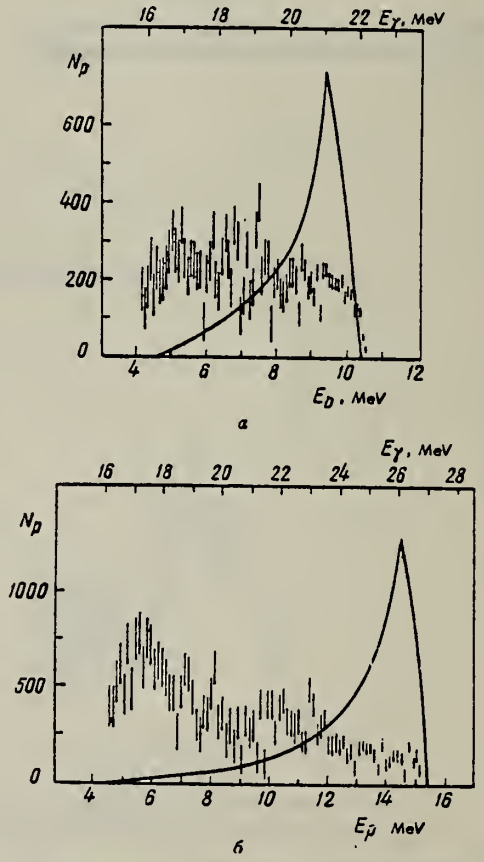

Fig. 4. Difference energy spectrum of protons, obtained from the energy distributions: a—for $E_{\gamma max}$ = 21 and 22 MeV; b—for $E_{\gamma max}$ = 26 and 27 MeV. The smooth curves are the photon spectrum corresponding to this proton energy distribution.

REF. N. Bezic, D. Jamnik, G. Kernel, J. Krajnik and J. Snajder
Nucl. Phys. A117, 124 (1968)

ELEM. SYM.	A	Z
Si		14

METHOD

REF. NO. 68 Be 4 egf

REACTION	RESULT	EXCITATION ENERGY	SOURCE		DETECTOR		ANGLE
			TYPE	RANGE	TYPE	RANGE	
G,MUT	ABX	10-30	C	35	MGC-D	10-30	4PI

103

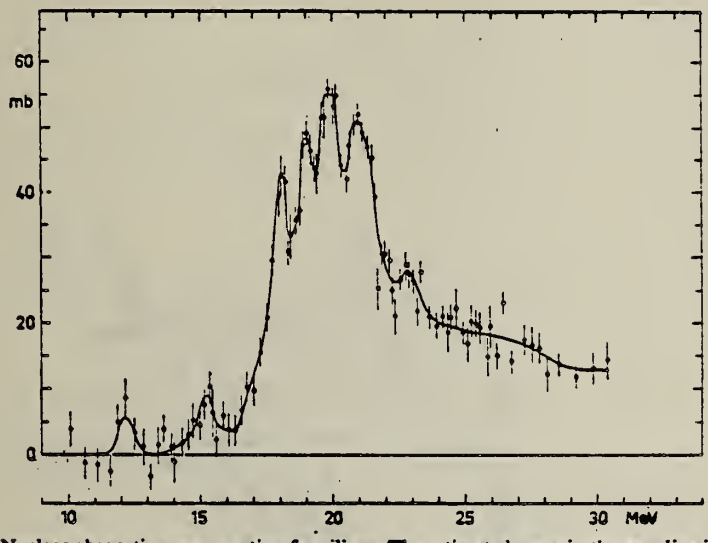

Fig. 1. Nuclear absorption cross section for silicon. The estimated error in the zero line is ±1.5 mb.

REF. B. C. Cook, D. W. Anderson, T. J. Englert
Phys. Letters 26B, 341 (1968)

ELEM. SYM.	A	Z
Si		14

METHOD

REF. NO. 68 Co 1 HMG

REACTION	RESULT	EXCITATION ENERGY	SOURCE		DETECTOR		ANGLE
			TYPE	RANGE	TYPE	RANGE	
G,N	RLX	THR- 65	C	13- 65	ACT-I		4PI

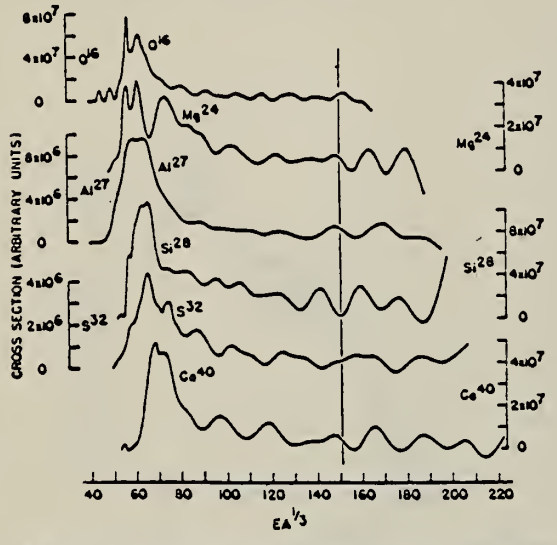

Fig. 1. Cross section for elements in the s-d shell as a function of $EA^{1/3}$. The vertical line is only an aid to the eye. Universal curves expected for the hydrodynamical model are not evident.

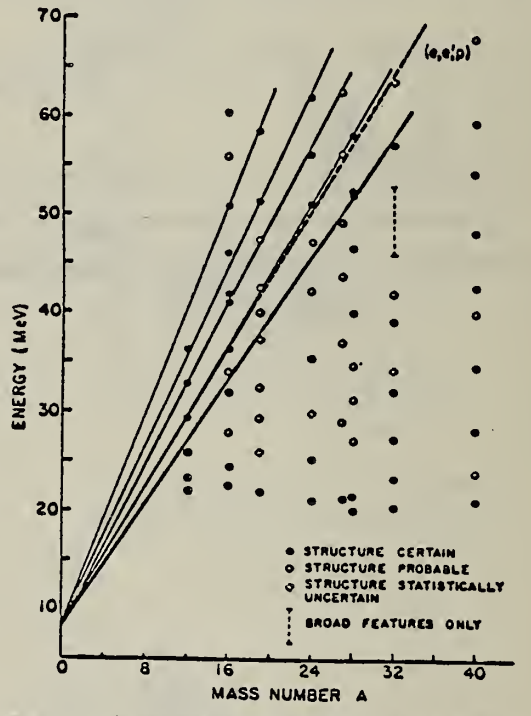

Fig. 2. A dependence of structure. A qualitative estimate for the statistical validity for structure is also indicated. The solid straight lines have the form mA + + 8 MeV while the dashed line represents the position of the 1s level as determined from (e,e'p) experiments.

B. I. Goryachev, B. S. Ishkhanov, V. G. Shevchenko and B. A. Yur'ev
Yad. Fiz. 7, 1168 (1968)
Sov. J. Nucl. Phys. 7, 698 (1968)

ELEM. SYM.	A	Z
Si		14

METHOD

REF. NO.	
68 Go 6	HMG

REACTION	RESULT	EXCITATION ENERGY	SOURCE		DETECTOR		ANGLE
			TYPE	RANGE	TYPE	RANGE	
G,XN	ABX	17-30	C	17-30	BF3-I		4PI

431+

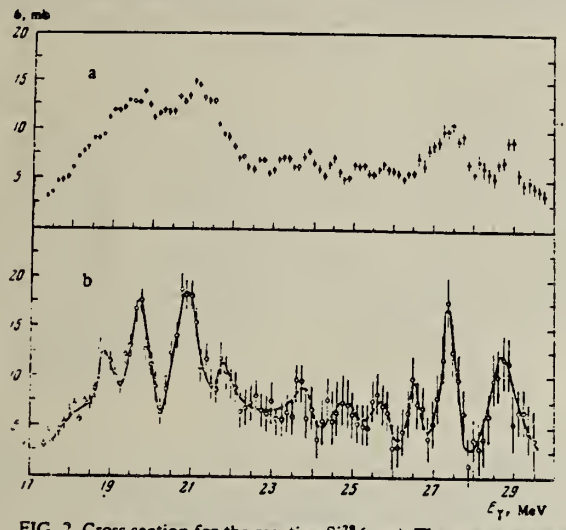

FIG. 2. Cross section for the reaction $Si^{28}(\gamma, n)$. The computational step is ΔE = 1 MeV (a) and 0.5 MeV (b).

Table I. Parameters of resonances observed in the cross section for $Si^{28}(\gamma, n)$

E^0, MeV (our data)	σ_{int}, MeV·mb	E^0, MeV [9]	E^0, MeV [10]	E^0, MeV (our data)	σ_{int}, MeV·mb	E^0, MeV [9]	E^0, MeV [10]
17.85±0.1	2.4		18.1	20.9±0.1	16.4	20.75	20.9
18.25±0.1	2.2		18.6	(21.6)	6.6	(22.75)	
18.8±0.1	7.5	18.50	19.0	27.4±0.2	15	(24.75)	
19.75±0.1	14.8	19.75	19.8	28.8±0.2	13		

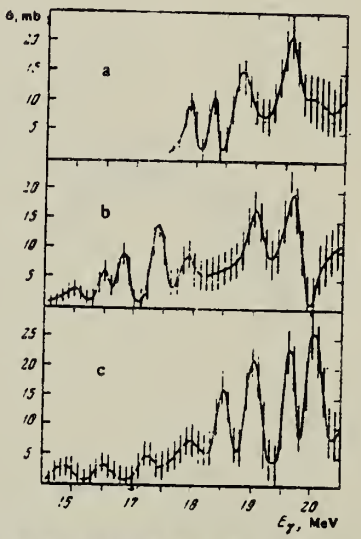

FIG. 5. Cross sections for the reactions: a – Si^{28} (γ, n), b – S^{32} (γ, n), c – Ca^{40} (γ, n). Computational step ΔE = 0.2 MeV.

	Punched	Checked w/ PO
IFM Card DATA	10/14	10/15/69
IFM Card REFERENCE	"	"

REF.

G. A. Savitskii, N. G. Afanas'ev, I. S. Gul'karov, V. D. Kovalev, A. S. Omelaenko, V. M. Khvastunov, and N. G. Shevchenko
Yad. Fiz. 8, 648 (1968)
Sov. J. Nucl. Phys. 8, 376 (1969)

ELEM. SYM.	A	Z
Si		14

METHOD

REF. NO.	
68 Sa 2	HMG

REACTION	RESULT	EXCITATION ENERGY	SOURCE		DETECTOR		ANGLE
			TYPE	RANGE	TYPE	RANGE	
E,E/	FMF	1-13	D	114-260	MAG-D	100-260	DST
		(1.78-12.7)					(30-130)

5 LEVELS 1.78-12.7

Table III. Squared form factor for inelastic scattering of electrons with excitation in Si^{28} of levels at 1.78, 4.62, 6.9 ± 0.2, and 9.7 ± 0.1 MeV.

q', F^{-1}	$F^2_\lambda \cdot 10^{-6}$	q', F^{-1}	$F^2_\lambda \cdot 10^{-6}$	q', F^{-1}	$F^2_\lambda \cdot 10^{-6}$	q', F^{-1}	$F^2_\lambda \cdot 10^{-6}$
0.67	510±50	1.00	42.6± 8.7	0.80	344±69	0.79	66.5±18.7
0.80	575±50	1.08	37.9±11.7	0.90	292±39	0.89	92.6±19.4
0.90	597±48	1.08	51.8±10.0	0.99	290±36	1.07	102±15
1.00	579±46	1.10	64.1±10.2	1.08	269±33	1.07	122±16
1.08	528±42	1.11	55.2±11.3	1.07	211±26	1.08	83.4±12.2
1.08	530±42	1.17	71.9±14.0	1.09	219±27	1.16	109±14
1.10	492±38	1.26	55.3± 7.0	1.09	150±19	1.25	96.9±12.1
1.11	413±35	1.34	54.9± 6.8	1.17	234±28	1.33	77.5±10.3
1.17	418±33	1.44	49.4± 6.1	1.25	201±24	1.42	74.6± 9.2
1.17	321±25	1.53	45.2± 4.7	1.34	182±22	1.53	67.3± 8.3
1.17	349±27	1.64	35.8± 3.7	1.43	132±16	1.61	59.5± 7.3
1.26	327±18	1.72	30.5± 3.1	1.53	94.0±11.2	1.71	44.4± 5.8
1.34	166±13	1.92	24.4± 2.4	1.62	66.6± 8.0	1.80	27.1± 3.3
1.41	84.7±7.0			1.71	47.3± 5.7		
1.53	35.5±3.1			1.81	24.7± 3.0		
1.64	20.4±1.8						
1.72	10.5±1.1						
1.82	6.71±0.73						

Table IV. Parameters obtained from analysis of data on electron scattering by Si^{28} with excitation of levels at 1.78, 4.62, 6.9 ± 0.2, and 9.7 ± 0.1 MeV

Level energy, MeV; spin and parity	Parameters								Kokame et al. [12]		
	Heim's model [1]			Schucan's model [2]							
	$B_\lambda \cdot 10^{-6}$	$B(E\lambda)\uparrow$, $e^2 \cdot F^{2\lambda}$	G	$B'_\lambda \cdot 10^{-6}$	$B(E\lambda)\uparrow$, $e^2 \cdot F^{2\lambda}$	D_λ, Mev-sec^2	C_λ, MeV	β^d_λ	C_λ, MeV	G	β^d_λ
1.78; 2+	11±1	295	11.3	15.6±2.3	292.5	$5.5 \cdot 10^{-43}$	40.9	0.33	51.4	6.7	0.29
4.62; 4+	9.1±0.7	$2.42 \cdot 10^3$	6.0	1.53±0.22	$1.25 \cdot 10^3$	$2.2 \cdot 10^{-41}$	1081	0.14			
6.9; 3−	14.1±1.5	$3.28 \cdot 10^3$	10.1	5.9±0.7	$2.39 \cdot 10^3$	$3.8 \cdot 10^{-43}$	422	0.24	319	6.1	0.28
9.7; 3−	5.5±0.8	$1.30 \cdot 10^3$	4.0	2.4±0.4	$9.71 \cdot 10^2$	$6.8 \cdot 10^{-42}$	1452	0.15			
9.7; 5−	13.1±2.0	$3.93 \cdot 10^3$	7.8	1.0±0.2	$1.60 \cdot 10^3$	$1.6 \cdot 10^{-41}$	3424	0.13			

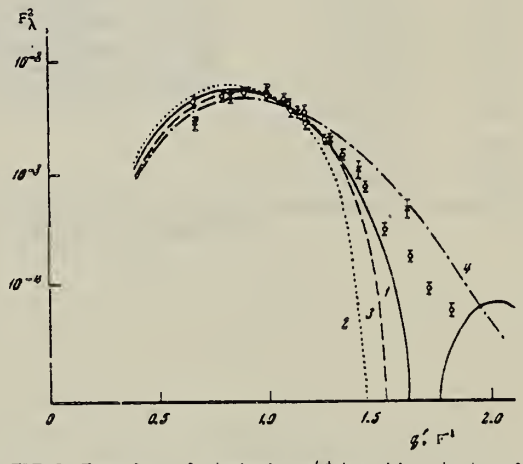

FIG. 3. Form factor for inelastic scattering with excitation of 1.78-MeV level. The curves have been calculated from the following formulas: Curve 1 – (4), Curve 2 – (8), Curve 3 – (12), Curve 4 – (13). Points: O – our data, X – data of Heim.[1]

[over]

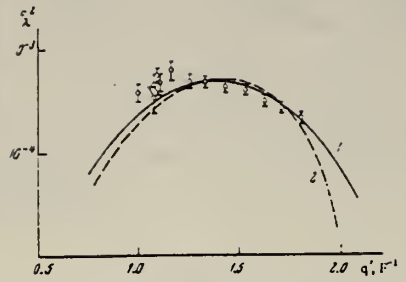

FIG. 4. Form factor for inelastic scattering with excitation of 4.62-MeV level. Curves 1 and 2 were calculated respectively from Eqs. (4) and (8).

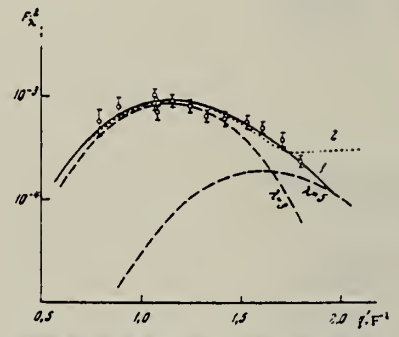

FIG. 6. Inelastic-scattering form factor corresponding to the peak at 9.7 ± 0.1 MeV. Curves 1 and 2 for a mixture of multiples with λ = 3 and λ = 5 have been calculated respectively from formulas (4) and (8). The dashed curves give the contributions of the individual multipoles, calculated from formula (4).

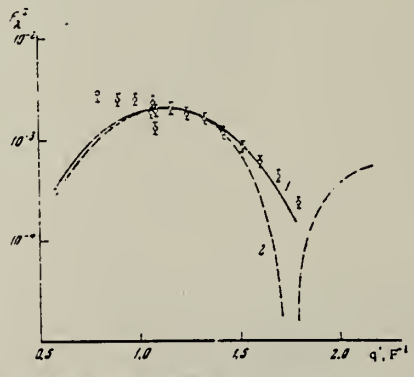

FIG. 5. Inelastic-scattering form factor corresponding to the peak at 6.9 ± 0.2 MeV. Curves 1 and 2 have been calculated respectively from Eqs. (4) and (8).

REF.

D. W. Anderson, A. J. Bureau, B. C. Cook, T. J. Englert
Phys. Rev. 183, 978 (1969)

ELEM. SYM.	A	Z
Si		14

METHOD

REF. NO.	
69 An 3	hmg

REACTION	RESULT	EXCITATION ENERGY	SOURCE		DETECTOR		ANGLE
			TYPE	RANGE	TYPE	RANGE	
G,XN	RLX	THR-65	C	16-65	ACT-I		4PI

Data normalized to measurements previously reported.

828

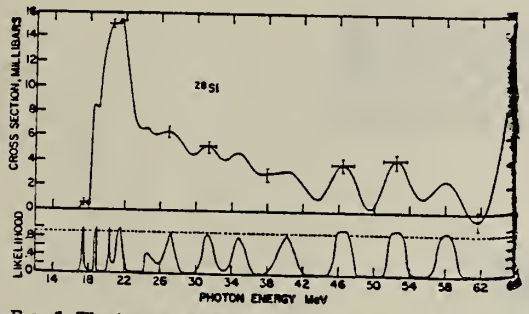

FIG. 5. The least-structure cross section, $\sigma=\sigma_a+2.0\sigma_{2a}+\sigma_{pn}$, for the silicon data. Vertical bars indicate errors in cross section. Horizontal bars indicate the resolution function width. The coefficient for σ_{2a} arises because of enhancement of the yield due to formation of Si^{28} as discussed in Sec. II. A likelihood estimate of the statistical certainty of the indicated structure is also shown.

TABLE I. Peak energies for the cross-section maxima of Figs. 4 and 5. All maxima with greater than 70% likelihood as computed from the cross-section errors[a] are shown. Maxima with less than 90% likelihood are doubtful.

Al^{27} Energy (MeV)	Likelihood	Si^{28} Energy (MeV)	Likelihood
(41.6±1.0)	0.72	(27.1±0.5)	0:90
49.4±0.8	0.96	(31.4±0.4)	0.88
56.3±0.9	0.98	(3.47±0.6)	0.86
		(40.1±0.9)	0.89
		(46.4±0.8)	1.00
		52.2±0.8	1.00
		58.2±1.0	0.98

[a] B. C. Cook (to be published).

REF.

Yu. P. Antuf'ev, V. L. Agranovich, V. B. Ganenko, V. S. Kuzmenko, I. I. Miroshnichenko, and P. V. Sorokin
Ukr. Fiz. Zh. 14, 248 (1969)

ELEM. SYM.	A	Z
Si		14

METHOD

REF. NO. 69 An 6 egf

REACTION	RESULT	EXCITATION ENERGY	SOURCE		DETECTOR		ANGLE
			TYPE	RANGE	TYPE	RANGE	
G,P	ABY	109-999	C	700,999	TEL-D	97-230	DST
G,D	ABY	120-999	C	700,999	TEL-D	97-205	DST

999 = 1.2 GEV

Summary

The cross-sections of the (γ, p) (γ, d) reactions were investigated. Li^7, Be^9, C^{12}, Si^{28}, Cu^{63}, Mo^{96} and Ta^{181} targets were irradiated with the bremsstrahlung of 700 and 1200 MeV maximum energy from the Kharkov PhTI Ac. Sci. UkrSSR linear accelerator. The photoprotons and deuterons were detected by the scintillation telescope at 30°, 60°, and 120° with the beam. Possible mechanisms of the proton and deuteron photoproduction are discussed. The qualitative agreement of A dependence of the cross-sections is observed with a suggestion on the meson mechanism for these reactions.

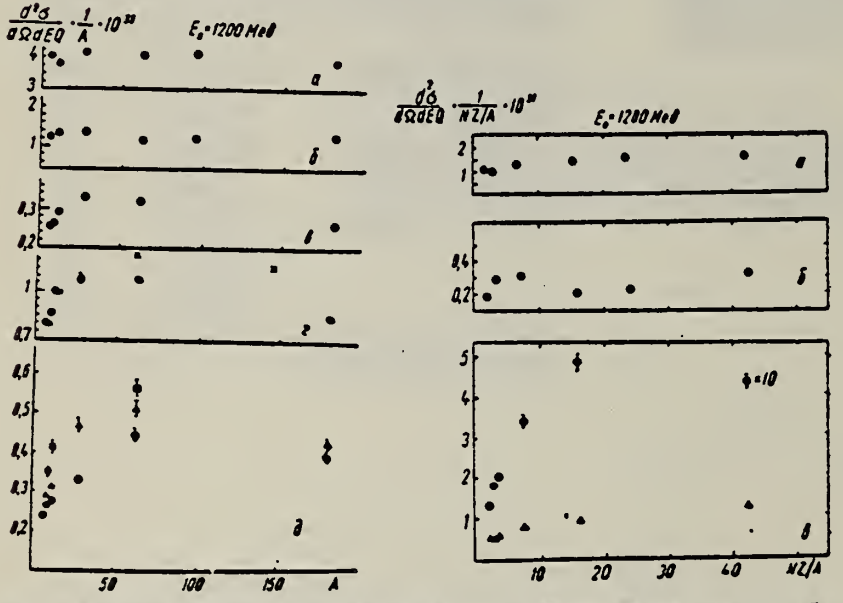

Рис. 1. Залежність перерізу (γ, p)-реакції від A: $а$ — ϑ=30°, E_p=97 *Мев*; $б$ — E_p=205 *Мев*; $в$ — ϑ=60°, E_p=230 *Мев*; $г$ — E_p=157 *Мев* (× — дані [3]); $д$ — ϑ=120°, ○ — E_p=120 *Мев*, △ — E_p=157 *Мев*, ■ — E_p=230 *Мев*. Абсолютне значення перерізу наведено при енергії протонів E_p=120 *Мев*. Інші дані нормовані до перерізу для Li^7 при E_p=120 *Мев*.

Рис. 2. Залежність перерізу (γ, d)-реакції від NZ/A: $а$ — ϑ=30°, E_d=97 *Мев*; $б$ — ϑ=30°, E_d=205 *Мев*; $в$: △ — ϑ=60°, E_d=97 *Мев*, ○ — ϑ=120°, E_d=97 *Мев* (перерізи наведені в одиницях 10^{-33} *см²/стер · Мев · Q*).

S. Costa, L. Ferrero, L. Pasqualini, F. Ferrero, C. Manfredotti
Lettere al Nuovo Cimento 1, 346 (1969)

Si		14

METHOD

REF. NO. 69 Co 1 egf

REACTION	RESULT	EXCITATION ENERGY	SOURCE TYPE	SOURCE RANGE	DETECTOR TYPE	DETECTOR RANGE	ANGLE
G,XN	ABX	14-38	C	14-38	BF3-I		4PI

83c

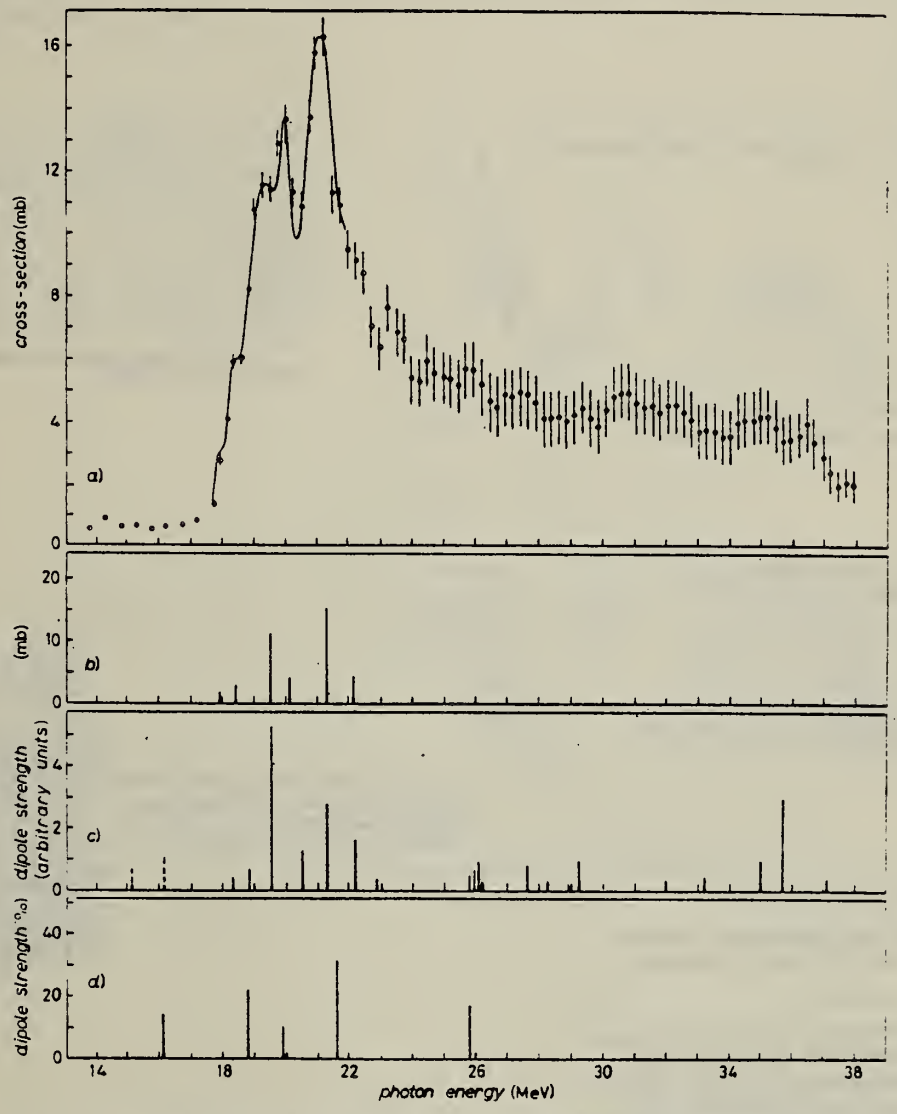

Fig. 1. – *a*) Experimental (γ, Tn) cross-section of Si. *b*) Height and position of the Lorentz lines used to fit the experimental results between 17.2 and 22 MeV. *c*) Dipole strengths calculated with the DTCM. *d*) Dipole strengths calculated with the particle-hole model.

REF.

V. I. Noga, Yu. N. Ranyuk, and P. V. Sorokin
Yad. Fiz. 2, 1152 (1969)
Sov. J. Nucl. Phys. 2, 673 (1969)

ELEM. SYM.	A	Z
Si		14

METHOD

REF. NO.	
69 No 1	egf

REACTION	RESULT	EXCITATION ENERGY	SOURCE		DETECTOR		ANGLE
			TYPE	RANGE	TYPE	RANGE	
G,NA24	ABY	43-999	C	100-999	ACT-I		4PI
							822

999 = 1.2 GEV

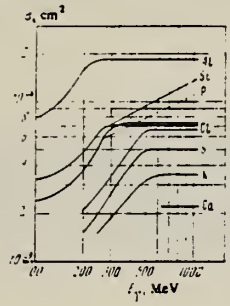

FIG. 2. Cross sections as a function of γ-ray energy.

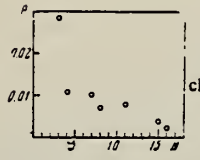

FIG. 3. Dependence of P on number of nucleons which have left the nucleus.

Table I

Reaction	Nucleons emitted	Threshold*, MeV	Target	Distribution of isotopes, %
$Al^{27} \rightarrow Na^{24}$	2p, n	31	Al	100
$Si^{28} \rightarrow Na^{24}$	3p, n	43	Si	92.27
$P^{31} \rightarrow Na^{24}$	4p, 3n	69	P	100
$S^{32} \rightarrow Na^{24}$	5p, 3n	78	S	95.02
$Cl^{35} \rightarrow Na^{24}$	6p, 5n	104	NH_4Cl	75.4
$K^{39} \rightarrow Na^{24}$	8p, 7n	140	K_2CO_3	93.08
$Ca^{40} \rightarrow Na^{24}$	9p, 7n	148	CaO	96.97

*The threshold was calculated as the binding energy of the emitted nucleons.

Table II. Cross sections for reactions in the saturation region

Reaction	σ_k, 10^{-28} cm²	Reaction	σ_k, 10^{-28} cm²
$Al^{27} \rightarrow Na^{24}$	185±20	$Cl^{35} \rightarrow Na^{24}$	68±7
$Si^{28} \rightarrow Na^{24}$	72±8	$K^{39} \rightarrow Na^{24}$	35±5
$P^{31} \rightarrow Na^{24}$	74±8	$Ca^{40} \rightarrow Na^{24}$	22±5
$S^{32} \rightarrow Na^{24}$	52±6		

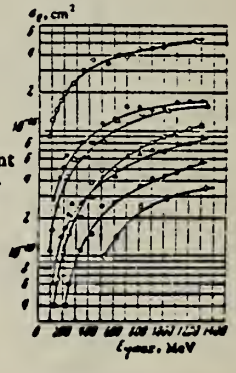

FIG. 1. Cross section σ_0 per equivalent photon as a function of maximum bremsstrahlung energy. Points: ○ – Al, ● – Si, △ – P, ▲ – S, □ – Cl, ■ – K, ◇ – Ca.

According to the photomesonic mechanism, the cross section for the reaction can be written in the form

$$\sigma = \sigma_0 AP. \qquad (1)$$

Here σ_0 is the total cross section for interaction of the photon with a free nucleon with inclusion of the nucleon motion in the nucleus (σ_0, as has been shown by Roos and Peterson,[8] depends only weakly on photon energy for $E_\gamma > 300$ MeV); A is the number of nucleons in the nucleus, and P is the probability that the reaction will proceed by a given channel.

REF. C. -P. Wu, F. W. K. Firk, and T. W. Phillips
Nucl. Phys. A147, 19 (1970)

ELEM. SYM.	A	Z
Si		14

METHOD

REF. NO.: 70 Wu 1 egf

REACTION	RESULT	EXCITATION ENERGY	SOURCE		DETECTOR		ANGLE
			TYPE	RANGE	TYPE	RANGE	
G,N	ABX	18-21	C	16-22	TOF-D		90
							819

Cross section relative to D(γ,n)p

GROUND STATE

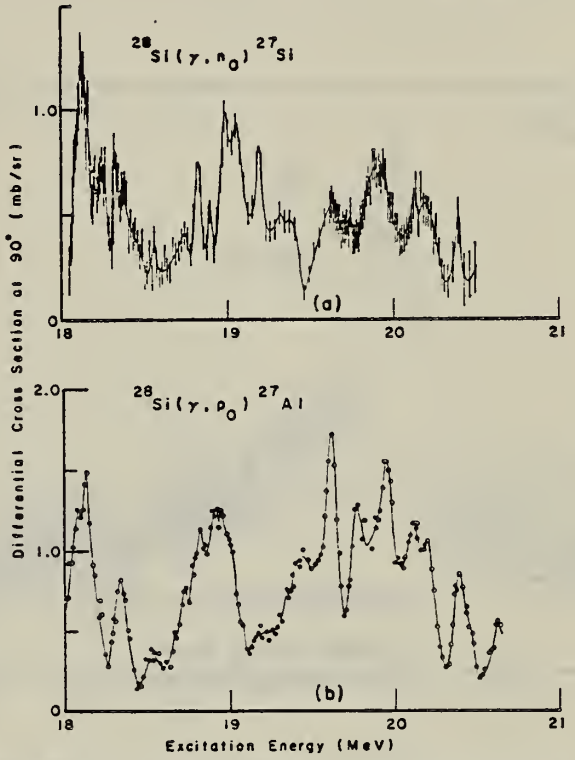

Fig. 4a. The observed $^{28}Si(\gamma, n_0)^{27}Si$ differential cross section at 90°. 4b. The $^{28}Si(\gamma, p_0)^{27}Al$ differential cross section at 90° deduced from the inverse reaction [1]).

REF.

J. Ahrens, H. Borchert, H.B. Eppler, H. Gimm, H. Gundrum, P. Riehn, G. Sita Ram, A. Zieger, and B. Ziegler
Elba-71, Tagungsbericht Elektronen Beschleuniger Arbeits Gruppen (Sept. 1971) Justus Liebig-Universitat Giessen.

ELEM. SYM.	A	Z
Si		14

METHOD

REF. NO.	
71 Ah 1	hmg

REACTION	RESULT	EXCITATION ENERGY	SOURCE		DETECTOR		ANGLE
			TYPE	RANGE	TYPE	RANGE	
G,MU-T	ABX	THR-150	C	10-150	MGC-D		4PI

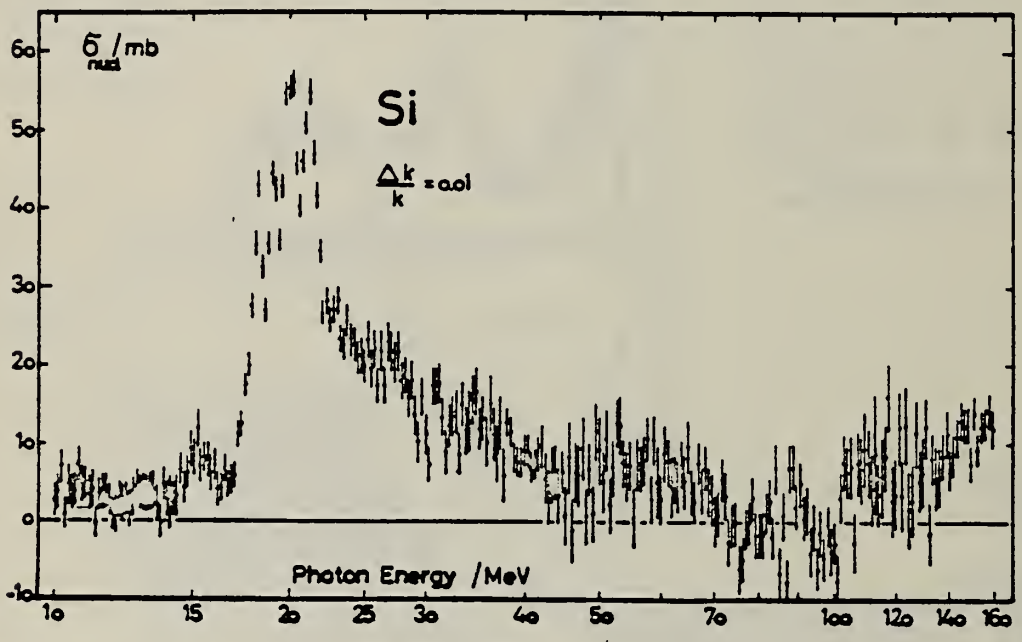

fig. 7

REF.

Yu. P. Antuf'ev, V. L. Agranovich, V. B. Ganenko, V. S. Kuz'menko, I. I. Miroshnichenko, and P. V. Sorokin
Yad. Fiz. 13, 473 (1971): Sov. J. Nucl. Phys. 13, 265 (1971)

ELEM. SYM.	A	Z
Si		14

METHOD

REF. NO.	
71 An 1	hmg

REACTION	RESULT	EXCITATION ENERGY	SOURCE		DETECTOR		ANGLE
			TYPE	RANGE	TYPE	RANGE	
G,P	SPC	45-999	C	700,999	TEL-D	25-400	DST
G,D	SPC	55-999	C	700,999	TEL-D	25-400	DST

999=1.2 GEV, REL D/P

Yield of protons 30-400 MeV, deuterons 30-200 MeV.

Table I. Values of the parameter τ, MeV

Target	E_0 = 700 MeV										E_0 = 1200 MeV					
	Protons					Deuterons					Protons			Deuterons		
	60°	80°	90°	100°	120°	60°	80°	90°	100°	120°	30°	60°	120°	30°	60°	120°
Li	46	42	34	30	27	28	24	22	21	20		45	28		27	24
Be	48	43	36	30	27	28	26	24	22	19		45	28		27	24
C	50	44	38	30	26	34	33	29	23	19	60	48	35	37	34	22
Si		43			28		27			22		46	35		28	25
Ca												45	29		27	24
Ta					28					21		45	34		27	24
Pb											51		29	36		22

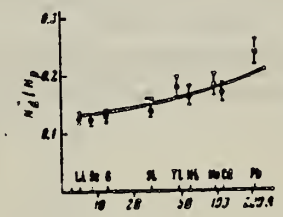

FIG. 4. The ratios N_d/N_p as a function of target-nucleus mass number A at an angle $\theta = 60°$ for $E_0 = 1200$ MeV. Solid curve—$A^{0.13}$.

The measured secondary-particle spectra for kinetic energies $T > 80$ MeV are well described by the expression

$$d^2\sigma / d\Omega dTQ = \text{const}\, T \exp(-T/\tau), \qquad (1)$$

which is identical to the formula for the evaporation process.[4] In Table I we have given the values of the parameter τ for the nuclei studied, at various angles. The accuracy in determination of τ is about 10%.

S. Costa, L. Ferrero, L. Pasqualini, and E. Mancini
Lettere al Nuovo Cimento 2, 665 (1971)

ELEM. SYM.		
Si		14

METHOD

REF. NO. 71 Co 2 egf

REACTION	RESULT	EXCITATION ENERGY	SOURCE		DETECTOR		ANGLE
			TYPE	RANGE	TYPE	RANGE	
G,XN	ABI	36-64	C	10-64	BF3-I		4PI

FAST N YIELD

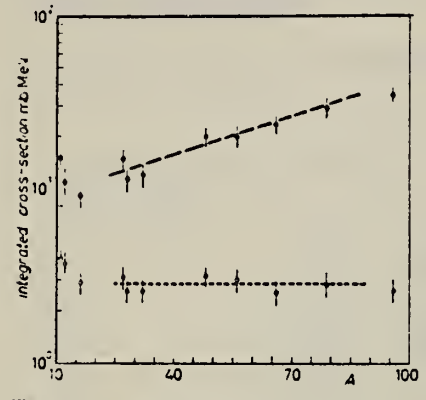

Fig. 2.

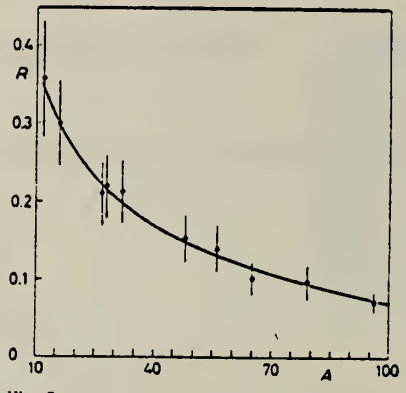

Fig. 3.

Fig. 2. – Experimental photoneutron cross-sections integrated over photon energy between 36 and 64 MeV and divided by NZ/A are plotted as a function of the mass number. Black dots are total cross-sections not corrected for neutron multiplicity; open circles represent fast neutron cross-sections (see text). The dashed lines are drawn only to guide the eye.

Fig. 3. – The ratio between «fast» and total photoneutron integrated cross-sections as a function of the mass number A. The solid line represents a fit of the ratios calculated for some nuclei by taking into account the theoretical neutron energy spectra given by GABRIEL and ALEMILLER (*) and the efficiencies of our detector (see Fig. 1).

REF.

Tatsuya Saito
Bull. Chem. Soc. Japan 44, 1800 (1971)

ELEM. SYM.	A	Z
Si		14

METHOD

REF. NO.	
71 Sa 2	egf

REACTION	RESULT	EXCITATION ENERGY	SOURCE		DETECTOR		ANGLE
			TYPE	RANGE	TYPE	RANGE	
G,NA24	ABX	THR-250	C	20-250	ACT-I		4PI
G,2P 609	ABX	THR-250	C	20-250	ACT-I		4PI

609

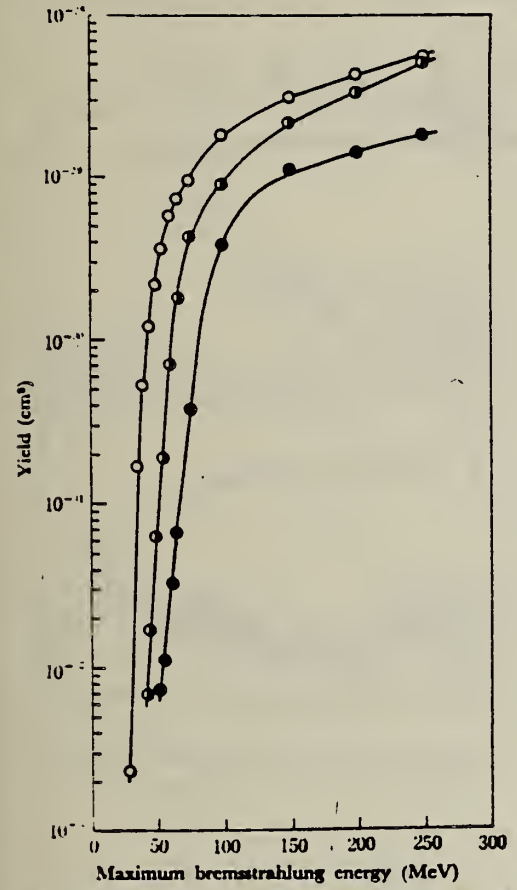

Fig. 4. The yield curves for the reactions $^{28}Si \rightarrow ^{24}Na$, $^{31}P \rightarrow ^{24}Na$, and $^{32}S \rightarrow ^{24}Na$.
○: $^{28}Si \rightarrow ^{24}Na$, ◑: $^{31}P \rightarrow ^{24}Na$, ●: $^{32}S \rightarrow ^{24}Na$

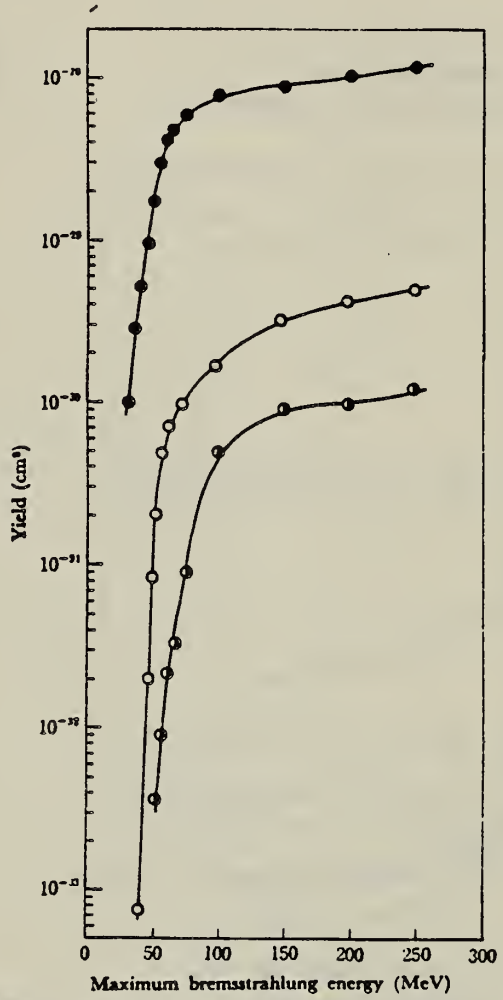

Fig. 5. The yield curves for the reactions $^{28}Si(\gamma,2p)^{26}Mg$, $^{31}P(\gamma,3p)^{26}Mg$, and $^{32}S(\gamma,4p)^{26}Mg$.
●: $^{28}Si(\gamma,2p)^{26}Mg$, ○: $^{31}P(\gamma,3p)^{26}Mg$, ◑: $^{32}S(\gamma,4p)^{26}Mg$

(over)

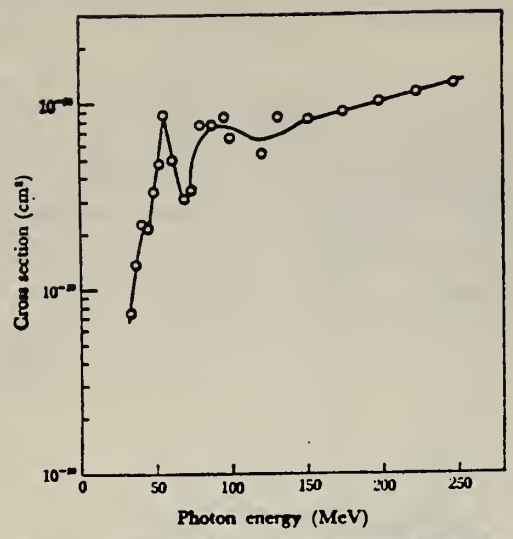

Fig. 7. The excitation function for the reaction $^{28}Si \rightarrow ^{24}Na$.

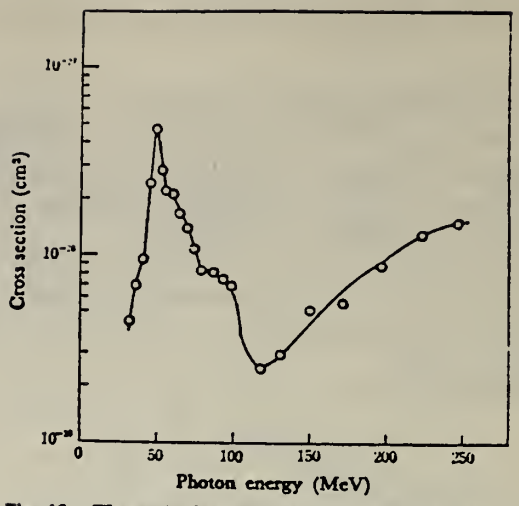

Fig. 10. The excitation function for the reaction $^{28}Si(\gamma,2p)^{26}Mg$.

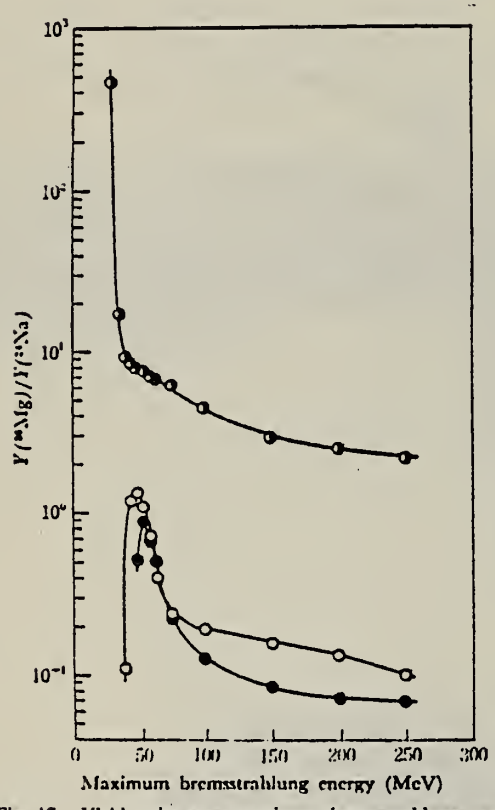

Fig. 13. Yield ratios *versus* maximum bremsstrahlung energy.
◑: $Y(^{28}Si(\gamma,2p)\ ^{26}Mg)/Y(^{28}Si \rightarrow ^{24}Na)$
○: $Y(^{31}P(\gamma,3p)\ ^{28}Mg)/Y(^{31}P \rightarrow ^{24}Na)$
●: $Y(^{32}S(\gamma,4p)\ ^{28}Mg)/Y(^{32}S \rightarrow ^{24}Na)$

REF. J. Ahrens, H. Borchert, H. B. Eppler, H. Gimm, H. Gundrum, P. Riehn, G. Sita Ram, A. Zieger, M. Kroning, B. Ziegler
Proc. International Conference on Nuclear Structure Studies Using Electron Scattering and Photoreaction, Sendai, Japan p. 213 (1972)

ELEM. SYM.	A	Z
Si		14

METHOD

REF. NO.	
72 Ah 7	egf

REACTION	RESULT	EXCITATION ENERGY	SOURCE		DETECTOR		ANGLE
			TYPE	RANGE	TYPE	RANGE	
G,MUT	ABX	10-140	C	140	MGC-D		4PI

596

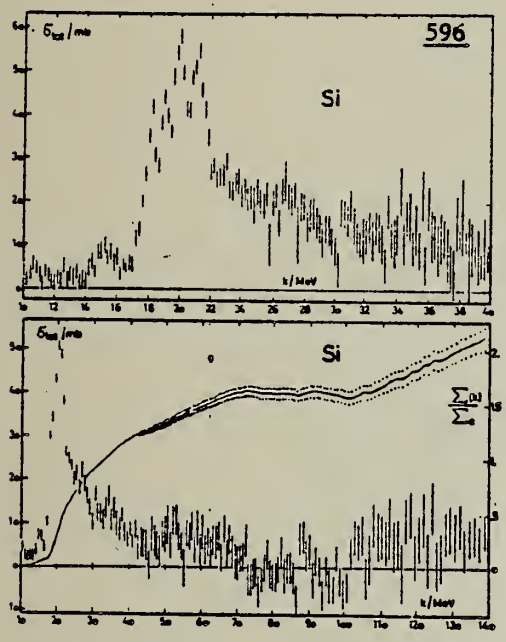

Fig.1o Total nuclear cross-sections for Si

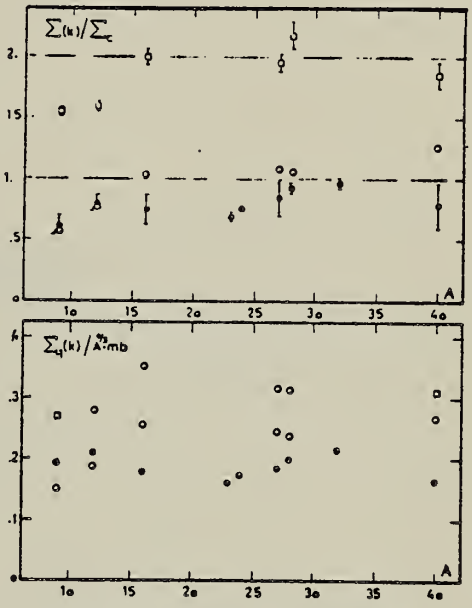

$\Sigma_c = 6o\frac{NZ}{A}$, $\Sigma(k) = \int_{1o}^{k}\delta(\tilde{k})d\tilde{k}$, $\Sigma_1(k) = \int_{1o}^{k}\delta(\tilde{k})\frac{d\tilde{k}}{\tilde{k}}$

ø NBS k=35MeV, o k=35 MeV, □ k=14o MeV

Fig.11 Integrated cross-sections

REF. J. Ahrens, H.B. Eppler, H. Gimm, H. Gundrum, M. Kroning, P. Riehn, G. SitaRam, A. Zieger, and B. Ziegler
PICNS-73, Vol.I, p.23 Asilomar

ELEM. SYM.	A	Z
Si		14

METHOD

REF. NO. 73 Ah 4 hmg

REACTION	RESULT	EXCITATION ENERGY	SOURCE		DETECTOR		ANGLE
			TYPE	RANGE	TYPE	RANGE	
G,MU-T	ABX	10-140	C	140	MGC-D		4PI

Statistics may have been improved over those of 72Ah7.

See figure on other side.

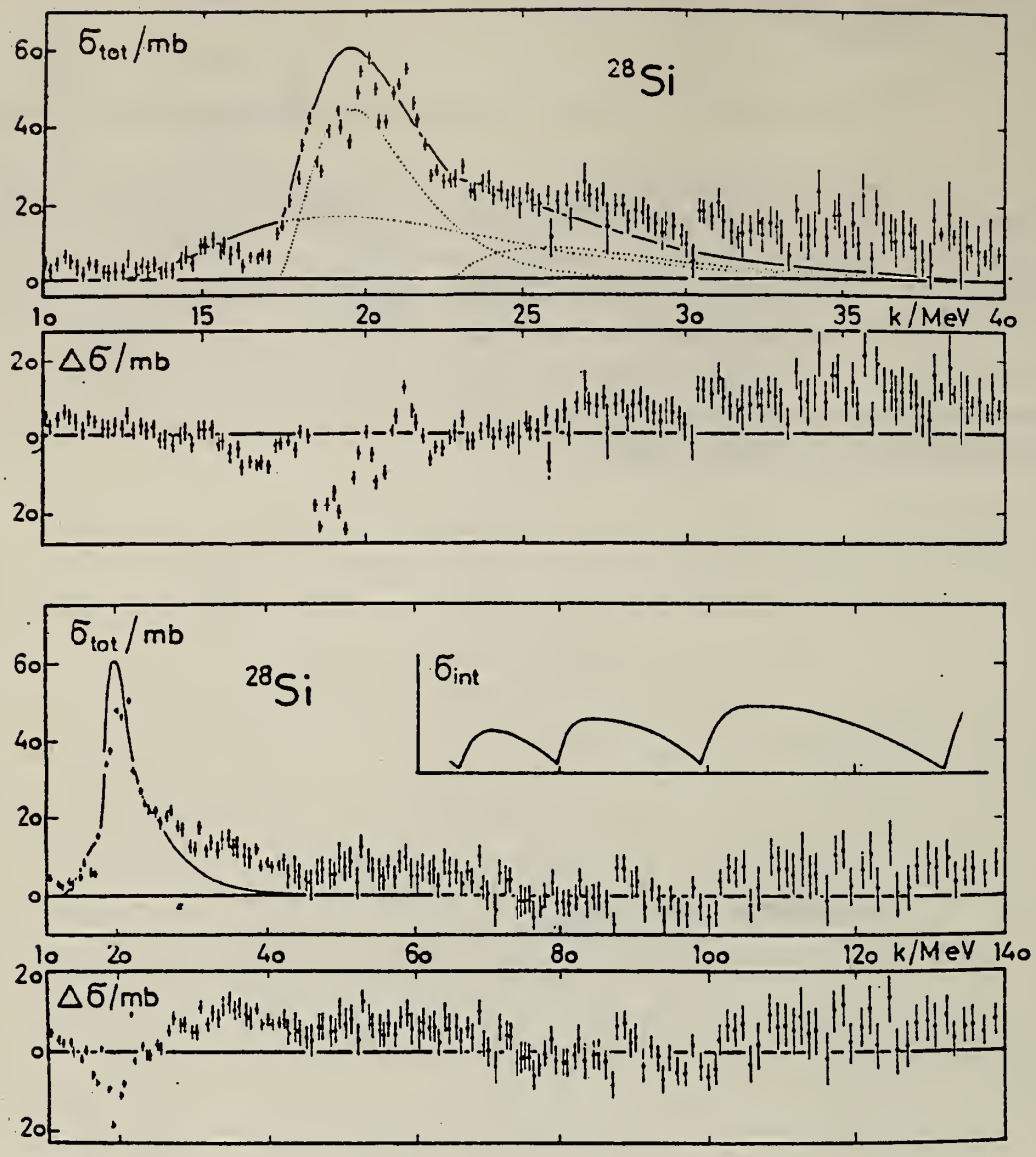

Fig. 7. Same as Fig. 2 for Si. The Si-target consisted of monocrystalline Si-rods in which occurs coherent pair production. As this effect has not been taken into account when subtracting the pair cross section from the measured data it appears in the data given here. The predicted shape of the interference term 6_{int} from theory 5 is given in the insert.

REF. N. V. Goncharov, A. I. Derebchinskii, O. G. Konovalov, S. G. Tonapetyan, and V. M. Khvorostyan
Yad. Fiz. 17, 242 (1973)
Sov. J. Nucl. Phys. 17, 124 (1973)

EL.EM. SYM.	A	Z
Si		14

METHOD

REF. NO. 73 Go 5 hmg

REACTION	RESULT	EXCITATION ENERGY	SOURCE		DETECTOR		ANGLE
			TYPE	RANGE	TYPE	RANGE	
G,PI+	ABY	170-400	C	400	BBL-D		90
G,PI-	ABY	170-400	C	400	BBL-D		90
G,P	ABY	82-400	C	400	BBL-D		90

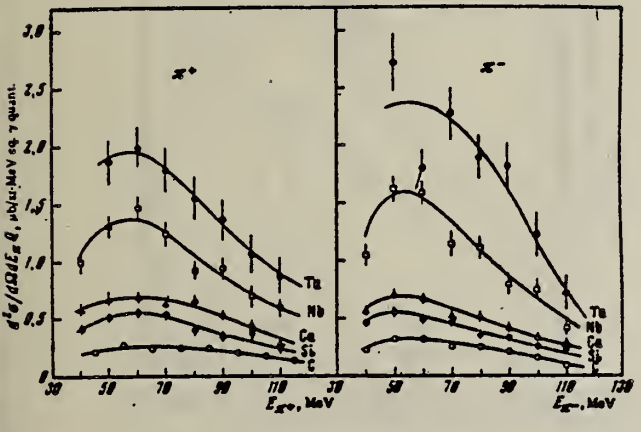

FIG. 2. Energy spectra of π^+ and π^- mesons, $E_\gamma^{max} = 400$ MeV, $\theta_{lab} = (90 \pm 7)°$.

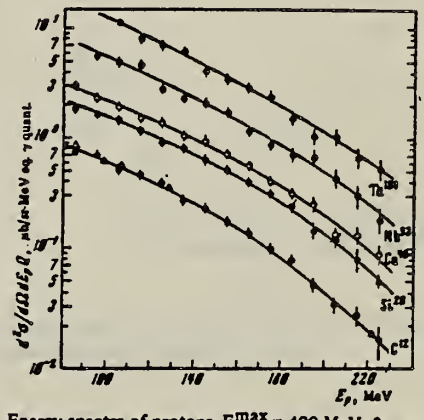

FIG. 3. Energy spectra of protons, $E_\gamma^{max} = 400$ MeV, $\theta_{lab} = (90 \pm 7)°$. Circles—present data, triangles—from [18].

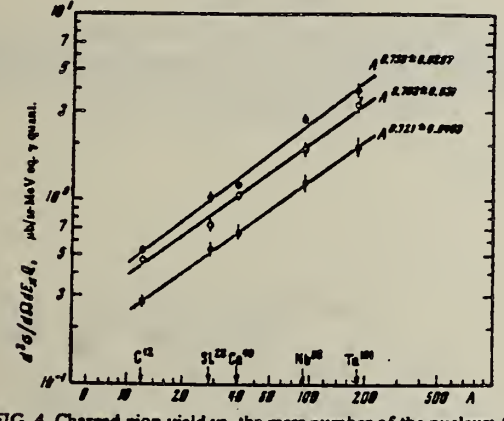

FIG. 4. Charged pion yield vs. the mass number of the nucleus: ●—$E_\gamma = 105 \pm 10$ MeV, ○—$E_\gamma = 85 \pm 10$ MeV, ◐—$E_\gamma = 65 \pm 10$ MeV.

[18] P. Dougan, W. Stiefler, LUSY preprint, 1001-1003, 1970.

(over)

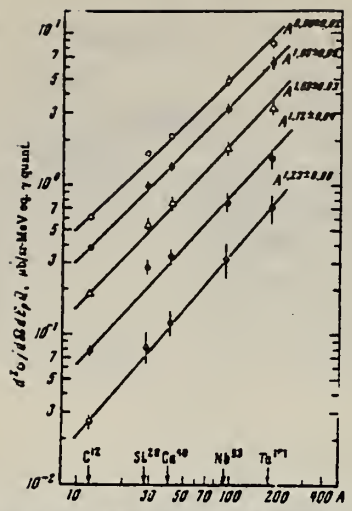

FIG. 5. Proton yields vs. mass number of the nucleus: ○–E_p = 100 ± 10 MeV, ●–E_p = 125 ± 15 MeV, Δ–E_p = 155 ± 15 MeV, ◐–E_p = 185 ± 15 MeV, ◒–E_p = 215 ± 15 MeV.

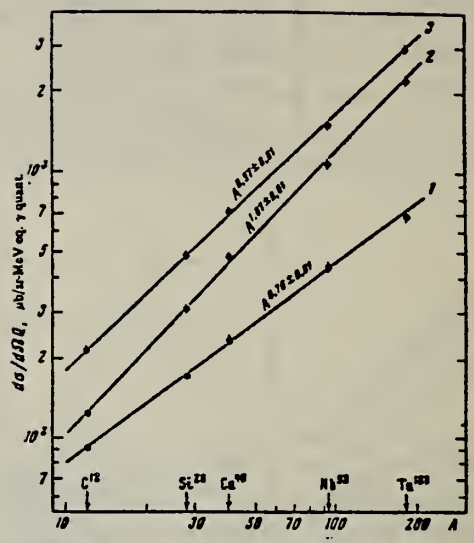

FIG. 6. Pion yield (1), proton yield (2), and summary pion and proton yield (3) vs. the mass number of the nucleus.

REF. A. Järund, B. Friberg, and B. Forkman
Z. Physik 262, 15 (1973)

ELEM. SYM.	A	Z
Si		14

METHOD

REF. NO. 73 Ja 3 egf

REACTION	RESULT	EXCITATION ENERGY	SOURCE TYPE	SOURCE RANGE	DETECTOR TYPE	DETECTOR RANGE	ANGLE
G,XXX	ABY	THR-999	C	100-999	ACT-I		4PI

XXX = NA-24, 999=1 GEV

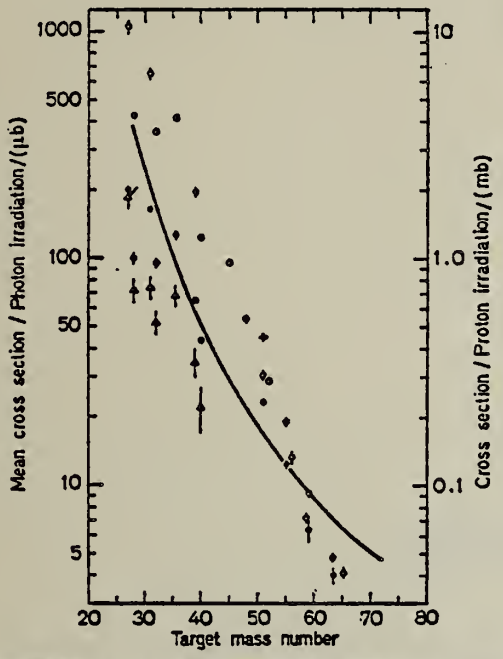

Fig. 7. Mean cross sections for ^{24}Na production as a function of target mass number. Present work filled circles. Noga *et al.* [3] open triangles, Kumbartzki *et al.* [13] cross and Korteling *et al.* [1] 400 MeV protons open circles. The solid line gives the mean cross sections calculated by Jonsson *et al.* [17]

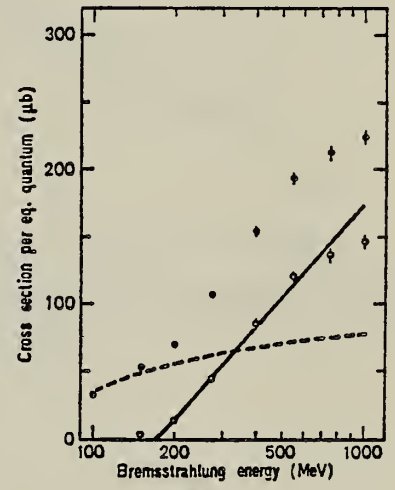

Fig. 2

Fig. 2. The determined yield for the reaction ^{28,29,30}Si → ^{24}Na (filled circles). Dashed line, solid line and open circles are interpreted as in Fig. 1

[1] Korteling, R.G. et al., J. Inorg. Nucl. Chem. 29, 2863 (1967).

[3] Noga, V.I. et al., Sov. J. Nucl. Phys. 9, 637 (1969).

[13] Kumbartzki, G. et al., Nucl. Phys. A176, 23 (1971).

[17] Jonsson, G.G. et al., LUNP7212, Oct. 1972, to be published in Physica Scripta.

REF.

A. Veyssiere, H. Beil, R. Bergere, P. Carlos, A. Lepretre, and A. De Miniac
Nucl. Phys. A227, 513 (1974)

C.M. SYM.	A	Z
Si		14

METHOD

REF. NO.	
74 Ve 1	egf

REACTION	RESULT	EXCITATION ENERGY	SOURCE		DETECTOR		ANGLE
			TYPE	RANGE	TYPE	RANGE	
G,N *	ABX	17- 30	D	17- 30	BF3-I		4PI

* 888

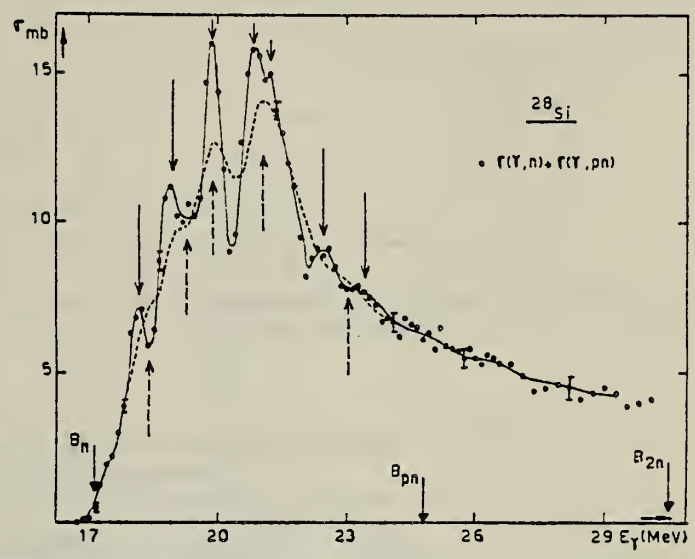

Fig. 2. Photoneutron cross section $\sigma_{Ta} = [\sigma(\gamma, n)+\sigma(\gamma, pn)]$ of ^{28}Si obtained with an energy resolution of $\Delta E = 180$ keV (full line and arrows) and with $\Delta E = 350$ keV (dashed line and arrows).

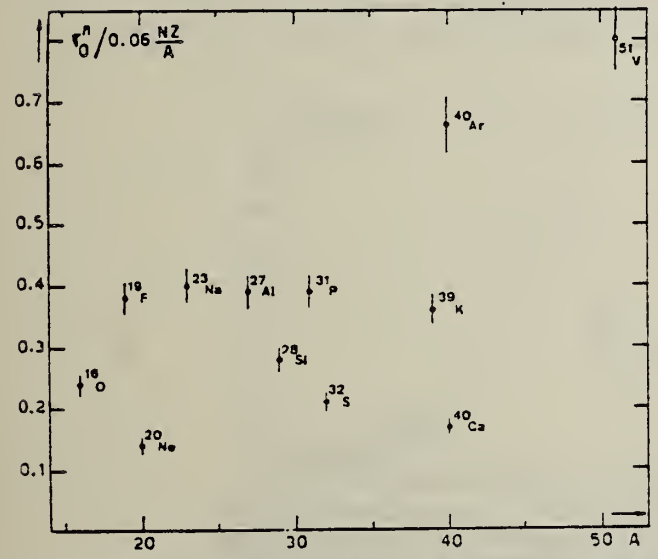

Fig. 22. Ratio of experimental integrated photoneutron cross section σ_0^n over the Thomas, Reiehe and Kuhn sum rule [0.06 NZ/A]. Numerical values and upper integration limits E_M are taken from table 3. Also $\Delta\sigma_0^n = \pm 7\%$ for all nuclei.

(over)

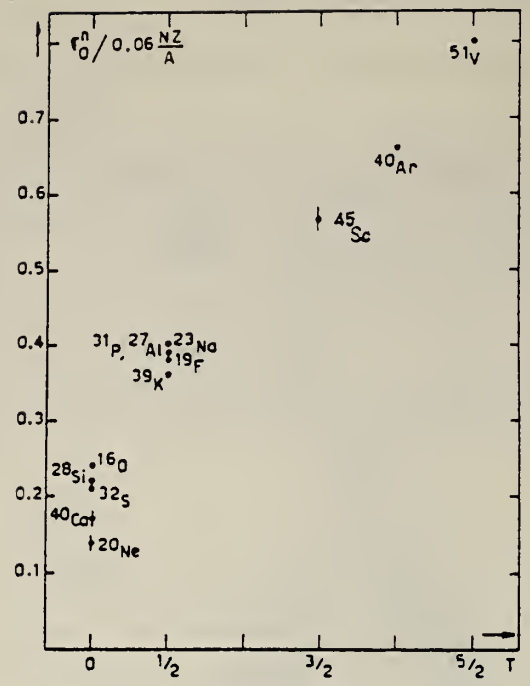

Fig. 24. The $[\sigma_0^n/(0.06\,NZ/A)]$ ratio as a function of isospin T. Possible overall errors of $\pm 7\%$ are to be applied to all nuclei shown.

TABLE 3

Experimental integrated photoneutron cross sections $\sigma_0^n = \int_0^{E_M} \sigma_{Tn}(E)\mathrm{d}E$ compared with the classical sum rule $[0.06\,NZ/A]$ of Thomas, Reich and Kuhn

	$T=0$					$T=\frac{1}{2}$					$T=\frac{3}{2}$	$T=2$	$T=\frac{5}{2}$
Nucleus	^{16}O	^{20}Ne	^{28}Si	^{32}S	^{40}Ca	^{19}F	^{23}Na	^{27}Al	^{31}P	^{39}K	^{45}Sc	^{40}Ar	^{51}V
σ_0^n (MeV · mb)	58 ±4	42 ±3	94 ±7	98 ±7	100 ±7	108 ±7	137 ±9	158 ±10	182 ±12	210 ±14	383 ±25	393 ±28	602 ±42
$\sigma_0^n/(0.06NZ/A)$	0.24	0.14	0.22	0.21	0.17	0.38	0.40	0.39	0.39	0.36	0.57	0.66	0.8
E_M (MeV)	30	26.7	30	30	29.5	29	30	30	29	30	28.1	26.7	28

REF.		ELEM. SYM.	A	Z
	J. Ahrens, H. Borchert, K.H. Czock, H.B. Eppler, H. Gimm, H. Gundrum, M. Kroning, P. Riehn, G. Sita Ram, A. Zieger, and B. Ziegler Nucl. Phys. A251, 479 (1975)	Si		14

METHOD	REF. NO.	
	75 Ah 3	egf

REACTION	RESULT	EXCITATION ENERGY	SOURCE		DETECTOR		ANGLE
			TYPE	RANGE	TYPE	RANGE	
G,MU-T	ABX	10- 30	C	140-275	MGC-D		4PI

932+

TABLE 2

The moments of the experimental nuclear cross section distributions integrated from 10 MeV to the energy E, and their statistical errors

	E (MeV)	$\sum_{-2}$ (mb/MeV)	±(%)	$\sum_{-1}$ (mb)	±(%)	$\sum_{0}$ (mb·MeV)	±(%)	$\sum_{+1}$ (b·MeV^{-1})	±(%)	$\sum_{+2}$ (b·MeV^{2})	±(%)
Li	100	0.196	1.1	4.64	1.0	143	1.7	5.82	3.1	305	5
	140	0.197	1.1	4.79	1.0	161	1.9	8.03	3.4	577	5
	210	0.198	1.1	5.03	1.0	206	2.0	16.60	3.7	2220	5
Be	100	0.192	2.5	5.19	1.5	173	2.0	7.11	3.4	362	5
	140	0.194	2.5	5.33	1.5	189	2.1	9.09	3.6	600	6
	210	0.195	2.5	5.58	1.5	236	2.1	17.80	3.5	2240	5
C	100	0.313	1.7	8.81	1.1	291	1.6	12.00	2.9	630	4
	140	0.316	1.7	9.18	1.2	334	2.2	17.10	5	1250	7
O	100	0.580	1.6	14.50	1.3	432	2.0	16.00	4	748	8
	140	0.585	1.6	15.10	1.3	508	2.5	25.20	5	1880	8
Al	100	1.10	1.8	25.70	1.5	739	2.6	27.9	5	1400	8
	140	1.11	1.8	26.3	1.7	807	3.9	36.4	9	2450	16
Ca	100	2.22	1.2	45.5	1.5	1120	3.6	34.9	9	1430	18
	140	2.23	1.2	46.8	1.7	1290	4.6	56.6	11	3710	19

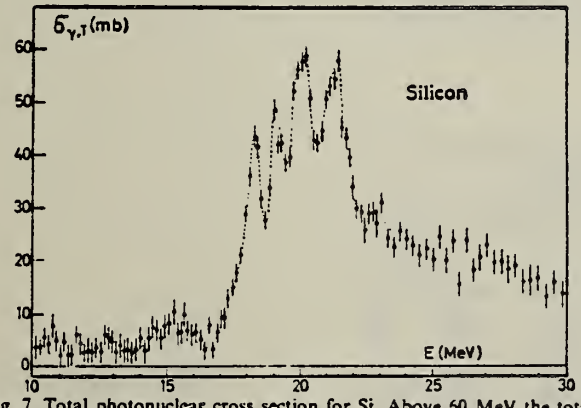

Fig. 7. Total photonuclear cross section for Si. Above 60 MeV the total attenuation cross section of Si displays a structure which can qualitatively be described by coherent pair production in the monocrystalline absorber rods (Überall effect) [11]). A more accurate measurement of this effect is in preparation. An unambiguous determination of the nuclear cross section above 50 MeV therefore turned out to be impossible.

REF.

V. di Napoli, G. Rosa, F. Salvetti, M. L. Terranova, H. G. de Carvalho, J. B. Martins, O. A. P. Tavares
J. Inorg. Nucl. Chem. 37, 1101 (1975)

ELEM. SYM.	A	Z
Si		14

METHOD

REF. NO. 75 Di 4 egf

REACTION	RESULT	EXCITATION ENERGY	SOURCE		DETECTOR		ANGLE
			TYPE	RANGE	TYPE	RANGE	
G,F18	ABY	THR-999	C	300-999	ACT-I		4PI
G,NA22	ABY	THR-999	C	300-999	ACT-I		4PI
G,NA24	ABY	THR-999	C	300-999	ACT-I		4PI

999 = 1 GEV

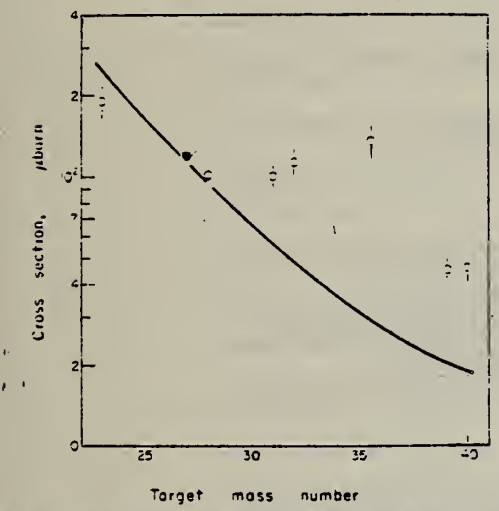

Fig. 2. Mean absolute cross section of ^{18}F photoproduction vs the target mass number. Open triangle: energy range 0·15–0·72 GeV, Ref. [18]. Filled circle: energy range 0·3–1 GeV. Ref. [3]. Open circles: present work. The curve has been calculated by means of Eqn (1).

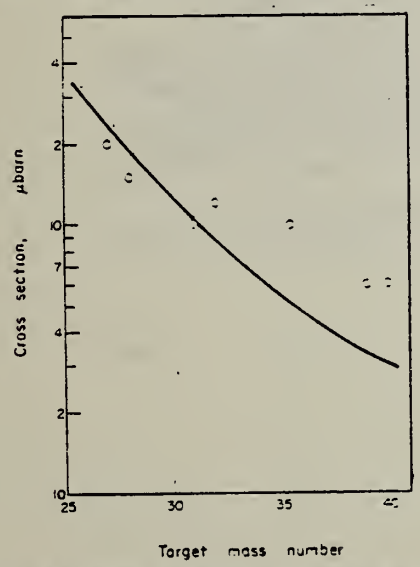

Fig. 3. Mean absolute cross section of ^{22}Na photoproduction vs the target mass number. The curve has been calculated by means of Eqn (1).

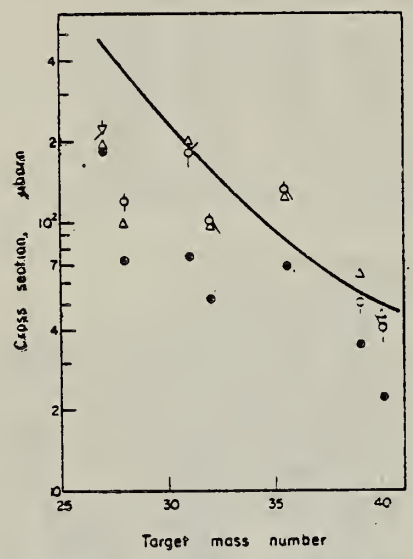

Fig. 4. Mean absolute cross section of ^{24}Na photoproduction vs the target mass number. Filled circles: energy range 0·1–1 GeV. Ref. [20]. Reversed open triangle: energy range 0·3–1 GeV, Ref. [8]. Open triangles: energy range 0·25–1 GeV, Ref. [19]. Open circles: present work. The curve has been calculated by means of Eqn (1).

Table 2. Cross-section per equivalent quantum $\alpha_0(\mu b)$ of photoproduction of ^{18}F

Target nucleus	Bremsstrahlung maximum energy E_0(GeV)				
	0·30	0·40	0·55	0·75	1·00
^{23}Na	590 ± 30	640 ± 30	720 ± 30	780 ± 30	830 ± 30
^{27}Al*	116 ± 7	172 ± 6	202 ± 6	245 ± 5	270 ± 5
^{28}Si	80 ± 10	110 ± 10	145 ± 10	170 ± 10	200 ± 10
^{31}P	60 ± 10	90 ± 10	130 ± 10	150 ± 10	180 ± 10
^{32}S	55 ± 10	90 ± 10	125 ± 10	160 ± 10	190 ± 10
^{35,37}Cl	185 ± 20	230 ± 20	270 ± 20	310 ± 20	350 ± 20
^{39}K	35 ± 5	50 ± 5	65 ± 5	75 ± 5	90 ± 5
^{40}Ca	5 ± 2	20 ± 3	35 ± 5	45 ± 5	60 ± 5

*The results for ^{27}Al have already been published (see[3]) and are reported for comparison.

(over)

Table 3. Cross-section per equivalent quantum $\sigma_Q(\mu b)$ of photoproduction of ^{22}Na

Target nucleus	Bremsstrahlung maximum energy E_0 (GeV)				
	0·30	0·40	0·55	0·75	1·00
^{27}Al	490 ± 20	560 ± 20	667 ± 20	690 ± 20	745 ± 20
^{28}Si	290 ± 20	330 ± 20	380 ± 20	430 ± 20	470 ± 20
^{31}P	230 ± 20	250 ± 20	290 ± 20	330 ± 20	350 ± 20
^{32}S	206 ± 10	240 ± 10	280 ± 10	320 ± 10	350 ± 10
$^{35,37}Cl$	230 ± 10	260 ± 10	290 ± 10	320 ± 10	350 ± 10
^{39}K	30 ± 3	50 ± 5	65 ± 5	80 ± 5	100 ± 5
^{40}Ca	5 ± 2	20 ± 3	45 ± 5	60 ± 5	60 ± 5

Table 4. Cross-section per equivalent quantum $\sigma_Q(\mu b)$ of photoproduction of ^{24}Na

DI Target nucleus	Bremsstrahlung maximum energy E_0 (GeV)				
	0·30	0·40	0·55	0·75	1·00
$^{27}Al^*$	370 ± 10	440 ± 10	500 ± 20	550 ± 20	660 ± 20
^{28}Si	100 ± 10	140 ± 10	160 ± 10	210 ± 10	240 ± 10
^{31}P	100 ± 20	160 ± 20	200 ± 20	270 ± 20	310 ± 20
^{32}S	120 ± 10	160 ± 10	180 ± 10	210 ± 10	240 ± 10
$^{35,37}Cl$	65 ± 10	100 ± 10	140 ± 10	190 ± 10	220 ± 10
^{39}K	20 ± 5	35 ± 5	55 ± 5	65 ± 5	80 ± 5
^{40}Ca	12 ± 3	25 ± 5	35 ± 5	50 ± 5	60 ± 5

*The results for ^{27}Al have already been published (see [8]) and are reported for comparison.

Table 5. Mean absolute cross-section $\bar{\sigma}_x(\mu b)$ in the energy range 0·3–1 GeV

Target nucleus	Produced radionuclide		
	^{18}F	^{22}Na	^{24}Na
^{23}Na	190 ± 30		
$^{27}Al^*$	120 ± 10	200 ± 20	220 ± 20
^{28}Si	100 ± 10	150 ± 20	120 ± 10
^{31}P	100 ± 10	100 ± 20	180 ± 20
^{32}S	110 ± 10	120 ± 10	100 ± 10
$^{35,37}Cl$	135 ± 20	100 ± 10	130 ± 10
^{39}K	45 ± 5	60 ± 5	50 ± 5
^{40}Ca	46 ± 5	60 ± 5	40 ± 5

*The results for the photoproduction of ^{18}F and ^{24}Na from ^{27}Al have already been published (Ref. [3] and [8], respectively).

2. V. di Napoli and M. L. Terranova, *J. inorg. nucl. Chem.* 36, 3633 (1974).
3. V. di Napoli, A. M. Lacerenza, F. Salvetti, S. M. Terenzi, H. G. de Carvalho and J. B. Martins, *J. inorg. nucl. Chem.* 35, 1419 (1973).
4. C. M. Lederer, J. M. Hollander and I. Perlman, *Table of Isotopes.* 6th Edn Wiley, New York (1967).
5. R. G. Korteling and A. A. Caretto, Jr., *J. inorg. nucl. Chem.* 29, 2863 (1967).
6. R. G. Korteling and A. A. Caretto, Jr., *Phys. Rev.* C1, 193 (1970).
7. R. G. Korteling and A. A. Caretto, Jr., *Phys. Rev.* C1, 1960 (1970).
8. V. di Napoli, A. M. Lacerenza, F. Salvetti, H. G. de Carvalho and J. B. Martins, *Lett. Nuovo Cimento* 1, 835 (1971).
9. I. Halpern, R. J. Debs, J. T. Eisinger, A. W. Fairhall and H. G. Richter, *Phys. Rev.* 97, 1327 (1955).
10. C. B. Fulmer, K. S. Toth, I. R. Williams, T. H. Handley, C. F. Dell, E. L. Callis, T. M. Jenkins and J. M. Wyckoff, *Phys. Rev.* C2, 1371 (1970).
11. G. J. Kumbartzki, U. Kim and C. K. Kwan, *Nucl Phys.* A160, 237 (1970).
12. G. J. Kumbartzki and U. Kim, *Nucl. Phys.* A176, 23 (1971).
13. K. Lindgren and G. G. Jonsson, *Nucl. Phys.* A197, 71 (1972).
14. C. E. Roos and V. Z. Peterson, *Phys. Rev.* 124, 1610 (1961).
15. T. A. Gabriel and R. G. Alsmiller, Jr., *Phys. Rev.* 182, 1035 (1969).
16. G. G. Jonsson and K. Lindgren, *Phys. Scr.* 7, 49 (1973).
17. G. Rudstam, *Z. Naturf.* 21a, 1027 (1966).
18. A. Masaike, *J. phys. Soc. Japan* 19, 427 (1964).
19. A. Jārund, B. Friberg and B. Forkman, Private communication to G. G. Jonsson and K. Lindgren, quoted in Ref. [16]; see also A. Jārund, B. Friberg and B. Forkman, University of Lund Report No. LUNP-7303, 1973 (unpublished).
20. V. I. Noga, Yu. N. Ranyuk and P. V. Sorokin, *Yad. Fiz.* 9, 1152 (1969) (transl.: *Sov. J. Nucl. Phys.* 9, 673 (1969)).
21. T. Methasiri and S. A. E. Johansson, *Nucl. Phys.* A167, 97 (1971).
22. J. R. Nix and E. Sassi, *Nucl. Phys.* 81, 61 (1966).
23. W. D. Myers and W. J. Swiatecki, *Nucl. Phys.* 81, 1 (1966).

REF. A. S. Danagulyan, N. A. Demekhina
Yad. Fiz. 24, 681 (1976)
Sov. J. Nucl. Phys. 24, 355 (1976)

ELEM. SYM.	A	Z
Si		14

METHOD

REF. NO. 76 Da 4 hmg

REACTION	RESULT	EXCITATION ENERGY	SOURCE TYPE	SOURCE RANGE	DETECTOR TYPE	DETECTOR RANGE	ANGLE
G,NA24	ABX	THR* 5	C	2* 5	ACT-I		4PI

*ENERGY, GEV

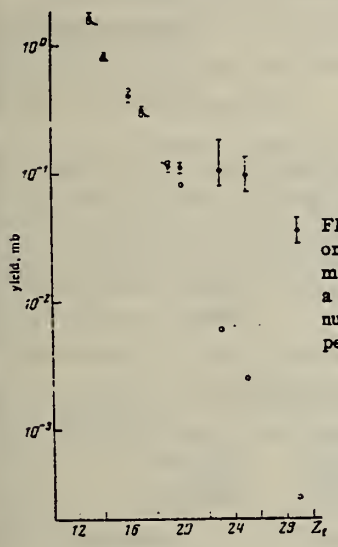

FIG. 2. Yield values and theoretical values according to the modified Rudstam formula as a function of the target charge number Z_t. Points: ●—experiment, ○—theory.

TABLE I. Experimental yields and reaction cross sections obtained in the measurements at the Erevan electron accelerator.

Target nucleus	Reaction yield, mb $E_{\gamma\ max}$, GeV					Reaction cross section, mb
	2	3	4	4.5	5	
^{27}Al	0.81±0.08	0.87		0.87		0.07213±0.0346
^{28}Si	0.27±0.02	0.28		0.29		0.0267±0.013
^{32}S	0.24±0.02	0.22		0.27		0.0323±0.0155
Cl	0.28±0.03	0.30		0.28		–
^{39}K	0.1±0.01	0.125		0.15		0.06±0.0288
^{40}Ca	0.066±0.01	0.09		0.115		0.035±0.0168
^{51}V	0.085±0.02	0.094±0.02	0.098±0.02		0.082±0.025	0.019
^{55}Mn	0.079±0.02	0.075±0.02	0.087±0.017		0.088±0.015	0.01076±0.0056
Cu	0.029±0.006	0.037±0.007	0.036±0.007		0.034±0.007	0.00547±0.0028

Note. The reaction cross sections have been calculated in the $1/E$ approximation of the bremsstrahlung spectrum.

REF.

J. Mougey, M. Bernheim, A. Bussiere, A. Gillebert, Phan Xuan Ho, M. Priou, D. Royer, I. Sick, G. J. Wagner
Nucl. Phys. A262, 461 (1976)

ELEM. SYM.	A	Z
Si		14

METHOD

REF. NO.: 76 Mo 5 egf

REACTION	RESULT	EXCITATION ENERGY	SOURCE		DETECTOR		ANGLE
			TYPE	RANGE	TYPE	RANGE	
E,E/P	ABX	10* 65	D	497	MAG-D		53

*MISSING ENERGY

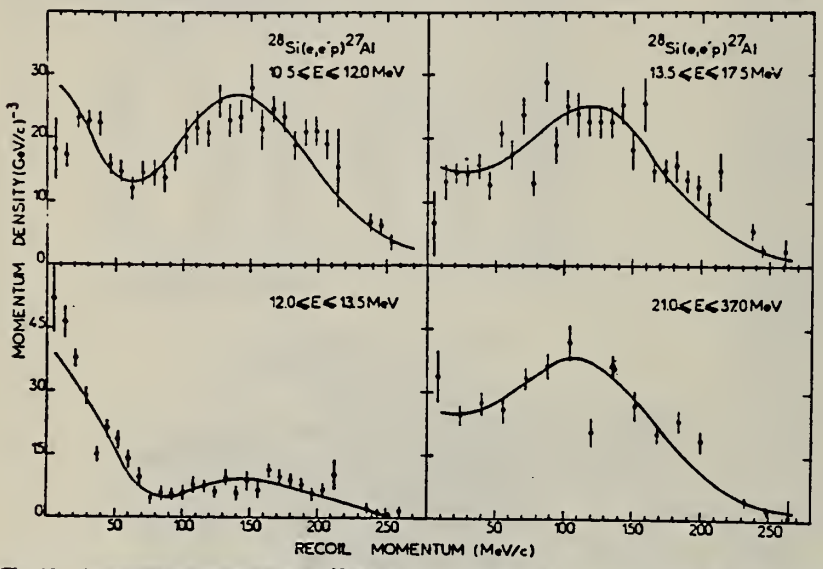

Fig. 12. Momentum distributions from ^{28}Si(e, e'p); (a) $10.5 \leq E \leq 12$ MeV, (b) $12 \leq E \leq 13.5$ MeV, (c) $13.5 \leq E \leq 17.5$ MeV and (d) $21 \leq E \leq 37$ MeV. The solid line represents the DWIA calculation.

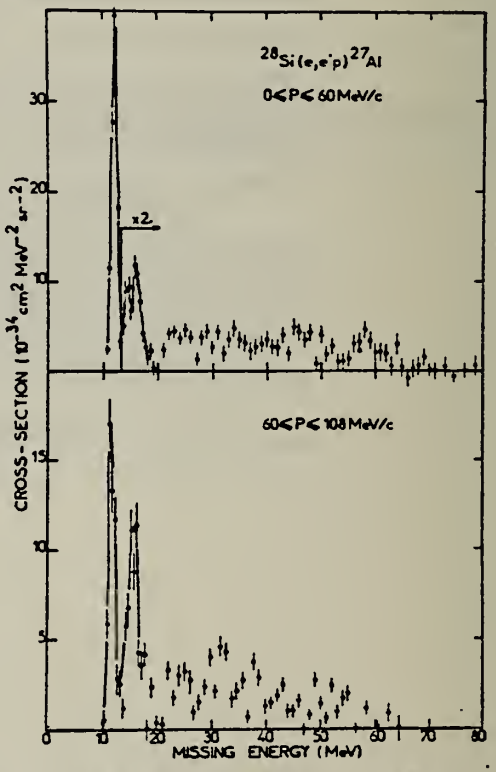

Fig. 11. Missing energy spectra from ^{28}Si(e, e'p); (a) $0 \leq P \leq 60$ MeV/c and (b) $60 \leq P \leq 180$ MeV/c.

REF.	ELEM. SYM.	A	Z
B.S. Ishkhanov, Yu.A. Novikov, E.S. Omarov, I.M. Piskarev Sov. J. Nucl. Phys. 32, 757 (1980) Yad. Fiz. 32, 1465 (1980)	Si		14

METHOD	REF. NO.
	80 Is 6 hg

REACTION	RESULT	EXCITATION ENERGY	SOURCE		DETECTOR		ANGLE
			TYPE	RANGE	TYPE	RANGE	
G,G	ABX	13 - 31	C	13 - 31	NAI-D		90

Natural isotopic composition target

B. S. Ishkhanov, Yu. A. Novikov, E. S. Omarov, and I. M. Piskarev

Institute of Nuclear Physics, Moscow State University

(Submitted 21 February 1980)
Yad. Fiz. 32, 1465–1475 (December 1980)

The energy spectra of photons scattered at 90° by ^{28}Si and ^{52}Cr targets have been measured in the betatron bremsstrahlung beam at 16 values of the maximum bremsstrahlung energy from 13.1 to 31 MeV. The photon elastic scattering cross sections in the vicinity of the giant resonance, as well as the cross sections for photon inelastic scattering with excitation of the 1.75 and 4.98 MeV levels of ^{28}Si and the 1.43 and 2.98 MeV levels of ^{52}Cr, were calculated from the spectra. A dispersion-theory analysis of the results enabled us to identify the peaks in the cross sections for which $E1$ photoabsorption is dominant. The experimental data are compared with the results of shell-model and simple-rotator-model calculations. The nature of the peaks observed in the scattering cross sections is discussed.

PACS numbers: 25.20. + y, 27.30. + t, 27.40. + z

TABLE I. Integrated characteristics of scattering process for ^{28}Si and ^{52}Cr targets.

Target nucleus	Process	Integrated cross section (MeV · mb) out to 32 MeV: The present work	Other studies
^{28}Si, mass, 159 g	Elastic scattering	2.2±0.4	2.8±0.4 [1] 2.0±0.5 [2]
	NRE (1.78 MeV, $J^\pi = 2^+$)	0.8±0.3	Not observed [1]
	Inelastic scattering to the 4.98 MeV 0^+ level	0.7±0.4	–
	Inelastic scattering to the 5.3 MeV 2^+ level	0.24±0.02	–
^{52}Cr, mass, 150 g	Elastic scattering	6.0±0.5	5.5±0.5 [2]
	NRE (1.43 MeV $J^\pi = 2^+$)	3.0±0.5	3.8±0.7 [1] 0.6±0.2 [2]
	Inelastic scattering to the 2.96 MeV 2^+ level	1.2±0.5	

[1] J. - M. Loisequx *et al.*, J. Phys. (Paris) 28, 11 (1967).
[2] J. Ahrens *et al.*, Phys. Lett. 31B, 570 (1979).

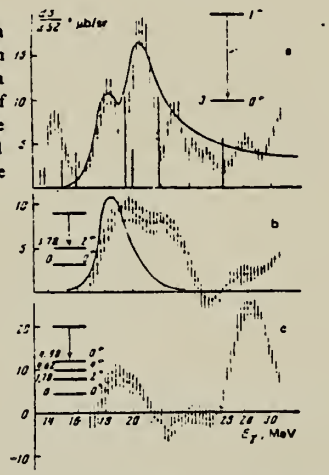

FIG. 1. a) Photon elastic scattering differential cross section for ^{28}Si. The full curve was calculated using the simple rotator model. The vertical bars were calculated using the shell model.[25] b) The NRE differential cross section for ^{28}Si. The full curve was calculated using the simple rotator model. c) Photon inelastic scattering differential cross section for excitation of the 4.98 MeV $J^\pi = 0^+$ level of ^{28}Si.

TABLE II. Levels populated in photon elastic and inelastic scattering from ^{28}Si.

Total absorption		Elastic scattering (the present work)		Inelastic scattering to the indicated levels (the present work)				$\frac{\sigma_{tot}}{\sigma_{el}}$, b	σ_{tot}, b
Total absorption [1]				1.78 MeV		4.98 MeV			
E_γ, MeV	σ, mb	E_γ, MeV	σ, μb	E_γ, MeV	σ, μb	E_γ, MeV	σ, μb		
–	–	14.5±0.3	80±20	–	–	–			
15.3	10	–	–	–	–	–	–	–	
18.2	40	18.2±0.3	80±20	–	–	–	–	20±5	22
19.0	45	–	–	19.0±0.5	80±20	19.0±0.5	80±20	–	–
20.0	55	20.5±0.5	210±40	–	–	–	–	14.5±4	17.1
21.5									
23.0	25.0	23.0±0.5	60±20	23.0±0.5	70±20	–	–	10.4±3	13.7
27.4	–	28.0±0.5	50±15	–	–	28.0±0.5	280±50	–	–
28.8									

[1] According to (γ, n) data.[3]

A=28

A=28

REF.

R. H. Helm
Phys. Rev. 104, 1466 (1956)

ELEM. SYM.	A	Z
Si	28	14

METHOD

REF. NO. 56 He 3 hmg

REACTION	RESULT	EXCITATION ENERGY	SOURCE		DETECTOR		ANGLE
			TYPE	RANGE	TYPE	RANGE	
E,E/	FMF	1-7	D	187	MAG-D		DST

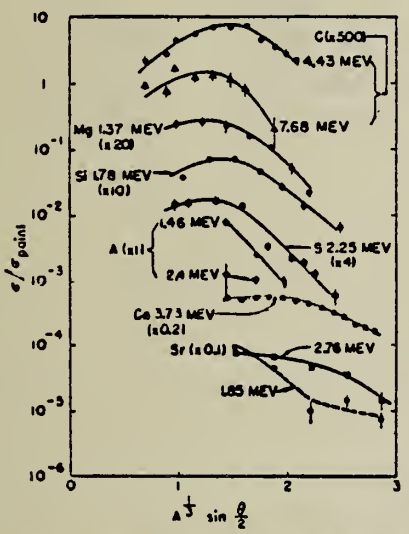

FIG. 3. Inelastic angular distributions (observed cross section divided by Feshbach point-charge cross sections). The results of Hahn *et al.* (reference 8) for Ca and of Fregeau and Hofstadter (reference 11) are included for comparison.

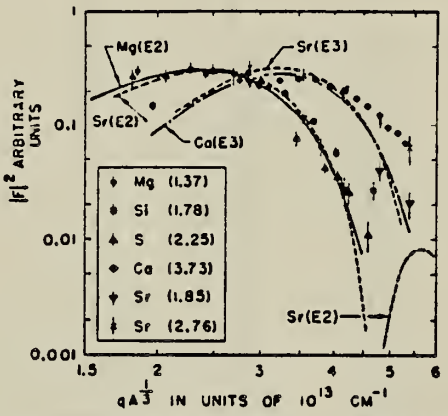

FIG. 7. Inelastic "universal curves." A composite plot of inelastic data from Mg, Si, S, Ca, and Sr against $qA^{\frac{1}{3}}$. The various form factors are arbitrarily normalized to minimize the spread of points. The point from sulfur and the point from silicon which seem to deviate from the "universal curve" are assumed to contain undetected experimental errors. The curves labeled Mg($E2$), Sr($E2$), Ca($E3$), and Sr($E3$) are calculated for electric-quadrupole and-octupole transitions using the "smeared δ-function" transition charge densities of Sec. V, and are arbitrarily normalized.

Ref. W.C. Barber, F. Berthold, G. Fricke, F.E. Gudden
Phys. Rev. 120, 2081 (1960)

Elem. Sym.	A	Z
Si	28	14

Method Stanford Mark II Linac; magnetic spectrometer; plastic scintillator counter telescope

Ref. No. 60 Ba 4 JHH

Reaction	E or ΔE	E_o	Γ	$\int \sigma dE$	Jπ	Notes
$(e^-,e^{-\prime})$	42.5	11.6				Both E_o measurement at $\theta = 160^\circ$
		20		125^{+125}_{-40} MeV-mb		(Giant Resonance)

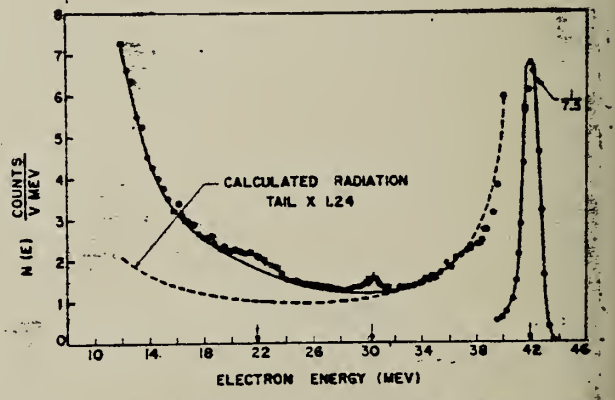

FIG. 9. Energy distribution of electrons, which were initially 42.5 Mev, after 160° scattering from a Si target.

M. Kimura, K. Shoda, N. Mutsuro, T. Tohei, K. Sato, K. Kuroda, K. Kuriyama, T. Ariba
J. Phys. Soc. Japan 15, 1128 (1960)

ELEM. SYM.	A	Z
Si	28	14

METHOD: Cyclotron; inverse; NaI spectrometer

REF. NO.: 60 Ki 3 NVB

REACTION	RESULT	EXCITATION ENERGY	SOURCE TYPE	SOURCE RANGE	DETECTOR TYPE	DETECTOR RANGE	ANGLE
P,G	RLX	19-26	D	8-15 (7.5-14.7)	NAI-D	,	90°

Resonances at:

E_p	E_γ
7.61 MeV	18.94 MeV
8.75 MeV	20.04 MeV
10.13 MeV	21.37 MeV

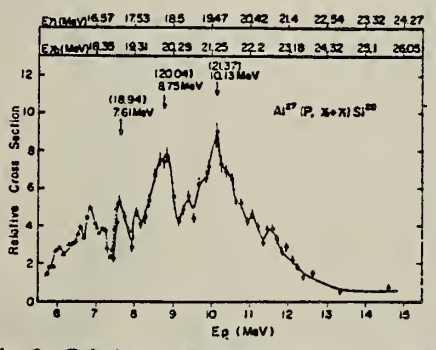

Fig. 2. Relative cross section curve for $Al^{27}(p, \gamma_0+\gamma_1)Si^{28}$ as a function of proton energy.

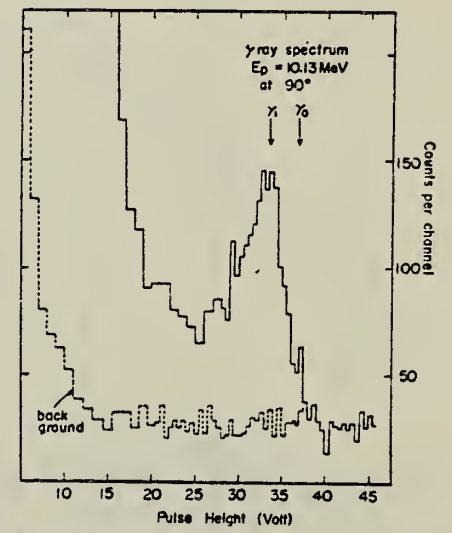

Fig. 1. Example of the gamma ray spectrum and the background spectrum without target.

Ref. **R.A. Tobin**
Phys. Rev. 120 (175 (1960)

Elem. Sym.	A	Z
Si	28	14

Method
Betatron, Si absorber and scatterer; NaI

Ref. No. **60 To 1** **JH**

Reaction	E or ΔE	E_o	Γ	∫σdE	Jπ	Notes
(γ,γ)	**Bremss; 13.1**		$2.89^{+0.99}_{-0.78}$ eV		1	$E_{thresh.}$ = 11.40 ± 0.06 MeV

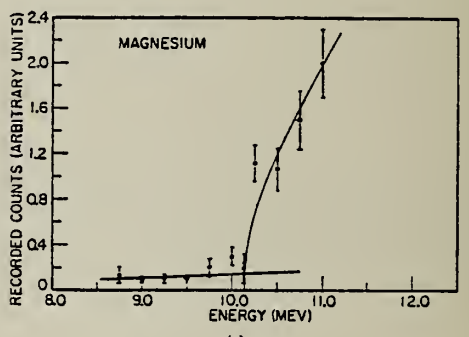

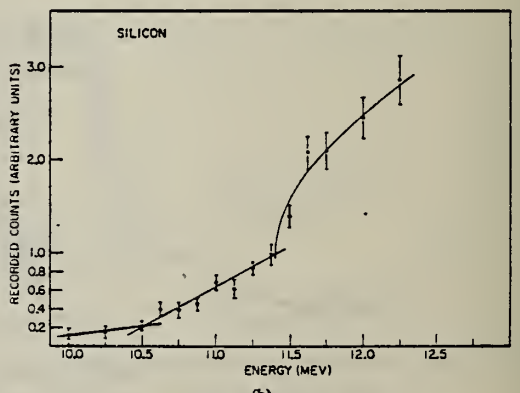

FIG. 4. Thresholds for the levels in Mg and Si.

REF.

T.G. Walker, W.T. Morton
Proc. Phys. Soc. 75, 4 (1960)

ELEM. SYM.	A	Z
Si	28	14

METHOD

Synchrotron; proton-neutron cross section; radioactivity

REF. NO. 60 Wa 2 NVB

REACTION	RESULT	EXCITATION ENERGY	SOURCE		DETECTOR		ANGLE
			TYPE	RANGE	TYPE	RANGE	
G, 5P4N	ABX	0-240	C	240	ACT-I		4PI

$\sigma = (0.06 \pm 0.01)\ 10^{-27} cm^2$/equivalent quantum

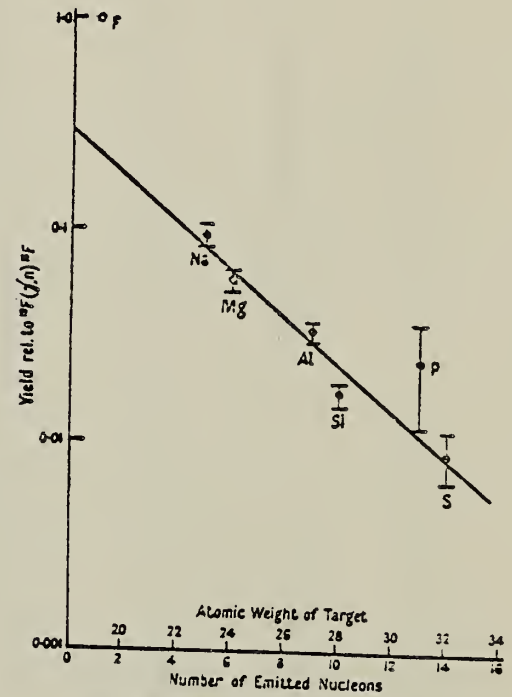

Yields relative to $^{19}F(\gamma, n)^{18}F$ at 240 Mev.

Ref. A.K. Berzin, R.P. Meshcheryakov
Zhur. Eksp. i Teoret. Fiz. 41, 1013 (1961)
Soviet Phys. JETP 14, 721 (1962)

Elem. Sym.	A	Z
Si	28	14

Method
Betatron; activation

Ref. No. 61 Be 1 JH

Reaction	E or ΔE	E_o	Γ	$\int \sigma dE$	Jπ	Notes
(γ,n)						$E_{thresh.}$ = 17.14 ± .12 MeV

REF.

A. Bussiere de Nercy
Ann. Phys. (Paris) Third Series 6, 1379 (1961)

ELEM. SYM.	A	Z
Si	28	14

METHOD

REF. NO.	
61 Bu 4	egf

REACTION	RESULT	EXCITATION ENERGY	SOURCE		DETECTOR		ANGLE
			TYPE	RANGE	TYPE	RANGE	
G,G *	ABX	11	C	11-16	NAI -D		UNK
G,G	ABX	15-30	C	32	NAI-D		140

*σ° = 19.7 ± 2.5 b

WIDTHS

Γ_0 = 114 ± 30 eV Γ_1 = 87 ± 25 eV

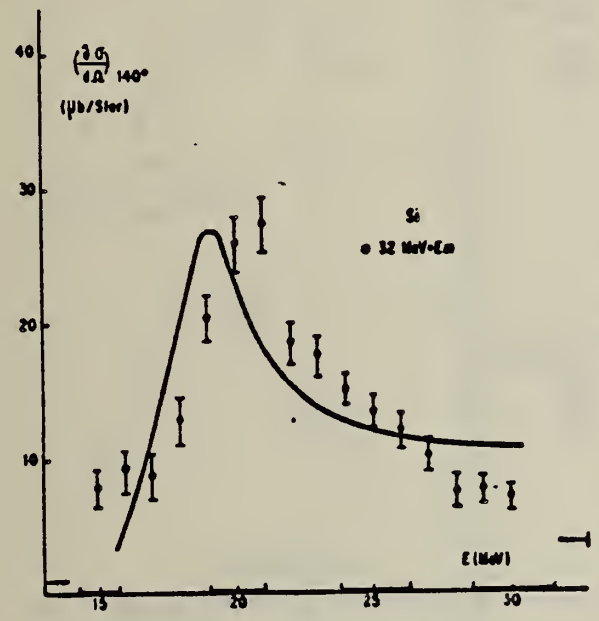

Fig. 20. — Section efficace différentielle de diffusion (γ, γ) à 140° pour le silicium.

REF.

C. C. Gardner and P. C. Gugelot
Proc. Int. Conf. Manchester 263 (1961)

ELEM. SYM.	A	Z
Si	28	14

METHOD

Cyclotron

REF. NO. 61 Ga 1 JDM

REACTION	RESULT	EXCITATION ENERGY	SOURCE		DETECTOR		ANGLE
			TYPE	RANGE	TYPE	RANGE	
P,G	ABX	16-25	D	5-13	NAI-D		90

8234

$\sigma_{int}(\gamma,p_o)$ = 0.10 MeV-barns.

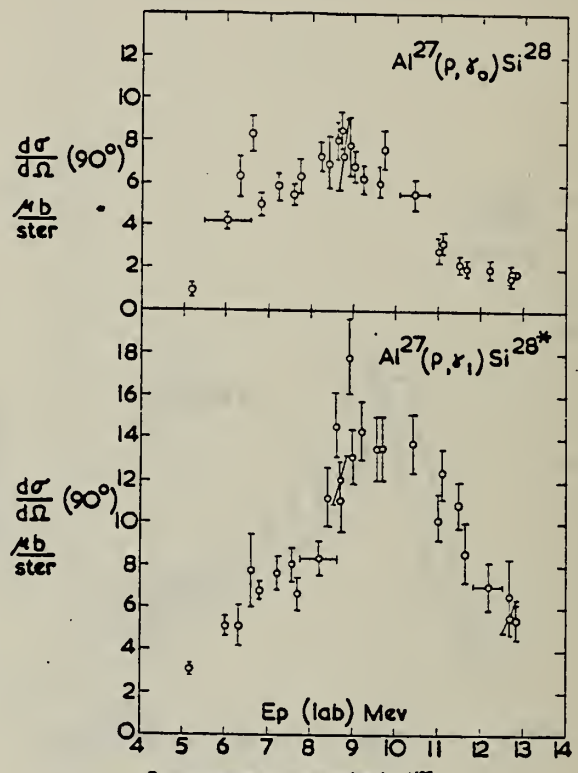

Proton capture cross-section in Al^{27}

γ_0, ground state transition; $E_{\gamma 0} = E_p(cm) + 11{\cdot}6$ MeV
γ_1, first excited state transition $E_{\gamma 1} = E_p(cm) + 9{\cdot}8$ MeV

Ref. H.E. Gove, A.E. Litherland, R. Batchelor
Nuclear Phys. 26, 480 (1961)

Elem. Sym.	A	Z
Si	28	14

Method Tandem accelerator; NaI

Ref. No. 61 Go 1 EH

Reaction	E or ΔE	E_o	Γ	∫σdE	Jπ	Notes
$Al^{27}(p,\gamma)$	2.6-11.4		Γ_p = 4.3MeV			Resolution limited by the target thickness.
		~ 19 MeV				E_{p_o} = 7.68 MeV; $\omega(\theta_\gamma)=1+(0.01\pm0.05)P_1+(0.35\pm0.07)P_2$
		~ 19.6				E_{p_o} = 8.27 MeV; $\omega(\theta_\gamma)=1-(0.09\pm0.05)P_1+(0.07\pm0.06)P_2$

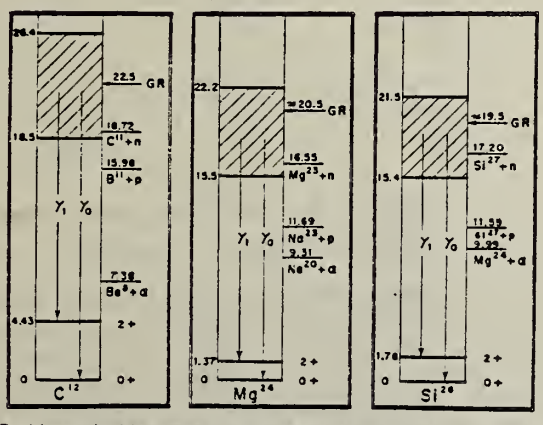

Fig. 1. Partial energy level diagrams for C^{12}, Mg^{24} and Na^{23} showing the region of excitation energy covered (shaded), the positions of the first excited states and the energies at which each nucleus becomes unstable against neutron, proton and alpha particle emission. The approximate position of the peak of the giant resonance (GR) is also indicated.

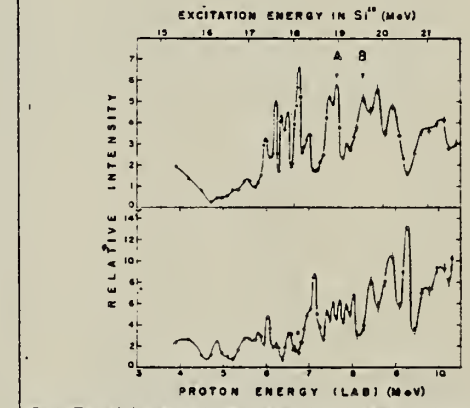

Fig. 16. The yield of gamma rays leading to the ground state (upper curve) and to the first excited state (lower curve) of Si^{28} resulting from proton capture in Al^{27} and measured at 90° to the incident beam. The ordinates of the two yield curves are correct relative to each other. The abscissae are marked both in terms of the incident laboratory proton energy and in excitation energy in the compound nucleus Si^{28}. A and B mark the energies at which angular distributions were measured.

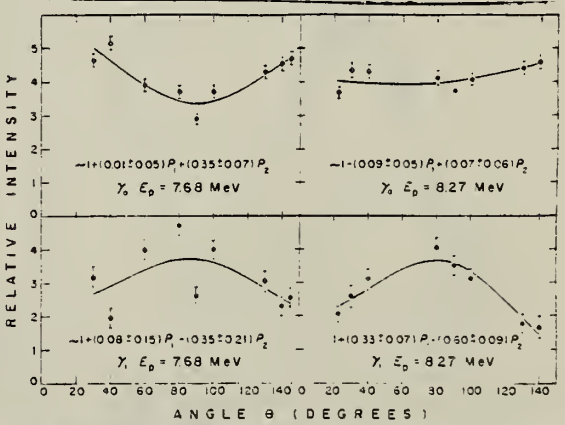

Fig. 17. Angular distributions of gamma rays leading to the ground state (γ_0) and to the first excited state (γ_1) of Si^{28} from the reaction Al^{27} (p, γ) measured at two proton energies of 7.68 and 8.27 MeV (corresponding to the positions A and B on the yield curve of fig. 14). The solid lines are least square Legendre polynomial fits and, in each case, values of the coefficients are given in the expressions $1+a_1P_1+a_2P_2$.

FORM NBS-418
(8-1-63)
USCOMM-DC 18556-P63

Ref. M. Kimura, K. Shoda, N. Mutsuro, T. Tohei, K. Sato, K. Kuroda, K. Kuriyama, T. Akiba
Nuclear Phys. 23, 338 (1961)

Elem. Sym.	A	Z
Si	28	14

Method: Variable energy cyclotron; NaI

Ref. No.: 61 Ki 1 EH

Reaction	E or ΔE	E_o	Γ	$\int \sigma dE$	Jπ	Notes
$Al^{27}(p,\gamma)$	7.5-14.7	..				$E_{\gamma o}$(calculated)=
		7.61				18.94 MeV
		8.75				20.04 MeV
		10.13				21.37 MeV
						$\sigma_{p,\gamma;max}$(10.13MeV) = (170±35) μb.
						Detector at 90°.

821

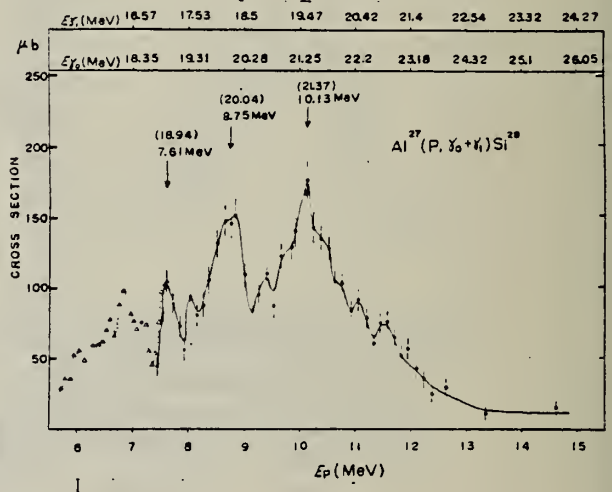

Figure 3: Relative cross section of the $Al^{27}(p,\gamma_o+\gamma_1)Si^{28}$ reaction. The lower abscissa is the laboratory photon energy, the upper abscissa, the calculated energy of γ_o and γ_1. The full line gives the present results; the broken line gives the Canberra results continued smoothly to the present results, neglecting the discrepancy in absolute cross sections.

Ref. K. Shoda, K. Kobayashi, S. Siina, K. Abe, M. Kimura
J. Phys. Soc. Japan 16, 1031 (1961)

Elem. Sym.	A	Z
Si	28	14

Method 24 MeV Bremss; emulsions; proton spectrum

Ref. No. 61 Sh 1 EH

Reaction	E or ΔE	E_o	Γ	$\int \sigma dE$	Jπ	Notes
$Si^{28}(\gamma,p)$	Bremss. 24					853

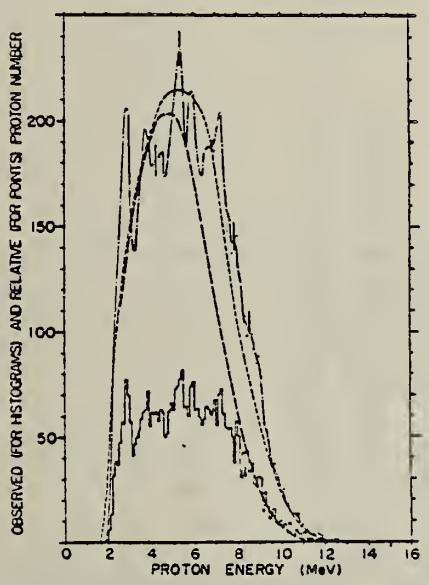

Fig. 1. The energy spectrum of photoprotons from Si. The solid line is a smoothed curve. The broken line and the dotted one are calculated curves of the statistical model with the level densities $\omega = C \exp[2\sqrt{0.45E}]\,MeV^{-1}$ and $\omega = C \exp[E/2.8]\,MeV^{-1}$, respectively.

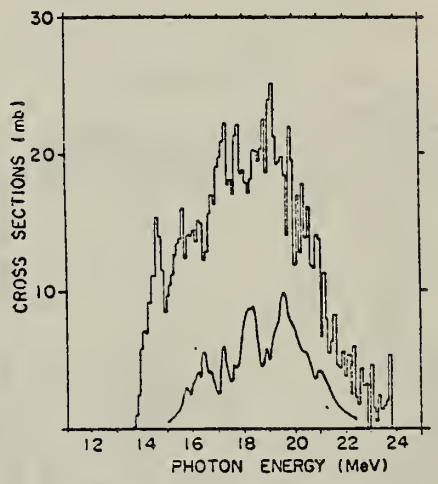

Fig. 2. The comparison of cross section of $Si^{28}(\gamma, p)Al^{27}$ (histogram) and that from $Al^{27}(p, \gamma)Si^{28}$ (solid line).

Ref.	Elem. Sym.	A	Z
P.G. Bizzeti, A.M. Bizzeti-Sona, M. Bocciolini, G. Di Caporiacco, M. Mandò, Nuovo Cimento 26, 1412 (1962)	Si	28	14

Method	Ref. No.
Van de Graaff; γ's from $Li^7(p,\gamma)$ reaction; solid state (silicon junction) detector	62 Bi 1 JHH

Reaction	E or ΔE	E_o	Γ	$\int \sigma dE$	Jπ	Notes
$Si^{28}(\gamma,p)$	17.6					E_p spectra in Figure 1, with E_α peaks included.
$Si^{28}(\gamma,\alpha)$	ΔE = 100 keV					Si detector irradiated giving 4π detector. σ fluctuations studied.

TABLE I.

Values of relative intensity of the various peaks with respect to p_0 (*)

θ	cos θ	Energy shift (keV)	$(p_1+p_2)/p_0$	p_1/p_0	p_2/p_0	α_0/p_0
0°	+1.00	+67.8	0.70±0.06	0.53±0.05	0.17±0.03	0.17±0.02
41° 30′	+0.75	+50.8	1.04±0.06	0.77±0.05	0.27±0.03	0.16±0.02
60°	+0.50	+33.9	1.44±0.08	0.90±0.05	0.54±0.03	0.15±0.02
75° 30′	+0.25	+16.9	1.73±0.10	0.87±0.06	0.86±0.06	0.17±0.02
90°	0	0	1.41±0.08	0.71±0.05	0.70±0.05	0.15±0.02
104° 30′	−0.25	−16.9	0.84±0.04	0.38±0.03	0.46±0.03	0.06±0.01
120°	−0.50	−33.9	0.84±0.05	0.43±0.03	0.41±0.03	< 0.03

(*) Errors shown are only statistical errors: maximum uncertainties of other origin (background evaluation, separation of neighbouring peaks, wall effects, etc.) are estimated to range from 15 to 7% for lower and higher values respectively. In addition a possible uncertainty in the geometrical conditions (estimated to be less than 2°) may introduce a systematic error in the value of the energy shift which ranges from 1.5 keV at 0° to 3.5 keV at 90°. The energy spread for every single point, however, is determined essentially by the width of the resonance as ±6 keV. The ratios shown were evaluated through an objective criterion suitably chosen for the best separation of the peaks: as a result, the values may be expected to differ somewhat from the cross-section ratios for transitions to the corresponding final levels. They are, however, proportional to them through a factor which is about 1 and does not depend on energy.

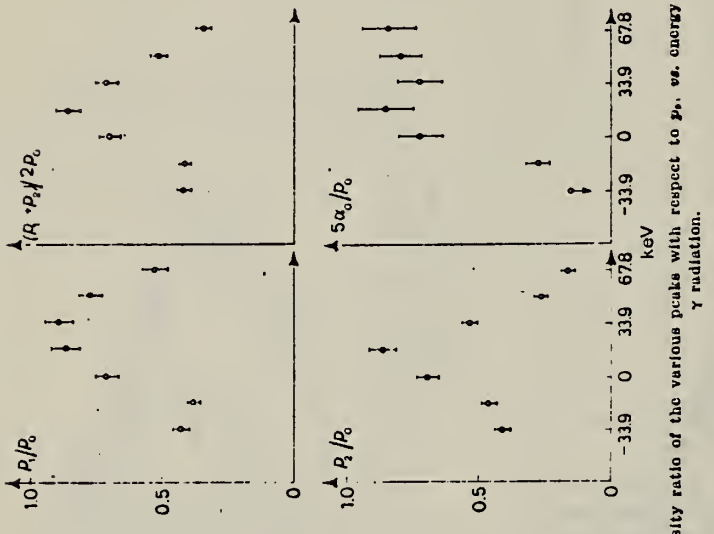

Fig. 2. – Intensity ratio of the various peaks with respect to p_0 vs. energy shift of incident γ radiation.

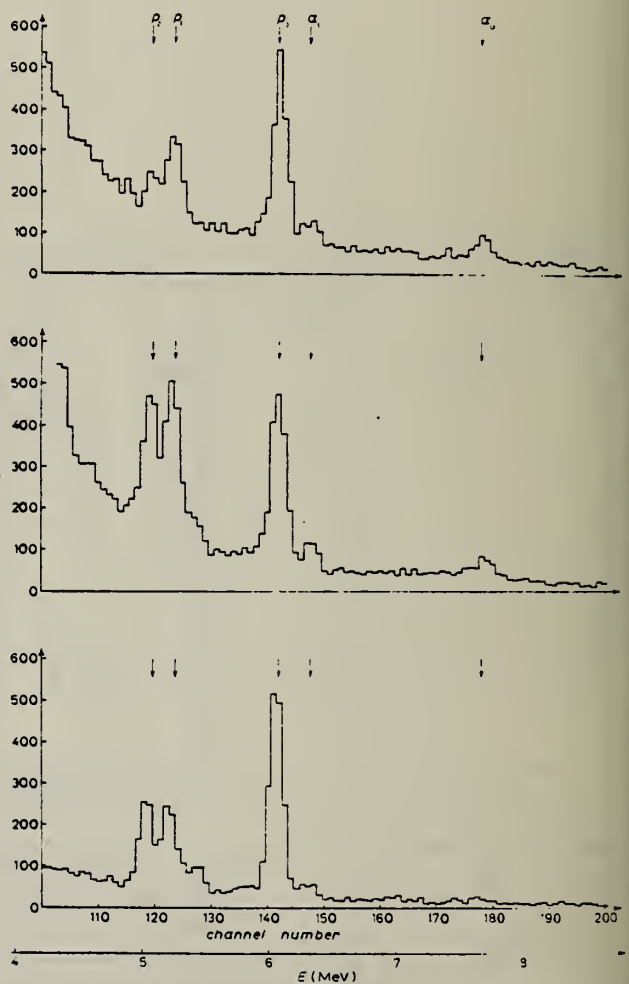

Fig. 1. – Typical $^{28}Si(\gamma,p)$ and (γ,α) energy spectra at various excitation energies near 17.64 MeV. The energy shifts ΔE of incident γ-rays are, from the top, +67.8, +16.9 and −33.9 keV, respectively. Note shifted energy-zero.

FORM NBS-418
(1-63)
ICOMM-DC 18556-P63

U.S. DEPARTMENT OF COMMERCE
NATIONAL BUREAU OF STANDARDS

Ref. E.C. Booth, K.A. Wright
Nuclear Phys. 35, 472 (1962)

Elem. Sym.	A	Z
Si	28	14

Method 4 MeV electron Van de Graaff; bremss.; nuclear resonance scattering, ring scatterer; NaI

Ref. No. 62 Bo 6 JHH

Reaction	E or ΔE	E_o	Γ	$\int \sigma dE$	Jπ	Notes
$Si^{28}(\gamma,\gamma)$	Bremss. 0 4					Detector at 110°

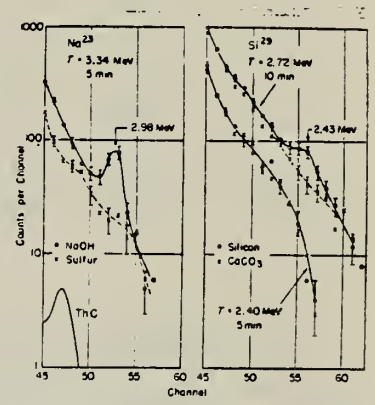

Fig. 3. Resonance fluorescence from the 2.98 MeV state of Na^{23} and the 2.43 MeV state of Si^{29}. The ThC peak is at 2.615 MeV. T is the maximum bremsstrahlung energy.

TABLE 2
Comparison of mean lifetime measurements

Nucleus	Energy	%	Spins	g	Γ_o/Γ	$W'(\theta)$	τ × 10¹⁴ sec This work	Other
Li^6	3.56	7	$1^+ - 0$	½	(1)	1	0.012	0.0072 $^{+0.0015}_{-0.0013}$ [10]
								0.0105 ±0.001 [15]
B^{11}	2.14	81	$\frac{1}{2}^- - (\frac{1}{2})$	½	1	1	0.53	0.47 ±0.06 [14]
Al^{27}	2.21	100	$\frac{1}{2}^+ - \frac{1}{2}^-$	½	(1)	1	3.2	2.7 ±0.3 [15]
Al^{27}	1.01	100	$\frac{1}{2}^+ - \frac{1}{2}^+$	½	0.98	1	320	170 ±50 [15]
Si^{28}	1.78	92	$0^+ - 2^+$	5	1	0.63	88	73 ±22 [16]
S^{32}	2.24	95	$0^+ - 2^+$	5	1	0.63	26	≈16 [16]
Mg^{24}	1.37	78.6	$0^+ - 2^+$	5	1	0.63	220	153 ±40 [15]
Mg^{25}	1.61	25	$\frac{1}{2}^+ - \frac{1}{2}^-$	½	(1)	1	3.6	2.5 $^{+0.6}_{-0.4}$ [17]
Cu^{65}	0.963	69	$\frac{1}{2} - \frac{1}{2}$	½	1	0.92	230	72 ±18 [18]
								90 ±15 [15]
Cu^{63}	0.67	69	$\frac{1}{2} - \frac{1}{2}$	½	1	1	100	31 ±3 [19]

The factor g equals $(2I+1)(2I_o+1)^{-1}$.

10) B. G. Hulet, Phys. Rev. 140 (1965) 1468
11) G. Vegors, L. Marsden and R. Heath, IDO-16370
12) Leslie Cohen and Ralph Tobias, Nuclear Physics 16 (1960) 245
13) W. C. Barber, F. Berthold, G. Friein and F. E. Gudden, Phys. Rev. 120 (1960) 2120
14) F. R. Metzger, C. P. Swann and V. K. Rasmussen, Phys. Rev. 110 (1958) 908.
15) F. R. Metzger, C. P. Swann and V. K. Rasmussen, Nuclear Physics 16 (1960) 620.
16) S. Ofer and A. Schwarzschild, Phys. Rev. Lett. 3 (1959) 216
17) V. K. Rasmussen, F. R. Metzger and C. P. Swann, Phys. Rev. 120 (1961) 1306
18) J. B. Cumming, A. Schwarzschild, A. W. Sunyar and N. T. Porile, Phys. Rev. 120 (1960) 2139
19) T. Rothen, F. R. Metzger and C. P. Swann, Nuclear Physics 22 (1961) 305

TABLE 3
Mean lifetimes of excited states deduced from the resonance scattering and bremsstrahlung measurements

Nucleus	%	Energy (MeV)	Spins	g	Γ_o/Γ	$W'(\theta)$	τ × 10¹⁴ ± 90% (sec)
Si^{28}	100	1.66	$1^+ - ?$	?	0.15	(1)	0.22
Na^{23}	100	2.08	$\frac{3}{2}^+ - \frac{1}{2}$	2	0.8	0.79	>0.60
		2.39	$-?$	?	0.89	(1)	>1.6
		2.64	$-?$	?	0.8	(1)	>0.8
		2.79	$-?$	?	(0.1)	(1)	>0.089
		2.98	$-?$	?	0.66	(1)	0.09
Al^{27}	100	2.72	$\frac{5}{2}^+ - \frac{1}{2}^+$	1	≤0.3	0.91	>0.35
		2.98	$-\frac{1}{2}$	2	0.229	1	0.3 × 10⁻³
Si^{29}	4.71	1.28	$\frac{1}{2}^+ - \frac{1}{2}^+$	2	1	0.89	1.8
		2.43	$-\frac{3}{2}^+$	2	(1)	0.85	0.5
Si^{28}	100	1.26	$1^+ - 0^+$	3	1	0.85	2.5
		2.23	-2	5	1	0.75	0.8
		2.15	-2	5	(1)	0.89	0.5
		2.59	-2	5	?	0.75	>1.6
		2.61	$-?$	?	?	(1)	>1.6
		2.91	-2	5	?	0.85	0.05
Si^{30}	96.	2.78	$0^+ - ?$	?	?	(1)	>0.6
Cu^{65}	6.9	2.127	$0^+ - 2$	5	1	0.89	>1.0
Cu^{63}	74.5	1.32	$\frac{3}{2}^+ - ?$	?	1	(1)	40
		1.76	$-?$	?	(1)	(1)	40
		2.7(3.68)	$-?$	?	?	(1)	0.24
		2.91	$-?$	?	?	(1)	0.32
Cu^{65}	30.8	2.1	?	?	?	(1)	>0.7
		2.17	?	?	?	(1)	>1.4
Cu^{63}	34.5	0.669	$\frac{3}{2}^+ - ?$	?	?	(1)	>1.6
		1.73	$-?$	?	?	(1)	>0.8
Si^{28}	92	1.78	$2^+ - ?$	?	?	(1)	>1.6
		2.28	$-?$	?	?	(1)	>1.6
		2.68	$-?$	?	1	(1)	0.37
		2.89	$-?$	?	1	(1)	>0.7
		2.85(3.06)	$-?$	?	?	(1)	0.14
		4.08–4.13	$-?$	?	?	(1)	>0.5
Cu^{65}	30	2.09	$2^+ - 2^+$	3	1	0.85	0.25
Cu^{63}	69	1.33	$2^+ - ?$	3	(1)	0.8	40>?>11

The factor g equals $(2I+1)(2I_o+1)^{-1}$.

Ref. R.D. Edge, G.A. Peterson
Phys. Rev. 128, 2750 (1962)

Elem. Sym.	A	Z
Si	28	14

Method: Linac; counter telescope

Ref. No.: 62 Ed 1 BG

Reaction	E or ΔE	E_o	Γ_γ(eV)	$\int \sigma dE$(MeV-mb)	Jπ	Notes
$Si^{28}(e,e')$	41.5	11.6	33	2.8±1.12		Nuclear states excited by 180° electron scattering; M1 transitions assumed. Inelastic electron scattering cross sections obtained by comparing inelastic peaks to e-p eleastic scattering peak. Γ_γ from virtual photon theory. Limits not given for cross sections. Γ_γ = 33 eV corresponds to transition from 1^+ excited state to 0^+ ground state.

REACTION	RESULT	EXCITATION ENERGY	SOURCE TYPE	SOURCE RANGE	DETECTOR TYPE	DETECTOR RANGE	ANGLE
A,G	ABY	11-13	D	1-3	NAI-D	8-13	DST
		(11.3 - 12.8)		(1.2 - 3.2)			

J-PI, SEP ISOTPS

TABLE III

Partial widths of ^{28}Si resonant states.

1 Resonance number	2 J^{π} [a]	3 $(2J+1)\times\Gamma_\alpha\Gamma_\gamma/\Gamma$ [b] (eV)	4 $(2J+1)\times\Gamma_p\Gamma_\gamma/\Gamma$ [c] (eV)	5 $(2J+1)\times\Gamma_p\Gamma_\alpha/\Gamma$ [c] (eV)	6 Γ [c] (eV)	7 Γ_α [d] (eV)	8 Γ_p [d] (eV)	9 Γ_γ (eV)	10 ϑ_α^2 [d] $\times 10^3$
1	1⁻	0.11				(0.037)			(85)
2	2⁺	0.065				(0.013)			(5)
3	3⁻	0.05				(0.007)			(7)
4	2⁺	0.075				(0.015)			(1.5)
5	1⁻	0.30				(0.10)			(4)
6	2⁺	0.045	0.00017			(0.009)	(3×10^{-5})		(0.4)
7	(4⁺)	0.035	0.028			(0.004)	(0.003)		(1.3)
8	(4⁺)	0.07	0.15			(0.008)	(0.017)		(1.4)
9		0.035	< 0.004						
10	2⁺	0.50	0.95	1.5	< 200	0.6	1.1	0.35	2.3
11	1⁻	0.07	< 0.002						
12	3⁻	0.23	5.4	5.0	< 60	0.8	18	0.8	5.1
13	4⁺	0.75		< 0.4	< 1000				
14	2⁺	0.09	4.0	5.9	< 160	1.2	54	0.8	1.3
15	2⁺	0.075	0.4	< 0.4	< 1000				
16	2⁺	1.25	1.0	10	< 1000	4.8	3.8	0.48	2.4
17	4⁺	2.0	4.3	4	< 190	0.9	1.9	0.9	7.0
18	3⁻	0.10	4	65	340 ± 110	9.5	380	0.6	14
19	4⁺	0.68	1.0	2.4	< 1000	0.5	0.8	0.22	2.4
20	2⁺	5.7	4.7	940	710 ± 130	420	340	2.1	65

[a] Combined results from (α,γ), (p,γ), and (p,α) measurements.
[b] From table II, column 6, after converting "partial" yields into total yields (see text).
[c] From ref. 9, except for resonances 6, 9, and 11 (present work).
[d] The values put in brackets were computed making the assumptions $\Gamma_\gamma \gg \Gamma_\alpha$ and $\Gamma_\gamma \gg \Gamma_p$. If the assumptions are not fulfilled the bracketed values can always be regarded as lower limits.

Ref 9: P.M. Endt, C. Van der Leun, Nuclear Phys. 34, 1 (1962)

Ref 15: S. Anderson, H. Bo, T. Holtebekk, O. Lonsjo, R. Tangen, Nuclear Phys. 19, 509 (1959)

Ref 16: P.F. Dahl, D.G. Costello, W.L. Walters, Nuclear Phys. 21, 106 (1960)

Ref 17: J.B. Marion, Rev. Mod. Phys. 33, 139 (1961), erratum on p. 623.

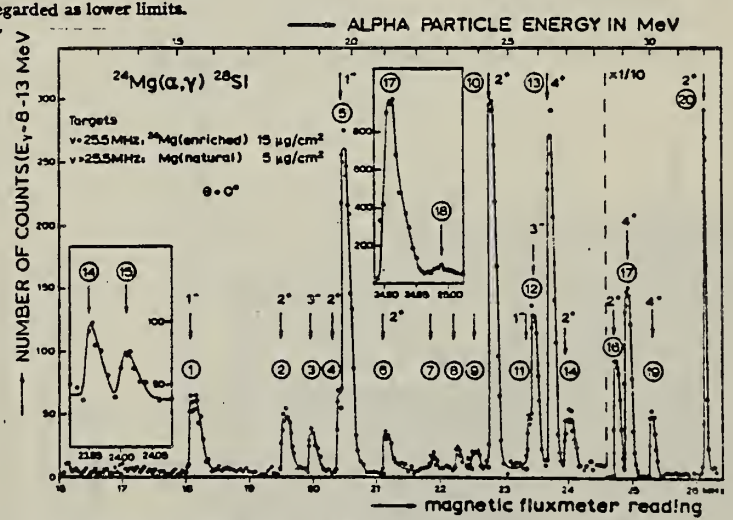

Fig. 2. Yield curve of the ^{24}Mg$(\alpha,\gamma)^{28}$Si reaction in the E_α = 1.2–3.2 MeV region. High-energy γ radiation ($E_\gamma \approx$ 8–13 MeV) is detected with a NaI scintillation crystal (10 cm long and 10 cm in diameter), as close to the target as possible at 0° to the beam. For $E_\alpha < 3.1$ MeV an enriched ^{24}Mg target was used of 15 μg/cm²; for $E_\alpha > 3.1$ MeV the target was natural Mg of 5 μg/cm² thickness; the parts of the yield curve shown in the two inserts were taken with a natural Mg target of about 3 μg/cm² thickness.

TABLE II

Resonances in the $^{24}Mg(\alpha, \gamma)^{28}Si$ reaction.

1	2	3	4	5	6	7	8	9	10	11	12
								$^{27}Al(p, \gamma)^{28}Si$			
Resonance number	E_α (MeV ± keV)	$E_x(^{28}Si)$ (MeV)	Main γ transitions (MeV)	$\frac{\Gamma_{\gamma 0}}{\Gamma_{\gamma 1}}$	$(2J+1) \times \frac{\Gamma_\alpha \Gamma_\gamma}{\Gamma}$ [e] (eV)	J^π	Quadrupole/dipole amplitude mixing ratio for γ_1	E_p (keV)	$E_x(^{28}Si)$ (MeV)	J^π	$E_x(\alpha, \gamma) - E_x(p, \gamma)$ (keV)
1	1.529 ± 5	11.296	γ_0, γ_1; 1.77 [a]	2.5	0.11	1⁻					
2	1.785 ± 6	11.516	γ_1;	< 0.05	0.065	2⁺	−3.0 ± 0.5				
3	1.865 ± 6	11.584	γ_1; 1.77	< 0.05	0.05	3⁻	+0.02 ± 0.02				
4	1.950 ± 6	11.657	γ_0, γ_1; 7.85, (4.8), (3.7), 1.77	0.5	0.075	2⁺					
5	1.964 ± 6	11.670	γ_0, γ_1; 1.77 [b]	0.06	0.30	1⁻	−0.09 ± 0.04				
6	2.093 ± 6	11.780	γ_1;	< 0.05	0.045	2⁺	−0.10 ± 0.10	202.3 ± 0.9 [n]	11.776		4
7	2.234 ± 7	11.901	γ_2;		0.025			326.0 ± 0.4 [h]	11.895	4(⁻) [i]	6
8	2.323 ± 6	11.977	γ_2; 6.9, 5.1		0.05			404.9 ± 0.4 [h]	11.971	4⁻ [i]	6
9	2.378 ± 6	12.024	6.9, 5.1 [c];		0.035						
10	2.435 ± 5	12.073	γ_0, γ_1; 5.15, 4.5	6	0.40	2⁺		504.8 ± 0.3 [h]	12.067	2⁺ [k] [j]	6
11	2.566 ± 5	12.185	γ_0, 10.9, γ_1; 1.77, 1.28 ± 0.02 [d]	3	0.07	1⁻					
12	2.580 ± 5	12.197	γ_1; (7.6)	< 0.10	0.18	3⁻	+0.03 ± 0.03	632.1 ± 0.5 [n]	12.190	3⁻ [k]	7
13	2.634 ± 5	12.243	γ_1; see also fig. 13	< 0.05	0.38	4⁺		679.2 ± 0.5 [n] [m]	12.236 [m]	3⁺ [k] [m]	7 [m]
14	2.692 ± 5	12.293	γ_1;	< 0.15	0.05	2⁺	+0.60 ± 0.05	731.2 ± 0.5 [n]	12.286	2⁺ [k]	7
15	2.704 ± 5	12.304	γ_1;	< 0.20	0.035			742.1 ± 0.7 [h]	12.296	2⁺ [k]	8
16	2.869 ± 5	12.445	γ_0, γ_1; (7.5) [a]	10	1.25	2⁺		885 ± 2 [h]	12.434		11
17	2.909 ± 5	12.479	γ_1; [a]	< 0.07	2.0	4⁺		923.1 ± 0.3 [h]	12.471		8
18	2.926 ± 5	12.494	[f]		0.10			937.6 ± 0.3 [h]	12.485	3⁻ [i]	9
19	2.998 ± 5	12.556	γ_1; 7.5, 5.6, 5.1, 4.65, 2.84, 2.01	< 0.05	0.68	4⁺		1002.5 ± 0.5 [h]	12.547		9
20	3.204 ± 6	12.732	γ_0, γ_1 [a];	3.0	5.7	2⁺		1183.4 ± 0.4 [h]	12.722	2⁺ [i]	10

[a] $\Gamma_{\gamma 0} + \Gamma_{\gamma 1} < 0.85\,\Gamma_\gamma$.
[b] $\Gamma_{\gamma 1} > 0.8\,\Gamma_\gamma$.
[c] The two lines are of equal intensity.
[d] The 10.9 and 1.28 MeV transitions are in coincidence. The intensity ratio of γ_0, $\gamma_{10\text{-}9}$ and γ_1 is 2 : 1 : 0.7.
[e] $\Gamma_{\gamma 1} > 0.9\,\Gamma_\gamma$.
[f] No spectrum has been taken at this weak resonance.
[g] Only those lines are included in Γ_γ which are indicated in column 4 to the left of the semicolon.
[h] Averages of measurements by several authors (see text).
[i] Ref. 15.
[j] Ref. 16.
[k] Ref. 17.
[l] These two J^π determinations are from $^{27}Al(p, \alpha)^{24}Mg$ [18].
[m] This resonance does *not* correspond to the (α, γ) resonance 13, see text.
[n] Present work.

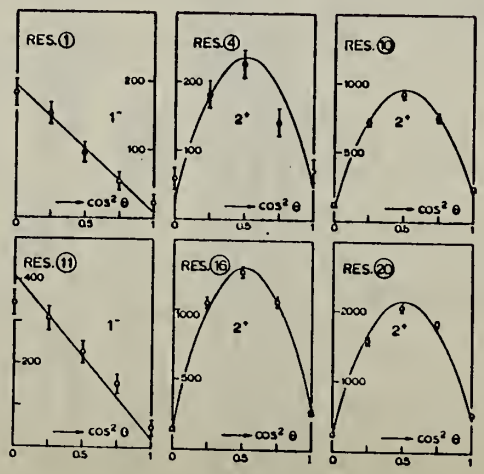

Fig. 5. Measured angular distributions of γ_0 at resonances 1, 4, 10, 11, 16, and 20. The curves correspond to the theoretical expressions given in fig. 2*a*, normalized to the measured total number of counts. Background has been subtracted. Distance between target and front of crystal D = 10 cm.

Ref. Y.P. Antoufiev, L.M. El-Nadi, D.A.E. Darwish, O.E. Badawy, P.V. Sorokin
Nuclear Phys. 46, 1 (1963)

Elem. Sym.	A	Z
Si	28	14

Method: Van de Graaff; NaI

Ref. No.: 63 An 2 JHH

Reaction	E or ΔE	E_o	Γ	$\int \sigma dE$	Jπ	Notes
$Al^{27}(p,\gamma)$	0.9-2.5					Detector at 90°.
	1.184	12.729				

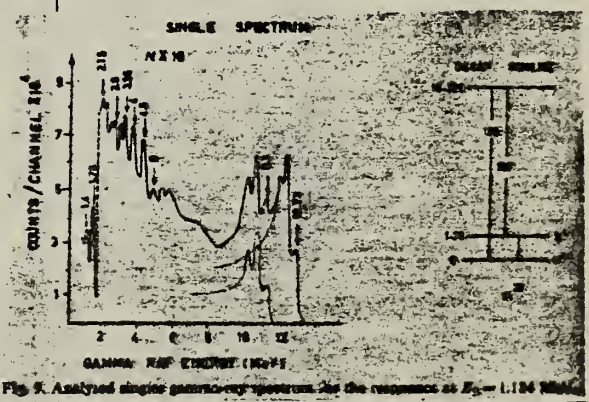

Fig. 9. Analyzed singles gamma-ray spectrum for the resonance at E_p = 1.184 MeV.

Ref. L.Simons, K.E.Nysten, M.Koskelin, O.Siltanen, E.Spring, G.Wendt

Phys.Letters 3, 306 (1963)

Elem. Sym.	A	Z
Si	28	14

Method

Van de Graff - 2 NaI(Tl)

Ref. No. 63Sil BG

Reaction	E or ΔE	E_o	Γ	$\int \sigma dE$	Jπ	Notes
$Al^{27}(p,\gamma)Si^{28}$		1.77			2^+	E2 radiation
		7.95±0.10			2^+	
						Angular distribution fitted to $w(\theta) = 1 + a_2 P_2(\cos\theta)$

Table 1
Results of γ-rays obtained at the 992 keV resonance in present and earlier investigations.

Present investigation		Bashkin and Ophel [4]		Brenner [3]		Gove et al. [2]	Hattori et al. [1]
Energy (MeV)	Int. (%)	Energy (MeV)	Int. (%)	Energy (MeV)	Int. (%)	Energy (MeV)	Energy (MeV)
1.77	123	1.78	124	1.80	100 *	1.77 **	
2.84±0.05	7.5	2.84±0.05	10	2.86	6 *	2.85 **	
3.08±0.10	3	3.12±0.10	<5				
4.58±0.05	10	4.52±0.10	10	} 4.66	21	4.62 **	4.5
4.75±0.05	11	4.78±0.075	13				
5.15±0.05	~2	5.12±0.10	<2				5.1
5.60±0.10	~1						
6.05±0.05	8	6.04±0.05	10	6.07	20		5.7
6.25±0.10	3	6.3 ±0.10	<3				6.7
7.40±0.10	~1	7.40±0.10	<2	7.21	} 17		7.5
7.95±0.10	13	7.95±0.05	8	8.04			8.3
9.49±0.10	3	8.98±0.15	<3				
10.76	100	10.76	100	10.8	100	10.77	10.7
				12.6	<5		12.1

* Separate measurement which is not related to other intensities.
** Coincidence with $6.5 < E_\gamma < 8.5$ (MeV).

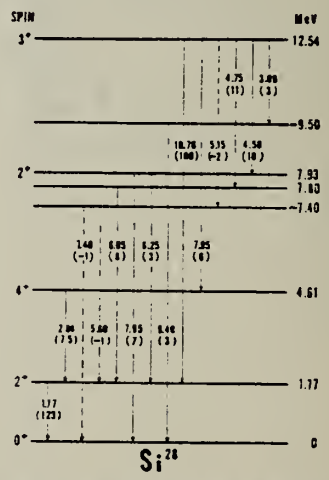

Fig. 2. Proposed decay scheme for the levels excited at the 992 keV resonance of the $Al^{27}(p,\gamma)Si^{28}$.

REF. R.G. Allas, S.S. Hanna, L. Meyer-Schutzmeister, R.E. Segel, P.P. Singh, and Z. Vager
Phys. Rev. Letters 13, 628 (1964)

ELEM. SYM.	A	Z
Si	28	14

METHOD
$Al^{27}(p,\gamma_0)Si^{28}$; tandem

[Page 1 of 2]

REF. NO. 64 Al 3 JOC

REACTION	RESULT	EXCITATION ENERGY	SOURCE		DETECTOR		ANGLE
			TYPE	RANGE	TYPE	RANGE	
P,G	ABX	15 - 24	D	4-13	NAI-D		DST

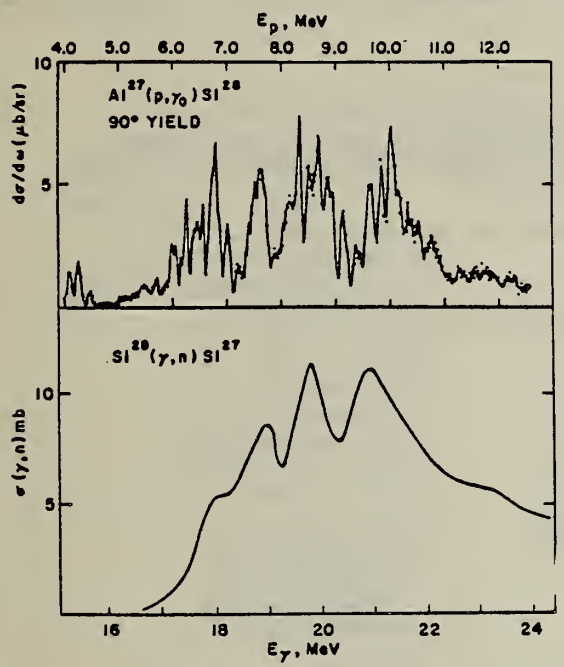

FIG. 1. Top curve: 90° yield of the ground-state gamma ray from the reactions $Al^{27}(p,\gamma)Si^{28}$. This yield curve was taken in 15-keV steps using a target about 10 keV thick. Bottom curve: yield of Si^{27} from the reaction $Si^{28}(\gamma,n)Si^{27}$ taken with a gamma-ray energy resolution of about 600 keV. The data are those of Caldwell et al. (reference 8). The two curves are plotted so as to be on the same gamma-ray energy scale.

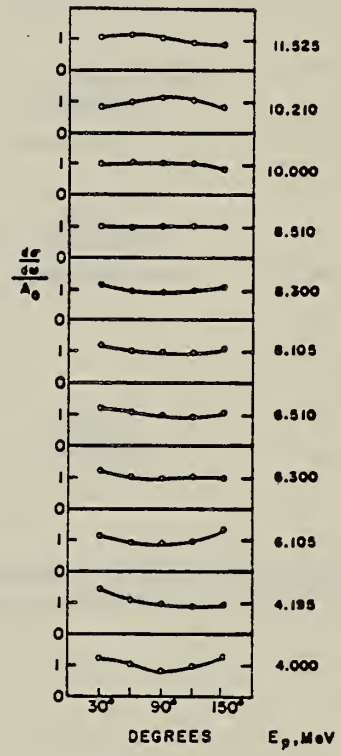

FIG. 2. Sample angular distributions of the ground state gamma ray from the reaction $Al^{27}(p,\gamma)Si^{28}$.

REF.	ELEM. SYM.	A	Z
R.G. Allas, S.S. Hanna, L. Meyer-Schützmeister, R.E. Segel, P.P. Singh, and Z. Vager Phys. Rev. Letters 13, 628 (1964)	Si	28	14

METHOD	REF. NO.	
$Al^{27}(p,\gamma_0)Si^{28}$; tandem [Page 2 of 2]	64 Al 3	JOC

REACTION	RESULT	EXCITATION ENERGY	SOURCE		DETECTOR		ANGLE
			TYPE	RANGE	TYPE	RANGE	
P,G	ABX	15 - 24	D	4 - 13	NAI-D		DST

Table I. Summary of experimental results on the (p,γ) giant resonance (references 9-11). The angular distributions that are quoted generally characterize the data to within 15% throughout the giant-resonance region.

Nucleus	Type of observation	Energy interval and range	Result
C^{12}	90° yield curve	50-keV steps 4.0-14 MeV	Broad ($\Gamma \approx 1$ MeV) overlapping levels; no correlation between γ_0 and γ_1.
	Angular distribution[a]	50-keV steps 4.0-14 MeV	$W(\theta)_{\gamma_0} = 1 + 0.15P_1 - 0.6P_2$ $W(\theta)_{\gamma_1} = 1 + 0.15P_1$
Ne^{20}	90° yield curve	30-keV steps 4.3-9.1 MeV	Broad ($\Gamma \approx 400$ keV) levels usually well isolated, γ_0 and γ_1 well correlated.
	Angular distribution	100-keV steps 4.0-10.5 MeV	$W(\theta)_{\gamma_0} = 1 + 0.05P_1 - 0.7P_2$ $W(\theta)_{\gamma_1} = 1 + 0.05P_1 + 0.2P_2$
Si^{28}	90° yield curve	15-keV steps 4.0-12.5 MeV	Narrow ($\Gamma \approx 50$ keV) Ericson fluctuations, superimposed on intermediate structure; no correlation between γ_0 and γ_1.
	Angular distribution	15-keV steps 4.0-4.32 MeV 6.0-6.62 MeV 8.0-8.54 MeV 10.0-10.28 MeV 11.54-11.58 MeV	$W(\theta)_{\gamma_0} = 1 + 0.07P_1$ $W(\theta)_{\gamma_1} = 1 + 0.1P_1 - 0.45P_2 - 0.1P_3$

[a]The coefficients of P_1 are average values. They actually increase by about 0.03/MeV over the giant resonance.

REF. E.C. Booth, B. Chasan and K.A. Wright
Nucl. Phys. 57, 403-420 (1964)

ELEM. SYM.	A	Z
Si	28	14

METHOD
Van de Graaff; resonance fluorescence

REF. NO. 64 Bo 1 NVB

REACTION	RESULT	EXCITATION ENERGY	SOURCE		DETECTOR		ANGLE
			TYPE	RANGE	TYPE	RANGE	
G,G	LFT	1-3	C	1-3	NAI-D		100
		(0.5 - 3.0)		(0.5 - 3.0)			

ABI

TABLE 1
Cases of observed resonance fluorescence

Nucleus multipol.	State (MeV)	Spin	Γ_0/Γ	$T(gw\Gamma_0^2/\Gamma^2)^{-1}$ (sec).	Mean lifetime T BCW (sec)	Mean lifetime T other (sec)	Ref.	Γ_0/Γ_W BCW
[illegible]	0.00	0+						
E2	1.78	2+	1	$17.5\pm5\times10^{-14}$	$56\pm15\times10^{-14}$	$73\pm22\times10^{-14}$	13)	12

REF.
P. Brix, H. G. Clerc, R. Engfer, G. Fricke, F. Gudden, H. Liesem and E. Spamer
Proc. Paris Conf. 372 (1964)

ELEM. SYM.	A	Z
Si	28	14

METHOD

REF. NO.	
64 Br 2	JDM

REACTION	RESULT	EXCITATION ENERGY	SOURCE		DETECTOR		ANGLE
			TYPE	RANGE	TYPE	RANGE	
E,E/	SPC	0-12	D	41	SCI-D		152

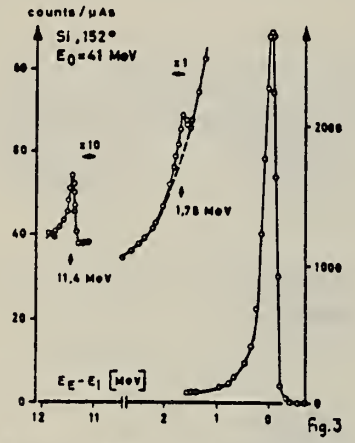

FIG. 3. — Electron scattering from a silicon foil ($d_{eff} = 0.30$ g/cm^2). $q_I = 0.46$ fm^{-1} for 1.78 MeV and 0.39 fm^{-1} for 11.4 MeV level. (From separate runs).

REF.

F. Rauch and E. Rössle
Phys. Letters 12, 217 (1964)

ELEM. SYM.	A	Z
Si	28	14

METHOD

$Al^{27}(p,\gamma)Si^{28}$

REF. NO. 64 Ra 1 JOC

REACTION	RESULT	EXCITATION ENERGY	SOURCE		DETECTOR		ANGLE
			TYPE	RANGE	TYPE	RANGE	
P,G	RLX	16-18	D	5-7	NAI-D		90
		(16.5-18.3)		(4.9-6.7)			

FLUCTUATIONS

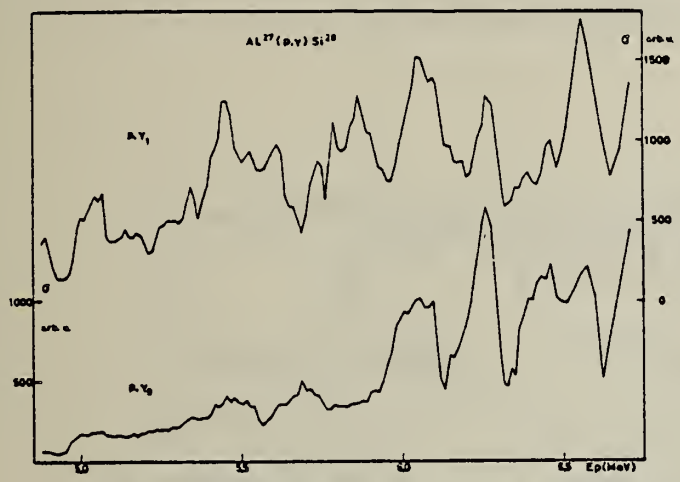

Fig. 1. Excitation function of the transitions to the ground state (γ_0) and first excited state (γ_1) in arbitrary units.

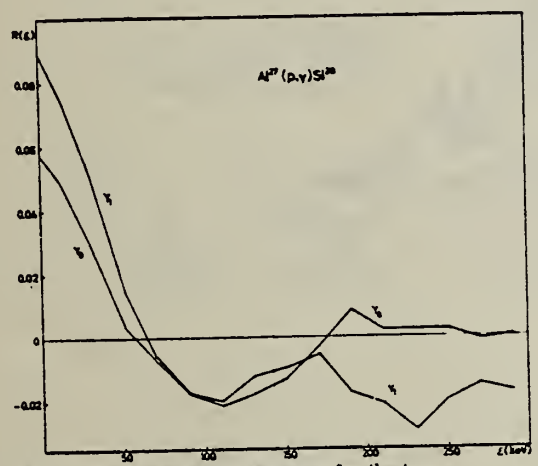

Fig. 2. Auto-correlation function for the two transitions.

REF. H. Ullrich
Proc. Paris Conf. 1038 (1964)

ELEM. SYM.	A	Z
Si	28	14

METHOD

32 MeV Betatron

REF. NO. 64 U1 3 JDM

REACTION	RESULT	EXCITATION ENERGY	SOURCE		DETECTOR		ANGLE
			TYPE	RANGE	TYPE	RANGE	
G,P	SPC	13-23	C	24	SCD-D	1-11	4PI

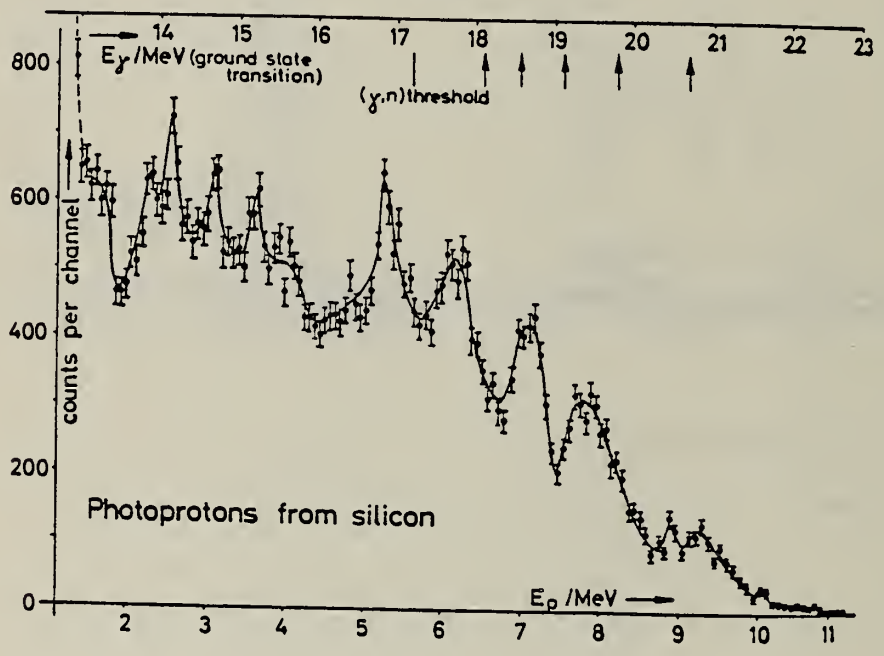

REF.

J.A. Weinman, L. Meyer-Schützmeister, L.L. Lee, Jr.
Phys. Rev. 133, B590-97 (1964)

EL EM. SYM.	A	Z
Si	28	14

METHOD

Van de Graaff

[Page 1 of 2]

REF. NO. 64 We 1 NVB

REACTION	RESULT	EXCITATION ENERGY	SOURCE TYPE	SOURCE RANGE	DETECTOR TYPE	DETECTOR RANGE	ANGLE
A,G	NØX	12 - 14	D	3-5	NAI-D		DST
		(12.7 - 13.7)					

1^-, 2^+ resonances have ground state transitions.

WIDTHS

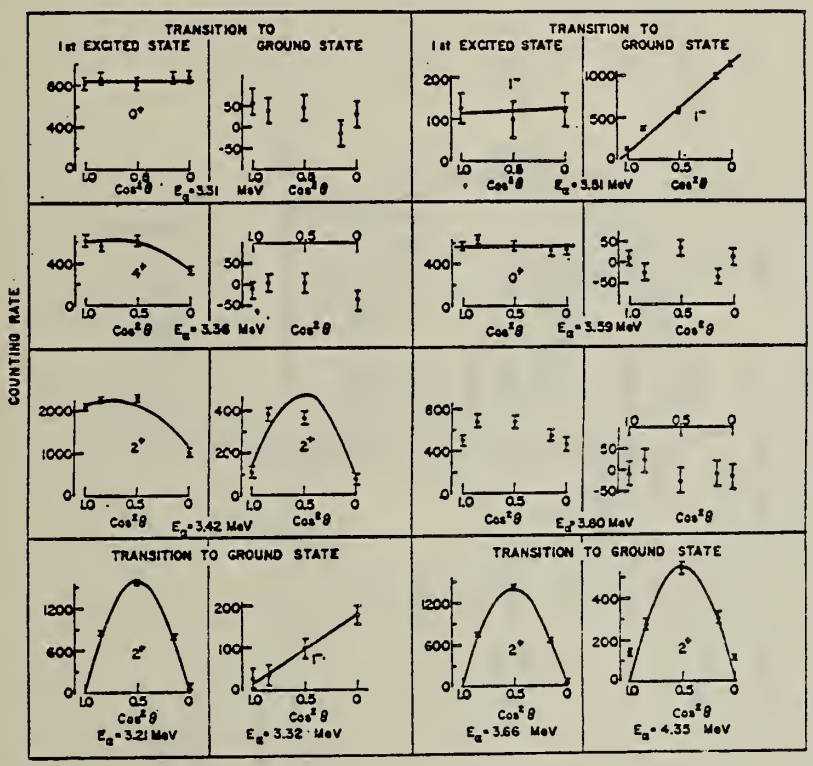

FIG. 5. Gamma-ray angular distributions measured on the peaks of the various resonances studied. Alpha-particle energies and observed transitions (to ground state or excited state) are indicated with each plot. The solid curves are theoretical curves calculated for a resonance having the spin and parity indicated and corrected for finite solid angle of the detector. At the resonance at $E_\alpha = 3.42$ MeV, the transition to the first excited state is of mixed multipolarity, the intensity ratio being $I(E2)/I(M1) = 4$.

REF.

J.A. Weinman, L. Meyer-Schützmeister, L.L. Lee, Jr.
Phys. Rev. 133, B590-97 (1964)

EL EM. SYM.	A	Z
Si	28	14

METHOD

Van de Graaff

REF. NO.

64 We 1 NVB

REACTION

RANGE

ANGLE

TABLE I. Experimental results of the $Mg^{24}(\alpha,\gamma)Si^{28}$ and $Mg^{24}(\alpha,\alpha)Mg^{24}$ reactions. For comparison, the values of other authors are given.

E_α(lab) (MeV)	E_x[a] (MeV)	I^π (α,γ)	I^π (α,α)	I^π (p,α)[b]	(α,α)	Γ_γ (keV) (α,γ)	(p,γ)[c]	$\Gamma_\alpha/\Gamma_\gamma$ (α,α)	$(2I+1)\Gamma_p\Gamma_\alpha/\Gamma_\gamma$ (eV)	Γ_α (keV)	Γ_p (keV)	$(2I+1)\Gamma_\alpha\Gamma_\gamma/\Gamma$ (eV)		Γ_γ (eV) measured		Γ_γ (eV) calculated	
												g.s.	exc.	g.s.	exc.	g.s.	exc.
3.213	12.740	2^+	2^+	2^+	1.1±0.3	0.8±0.5	0.710±0.130	0.4±0.2	940	0.42[d]	0.34[d]	4.6	1.5	2.3	0.75	1.38(E2)	0.65(E2)
3.307	12.820	$(0^+,3^-)$	•	[f]		⩽0.6	<0.200		1.7			<0.02	0.18				
3.318	12.830	1^-	1^-	[f]	$2.0^{+0.6}_{-0.3}$	2.8±0.5		0.7±0.1	3.4	2.0±0.4	0.0016±0.0002	0.26	<0.01	0.13		1320(E1)	
3.363	12.869	4^+	•	4^+		⩽0.6	<0.160		35			<0.02	0.09				
3.418	12.919	2^+	2^+	2^+	0.7±0.3	1.3±0.5	~1.100	0.3±0.2	1640	0.6[b]	0.6[b]	0.14	0.86	0.17	0.57	1.48(E2)	0.71(E2)
3.447	12.941	•	•	$(2^+,3^-)$		•	0.290±0.070		206								
3.504	12.989	1^-	(1^-)			1.5±0.5		⩽0.5	<860	⩾2.9	⩽1.7	0.29	0.04				
		•	0^+		⩾2.9												
3.583	13.056	(0^+)	0^+		$2.2^{+0.8}_{-0.4}$	2.4±0.5		0.9±0.1	<40	2.2±0.4	⩽0.05	<0.02	0.22	0.2		0.75(E2)	
3.660	13.123	2^+	(2^+)			0.8±0.5		0.8±0.2				3.4	⩽0.3	0.85		1.59(E2)	
3.737	13.189	•	[f]			•											
3.807	13.249	(0^+)	0^+		⩾2.1	2.3±0.6		0.9±0.1	<580	2.1±0.4	<0.73	<0.03	0.14	0.13		0.82(E2)	
3.827	13.266	•	(1^-)			•		[f]									
3.961	13.381	[f]				3.0±0.7											
4.349	13.714	2^+															

[a] Computed on the assumption that Q_0=9.986 MeV.
[b] From Anderson *et al.*, Ref. 3.
[c] From Anderson *et al.*, Ref. 2.
[d] From P. J. M. Smulders (private communication).
[e] Not observed.
[f] Not measured although resonance observed.

REACTION	RESULT	EXCITATION ENERGY	SOURCE		DETECTOR		ANGLE
			TYPE	RANGE	TYPE	RANGE	
G,P	RLX	18	D	18	SCD-D	4-8	4PI
G,A	RLX	18	D	18	SCD-D	6-8	4PI

Energy of photon varied around 17.62 MeV.

In Table 3, ΣT_ℓ = sum of transmission coefficients.

Cross sections are averaged.

TABLE 3
Average cross sections

Transition [a])	Experimental cross sections	ΣT_i E1	ΣT_i E2	$\langle\sigma\rangle/\Sigma T_i$ E1	$\langle\sigma\rangle/\Sigma T_i$ E2
$p_0(\frac{1}{2}^+)$	4.26	0.652	1.098	6.53	3.88
$p_1(\frac{1}{2}^+)$	1.44	0.960	0.366	1.50	3.94
$p_2(\frac{3}{2}^+)$	1.33	0.971	0.684	1.37	1.95
$p_3(\frac{7}{2}^+)$	0.3	0.019	0.094		
$p_4(\frac{5}{2}^+)$	0.76	0.335	0.193	2.27	3.94
$\alpha_0(0^+)$	0.25	0.973	0.729	0.26	0.34
$\alpha_1(2^+)$	0.28	1.161	1.117	0.24	0.25

[a]) Spin and parity of the final level are shown in parentheses.

REACTION	RESULT	EXCITATION ENERGY	SOURCE		DETECTOR		ANGLE
			TYPE	RANGE	TYPE	RANGE	

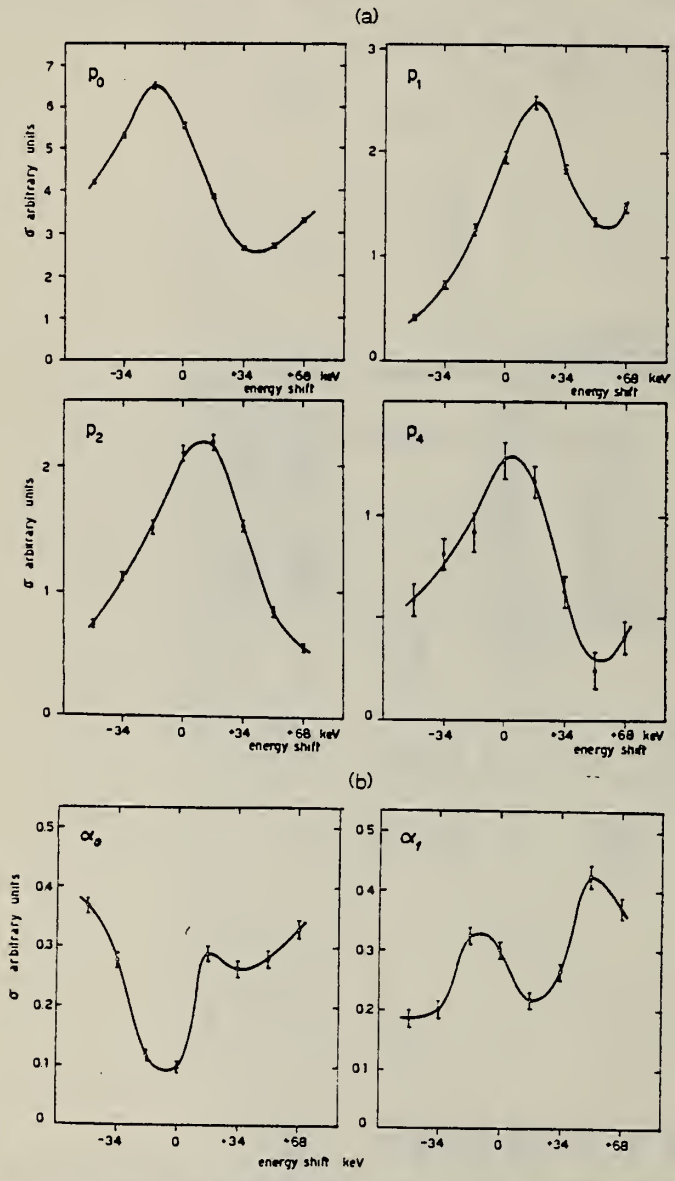

Fig. 3. Experimental cross sections versus energy for the six transitions observed.
a) proton transitions, b) α transitions.

REF. S. Matsumoto, H. Yamashita, T. Kamae and Y. Nogami
J. Phys. Soc. Japan 20, 1321 (1965)

ELEM. SYM.	A	Z
Si	28	14

METHOD

REF. NO. 65 Ma 6 EGF

REACTION	RESULT	EXCITATION ENERGY	SOURCE		DETECTOR		ANGLE
			TYPE	RANGE	TYPE	RANGE	
G,P	ABX	17-22	D	17-22	SCD-D	4-12	4PI
G,A	ABX	17-22	D	17-22	SCD-D	4-12	4PI

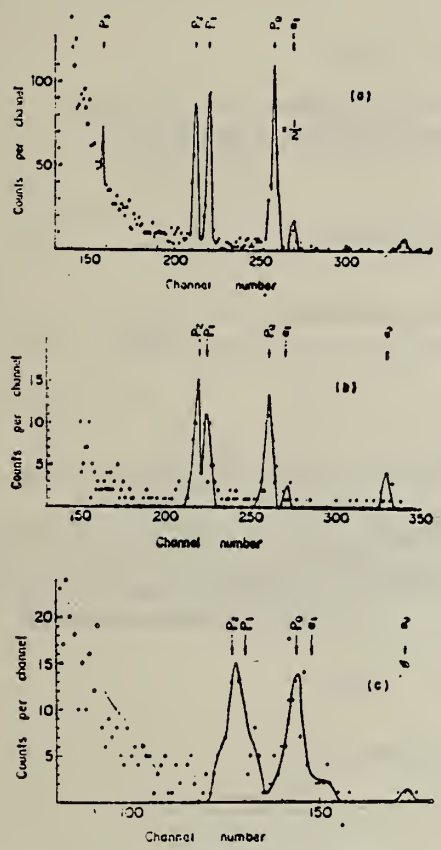

Fig. 4. Typical pulse-height distributions of charged particles: (a) E_γ=17.62 Mev (1), Li (p, γ) resonance radiation, (b) and (c) E_γ=18.17 (3), 19.82 MeV (10), Li (p, γ) radiation (1, 3, 10, see Table I). p_0, p_1 and p_2 represent the proton groups leading to the ground, first, and second-excited states of ^{27}Al; α_0 and α_1 represent the alpha-particle groups leading to the ground and first-excited states of ^{24}Mg.

REF. S. Matsumoto, H. Yamashita, T. Kamae and Y. Nogami
J. Phys. Soc. Japan 20, 1321 (1965)

ELEM. SYM.	A	Z
Si	28	14

METHOD

REF. NO. 65 Ma 6

EGF

REACTION	RESULT	EXCITATION ENERGY	SOURCE		DETECTOR		ANGLE
			TYPE	RANGE	TYPE	RANGE	

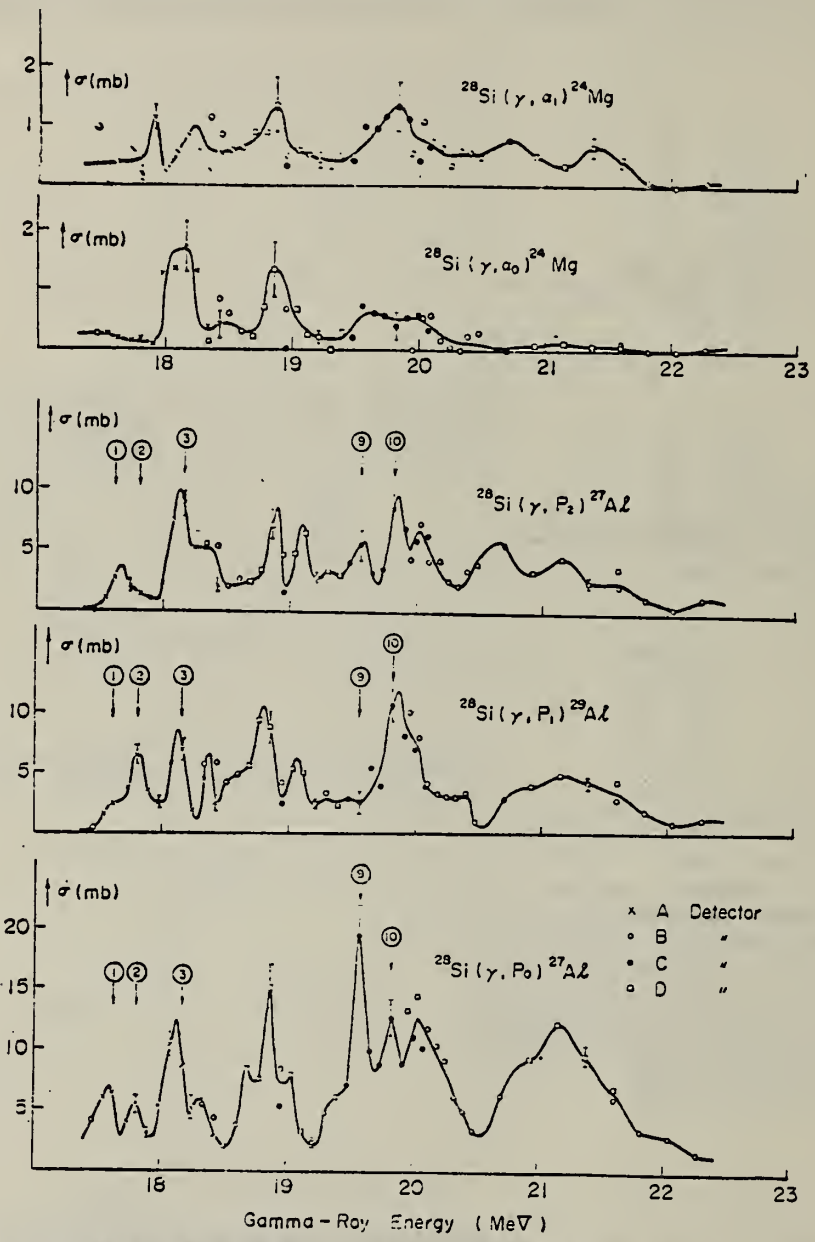

Fig. 5. The cross sections for the ^{28}Si(γ, p) ^{27}Al and the ^{28}Si(γ, α) ^{24}Mg reactions. (Numbering of peaks, see Table I.)

REF. A. W. Parker, R. R. Whitehead, G. G. Shute
Aust. J. Phys. 18, 15 (1965)

EL EM. SYM.	A	Z
Si	28	14

METHOD

REF. NO. 65 Pa 2 egf

REACTION	RESULT	EXCITATION ENERGY	SOURCE		DETECTOR		ANGLE
			TYPE	RANGE	TYPE	RANGE	
P,G	ABX	19-22	D	8-11	NAI-D	8-25	90

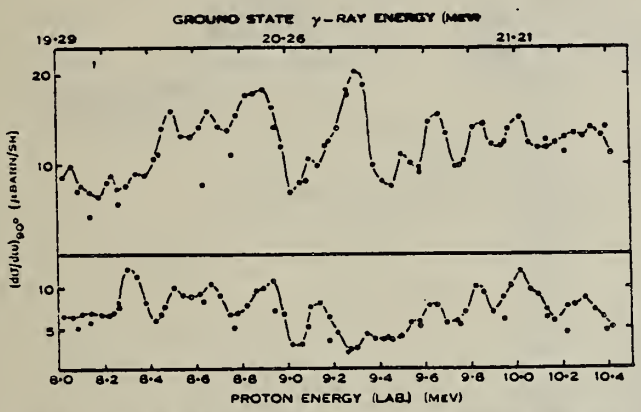

Fig. 2.—Yield curves of ground state γ-rays (lower curve) and first excited state γ-rays (upper curve). The full circles are the present results, and the open circles are the results of Gove, Litherland, and Batchelor (1961). The target-thickness correction (~ 14 keV) to the energy scale has not been applied.

REF.

P. P. Singh, R. E. Segel, L. Meyer-Schützmeister, S. S. Hanna and R. G. Allas
Nuclear Phys. 65, 577 (1965)

ELEM. SYM.	A	Z
Si	28	14

METHOD

[Page 1 of 3]

REF. NO. 65 Si 1 EGF

REACTION	RESULT	EXCITATION ENERGY	SOURCE		DETECTOR		ANGLE
			TYPE	RANGE	TYPE	RANGE	
P,G	ABX	16-24	D	4-13	NAI-D	16-24	90

104

TABLE 1

Cross-section measurements for $Si^{28}(\gamma, p)Al^{27}$ compared with those for $C^{12}(\gamma, p)B^{11}$

Nucleus	Peak value of $\sigma(\gamma, p)$ (mb)	$\int\sigma(\gamma, p)dE$ (dipole sum)	Upper limit of integration (MeV)	Reaction	Ref.
Si^{28}	13	0.14	23.2	(p, γ_0)	a)
Si^{28*}	5	0.06	23.2 b)	(p, γ_1)	a)
Si^{28}	22	0.24	24.1	(p, γ_0)	12)
Si^{28*}	8	0.09	24.1 b)	(p, γ_1)	12)
$Si^{28}+Si^{28*}$	16	0.17	26.0, 24.2	$(p, \gamma_0+\gamma_1)$	11)
Si^{28}	31	0.33	23.0	(γ, p)	3)
Si^{28}		0.64	28.0	(γ, p)	9)
C^{12}	12.5	0.29	29.0	(p, γ_0)	3)
C^{12*}	2.7	0.09	29.0 b)	(p, γ_1)	3)
C^{12}	13.5	0.31	29.0 b)	(p, γ_0)	1)
C^{12}	3.5	0.12	29.0 b)	(p, γ_1)	1)
C^{12}	21.6	0.49	29.0 b)	(p, γ_0)	38)
C^{12}	11.0	0.28	29.3	(e, pe')	16)
C^{12}	14.7	0.26	24.0	(γ, p)	40)
C^{12}	12.7	0.23	24.0	(γ, p)	41)
C^{12}	8.1	0.20	30.7	(γ, p_0)	42)

Results for the (p, γ) reaction have been converted to the inverse (γ, p) process by means of the detailed-balance theorem. In general the (γ, p) measurements may include transitions to excited states in the final nucleus. Whenever appropriate, the results have been corrected for the observed angular distributions. The integrated cross sections are in units of the electric-dipole sum $(2\pi^2 e^2 \hbar/Mc)(NZ/A) = 0.42$ and 0.18 MeV · b for Si^{28} and C^{12}, respectively.

a) Present work.
b) By extrapolation of the yield curve.

TABLE 6

Values of Γ in Si^{28} from various reactions

Reaction	E_{ex} in Si^{28} (MeV)	Method	Γ (keV)	Ref.
$Al^{27}(p, \gamma_0)Si^{28}$	17.4 –21.7	autocorr.	50±10	a
$Al^{27}(p, \gamma_0)Si^{28}$	17.4 –22.2	peak spacing	65±10	a)
$Al^{27}(p, \gamma_1)Si^{28*}$	17.4 –21.7	autocorr.	55±10	a)
$Al^{27}(p, \gamma_1)Si^{28*}$	17.4 –22.2	peak spacing	60±10	a)
$Si^{28}(\gamma, p_0 \ldots)Al^{27}$ $Si^{28}(\gamma, \alpha_0\alpha_1)Mg^{24}$	17.56–17.68	peak spacing	40	36)
$Al^{27}(p, \alpha_0 \ldots)$	20.6 –22.1	autocorr.	65	34)
$Al^{27}(p, \alpha_0\alpha_1)Mg^{23}$	20.3 –23.2	autocorr.	45	35)
$C^{12}(O^{16}, \alpha_0 \ldots)Mg^{24}$	23.9 –30.9	autocorr.	116	37)

a) Present work.

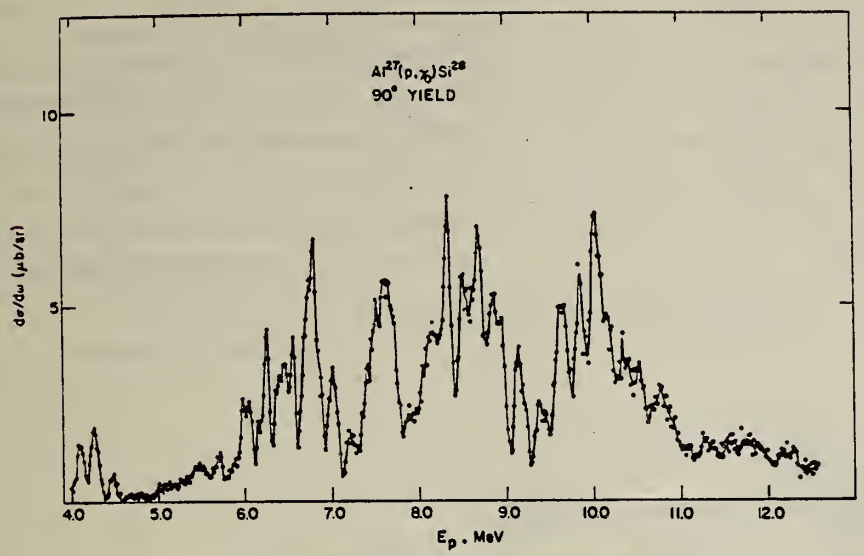

Fig. 3. Differential yield curve for $Al^{27}(p, \gamma_0)Si^{28}$.

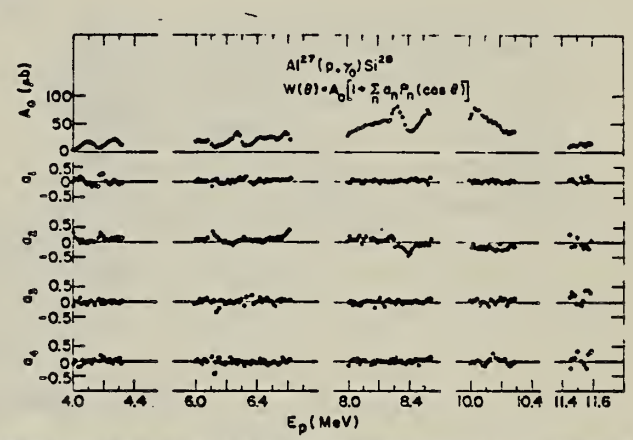

Fig. 6. Coefficients obtained in fitting series of Legendre polynomials to the angular distributions for $Al^{27}(p, \gamma_0)Si^{28}$.

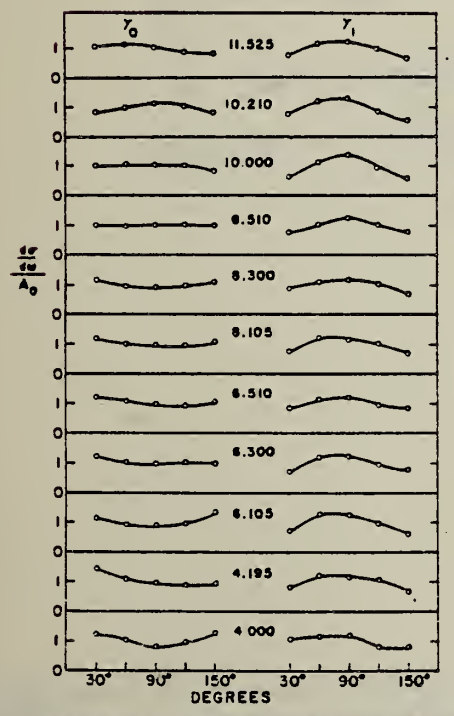

Fig. 5. Typical angular distributions observed for $Al^{27}(p, \gamma)Si^{28,29,30}$.

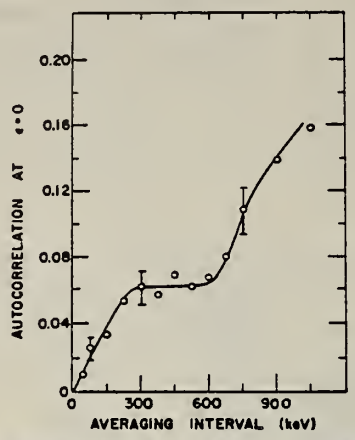

Fig. 14. Dependence of the autocorrelation at $\varepsilon = 0$ (mean squared deviation) on the averaging interval for $Al^{27}(p, \gamma_0)Si^{28}$.

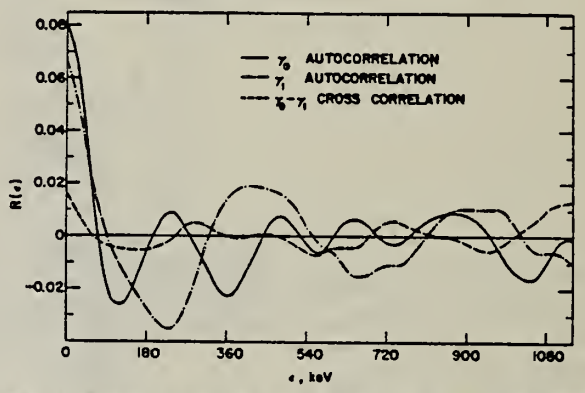

Fig. 15. Correlation functions for the yield curves from $Al^{27}(p, \gamma)Si^{28}$.

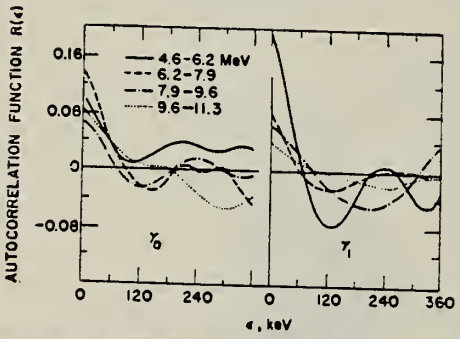

Fig. 16. Autocorrelation functions for γ_0 and γ_1 for limited energy ranges.

REF.

C. P. Swann
Phys. Rev. 139, B271 (1965)

ELEM. SYM.	A	Z
Si	28	14

METHOD Van de Graaff, $F^{19}(p,\alpha\gamma)O^{16}$ source; resonant scattering, not self-absorption

REF. NO. 65 Sw 1 NVB

REACTION	RESULT	EXCITATION ENERGY	SOURCE TYPE	SOURCE RANGE	DETECTOR TYPE	DETECTOR RANGE	ANGLE
G,G	LFT	7	D	7	NAI-D		DST
		(6.880)		(6.890)			

Mean lifetime τ: J

1.93×10^{-13} sec $< \tau < 2.48 \times 10^{-13}$ sec, assuming ground state branching to be between 70% and 90%.

J = 2.

TABLE I. Ratio of the effective cross section at 121.5° to that at 90°. The calculated values are for the spin sequences 0-1-0, 0-2-0, and 0-3-0, respectively.

Calculated values			
Spin 1	Spin 2	Spin 3	Expt. value
1.27	0.60	2.68	0.55±0.23

REF. H. Artus, P. Brix, H. G. Clerc, F. Eigenbrod, A. Goldmann, F. Gudden, E. Spamer, P. Strehl, M. Stroetzel, O. Titze, and K. J. Wetzel
Proc. Gatlinburg Conference, 314 (1966)

ELEM. SYM.	A	Z
Si	28	14

METHOD

REF. NO. 66 Ar 2 hmg

REACTION	RESULT	EXCITATION ENERGY	SOURCE TYPE	SOURCE RANGE	DETECTOR TYPE	DETECTOR RANGE	ANGLE
E,E/	LFT	5	D		MAG-D		
		(4.97)					

TABLE 1

Summary of Experimental Results[a]

Nuclide	E_x (MeV)	Type	Γ_γ^0(eV)	Γ_γ^0/Γ_w	R_σ (F)
^{6}Li	2.18	E2	$(3.9 \pm 0.5) \times 10^{-4}$	14.4	3.77 ± 0.48
	3.56	M1	8.9 ± 0.4	9.4	2.96 ± 0.11
^{7}Li	11.28 ± 0.05	(M1) or	(1.3 ± 0.4)/g[b]	0.043/g	—
		(M2)	(0.026 ± 0.008)/g	2.6/g	—
^{9}Be	15.97 ± 0.03	M1	(3.7 ± 0.8)/g	0.043/g	—
^{11}B	4.46	E2 and	0.0173 ± 0.0021	8.2	3.44 ± 0.50
		M1	0.64 ± 0.08	0.34	2.60 ± 0.35
	5.04	M1	1.84 ± 0.14	0.69	2.60 ± 0.11
^{12}C	4.43	E2	0.0122 ± 0.0008	5.30	3.14 ± 0.30
^{16}O	6.92	E2	0.100 ± 0.015	3.28	3.82 ± 0.46
	11.52	E2	0.52 ± 0.13	1.31	—
^{24}Mg	9.85 ± 0.04	M1	7.95 ± 1.2	0.38	3.50 ± 0.49
	9.97 ± 0.03				
	10.35 ± 0.03	E2	0.24 ± 0.05	0.58	5.05 ± 0.50
	10.70 ± 0.03	M1	22.2 ± 2.4	0.86	3.60 ± 0.36
	10.93 ± 0.04	E2	0.26 ± 0.11	0.50	—
^{28}Si	4.97 ± 0.02	C0	$(2.0 \pm 0.5) \times 10^{-5}$[c]	—	6.90 ± 1.20
^{40}Ca	6.89 ± 0.05	E2	0.29 ± 0.04	2.85	4.60 ± 0.50

[a] The Born approximation has been used except for ^{16}O and ^{40}Ca.
[b] $g = (2I_f + 1)/(2I_i + 1)$.
[c] Γ_e^2 equivalent to ME = (8.87 ± 1.00) F^2.

REF. B.I. Goryachev, B.S. Ishkanov, V.G. Shevchenko, and B.A. Yur'ev
ZhETF Pis'ma 4, No. 11, 491 (1966)
JETP Letters 4, No. 11, 330 (1966)

ELEM. SYM.	A	Z
Si	28	14

METHOD

REF. NO. 66 Go 3 EGF

REACTION	RESULT	EXCITATION ENERGY	SOURCE		DETECTOR		ANGLE
			TYPE	RANGE	TYPE	RANGE	
G,N	ABX	17-30	C	17-30	BF3-I		4PI

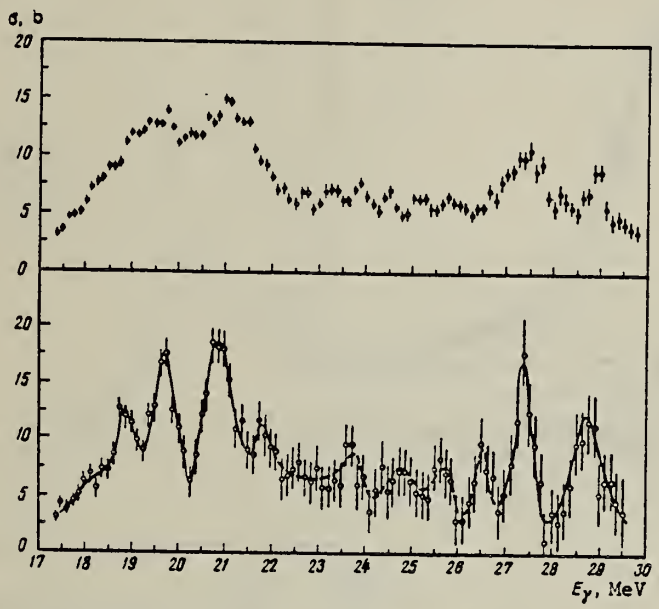

Cross section of the reaction $Si^{28}(\gamma, n)$, measured every 125 keV: a) counted in steps ΔE = 1 MeV, b) counted in steps ΔE = 0.5 MeV.

H. Lichtblau and B.M. Spicer
Aust. J. Phys. 19, 297 (1966)

ELEM. SYM.	A	Z
Si	28	14

METHOD

5 MeV Betatron; NBS ionization chamber

REF. NO. 66 Li 1 JDM

REACTION	RESULT	EXCITATION ENERGY	SOURCE		DETECTOR		ANGLE
			TYPE	RANGE	TYPE	RANGE	
G,P	SPC	THR - 32	C	21,32	SCI-D	1 - 19	90

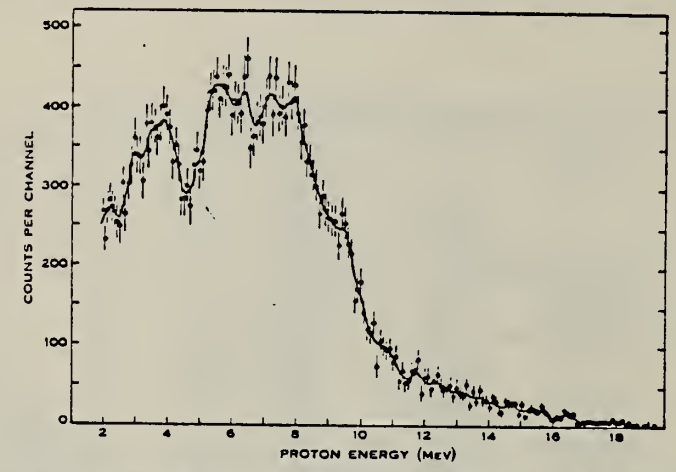

Fig. 7.—Energy spectrum of photoprotons from silicon, with bremsstrahlung end-point energy 32 MeV.

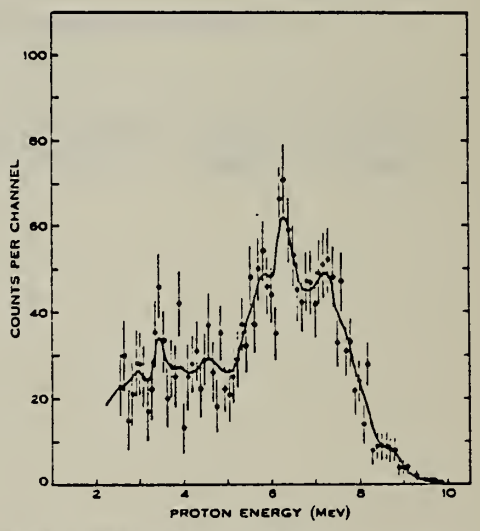

Fig. 8.—Energy spectrum of photoprotons from silicon, with bremsstrahlung end-point energy 21·2 MeV.

REF.	ELEM. SYM.	A	Z
H. Liesem Z. Physik, 196, 174 (1966)	Si	28	14

METHOD	REF. NO.	
Linac	66 Li 2	JDM

REACTION	RESULT	EXCITATION ENERGY	SOURCE		DETECTOR		ANGLE
			TYPE	RANGE	TYPE	RANGE	
E,E/	LFT	2,11	D	30-56	MAG-D		DST

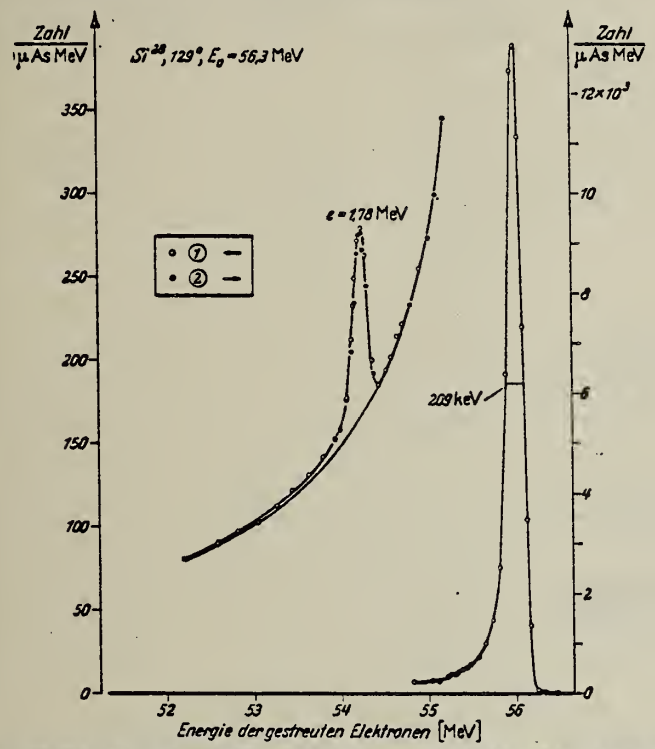

Fig. 1. Spektrum der gestreuten Elektronen mit 0 bis 3,5 MeV Energieverlust (q=0,510 fm^{-1} für ε=1,78 MeV). Die relative Energieunschärfe von Primärstrahl und Spektrometer betrug $(\Delta E/E)_A = (\Delta E/E)_S = 3‰$. Zur Prüfung der Reproduzierbarkeit wurde das Spektrum zweimal durchgemessen (offene Kreise von rechts, ausgefüllte von links kommend). Auf der Ordinate aufgetragen ist die Zahl der registrierten Elektronen pro Energieintervall bezogen auf die vom Strahlfänger aufgesammelte Ladung. Die linke Skala gilt für die unelastische, die rechte für die elastische Linie. Das Target stand in Transmissionsstellung

Tabelle 2. *Meßergebnisse*

Definition von R_{tr} s. Gl. (5). Weisskopf-Abschätzung Γ_W nach WILKINSON — in AJZENBERG-SELOVE, F.: Nuclear Spectroscopy, Part B, NewYork and London: Academic Press 1960 — mit R=1,2 fm. Werte in eckigen Klammern: Auswertung unter Einbeziehung des „Photonenpunktes" nach [15] (vgl. Fig. 4).

Anregungsenergie (MeV)	Übergang	R_{tr} (fm)	Γ_γ^0 (eV)	Γ_γ^0/Γ_W
1,77±0,01	C2	4,7±0,5 [4,3]	(1,21±0,17)·10^{-3} [1,05·10^{-3}]	16 [14]
11,42±0,02	M1	3,2±0,3	32,4±4,5	1,0

REACTION	RESULT	EXCITATION ENERGY	SOURCE TYPE	SOURCE RANGE	DETECTOR TYPE	DETECTOR RANGE	ANGLE

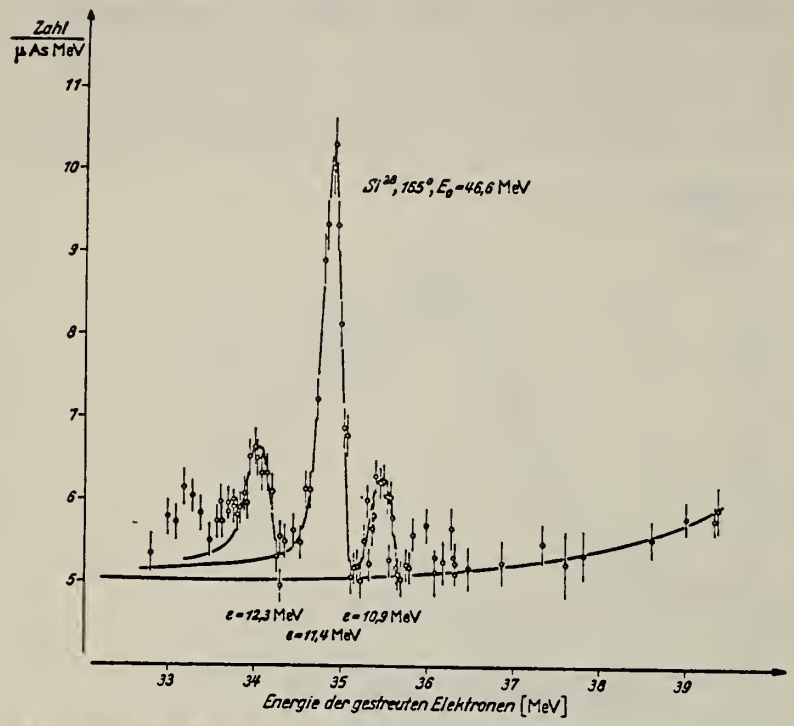

Fig. 2. Energieverteilung der mit 7 bis 13 MeV Energieverlust unelastisch gestreuten Elektronen (q= 0,410 fm^{-1} für ε=11,4 MeV). Man beachte, daß der Nullpunkt des Ordinatenmaßstabes unterdrückt worden ist. Das Target befand sich in Reflexionsstellung

Tabelle 3. *Experimentelle Parameter und Meßwerte für 10,9 und 12,3 MeV-Niveau. Die bei A_I/A_E angegebenen Fehler wurden geschätzt, sie gelten auch annähernd für die beiden letzten Spalten*

	Θ (°)	E_0 (MeV)	q (fm^{-1})	A_I/A_E (10^{-3})	$F_L^2(qE)$ (berechnet)	$R(d\sigma/d\Omega)$ (10^{-32} cm^2/sr)	$B(M1,q)$ (10^{-28} cm^2)
Si^{28}	152,45	53,74	0,471	0,72 ± 50%	0,380	0,66	0,54
10,9 MeV	152,45	35,83	0,294	0,21 ± 30%	0,635	0,73	0,68
($M1$)	152,45	46,52	0,400	0,42 ± 30%	0,486	0,67	0,57
	164,55	53,84	0,482	2,8 ± 30%	0,363	0,72	0,60
	164,55	53,82	0,482	2,3 ± 25%	0,363	0,59	0,49
	152,45	45,85	0,393	0,32 ± 25%	0,495	0,52	0,45
	152,45	55,16	0,485	0,81 ± 20%	0,360	0,67	0,55
	153,15	47,23	0,413	0,74 ± 20%	0,474	1,05	0,86
	165,05	46,55	0,413	1,9 ± 15%	0,471	0,79	0,67
Si^{28}	152,45	53,74	0,463	0,69 ± 50%	0,380	0,63	0,56
12,3 MeV	164,55	53,84	0,474	2,0 ± 50%	0,363	0,48	0,43
($M1$)	164,55	53,82	0,474	2,2 ± 50%	0,363	0,56	0,50
	152,45	55,16	0,477	0,80 ± 25%	0,360	0,66	0,58
	153,15	47,23	0,404	0,61 ± 20%	0,474	0,86	0,76
	165,05	46,55	0,405	2,1 ± 15%	0,471	0,90	0,82

REF. R. B. Begzhanov and A. A. Islamov
J. Nucl. Phys. (USSR) 5, 483 (1967)
Sov. J. Nucl. Phys. 5, 339 (1967)

ELEM. SYM.	A	Z
Si	28	14

METHOD

REF. NO. 67 Be 5 HMG

REACTION	RESULT	EXCITATION ENERGY	SOURCE		DETECTOR		ANGLE
			TYPE	RANGE	TYPE	RANGE	
G,G	LFT	2.0	D	2.0	NAI-D		120

$\tau_\gamma = (6.0 \pm 1.2) \cdot 10^{-13}$ sec. 1.78 MeV

REF.

H. W. Kuehne, P. Axel, and D. C. Sutton
Phys. Rev. 163, 1278 (1967)

ELEM. SYM.	A	Z
Si	28	14

METHOD

REF. NO.
67 Ku 2 HMG

REACTION	RESULT	EXCITATION ENERGY	SOURCE		DETECTOR		ANGLE
			TYPE	RANGE	TYPE	RANGE	
G,G	LFT	11-13	D	11-13	NAI-D	11-13	135

Photons, defined in energy to about 1% with the aid of a bremsstrahlung monochromator, were scattered by isolated energy levels in C, Mg, and Si. Parameters for the six observed levels are:

Isotope	Energy (MeV)	Γ_0^2/Γ (eV)	Γ_0/Γ	$B(M1)/(e\hbar/2M_pc)^2$
C^{13}	15.11	36	1	0.93
Mg^{24}	10.66±0.02	14	0.8	1.21
Si^{28}	11.42±0.02	23	1	1.33
Si^{28}	12.33±0.03			
Mg^{24}	9.92±0.03	3.0	0.5	0.49
Mg^{26}	10.07±0.05	4.2		≥0.36

The 15.11-MeV level in C^{13}, the 9.92- and 10.66-MeV levels in Mg^{24}, and the 11.42-MeV level in Si^{28} are $T=1$, $T_z=0$ analogs of low-lying 1+ states in the neighboring odd-odd nuclei. These levels exhaust most of of the magnetic dipole transition strength of the respective nuclei, and therefore give information about the expectation value of $l\cdot s$ in the ground state.

REF.

J. M. Loiseaux, J. M. Maison, and M. Langevin
J. de Physique 28, 11 (1967)

EL EM. SYM.	A	Z
Si	28	14

METHOD

REF. NO. 67 Lo 1 JOC

REACTION	RESULT	EXCITATION ENERGY	SOURCE		DETECTOR		ANGLE
			TYPE	RANGE	TYPE	RANGE	
G,G/	ABX	15-32	C	34	NAI-D		DST

TABLEAU I

COEFFICIENT a DES DISTRIBUTIONS ANGULAIRES

$W(\theta) = 1 + a\cos^2\theta$

^{16}O.....	a(19-25 MeV) $= 1 \pm 0,1$				
^{23}Na.....	a(15-18 MeV) $= 0,1 \pm 0,1$	a(18,5-23 MeV) $= -0,1 \pm 0,15$	a(25-30 MeV) $= 0,85 \pm 0,2$		
^{24}Mg	a(16,5-20 MeV) $= 0,3 \pm 0,1$	a(20-25 MeV) $= -0,5 \pm 0,1$	a(25,5-32 MeV) $= -0,5 \pm 0,1$		
^{28}Si	a(15-17,5 MeV) $= 0,87 \pm 0,1$	a(18-23 MeV) $= 0,7 \pm 0,1$	a(25,5-32 MeV) $= -0,5 \pm 0,1$		
^{39}K	a(14,5-18,5 MeV) $= -0,5 \pm 0,1$	a(19-24,5 MeV) $= 1 \pm 0,1$	a(25-32 MeV) $= 1 \pm 0,1$		

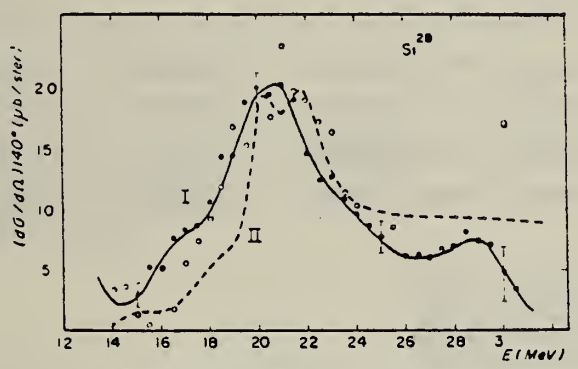

FIG. 7. — ^{28}Si Section efficace différentielle de diffusion à 140° (courbe I) (∘ $E_m = 25$ MeV ; • $E_m = 32$ MeV).

REF. G. A. Savitskii, N. G. Afanas'ev, I. S. Gul'karov, V. D. Kovalev, A. S. Omelaenko, V. M. Khvastunov, N. G. Shevchenko
J. Nucl. Phys. (USSR) 6, 685 (1967)
Soviet J. Nucl. Phys. 6, 499 (1968)

ELEM. SYM.	A	Z
Si	28	14

METHOD

REF. NO. 67 Sa 1 HMG

REACTION	RESULT	EXCITATION ENERGY	SOURCE		DETECTOR		ANGLE
			TYPE	RANGE	TYPE	RANGE	
E,E/	FMF	1-10	D	100-260	MAG-D		DST

B(EL), widths, and lifetimes also given.

Transition Matrix Elements and Characteristics of Excited Si^{28} States Obtained with a Model-dependent[21] and a Model-independent[20] Method

Energy, MeV	Level Spin and Parity	A_λ	B_λ	$\langle f\|r^\lambda\|i\rangle / F^\lambda$	$\langle f\|r^{\lambda+2}\|i\rangle / F^{\lambda+2}$	R_{trans}/F	$B(E\lambda, J_i \to J_f)/e^2F^{2\lambda}$	Γ, eV	τ, sec	G	Method of determining Parameters
1.78	2+	2.19±0.06	0.43±0.03	14.5±0.4	216.8±12.7	3.87±0.17	293±20 208.5±11.6	$(0.82\pm0.06)\cdot10^{-9}$ $(0.60\pm0.03)\cdot10^{-9}$	$(8.0\pm0.5)\cdot10^{-13}$ $(1.09\pm0.06)\cdot10^{-12}$	11.3±0.8 8.3±0.5	[*] [*]
4.62	4+	0.37±0.03	0.28±0.02	152.4±3.2	3037.5±119.2	4.50±0.13	$(2.42\pm0.19)\cdot10^4$ $(2.32\pm0.10)\cdot10^4$	$(2.58\pm0.22)\cdot10^{-10}$ $(2.77\pm0.12)\cdot10^{-10}$	$(2.29\pm0.16)\cdot10^{-6}$ $(2.38\pm0.10)\cdot10^{-6}$	6.0±0.5 5.8±0.3	[*] [*]
6.9±0.2	3−	1.01±0.08	0.31±0.07	46.8±3.7	800.0±125.5	4.14±0.49	$(3.28\pm0.35)\cdot10^3$ $(2.15\pm0.35)\cdot10^3$	$(1.31\pm0.14)\cdot10^{-4}$ $(0.83\pm0.14)\cdot10^{-4}$	$(5.02\pm0.48)\cdot10^{-12}$ $(7.47\pm1.18)\cdot10^{-12}$	10.1±1.1 6.8±1.1	[*] [*]
9.7±0.1	3−	0.79±0.05	0.35±0.07	35.3±2.3	647.2±83.5	4.23±0.44	$(1.30\pm0.19)\cdot10^3$ $(1.32\pm0.17)\cdot10^3$	$(5.63\pm0.82)\cdot10^{-4}$ $(5.72\pm0.73)\cdot10^{-4}$	$(1.17\pm0.16)\cdot10^{-12}$ $(1.15\pm0.15)\cdot10^{-12}$	4.0±0.6 4.1±0.5	[*] [*]

REF. N. G. Afanas'ev, I. S. Gul'karov, G. A. Savitskii, V. M. Khvastunov and N. G. Shevchenko
Yad. Fiz. 7, 13 (1968)
Sov. J. Nucl. Phys. 7, 8 (1968)

EL EM. SYM.	A	Z
Si	28	14

METHOD

REF. NO. 68 Af 1

hmg

REACTION	RESULT	EXCITATION ENERGY	SOURCE		DETECTOR		ANGLE
			TYPE	RANGE	TYPE	RANGE	
E,E/	FMF	10-30	D	150-225	MAG-D	120-225	DST

B(EL)

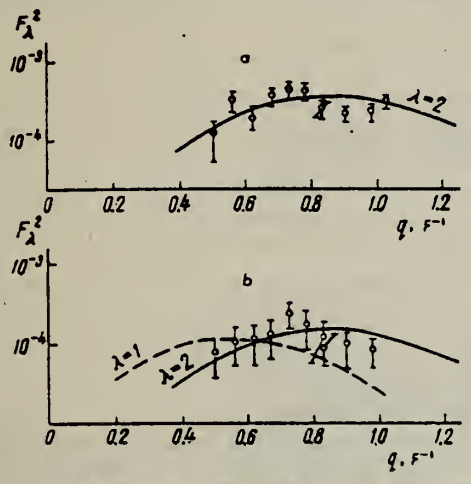

Fig. 2. Dependence of the square of the form factor of inelastic electron scattering with excitation of the levels 12.7 ± 0.2 MeV (a) and 15.0 ± 0.2 MeV (b) on the momentum transfer (points). The curves were calculated from the phenomenological model.[9]

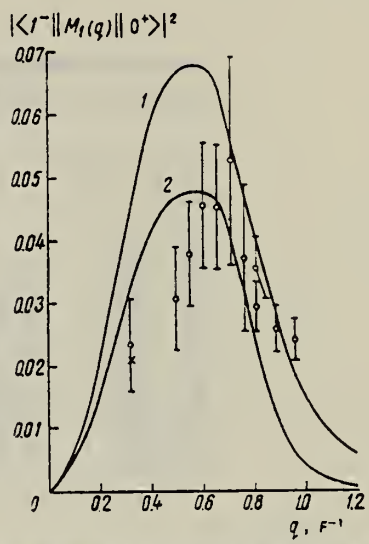

Fig. 3. Dependence of the square of the longitudinal form factor $|\langle 1^-\|M_1(q)\|0^+\rangle|^2$ on the momentum transfer. Circles—experimental points, containing also a small addition of the square of the transverse form factor; cross—experimental value of the square of the longitudinal form factor. Curves 1 and 2—calculated from the collective models of the longitudinal form factor.

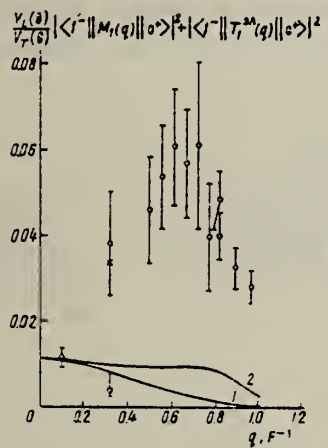

Fig. 4. Dependence of $(d\sigma/d\Omega)$ $(\Delta^4 E/8\pi\alpha^2 E' V_T(\theta))$ on the momentum transfer. Points: △—photon point;[3,4] □—point of Barber et al.[5]; ×—value of $(V_L(\theta)/V_T(\theta))|\langle 1^-\|M_1(q)\|0^+\rangle|^2$; ○—our experimental data. Curves 1 and 2—calculated from the collective models of the square of the transverse form factor (1—Goldhaber-Teller model, 2—Czyz model).

REACTION	RESULT	EXCITATION ENERGY	SOURCE		DETECTOR		ANGLE
			TYPE	RANGE	TYPE	RANGE	

Table I
Absolute differential cross sections for inelastic scattering of electrons with excitation of the 12.7 and 15.0 MeV peaks and the giant-resonance peak.

θ, deg	E, MeV	dσ/dΩ, cm²/sr		
		12.7±0.2 MeV	15.0±0.2 MeV	Giant resonance
25	150.0			$(2.53\pm0.80)\cdot10^{-29}$
40	150.7	$(3.46\pm1.81)\cdot10^{-31}$	$(2.31\pm1.21)\cdot10^{-31}$	$(5.46\pm1.47)\cdot10^{-30}$
45	151.0	$(5.93\pm1.72)\cdot10^{-31}$	$(1.99\pm1.04)\cdot10^{-31}$	$(4.17\pm0.92)\cdot10^{-30}$
50	150.8	$(2.43\pm0.78)\cdot10^{-31}$	$(1.36\pm0.71)\cdot10^{-31}$	$(3.30\pm0.73)\cdot10^{-30}$
55	150.8	$(2.91\pm0.72)\cdot10^{-31}$	$(1.06\pm0.55)\cdot10^{-31}$	$(2.24\pm0.49)\cdot10^{-30}$
60	150,6	$(2.42\pm0.60)\cdot10^{-31}$	$(1.35\pm0.45)\cdot10^{-31}$	$(1.82\pm0.57)\cdot10^{-30}$
65	150.1	$(1.67\pm0.41)\cdot10^{-31}$	$(6.87\pm3.59)\cdot10^{-32}$	$(9.21\pm2.90)\cdot10^{-31}$
50	199.1	$(1.72\pm0.42)\cdot10^{-31}$	$(8.50\pm4.45)\cdot10^{-32}$	$(1.52\pm0.21)\cdot10^{-30}$
50	199.1	$(1.73\pm0.35)\cdot10^{-31}$	$(5.96\pm2.54)\cdot10^{-32}$	$(1.25\pm0.17)\cdot10^{-30}$
55	199.3	$(1.01\pm0.21)\cdot10^{-31}$	$(4.60\pm2.39)\cdot10^{-32}$	$(7.42\pm1.02)\cdot10^{-31}$
60	199.3	$(7.42\pm1.89)\cdot10^{-32}$	$(2.65\pm1.13)\cdot10^{-32}$	$(4.81\pm0.66)\cdot10^{-31}$
55	225.0	$(1.13\pm0.13)\cdot10^{-31}$		

Table II
Matrix elements of transition and characteristics of highly excited Si^{28} states, obtained by the model-dependent[9] and model-independent[10] methods

Spin and parity of levels	Energy, MeV	$\langle f\|\|r^\lambda\|\|i\rangle F^\lambda$	$\langle f\|\|r^{\lambda+2}\|\|i\rangle / F^{\lambda+2}$,	R_{trans}, F	$B(E\lambda;J_i\to J_f)$, $e^2\cdot F^{2\lambda}$	Γ_{γ_0}	τ_{exp}	G	Method of determining the parameters (see reference)
2+	12.7±0.2	3.31±0.23	51.6±8.9	3.95±0.48	15.3±4.3	0.81±0.23	$(8.1\pm2.3)\cdot10^{-16}$	0.61±0.17	[9]
					11.0±1.5	0.58±0.08	$(11.3\pm1.6)\cdot10^{-16}$	0.44±0.06	[10]
2+	15.0±0.2	2.86±0.25	54.1±11.9	4.35±0.67	6.7±1.9	0.82±0.24	$(8.0\pm2.3)\cdot10^{-16}$	0.27±0.08	[9]
					8.2±1.4	1.0±0.2	$(6.6\pm1.2)\cdot10^{-16}$	0.33±0.06	[10]
1−	15.0±0.2	0.29±0.02	2.8±0.3	3.11±0.24	$(14.3\pm4.3)\cdot10^{-2}$	167.7±50.3	$(3.9\pm1.2)\cdot10^{-14}$	0.08±0.02	[9]
					$(8.4\pm0.7)\cdot10^{-2}$	98.5±8.2	$(6.7\pm0.6)\cdot10^{-18}$	0.05±0.01	[10]

REF. T. E. Drake, E. L. Tomusiak and H. S. Caplan
Nucl. Phys. A118, 138 (1968)

ELEM. SYM.	A	Z
Si	28	14

METHOD

REF. NO. 68 Dr 1 egf

REACTION	RESULT	EXCITATION ENERGY	SOURCE		DETECTOR		ANGLE
			TYPE	RANGE	TYPE	RANGE	
E,E/	FMF	11	D	140	MAG-D		DST

11=11.4

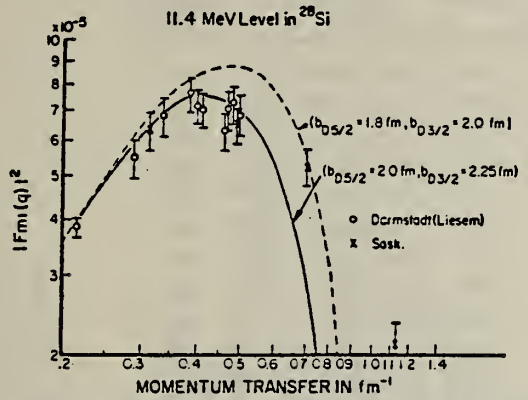

Fig. 11. The momentum-transfer dependence of the square of the form factor for the 11.4 MeV magnetic dipole level in ^{28}Si. The theoretical curves were calculated using harmonic-oscillator wave functions with the oscillator parameters b as shown.

REF. I.S. Gulkarov, N.G. Afanasyev, G.A. Savitsky, V.M. Khvastunov and N.G. Shevchenko
Phys. Letters 27B, 417 (1968)

ELEM. SYM.	A	Z
Si	28	14

METHOD

REF. NO. 68 Gu 1 egf

REACTION	RESULT	EXCITATION ENERGY	SOURCE		DETECTOR		ANGLE
			TYPE	RANGE	TYPE	RANGE	
E,E/	ABX	10-30	D	150-225	MAG-D	100-225	DST

$q^2 = 0.09 - 0.9$ fm^{-2}

Table 1
Absolute differential cross sections of the inelastic electron scattering with the giant resonance excitation
Integration limits from 14 to 30 MeV.

θ^o	E (MeV)	q(fm^{-1})	$\frac{d\sigma}{d\Omega}$ (cm^2/sr)	$\frac{V_L(\theta)}{V_T(\theta)}$
25	150.0	0.32	$(2.53 \pm 0.80) \times 10^{-29}$	1.65
40	150.7	0.50	$(5.46 \pm 1.47) \times 10^{-30}$	1.52
45	151.0	0.56	$(4.17 \pm 0.92) \times 10^{-30}$	1.43
50	150.8	0.61	$(3.30 \pm 0.73) \times 10^{-30}$	1.34
55	150.8	0.67	$(2.24 \pm 0.49) \times 10^{-30}$	1.26
60	150.6	0.72	$(1.82 \pm 0.57) \times 10^{-30}$	1.17
65	150.1	0.77	$(9.21 \pm 2.90) \times 10^{-31}$	1.08
50	199.1	0.82	$(1.52 \pm 0.21) \times 10^{-30}$	1.37
50	199.1	0.82	$(1.25 \pm 0.17) \times 10^{-30}$	1.37
55	199.3	0.89	$(7.42 \pm 1.02) \times 10^{-31}$	1.28
60	199.3	0.96	$(4.81 \pm 0.66) \times 10^{-31}$	1.18
50	224.3	0.92	$(1.01 \pm 0.14) \times 10^{-30}$	1.37

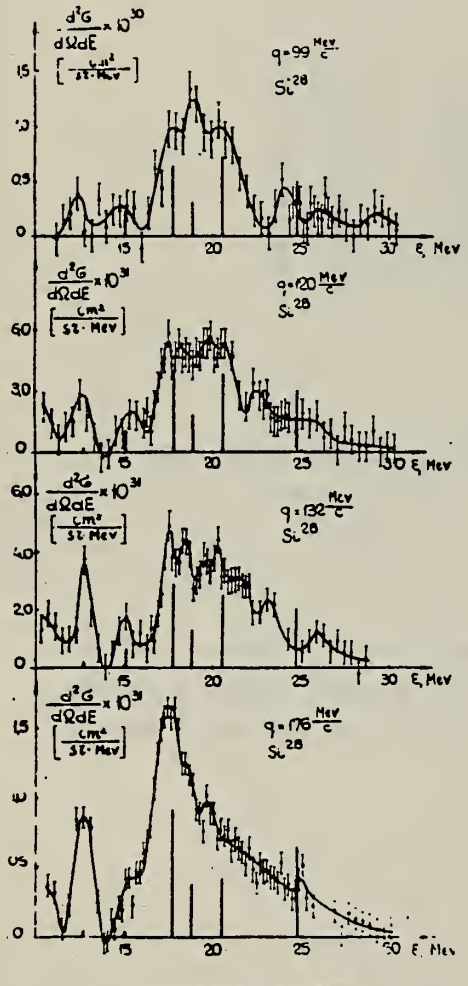

Fig. 1. Inelastic electron spectra in ^{28}Si measured for different momentum transfers. Radiative tails from elastic and inelastic peaks are subtracted; ϵ is the excitation energy. Vertical lines represent the particle-hole model calculations of the longitudinal formfactor [3]. In order to get better agreement with experiment all vertical lines were 1 MeV shifted to the left. The length of the lines is given in relative units.

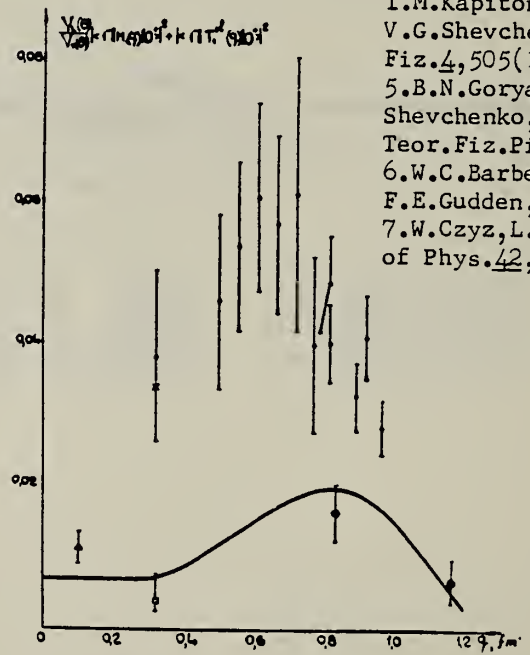

Fig. 2. Dependence of $(d\sigma/d\Omega)/(\Delta^4/8\pi\alpha^2 V_T(\theta))\ E/E'$ on the momentum transfer. The solid curve is the particle-hole calculation of the transverse formfactor [3,7].
○ - our data; △ - photon point [4,5] ;
□ - Barber et al. [6] ; ⊙ - ref. 7.

3. I.B.Seaborn, I.M. Eisenberg, Nucl.Phys.63,496 (1965).
4. B.N.Goryachev, B.S.Ishkanov, I.M.Kapitonov,Zh.M.Seliverstova, V.G.Shevchenko,B.A.Yuryev, Yad. Fiz.4,505(1966).
5.B.N.Goryachev,B.S.Ishkhanov,V.G. Shevchenko,B.A.Yuryev,Zh.Eksp.i Teor.Fiz.Pis'ma Redakt.4,491(1966).
6.W.C.Barber,F.Berthod,C.Fricke, F.E.Gudden,Phys.Rev.120,2081(1960).
7.W.Czyz,L.Lesniak,A.Malecki,Ann. of Phys.42, 97 (1967).

REF. L. Meyer-Schutzmeister, Z. Vager, R. E. Segel and P. P. Singh
Nucl. Phys. A108, 180 (1968)

ELEM. SYM.	A	Z
Si	28	14

METHOD

[Page 1 of 2]

REF. NO. 68 Me 1 EGF

REACTION	RESULT	EXCITATION ENERGY	SOURCE		DETECTOR		ANGLE
			TYPE	RANGE	TYPE	RANGE	
G,A	ABX	15-22	D	5.3-14	NAI-D	10-22	DST

777

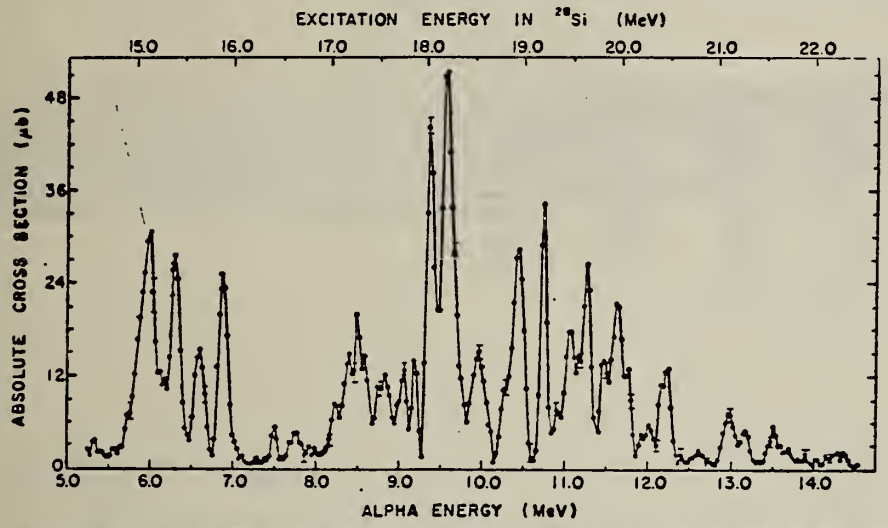

Fig. 3. The absolute cross section for the reaction $^{24}Mg(\alpha,\gamma_0)^{28}Si$, plotted as a function of the bombarding energy E_α. In integrating the γ_0 intensity over all angles to obtain these cross sections, the measured angular distribution of the $\sin^2\theta$ form – characteristic of pure electric-dipole transitions – has been used. A slight correction for the solid angle of the detector is included.

TABLE 1

The averaged absolute cross sections $\overline{\sigma(\alpha,\gamma_0)}$ and $\overline{\sigma(\alpha,\gamma_1)}$ for the reactions $^{24}Mg(\alpha,\gamma_0)$, $^{24}Mg(\alpha,\gamma_1)$, $^{26}Mg(\alpha,\gamma_0)$ and $^{28}Si(\alpha,\gamma_0)$

	$^{24}Mg(\alpha,\gamma)^{28}Si$		$^{26}Mg(\alpha,\gamma_0)^{30}Si$		$^{32}Si(\alpha,\gamma_0)^{32}S$	
ΔE_x (MeV)	$\overline{\sigma(\alpha,\gamma_0)}$ (μb)	$\overline{\sigma(\alpha,\gamma_1)}$ (μb)	ΔE_x (MeV)	$\overline{\sigma(\alpha,\gamma_0)}$ (μb)	ΔE_x (MeV)	$\overline{\sigma(\alpha,\gamma_0)}$ (μb)
14.65–16.65	8.5	5.0	14.1–16.1	6.1	13.1–15.5	1.7
16.65–18.65	12.9	6.1	16.1–18.1	9.7	15.5–17.5	2.2
18.65–20.65	11.0	8.6	18.1–20.1	4.6		
20.65–22.65	2.1	5.6	20.1–22.1	1.0		
14.65–22.65	8.6	6.3	14.1–22.1	5.3	13.1–17.5	1.9

The cross sections in the first four rows were obtained from the data in figs. 3–6 and 15 by averaging over the indicated ≈ 2 MeV ranges of excitation energy E_x in the product nucleus (^{28}Si, ^{30}Si or ^{32}S). The last line gives the average for the entire energy range that was studied.

REACTION	RESULT	EXCITATION ENERGY	SOURCE		DETECTOR		ANGLE
			TYPE	RANGE	TYPE	RANGE	

TABLE 3

The cross sections $\overline{\sigma(\gamma, \alpha_0)}$ for the α-decay of the nuclei ^{28}Si, ^{29}Si and ^{32}S

Target nucleide	ΔE (MeV)	$\overline{\sigma(\gamma, \alpha_0)}$ (mb)	$\overline{\sigma(\gamma, p_0)}$ (mb)	$\frac{\overline{\sigma(\gamma, \alpha_0)}}{\overline{\sigma(\gamma, p_0)}}$	$\gamma^2(\alpha_0)/\gamma^2(p_0)$	
					$l = 1$	$l = 3$
^{28}Si	16.65–18.65	1.01	6.2	0.16	0.35	0.12
	18.65–20.65	0.94	11.7	0.080	0.095	0.041
	20.65–22.65	0.22	9.6	0.023	0.019	0.011
	16.65–22.65	0.72	9.2	0.08		
^{29}Si	14.1 –16.1	0.43				
	16.1 –18.1	0.69				
	18.1 –20.1	0.35				
	18.1 –20.1	0.35				
	20.1 –22.1	0.08				
	14.1 –22.1	0.38				
^{32}S	13.1 –15.5	0.20	1.7	0.12		
	15.5 –17.5	0.27	2.1	0.13		
	17.5 –19.5		3.0			
	13.1 –17.5	0.23	1.9	0.12		

The averages were taken over ≈ 2 MeV wide energy regions ΔE and over the total studied energy region of the giant dipole resonance. These cross sections were obtained by detailed balance from the α-capture in ^{24}Mg, ^{25}Mg and ^{26}Si. For comparison, the average cross sections $\overline{\sigma(\gamma, p_0)}$ over the same energy regions ΔE for the reactions ^{28}Si$(\gamma, p_0)^{27}$Al and ^{32}S$(\gamma, p_0)^{31}$P are also presented. These likewise were obtained by detailed balance from the inverse reactions as measured by Singh *et al.* [5]) and by Dearnaley *et al.* [4]). For the calculation, we assumed an isotropic angular distribution for the ^{28}Si(γ, p_0) reaction, a $\sin^2\theta$ distribution for ^{32}S(γ, p_0). In addition, the ratios $\overline{\sigma(\gamma, \alpha_0)}/\overline{\sigma(\gamma, p_0)}$ are given for both ^{28}Si and ^{32}S and also the calculated reduced width $\gamma^2(\alpha_0)/\gamma^2(p_0)$ for an orbital-angular-momentum transfer of $l = 1$ and of $l = 3$ in the decay of ^{28}Si.

Yu. P. Antuf'ev, V. L. Agranovich, V. B. Ganenko, V. S. Kuzmenko, I. I. Miroshnichenko, and P. V. Sorokin
Ukr. Fiz. Zh. 14, 248 (1969)

Si	28	14

METHOD

REF. NO. 69 An 6 egf

REACTION	RESULT	EXCITATION ENERGY	SOURCE		DETECTOR		ANGLE
			TYPE	RANGE	TYPE	RANGE	
G,P	ABY	109-999	C	700,999	TEL-D	97-230	DST
G,D	ABY	120-999	C	700,999	TEL-D	97-205	DST

999 = 1.2 GEV

Summary

The cross-sections of the (γ, p) (γ, d) reactions were investigated. Li^7, Be^9, C^{12}, Si^{28}, Cu^{63}, Mo^{96} and Ta^{181} targets were irradiated with the bremsstrahlung of 700 and 1200 MeV maximum energy from the Kharkov PhTI Ac. Sci. UkrSSR linear accelerator. The photoprotons and deuterons were detected by the scintillation telescope at 30°, 60°, and 120° with the beam. Possible mechanisms of the proton and deuteron photoproduction are discussed. The qualitative agreement of A dependence of the cross-sections is observed with a suggestion on the meson mechanism for these reactions.

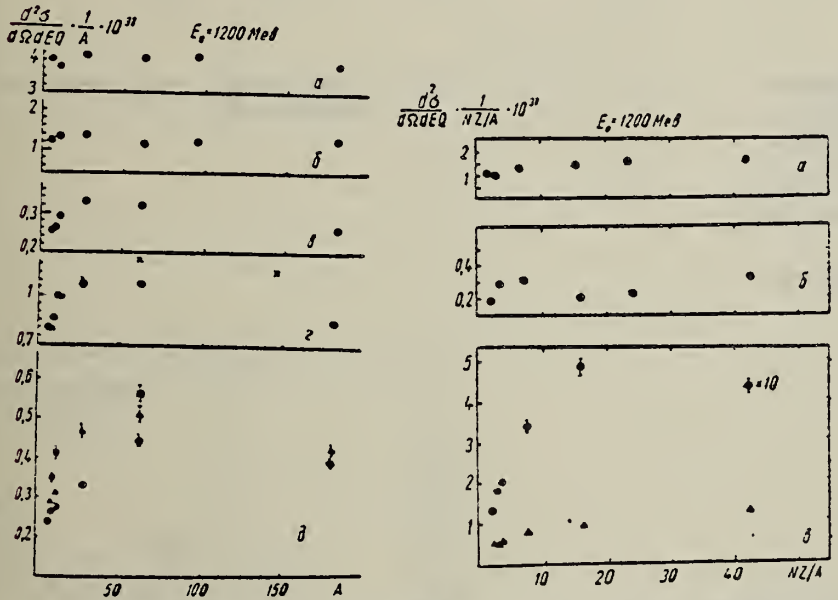

Рис. 1. Залежність перерізу (γ, p)-реакції від A: а — ϑ=30°, E_p=97 *Мев*; б — E_p=205 *Мев*; в — ϑ=60°, E_p=230 *Мев*; г — E_p=157 *Мев* (× — дані [3]); д — ϑ=120°, ○ — E_p=120 *Мев*, △ — E_p=157 *Мев*, □ — E_p=230 *Мев*. Абсолютне значення перерізу наведено при енергії протонів E_p=120 *Мев*. Інші дані нормовані до перерізу для Li^7 при E_p=120 *Мев*.

Рис. 2. Залежність перерізу (γ, d)-реакції від *NZ/A*: а — ϑ=30°, E_d=97 *Мев*; б — ϑ=30°, E_d=205 *Мев*; в: △ — ϑ=60°, E_d=97 *Мев*, ○ — ϑ=120°, E_d=97 *Мев* (перерізи наведені в одиницях 10^{-32} *см²/стер · Мев · Q*).

L. W. Fagg, W. L. Bendel, E. C. Jones, Jr., and S. Numrich
Phys. Rev. 187, 1378 (1969)

ELEM. SYM.	A	Z
Si	28	14

METHOD

REF. NO.	
69 Fa 1	hmg

REACTION	RESULT	EXCITATION ENERGY	SOURCE		DETECTOR		ANGLE
			TYPE	RANGE	TYPE	RANGE	
E,E/	ABX	9-16	D	39,56	MAG-D	30-56	180
				(38.9,55.9)			

J-PI, B(ML)

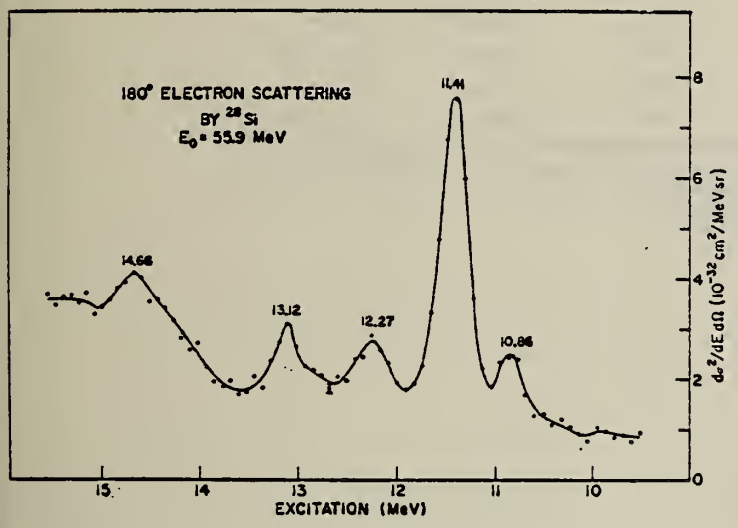

FIG. 2. Differential cross section for 180° electron scattering from ^{28}Si at E_0 = 55.9 MeV covering the excitation energy range 10–15 MeV.

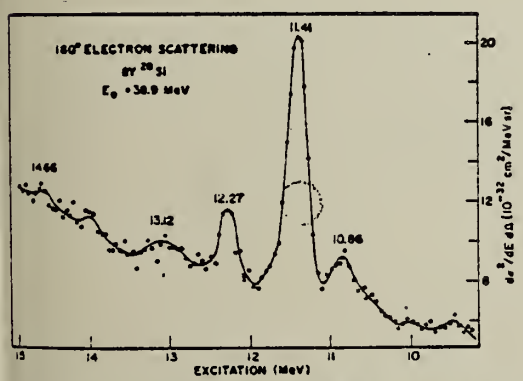

FIG. 3. Differential cross section for 180° electron scattering from ^{28}Si at E_0 = 38.9 MeV covering the excitation energy range 9-15 MeV.

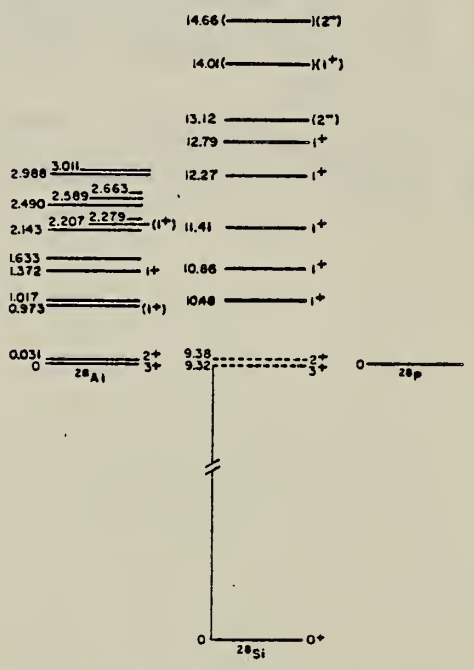

FIG. 4. Energy-level diagram adjusted for the Coulomb displacement so that the ^{28}Si and ^{28}Al analog states are approximately aligned. Only the ^{28}Si states denoted with a solid line were excited in this experiment. The energies given in the ^{28}Al-level scheme are those quoted from Endt and Van der Leun (Ref. 22). The parentheses around the states at 14.66 and 14.01 MeV indicate a considerable degree of uncertainty as to their existence and position.

[over]

TABLE I. Values of differential cross sections, spin and parity, transition radii, and radiation widths for energy levels excited in ^{28}Si.

Level energy (MeV)	$d\sigma/d\Omega)_{56}$ (10^{-34} cm^2/sr)	$(d\sigma/d\Omega)_{28}$ (10^{-34} cm^2/sr)	J^π	PWBA R_M (fm)	PWBA Γ_0 (eV)	DWBA corrected R_M (fm)	DWBA corrected Γ_0 (eV)
10.48±0.06	10±3	39±9	1$^+$	4.1	3.3	3.9±0.4	$2.4_{-0.9}^{+1.3}$
10.86±0.04	60±5	117±10	1$^+$	3.25	8.0	$2.98_{-0.27}^{+0.23}$	$5.7_{-1.1}^{+1.3}$
10.90±0.06[a]					4.8±1.3[a]		
11.41±0.03	250±14	408±28	1$^+$	2.93	29.2	$2.58_{-0.25}^{+0.21}$	$20.8_{-3.7}^{+4.3}$
11.42±0.02[e]				3.2±0.3[e]	32.4±4.5[a]	3.0±0.3[b]	25.7±3.6[b]
11.42±0.02[e]					47±12[d] 33[e]		22.9±4[c]
12.27±0.04	55±6	103±12	1$^+$	3.22	10.1	$2.93_{-0.23}^{+0.23}$	$7.3_{-1.8}^{+2.0}$
12.32±0.06[a]					7.5±1.9[a]		
12.79±0.10	17±5	37±12	1$^+$	3.5	4.5	$3.2_{-1.2}^{+0.7}$	$3.3_{-1.7}^{+2.3}$
13.12±0.05	53±10	55±18	(2$^-$)	5.0	0.20	$4.6_{-1.3}^{+0.9}$	$0.14_{-0.07}^{+0.10}$
14.01±1.10	20±10	62±24	(1$^+$)	4.0	12.2	$3.8_{-1.1}^{+0.8}$	$8.9_{-5.0}^{+7.2}$
14.66±0.08	110±35	62±26	(2$^-$)	3.3	0.28	$2.7_{-2.7}^{+1.8}$	$0.20_{-0.10}^{+0.20}$

[a] Reference 5. In this reference the value of R_M found for the 11.4-MeV level was also used to find Γ_0 for other levels.
[b] Reference 18 using the data of Ref. 5.
[c] Reference 11. Photon scattering result using $\Gamma_0/\Gamma = 1$, where Γ is the total level width.
[d] Reference 6.
[e] Reference 7.

[5] H. Leisem, Z. Physik 196, 174 (1966).
[6] W. C. Barber, F. Berthold, G. Fricke, and F. E. Gudden, Phys. Rev. 120, 2081 (1968).
[7] R. D. Edge and G. A. Peterson, Phys. Rev. 128, 2750 (1962).
[11] H. W. Kuehne, P. Axel, and D. L. Sutton, Phys. Rev. 163, 1278 (1967).
[22] P. M. Endt and C. Van der Leun, Nucl. Phys. A105, 1 (1967).

REF. S.V. Dementii, N.G. Afanas'ev, I.M. Arkatov, V.G. Vlasenko, V.A. Gol'dshtein, and E.L. Kuplennikov
Yad. Fiz. 11, 19 (1970)
Sov. J. Nucl. Phys. 11, 10 (1970)

ELEM. SYM.	A	Z
Si	28	14

METHOD

REF. NO. 70 De 1 hmg

REACTION	RESULT	EXCITATION ENERGY	SOURCE		DETECTOR		ANGLE
			TYPE	RANGE	TYPE	RANGE	
E,E/	ABX	400-999	D	690-999	MAG-D		DST
		(400-1115)		(690-1115)			

NO DATA, SEE C12

Results for ^{28}Si are claimed to be similar to those for ^{12}C.

REF. T. W. Donnelly Jr., J. D. Walecka, G. E. Walker and I. Sick
Phys. Letters 32B, 545 (1970)

ELEM. SYM.	A	Z
Si	28	14

METHOD

REF. NO. 70 Do 1 egf

REACTION	RESULT	EXCITATION ENERGY	SOURCE		DETECTOR		ANGLE
			TYPE	RANGE	TYPE	RANGE	
E,E/	FMF	11-24	D	100-300	MAG-D		145

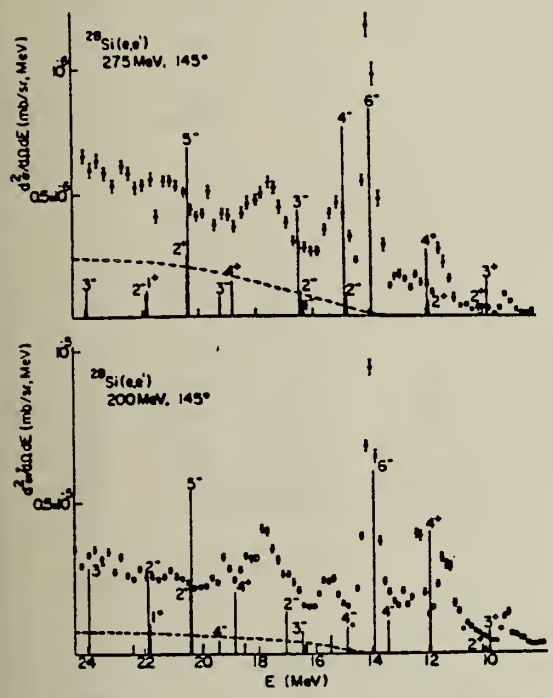

Fig. 1a. The cross section $d^2\sigma/d\Omega dE$ for inelastic electron scattering from ^{28}Si at E_e = 275 MeV, $\theta = 145^\circ$ unfolded for radiative processes. The non-negligible cross sections predicted by the p-h model for q = = 525 MeV/c are shown as spikes (arbitrary overall scale). The dashed line is the computed quasi-elastic spectrum; b) Same as (a), except E_e = 200 MeV and theoretical cross sections computed for q = 375 MeV/c.

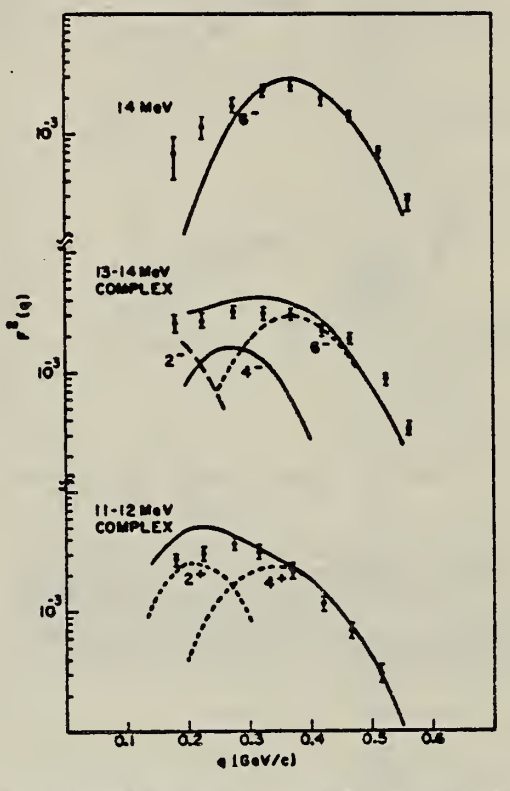

Fig. 2. Form factors for the 11-12 MeV, 13-14 MeV and 14 MeV complexes. The p-h states comprising each complex and the experimental energy intervals are given in the text. All theoretical T = 1 form factors have been reduced by $\frac{1}{2}$.

[over]

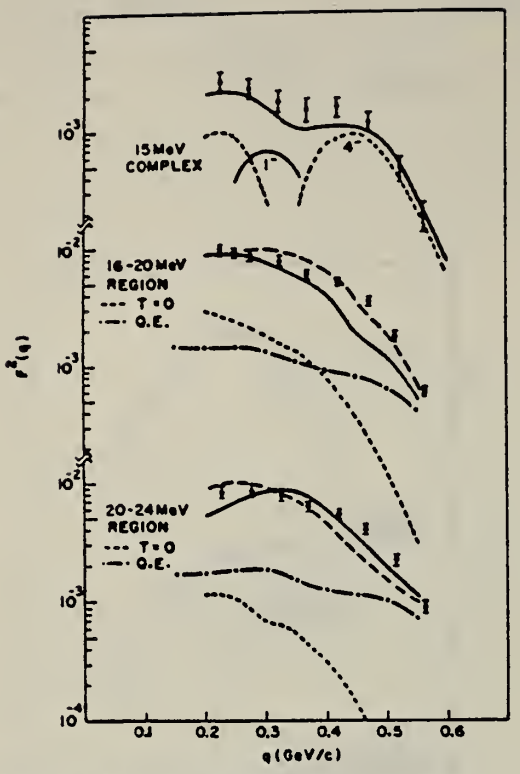

Fig. 3. Form factors for the 20-24 MeV, 16-20 MeV and 15 MeV complexes. For the first two complexes, the quasi-elastic (see text) and $T = 0$ p-h contributions are also shown. The $T = 1$ p-h contributions have been reduced by $\frac{1}{2}$. The results of moving the $1f_{5/2}$ configuration energy down by 1 MeV is indicated by the heavy dashed line.

REF.

M. A. Meyer, N. S. Wolmarans, D. Reitmann
Nucl. Phys. A144, 261 (1970)

ELEM. SYM.	A	Z
Si	28	14

METHOD

REF. NO.	
70 Me 1	egf

REACTION	RESULT	EXCITATION ENERGY	SOURCE		DETECTOR		ANGLE
			TYPE	RANGE	TYPE	RANGE	
P,G	RLY	12-13	D	1-2	SCD-D	0-13	

TABLE 2

Gamma decay of $^{27}Al(p,\gamma)^{28}Si$ resonances in the energy range E_p = 1.01–2.00 MeV

Resonance			Gamma decay in percentages to E_x (MeV) in ^{28}Si												
E_p [a] (keV)	E_x [b] (keV)	J^π [c]	0 0^+	1.78 2^+	4.62 4^+	4.98 0^+	6.28 3^+	6.69 0^+	6.88 3^-	6.89 4^+	7.38 2^+ [d]	7.42 2^+	7.80 3^+	7.93 2^+	Other levels E_x (%)
1025	12574	$1^+, 2$	2	28		1	2				1	6	47		8.26(8), 8.33(1), 8.59(2), 8.90(1), 9.50(1)
1090	12636	(3^-) [e]		19	21		14		1		6			1	8.33(5), 9.32(6), 9.38(4), 10.38(23)
1098	12644	(4^-) [e]			13				41	17					8.95(4), 9.42(3), 9.70(22)
1118	12664	4^- [e]			0.7		29		6						8.41(48), 8.59(12), 9.32(0.3) 9.70(1), 11.43(3)
1172	12715	$1, 2^+$	0.5	70			2	7	1		1	6		0.5	8.26(1), 9.38(6), 9.50(2), 10.59(3)
1183	12726	2^+ [f]	68	21		6	1		2						9.32(2)
1199	12742	3^- [e]		22			30		26			2	2	7	8.41(1), 8.59(2), 9.32(3), 9.38(3), 9.42(1), 9.70(1)
1213	12755	$1^-, 2^+$		76		1		12	1		4	1		0.5	8.26(2), 9.50(2), (10.72(0.5))
1262	12802	3^- [e]		43	5		1		41			6			8.41(2), 9.32(0.5), 9.38(1), 9.42(0.5)
1278	12817	$4^+, 5^-$			32		4			20					8.54(2), 8.59(22), 9.16(5), 9.42(14), 10.31(1)
1317	12855	4^+ [e]		13	13		52		2	6			5		8.59(2), 8.95(1), 9.32(6)
1328	12866	$2^+, 3, 4^+$		89	7						2	2			
1364	12900	(4^+) [e]		25	10		42			15					8.59(2), 9.32(3), 9.38(3)
1365	12901	2^+ [e]													
1381	12917	$2^+, 3, 4^+$		86	5		4					2	1		8.59(2)
1388	12924	$2^+, 3^-$		83	1		3			3	3	1		3	8.26(1), 8.59(1), 9.16(1)
1457	12991	$2, 3, 4^+$		3	13		1		4				9		8.41(5), 8.59(8), 9.32(57)
1502	13034	2^+	5	38	23				12		5	6	1	4	8.26(2), 8.41(1), 9.32(1), 9.38(2)
1520	13051			76			1		18		1		2		8.33(1), 9.76(1)
1566	13095	$(3^-, 4^+)$ [f]		3	6		5			9		2	25		8.26(8), 8.41(2), 9.32(36), 10.38(4)
1578	13107	2^+	43	6			3		7				7		8.54(4), 8.59(11), 9.32(14), 10.18(5)
1588	13117	$2^+, 3, 4^+$		45	22		3		6		9	2			8.26(1), 8.41(3), 9.16(3), 10.21(6)
1647	13173	3^- [f]		23	6		16				4	6	10	2	9.32(30), 9.38(3)
1662	13188			82			3				5		2	2	8.26(1), 9.50(5)
1663	13189														
1680	13205	$2, 3, 4^+$		91	3				1	1	3				9.32(1)
1684	13209	$3^-, 4^+$		79					10						9.70(11)
1706	13230	$2^+, 3, 4^+$		23	5		8			27		1			8.59(3), 8.95(3), 9.32(17), 9.38(9), 9.70(4)
1724	13248	3^- [f], 5^- [g]			2		2			6				(1)	9.70(89)
1749	13272			78										8	9.32(11), 9.38(1), 10.38(2)
1800	13321	$(1, 2, 3^-)$	2	95										3	
1842	13361	3^- [f]	2	11	3		4			11		18	1	2	8.59(1), 9.32(21), 9.42(2), 10.38(24)
1899	13416	2^+	19	22	5		7		11						10.38(36)
1910	13427				62					21					8.59(4), 8.95(6), 10.42(7)
1969	13483			40			17		10		4	5		4	8.33(1), 8.59(7), 9.32(3), 9.38(2), 9.50(4), 10.21(3)

[a]) Ref. [9]) and the present experiment, see table 1.
[b]) As computed with the Q-value from ref. [1]).
[c]) Present experiment (see subsect. 4.1) unless indicated otherwise.
[d]) Ref. [1]).
[e]) Ref. [9]) and ref. [14]).
[f]) Ref. [15]).
[g]) Ref. [16]).

REF. P. Strehl
Z. Physik 234, 416 (1970)

ELEM. SYM.	A	Z
Si	28	14

METHOD

REF. NO. 70 St 2 egf

REACTION	RESULT	EXCITATION ENERGY	SOURCE TYPE	SOURCE RANGE	DETECTOR TYPE	DETECTOR RANGE	ANGLE
E,E/	ABX	5,6	D	30-58	MAG-D		DST
		(4.98, 6.69)					

5=4.98, 6=6.69 0+

Tabelle 3. *Experimentelle Parameter und Meßwerte. E_0, Θ Primärenergie, Streuwinkel im Laborsystem. q unelastischer Impulsübertrag. σ/σ_E gemessenes Verhältnis von unelastischem zu elastischem differentiellen Wirkungsquerschnitt; in Klammer ist der statistische Fehler in % angegeben. $d\sigma/d\Omega$ unelastischer differentieller Wirkungsquerschnitt; wegen der Fehlerangaben vgl. Text. Die Meßwerte für Si und S sind als Ergebnisse für ^{nat}Si und ^{nat}S aufzufassen (vgl. Text)*

	E_0 (MeV)	Θ (°)	q^2 (fm^{-2})	σ/σ_E (10^{-4})	$d\sigma/d\Omega$ (10^{-33} cm^2/ster.)
^{12}C 7,65 MeV	59,58	117,04	0,231	14,90 (0,6)	24,69 ±1,60
	56,94	129,02	0,231	13,79 (1,0)	13,68 ±0,96
	54,12	141,11	0,229	14,98 (0,7)	8,15 ±0,55
	52,75	153,15	0,231	15,24 (1,0)	6,62 ±0,47
	51,90	165,05	0,231	15,78 (1,8)	1,16 ±0,09
	51,18	104,98	0,145	5,80 (0,7)	28,80 ±1,69
	47,90	117,04	0,145	5,51 (0,7)	17,19 ±1,01
	45,48	129,02	0,145	5,97 (1,2)	11,14 ±0,71
	43,57	141,11	0,143	5,95 (1,1)	6,09 ±0,38
	42,54	153,15	0,145	5,82 (1,4)	2,67 ±0,18
	37,51	104,98	0,074	1,41 (1,4)	15,38 ±1,07
	35,08	117,04	0,073	1,33 (1,6)	9,14 ±0,57
	33,39	129,02	0,073	1,44 (1,7)	5,89 ±0,37
	32,04	141,11	0,073	1,39 (2,0)	3,11 ±0,21
	31,36	153,15	0,073	1,39 (3,2)	1,39 ±0,11
^{24}Mg 6,44 MeV	59,01	116,94	0,232	5,53 (2,2)	28,28 ±2,24
	55,81	129,03	0,231	5,41 (1,5)	16,65 ±1,20
	53,64	140,95	0,231	5,65 (1,6)	9,51 ±0,70
	52,14	153,00	0,231	5,17 (2,1)	3,95 ±0,32
	36,98	104,96	0,074	0,59 (2,6)	25,08 ±1,78
	34,59	116,94	0,074	0,56 (3,2)	15,09 ±1,16
	32,87	129,03	0,074	0,58 (2,8)	9,37 ±0,68
	31,72	140,95	0,074	0,58 (3,1)	5,10 ±0,39
	30,86	153,00	0,074	0,68 (5,5)	2,69 ±0,27
Si 4,98 MeV	58,38	116,94	0,232	5,61 (1,9)	38,70 ±2,68
	55,12	129,03	0,231	5,27 (0,9)	21,98 ±1,34
	52,87	141,11	0,231	5,58 (1,3)	12,72 ±0,81
	51,28	153,00	0,230	5,69 (1,9)	6,00 ±0,42
	49,93	104,96	0,145	2,05 (1,6)	49,60 ±3,13
	49,97	104,96	0,146	2,10 (1,4)	50,68 ±3,09
	46,77	116,94	0,146	2,23 (2,2)	33,90 ±2,31
	44,28	129,03	0,146	2,14 (2,0)	19,48 ±1,29
	42,44	141,11	0,146	2,20 (1,7)	10,98 ±0,70
	41,23	153,00	0,145	2,45 (2,1)	5,64 ±0,38
	41,37	153,00	0,146	2,48 (2,5)	5,67 ±0,40
	36,28	104,96	0,074	0,53 (4,5)	32,51 ±2,90
	36,26	104,96	0,074	0,56 (4,0)	34,35 ±2,89
	33,98	116,94	0,074	0,55 (4,3)	21,28 ±1,83
	32,17	129,03	0,074	0,52 (4,0)	11,98 ±1,00
	30,87	141,11	0,073	0,59 (5,3)	7,54 ±0,73
	29,96	153,00	0,073	0,66 (5,7)	3,89 ±0,39
	30,09	153,00	0,074	0,60 (5,0)	3,52 ±0,33
Si 6,69 MeV	58,38	116,94	0,225	0,48 (25)	3,30 ±1,00
S 3,78 MeV	59,19	104,96	0,210	0,32 (37)	5,17 ±3,36
	58,80	104,96	0,209	0,27 (45)	4,40 ±3,30
^{40}Ca 3,35 MeV	53,98	140,95	0,250	0,92 (9)	3,03 ±1,21

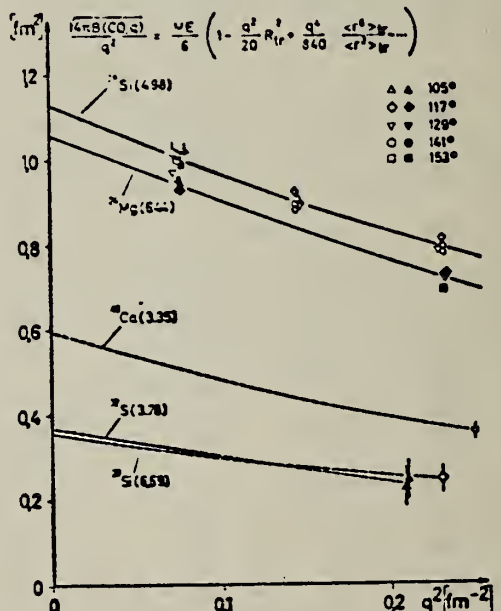

Fig. 3. Meßergebnisse für Monopolübergänge in ^{24}Mg(6,44 MeV), ^{28}Si(4,98 und 6,69 MeV), ^{32}S(3,78 MeV) und ^{40}Ca(3,35 MeV) als Funktion von q^2. Die eingetragenen Meßpunkte und die zugehörigen Kurven gelten für eine Auswertung mit f_c, x_1 und x_2 nach Modell I. Für ^{28}Si(4,98) sind nur die aus σ/σ_E und D_{exp}^{BA} berechneten longitudinalen Anteile aufgetragen (vgl. 5.1), wobei die Meßpunkte bei gleicher Impulsübertragung und gleichem Streuwinkel (vgl. Tabelle 3) zusammengefaßt wurden. Die gestrichelten Kurven zeigen die Extrapolation nach $q=0$ mit vorgegebenem Übergangsradius

REF. D. V. Webb, E. G. Muirhead and B. M. Spicer
Nucl. Phys. A159, 81 (1970)

ELEM. SYM.	A	Z
Si	28	14

METHOD

REF. NO. 70 We 1 egf

REACTION	RESULT	EXCITATION ENERGY	SOURCE		DETECTOR		ANGLE
			TYPE	RANGE	TYPE	RANGE	
G,N	ABX	17-32	C	17-32	ACT-I		4PI

356+

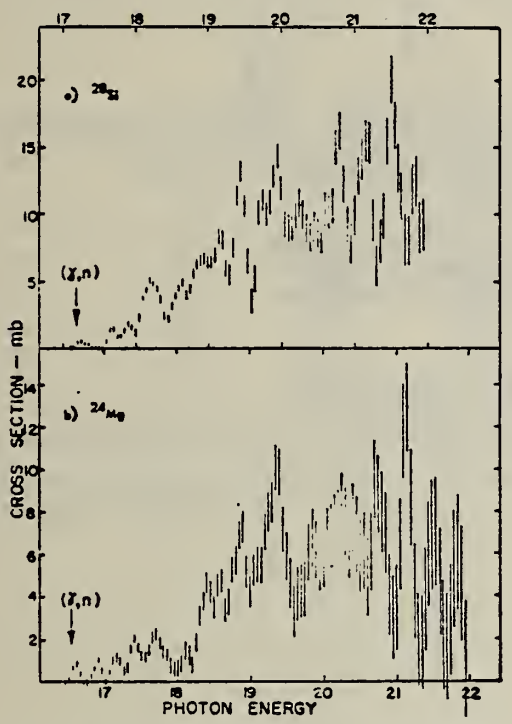

Fig. 2. Analysis of the Δ_c = 50 keV data to 22 MeV in Δ_s = 100 keV bins for the photoneutron cross sections of (a) silicon and (b) magnesium.

TABLE 2

Integrated cross sections for silicon

Source	$\int_0^{24\,MeV} \sigma dE$ (MeV · mb)	$\int_0^{31\,MeV} \sigma dE$ (MeV · mb)
this experiment	53±5	93±8
Caldwell *et al.* [21])	45	69
Goryachev *et al.* [20])	63	105
Bolen and Whitehead [23])	64	

[20])B.I.Goryachev, B.S.Ishkhanov, V.G.Shevchenko, B.A.Yur'ev, JETP Lett.4 (1966)330.
[21])J.T.Caldwell, R.R.Harvey, R.L.Bramblett, S.C.Fultz, Phys. Lett.6(1963)213.
[23])L.N. Bolen, W.D.Whitehead, Phys.Rev.132 (1963)2251.

[over]

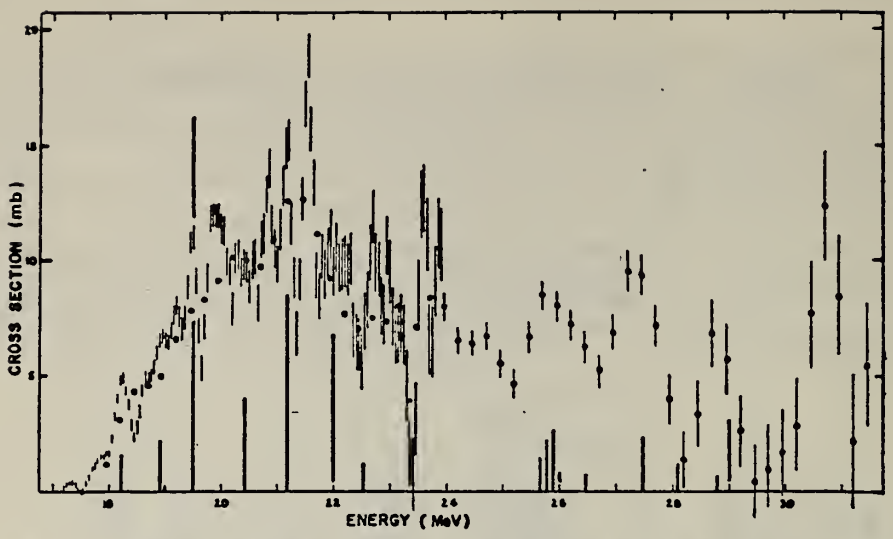

Fig. 1. The photoneutron cross section of silicon. The full circles indicate the coarse resolution measurement (Δ_e = 250 keV, Δ_a = 500 keV). The higher resolution measurement (Δ_e = 50 keV, Δ_a = 200 keV) is presented by the error bars up to 24 MeV. The heavy vertical bars show the predictions of Drechsel *et al.* [10].

[10] D. Drechsel, J.B. Seaborn and W. Greiner, Phys. Rev. 162 (1967) 983.

REF. W. F. Davidson, J. L. Black, M. R. Najam, B. M. Spicer
Nucl. Phys. A168, 399 (1971)

ELEM. SYM.	A	Z
Si	28	14

METHOD

REF. NO. 71 Da 2 egf

REACTION	RESULT	EXCITATION ENERGY	SOURCE		DETECTOR		ANGLE
			TYPE	RANGE	TYPE	RANGE	
HE,G	ABX	27-31	D	4-8	NAI-D		DST

HE=HE3

TABLE 1

Summary of differential cross sections for γ_0 and γ_1 observed in the reaction $^{25}Mg(\tau,\gamma)^{28}Si$

E_τ [a] (MeV)	Angle	Target thickness (keV)	E_x [b] (MeV)	$\frac{(d\sigma)}{(d\Omega)}_{\gamma_0}$ (nb/sr)	$\frac{(d\sigma)}{(d\Omega)}_{\gamma_1}$ (nb/sr)
4.44	90°	110	27.20	20±10	25±10
6.08	90°	450	28.64	9± 6	26±15
6.08	55°	450	28.64	17± 8	40±20
6.08	55°	450	28.64	12± 7	26±15
6.15	90°	90	28.73	22±15	70±30
8.26	90°	75	30.61	< 20	< 20

[a]) The ^{3}He bombarding energies quoted here have been adjusted for energy degradation in the target.

[b]) The excitation in ^{28}Si has been corrected for energy loss in the target, and is synonymous with the energy of the ground state capture γ-ray.

REF. N.V. Goncharov, A.I. Derebchinskii, O.P. Konovalov, S.G. Tonapetyan, and V.M. Khvorostyan
Yad. Fiz. 14, 31 (1971)
Sov. J. Nucl. Phys. 14, 18 (1972)

EL EM. SYM.	A	Z
Si	28	14

METHOD

REF. NO.	
71 Go 2	hmg

REACTION	RESULT	EXCITATION ENERGY	SOURCE		DETECTOR		ANGLE
			TYPE	RANGE	TYPE	RANGE	
G,PI+	RLY	150-500	C	500	CCH-D		DST

PI-/PI+ YIELD RATIO

Measurements are reported of the relative yield of π^0 mesons and the π^-/π^0 yield ratio for mesons with energy 40 ± 10 MeV emitted in the angular range θ_{lab} = 50–160° in photon-induced reactions with E_γ^{max} = 500 MeV with light and medium nuclei. The charged π-meson detector was a 34-cm Freon bubble chamber with a tube for the beam. The π^-/π^+ yield ratio for He^4, Li^7, C^{12}, Si^{28}, S^{32}, Ca^{40}, and Nb^{93} was found to be respectively 0.94 ± 0.14, 2.15 ± 0.31, 1.22 ± 0.21, 1.25 ± 0.15, 1.0 ± 0.13, 1.11 ± 0.13, and 1.53 ± 0.25. It was established that the π^0-meson yield follows a $ZA^{-1/3}$ law.

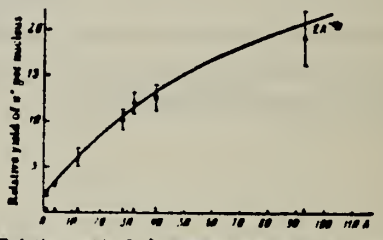

FIG. 2. Relative yield of π^0 mesons per nucleus as a function of mass number A.

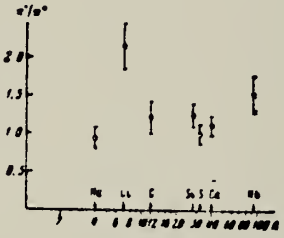

FIG. 3. π^-/π^0 yield ratio as a function of mass number A.

Y. Horikawa, Y. Torizuka, A. Nakada, S. Mitsunobu, Y. Kojima, and M. Kimura
Phys. Letters 36B, 9 (1971)

Si	28	14

METHOD

REF. NO. 71 Ho 1 egf

REACTION	RESULT	EXCITATION ENERGY	SOURCE TYPE	SOURCE RANGE	DETECTOR TYPE	DETECTOR RANGE	ANGLE
E,E/	FMF	2,5	D	183,250	MAG-D		DST

1.78,4.61 MEV

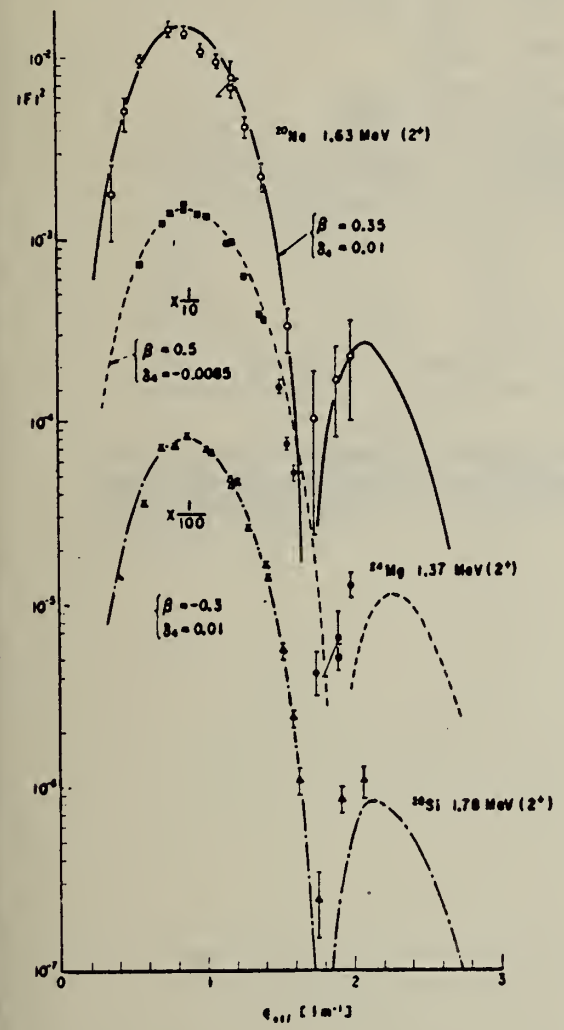

Fig.1. The experimental form factors for the 2$^+$ members of the ground-state rotational bands in ^{20}Ne, ^{24}Mg and ^{28}Si are shown as a function of the q_{eff} [3].

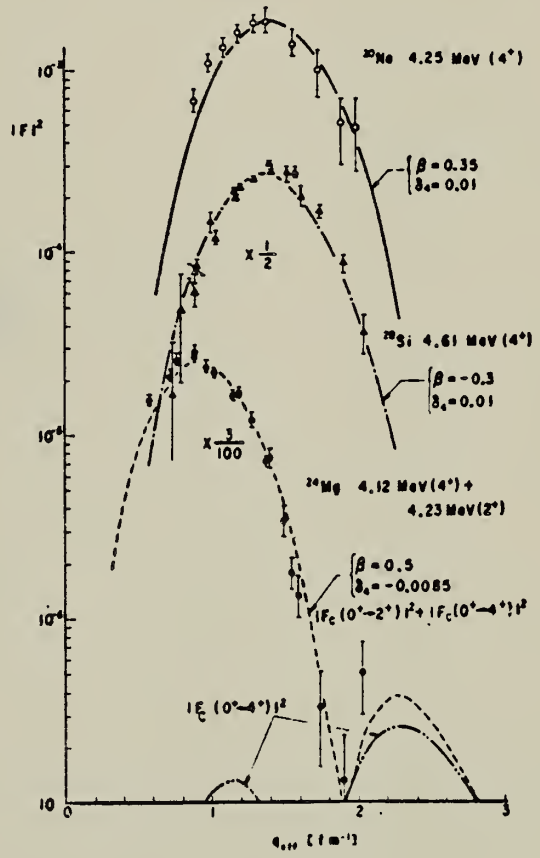

Fig.2. The same as for fig. 1 except for the 4$^+$ members. The unresolved data of the 4.12 MeV (4$^+$) and 4.23 MeV(2^+_2) states is presented in the case of ^{24}Mg.

(over)

(2) R. de Swiniarski, D. Glashausser, D. L. Hendrie, J. Sherman, A D. Bacher, and E. A. McClatchie, Phys. Rev. Letters 23 (1964) 317.
(3) D. G. Ravenhall, quoted in: R. Hofstater, Rev. Mod. Phys. 28 (1956) 214.
(5) H. Rebel, G. W. Schweimer, J. Specht, G. Schatz, R. Lohken, D. Habs, G. Hanser and H. Klewe-Nebenius, Phys. Rev. Letters 26 (1971) 1190.

Table 1

The values obtained from the Nilsson orbits which provide the best fit form factors. The signs of the moments were determined by the characteristic of the orbits. The β_2 and β_4 values of the present study are compared with those of the (p,p') [2] and (α,α') [5] reactions.

	$\langle r^2\rangle^{1/2}$	$\langle r^4\rangle^{1/4}$	Q_o	H_o	β_2			β_4		
	(fm)	(fm)	(efm^2)	(efm^4)	present (e,e')	(p,p')	(α,α')	present (e,e')	(p,p')	(α,α')
^{20}Ne	2.91	3.14	+58 ± 3	+249 ± 27	+0.40	+0.47	+0.35 ±0.01	+0.19	+0.28 ±0.05	+0.11 ±0.01
^{24}Mg	3.03	3.24	+69 ± 3	+ 48 ± 16	+0.45	+0.47		-0.06	-0.05 ±0.08	
^{28}Si	3.14	3.35	-64 ± 3	+205 ± 33	-0.39	-0.37	-0.32 ±0.01	+0.10	+0.25 ±0.08	+0.08 ±0.01

REF. V. G. Vlasenko, N. G. Afanas'ev, V. A. Gol'dshtein, S. V. Dementii, and E. L. Kuplennikov
Yad. Fiz. 13, 259 (1971); Sov. J. Nucl. Phys. 13, 144 (1971)

ELEM. SYM.	A	Z
Si	28	14

METHOD

REF. NO. 71 V1 1 hmg

REACTION	RESULT	EXCITATION ENERGY	SOURCE		DETECTOR		ANGLE
			TYPE	RANGE	TYPE	RANGE	
E,E/	FMF	0-300	D	592- 999	MAG-D		DST

999 = 1143 QUASIELASTIC SCTNG

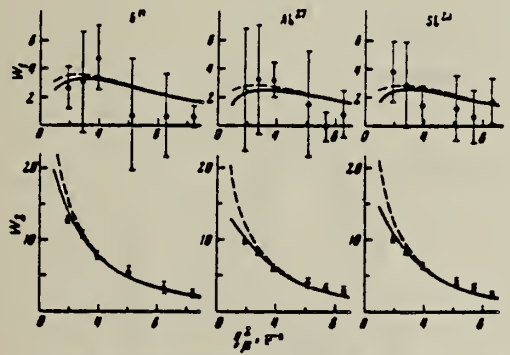

FIG. 3. Inelastic electromagnetic form factors of B^{11}, Al^{27}, and Si^{28}, measured in the region of the continum. The dashed curves are the result of a calculation based on Eqs. (2), (7), and (8), and the solid curves based on Eqs. (3), (7), and (8).

REF.

A. Nakada & Y. Torizuka
J. Phys. Soc. Japan 32, 1 (1972)

ELEM. SYM.	A	Z
Si	28	14

METHOD

REF. NO.: 72 Na 1 egf

REACTION	RESULT	EXCITATION ENERGY	SOURCE TYPE	SOURCE RANGE	DETECTOR TYPE	DETECTOR RANGE	ANGLE
E,E/	LFT	1-10	D	183-250	MAG-D		DST

1.78,4.6,6.9,9.7 MEV

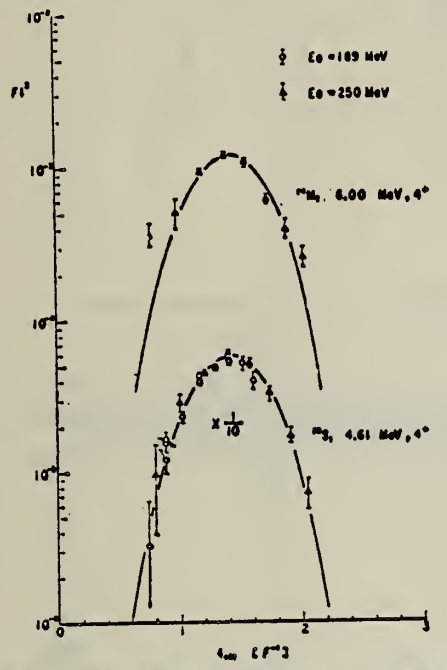

Fig. 7. The inelastic form factors for the 6.00-MeV(4+) state in ^{24}Mg and 4.61-MeV(4+) state in ^{28}Si.

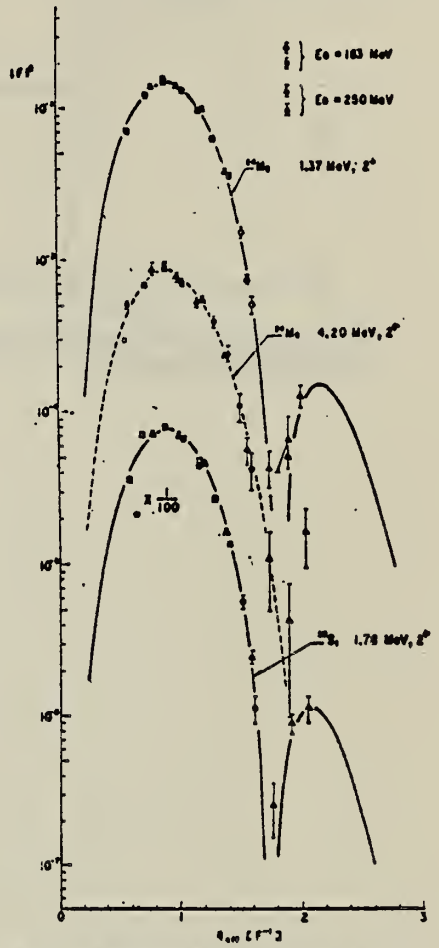

Fig. 5. The inelastic form factors for the 1.37-(2+ 4.20-MeV (2+) states in ^{24}Mg and for the 1.7 MeV (2+) in ^{28}Si are shown as a function of q_{eff}. The curves are the best fit form factors calculate with the Born approximation.

Table II. The $B(EL)$ values extracted from the experimental form factors.

			Born approx.		DWBA	
Nucleus	E_x (MeV)	J^π	$B(EL)$ (W.U.)	$B(EL)$ (e^2F^{2L})	$B(EL)$ (W.U.)	$B(EL)$ (e^2F^{2L})
^{24}Mg	1.37	2+	18.1±1.7	(3.27±0.35)×10^3	21.7±2.2	(4.46±0.45)×10^3
	4.23	2+	1.11±0.18	(2.28±0.37)×10		
	6.00	4+	10.6	2.87×10^4		
^{28}Si	1.78	2+	11.1±1.5	(2.80±0.38)×10^3	13.7±1.3	(3.46±0.33)×10^3
	4.61	4+	4.35±0.49	(1.78×0.20)×10^4		
	6.88	3−	8.99±0.71	(2.93±0.23)×10^3		
	9.70	3−	1.88±0.30	(6.13±0.98)×10^3		

(over)

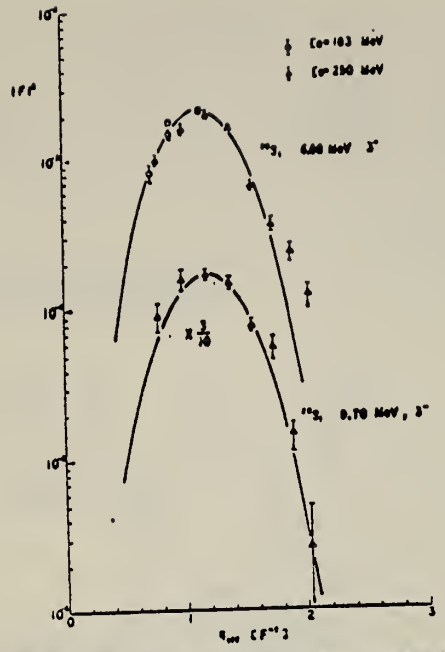

Fig. 6. The inelastic form factors for the 6.88-(3⁻) and 9.70-MeV (3⁻) states in ^{28}Si.

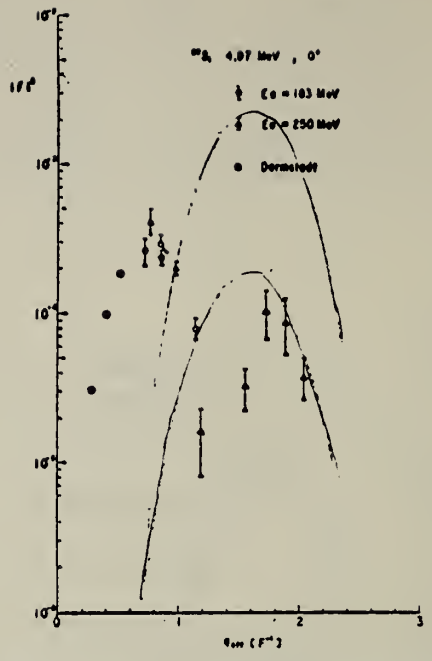

Fig. 8. The inelastic form factor for the 4.97-MeV(0+) state in ^{28}Si. The data of Darmstadt, Phys. Letters 27B (1968) 641, are also plotted.

REF.

J.E.M. Thomson, N.D. Champion, R.J.J. Stewart, M.N. Thompson
Aust. J. Phys. 25, 669 (1972)

ELEM. SYM.	A	Z
Si	28	14

METHOD

REF. NO.	
72 Th 8	egf

REACTION	RESULT	EXCITATION ENERGY	SOURCE		DETECTOR		ANGLE
			TYPE	RANGE	TYPE	RANGE	
G,NG	ABI	18- 28	C	28	SCD-D		140
G,PG	ABI	12- 28	C	28	SCD-D		140

TABLE 1

RESULTS FOR STATES POPULATED IN ^{27}Si AND ^{27}Al

(a) ^{27}Si

E (MeV)	J^π	$\int_0^{28} \sigma\, dE$ (MeV mb)	Spectroscopic factor C^2S (^{3}He, α)*	(p, d)†
0	5/2+	53±1‡	2·99	2·14
0·784	1/2+	14	0·42	0·65
0·954	3/2+	7	0·38	0·37
2·17	7/2+	—	—	—
2·65	5/2	<2·3	0·78	0·23
2·86	—	3·4	1·43	0·82
2·91	—	—	—	—

(b) ^{27}Al

E (MeV)	J^π	$\int_0^{23} \sigma\, dE$ (MeV mb)	(d, ^{3}He)§ l	C^2S
0	5/2+	50±5‡	2	3·1
0·843	1/2+	32	0	0·58
1·013	3/2+	19	2	0·60
2·21	7/2+	<2	—	—
2·73	5/2+	12	2	0·63
2·98	3/2+	13	(2)	<0·3
3·001	9/2+	—	—	—
3·68	1/2+	8	—	—
3·96	(3/2)	(3)	—	—
4·05	(1/2, 3/2)−	9	1	—

* Data from Swenson, Zurmuhle, and Fou (1967).
† Data from Jones, Johnson, and Griffiths (1968).
‡ See text for derivations of ground state integrated cross sections.
§ Averages of the data from Gove *et al.* (1968) and Wildenthal and Newman (1968).

REF. J. Ahrens, H.B. Eppler, H. Gimm, H. Gundrum, M. Kroning, P. Riehn, G. SitaRam, A. Zieger, and B. Ziegler
PICNS-73, Vol. I, p. 23 Asilomar

ELEM. SYM.	A	Z
Si	28	14

METHOD

REF. NO.	
73 Ah 4	hmg

REACTION	RESULT	EXCITATION ENERGY	SOURCE		DETECTOR		ANGLE
			TYPE	RANGE	TYPE	RANGE	
G,MU-T	ABX	THR-140	C	10-140	MGC-D		4PI

Statistics may have been improved over those of 72Ah7.

See figure on other side.

(OVER)

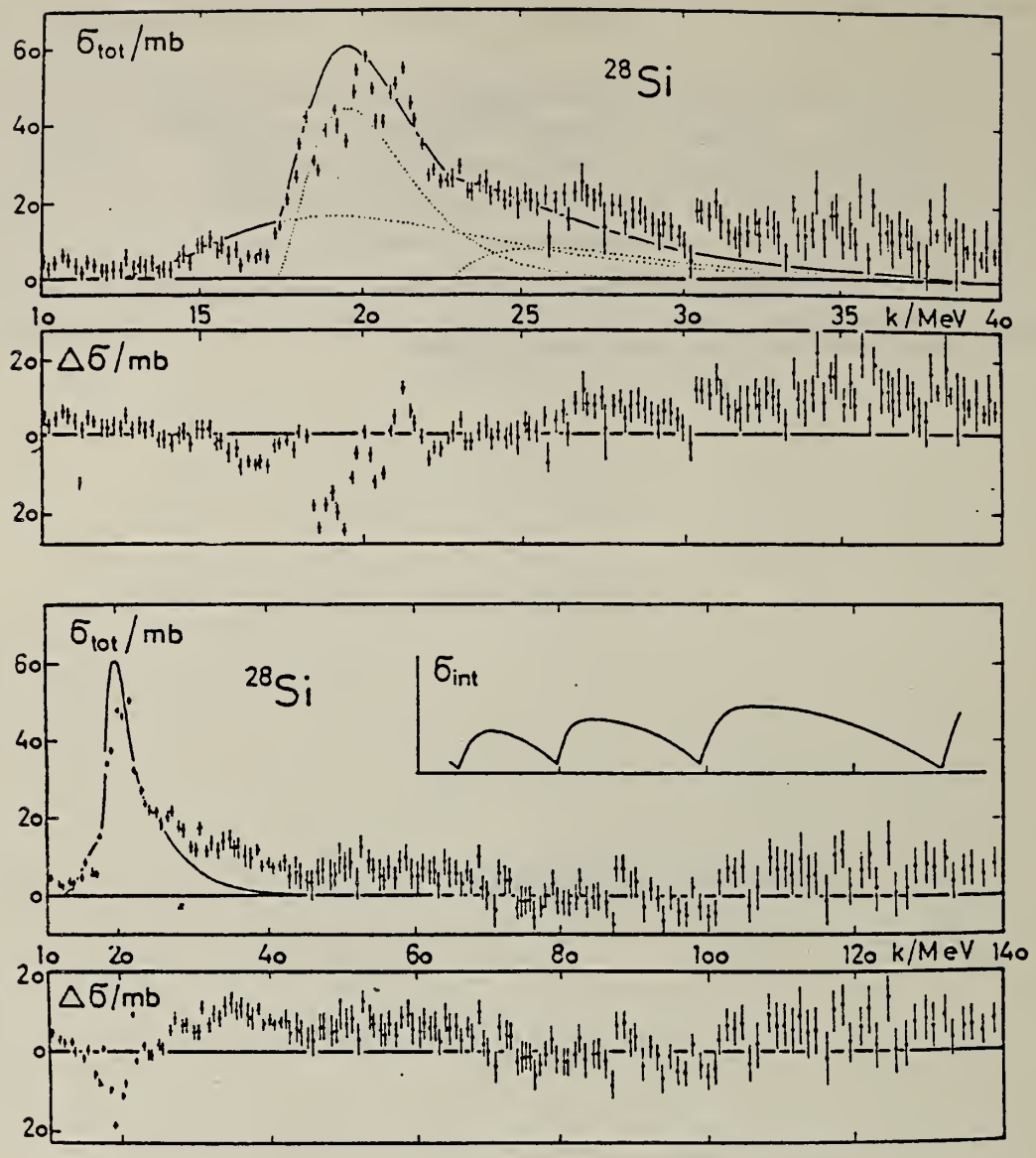

Fig. 7. Same as Fig. 2 for Si. The Si-target consisted of monocrystalline Si-rods in which occurs coherent pair production. As this effect has not been taken into account when subtracting the pair cross section from the measured data it appears in the data given here. The predicted shape of the interference term σ_{int} from theory [5] is given in the insert.

REF.	ELEM. SYM.	A	Z
R. Bergere, H. Beil, P. Carlos, A. Lepretre, A. Veyssiere PICNS - 73, Vol.I, p. 525 Asilomar	Si	28	14

METHOD	REF. NO.	
	73 Be 10	hmg

REACTION	RESULT	EXCITATION ENERGY	SOURCE		DETECTOR		ANGLE
			TYPE	RANGE	TYPE	RANGE	
G,N	ABX	16- 30	D	16- 30	BF3-I		4PI

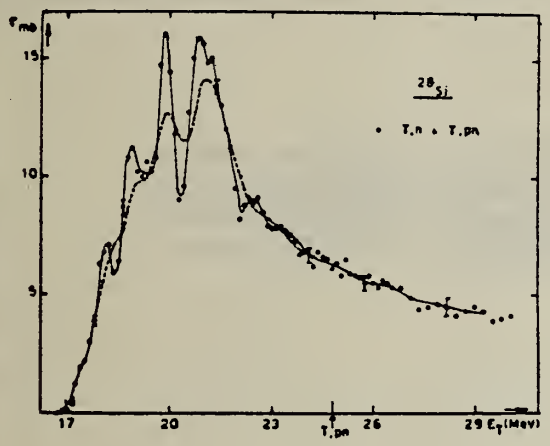

Fig. 1 ^{28}Si[(γ,n) + (γ,pn)] cross sections measured with an energy resolution
1) ΔE = 350 keV (dotted line)
2) ΔE = 180 keV (solid line)

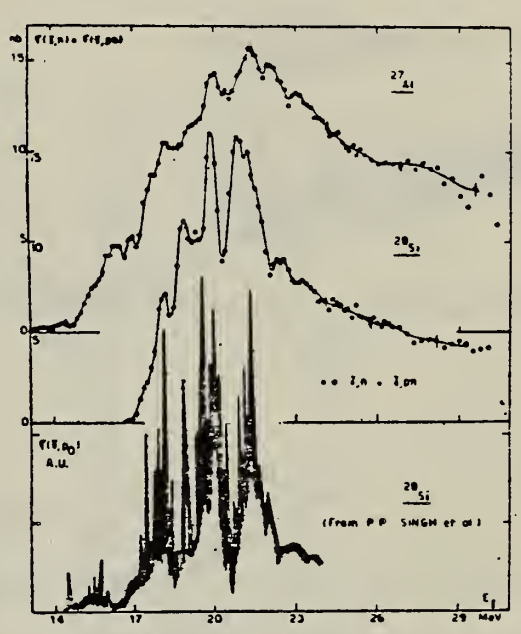

Fig. 3 ^{28}Si and ^{27}Al [(γ,n) + (γ,pn)] cross-sections compared to ^{27}Al(p,γ$_0$)^{28}Si measured by Singh.[6]

[6] P.P. Singh et al., Nucl. Phys. 65, 577 (1965)

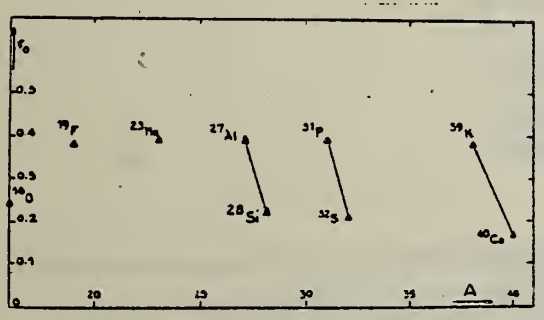

Fig. 13 Integrated photoneutron cross-sections for s-d shell nuclei.

REF. I.I. Chkalov, N.G. Shevchenko, N.G. Afanas'ev, I.I. Zalyubovskii, A.A. Khomich, V.N. Polishchuk, A.S. Litvinenko, A. Yu. Buki
Yad. Fiz. 18, 945 (1973)
Sov. J. Nucl. Phys. 18, 487 (1974)

ELEM. SYM.	A	Z
Si	28	14

METHOD

REF. NO. 73 Ch 7 hmg

REACTION	RESULT	EXCITATION ENERGY	SOURCE TYPE	SOURCE RANGE	DETECTOR TYPE	DETECTOR RANGE	ANGLE
E,E/	FMF	11- 30	D	108-220	MAG-D		135

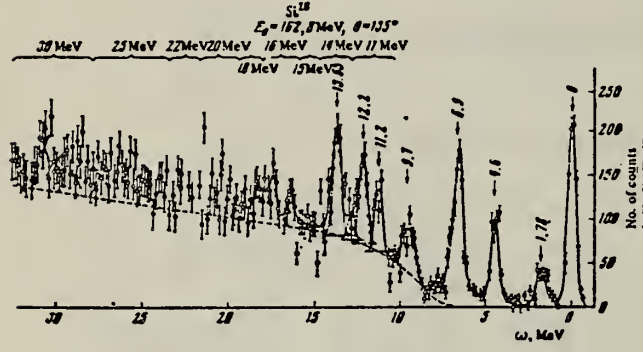

FIG. 2. The spectrum of Fig. 1 after correction for the ionization and radiation effects. The full curve was drawn freehand through the experimental points; the dash-dot curves show the separated states at 11.2, 12.2, and 13.65 MeV; and the dashed curve separates the spectrum into resonance and nonresonance parts. The braces at the top mark the limits of the several complexes, as indicated.

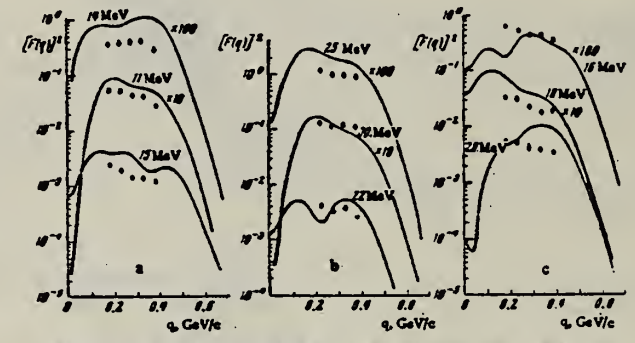

FIG. 3. The squares of the form factors for the complexes as functions of the momentum transfer. The curves are theoretical, while the points give the squares of the experimental total form factors. To separate the curves, the ordinates (both theoretical and experimental) for some of the complexes have been multiplied by 10 or 100 (as indicated at the curves).

Theoretical and experimental values of the form factors for the 16-18 MeV complex

q, MeV/c	$F^2(\Phi_{theor})\cdot 10^3$	$F^2(\Phi)_{exp}\cdot 10^3$	q, MeV/c	$F^2(\Phi_{theor})\cdot 10^3$	$F^2(\Phi)_{exp}\cdot 10^3$
181.25	8.91	9.0±0.38	334.95	6.7	5.82±0.28
231.8	7.95	7.75±0.34	387.2	4.97	5.21±0.25
283.15	7.57	6.22±0.28			

REF.

G. C. Li, M. R. Yearian, and I. Sick
Phys. Rev. C9, 1861 (1974)

ELEM. SYM.	A	Z
Si	28	14

METHOD

REF. NO.: 74 Li 2 hmg

REACTION	RESULT	EXCITATION ENERGY	SOURCE TYPE	SOURCE RANGE	DETECTOR TYPE	DETECTOR RANGE	ANGLE
E,E/	FMF	2	C	250,500	MAG-D		DST
		(1.778)					

LEVEL 1.778 MEV

Detailed elastic scattering data tables for ^{24}Mg, ^{27}Al, ^{28}Si, and ^{32}S.

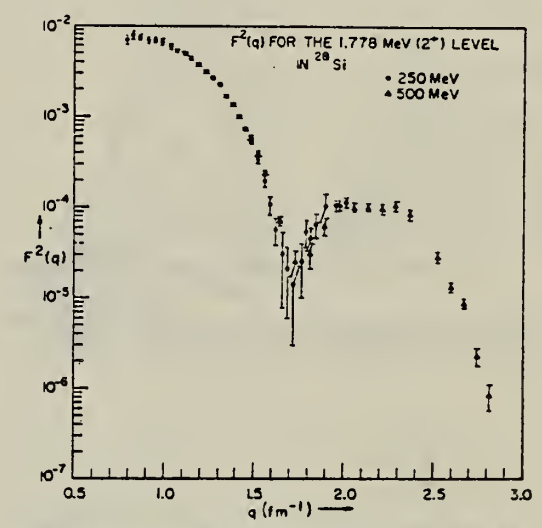

FIG. 12. Experimental form factor of the 1.778-MeV (2^+) level in ^{28}Si.

REF. S. G. Tonapetyan, N. V. Goncharov, and V. M. Khvorostyan
Yad. Fiz. 22, 440 (1975)
Sov. J. Nucl. Phys. 22, 226 (1976)

ELEM. SYM.	A	Z
Si	28	14

METHOD

REF. NO. 75 To 4 egf

REACTION	RESULT	EXCITATION ENERGY	SOURCE		DETECTOR		ANGLE
			TYPE	RANGE	TYPE	RANGE	
G,PI+	ABY	150-400	C	300,400	BBL-D		90
G,PI-	ABY	150-400	C	300,400	BBL-D		90
G,P	ABY	91-400	C	300,400	BBL-D		90

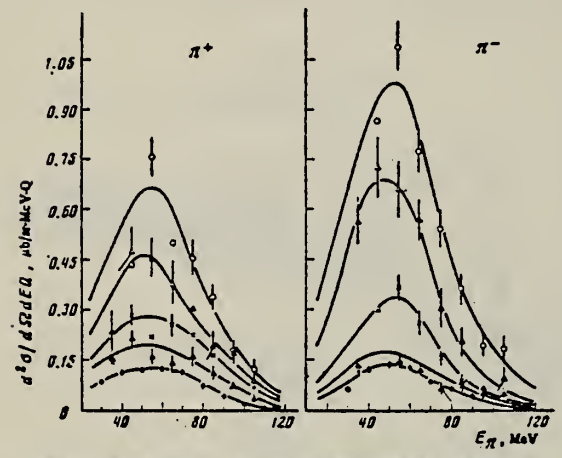

FIG. 1. Energy spectra of π^+ and π^- mesons. E_γ^{max} = 300 MeV, θ_{lab} = 90 ± 7°. Points: ●—^{12}C, ▲—^{28}Si, X—^{40}Ca, △—^{93}Nb, ○—^{181}Ta.

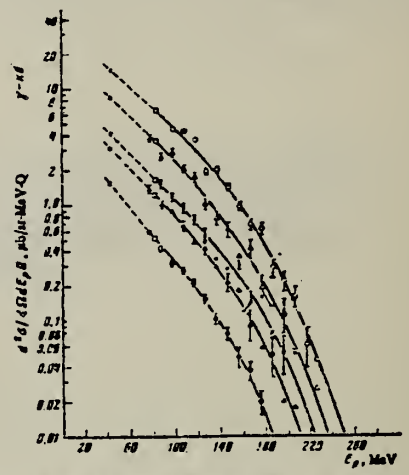

FIG. 3. Energy spectra of protons, E_γ^{max} = 300 MeV, θ_{lab} = 90 ± 7°. Points: ●—^{12}C, ▲—^{28}Si, X—^{40}Ca, △—^{93}Nb, ○—^{181}Ta, □—data from ref. 5, *—data from ref. 6.

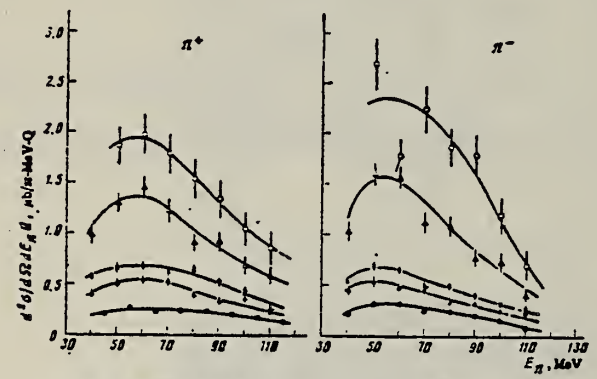

FIG. 2. Energy spectra of π^+ and π^- mesons. E_γ^{max} = 400 MeV, θ_{lab} = 90 ± 7°. The points are the same as in Fig. 1.

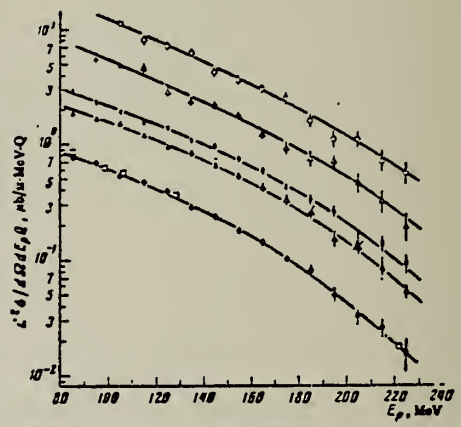

FIG. 4. Energy spectra of protons, E_γ^{max} = 400 MeV, θ_{lab} = 90 ± 7°. The points are the same as in Fig. 1; □—data from ref. 7.

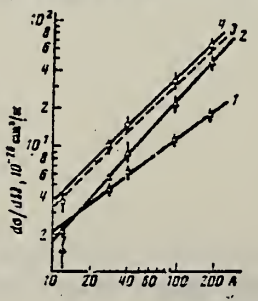

FIG. 5. Dependence of yields of π mesons 1, protons 2, and the sum of π-meson and proton yields 4 as a function of mass number of the nucleus. The dashed line 3 is the theory. Points: □—experimental differential cross sections for pions of all signs, △—differential cross sections for protons emitted at the same angle θ_{lab} = 90°, ○—combined values of these differential cross sections. The statistical errors are shown.

[5] P.C.Murray et a., Phys.Rev.94,764 (54).
[6] C.Levinthal et al.,Phys.Rev.82,822 (51).
[7] P.Dougan et al.,LUSY Prep.1002 (1970).

REF. V.D. Epaneshnikov, V.M. Kuznetsov, O.I. Stukov
Yad. Fiz. 23, 249 (1976)
Sov. J. Nucl. Phys. 23, 129 (1976)

ELEM. SYM.	A	Z
Si	28	14

METHOD

REF. NO. 76 Ep 4 hmg

REACTION	RESULT	EXCITATION ENERGY	SOURCE		DETECTOR		ANGLE
			TYPE	RANGE	TYPE	RANGE	
G,P-	ABX	150-400	C	180-400	ACT-I		4PI

The activation method has been used to measure the yields of the reactions $^{28}Si(\gamma,\pi^-)^{28}P$ and $^{11}B(\gamma,\pi^-)^{11}C$ from the π-meson production threshold to 400 MeV. The results obtained are in satisfactory agreement with theoretical calculations based on the model of surface production of mesons.

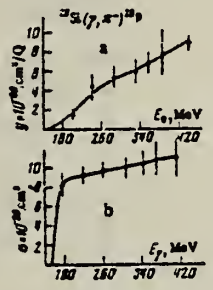

FIG. 1. Yield curve (a) and total cross sections (b) for the reaction $^{28}Si(\gamma,\pi^-)^{28}P$.

REF.	ELEM. SYM.	A	Z
V.M. Asaturyan, E.O. Grigoryan, G.A. Vartapetyan, A.S. Danagulyan, N.A. Demëkhina & A.G. Khudaverdyan Sov. J. Nucl. Phys. 25, 601 (1977) Yad. Fiz. 25, 1133 (1977)	Si	28	14

METHOD	REF. NO.	
	77 As 10	hmg

REACTION	RESULT	EXCITATION ENERGY	SOURCE TYPE	SOURCE RANGE	DETECTOR TYPE	DETECTOR RANGE	ANGLE
G,Be7 G,C11	ABY	THR*5	C	2*5	SCD-D		UKN
G,N13 G,F18				(4.5)			
G,Na22 G,Na24							

Photonuclear reactions in the targets ^{27}Al, ^{28}Si, ^{31}P, ^{32}S, and ^{40}Ca have been studied for maximum bremsstrahlung energies of 2, 2.4, 3, and 4.5 GeV. The yields of the residual nuclei ^{7}Be, ^{11}C, ^{13}N, ^{18}F, ^{22}Na, and ^{24}Na were measured by means of a germanium-lithium semiconductor detector with a sensitive volume of 30 cm^3. In discussion of the results we took into account the contribution of the low energy part of the bremsstrahlung spectrum. Comparison of the measured yields with estimates calculated by Rudstam's formula permitted us to conclude that there is a difference in the mechanism of formation of the light fragments ^{7}Be, ^{11}C, and ^{13}N from that of the other residual nuclei ^{18}F, ^{22}Na, and ^{24}Na.

*GEV 5=4.5 GEV

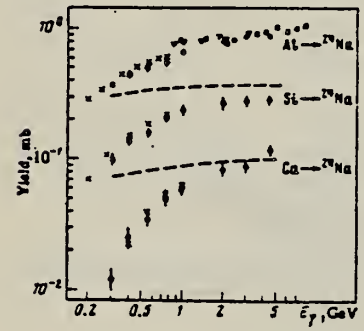

FIG. 1. Yields of the isotope ^{24}Na from targets of Al, Si, and Ca. ×—Data of Ref. 4, ○—data of Ref. 2, ▽—data of Ref. 6, □—data of Ref. 10, ●—data of the present work. The dashed lines show the contributions of the low energy part of the bremsstrahlung spectrum to the yields of the reactions Al—^{24}Na, Si—^{24}Na according to the data of Ref. 4 and the results of the calculations of the present work.

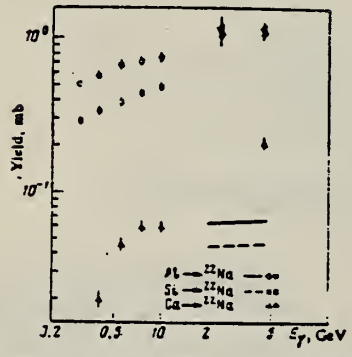

FIG. 2. Yields of ^{22}Na from targets of Al, Si, and Ca. The hollow symbols show the data of Ref. 2, and the solid symbols the data of the present work. The lines indicate the results of the calculations of the present work, which determine the contribution of the low-energy part of the bremsstrahlung spectrum to the yields of the reactions Al—^{22}Na and Si—^{22}Na for 2 GeV $\leq E_{\gamma_{max}} \leq$ 4.5 GeV.

TABLE II.

Residual nucleus	Reaction yields, mb/Q: $E_{\gamma max}$ = 1 GeV	2 GeV	2.4 GeV	3 GeV	4.5 GeV	Normalized yields	$\sigma_{exp}/\sigma_{theor}$
Al target							
^{24}Na	0.66±0.02	0.81	0.81	0.87	0.87	0.98	0.53
^{22}Na	0.745±0.02		1.02±0.15		1.07±0.1	0.668	0.98
^{18}F	0.27±0.005	0.38±0.02		0.4±0.02	0.39±0.01	0.296	1.8
^{13}N		0.021±0.004		0.025±0.005	0.022±0.004	0.0127	2.54
^{11}C	0.117±0.013	0.104±0.015		0.12±0.02	0.107±0.015	0.081	3.3·10^3
^{7}Be	0.29±0.05		0.37±0.08		0.3±0.05	0.246	1.58·10^3
Si target							
^{24}Na	0.24±0.01	0.274±0.024	0.27±0.02	0.28±0.02	0.29±0.02	0.54	0.43
^{22}Na	0.47±0.02		1.22±0.2		1.22±0.1	1.17	2.39
^{18}F	0.2±0.01	0.36±0.03		0.39±0.02	0.39±0.02	0.38	2.69
^{13}N		0.033±0.01		0.037±0.01	0.039±0.01	0.0297	7.28
^{11}C		0.104±0.02		0.115±0.025	0.121±0.027	0.107	5.2·10^3
^{7}Be			0.368±0.05		0.32±0.04	0.291	8.2·10^3
P target							
^{24}Na	0.31±0.02				0.35±0.03	0.428	0.72
^{22}Na	0.35±0.02				0.35±0.06	0.421	2.03
^{7}Be					0.33±0.03	0.296	8.81·10^3
S target							
^{24}Na	0.24±0.01	0.23±0.02	0.23±0.02	0.24±0.02	0.27±0.02	0.417	1.1
^{22}Na	0.53±0.04				0.64±0.06	0.588	3.68
^{18}F	0.19±0.01	0.26±0.01		0.22±0.01	0.27±0.01	0.284	4.73
^{13}N		0.047±0.03		0.063±0.03	0.08±0.025	0.054	2.86·10^3
^{11}C	0.122±0.013	0.183±0.038		0.142±0.029	0.15±0.03	0.126	1.23·10^3
^{7}Be	0.25±0.05		0.38±0.05		0.34±0.04	0.314	1·10^3
Cl target							
^{24}Na	0.22±0.01	0.28±0.03		0.3±0.03	0.38±0.03	0.297	1.8
^{18}F	0.35±0.02	0.21±0.01				0.18	7.82
K target							
^{24}Na	0.08±0.005	0.1±0.01		0.123±0.012	0.15±0.015	0.16	2
^{18}F	0.08±0.008	0.11±0.05				0.1	7.58
Ca target							
^{24}Na	0.08±0.005	0.086±0.01		0.08±0.01	0.12±0.012	0.147	2.2
^{22}Na	0.08±0.005				0.21±0.02	0.21	6.37
^{7}Be					0.245±0.025	0.23	1.5·10^3

Data for Cl and K targets previously published in Reference 11.

[11]G. A. Vartapetyan *et al.*, Yad. Fiz. 17, 685 (1973) [Sov. J. Nucl. Phys. 17, 350 (1973)].

REF. J.E.M. Thomson and M.N. Thompson
Nucl. Phys. A285, 84 (1977)

ELEM. SYM.	A	Z
Si	28	14

METHOD

REF. NO. 77 Th 1

egf

REACTION	RESULT	EXCITATION ENERGY	SOURCE		DETECTOR		ANGLE
			TYPE	RANGE	TYPE	RANGE	
G,NG	ABY	18-28	C	28	SCD-D		140
G,PG	ABY	13-28	C	28	SCD-D		140
G,AG	ABY	11-28	C	28	SCD-D		140

TABLE 1

Population of ^{27}Si and ^{27}Al states following photodisintegration and particle pick-up reactions

MeV	J^π	Relative population	$\int_0^{28}\sigma dE$ (MeV · mb) [a]	Spectro factor [b,c]	Ang. mom. transfer
		^{27}Al levels			
g.s.	$\frac{5}{2}^+$		56±10*	3.5	2
0.842	$\frac{1}{2}^+$	54±22	35±15	0.64	0
1.013	$\frac{1}{2}^+$	32±10	20±6	0.66	2
2.210	$\frac{7}{2}^+$	< 4	< 2		
2.734	$\frac{3}{2}^+$	19±5	13±2	0.68	2
2.981	$\frac{3}{2}^+$	18±3	12±2	< 0.4	(2)
3.004	$\frac{9}{2}^+$				(4)
3.678	$\frac{1}{2}^+$	12±3	8±2	< 0.02	
3.955	$(\frac{1}{2}, \frac{3}{2})^+$				
4.054	$(\frac{1}{2}, \frac{3}{2})^-$	13±3	9±2	1.8	1
4.409	$\frac{3}{2}^+$	v. weak	v. small	0.35	2
4.510	$\frac{11}{2}^+$				
4.580	$\frac{7}{2}^+$				
4.812	$\frac{3}{2}^+$	weak			
5.155	$(\frac{1}{2}, \frac{3}{2})^-$			1.2	1
5.434		weak			
		^{27}Si levels			
g.s.	$\frac{5}{2}^+$		48±14*	5.6	2
0.780	$\frac{1}{2}^+$	22±7	14±5	1.3	0
0.956	$\frac{3}{2}$	11±4	7±2	0.7	2
2.163	$\frac{7}{2}$				
2.647	$\frac{3}{2}$	< 3.5	< 2.3	0.7	2
2.864	$(\frac{1}{2}, \frac{3}{2})^+$	5±1.5	3.4±1	1.6	2
2.96					
		^{24}Mg levels			
1.368	2^+	9±3	6±2		

[a]) Relative errors only see text.
[b]) Refs. [17,18]).
[c]) Refs. [19,20]).
* Deduced from published total cross sections using present data for excited state cross sections.

[17] J.E.M. Thomson, R.J.J. Stewart and M.N. Thompson, Proc. Int. Conf. on nuclear structure, Sendai 297 (1972)

[18] H.E. Grove, K.H. Purser, J.J. Schwartz, W.P. Alford and D. Cline, Nucl. Phys. A116 369 (1968)

[19] B.H. Wildenthal and E. Newman, Phys. Rev. 167, 1027 (1967)

[20] G.D. Jones, R.R. Johnson and R.J. Griffith, Nucl. Phys. A107, 659 (1968)

REF. V. Di Napoli, J. B. Martins, G. Rosa, F. Salvetti, O. A. P. Tavares, M. L. Terranova and H. G. De Carvalho
J. Inorg. Nucl. Chem. 40, 1619 (1978)

ELEM. SYM.	A	Z
Si	28	14

METHOD

REF. NO.	
78 Di 10	hg

REACTION	RESULT	EXCITATION ENERGY	SOURCE		DETECTOR		ANGLE
			TYPE	RANGE	TYPE	RANGE	
G,C11	ABY	31(31.33)-999	C	300-999	ACT-I		4PI
G,Be7	ABY	31(31.53)-999	C	300-999	ACT-I		4PI

Abstract—Mean cross sections for the photoproduction of ^{7}Be and ^{11}C from ^{19}F, ^{27}Al, ^{28}Si and ^{32}S targets, ^{7}Be from ^{10,11}B, and ^{11}C from ^{14}N and ^{16}O targets have been measured using bremsstrahlung beams in the energy range 0.3–1.0 GeV. The results have been compared with previous measurements and an excellent agreement has been found. In most cases, the values obtained turned out to be much larger than those expected from a simple spallation mechanism. A fragmentation and/or a fission-like process has been suggested in explaining the mechanism of such reactions.

999=1 GEV

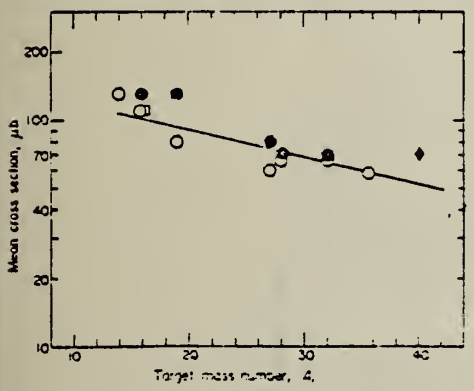

Fig. 1. Mean cross sections per photon, $\bar{\sigma}_A$, of ^{11}C photoproduction vs the target mass number A. Experimental data are taken from: ●, Ref. [9]; □, Ref. [13]; ◆, Ref. [2]; ○, present work. The straight line is a least squares fit of the experimental points.

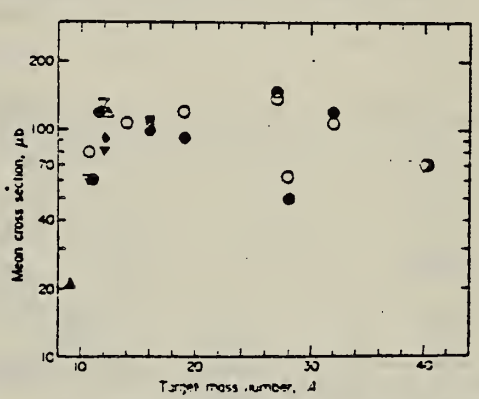

Fig. 2. The same as in Fig. 1 for ^{7}Be photoproduction. Experimental data are taken from: ▲, Refs. [6, 7]; ▽, Ref. [8]; ⊖, Ref. [9]; △, Ref. [10]; ◆, Ref. [11]; ▼, Ref. [12]; □, Ref. [13]; ■, Ref. [14]; ◇, Ref. [2]; ○, present work.

Table 1. Cross sections per equivalent quantum of ^{11}C photoproduction

E_0 (GeV)	Cross Section, σ_Q (μb)						
	^{14}N	^{16}O	^{19}F	^{27}Al	^{28}Si	^{32}S	^{35,37}Cl
0.30	520±30	200±20	110±20	28±10	35±10	45±10	30±10
0.32	520±30	210±20	120±20	30±10	42±10	50±10	30±10
0.35	530±30	230±20	125±20	38±10	45±10	60±10	40±10
0.40	530±30	230±20	130±20	42±10	52±10	65±10	50±10
0.48	550±30	255±20	150±20	60±10	70±10	80±10	60±10
0.55	570±30	260±20	160±20	60±10	78±10	85±10	60±10
0.65	600±30	290±20	180±20	70±10	85±10	98±10	75±10
0.75	620±30	300±20	180±20	79±10	95±10	110±10	85±10
0.90	650±30	320±20	190±20	90±10	110±10	120±10	95±10
1.00	690±30	330±20	210±20	100±10	115±10	125±10	100±10

Table 2. Cross sections per equivalent quantum of ^{7}Be photoproduction

E_0 (GeV)	Cross Section, σ_Q (μb)						
	^{10,11}B	^{14}N	^{16}O	^{19}F	^{27}Al	^{28}Si	^{32}S
0.30	150±20	200±20	113±20	152±20	40±20	20±20	50±20
0.32	160±20	200±20	120±20	150±20	45±20	30±20	54±20
0.35	160±20	210±20	130±20	159±20	42±20	30±20	60±20
0.40	175±20	226±20	145±20	170±20	98±20	20±20	70±20
0.48	190±20	245±20	163±20	186±20	100±20	50±20	140±20
0.55	200±20	260±20	187±20	200±20	93±20	48±20	90±20
0.65	220±20	280±20	197±20	214±20	140±20	68±20	130±20
0.75	225±20	300±20	215±20	227±20	180±20	70±20	130±20
0.90	240±20	318±20	230±20	245±20	186±20	88±20	165±20
1.00	250±20	330±20	242±20	260±20	200±20	97±20	190±20

Table 3. Comparison between experimentally determined and calculated cross sections of ^{7}Be and ^{11}C photoproduction and indication of the dominant reaction channels

Target Nucleus	Product Nucleus	Nominal Nucleon Loss, ΔA	$\Delta A/A_t$ (x100)	$\bar{\sigma}_{exp}$ (*) (μb)	$\bar{\sigma}_{CDMD}$ (**) (μb)	$\frac{\bar{\sigma}_{exp}}{\bar{\sigma}_{CDMD}}$	Apparent Threshold (Exp.) E_{th}(MeV)	Possible Mechanism of Production
$^{10,11}B$	^{7}Be	(3)	(30).36	67	28	2	≤ 50	Spallation
^{12}C	^{7}Be	5	42	110	20	5	≤ 50	Spallation
^{14}N	^{7}Be	7	50	108	12	9	≤ 50	Fission Spallation
^{14}N	^{11}C	3	21	130	60	2	≤ 50	Spallation
^{16}O	^{7}Be	9	56	107	8	13	$50<E_{th}<200$	Fission Fragmentation
^{16}O	^{11}C	5	31	117	33	3	≤ 50	Spallation
^{19}F	^{7}Be	12	63	106	5	21	$50<E_{th}<200$	Fission Fragmentation
^{19}F	^{11}C	8	42	105	16	7	$50<E_{th}<200$	Fission Fragmentation Spallation
^{27}Al	^{7}Be	20	74	142	2	71	> 200	Fragmentation
^{27}Al	^{11}C	16	59	70	5	14	$50<E_{th}<200$	Fission Fragmentation
^{28}Si	^{7}Be	21	75	56	2	28	> 200	Fragmentation
^{28}Si	^{11}C	17	61	68	4	17	$50<E_{th}<200$	Fission Fragmentation
^{32}S	^{7}Be	25	78	114	2	57	> 200	Fragmentation
^{32}S	^{11}C	21	66	68	3	23	$50<E_{th}<200$	Fission Fragmentation
$^{35,37}Cl$	^{11}C	24.(26)	69.(70)	59	3	20	$50<E_{th}<200$	Fission Fragmentation
^{40}Ca	^{7}Be	33	83	70	1	70	> 200	Fragmentation
^{40}Ca	^{11}C	29	73	70	2	35	> 200	Fragmentation

(*) Mean values of the different measurements (see Figs. 1 and 2).

(**) Calculated values according to Ref. [1].

REF. W. Knupfer, Phys. Lett. 77B, 367 (1978)

ELEM. SYM.	A	Z
Si	28	14

METHOD

REF. NO. 78 Kn 7 rs

REACTION	RESULT	EXCITATION ENERGY	SOURCE		DETECTOR		ANGLE
			TYPE	RANGE	TYPE	RANGE	
E,E/	RLY	13-16	D	UKN.	MAG-D		DST

M2 LEVELS

The location of the M2 giant resonance in ^{28}Si, ^{90}Zr and ^{208}Pb, predicted within the framework of the MSI-RPA particle–hole model, has been confirmed by high-resolution inelastic electron scattering ($E_x \approx 44A^{-1/3}$ MeV). The fragmented M2 strength distribution can only be described assuming a mass-dependent quenching of the intrinsic g_s factor. This has the consequence that the long sought M1 strength is much reduced in heavy nuclei, an effect which is supported experimentally.

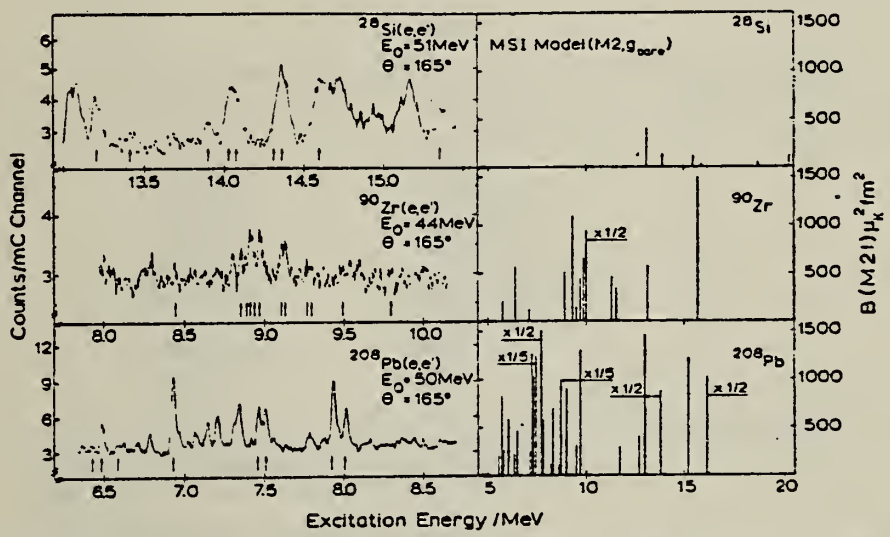

Fig. 1. The left part shows selected (e, e') spectra on ^{28}Si, ^{90}Zr and ^{208}Pb at various energies but all at $\theta = 165°$. The 2^- states are marked by arrows. The right part displays the model prediction for the M2 strength.

REF. J.W. Maas, E. Somorjai, H.D. Graber, C.A. Van Den Wijngaart, C. Van Der Leun and P.M. Endt
Nucl. Phys. A301, 213 (1978)

ELEM. SYM.	A	Z
Si	28	14

METHOD

REF. NO. 78 Ma 3 rs

REACTION	RESULT	EXCITATION ENERGY	SOURCE TYPE	SOURCE RANGE	DETECTOR TYPE	DETECTOR RANGE	ANGLE
P,G	NOX	2- 13	D	1- 2	SCD-D		DST
A,G	NOX	11- 13	D	2- 4	SCD-D		DST

J-PI

TABLE 3

Excitation energies (in keV) of ^{28}Si levels determined in the present work

Present exp.	Ref. [23])	J^π; T [a])
1778.61 ± 0.15	1778.88 ± 0.09	2^+
4616.81 ± 0.17	4617.8 ± 0.2	4^+
6275.9 ± 0.3	6276.5 ± 0.2	3^+
9315.7 ± 0.5	9316.1 ± 0.5	3^+; 1
9379.8 ± 0.5	9381.2 ± 0.6	2^+; 1
10375.8 ± 0.4	10377.1 ± 1.0	3^+; 1 [c])
10598.9 ± 1.0 [a])	10598.2 ± 2.0 [d])	1^+; 1
10724.7 ± 0.4	10724.6 ± 1.3	1^+; 1
10901.9 ± 1.0 [a])	10901 ± 3	1^+; 1
11446.2 ± 0.5 [b])	11445 ± 3	1^+; 1
12635.0 ± 0.4	12635	

[a]) The J^π values are taken from ref. [23]) if not indicated otherwise: the T-values are from table 9.
[b]) Resulting from an unpublished resonant absorption experiment.
[c]) The J^π value has been determined in the present work.
[d]) Ref. [27]).
[e]) Measured relative to E_x = 10.72 MeV; see subsect. 3.1.2.

[25] P.M. Endt and C. Van der Leun, Nucl. Phys. A214 (1973) 1; A105 (1967) 1

[27] M.A. Meyer, I. Venter and D. Reitmann, Nucl. Phys. A250 (1975) 235

over

TABLE 5

Gamma-ray decay of $^{24}Mg(\alpha, \gamma)^{28}Si$ resonances

Resonances			γ-decay (%) to E_x (MeV) in ^{28}Si											
E_α (keV)	E_x (keV)	$J^\pi; T$ [a])	0 0^+	1.78 2^+	4.62 4^+	4.98 0^+	6.28 3^+	6.69 0^+	6.88 3^-	6.89 4^+	7.80 3^+	9.32 3^-;1	9.38 2^+;1	other levels E_x (%)
1530	11296	1^-	75	21		<3		2	2					
1787	11516	2^+		64	12	3		9					12	
1866	11584	3^-		90	5				5					
1952	11657	2^+	14	27	6		6	11	8				4	7.38(3), 7.42(3), 7.93(12), 8.33(5), 9.48(1)
1966	11670	1^-	7	82		3			4				4	
2094	11779	2^+		100			<1							
2235	11900	$(2^+, 3^-, 4^+)$			81					14				8.59(5)
2323	11975	$(2^+, 3^-, 4^+)$		2	76				1	15				8.59(4), 9.42(2)
2378	12023	5^-			5				51	6				8.41(16), 9.16(13) 10.18(9)
2435	12071	2^+	58	13	2		4			9	2			8.26(1), 8.59(1) 10.38(10)
2564	12182	1^-	36	6		9							7	7.38(12), 8.90(13) 10.90(17)
2578	12194	3^-		77	16				4				3	
2633	12241	4^+		52	23		2			2				7.38(17), 8.59(4)
2690	12290	2^+		54			1	3				11	30	7.93(1)
2703	12301	$(1^-, 2^+)$		27										8.33(3), 8.90(42) 9.50(19), 10.60(3) 10.72(6)
2866	12440	2^+	74	5	3		4			1	3	9	1	
2906	12474	4^+		94	2		1				1			7.93(1), 8.26(1)
2921	12488	3^-		75	25									
2994	12550	4^+		61	3		5			2				7.38(5), 7.42(11) 7.93(5), 8.26(3) 10.38(3), 10.42(2)
3198	12725	2^+	68	21		6	1		2			2		
3291	12805	$(1^-, 2^+)$	13	27		6								7.42(6), 10.60(38) 10.90(10)
3303	12815	1^-	70			20							2	10.27(8)
3349	12854	4^+		13	13		49		1	6	5	6		8.59(2), 8.94(1) 10.67(4)
3354	12859	$(2^+, 3^-, 4^+)$		7			19			31				9.16(35), 10.945(8)
3402	12899	2^+	7	26	7	1	31	1				5	10	7.80(11), 8.59(1)
3429	12923	$(2^+, 3^-, 4^+)$					53							8.26(40), 9.48(7)
3486	12972	1^-	43	3		17		1	4					7.42(1), 7.93(2) 8.33(3), 8.90(2) 9.48(2), 10.27(20) 10.60(..)
3565	13039	0^+		56										7.42(3), 8.90(41)
3628	13093	4^+			10		7			12	13	40		8.26(8), 8.41(3) 9.48(2), 10.38(5)
3642	13105	2^+	88	6		3			2				1	
3787	13230	2^+	3	18	8		8			47		5	11	

[a]) All resonances have π = natural and are (predominantly) of $T = 0$ character; for the J^π assignments, see table 4.

REF. M.A. Kovash, S.L. Blatt, R.N. Boyd, T.R. Donoghue, H.J. Hausman
A.D. Bacher
Phys. Rev. Lett. 42, 700 (1979)

ELEM. SYM.	A	Z
Si	28	14

METHOD

REF. NO. 79 Ko 1 hg

REACTION	RESULT	EXCITATION ENERGY	SOURCE		DETECTOR		ANGLE
			TYPE	RANGE	TYPE	RANGE	
P,G	SPC	50-89	D	40-80	NAI-D		60

Observations are reported from the first systematic studies of proton radiative capture at intermediate energies. In addition to captures to the ground and first few excited states, the reactions $^{11}B(p,\gamma)^{12}C$ and $^{27}Al(p,\gamma)^{28}Si$ reveal unexpectedly strong transitions to isolated high-lying states. These latter transitions could take place via "second-harmonic" giant resonances. Protons on ^{12}C produce a rich spectrum of γ rays which may arise from captures to high-lying single-particle states.

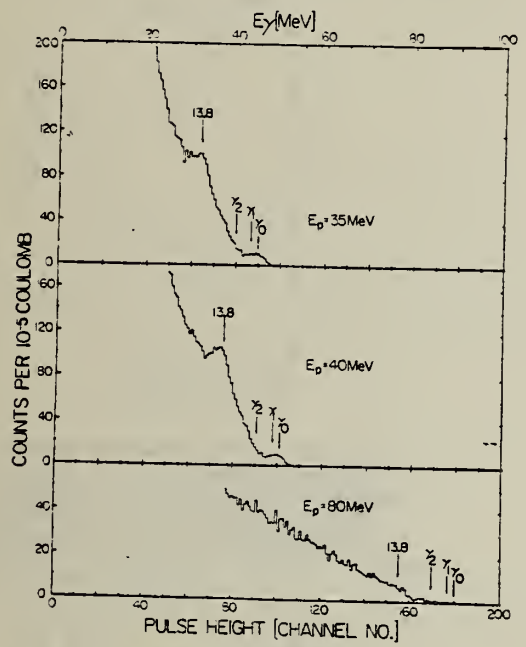

FIG. 2. γ-ray spectra from 35-, 40-, and 60-MeV protons on ^{27}Al observed at 60°. See Fig. 1 for notation.

REF. R. Pitthan, F.R. Buskirk, J.N. Dyer, E.E. Hunter and G. Pozinsky
Phys. Rev. C 19, 299 (1979)

ELEM. SYM.	A	Z
Si	28	14

METHOD

REF. NO. 79 Pi 1 hg

REACTION	RESULT	EXCITATION ENERGY	SOURCE		DETECTOR		ANGLE
			TYPE	RANGE	TYPE	RANGE	
E,E/	FMF	4- 50	D	91	MAG-D		DST
				(91.2)			

Inelastic electron scattering in ^{28}Si between 4 and 50 MeV excitation energy reveals two concentrations of $E2$ strength in the continuum. One is between 15 and 20 MeV, with a peak at 17 MeV, and can be identified with the giant quadrupole resonance in the ground state oblate well. A broad distribution of $E2$ strength between 22 and 42 MeV is predominantly isovector in nature. In addition, a small but persistent $E2$ peak at 24 MeV was found, which may be interpreted as being the corresponding state in the prolate well to the 17 MeV resonance. It is shown that 50% or more of the photon cross section in excess of the classical dipole sum rule between 10 MeV and the pion threshold may be due to $E2$ absorption.

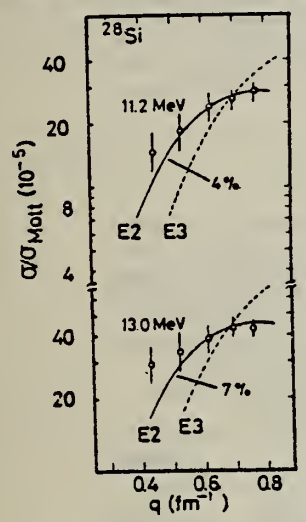

FIG. 2. The cross section divided by the Mott cross section for the states (or group of states) at 11.2 and 13.0 MeV. Comparison with a DWBA calculation based on the Tassie (identical with the Goldhaber-Teller) model and normalized to the percentage exhaustion of the isoscalar EWSR as indicated shows clearly that these states are quadrupole excitations.

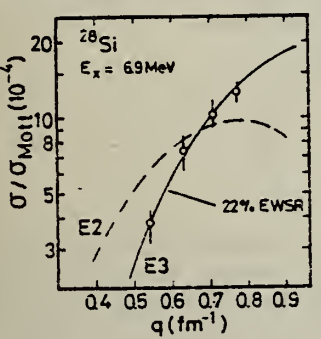

FIG. 3. Similar to Fig. 2 but for the level at 6.9 MeV. Comparison with DWBA calculations shows this state to be $E3$. This state agrees very well with the $1\hbar\omega$, isoscalar $E3$ state predicted by the shell model at $24A^{-1/3}$ MeV with a strength of 28% of the EWSR ($\Delta T = 0$) (see Ref. 22).

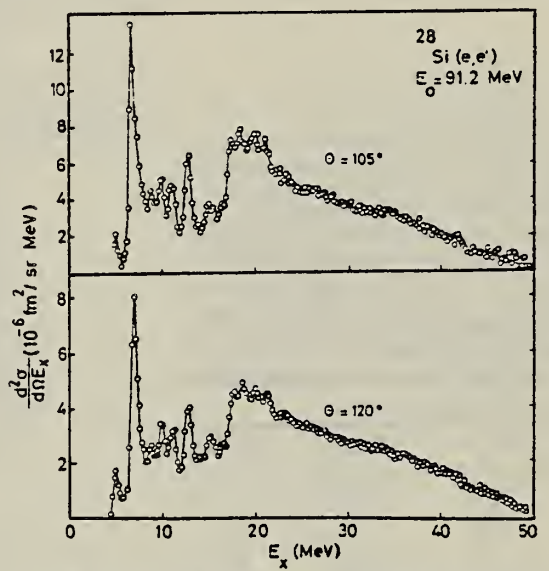

FIG. 5. Data of Fig. 1 after subtraction of a background described in the text and correction for the constant dispersion of the magnetic spectrometer. Some similarity to the photon data of Fig. 4 in the 17 to 22 MeV region can be recognized, especially the four characteristic peaks at 17.7, 18.8, 20.2, and 21.4 MeV. The ghost peak located at 92% of the elastic energy (E_x = 7.3 MeV) has been subtracted. The spectra were taken and fitted with 10 points per MeV, which have been reduced by a factor of 2 for graphical purposes. The statistical error is equal to the size of the circles in the 120° spectrum and slightly larger for 105°.

22 I. Hamamoto, in Proceedings of the International Conference on Nuclear Structure Studies Using Electron Scattering and Photoreaction, Sendai, 1972, edited by K. Shoda and H. Ui [(Suppl. Res. Rep. Lab. Nucl. Sci, Tohoku Univ. 5, 208 (1972)]

over

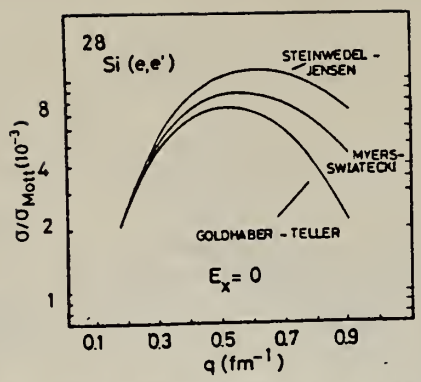

FIG. 7. Comparison of DWBA calculations based on the three models indicated. It is evident that, e.g., use of the Goldhaber-Teller model instead of the Myers-Swiatecki model would influence the quantitative results because the relative difference $[\sigma(MS)-\sigma(GT)]/\sigma(MS)$ changes from 8% for 60° to 28% for 120°, lowering the $E1$ strength subtracted by approximately 20%. However, measurements in other nuclei indicate that the MS model describes the GDR better, and, furthermore, the qualitative features do not change no matter what model is used.

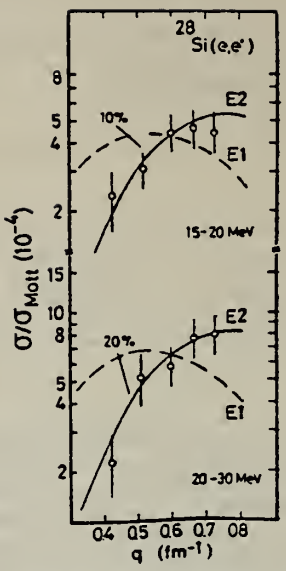

FIG. 8. Comparison of (e,e') strength between 15 to 20 and 20 to 30 MeV with DWBA calculations based on the MS model for the $E1$ and the GT model for the $E2$. The data correspond to the R_{min} values of Table I, but the 15 to 20 MeV data do not include half of the $E2$ strength found between 14 and 16 MeV.

TABLE I. Distribution of $E2$ strength in ^{28}Si into the various regions discussed in the text. Although isospin cannot be directly inferred from (e,e'), the strength below 20 MeV should be predominantly isoscalar and the one above isovector, based on macroscopic and microscopic considerations and comparison with heavier nuclei. The subscripts max and min refer to maximum and minimum values of the sum rule extracted under the background assumptions discussed in the text, ΔR shows the error (in %) if one does not take into account contributions to the error from the background assumptions.

E_x (MeV)	R_{max} [a]	R_{min} [a]	ΔR (%)
0–15	30 [b]	30 [b]	10
15–20	26 [b]	14 [b]	20
20–30	32	10	20
30–50	70	50	30
	50 [c]	30 [c]	

[a] $R = E_x B(E2)/\mathrm{EWSR}(E2,\Delta T = 0,1)\times 100$.
[b] Includes 3.5% EWSR from 14–16 MeV complex.
[c] Lower value derived by assuming 70% of isoscalar $3\hbar\omega_0 E3$ strength between 30 and 50 MeV (Ref. 22).

TABLE II. Comparison of the strength of the isoscalar $E2$ resonance around 17 to 20 MeV from various reactions. It is evident that the strength is grouped around two values, (12 to 14)% and (25 to 31)% of the isoscalar sum rule. As outlined in the text the higher value in hadronic experiments is from measurements where the $E1$ was not taken into consideration. If we use the equivalent background procedure as in (α,α'), the lower value of (14±3)% EWSR results.

E_x (MeV)	Reaction	R [a]	Reference
16.9–24.8	(α,α')	31±5	Knö76
15.5–23.0	(α,α')	27±6	VanB77
	(p,p')	12±4 [b]	
~19.4	(α,α')	~25	YouR77
15–22	^{24}Mg(α,γ)	~13	Han76
15–20	(e,e')	26±5 [c]	this
		14±3 [d]	work

[a] $R = E_x B(E2)/\mathrm{EWSR}(E2,\Delta T = 0)\times 100$.
[b] Value corrected for Myers-Swiatecki model.
[c] Including nonresonant strength.
[d] Background consistent with (α,α').

REF. R. Schneider, A. Richter, A. Schwierczinski, E. Spamer, O. Titze, W. Knüpfer
Nucl. Phys. A323, 13 (1979)

ELEM. SYM.	A	Z
Si	28	14

METHOD

REF. NO. 79Sc7 hg

REACTION	RESULT	EXCITATION ENERGY	SOURCE		DETECTOR		ANGLE
			TYPE	RANGE	TYPE	RANGE	
E,E/	LFT	10-13	D	38-58	MAG-D	26-48	DST
		(10.594-12.331)		(38.7-57.5)			

Abstract: High resolution inelastic electron scattering at low momentum transfer yields the precise location of states with J^π, $T = 1^+$, 1 in ^{28}Si at excitation energies E_x = 10.594, 10.725, 10.901, 11.445 and 12.331 MeV with an overall energy uncertainty of about ±1 keV. An analysis of the inelastic cross sections to these states in terms of the DWBA with RPA wave functions from the model of separable interaction (MSI) yields a total isovector strength of $\sum\Gamma_\gamma^0$ = 34.40±1.37 eV. This result is compared to RPA and open-shell model calculations and it is shown that M1 spin-flip transitions seem to be a sensitive tool to investigate ground state correlations. A qualitative comparison of the M1 transitions with analogous charge exchange reactions involving hadrons and radiative pion and muon capture is also made.

LEVELS 5 J-PI, B(ML)

E NUCLEAR REACTIONS ^{28}Si(e, e'). E = 38.7–57.5 MeV; measured $\sigma(E_1, \theta)$. ^{28}Si deduced levels with $J^\pi = 1^+$, transition probability; performed shell-model calculations.

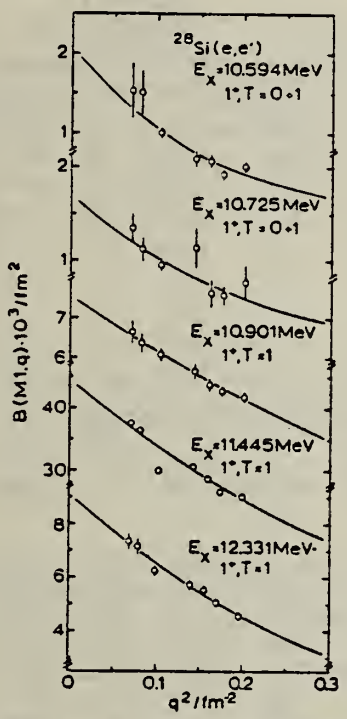

Fig. 4. The B(M1, q) values determined from experiment with the help of eq. (1) in the main text plotted as a function of q^2. In the momentum range $q^2 < 0.2$ fm^{-2} the influence of the higher moments $R_{tr}^4 = \langle r^5\rangle/\langle r\rangle$ and $R_{tr}^6 = \langle r^7\rangle/\langle r\rangle$ in eq. (2) is small. Therefore for the fit we have used the estimates $R_{tr}^4 = 1.32[R_{tr}^2]^2$ and $R_{tr}^6 = 2.25[R_{tr}^2]^3$ following from the prediction of a phenomenological model which reproduces the experimental value of $R_{tr}^2 = \langle r^3\rangle/\langle r\rangle$. Fitted to the experimental values is expression (2) which yields extrapolated to $q = k = E_x/\hbar c$ the B(M1, k) value at the photon point.

TABLE 1
Magnetic dipole transition strengths, transition radii and ground state radiative widths for various 1^+ levels in ^{28}Si

E_x (MeV)	$B(M1, k)(\mu_k^2)$	R_{tr} (fm)	Γ_γ^0 (eV)
10.594	0.19±0.04	3.94±0.35	0.86±0.16
10.725	0.15±0.03	3.58±0.50	0.73±0.13
10.901	0.68±0.05	2.27±0.19	3.41±0.26
11.445	4.07±0.22	2.68±0.12	23.50±1.27
12.331	0.81±0.06	2.86±0.16	5.90±0.39
	$\sum B(M1, k)\uparrow$ = 5.90±0.24 μ_k^2		$\sum\Gamma_\gamma^0$ = 34.40±1.37 eV

REF. V.V. Varlamov, B.S. Ishkhanov, I.M. Kapitonov, A.N. Panov, V.I. Shvedunov
Izv. Akad. Nauk SSSR 43, 186 (1979)
Bull Acad. Sci. 43, 157 (1979)

ELEM. SYM.	A	Z
Si	28	14

METHOD

REF. NO. 79 Va 5 hg

REACTION	RESULT	EXCITATION ENERGY	SOURCE		DETECTOR		ANGLE
			TYPE	RANGE	TYPE	RANGE	
G,P	ABX	11-29	C	18-29	SCD-D		UKN

Fig. 3 gives cross section for transitions to various states in ^{27}Al. The areas under these data are given in Table 2.

The many-channel method was used in the work to measure the energy spectra of photoprotons from the ^{28}Si nucleus at 16 values of the upper boundary of γ-bremsstrahlung from 18.1 to 29.0 MeV.

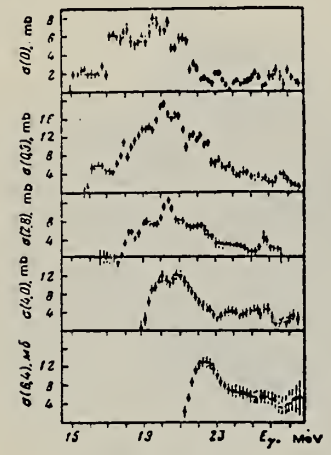

Fig. 3

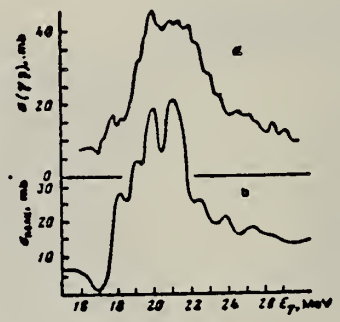

Fig. 4

Table 3

E_x, MeV	$(Nl_j)^{-1}$	C²S	$\sigma_{tot}(E_x)$, % 0—23 MeV	$\sigma_{tot}(E_x)$, % 0—28 MeV	E_x, MeV	$(Nl_j)^{-1}$	C²S	$\sigma_{int}(E_x)$, % 0—23 MeV	$\sigma_{int}(E_x)$, % 0—28 MeV
0	$1d_{5/2}^{-1}$	3,1	18	15	2,8	$1d_{5/2}^{-1}$	0,6	16	16
0,9	$2s_{1/2}^{-1}$	0,8	40	36		$1d_{3/2}^{-1}$	0,3		
	$1d_{3/2}^{-1}$	0,6			4,0	$1p_{1/2}^{-1}$	1,8	16	17
					6,4	$1p_{3/2}^{-1}$		10	16

Fig. 3. Partial cross sections of the photoproton reaction on the ^{28}Si nucleus.

Fig. 4. Total photoproton cross section obtained in the present work (a) and total-absorption cross section (b) for the ^{28}Si nucleus [12].

12. J. M. Wyckoff, B. Ziegler, H. W. Koch, and R. Uhlig, Phys. Rev., vol. 137, p. B576, 1965. 65 Wy 1

The principal results of the work, besides Figs. 3 and 4 and Table 2, are likewise summarized in Table 3 where the hole states $(Nl_j)^{-1}$ and their spectroscopic factors (c^2S) obtained in [11] for the corresponding excited states of the ^{27}Al nucleus are shown along with the fractions of the total cross section of the photoproton reaction represented by the integral cross sections in the ranges of excitation energy of the ^{28}Si nucleus extending from 0 to 23 MeV and from 0 to 28 MeV.

Table 2

E_x, MeV	ΔE, MeV	σ_{int}, MeV·mb	E_x, MeV	ΔE, MeV	σ_{int}, MeV·mb
0	0,5—0,7	34±5	4,0	4,0	33±8
0,9	0,5—0,7	78±8	6,4	4,0	20±6
2,8	0,5—0,7	32±10			

REF. K.E. Whitner, C.F. Williamson, B.E. Norum, S. Kowalski
Phys. Rev. C22, 374 (1980)

ELEM. SYM.	A	Z
Si	28	14

METHOD

REF. NO. 80 Wh 2 egf

REACTION	RESULT	EXCITATION ENERGY	SOURCE		DETECTOR		ANGLE
			TYPE	RANGE	TYPE	RANGE	
E,E/	FMF	2,5	D	126=293	MAG-D		DST

Natural Silicon Target

2=1.78, 5=4.62 MEV

Electron scattering from ^{28}Si and ^{29}Si has been performed at energies from 126 to 293 MeV and at angles of 45° and 90°. Form factors were extracted for levels below 5.0 MeV in ^{28}Si and ^{29}Si over an effective momentum transfer range of 0.6 to 2.1 fm^{-1}. A particle-phonon coupling calculation using harmonic-oscillator single-particle states and data from ^{28}Si give a reasonable description of the low-lying states of ^{29}Si.

[NUCLEAR REACTIONS ^{28}Si(e,e') first 2 excited states; ^{29}Si(e,e') first 5 excited states; measured form factors 45° and 90°, $0.6 \leq q \leq 2.1$ fm^{-1}; natural Si target; PWBA analysis, vibrating core and intermediate coupling for ^{29}Si.]

TABLE VI. Electron scattering squared form factors for levels in ^{28}Si.[a,b]

	0$^+$ (0.00 MeV)			2$^+$ (1.78 MeV)			4$^+$ (4.62 MeV)		
Run	q_{eff} (fm^{-1})	$\lvert F\rvert^2$ ×10^{-4}	± %	q_{eff} (fm^{-1})	$\lvert F\rvert^2$ ×10^{-5}	± %	q_{eff} (fm^{-1})	$\lvert F\rvert^2$ ×10^{-5}	± %
1	0.601	3270	0.72	0.597	443	0.72			
2	0.701	2000	0.67	0.698	617	0.94	0.692	4.10	21
3	0.796	1150	0.54	0.793	658	1.64	0.787	7.31	7.1
4	0.895	613	0.74	0.891	691	1.14	0.886	15.2	4.2
5	0.951	361	0.97	0.944	628	0.70	0.934	16.2	3.0
6	0.999	261	0.88	0.995	636	0.81	0.990	24.9	7.9
7	1.051	138	0.64	1.044	561	0.61	1.034	27.4	2.4
8	1.156	36.5	2.0	1.149	425	0.65	1.139	36.5	2.5
9	1.203	17.6	0.81	1.196	337	0.47	1.186	37.7	1.06
10	1.234	10.6	0.51	1.228	324	0.55	1.217	42.6	1.23
11	1.266	5.89	3.87	1.259	271	0.37	1.250	44.7	0.54
12	1.304	3.62	8.31	1.297	243	0.55	1.287	49.2	2.5
13	1.360	3.32	1.15	1.354	159	0.45	1.340	47.9	0.82
14	1.412	4.89	3.1	1.406	126	0.89	1.396	50.9	1.38
15				1.467	63.3	0.86	1.458	49.6	1.35
16	1.544	8.77	0.42	1.537	32.4	1.17	1.530	45.6	1.27
17	1.599	9.60	1.12	1.593	17.7	2.5	1.580	44.6	3.3
18	1.678	8.22	0.54	1.672	3.62	2.1	1.660	35.9	1.68
19	1.744	6.08	0.73	1.737	0.932	6.7	1.734	26.9	2.9
20	1.836	4.60	0.95	1.830	3.35	3.9	1.819	23.4	1.53
21	1.939	2.49	1.13	1.932	7.81	2.7	1.922	15.3	1.85
22	2.039	1.12	1.88	2.032	10.5	1.09	2.020	8.81	1.43
23	2.134	0.417	1.68	2.127	10.9	1.01	2.120	4.98	6.4
24				1.131	397	3.5			

[a] The squared form factor should be multiplied by the indicated factor.
[b] Percentage errors are statistical only.

(over)

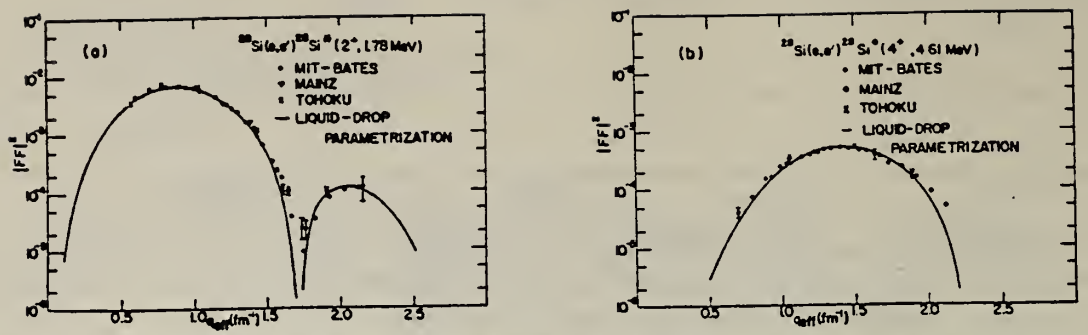

FIG. 4. Squared form factors for electron scattering from ^{28}Si. (a) 2$^+$(1.78 MeV) level. (b) 4$^+$(4.61 MeV) level. Data from three different laboratories are shown along with the fits to the diffuse edge vibrating liquid-drop model.

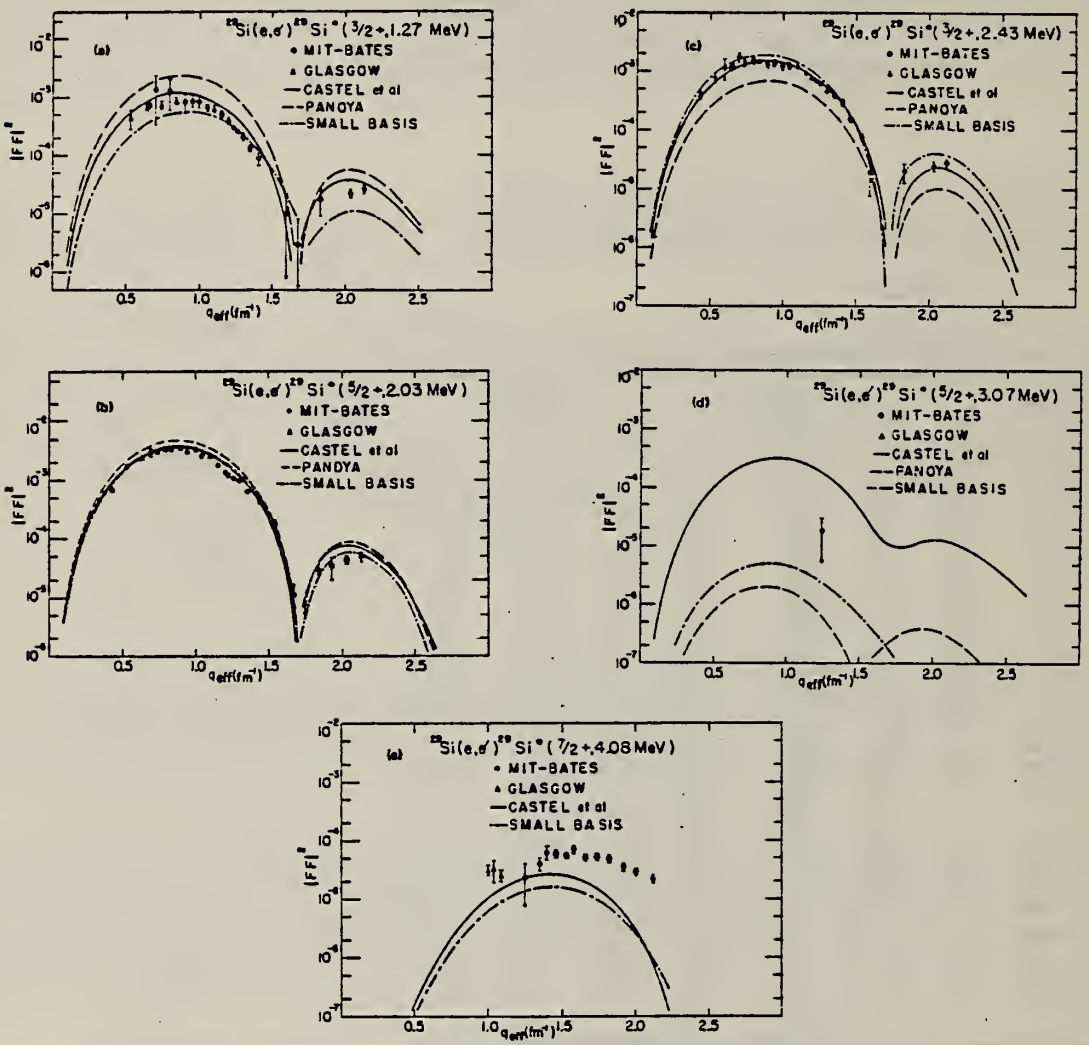

FIG. 5. Squared form factors for electron scattering from the low-lying levels in ^{29}Si. (a) $\frac{3}{2}^+$(1.27 MeV) level. (b) $\frac{5}{2}^+$(2.03 MeV) level. (c) $\frac{3}{2}^+$(2.43 MeV) level. (d) $\frac{5}{2}^+$(3.07 MeV) level. (e) $\frac{7}{2}^+$(4.08 MeV) level. The present data are shown as solid circles and the data of Ref. 17 are shown as solid triangles. Also shown are theoretical curves calculated from the three sets of eigenvectors as described in text.

REF. S. Yen, R. Sobie, H. Zarek, B.O. Pich, T.E. Drake, C.F. Williamson, S. Kowalski, C.P. Sargent
Phys. Lett. 93B, 250 (1980)

ELEM. SYM.	A	Z
Si	28	14

METHOD

REF. NO. 80 Ye 1 hg

REACTION	RESULT	EXCITATION ENERGY	SOURCE		DETECTOR		ANGLE
			TYPE	RANGE	TYPE	RANGE	
E,E/	FMF	15	D	1*3	MAG-D		DST
		(14.36)					

High-resolution (e,e') was used to measure the form factor of the 6^-, $T = 1$ resonance in ^{28}Si. The results disagree with previous experimental results and with theoretical calculations. The role of meson-exchange currents in producing the observed quenching of magnetic strength, and the relevance of (e, e') to other reactions are briefly discussed.

*Q IN FM-1

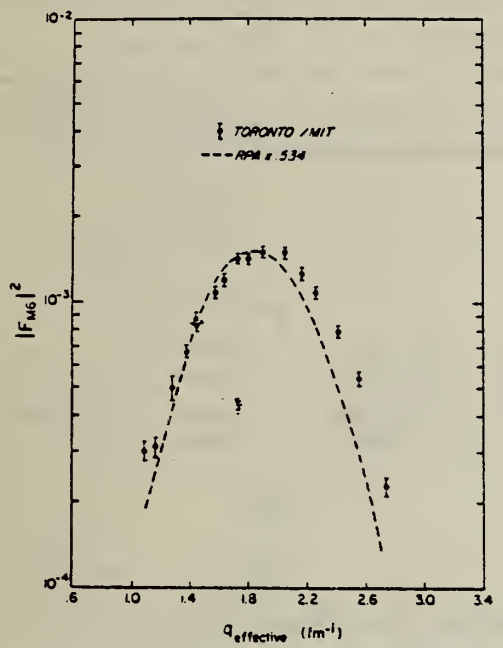

Fig. 3. The form factor $|F_{M6}|^2$ for the 6^- $T = 1$ resonance at 14.36 ± 0.02 MeV in ^{28}Si. The open-shell random phase approximation calculation, renormalized to fit the data, is shown as a dashed line.

REF. B.S. Ishkhanov, Yu.A. Novikov, E.S. Omarov, I.M. Piskarev
Izv. Akad. Nauk SSSR 45, 147 (1981)
Bull. Acad. Sci. 45, 129 (1981)

ELEM. SYM.	A	Z
Si	28	14

METHOD

REF. NO. 81 Is 5 hg

REACTION	RESULT	EXCITATION ENERGY	SOURCE		DETECTOR		ANGLE
			TYPE	RANGE	TYPE	RANGE	
G,G	ABX	5-17	C	6-17	NAI-D		90

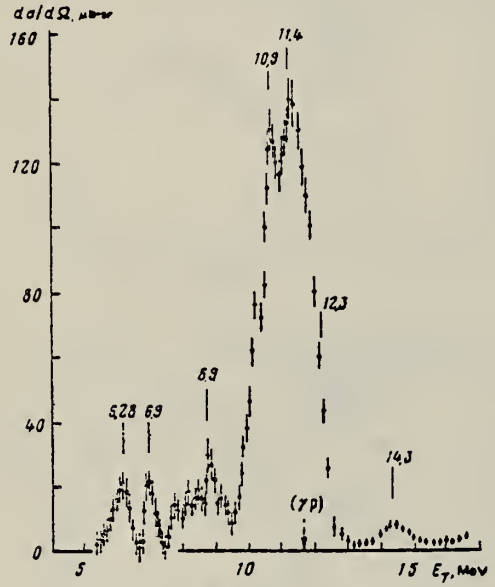

Fig. 1

Table 1

Levels Populated During Elastic Scattering of Protons by an ^{28}Si Nucleus

E_{i0}, MeV; T [11]	E_{i0}, MeV (present work)	Integral cross section, MeV·mb	
		present work	[4]
6,28; 3+	6,3±0,1	0,12±0,03	–
6,87; 3−	7,0±0,1	0,10±0,03	–
6,88; 4+			
7,39; 3+	7,8±0,1	0,03±0,02	–
7,93; 2+			
8,25; 2+	8,2±0,1	0,03±0,02	–
8,32; 1+			
8,9; 1−			
8,94; (4+,5+)	8,9±0,1	0,14±0,03	–
10,9; 1+; T=1	10,9±0,1	0,25±0,05	–
11,44; 1+, T=1			
12,33; 1+; T=1	11,4±0,2	2,2±0,2	2,0±0,3
—	14,3±0,5	0,06±0,02	–

Fig. 1. Cross section for the elastic scattering of photons by an ^{28}Si nucleus. The arrow denotes the threshold of the (γp)-reaction.

REF. G.W. Dodson, E.C. Booth, F.L. Milder, B.E. Parad, B.L. Roberts, D.R. Tieger, J. Comuzzi
Phys. Rev. C26, 2548 (1982)

ELEM. SYM.	A	Z
Si	28	14

METHOD

REF. NO. 82 Do 3 egf

REACTION	RESULT	EXCITATION ENERGY	SOURCE TYPE	SOURCE RANGE	DETECTOR TYPE	DETECTOR RANGE	ANGLE
G,PIØ	ABY	THR*20	C	140-155	CKV-I		1PI

Photoproduction of π^0 mesons off targets of ^{6}Li, ^{12}C, ^{28}Si, ^{40}Ca, natural Cd, and natural Pb was studied using a bremsstrahlung beam with endpoint energies of 140, 145, 150, and 155 MeV. Photoproduction from a liquid hydrogen target was employed as a normalization. The measured yields were found to be in disagreement with published theoretical cross sections for ^{6}Li$(\gamma,\pi^0)^6$Li and also in disagreement with a simple schematic model which assumed only coherent contributions from the M_{1+} multipole. The schematic model, however, did approximately predict the relative magnitudes of the yield curves for the energy range 14—20 MeV over threshold.

*MEV ABOVE THR

[NUCLEAR REACTIONS ^{6}Li, ^{12}C, ^{28}Si, ^{40}Ca, Cd, Pb, (γ,π^0); E_γ=140—155 MeV; measured σ; test of reaction model.]

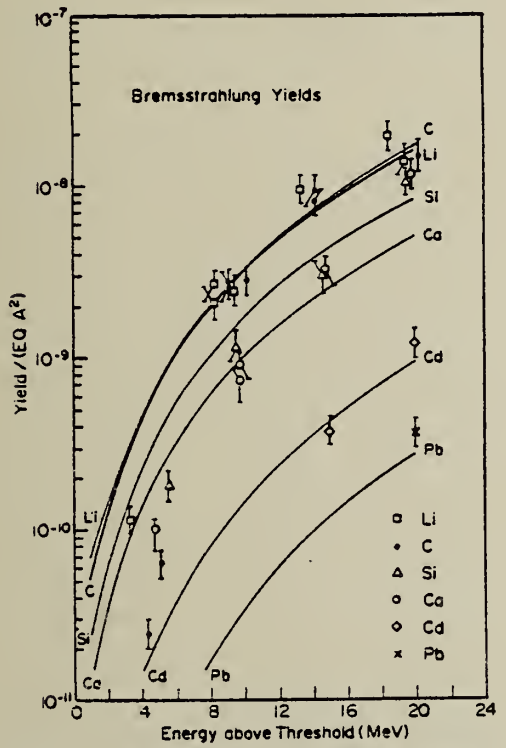

FIG. 6. The experimental and calculated yields for (γ,π^0) off a range of complex nuclei. The data were scaled so that the ^{12}C$(\gamma,\pi^0)^{12}$C experimental yield fit the calculated yield at 9.7 MeV over threshold (see text).

A=29

A=29

Ref. A.E. Berzin, L.P. Mashcheryakov
Zhur. Eksp. i Teoret. Fiz. 41, 1013 (1961)
Soviet Phys. JETP 14, 721 (1962)

Elem. Sym.	A	Z
Si	29	14

Method: Betatron; activation

Ref. No.: 61 Be 1 JR

Reaction	E or ΔE	E_o	Γ	$\int \sigma dE$	Jπ	Notes
(γ,n)						$E_{thresh.}$ = 8.47 ± 0.07 MeV

Ref. E.C. Booth, K.A. Wright
Nuclear Phys. 35, 472 (1962)

Elem. Sym.	A	Z
Si	29	14

Method 4 MeV electron Van de Graaff; bremss.; nuclear resonance scattering, ring scatterer; NaI

Ref. No. 62 Bo 6 JHH

Reaction	E or ΔE	E_0	Γ	$\int \sigma dE$	Jπ	Notes
$Si^{29}(\gamma,\gamma)$	Bremss. 0 - 4					

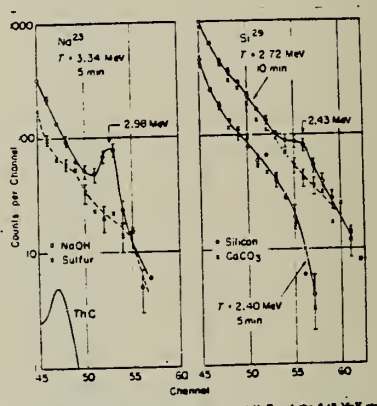

Fig. 3. Resonance fluorescence from the 2.98 MeV state of Na^{23} and the 2.43 MeV state of Si^{29}. The ThC peak is at 2.615 MeV. T is the maximum bremsstrahlung energy.

TABLE 2

Mean lifetimes of excited states deduced from the resonance scattering of bremsstrahlung

Nucleus	%	Energy (MeV)	Spins	g	Γ_0/Γ	$W'(\theta)$	$\tau \times 10^{12} \pm 35\%$ (sec)
F^{19}	100	1.46	$\frac{1}{2}^+ - ?$	?	0.13	(1)	$0.25g$
Na^{23}	100	2.08	$\frac{3}{2}^+ - \frac{1}{2}$	2	0.1	0.79	>0.04
		2.39	$-?$	?	0.53	(1)	$>1.6g$
		2.64	$-?$	?	0.8	(1)	$>0.3g$
		2.70	$-?$	?	(0.1)	(1)	$>0.008g$
		2.98	$-?$	?	0.46	(1)	$0.03g$
Al^{27}	100	2.73	$\frac{1}{2}^+ - \frac{1}{2}^+$	1	$\leqq 0.3$	0.91	>0.22
		2.98	$-\frac{1}{2}$	$\frac{1}{2}$	0.218	1	2.2×10^{-3}
Si^{29}	4.71	1.28	$\frac{1}{2}^+ - \frac{1}{2}^+$	2	1	0.88	1.5
		2.43	$-\frac{3}{2}^+$	2	(1)	0.88	0.2
P^{31}	100	1.28	$\frac{1}{2}^+ - \frac{1}{2}^+$	2	1	0.88	2.2
		2.23	$-\frac{5}{2}$	3	1	0.79	4.5
		3.13	$-\frac{3}{2}$	2	(1)	0.88	0.2
		3.29	$-\frac{5}{2}$	3	?	0.79	$>1.8(\Gamma_0/\Gamma)^2$
		3.41	$-?$	?	?	(1)	$>1.3g(\Gamma_0/\Gamma)^2$
		3.51	$-\frac{3}{2}$	2	?	0.88	$0.02(\Gamma_0/\Gamma)^2$
S^{32}	95	3.78	$0^+ - ?$	?	?	(1)	$>0.6g(\Gamma_0/\Gamma)^2$
S^{34}	4.2	2.127	$0^+ - 2$	5	1	0.63	>1.0
Cl^{35}	75.5	1.22	$\frac{1}{2}^+ - ?$	?	1	(1)	$6g$
		1.78	$-?$	?	(1)	(1)	$4g$
		2.7(2.65)	$-?$	?	?	(1)	$0.31g(\Gamma_0/\Gamma)^2$
		3.01	$-?$	?	?	(1)	$0.37g(\Gamma_0/\Gamma)^2$
Cl^{35}	75.5	3.1	?	?	?	(1)	$>0.74g(\Gamma_0/\Gamma)^2$
		3.17	?	?	?	(1)	$>1.5g(\Gamma_0/\Gamma)^2$
Cl^{37}	24.5	0.838	$\frac{1}{2}^+ - ?$	?	1	(1)	$>13g$
		1.72	$-?$	?	?	(1)	$>0.8g(\Gamma_0/\Gamma)^2$
K^{39}	93	2.53	$\frac{1}{2}^+ - ?$	?	1	(1)	$>1.6g$
		2.82	$-?$	?	1	(1)	$>1.5g$
		3.02	$-?$	?	1	(1)	$0.37g$
		3.60	$-?$	?	1	(1)	$>0.7g$
		3.88(3.94)	$-?$	?	?	(1)	$0.14g(\Gamma_0/\Gamma)^2$
		4.08–4.12	$-?$	?	?	(1)	$>0.2g(\Gamma_0/\Gamma)^2$
Ca^{40}	96	3.90	$0^+ - 2^+$	5	1	0.63	>0.46
Cu^{63}	69	1.33	$\frac{3}{2}^- - \frac{1}{2}$	2	(1)	0.8	$44 > \tau > 11$

The factor g equals $(2I+1)(2I_0+1)^{-1}$.

TABLE 3

Comparison of mean lifetime measurements

Nucleus	Energy	%	Spins	g	Γ_0/Γ	$W'(\theta)$	$\tau \times 10^{14}$ sec This work	Other	
Li^6	3.56	7	$1^+ - 0$	$\frac{1}{3}$	(1)	1	0.013	$0.0073^{+0.0015}_{-0.0013}$	[15]
								0.0106 ± 0.001	[16]
B^{11}	2.14	81	$\frac{1}{2}^- - (\frac{1}{2})$	$\frac{1}{2}$	1	1	0.53	0.47 ± 0.06	[16]
Al^{27}	2.21	100	$\frac{1}{2}^+ - \frac{1}{2}^-$	$\frac{1}{2}$	(1)	1	3.2	2.7 ± 0.3	[15]
Al^{27}	1.01	100	$\frac{1}{2}^+ - \frac{3}{2}^+$	$\frac{1}{2}$	0.96	1	520	170 ± 50	[15]
Si^{28}	1.78	92	$0^+ - 2^+$	5	1	0.63	88	73 ± 22	[15]
S^{32}	2.24	95	$0^+ - 2^+$	5	1	0.63	26	≈ 16	[16]
Mg^{26}	1.37	78.6	$0^+ - 2^+$	5	1	0.63	220	155 ± 40	[15]
Mg^{26}	1.61	26	$1^+ - \frac{1}{2}$	$\frac{1}{3}$	(1)	1	3.8	$2.5^{+0.6}_{-0.4}$	[17]
Cu^{65}	0.963	69	$\frac{3}{2} - \frac{1}{2}$	$\frac{1}{3}$	1	0.92	230	73 ± 18	[15]
								90 ± 15	[16]
Cu^{65}	0.67	69	$\frac{3}{2} - \frac{1}{2}$	$\frac{1}{3}$	1	1	100	31 ± 3	[18]

The factor g equals $(2I+1)(2I_0+1)^{-1}$.

10) R. C. Thiele, Phys. Rev. 148 (1966) 1469.
11) S. Vegors, L. Marsden and R. Heath, IDO-16870
12) Leslie Cohen and Ralph Tobias, Nuclear Physics 14 (1959) 242
13) W. C. Barber, F. Berthold, G. Friels and F. E. Gaddes, Phys. Rev. 120 (1960) 2128
14) F. R. Metzger, C. P. Swann and V. K. Rasmussen, Phys. Rev. 110 (1958) 909
15) F. R. Metzger, C. P. Swann and V. K. Rasmussen, Nuclear Physics 16 (1960) 568
16) S. Ofer and A. Schwarzschild, Phys. Rev. Lett. 3 (1959) 364
17) V. K. Rasmussen, F. R. Metzger and C. P. Swann, Phys. Rev. 123 (1961) 1330
18) J. B. Cummings, A. Schwarzschild, A. W. Sunyar and N. T. Porile, Phys. Rev. 126 (1962) 2130
19) T. Rothen, F. R. Metzger and C. P. Swann, Nuclear Physics 23 (1961) 206

REF.

T. W. Retz-Schmidt, S. J. Skorka, J. Morgenstern and H. Schmidt
Proc. Paris Conf. 396 (1964)

EL EM. SYM.	A	Z
Si	29	14

METHOD

Resonance Flurescence $^{29}Si(p,p'\gamma)$

REF. NO.

64 Re 1 JDM

REACTION	RESULT	EXCITATION ENERGY	SOURCE		DETECTOR		ANGLE
			TYPE	RANGE	TYPE	RANGE	
G,G	LFT	1	D	1	NAI-D	1	90

For the 1.277 MeV level in ^{29}Si $3/2^+$

$$\Gamma = (2.16 \,{}^{+0.83}_{-0.61}) \text{ MeV}$$

$$\tau_m = (3.05 \,{}^{+1.20}_{-0.85}) \times 10^{-13} \text{ secs.}$$

$$|M|^2_{E2} = (6.5 \,{}^{+2.4}_{-1.8})$$

$$|M|^2_{M1} = (0.048 \,{}^{+0.018}_{-0.014})$$

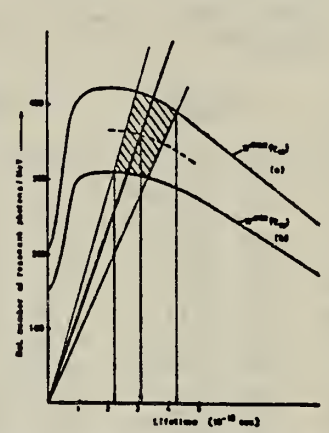

Fig. 2. — Calc. rel. number of resonant photons/MeV *vs.* lifetime of 3/2+ state in Si^{29}. Curves a) and b) see text. Slope of straight line results from experiment.

REF.

Y. Oka, T. Kato, K. Nomura, T. Saito, Hui-Tuh Tsai
Bull. Chem. Soc. Japan 41, 380 (1968)

ELEM. SYM.	A	Z
Si	29	14

METHOD

REF. NO.	
68 Ok 3	egf

REACTION	RESULT	EXCITATION ENERGY	SOURCE		DETECTOR		ANGLE
			TYPE	RANGE	TYPE	RANGE	
G,P	ABY	THR-20	C	20	ACT-I		4PI

TABLE 1. SUMMARY OF DATA ON (γ, p) REACTIONS WITH 20 MeV BREMSSTRAHLUNG

Nuclide: Parent (Natural abundance, %)	Nuclide: Residual (Half-life)	S_p (MeV)	Observed γ-ray: Energy (MeV)	Observed γ-ray: Branching ratio (%)	Observed γ-ray: Type of multipole transition	Yield determined: μCi/mg[a]	Yield determined: Yield/mol·R
^{25}Mg (10.11)	^{24}Na (15 hr)	12.06	1.37	100	$E2$	1.48×10^{-1}	1.7×10^{5}
^{29}Si (4.71)	^{28}Al (2.27 min)	12.33	1.78	100	$E2$	1.91	2.8×10^{5}
^{30}Si (3.12)	^{29}Al (6.56 min)	13.59	1.28	93.8	$E2+M1$	6.51×10^{-1}	1.5×10^{5}
^{44}Ca (2.06)	^{43}K (22.4 hr)	12.17	0.374	85	$E2+M1$	7.86×10^{-3}	1.3×10^{5}
^{47}Ti (7.32)	^{46}Sc (84.1 d)	10.47	0.887	100	$E2$	7.11×10^{-4}	3.1×10^{5}
^{48}Ti (73.99)	^{47}Sc (3.4 d)	11.44	0.160	100	$E2+M1$	6.83×10^{-3}	1.2×10^{5}
^{49}Ti (5.46)	^{48}Sc (1.8 d)	11.35	1.31	100	$E2$	4.40×10^{-3}	5.8×10^{4}
^{53}Cr (9.55)	^{52}V (3.8 min)	11.15	1.43	100	$E2$	5.01×10^{-1}	6.6×10^{4}
^{57}Fe (2.17)	^{56}Mn (2.58 hr)	10.57	1.81	23.5	$E2+M1$	8.10×10^{-3}	2.1×10^{5}
^{74}Ge (36.74)	^{73}Ga (4.8 hr)	10.92	0.295	97	$(E2)$	3.70×10^{-1}	1.3×10^{5}
^{77}Se (7.58)	^{76}As (26.5 hr)	9.61	0.559	41	$E2$	1.48×10^{-3}	1.3×10^{5}
^{87}Sr (7.02)	^{86}Rb (19 d)	9.41	1.08	9	$E2$	5.15×10^{-4}	9.9×10^{4}
^{113}Cd (12.26)	^{112}Ag (3.2 hr)	9.74	1.39	35	$E2$	1.91×10^{-3}	2.1×10^{4}
^{117}Sn (7.57)	^{116m}In (54 min)	9.58	1.27	84	$E2$	9.80×10^{-3}	6.9×10^{3}
^{137}Ba (11.32)	^{136}Cs (13 d)	8.67	0.830	100	$E2$	1.68×10^{-4}	2.2×10^{4}
^{199}Hg (16.84)	^{198}Au (2.7 d)	7.27	0.412	100	$E2$	8.43×10^{-4}	2.2×10^{4}

a) The value corrected at the end of 1 hr irradiation (9.4×10^{6} R/min).

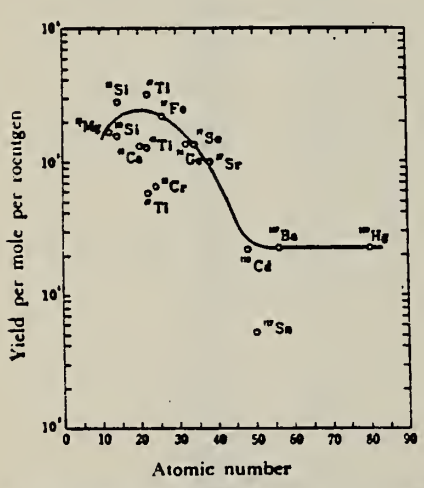

Fig. 2. The yield curve for the (γ, p) reaction with 20 MeV bremsstrahlung.

REF.

H. E. Jackson and R. E. Toohey
Phys. Rev. Letters 29, 379 (1972)

ELEM. SYM.	A	Z
Si	29	14

METHOD

REF. NO. 72 Ja 2 hmg

REACTION	RESULT	EXCITATION ENERGY	SOURCE		DETECTOR		ANGLE
			TYPE	RANGE	TYPE	RANGE	
G,N	SPC	8- 11	C	11	TOF-D		DST
		(8.5 - 10.4)		(10.42)			

A study of the reaction $^{29}Si(\gamma,n)$ near threshold suggests that a doorway state with $J^\pi = \frac{3}{2}^-$ common to the channels $^{28}Si + n$ and $^{29}Si + \gamma$ lies near 750 keV. We observe experimentally Lane's prediction of a significant nonresonant background cross section associated with strong partial-width correlations.

9.25 MEV DOORWAY

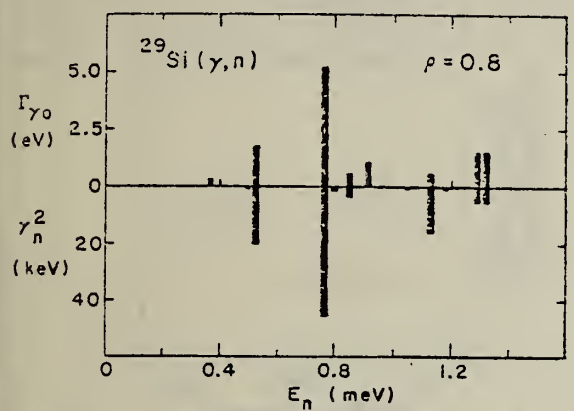

FIG. 2. Ground-state radiation widths Γ_{γ_0} and reduced neutron widths γ_n^2 for resonances in the ^{29}Si compound nucleus with $J^\pi = \frac{3}{2}^-$.

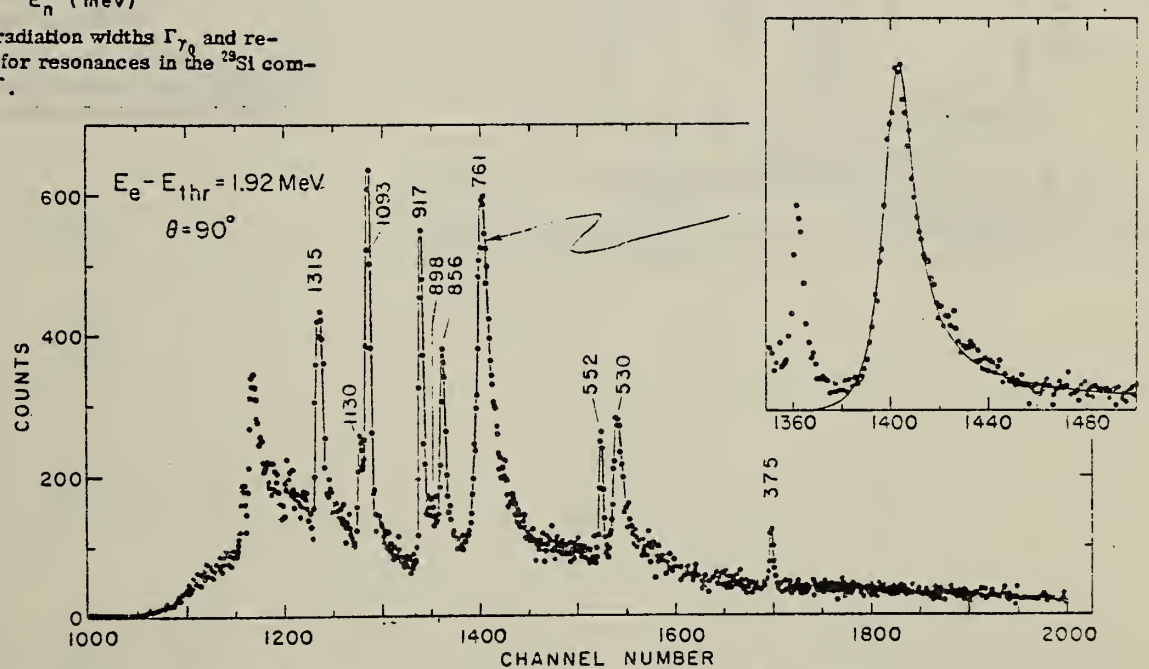

FIG. 1. Photoneutron time-of-flight spectrum for $^{29}Si(\gamma,n)$. Flight path, 9 m; bremsstrahlung pulse width, 6 nsec; pulse repetition rate, 800 pulses/sec; average linac current, ~25 μA. The spectrum was accumulated in a 24-h run. The data have not been corrected for variations in detector efficiency or for the energy dependence of the incident flux. Resonance energies are given in keV. Inset, expanded plot of the data in the region of the 761-keV resonance. The curve is the resonance shape resulting from the sum of a normal Breit-Wigner amplitude whose total width is $\Gamma = 26$ keV and a nonresonant amplitude corresponding to a background cross section of 0.32 mb.

REF. K. Fukuda and S. Okabe
J. Phys. Soc. Japan 34, 315 (1973)

ELEM. SYM.	A	Z
Si	29	14

METHOD

REF. NO. 73 Fu 2 egf

REACTION	RESULT	EXCITATION ENERGY	SOURCE TYPE	SOURCE RANGE	DETECTOR TYPE	DETECTOR RANGE	ANGLE
G,N	ABX	8- 13	C	8- 13	BF3-I		DST

$\sigma_o(13)$ = 11 MeV-mb

802

$d\sigma/d\Omega = a + b \sin^2\theta$

b/a = 2.1 ± 1.0 E_m = 11.7 MeV

= 3.9 ± 0.8 = 12.9 MeV

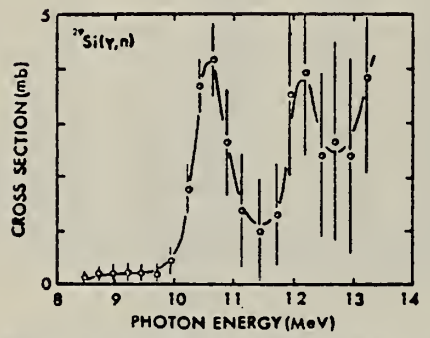

Fig. 2. The photoneutron cross-section for ^{29}Si using a bin width of 0.5 MeV.

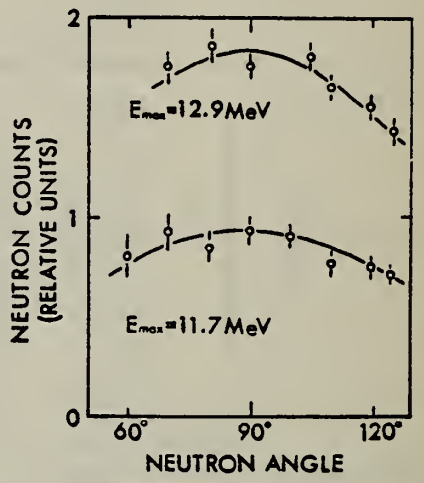

Fig. 3. Angular distributions of photoneutrons from ^{29}Si irradiated with bremsstrahlung spectra of 11.7 and 12.9 MeV maximum energies.

REF.

S. W. Brain, A. Johnston, W. A. Gillespie, E. W. Lees and R. P. Singhal
J. Phys. G 3, 681 (1977)

ELEM. SYM.	A	Z
Si	29	14

REF. NO. 77 Br 10 egf

REMARKS: Inelastic form factor plotted for all levels

REACTION	RESULT	EXCITATION ENERGY	SOURCE		DETECTOR		ANGLE
			TYPE	RANGE	TYPE	RANGE	
E,E/	LFT	1- 9	D	63-117	MAG-D		DST

13 STATES

Abstract. The excited states of ^{29}Si up to 8·3 MeV excitation energy have been studied by inelastic electron scattering in the momentum transfer range 0·4 to 1·05 fm^{-1}. Ground-state transition probabilities and transition radii were obtained for the levels excited. At lower excitation energies our transition probabilities agree with previous work. A number of high excitation and high-multipolarity levels are studied for the first time, and several previously tentative spin–parity assignments are confirmed. Transition probabilities for $L = 2$, 3 and 4 are compared with the predictions of the intermediate coupling model, and the Nilsson and shell models.

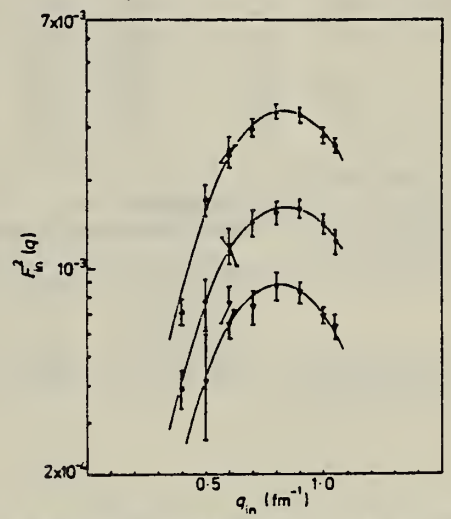

Figure 2. Inelastic form factors for the ^{29}Si E2 transitions at 1·27 MeV (▽), 2·03 MeV (△) and 2·43 MeV (○). The full curves are the best-fit DWBA form factors.

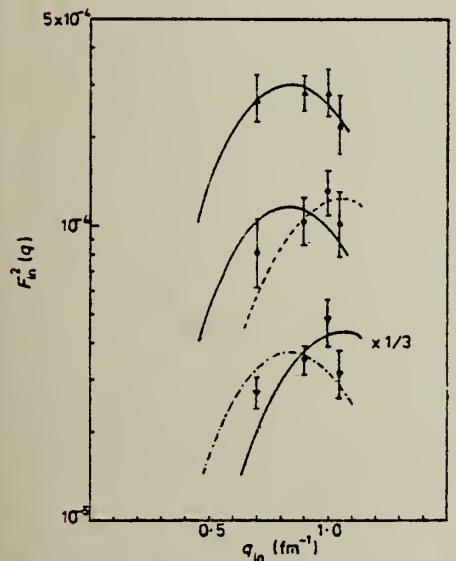

Figure 7. DWBA fits to the form factor data for the 7·91 MeV (——, E2; – – –, E3), 8·13 MeV (——, E2) and 8·27 MeV (——, E3; – – –, E2) levels.

over

Table 5. Results for the present analysis of ^{29}Si using the Tassie model.

E_x (MeV)	J^π	Transition	c_{tr} (fm)	t_{tr} (fm)	R_{tr} (fm)	$B(XL, \omega\uparrow)$§ (e^2 fm^{2L})	G_{sp} (Wu)¶
1·276	$\frac{3}{2}^+$	E2	2·979	2·23‡	4·35	42 ± 10	3·9 ± 0.9
2·022	$\frac{5}{2}^+$	E2	2·841	2·23‡	4·26	148 ± 21	9·1 ± 1·3
2·418	$\frac{1}{2}^+$	E2	2·844	2·23‡	4·27	71 ± 11	6·6 ± 1·0
3·627	$\frac{7}{2}^-$	E3	2·968	2·23‡	4·94	680 ± 90	3·3 ± 0·4
4·107	$\frac{7}{2}^+$	E4	2·85‡	2·39‡	5·97	(7 ± 4) × 10^3	3·6 ± 2·0
4·90	†						
5·280	$\frac{7}{2}^+$	E4	2·85‡	2·39‡	5·97	(2·1 ± 0·8) × 10^4	1·0 ± 0·5
6·514	$(\frac{3}{2}, \frac{5}{2})^+$	E2	2·230	2·23‡	3·90	11 ± 2	
7·019	$(\frac{3}{2}, \frac{7}{2})^-$	E3	2·427	2·23‡	4·71	(1·2 ± 0·2) × 10^3	
7·621	$(\frac{5}{2}, \frac{7}{2})^-$	E3	2·818	2·23‡	4·87	(1·8 ± 0·2) × 10^3	
7·905	$(\frac{3}{2}, \frac{5}{2})^+$	E2	2·841‡	2·23‡	4·26	5·0	
		E3	2·968‡	2·23‡	4·94	2·8 × 10^2	
8·132	$(\frac{1}{2}, \frac{3}{2}, \frac{5}{2})^+$	E2	2·841‡	2·23‡	4·26	3·3	
8·272	$(\frac{5}{2}, \frac{7}{2})^-$	E2	2·841‡	2·23‡	4·26	4·9	
		E3	2·968‡	2·23‡	4·94	3·0 × 10^2	

† See table 6 and text.
‡ This parameter was fixed during fitting.
§ $B(XL, \omega\uparrow)$ (X = E or M) is the reduced transition probability for excitation from the ground state to the level of spin L.
¶ The collectivity of the levels are given in Weisskopf units as defined in Wilkinson (1960).

Wilkinson D.H. 1960 Nuclear Spectroscopy (New York: Academic) part B 852-89

REF. S. Joly, G. Grenier, J. Voignier, J.W. Boldeman
Nucl. Phys. A334, 269 (1980)

ELEM. SYM.	A	Z
Si	29	14

METHOD

REF. NO. 80 Jo 5 hg

REACTION	RESULT	EXCITATION ENERGY	SOURCE		DETECTOR		ANGLE
			TYPE	RANGE	TYPE	RANGE	
N,G	LFT	9, 10	D	565*813	SCD-D		100
		(9.34,9.28)					

γ-Transitions assumes E1 for the angular distribution effect. *ENERGY IN KEV

Abstract: Gamma-ray spectra from the neutron capture by natural silicon have been measured with Ge(Li) and NaI detectors for neutron resonances at 565 and 813 keV. Absolute partial and total radiative widths have been obtained and compared with previous results and with recent valence and shell-model calculations.

E NUCLEAR REACTIONS ^{28}Si(n, γ), E = 565, 813 keV; measured $\sigma(E, E_\gamma)$. ^{29}Si deduced $\Gamma_{\gamma 0}$, Γ_γ. Natural target.

TABLE 3

Ground-state radiative widths $\Gamma_{\gamma 0}$

Resonance energy (keV)	$\Gamma_{\gamma 0}$		Weighted mean (eV)
	Ge(Li) exp. (eV)	NaI exp. (eV)	
565	0.70±0.25	0.55±0.15	0.60±0.15
813	2.40±0.65	2.10±0.50	2.20±0.40

REF. K.E. Whitner, C.F. Williamson, B.E. Norum, S. Kowalski
Phys. Rev. C22, 374 (1980)

ELEM. SYM.	A	Z
Si	29	14

METHOD

REF. NO. 80 Wh 2 egf

REACTION	RESULT	EXCITATION ENERGY	SOURCE		DETECTOR		ANGLE
			TYPE	RANGE	TYPE	RANGE	
E,E/	FMF	1,4	D	126-293	MAG-D		DST

Natural Silicon Target

4 STATES 1.27-4.08

Electron scattering from ^{28}Si and ^{29}Si has been performed at energies from 126 to 293 MeV and at angles of 45° and 90°. Form factors were extracted for levels below 5.0 MeV in ^{28}Si and ^{29}Si over an effective momentum transfer range of 0.6 to 2.1 fm^{-1}. A particle-phonon coupling calculation using harmonic-oscillator single-particle states and data from ^{28}Si give a reasonable description of the low-lying states of ^{29}Si.

[NUCLEAR REACTIONS ^{28}Si(e,e') first 2 excited states; ^{29}Si(e,e') first 5 excited states; measured form factors 45° and 90°, $0.6 \leq q \leq 2.1$ fm^{-1}; natural Si target; PWBA analysis, vibrating core and intermediate coupling for ^{29}Si.]

TABLE VII. Electron scattering squared form factors for levels in ^{29}Si.[a,b]

	$\frac{1}{2}^+$ (1.27 MeV)			$\frac{5}{2}^+$ (2.03 MeV)			$\frac{3}{2}^+$ (2.43 MeV)			$\frac{1}{2}^+$ (4.08 MeV)		
Run	q_{eff} (fm^{-1})	$\lvert F\rvert^2$ $\times 10^{-5}$	± %	q_{eff} (fm^{-1})	$\lvert F\rvert^2$ $\times 10^{-5}$	± %	q_{eff} (fm^{-1})	$\lvert F\rvert^2$ $\times 10^{-5}$	± %	q_{eff} (fm^{-1})	$\lvert F\rvert^2$ $\times 10^{-5}$	± %
1							0.596	113	38			
2	0.698	130	75	0.697	294	13	0.696	169	18.4			
3	0.794	129	55	0.792	331	8.8	0.791	147	15.1			
4	0.892	81.8	36	0.890	355	5.9	0.890	128	11.7			
5	0.946	84.7	21	0.943	304	5.8	0.942	136	9.1			
6	0.996	82.1	24	0.995	331	6.0	0.994	120	9.7			
7	1.046	64.8	13.3	1.044	252	5.9	1.041	124	7.2			
8	1.151	48.6	10.0	1.149	181	6.4	1.148	88.1	8.4			
9	1.198	37.3	10.3	1.195	137	5.2	1.193	73.0	6.2			
10	1.229	29.1	5.0	1.226	122	6.7	1.225	67.5	7.8	1.219	2.42	62
11	1.261	24.3	5.2	1.258	108	4.4	1.257	61.4	4.8	1.251	2.33	66
12	1.299	20.1	10.5	1.296	97.2	6.9	1.295	44.3	8.9			
13	1.356	13.0	5.6	1.352	64.2	5.3	1.351	37.5	5.7	1.348	4.05	25
14	1.408	8.63	25	1.405	46.9	10.3	1.403	28.9	10.5	1.397	6.29	25
15							1.464	15.5	10.8	1.458	5.89	16.5
16				1.536	10.7	12.5	1.535	7.60	11.5	1.530	5.51	10.2
17	1.595	0.96	121				1.590	1.88	61	1.584	7.07	14.8
18	1.673	0.28	179	1.670	1.10	49				1.663	5.07	9.9
19										1.736	5.32	12.9
20	1.831	1.72	49	1.829	2.98	18.7	1.827	1.94	36	1.821	4.95	15.5
21				1.931	3.36	41				1.923	3.48	15.8
22	2.034	2.11	11.0	2.031	4.39	15.8	2.029	2.41	17.2	2.024	3.00	11.6
23	2.129	2.63	10.6	2.126	4.86	17.5	2.125	2.68	16.3	2.119	2.18	14.1
24												

[a] The squared form factor entries should be multiplied by the indicated factor.
[b] Percentage errors are statistical only.

(over)

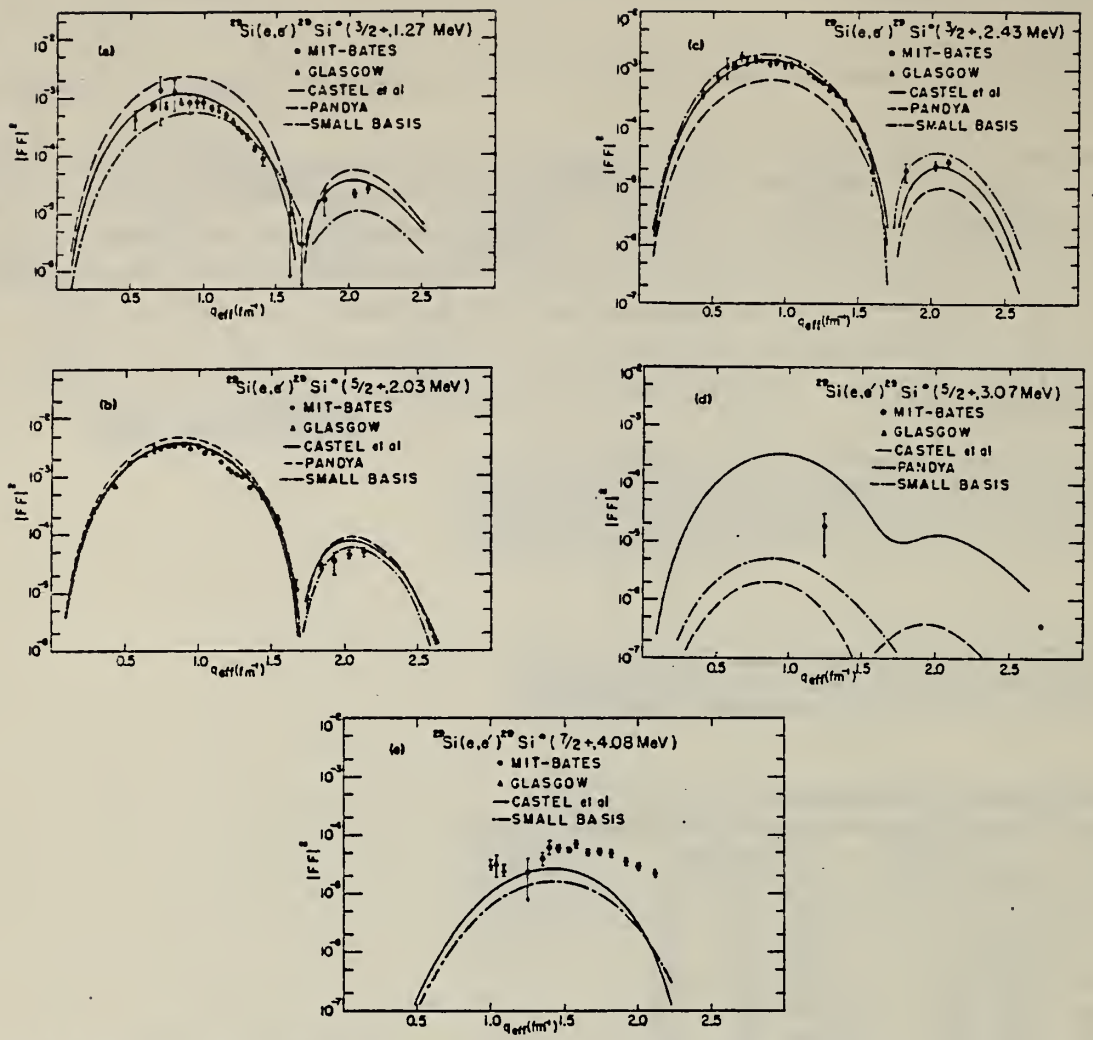

FIG. 5. Squared form factors for electron scattering from the low-lying levels in ^{28}Si. (a) $\frac{3}{2}^+$(1.27 MeV) level. (b) $\frac{5}{2}^+$(2.03 MeV) level. (c) $\frac{3}{2}^+$(2.43 MeV) level. (d) $\frac{5}{2}^+$(3.07 MeV) level. (e) $\frac{7}{2}^+$(4.08 MeV) level. The present data are shown as solid circles and the data of Ref. 17 are shown as solid triangles. Also shown are theoretical curves calculated from the three sets of eigenvectors as described in text.

REF. R.E. Pywell, B.L. Berman, P. Kean, M.N. Thompson
Nucl. Phys. A369, 141 (1981)

ELEM. SYM.	A	Z
Si	29	14

METHOD

REF. NO.	
81 Py 2	hg

REACTION	RESULT	EXCITATION ENERGY	SOURCE		DETECTOR		ANGLE
			TYPE	RANGE	TYPE	RANGE	
G,XN	ABX	8-29	C	8-29	BF3-I		4PI
		(8.5-29)					
G,N	ABX	8-16	C	8-16	BF3-I		4PI

Abstract: The photoneutron cross section of ^{29}Si has been measured over the energy range 8 to 28 MeV using the bremsstrahlung yield curve technique. The giant dipole resonance is observed to be centered at 21.2 MeV and is 5.5 MeV wide. In addition, a pygmy resonance containing much fine structure is observed below 17 MeV. An attempt is made to interpret these observations in terms of the weak coupling of the extra neutron to a ^{28}Si core. However, detailed comparisons of the structure and relative strengths of the ^{28}Si and ^{29}Si cross sections reveal that the coupling of the extra-core nucleon is large and significantly modifies the core wave function.

E NUCLEAR REACTIONS ^{29}Si(γ, xn), $E \approx$ 8-28 MeV, enriched sample; measured 4π neutron yield with bremsstrahlung. Deduced σ(E), observed GDR and pygmy resonance.

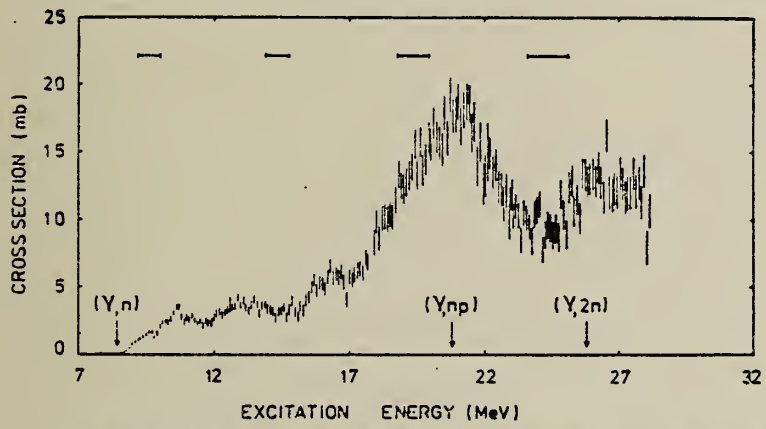

Fig. 1. The cross section ^{29}Si(γ, sn), obtained from the yield curve measured in 100 keV intervals. Error bars are statistical only. There is an uncertainty no greater than 10 % in the absolute magnitude of the cross section. Horizontal bars indicate the width of the interval used in data analysis.

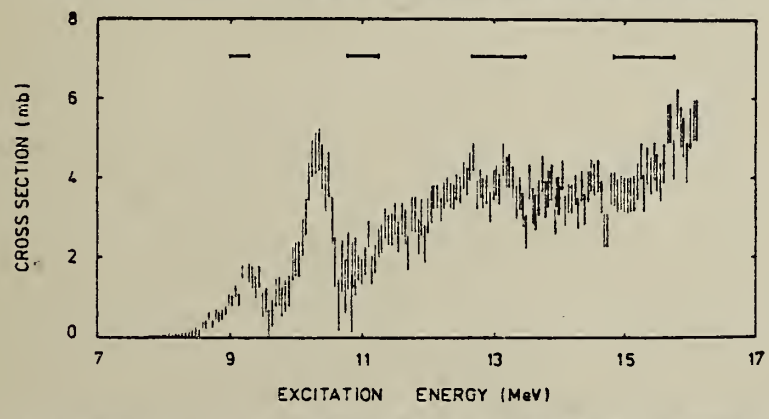

Fig. 2. The cross section for ^{29}Si(γ, n), obtained from the yield curve measured in 50 keV intervals. Error bars are statistical only. There is an uncertainty no greater than 10 %, in the absolute magnitude of the cross section. Horizontal bars indicate the width of the interval used in data analysis.

A=30

A=30

A=30

Ref. A.E. Berzin, R.P. Mashcheryakov
Zhur. Eksp. i Teoret. Fiz. 41, 1013 (1961)
Soviet Phys. JETP 14, 721 (1962)

Elem. Sym.	A	Z
Si	30	14

Method: Betatron; activation

Ref. No.: 61 Be 1 JE

Reaction	E or ΔE	E_o	Γ	$\int \sigma dE$	Jπ	Notes
(γ,n)						$S_{thresh.}$ = 10.618 ± 0.07 MeV

REF.
L. Meyer-Schutzmeister, Z. Vager, R. E. Segel and P. P. Singh
Nucl. Phys. A108, 180 (1968)

ELEM. SYM.	A	Z
Si	30	14

METHOD

REF. NO. 68 Me 1 EGF

REACTION	RESULT	EXCITATION ENERGY	SOURCE		DETECTOR		ANGLE
			TYPE	RANGE	TYPE	RANGE	
G,A	ABX	14-22	D	4-14	NAI-D	10-22	DST

759+

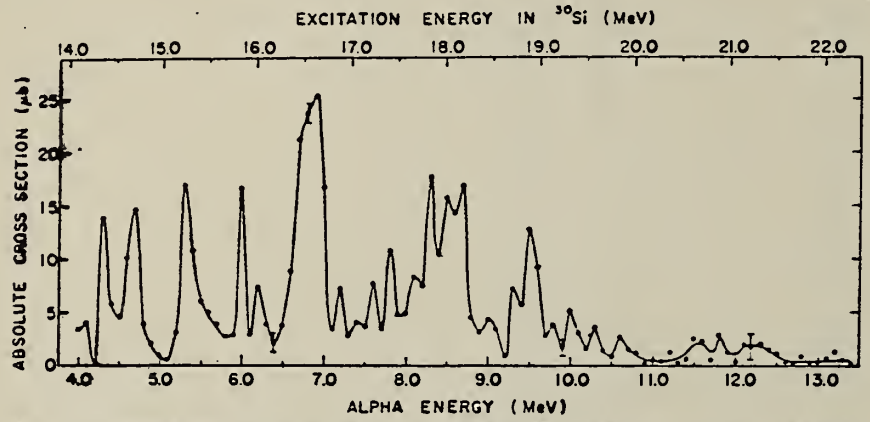

Fig. 5. The absolute cross section for the reaction ^{26}Mg$(\alpha,\gamma_0)^{30}$Si plotted as a function of the energy of the incident alpha. The data were taken in 100 keV steps. As in fig. 3, the angular distribution used was of the $\sin^2\theta$ form typical of an electric-dipole transition.

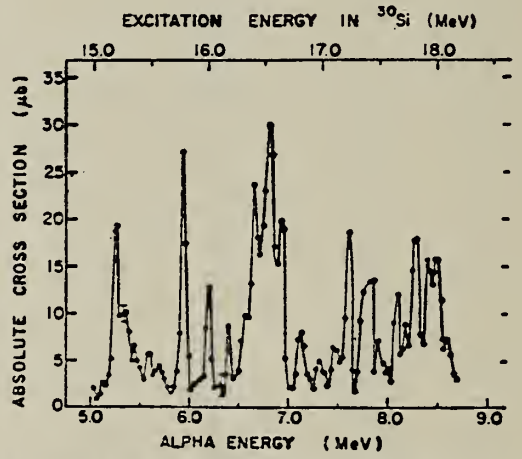

Fig. 6. Same as fig. 5 except that the measurements were taken in 30 keV steps instead of 100 keV and extend only from 5.0 to 8.7 MeV.

REACTION	RESULT	EXCITATION ENERGY	SOURCE		DETECTOR		ANGLE
			TYPE	RANGE	TYPE	RANGE	

TABLE 1

The averaged absolute cross sections $\overline{\sigma(\alpha,\gamma_0)}$ and $\overline{\sigma(\alpha,\gamma_1)}$ for the reactions $^{24}Mg(\alpha,\gamma_0)$, $^{24}Mg(\alpha,\gamma_1)$, $^{26}Mg(\alpha,\gamma_0)$ and $^{28}Si(\alpha,\gamma_0)$

	$^{24}Mg(\alpha,\gamma)^{28}Si$		$^{26}Mg(\alpha,\gamma_0)^{30}Si$		$^{28}Si(\alpha,\gamma_0)^{32}S$	
ΔE_x (MeV)	$\overline{\sigma(\alpha,\gamma_0)}$ (μb)	$\overline{\sigma(\alpha,\gamma_1)}$ (μb)	ΔE_x (MeV)	$\overline{\sigma(\alpha,\gamma_0)}$ (μb)	ΔE_x (MeV)	$\overline{\sigma(\alpha,\gamma_0)}$ (μb)
14.65–16.65	8.5	5.0	14.1–16.1	6.1	13.1–15.5	1.7
16.65–18.65	12.9	6.1	16.1–18.1	9.7	15.5–17.5	2.2
18.65–20.65	11.0	8.6	18.1–20.1	4.6		
20.65–22.65	2.1	5.6	20.1–22.1	1.0		
14.65–22.65	8.6	6.3	14.1–22.1	5.3	13.1–17.5	1.9

The cross sections in the first four rows were obtained from the data in figs. 3–6 and 15 by averaging over the indicated ≈ 2 MeV ranges of excitation energy E_x in the product nucleus (^{28}Si, ^{30}Si or ^{32}S). The last line gives the average for the entire energy range that was studied.

TABLE 3

The cross sections $\overline{\sigma(\gamma,\alpha_0)}$ for the α-decay of the nuclei ^{28}Si, ^{30}Si and ^{32}S

Target nucleide	ΔE (MeV)	$\overline{\sigma(\gamma,\alpha_0)}$ (mb)	$\overline{\sigma(\gamma,p_0)}$ (mb)	$\dfrac{\overline{\sigma(\gamma,\alpha_0)}}{\overline{\sigma(\gamma,p_0)}}$	$\gamma^2(\alpha_0)/\gamma^2(p_0)$	
					$l=1$	$l=3$
^{28}Si	16.65–18.65	1.01	6.2	0.16	0.35	0.12
	18.65–20.65	0.94	11.7	0.080	0.095	0.041
	20.65–22.65	0.22	9.6	0.023	0.019	0.011
	16.65–22.65	0.72	9.2	0.08		
^{30}Si	14.1 –16.1	0.43				
	16.1 –18.1	0.69				
	18.1 –20.1	0.35				
	18.1 –20.1	0.35				
	20.1 –22.1	0.08				
	14.1 –22.1	0.38				
^{32}S	13.1 –15.5	0.20	1.7	0.12		
	15.5 –17.5	0.27	2.1	0.13		
	17.5 –19.5		3.0			
	13.1 –17.5	0.23	1.9	0.12		

The averages were taken over ≈ 2 MeV wide energy regions ΔE and over the total studied energy region of the giant dipole resonance. These cross sections were obtained by detailed balance from the α-capture in ^{24}Mg, ^{26}Mg and ^{28}Si. For comparison, the average cross sections $\overline{\sigma(\gamma,p_0)}$ over the same energy regions ΔE for the reactions $^{28}Si(\gamma,p_0)^{27}Al$ and $^{32}S(\gamma,p_0)^{31}P$ are also presented. These likewise were obtained by detailed balance from the inverse reactions as measured by Singh *et al.* [6]) and by Dearnaley *et al.* [6]). For the calculation, we assumed an isotropic angular distribution for the $^{28}Si(\gamma,p_0)$ reaction, a $\sin^2\vartheta$ distribution for $^{32}S(\gamma,p_0)$. In addition, the ratios $\overline{\sigma(\gamma,\alpha_0)}/\overline{\sigma(\gamma,p_0)}$ are given for both ^{28}Si and ^{32}S and also the calculated reduced width $\gamma^2(\alpha_0)/\gamma^2(p_0)$ for an orbital-angular-momentum transfer of $l=1$ and of $l=3$ in the decay of ^{28}Si.

REF. Y. Oka, T. Kato, K. Nomura, T. Saito, Hui-Tuh Tsai
Bull. Chem. Soc. Japan 41, 380 (1968)

ELEM. SYM.	A	Z
Si	30	14

METHOD

REF. NO. 68 Ok 3 egf

REACTION	RESULT	EXCITATION ENERGY	SOURCE		DETECTOR		ANGLE
			TYPE	RANGE	TYPE	RANGE	
G,P	ABY	THR-20	C	20	ACT-I		4PI

TABLE 1. SUMMARY OF DATA ON (γ, p) REACTIONS WITH 20 MeV BREMSSTRAHLUNG

Nuclide: Parent (Natural abundance, %)	Nuclide: Residual (Half-life)	S_p (MeV)	Observed γ-ray: Energy (MeV)	Observed γ-ray: Branching ratio (%)	Observed γ-ray: Type of multipole transition	Yield determined: μCi/mg[a]	Yield determined: Yield/mol·R
^{25}Mg (10.11)	^{24}Na (15 hr)	12.06	1.37	100	$E2$	1.48×10^{-1}	1.7×10^{5}
^{29}Si (4.71)	^{28}Al (2.27 min)	12.33	1.78	100	$E2$	1.91	2.8×10^{5}
^{30}Si (3.12)	^{29}Al (6.56 min)	13.59	1.28	93.8	$E2+M1$	6.51×10^{-1}	1.5×10^{5}
^{44}Ca (2.06)	^{43}K (22.4 hr)	12.17	0.374	85	$E2+M1$	7.86×10^{-3}	1.3×10^{5}
^{47}Ti (7.32)	^{46}Sc (84.1 d)	10.47	0.887	100	$E2$	7.11×10^{-4}	3.1×10^{5}
^{48}Ti (73.99)	^{47}Sc (3.4 d)	11.44	0.160	100	$E2+M1$	6.83×10^{-2}	1.2×10^{5}
^{49}Ti (5.46)	^{48}Sc (1.8 d)	11.35	1.31	100	$E2$	4.40×10^{-3}	5.8×10^{4}
^{53}Cr (9.55)	^{52}V (3.8 min)	11.15	1.43	100	$E2$	5.01×10^{-1}	6.6×10^{4}
^{57}Fe (2.17)	^{56}Mn (2.58 hr)	10.57	1.81	23.5	$E2+M1$	8.10×10^{-2}	2.1×10^{5}
^{74}Ge (36.74)	^{73}Ga (4.8 hr)	10.92	0.295	97	$(E2)$	3.70×10^{-1}	1.3×10^{5}
^{77}Se (7.58)	^{76}As (26.5 hr)	9.61	0.559	41	$E2$	1.48×10^{-2}	1.3×10^{5}
^{87}Sr (7.02)	^{86}Rb (19 d)	9.41	1.08	9	$E2$	5.15×10^{-4}	9.9×10^{4}
^{113}Cd (12.26)	^{112}Ag (3.2 hr)	9.74	1.39	35	$E2$	1.91×10^{-2}	2.1×10^{4}
^{117}Sn (7.57)	^{116m}In (54 min)	9.58	1.27	84	$E2$	9.80×10^{-3}	6.9×10^{5}
^{137}Ba (11.32)	^{136}Cs (13 d)	8.67	0.830	100	$E2$	1.68×10^{-4}	2.2×10^{4}
^{199}Hg (16.84)	^{199}Au (2.7 d)	7.27	0.412	100	$E2$	8.43×10^{-4}	2.2×10^{4}

a) The value corrected at the end of 1 hr irradiation (9.4×10^{6} R/min).

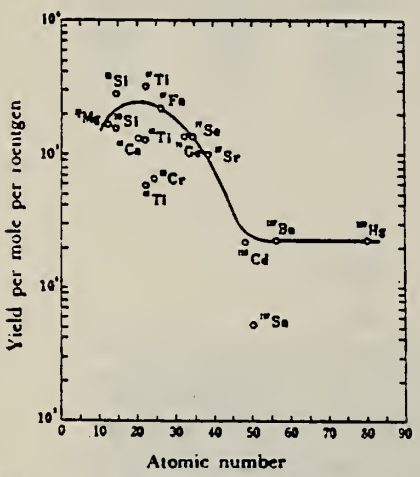

Fig. 2. The yield curve for the (γ, p) reaction with 20 MeV bremsstrahlung.

B. Friberg, G. Andersson, and B. Forkman
Nucl. Phys. A171, 551 (1971)

Si	30	14

METHOD

REF. NO. 71 Fr 1 egf

REACTION	RESULT	EXCITATION ENERGY	SOURCE		DETECTOR		ANGLE
			TYPE	RANGE	TYPE	RANGE	
G,P	ABX	14-800	C	100-800	ACT-I		4PI

$$Y_{R,\text{meson}} = \tfrac{1}{4} F_R \, y_{^{12}C,\text{meson}}$$

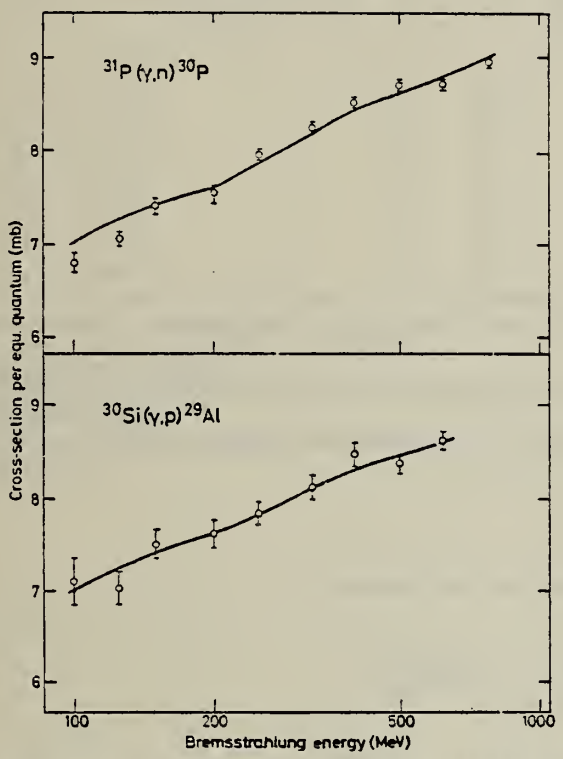

Fig. 2. Absolute yields for the reactions $^{30}Si(\gamma, p)^{29}Al$ and $^{31}P(\gamma, n)^{30}P$. Solid lines same as for fig. 1.

	Punched	Checked w/PO
IBM Card DATA	3/14/72	✓
IBM Card REFERENCE	3/14/72	✓

REF.

J. P. Russell, W. E. Taylor, F. E. Dunnam and H. A. Van Rinsvelt
Nucl. Phys. A187, 449 (1972)

ELEM. SYM.	A	Z
Si	30	14

METHOD

REF. NO.: 72 Ru 1 | egf

REACTION	RESULT	EXCITATION ENERGY	SOURCE		DETECTOR		ANGLE
			TYPE	RANGE	TYPE	RANGE	
A,G	ABY	13-14	D	3-4	NAI-D		DST

J-PI, LFT

TABLE 2

Summary of resonances observed in the $^{26}Mg(\alpha,\gamma)^{30}Si$ and $^{26}Mg(\alpha,\alpha)^{26}Mg$ reactions

Resonance number [a]	E_α (MeV)	E_x (MeV)	Observed in (α,γ)	Observed in (α,α)	J^π	Γ_α (keV) [c]	$\frac{(2J+1)}{\Gamma}\Gamma_\alpha\Gamma_{\gamma_0}$(eV)	Γ_{γ_0}(eV) [d]
9	3.285	13.495		×	1^-	0.75		
16	3.612	13.778		×	0^+	14.0		
18	3.709	13.862	×	×	1^-	1.5	0.1 [b]	0.4
19	3.750	13.903		×	(1^-)	0.5		
23	3.880	14.012		×	0^+	8.0		
24	3.981	14.102	×	×	1^-	1.0	1.0 [b]	6.1
	4.091	14.197		×	0^+	5.0		
28	4.160	14.258		×	(2^+)	0.5		
29	4.231	14.317	×	×	1^-	2.0	2.8 [b]	8.5

[a]) The resonance numbers correspond to the numbers of table 1, except for the resonance at E_α = 4.091 MeV which has not been identified in the (α, n) data.
[b]) The error is estimated to be ±40 %.
[c]) The values shown for Γ_α are the results from the multi-level multi-channel R-matrix calculation. The error is of the order of ±30 %.
[d]) The total widths used in the computation of the radiative widths Γ_{γ_0} are shown in table 1. It was also assumed that $\Gamma_p = 0$.

$^{26}Mg(\alpha,\gamma)^{30}Si$

GROUND STATE TRANSITION ANGULAR DISTRIBUTIONS

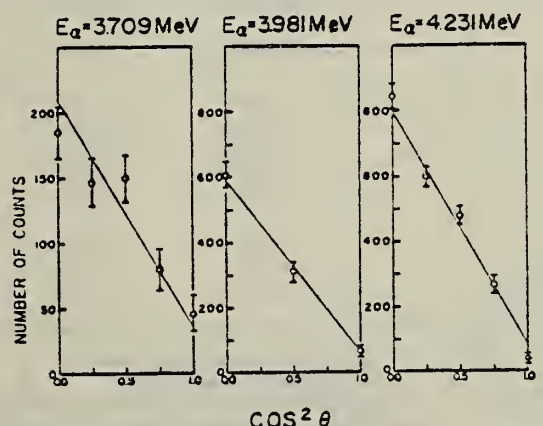

Fig. 3. Ground state transition angular distributions measured at the three $^{26}Mg(\alpha,\gamma)^{30}Si$ resonances. The solid lines represent the theoretical angular distributions for a 1^- resonance spin. The solid angle attenuation has been taken into account: $Q_2 = 0.79$ for the 3.709 MeV resonance and $Q_2 = 0.87$ for the two remaining resonances.

(over)

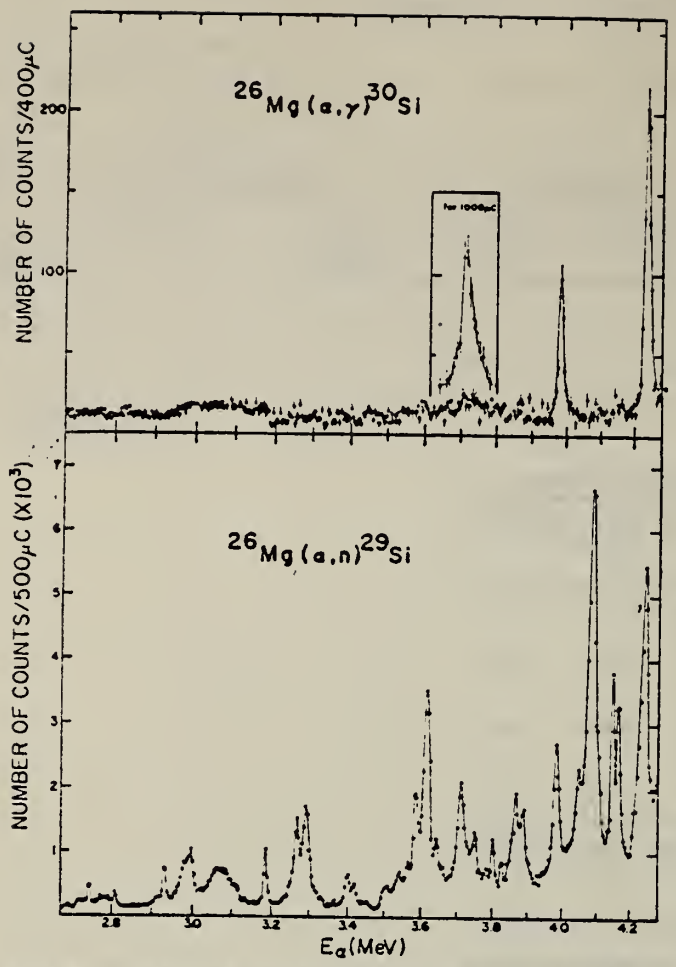

Fig. 1. Excitation functions for the reactions $^{26}Mg(\alpha, n)^{29}Si$ and $^{26}Mg(\alpha,\gamma)^{30}Si$. The weak 3.709 MeV resonance in $^{26}Mg(\alpha,\gamma)^{30}Si$ was measured with a 35 keV thick target and for a charge of 1000 μC accumulated at each energy: the results are shown in the insert.

TABLE 3

Radiative strengths of E1 radiation observed in ^{28}Si and ^{30}Si: resonance energies, excitation energies, resonance strengths for the ground state transition, radiative strengths in Weisskopf units

E_α (MeV)	E_x (MeV)	$(2J+1)\frac{\Gamma_\alpha\Gamma_{\gamma_0}}{\Gamma}$ (eV)	$\lvert M\rvert^2 \times 10^3$
	^{28}Si		
1.529 [a])	11.296	0.08	0.03 [a])
1.964 [a])	11.670	0.02	0.006 [a])
2.566 [a])	12.183	0.05	0.01 [a])
3.318 [b])	12.830	0.3	0.07 [c])
3.504 [b])	12.989	0.3	0.07 [c])
	^{30}Si		
3.709	13.862	0.1	0.2 [d])
3.981	14.102	1.0	3.3 [d])
4.231	14.317	2.8	4.4 [d])

[a]) Results from Smulders and Endt [14]).
[b]) Results from Weinman *et al.* [22]).
[c]) The radiative widths Γ_{γ_0} used in the calculation of the radiative strengths $|M|^2$ were extracted from the resonance strengths assuming Γ_γ and $\Gamma_p \ll \Gamma_\alpha$.
[d]) The radiative widths Γ_{γ_0} used here are shown in table 2.

[14] P.J.M. Smulders & P.M. Endt, Physica 28 (1962) 1093

[22] J.A. Weinman et al., Phys. Rev. 133 (1964) B590

REF. B. Bülow, B. Johnsson and M. Nilsson
Z. Physik A282, 261 (1977)

ELEM. SYM.	A	Z
Si	30	14

METHOD

REF. NO. 77 Bu 11 egf

REACTION	RESULT	EXCITATION ENERGY	SOURCE		DETECTOR		ANGLE
			TYPE	RANGE	TYPE	RANGE	
G,P	ABX	13-800	C	75-800	ACT-I		4PI

The yields of (γ, p) reactions on ^{30}Si, ^{68}Zn and ^{130}Te have been measured as a function of the bremsstrahlung end-point energy, $E_{\gamma,max}$, in the energy range 75–800 MeV, using the activation method. Cross sections have been deduced and are compared to results obtained using a semi-empirical model.

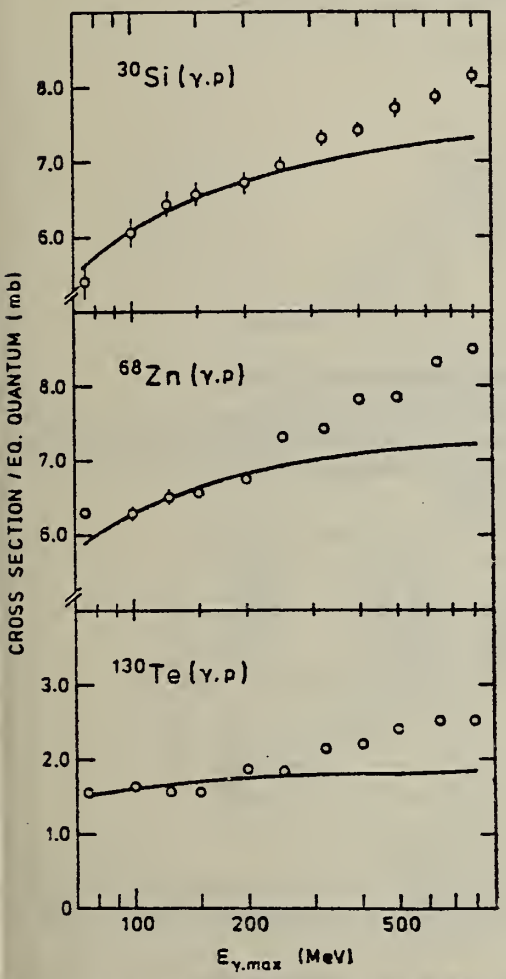

Fig. 1. Measured yields for the (γ, p) reactions in ^{30}Si, ^{68}Zn and ^{130}Te. The solid lines are the fitted yields due to the giant resonance and quasideuteron cross sections

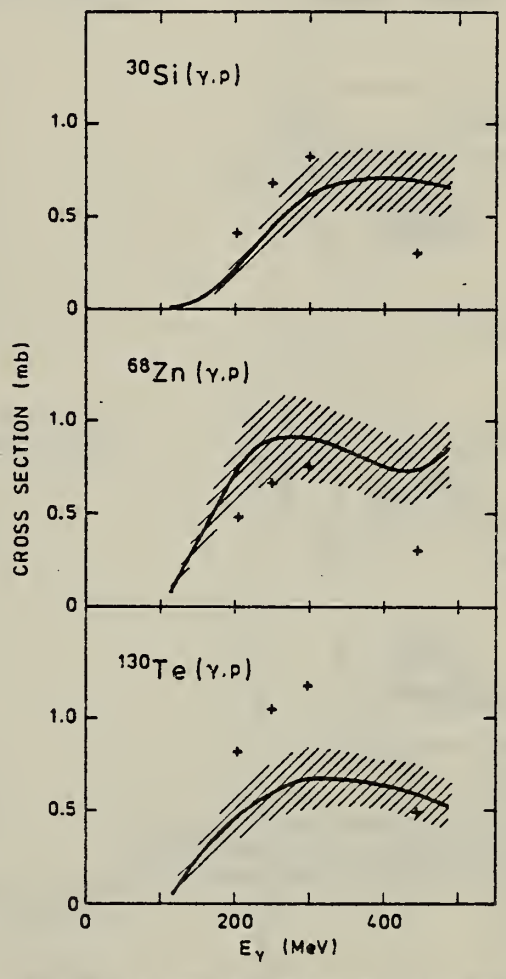

Fig. 2. The solid curves show the smoothed cross sections arising from photoproduction of mesons and the hatched areas indicate the estimated errors. +sings are values calculated using the semi-empirical formalism

REF. B. Bulow, B. Johnsson and M. Nilsson; Z Physik A285, 323 (1978)

ELEM. SYM.	A	Z
Si	30	14

METHOD

REF. NO. 78 Bu 9 RS

REACTION	RESULT	EXCITATION ENERGY	SOURCE		DETECTOR		ANGLE
			TYPE	RANGE	TYPE	RANGE	
G,2P	ABY	24-640	C	75-640	ACT-I		4PI

The yields of the $(\gamma,2p)$ reaction on ^{30}Si and of the $(\gamma,2p)$, $(\gamma,2pn)$, $(\gamma,3p)$ and $(\gamma,3pn)$ reactions on ^{31}P have been measured as a function of the maximum bremsstrahlung energy in the range 75–640 MeV. The cross sections have been deduced and are compared to Monte-Carlo calculations. The magnitude of the cross sections in the energy range above the threshold for the photoproduction of mesons is also discussed using a simple analytical approach.

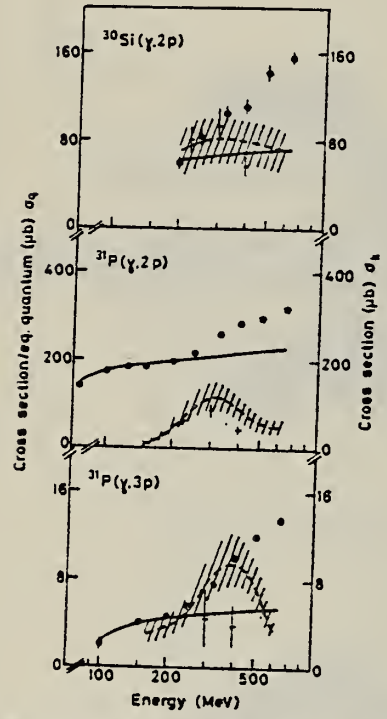

Fig. 1. The filled circles show measured yields as a function of the maximum bremsstrahlung energy. The meaning of the solid lines, the hatched areas and the plus signs is given in the text

Table 2. Reaction thresholds, *GR* and *QD* normalizationfactors and calculated mean cross sections for the different reactions

Reaction	Threshold (MeV)	Normalization-factor	$\bar{\sigma}_\gamma$ (200–640 MeV)	*GR* and *QD* reference
^{30}Si(γ, 2p)	24.0	0.67	72.5 ± 5.9	[12]
^{31}P(γ, 2p)	20.8	0.98	88.3 ± 7.8	[11]
(γ, 2pn)	30.2	1.3	197. ±19	[11]
(γ, 3p)	31.3	1.2	5.1 ± 1.0	[12]
(γ, 3pn)	39.8	1.0	41.6 ± 1.8	–

REF. G. Odgers, B.L. Berman, R.E. Pywell, M.N. Thompson
Nucl. Phys. A388, 445 (1982)

ELEM. SYM.	A	Z
Si	30	14

METHOD

REF. NO.	
82 0d 1	egf

REACTION	RESULT	EXCITATION ENERGY	SOURCE		DETECTOR		ANGLE
			TYPE	RANGE	TYPE	RANGE	
G,XN	ABX	10-28	C	10-28	BF3-I		4PI

Abstract: The photoneutron cross section for ^{30}Si has been measured over the energy range 10 to 28 MeV using the bremsstrahlung-yield-curve technique. The cross section is observed to be highly fragmented, consistent with systematic trends observed in other light nuclei consisting of two neutrons outside a self-conjugate core.

E NUCLEAR REACTIONS ^{30}Si(γ, xn), $E \sim 10$–28 MeV bremsstrahlung; measured neutron yield; deduced $\sigma(E)$. ^{30}Si deduced GDR fragmentation.

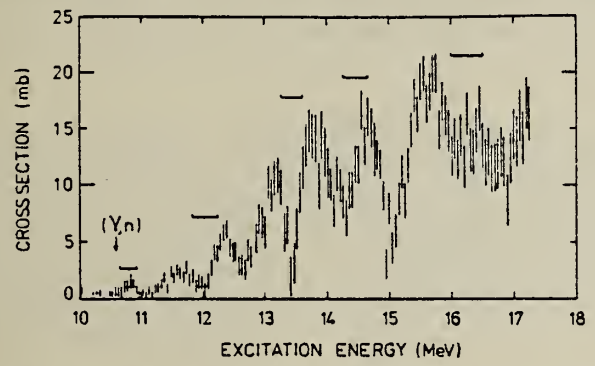

Fig. 1. Low-energy region of the ^{30}Si(γ, n) cross section determined from a yield measurement taken at 50 keV intervals. The vertical bars indicate statistical uncertainty and the horizontal lines give a measure of the resolution.

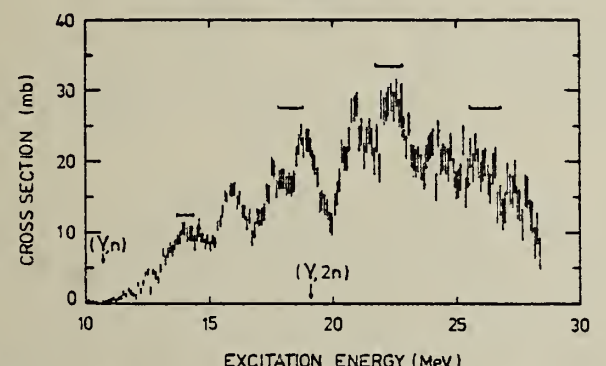

Fig. 2. The ^{30}Si(γ, xn) cross section. No correction has been made for double counting from the (γ, 2n) reaction. The vertical bars indicate statistical uncertainty and the horizontal lines give a measure of the resolution.

TABLE 1

Resonances observed in the reaction ^{30}Si(γ, xn)

Energy (MeV)	Peak height (mb)	FWHM (MeV)
10.8	1	0.15
11.6	2	0.4
12.4	4	0.3
13.1	8	0.4
13.8	12	0.5
14.6	8	0.5
15.8	14	0.8
17.5		
18.9		
21.0		
22.3		
(24.2)		

The widths and heights are values obtained from a fit of lorentzians to the high-resolution data.

TABLE 2

Integrated cross sections for the photoneutron reaction in the three silicon isotopes

1 Silicon isotope	2 $\int_{thr}^{17\,MeV} \sigma(E)\,dE$ (MeV · mb)	3 $\int_{thr}^{20\,MeV} \sigma(E)\,dE$ (MeV · mb)	4 $\int_{thr}^{28\,MeV} \sigma(E)\,dE$ (MeV · mb)	5 $\int_{17\,MeV}^{20\,MeV} \sigma(E)\,dE$ (MeV · mb)
^{28}Si [a])		26	87	25
^{29}Si [b])	27	59	162	32
^{30}Si [c])	51	100	264*	49

[a]) Ref. [2]). [b]) Ref. [8]). [c]) Present work.

* Uncorrected for double counting above the (γ, 2n) reaction threshold at 19.1 MeV.

The values for ^{30}Si are obtained from the present work. The absolute uncertainty is ±10%. Column 2 lists the values below 17 MeV (essentially the ^{28}Si(γ, n) threshold). Column 3 lists the values up to the energy where the ^{30}Si(γ, 2n) contribution becomes significant. Column 5 allows comparison of the (γ, n) strengths over a specific region of the GDR for these nuclei.

2) A. Veyssière, H. Beil, R. Bergère, P. Carlos, A. Leprêtre and A. de Miniac, Nucl. Phys. A227 (1974) 513

8) R.E. Pywell, B.L. Berman, P. Kean and M.N. Thompson, Nucl. Phys. A369 (1981) 141

PHOSPHOROUS
Z=15

The name phosphorous, derived from the Greek *phos* + *phoros* meaning "light bearing", indicates its properties of glowing in the dark when exposed to air.

Raimondo di Sangro (1710-1771) mentioned the "perpetual lamps" of Saint Augustine (354-430) which were found in the sepulchers of the early Christians. Di Sangro believed that these lamps contained phosphorous. Paracelsus (1493-1541) had a recipe for "the separation of the element from watery substances". He obtained "icicles which are the elements of fire" apparently from the distillation of urine. This probably was elemental phosphorous.

P
A=29

Most authorities attribute the discovery of phosphorous to Hennig Brand of Hamburg who used the residue from evaporated urine as the source of the element. No one knows what led this zealous alchemist to hope, that in human urine, he might find a liquid that might change silver into gold, but it is well known that his odd experiments, produced both startling and strangely beautiful results. News of the discovery spread across Germany but Brand kept his process secret —— at least for awhile.

Its history at this point is sprinkled with deceit and intrigue. Many alchemists sought the philosopher's stone and it was thought that such an unusual material as phosphorous might lead to this stone. Von Leibniz (1646-1716), the famous German mathematician and scientist, was personally acquainted with Brand and wrote a detailed account of the discovery of phosphorous as well as a biographical sketch of the people involved. It is interesting that an element so difficult to isolate should have been discovered through the unguided fumbling of an alchemist.

P
A=29

Ref. J.O. Newton
Nuclear Phys. 21, 529 (1960)

Elem. Sym.	A	Z
P	29	15

Method Van de Graaff; NaI

Ref. No. 60 Ne 1 JHH

Reaction	E or ΔE	E_o	Γ	$\int \sigma dE$	Jπ	Notes
(p,γ)	1.0-2.5	1.653 ±0.005	55.2±2kev		3/2	E_γ levels in P^{29}: 4.320±0.015 MeV; Γ_γ=1.75±0.35 ev
		2.09 ±0.015	14±2 kev			4.74±0.02 MeV

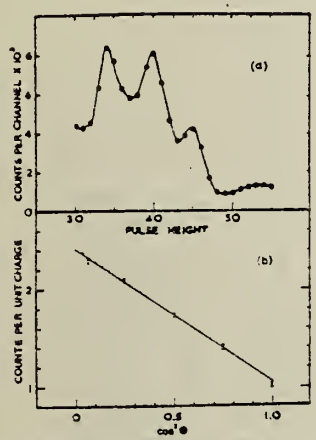

Fig. 1. (a). Typical pulse height spectrum of the 4.33 MeV gamma ray at a bombarding energy of 1.65 MeV. (b). Angular distribution of the 4.33 MeV gamma rays at the peak of the 1.65 MeV resonance. The full line is the least squares fit to the points.

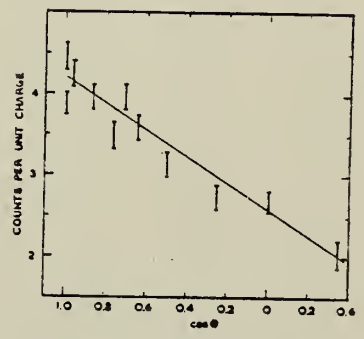

Fig. 4. Angular distribution of the 4.7 MeV gamma rays taken at the peak of the 2.09 MeV resonance.

Ref. K.J. Van Oostrum, N. Hazewindus, A.H. Wapstra, J.W. Olness, J.L. Parker
Nuclear Phys. 25, 409 (1961)

Elem. Sym.	A	Z
P	29	15

Method
2.5 MeV VandeGraaff; NaI

Ref. No.
61 Va 3

JHH

Reaction	E or ΔE	E_o	Γ	$\int \sigma dE$	Jπ	Notes
(p,γ)	0.3-2.3		Γ_γ = (ev)			
		0.371	$>0.8X10^{-3}$		$5/2^+$	E_{γ_o} = 3.09 MeV (very weak; mostly by cascade)
		1.65	1.85±0.40		$3/2^-$	E_{γ_o} = 4.34 MeV
		2.09	0.43±0.08		$1/2^+$	E_{γ_o} = 4.76 MeV

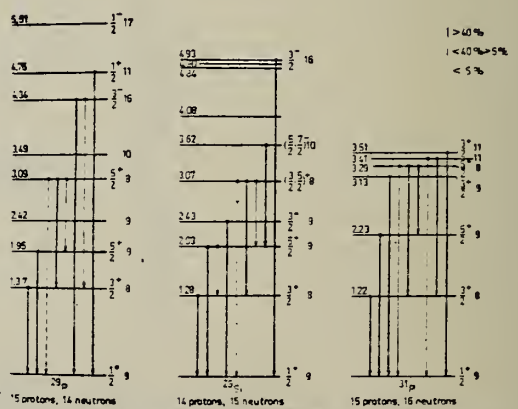

Fig. 7. Level schemes of three nuclei with the odd particle in Nilsson orbit 9/(4) in the ground state. For each level the excitation energy is given on the left side of the figure. The spin, parity and the Nilsson orbit-number are given on the right side. The relative intensities of the gamma transitions are indicated by the various line thicknesses.

REF.

D.H. Youngblood, G.C. Morrison and R.E. Segel
Phys. Letters 22, 625 (1966)

ELEM. SYM.	A	Z
P	29	15

METHOD

Van de Graaff; $^{28}Si(p,\gamma)^{29}P$

REF. NO. 66 Yo 1 JDM

REACTION	RESULT	EXCITATION ENERGY	SOURCE		DETECTOR		ANGLE
			TYPE	RANGE	TYPE	RANGE	
P,G	SPC	8 - 9	D	5 - 6	ACT		4PI

The lowest $T = \frac{3}{2}$ state in ^{29}P is at $E_p = 5.833 \pm 0.010$ MeV

$\Gamma_{total} = 2.5$ keV

$\Gamma_\gamma = 0.8 \pm 0.3$ eV

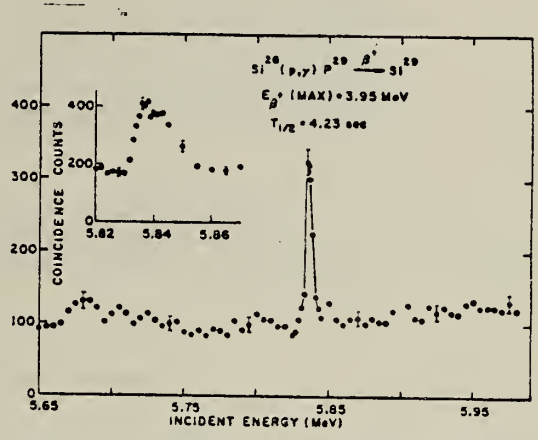

Fig. 1. Excitation curve for the reaction $^{28}Si(p,\gamma)^{29}P$ measured with a thin (~ 100 $\mu g/cm^2$) target. The inset shows the excitation curve over the 5.83 MeV resonance with a thick (~ 250 $\mu g/cm^2$) target.

REF. M. Riihonen, J. Keinonen, A. Anttila
Nucl. Phys. A313, 251 (1979)

ELEM. SYM.	A	Z
P	29	15

METHOD

REF. NO. 79 Ri 2 hg

REACTION	RESULT	EXCITATION ENERGY	SOURCE TYPE	SOURCE RANGE	DETECTOR TYPE	DETECTOR RANGE	ANGLE
P,G	NOX	3-5	D	0-2	SCD-D		DST
		(3.11-4.76)		(.37-2.09)			

Abstract: The absolute resonance strengths of the $^{28-30}$Si(p, γ)$^{29-31}$P reactions have been studied. New values for the frequently used standard resonances at E_p = 370, 416 and 620 keV in the above reactions, respectively, have been determined. In addition, the strengths of the ^{28}Si(p, γ)^{29}P resonances at E_p = 1381, 1652 and 2088 keV and of the four dominant ^{30}Si(p, γ)^{31}P resonances at E_p = 499, 777, 942 and 983 keV have been determined. The branching ratios and angular distributions of the γ-rays used in the determinations were obtained in the same experimental set-up as the strength measurements. Using these revised resonance strengths, the astrophysical reaction rates of hydrogen burning of ^{29,30}Si in explosive carbon burning have been deduced. The reaction rates found for hydrogen burning of $^{28-30}$Si in the stellar temperature region of $T = (0.3–10) \times 10^9$ K are compared with Hauser-Feshbach calculations.

STELLAR REACTION RATE

E NUCLEAR REACTIONS ^{28}Si(p, γ), E = 0.37, 1.38, 1.65, 2.09 MeV; ^{29}Si(p, γ), MeV, ^{30}Si(p, γ), E = 0.50, 0.62, 0.78, 0.94, 0.98 MeV; measured $\sigma(E_p)$, $I_\gamma(\theta)$. ^{29,30,31}P resonances deduced γ-branchings, resonance strengths. Ge(Li) detector. Natural and enriched targets.

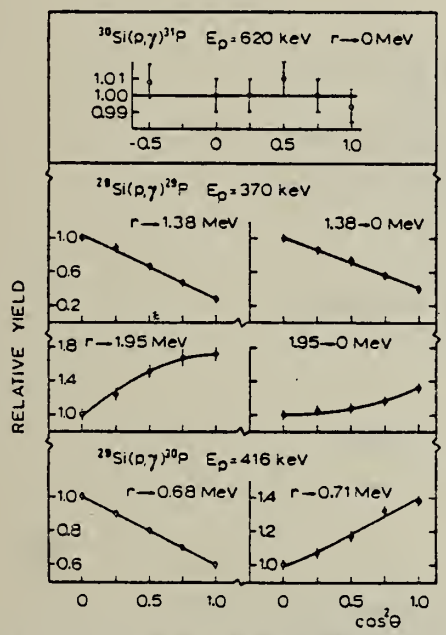

Fig. 1. The results of angular distribution measurements of the standard resonances at E_p = 370, 416 and 620 keV in the $^{28-30}$Si(p, γ)$^{29-31}$P reactions. In the case of the E_p = 620 keV resonance, the experimental points are shown without eccentricity or absorption corrections. In other cases these corrections have been made. The solid lines are the fitted curves of the form $W(\theta) = 1 + a_2 P_2(\cos\theta) + a_4 P_4(\cos\theta)$.

(over)

TABLE 1

Summary of the angular distribution results for $^{28-30}$Si(p, γ)$^{29-31}$P resonances and comparison with previous values

Reaction	E_p (MeV)	Transition (MeV)	a_2		a_4	
			present [a]	previous	present [a]	previous
^{28}Si(p, γ)^{29}P	0.37	r → 1.95	0.52 ± 0.02	0.372 ± 0.036 [b]	−0.19 ± 0.03	0.097 ± 0.071 [b]
		r → 1.38	−0.79 ± 0.02	−0.809 ± 0.041 [b]	−0.01 ± 0.03	0.026 ± 0.074 [b]
		1.38 → 0	−0.58 ± 0.03	−0.568 ± 0.017 [b]	−0.05 ± 0.04	−0.017 ± 0.031 [b]
		1.95 → 0	0.19 ± 0.02	0.211 ± 0.039 [b]	0.13 ± 0.03	0.120 ± 0.080 [b]
	1.38	r → 1.95	−0.83 ± 0.03	−0.55 ± 0.55 [c]	0.14 ± 0.05	0.01 ± 0.07 [c]
		r → 1.38	0.67 ± 0.02	0.51 ± 0.09 [c]	−0.47 ± 0.02	−0.25 ± 0.09 [c]
		1.38 → 0	−0.61 ± 0.03	−0.59 ± 0.05 [c]	−0.03 ± 0.04	
		1.95 → 0	0.41 ± 0.02	0.44 ± 0.07 [c]	−0.34 ± 0.03	−0.30 ± 0.07 [c]
	1.65	r → 0	−0.43 ± 0.03	−0.53 ± 0.04 [c]	−0.03 ± 0.04	
^{29}Si(p, γ)^{30}P	0.42	r → 0.71	0.30 ± 0.02		0.01 ± 0.03	
		r → 0.68	−0.37 ± 0.02		0.00 ± 0.04	
^{30}Si(p, γ)^{31}P	0.50	r → 0	−0.49 ± 0.03	−0.39 ± 0.01 [d])	0.00 ± 0.02	−0.01 ± 0.01 [d]
				−0.41 ± 0.02 [c]		
	0.62	r → 0	0		0	
	0.78	r → 0	−0.40 ± 0.02	−0.31 ± 0.01 [c]	0.01 ± 0.04	
	0.94	r → 0	−0.83 ± 0.03	−0.72 ± 0.02 [c]	0.05 ± 0.05	
	0.98	r → 0	−0.65 ± 0.03		0.07 ± 0.04	

The E_p and E_x values are taken from ref. [25]).

[a]) The coefficients are corrected for finite solid angle of the Ge(Li) detector [30]). The correction due to the finite size of the beam spot on the target is negligible and is considered to be included in the uncertainty of the target-to-detector distance, 50 ± 2 mm.

[b]) Ref. [12]). [c]) Ref. [14]). [d]) Ref. [5]). [e]) Ref. [31]).

TABLE 2

Summary of the present strength measurements

Reaction	E_p (keV)	Transitions (MeV)	Branching [a]) (%)	$W_{exp}(55°)$ [b])	$\varepsilon(E_p)$ [c]) eV/(10^{13} at/cm^2)	S_{lab} (eV)	
^{28}Si(p, γ)^{29}P	370	r → 1.95	30 ± 2	1.04	14.1	(5.5 ± 0.8) × 10^{-3}	
		r → 1.38	70 ± 2	1.00		(5.4 ± 0.5) × 10^{-3}	(5.6 ± 0.4) × 10^{-3}
		1.38 → 0	70 ± 2	1.01		(5.6 ± 0.4) × 10^{-3}	
		1.95 → 0	27 ± 2	0.97		(5.7 ± 0.8) × 10^{-3}	
	1381	r → 1.95	51 ± 1	0.97	6.8	(103 ± 8) × 10^{-3}	
		r → 1.38	46 ± 1	1.09		(84 ± 8) × 10^{-3}	(92 ± 8) × 10^{-3}
		1.38 → 0	49 ± 1	1.01		(89 ± 10) × 10^{-3}	
		1.95 → 0	51 ± 1	1.07		(93 ± 9) × 10^{-3}	
	1652	r → 0	93 ± 1	1.00	6.1	9.0 ± 0.7	
	2088	r → 0	91 ± 2	1.19	5.1	0.95 ± 0.14	
^{29}Si(p, γ)^{30}P	416	r → 0.71	33 ± 1	1.00	13.3	1.09 ± 0.35	1.04 ± 0.10
		r → 0.68	57 ± 1	1.00		0.99 ± 0.15	
^{30}Si(p, γ)^{31}P	499	r → 0	52 [d])	1.00	12.1	0.33 ± 0.05	
	620	r → 0	95 ± 1	1.00	10.8	5.0 ± 0.3	
	777	r → 0	68 [d])	1.00	9.5	1.2 ± 0.2	
	942	r → 0	66 [d])	1.00	8.5	2.0 ± 0.3	
	983	r → 0	70 [d])	1.00	8.3	2.0 ± 0.3	

The E_p and E_x values are taken from ref. [25]).

[a]) All values given are relative to the value of 100 % for the total intensity for the decays of the resonance state.

[b]) As deduced from the angular distribution data obtained in the present experimental geometry. Thus the solid angle attenuation is taken into account experimentally. Error limits are within 1 %.

[c]) Ref. [24]). Error limits estimated to be ± 5 %.

[d]) Ref. [9]). Error limits estimated to be ± 2 %.

A=30

A=30

Ref.		Elem. Sym.	A	Z
	A.K. Val'ter, Yu. P. Antuf'ev, E.G. Kopanets, A.N. L'vov, P. Tsytko Zhur. Eksp. i Teoret. Fiz. 41, 1449 (1961) Soviet Phys. JETP 14, 1035 (1962)	P	30	15

Method	Ref. No.	
4- MeV Van de Graaff; Na I	61 Va 2	JHH

Reaction	E or ΔE	E_o	Γ	$\int \sigma dE$	Jπ	Notes
(p,γ)	1.33	6.84±.08 1.97±.08 0.68±.05 (For transitions to ground state, see Table I below.)			2 + 0 +	Angular distribution of 6.84 MeV line (Figure 2) fitted by least squares to $W(0) = 1 - (0.485 \pm .015)\cos^2\theta$.

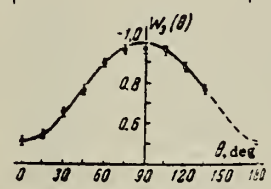

FIG. 2. Experimental angular distribution of the γ rays for the γ transition from the 6.847-Mev level to the ground state of P^{30} [see (1)].

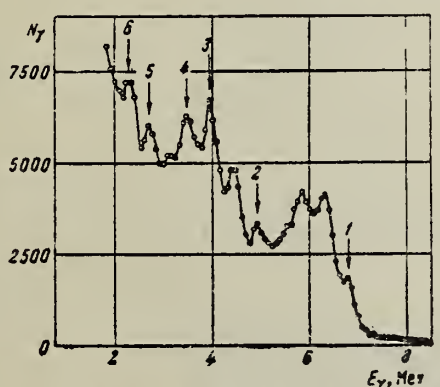

FIG. 1. Hard part of the γ-ray spectrum for the resonance at E_p = 1330 kev in the reaction Si^{29} (p, γ)P^{30}.

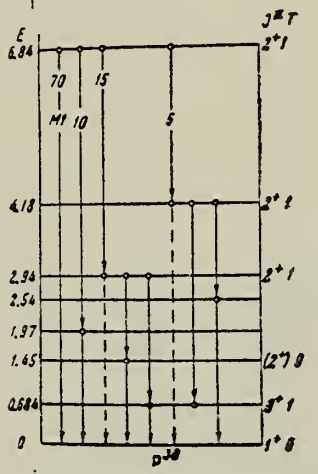

FIG. 3. γ-transition scheme in P^{30} from the 6.847-Mev resonant level.

Table I.

No.	γ lines observed in the spectrum, Mev	Level of P^{30} nucleus		Energy of γ transition and relative intensity*
		initial	final	
1	6.84±0.08	6.847	0	6.847; 70%
2	4.90±0.08	6.847	1.97	4.877; 10%
3	3.90±0.08	6.847	2.94	3.907; 15%
4	3.50±0.08	4.18	0.684	3.496; 5%
5	2.70±0.08	6.847	4.18	2.667
6	2.25±0.08	2.94	0.684	2.256
7	1.97±0.08	1.97	0	1.97
8	1.65±0.08	4.18	2.54	1.64
9	1.45±0.08	2.94	1.45	1.49
10	0.68±0.05	0.684	0	0.684

*The sum of all the transitions from the resonant level is taken to be 100 percent.

Ref. Yu.P.Antuf'ev, A.K.Val'ter, A.N.L.'Vov, E.G.Kopanets, S.P.Tsytko
Zhur.Eksptl. i Teoret.Fiz. 42, 386 (1962);
Soviet Phys.JETP 15, 268 (1962)

Elem. Sym.	A	Z
P	30	15

Method: NaI(Tl)

Ref. No.: 62An2 BG

Reaction	E or ΔE	E_o	Γ	$\int \sigma dE$	Jπ	Notes
	keV	keV				
$Si^{29}(p,\gamma)P^{30}$	E_p= 1.3-1.55	E_p= 1308				
		1330				
		1375			1^+	1375 KeV resonance corresponds to 6.89±.08 MeV level.
		(1470)				
		1500			2^+	1500 Kev corresponds to 7.01±.08 level.

Ref. A.K. Val'ter, E.G. Kopanets, A.N. L'vov, S.P. Tsytke
Izv. Akad. Nauk SSSR, Ser. Fiz. 27, 232 (1963)

Elem. Sym.	A	Z
P	30	15

Method: Monochromatic protons; NaI

Ref. No.: 63 Va 2

Reaction	E or ΔE	E_o	Γ	$\int \sigma dE$	Jπ	Notes
$Si^{29}(p,\gamma)P^{30}$						
	1.308	6.8			1 +	

Рис. 1. Жесткая часть спектра γ-лучей, соответствующих резонансу 1308 keV в реакции Si^{29} (p, γ)P^{30}. *A, B, C, D, G, H* — пики полного поглощения γ-лучей для монохроматических γ-лучей, полученные при разложении измеренного спектра

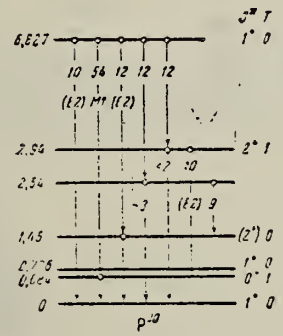

Рис. 2. Схема распада резонансного уровня P^{30} с энергией возбуждения 6,827 MeV (E_p = 1308 keV). Цифрами около стрелок указаны интенсивности γ-переходов

Энергии и интенсивности γ-переходов, возникающих при разрядке резонансного уровня 6,827 MeV P^{30}

E_γ, MeV	Обозначение γ-линии (на рис. 1)	Уровни P^{30}, MeV: начальный	конечный	Энергия γ-перехода (по схеме рис. 2)	Относительная интенсивность *	Мультипольность и характер γ-перехода
6,8 ± 0,08	*A*	6,827	0	6,827	10	(*E*2)
6,1 ± 0,08	*B*	6,827	0,684	6,14	54	*M*1
5,3 ± 0,08	*C*	6,827	1,45	5,28	12	(*E*2)
4,3 ± 0,08	*D*	6,827	2,54	4,29	12	
3,9 ± 0,08	*G*	6,827	2,94	3,89	12	
2,9 ± 0,08	*H*	2,94	0	2,94	4	
2,54 ± 0,05	—	2,54	0	2,54	3	
2,26 ± 0,05	—	2,94	0,684	2,26	10	*E*2
1,45 ± 0,05	—	1,45	0	1,45	12 ± 9	
1,10 ± 0,05	—	2,54	1,45	1,09	0	(*E*2)
0,684 ± 0,05	—	0,684	0	0,684	54	*M*1

* За 100% принята сумма интенсивностей всех γ-переходов с данного резонансного состояния 6,827 MeV.

REF. H. Ejiri, Y. Nakjima, K. Horie, S. Matsumoto and Y. Nogami
Nuc. Phys. 51, 470-480 (1964)

ELEM. SYM.	A	
P	30	1

METHOD
$Si^{29}(p,\gamma)P^{30}$ Electrostatic accelerator; NaI

REF. NO. 64 Ej 1

REACTION	RESULT	EXCITATION ENERGY	SOURCE		DETECTOR		ANGL
			TYPE	RANGE	TYPE	RANGE	
P, G	NØX	7	D	1	NAI-D		DST

Q = 5.57 ± 0.03 MeV

J-PI, WIDTHS

TABLE 1
Resonances in the reaction $^{29}Si(p,\gamma)^{30}P$ and the gamma ray de-excitation

Excited state	Gamma ray De-excitation		
	E_γ(MeV)	Initial state-Final state (MeV)	Reduced width Γ_{γ_i}(eV)
6.835 MeV	6.85	6.835–0	0.02 ±0.01
$J^\pi = 1^+, T = 0$	6.15	6.835–0.685	0.17 ±0.03
$\Gamma_p < 4$ keV	(3.9)	(6.835–2.94)	(0.015±0.008)
6.86 MeV	6.85	6.86 –0	0.22 ±0.04
$J^\pi = 2^\pm, T = 1$	5.4	6.86 –1.45	0.05 ±0.015
$\Gamma_p = 6\pm2$ keV	(6.15)	(6.86 –0.7)	(0.01 ±0.006)

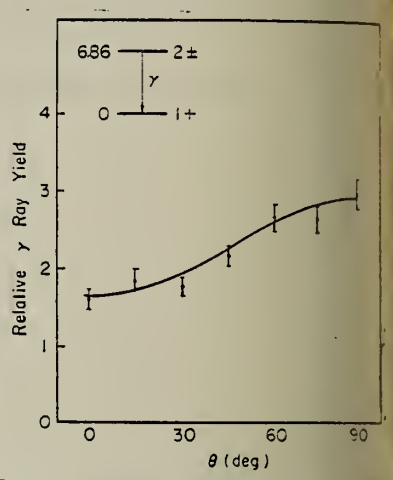

Fig. 10. Angular distribution of gamma rays to the ground state at E_p = 1.333 MeV resonance.

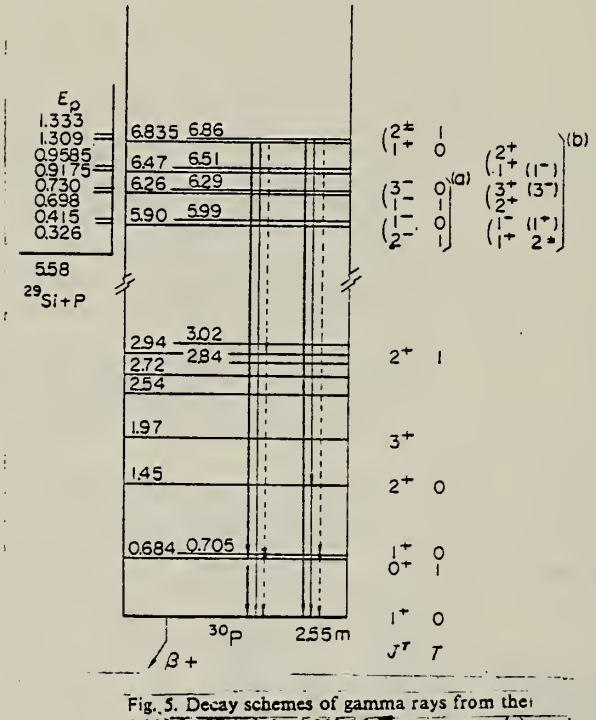

Fig. 5. Decay schemes of gamma rays from the 1.309 MeV and the 1.333 MeV resonances. (a) van

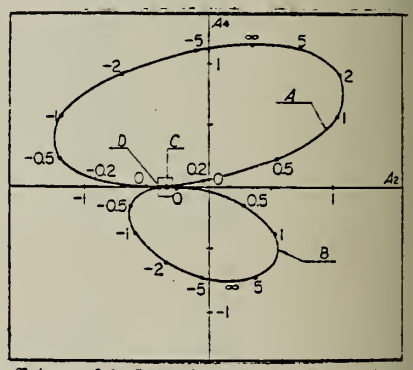

Fig. 11. Coefficients of the Legendre polynomial expansion of the angu distribution of gamma rays to the ground state at E_p = 1.333 MeV reson A_2 and A_4 indicate the coefficients of $P_2(\cos\theta)$ and $P_4(\cos\theta)$, respectively A and B represent the calculated coefficient of 2^+–1^+ transition for cha spin 0 and 1, respectively. C and D are those of 2^-–1^+ transition for l_p = 1 a respectively. Parameters on the lines of A and B indicate the ratio of the ampl of E2 transition to that of M1 transition. Experimental value and the error represented as the inner part of the rectangle.

REF. G. I. Harris, A. K. Hyder, Jr., and J. Walinga
Phys. Rev. 187, 1413 (1969)

ELEM. SYM.	A	Z
P	30	15

METHOD

REF. NO. 69 Ha 2 egf

REACTION	RESULT	EXCITATION ENERGY	SOURCE		DETECTOR		ANGLE
			TYPE	RANGE	TYPE	RANGE	
P,G	LFT	6-8	D	0-2	SCD-D	0-7	

J-PI

TABLE I. Resonances in the $Si^{29}(p,\gamma)P^{30}$ reaction for E_p = 300–1800 keV. The resonance strengths $S=(2J+1)\Gamma_\gamma\Gamma_p/\Gamma$ and the total widths Γ are given. For comparison, resonances reported in Refs. 22 and 23 for $Si^{29}(p,p)Si^{29}$ are also listed. The (p,p) data at 1505 keV is from recent work in this laboratory, to be published elsewhere (Ref. 17).

$Si^{29}(p,\gamma)P^{30}$				$Si^{29}(p,p)Si^{29}$		
E_p (keV)	$E_x(P^{30})$ (keV)	S (eV)	Γ (keV)	E_p (keV)	Γ (keV)	J^π
327	5.913	0.077±0.015	≤3			
416	5.999	0.70±0.10	≤5			
698	6.272	0.87±0.17	≤4			
731	6.304	0.44±0.09	≤3			
917	6.483	0.40±0.08	≤4			
958	6.523	0.19±0.04	≤2			
1111	6.671	0.21±0.04	≤2			
1302	6.856	1.4±0.3	≤2			
1324	6.877	0.36±0.07	≤2			
1327	6.880	2.4±0.5	5.7±1.0	1331	6	2^-
1374	6.925	4.0±0.8	7.1±0.7	1377	7	1^-
1470	7.018	0.73±0.15	≤4	1470	≤4[a]	$1^-, 2^-$
1502	7.049	(weak)				
1505	7.052	5.0±1.0	≤3	1505[b]	0.037	4^-
1643	7.185	14±3	17.2±2.0	1648	16	1^-
1654	7.206	0.83±0.16	≤1.5			
1669	7.210	0.59±0.12	≤3			
1686	7.227	11±2	5.9±0.7	1686	7	$1^-, 2^-$
1746	7.285	2.2±0.5	≤1.5			
1749	7.288	5.2±1.0	≤2			
1773	7.311	0.87±0.17	≤1.5			
1775	7.313	1.1±0.2	≤1.5			
1792	7.330	≃2.0		1796	20	1^-
				1967	≤3	1^+

[a] Preliminary analysis of (p,p) data obtained in this laboratory shows $\Gamma \simeq 0.5$ keV (Ref. 17).

[b] Doublet with nearly identical members separated by 700 eV. The separate values of Γ, determined in elastic-scattering measurements, are given in the Appendix.

over

TABLE II. Branching ratios of the γ decay of $Si^{29}(p,\gamma)P^{30}$ resonances in percent. See text for explanation of values in parentheses.

Resonances		Bound levels of P^{30} (E_x in MeV, J^π)																			
E_p (keV)	J^π	0 1^+	0.68 0^+ $T=1$	0.71 1^+	1.45 2^+	1.97 3^+	2.54 3^+	2.72 2^+	2.84 3^+	2.94 2^+ $T=1$	3.02 1^+	3.74	3.93	4.14 2^-	4.18 2^+ $T=1$	4.23 4^-	4.43 2^+	4.47 0^+ $T=1$	4.50 1^+ $T=1$	4.62 3^-	4.92 $(5)^-$	4.95 $1^{(+)}$
327	$1,2^-$	82		10	8																	
416	1	4	52	36						3	3							2				
698	2^-	1		2		42	21	25	4		5											
731	3^+	0.6			0.4					80					19							
917	1	6	51		2			2		7					10				22			
958		12		2	16	5	11		14	12					12				(16)			
1111		3					(8)			54					17				(18)			
1302	1	2	76					2		14								6				
1324	(3)				37	17		(9)		29					8							
1327	2^-	73		2	7				3	(3)	6			(6)								
1374	1^-	7	66		9			2										13	3			
1470	2^-	22		9			7				12		(2)	13					33	4		
1502						X^a	X		(X)													
1505[b]	4^-					6	4		4							59				13	14	
1643	1^-	25	11	45							12							3	4			
1664			(3)		5					≥80												
1669											≥70											
1686	2^-	22		13	6	1	2				4			41						11		
1746	3				25		15			50					10							
1749	2^+	21	2	3	5			18				3					35					13
1773				20		30									20				30			
1775	(3)	5			15	25		5		50												
1792	1^-	X																(X)	X			

[a] The presence of transitions suggested by NaI(Tl) data at the weak 1502- and 1792-keV resonances are indicated by the entry X. The $R\rightarrow 0$ transition at the 1792-keV resonance appears about twice as strong as the sum of the transitions to the pair of levels near 4.5 MeV.

[b] Doublet. See Sec. III and the Appendix.

A=31

A=31

Ref. R. Basile, C. Schuhl
Compt. Rend. 240, 2399 (1955)

Elem. Sym.	A	Z
P	31	15

Method Betatron; activity; ionization

Ref. No. 55 Ba 2 | EGF

Reaction	E or ΔE	E_o	Γ	$\int \sigma dE$	Jπ	Notes
$P^{31}(\gamma,n)$	Bremss 11.50-13.50					E_{th} = 12.33±0.05 MeV See Table 2 for breaks near threshold.

TABLEAU II.

Discontinuités dans la courbe d'activation de la réaction $^{31}P(\gamma, n)^{30}P$.

$(h\nu_c - h\nu_0)$.....	0,25±0,02	0,42±0,03	0,57±0,03	0,85±0,05	1,05±0,05
$h\nu_c$.....	12,58±0,07	12,75±0,08	12,90±0,08	13,18±0,10	13,38±0,10

$h\nu_0$, énergie du seuil, soit 12,33±0,05 et $h\nu_c$, énergie de cassure.

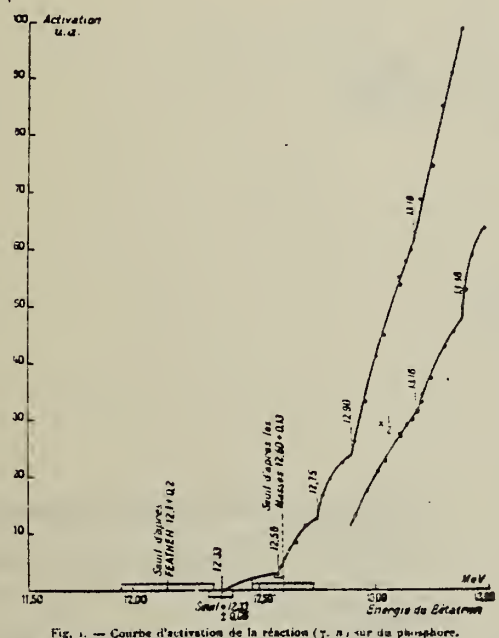

Fig. 1. — Courbe d'activation de la réaction (γ, n) sur du phosphore.

TABLEAU I.

Discontinuités dans la courbe d'activation de la réaction $^{16}O(\gamma, n)^{15}O$ (*).

Auteurs.	Seuil (MeV).	Énergie des cassures (MeV).				
Haslam (1).....	15,60	15,84	16,56	16,72	16,96	–
Katz (2).....	15,60	15,9	16,4	16,7	16,9	17,1
Basile et Schuhl...	15,60 ± 0,03	16,00 ± 0,05	16,54 ± 0,06	16,7 ± 0,1	16,82 ± 0,08	17,08 ± 0,05

(*) Nous avons arrêté le tableau aux valeurs maxima que nous avions obtenues.

(1) R. N. H. Haslam, L. Katz, B. J. Horsley, A. G. W. Cameron et R. Montalbetti, *B. A. P. S.*, 27, n° 3, 1952, p. 20.
(2) J. Goldemberg, L. Katz et L. Katz et J. Goldemberg, *B.A.P.S.*, 28, n° 4, 1953, p. 16.
(3) L. Katz, R. N. H. Haslam, B. J. Horsley, A. G. W. Cameron et R. Montalbetti, *Phys. Rev.*, 95, n° 2, 1954, p. 463.

REF.	ELEM. SYM.	A	Z
E. Basile Ann. Phys. (Paris) 2, 267 (1957	P	31	15

METHOD	REF. NO.	
	57 Ba 3	JOC

REACTION	RESULT	EXCITATION ENERGY	SOURCE		DETECTOR		ANGLE
			TYPE	RANGE	TYPE	RANGE	
G,N	ABY	11-14	C	11-14	ACT-I		4PI

BREAKS

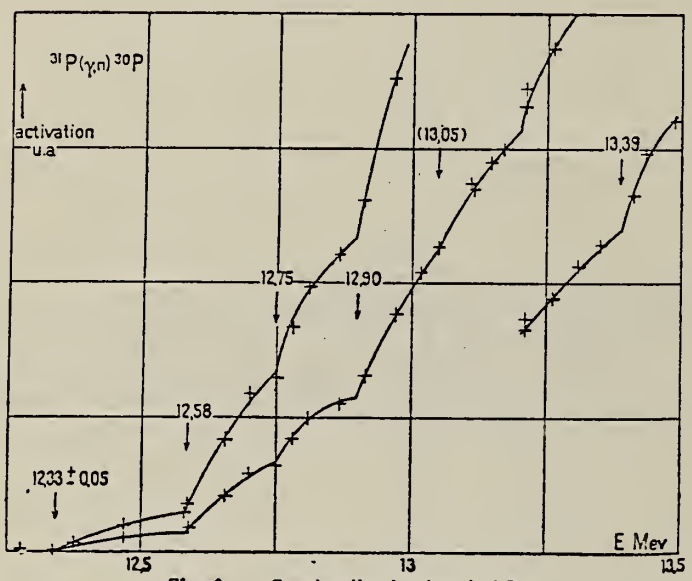

Fig. 6. — Courbe d'activation de ^{31}P.

Position des discontinuités dans la courbe d'activation de ^{31}P (fig. 6)

Seuil (MeV)	*Energie des discontinuités (MeV)*				
12,33 ± 0,05	12,58	12,75	12,90	13,18	13,38
	Ecart entre les discontinuités (keV)				
	250	170	150	280	200

Énergie en MeV des raies.	12,33	12,58	12,75	12,90	(13,05)	13,18
$\int \sigma(W)dW$ en keV. barns.	0,065	0,284	0,235	0,523	0,232	0,660

J.G. Chidley, L. Katz, S. Kowalski
Can. J. Phys. 36, 407 (1958)

ELEM. SYM.	A	Z
P	31	15

ACD
Betatron

REF. NO.
58 Ch 2
NVB

REACTION	RESULT	EXCITATION ENERGY	SOURCE		DETECTOR		ANGLE
			TYPE	RANGE	TYPE	RANGE	
G,N	RLY	THR	C	THR	BF3-I		4PI

See 58 Ka 1 for cross sections.

THRESHOLD

TABLE I

MEASURED PHOTONEUTRON THRESHOLDS

Reaction	Measured Q value, Mev.	Other Q values, Mev.	Method	Reference
$P^{31}(\gamma, n)P^{30}$	12.50±0.05 (12.45±0.08)			
		12.35 ±0.2	Threshold	McElhinney *et al.* (1949)
		12.4 ±0.2	Threshold	Katz and Penfold (1951)
		12.05 ±0.20	Threshold	Sher *et al.* (1951)
		12.40 ±0.08	Mass data	Wapstra (1955)
		12.391±0.030	Review	Mattauch *et al.* (1956)

TABLE II

COMPARISON OF THRESHOLDS FROM MASS DATA AND FROM PHOTONEUTRON REACTIONS

Reaction	Photoneutron threshold, Mev.	Mass data threshold, Mev.	Difference, Mev.
$Na^{23}(\gamma, n)Na^{22}$	12.47±0.05	12.417±0.014	−0.05±0.05
$Al^{27}(\gamma, n)Al^{26}$	12.96±0.06	13.03 ±0.06	+0.07±0.08
$P^{31}(\gamma, n)P^{30}$	12.48±0.05	12.39 ±0.03	−0.09±0.06
$Co^{59}(\gamma, n)Co^{58}$	10.44±0.05	10.49 ±0.01	+0.05±0.05
$Pr^{141}(\gamma, n)Pr^{140}$	9.46±0.05	9.30 ±0.06	−0.16±0.08

Ref.	Elem. Sym.	A	Z
J. Dular, G. Kernel, M. Kregar, M.V. Mihailović, G. Pregl, M. Rosina, C. Zupančič Nuclear Phys. 14, 131 (1959)	P	31	15

Method	Ref. No.	
Compton Spectrometer; 30 MeV Betatron	59 Du 1	EH

Reaction	E or ΔE	E_o	Γ	$\int \sigma dE$	Jπ	Notes 813
(μ_t)	Bremss. 28.9 30.3					

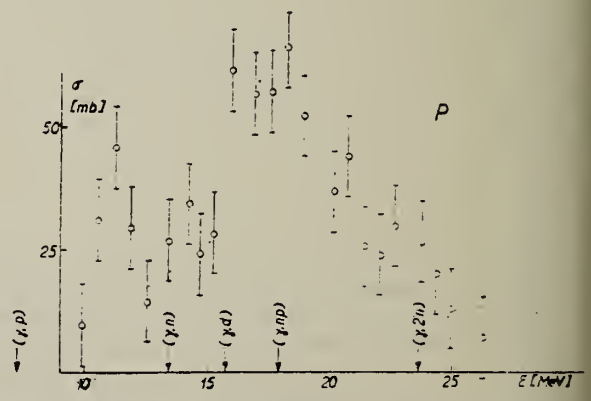

Fig. 6. Nuclear absorption cross section for P.

REF.

J. O'Connell, P. Dyal, J. Goldemberg
Phys. Rev. 116, 173 (1959)

ELEM. SYM.	A	Z
P	31	15

METHOD: Betatron

REF. NO.: 59 Oc 1 | NVB

REACTION	RESULT	EXCITATION ENERGY	SOURCE TYPE	SOURCE RANGE	DETECTOR TYPE	DETECTOR RANGE	ANGLE
G,2P	RLI	THR-100	C	THR-100	ACT-I		4PI
G,N2P	RLI	THR-100	C	THR-100	ACT-I		4PI

REL TØ G,N

TABLE II. Relative integrated cross sections.

Element	(γ,n)	Position of the peak for (γ,n)	$(\gamma,2n)$	Position of the peak for $(\gamma,2n)$
C^{12}	1	23 Mev	0.003	42 Mev
N^{14}	1	24 Mev	0.007[a]	
O^{16}	1	22 Mev	0.002	40 Mev
F^{19}	1	20 Mev	0.14	32 Mev
Na^{23}	1	20 Mev	0.05	32 Mev
P^{31}	1	20 Mev	0.06 $(\gamma,2p)$	45 Mev $(\gamma,2p)$
			0.08 $(\gamma,2pn)$	50 Mev $(\gamma,2pn)$

[a] The (γ,n) integrated cross section was taken from reference 4.

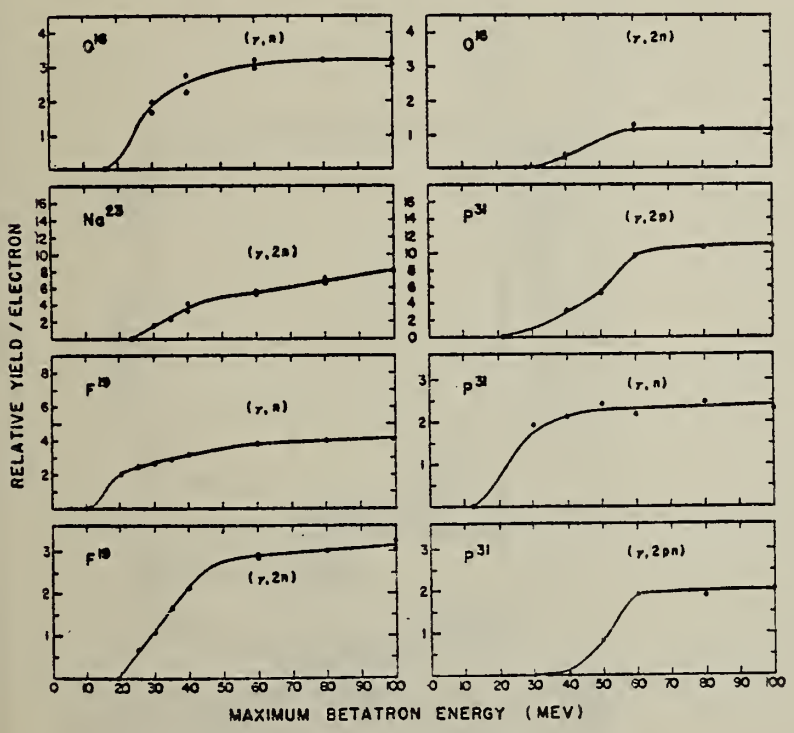

FIG. 1. The energy dependence of several photonuclear reactions. The relative yield scales of different graphs are independent.

Ref. E.C. Booth Nuclear Phys. 19, 426 (1960)	Elem. Sym.	A	Z
	P	31	15
Method Van de Graaff; electron bremss.; Ring scatterer; NaI	Ref. No.		
	60 Bo 3		JHH

Reaction	E or ΔE	E_o	Γ	$\int \sigma dE$	Jπ	Notes
(γ,γ)	Bremss. 0.5-2.2	1.26			3/2	Mean lifetime t/g: $= (3.4 \pm 1.5) 10^{-13}$ sec [resonance scattering] where $g = (1+2I)/(1+2I_o)$.

REF.

K.N. Geller, J. Halpern, E.G. Muirhead
Phys. Rev. 118, 1302 (1960)

ELEM. SYM.	A	Z
P	31	15

METHOD

Betatron; neutron threshold; ion chamber

REF. NO. 60 Ge 3 NVB

REACTION	RESULT	EXCITATION ENERGY	SOURCE		DETECTOR		ANGLE
			TYPE	RANGE	TYPE	RANGE	
G,N	NØX	THR	C	THR	ACT-I		4PI

THRESHØLD

TABLE I. Summary and comparison of neutron separation energies inferred from present threshold measurements with values predicted from mass data and reaction energies. All energies are expressed in the center-of-mass system in Mev.

Reaction	No. runs	Present results	Other results	Method	Reference
$P^{31}(\gamma,n)P^{30}$	5	$\leqslant 12.391 \pm 0.026$	12.40 ± 0.08	LSA	c
			12.391 ± 0.030	LSA	a
			12.359 ± 0.017	reaction cycle	e
			12.321 ± 0.009	mass data	g
			12.50 ± 0.05	threshold	i

[a] J. Mattauch, L. Waldmann, R. Bieri, and F. Everling, *Annual Review of Nuclear Science* (Annual Reviews, Inc., Palo Alto, 1956), Vol. 6, p. 179.
[b] R. W. Kavanagh and C. A. Barnes, Phys. Rev. 112, 503 (1958).
[c] A. H. Wapstra, Physica 21, 367 (1955).
[d] T. T. Scolman, K. S. Quisenberry, and A. O. Nier, Phys. Rev. 102, 1076 (1956).
[e] P. M. Van Patter and W. Whaling, Revs. Modern Phys. 26, 402 (1954); 29, 756 (1957).
[f] See reference 4.
[g] C. F. Giese and J. L. Benson, Phys. Rev. 110, 712 (1958).

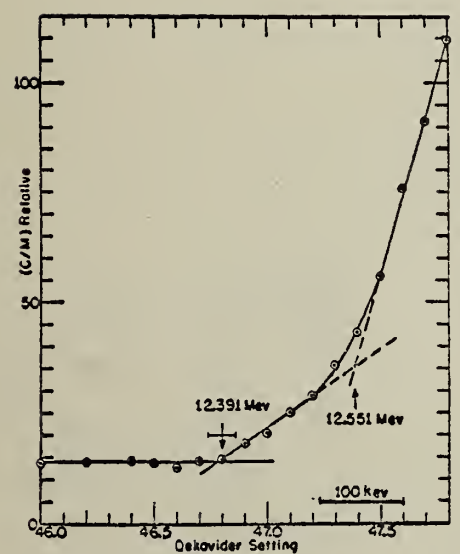

FIG. 6. Activation curve for phosphorus from 12.18 Mev to 12.66 Mev. Change in slope at 12.55 Mev is attributed to a level in the (γ,n) cross section at 12.59 Mev of width about 80 kev.

Ref.	Elem. Sym.	A	Z
A.M. Gorbunov, F.P. Denisov, V.A. Kolutkhin Zhur. Eksp. i Teoret. Fiz. 38, 1084 (1960) Soviet Phys. JETP 11, 783 (1960)	P	31	15

Method	Ref. No.	
260 MeV Synchrotron; activation; B ctrs. "photon difference"	60 Co 2	JHR

Reaction	E or ΔE	E_o	Γ	$\int \sigma dE$	Jπ	Notes
$P^{31}(\gamma,?)Na^{24}$	30-260					Observed threshold 60 MeV indicates substantial contribution from emission of bound nucleans, i.e., $(\gamma,He^4 2pn)$. Probably some (γ,Be^7). Refers to "quasi-neutron mechanism."

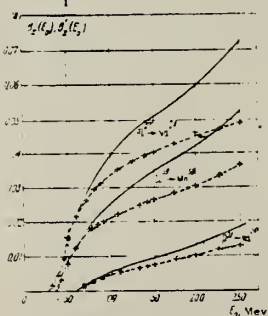

FIG. 1. Active yields of the $Al^{27} \rightarrow Na^{24}$, $Co^{59} \rightarrow Mn^{54}$, and $P^{31} \rightarrow Na^{24}$ reactions as a function of the peak bremsstrahlung energy. The values of $B_\gamma(E_0)$ are given by the continuous curves, of $B_\gamma(E_0)$ – by the dashed curves [the values of $B_\gamma(E_0)$ are given in arbitrary units].

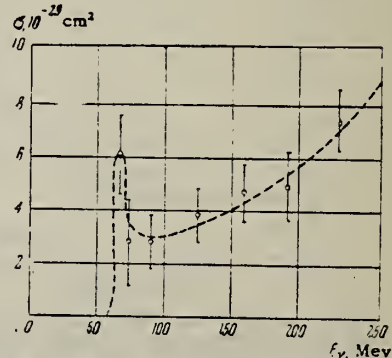

4. Effective cross section for the $P^{31} \rightarrow Na^{24}$ reaction.

REF. T.G. Walker, W.T. Morton
Proc. Phys. Soc. 75, 4 (1960)

ELEM. SYM.	A	Z
P	31	15

METHOD: Synchrotron; proton-neutron cross section; radioactivity

REF. NO.: 60 Wa 2 | NVB

REACTION	RESULT	EXCITATION ENERGY	SOURCE		DETECTOR		ANGLE
			TYPE	RANGE	TYPE	RANGE	
G,6P6N	ABX	0-240	C	240	ACT-I		4PI

$\sigma = (0.08 \pm 0.04)\ 10^{-27} cm^2$/equivalent quantum

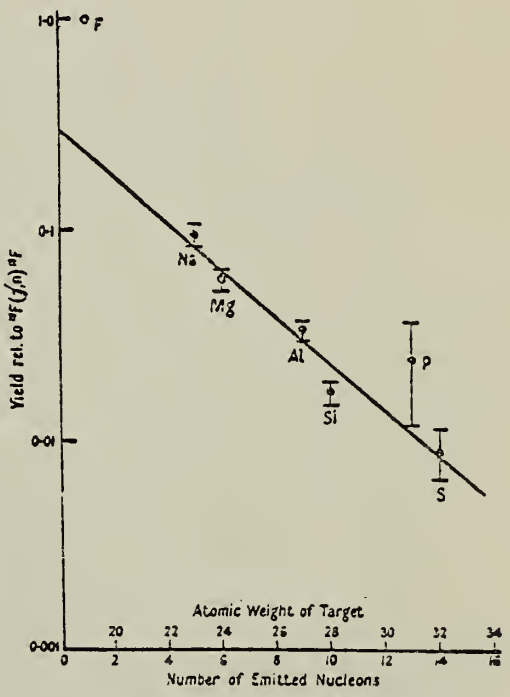

Yields relative to $^{18}F(\gamma, n)^{18}F$ at 240 Mev.

REF.

Ottavia Borello
Rev.Un.Mat.Argent.As.Fis.Argent.19, 251 (1961)

ELEM. SYM.	A	-
P	31	15

METHOD

REF. NO. 61 Bo 3 — EGF

REACTION	RESULT	EXCITATION ENERGY	SOURCE		DETECTOR		ANGLE
			TYPE	RANGE	TYPE	RANGE	
G,MU-T	ABX	11 - 20	C	11-20	ACT-I		

Used activity to measure total attenuation.

TABELA I

Reações	*Material*	*Meia vida* (Mev)	*Limiar* (Mev)	*Energia do Bétatron* P^{31} (Mev)	*Energia do Bétatron* P^{141} (Mev)	*Energia Média* (Mev) P^{31}	*Energia Média* (Mev) Pr^{141}
(a) $Cu^{63}(\gamma, n)\,Cu^{62}$	Cobre	10,1	10,6	11,4	11,8	11,0	11,2
(b) $Fe^{54}(\gamma, n)\,Fe^{53}$	Ferro	9,0	11,9	— —	16,0	—	14,6
(c) $O^{16}(\gamma, n)\,O^{15}$	Acido borico	2,1	15,6	17,4	17,6	16,5	16,6
(d) $C^{12}(\gamma, n)\,C^{11}$	Polietileno	20,5	18,7	20,3	20,1	19,5	19,6

TABELA II — P^{31}

Energia em Mev	μ(cm cm²/g)	σ(cm in barns)
11,0	0,0237 ± 0,0003	1220 ± 15
16,5	0,0235 ± 0,0002	1210 ± 10
19,5	0,0250 ± 0,0003	1287 ± 15

TABELA III Pr^{141}

Energia em Mev	μ(cm cm²/g)	σ(cm barns)
11,2	0,0435 ± 0,0009	10,19 ± 0,21
14,6	0,0481 ± 0,0008	11,26 ± 0,19
16,6	0,0505 ± 0,0008	11,83 ± 0,19
19,6	0,0550 ± 0,0005	13,00 ± 0,12

REF.

A. Bussiere de Nercy
Ann. Phys.(Paris) Third Series 6, 1379 (1961)

ELEM. SYM.	A	Z
P	31	15

METHOD

REF. NO. 61 Bu 4 egf

REACTION	RESULT	EXCITATION ENERGY	SOURCE		DETECTOR		ANGLE
			TYPE	RANGE	TYPE	RANGE	
G,G	ABX	15-30	C	32	NAI -D		140

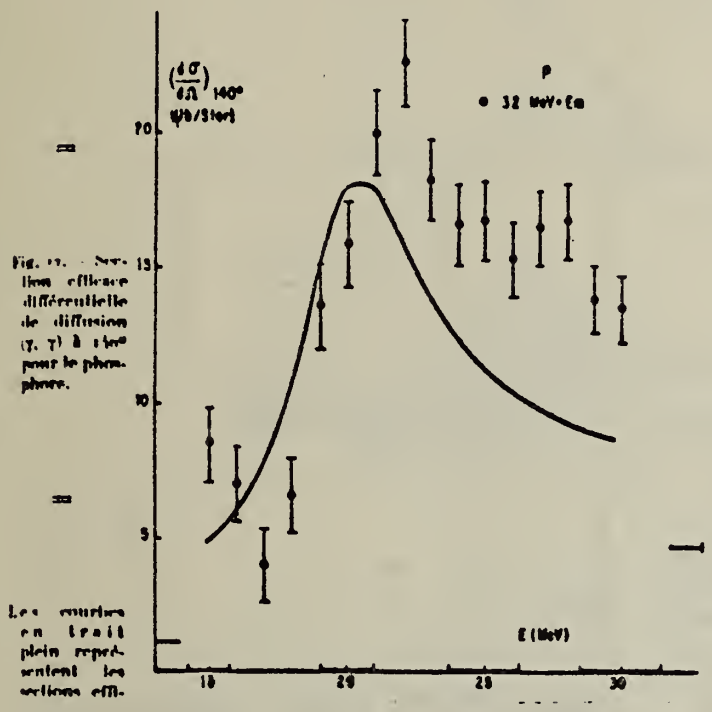

Fig. ... Section efficace différentielle de diffusion (γ, γ') à 140° pour le phosphore.

Les courbes en trait plein représentent les sections effi-

Ref. D. Sadeh
Phys. Rev. 123, 855 (1961)

Elem. Sym.	A	Z
P	31	15

Method: Betatron; activation; NaI for annihilation radium from P^{30} positrons.

Ref. No.: 61 Sa 1

EGF/JH

Reaction	E or ΔE	E_o	Γ	$\int \sigma dE$	Jπ	Notes
(γ,n)	12-14					"Breaks" shown in Figure 1 are list in Table 1. $E_{\gamma\ thresh.}$ = 12.23 ± 0.04 MeV.

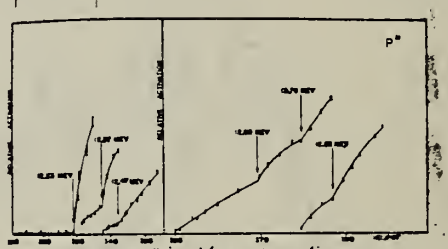

Fig. 1. "Breaks" in the activation curve of the $P^{31}(\gamma,n)P^{30}$ reaction

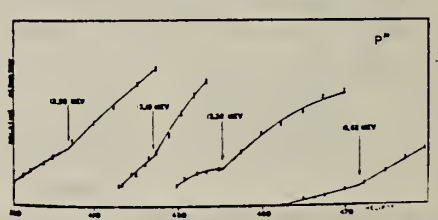

TABLE I. The energy of the breaks in the $P^{31}(\gamma,n)P^{30}$ reaction compared to the results of other groups.

Our results $P^{31}(\gamma,n)P^{30}$ ±0.04 Mev	Schull[a] $P^{31}(\gamma,n)P^{30}$ ±0.05 Mev	Geller *et al.*[b] $P^{31}(\gamma,n)P^{30}$ ±0.026 Mev	Bromley *et al.*[c] $Si^{29}(p,n)P^{30}$ ±0.007 Mev[d]
12.23			
12.37	12.33	12.39	12.41[e]
			12.44
			12.49
12.47	12.58	12.55	12.53[e]
			12.56
			12.63
12.68			12.66[e]
			12.73
			12.76
12.78	12.75		12.80[e]
12.83	12.90		
12.98			
13.18	13.18		
13.32	13.38		

[a] See reference 2.
[b] See reference 7.
[c] See reference 14.
[d] Results extracted from Bromley's graphs.
[e] Strong resonances.

Ref 14 Bromley et al, Can. J. Phys. 37, 153 (1959).
Ref 2: C.G. Schull, Suppl. Nuovo cimento 4, 1162 (1956)
Ref 7: Geller et al, Phys. Rev. 118, 1302 (1960)

TABLE II. Thresholds (in Mev) of the $P^{31}(\gamma,n)P^{30}$ and $Cl^{35}(\gamma,n)Cl^{34}$ reactions compared to the results of other groups.

References	$P^{31}(\gamma,n)P^{30}$	$Cl^{35}(\gamma,n)Cl^{34}$
Our results[a]	12.23 ±0.04	12.66±0.04
Schull[b]	12.33 ±0.05	12.79±0.05
Chidley *et al.*[c]	12.50 ±0.05	
Wapstra (mass data)[d]	12.40 ±0.08	12.71±0.12
Everling (mass data)[e]	12.316±0.02	12.57±0.04

[a] These results are given in the laboratory system. In the center-of-mass system the results will not decrease more than 3 kev.
[b] See reference 2.
[c] Can. J. Phys. 36, 407 (1956).
[d] Physica 21, 367 (1955).
[e] Nuclear Phys. 15, 342 (1960).

Ref 2: Schull, Suppl. Nuovo cimento 4, 1162 (1956

Ref.	Elem. Sym.	A	Z
K. Shoda, S. Shiina, K. Kobayashi, K. Abe, M. Kimura J. Phys. Soc. Japan 16, 1807 (1961)	P	31	15

Method	Ref. No.	
24 MeV betatron; proton spectrum; angular distribution; nuclear emulsion; r - chamber	61 Sh 4	NVI

Reaction	E or ΔE	E_0	Γ	$\int \sigma dE$	Jπ	Notes
$P^{31}(\gamma,xp)$	Bremss. 24					Yield = 3.2 c 10^5 protons/mole-r

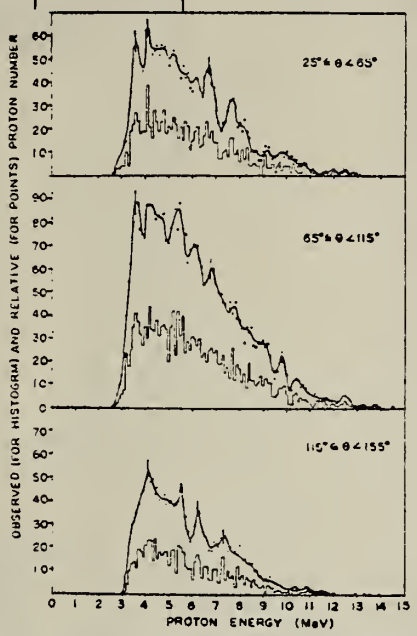

Fig. 5. Energy distributions of protons from P^{31} (γ, p) for three directional groups. The smoothed results are shown by the points.

Fig. 6. Energy distribution of total observed protons and calculated distributions by the statistical theory from P^{31}.
Full line: Observed spectrum smoothed out by the method of Ferreira and Valoshek.
Broken line: Calculated spectrum using $\omega = C \exp[2\sqrt{0.32E}]$ MeV^{-1}
Dotted line: Calculated spectrum using $\omega = C \exp[2\sqrt{2.42E}]$ MeV^{-1}.
Each curve is normalized to best fit to experimental points.

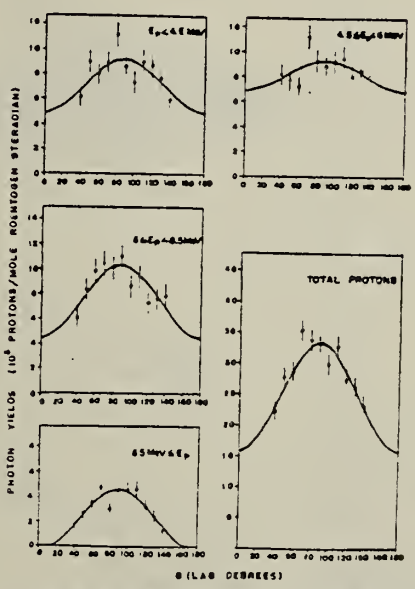

Fig. 7. Angular distributions of protons from P^{31}. Full lines are obtained by least squares.

Table II. Angular distributions calculated by least squares for $a+b\sin^2\theta$.

Element	Proton energy (MeV)	Augular distributions
Si^{29}	1.8—3.3	$1-(0.50\pm0.39)\sin^2\theta$
	3.3—4.7	$1-(0.09\pm0.44)\sin^2\theta$
	4.7—6.3	$1+(0.01\pm0.40)\sin^2\theta$
	6.3—7.7	$1+(0.06\pm0.49)\sin^2\theta$
	larger than 7.7	$1+(0.48\pm0.73)\sin^2\theta$
	Total	$1-(0.05\pm0.20)\sin^2\theta$
P^{31}	2.7—4.5	$1+(0.85\pm0.42)\sin^2\theta$
	4.5—6.0	$1+(0.35\pm0.34)\sin^2\theta$
	6.0—8.5	$1+(1.31\pm0.59)\sin^2\theta$
	larger than 8.5	$(-0.08\pm0.18)-\sin^2\theta$
	Total	$1+(1.10\pm0.27)\sin^2\theta$

FORM NBS-418
(8-1-63)
USCOMM-DC 18556-P63

U.S. DEPARTMENT OF COMMERC
NATIONAL BUREAU OF STANDARC

Ref. E.C. Booth, K.A. Wright
Nuclear Phys. 35, 472 (1962)

Elem. Sym.	A	Z
P	31	15

Method 4 MeV electron Van de Graaff; bremss.; nuclear resonance scattering, ring scatterer; NaI

Ref. No. 62 Bo 6 JHH

Reaction	E or ΔE	E_0	Γ	$\int \sigma dE$	Jπ	Notes
$P^{31}(\gamma,\gamma)$	Bremss. 0 - 4					Detector at 110°

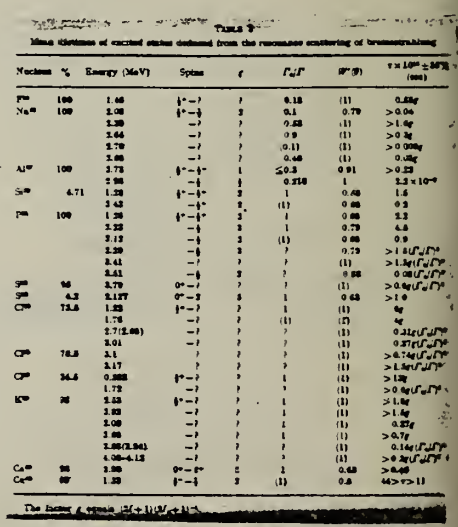

TABLE 3

Mean lifetimes of excited states deduced from the resonance scattering of bremsstrahlung

Nucleus	%	Energy (MeV)	Spins	ε	Γ_0/Γ	$W(\theta)$	$\tau \times 10^{15}$ s (fs)
F^{19}	100	1.46	$\frac{1}{2}^+ \to \frac{1}{2}^-$	1	0.18	(1)	0.88 η
Na^{23}	100	2.08	$\frac{1}{2}^+ \to \frac{3}{2}^-$	2	0.1	0.79	> 0.06
		2.39	$\to \frac{1}{2}^-$	1	0.53	(1)	$> 1.6\eta$
		2.64	$\to \frac{3}{2}^-$	1	0.9	(1)	$> 0.3\eta$
		2.79	$\to \frac{1}{2}^-$	1	(0.1)	(1)	$> 0.003\eta$
		2.98	$\to \frac{3}{2}^-$	1	0.68	(1)	0.35η
Al^{27}	100	1.73	$\frac{1}{2}^+ \to \frac{1}{2}^+$	1	≤ 0.3	0.91	> 0.23
		2.98	$\to \frac{3}{2}^+$	1	0.258	1	1.3×10^{-3}
Si^{28}	4.71	1.78	$1^- \to 1^+$	2	1	0.68	1.6
		3.43	$\to 2^+$	2	(1)	0.68	0.3
P^{31}	100	1.26	$\frac{1}{2}^+ \to \frac{1}{2}^+$	1	1	0.68	2.2
		2.23	$\to \frac{3}{2}^+$	1	1	0.79	0.6
		2.12	$\to \frac{1}{2}^+$	1	(1)	0.68	0.9
		2.29	$\to \frac{3}{2}^+$	1	?	0.79	$> 1.6(\Gamma_0/\Gamma)^2$
		2.41	$\to ?$	?	?	(1)	$> 1.3\eta(\Gamma_0/\Gamma)^2$
		2.61	$\to \frac{3}{2}^+$	2	?	0.68	$0.08(\Gamma_0/\Gamma)^2$
S^{32}	95	2.79	$0^+ \to ?$	?	?	(1)	$> 0.6\eta(\Gamma_0/\Gamma)^2$
S^{34}	4.2	2.127	$0^+ \to 2^+$	2	1	0.68	> 1.0
Cl^{35}	75.5	1.22	$\frac{1}{2}^+ \to ?$	?	1	(1)	4η
		1.76	$\to ?$	?	(1)	(1)	4η
		2.7(2.68)	$\to ?$	?	?	(1)	$0.31(\Gamma_0/\Gamma)^2$
		3.01	$\to ?$	?	?	(1)	$0.37(\Gamma_0/\Gamma)^2$
Cl^{37}	24.5	3.1	$\to ?$	?	?	(1)	$> 6.7\eta(\Gamma_0/\Gamma)^2$
		3.17	$\to ?$	?	?	(1)	$> 1.5\eta(\Gamma_0/\Gamma)^2$
Cl^{37}	24.5	0.3088	$\frac{3}{2}^+ \to ?$	?	1	(1)	$> 12\eta$
		1.72	$\to ?$	?	?	(1)	$> 0.4\eta(\Gamma_0/\Gamma)^2$
K^{39}	93	2.53	$\frac{1}{2}^+ \to ?$	?	1	(1)	$> 1.4\eta$
		2.82	$\to ?$	?	1	(1)	$> 1.4\eta$
		2.98	$\to ?$	?	1	(1)	0.27η
		3.02	$\to ?$	?	1	(1)	$> 0.7\eta$
		2.80(2.941)	$\to ?$	?	?	(1)	$0.14(\Gamma_0/\Gamma)^2$
		4.08-4.15	$\to ?$	?	?	(1)	$> 0.2\eta(\Gamma_0/\Gamma)^2$
Ca^{40}	96	3.35	$0^+ \to 1^+$	2	1	0.68	> 0.68
Ca^{42}	0.7	1.53	$0^+ \to \frac{1}{2}^+$	2	(1)	0.8	$4\pi > \tau > 1\eta$

The factor η equals $(E_0 + 1)(E_0 + 2)$.

Ref. V. Emma, C. Milone, S. Jannelli, F. Mezzanares
Nuovo Cimento 26, 890 (1962)

Elem. Sym.	A	Z
P	31	15

Method: Betatron; emulsions

Ref. No.: 62 Em 1 | JHH

Reaction	E or ΔE	E_o	Γ	$\int \sigma dE$	Jπ	Notes
$P^{31}(\gamma,n)$	Bremss. 30					Neutron spectrum for $E_n \geq 1.5$ MeV. 90° measurement. High-energy tail and wide peak around 5.5 MeV in E_n spectrum indicate that other processes besides evaporation must occur. 30% direct for $E_n > 1.5$; 60% direct for $E_n > 4$.

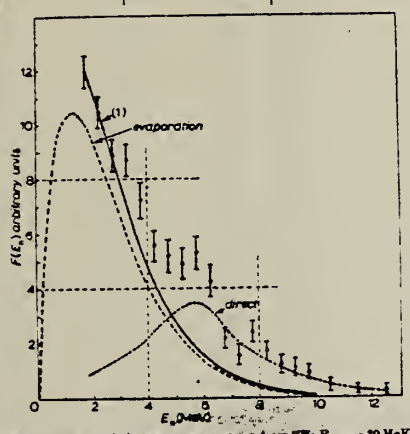

Fig. 1. – Points: experimental photoneutron spectrum from ^{31}P; $E_{\gamma\,max} = 30$ MeV. Curve (1) represents the function $F(E_n) = KE_n \exp[-E_n/1.3]$ which fits the experimental points for $E_n < 3$ MeV. The « evaporation » and « direct » curves represent the contribution of the evaporation and direct interaction to the experimental spectrum.

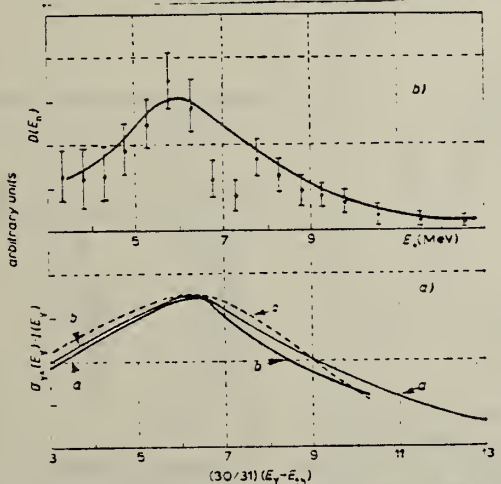

Fig. 3 a), b). – The curves *a*, *b*, *c*, represent the function $\sigma_{(\gamma,n)}(E_\gamma) \cdot D(E_n)$ assuming the $\sigma(\gamma, n)$ cross-section given in refs. [10,11,12] respectively; for the curve $D(E_n)$ see text.

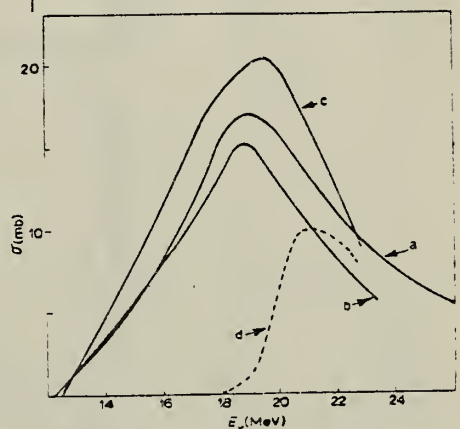

Fig. 2. – The curves *a*, *b*, and *c* represent the $^{31}P(\gamma, n)$ cross-section according to the refs. [10,11,12] respectively; the curve *d* represents the (γ, np) cross-section according to ref. [12].

[10] J. Halpern, A. K. Mann and R. Nathans: *Phys. Rev.*, **88**, 968 (1952).
[11] R. Montalbetti, L. Katz and J. Goldemberg: *Phys. Rev.*, **91**, 659 (1953).
[12] L. Katz and A. S. Penfold: *Phys. Rev.*, **81**, 815 (1951).

Ref. N. Mutsuro, K. Kageyama, M. Mishina, E. Tanaka, M. Kimura
J. Phys. Soc. Japan 17, 1673 (1962)

Elem. Sym.	A	Z
P	31	15

Method: Betatron; BF_3 counters; Al thin-wall ion chamber monitor

Ref. No.: 62 Mu 2 | NVB

Reaction	E or ΔE	E_0	Γ	$\int \sigma dE$	Jπ	Notes
P^{31} (γ.xn)	Bremss. 12.5-24	13.5 14.6 15.8 (17) 17.5 19.0 20.3		$\int_0^{22.5}$ = 120±10 MeV-mb		Suggested correspondence with observed proton energy peaks.

755+

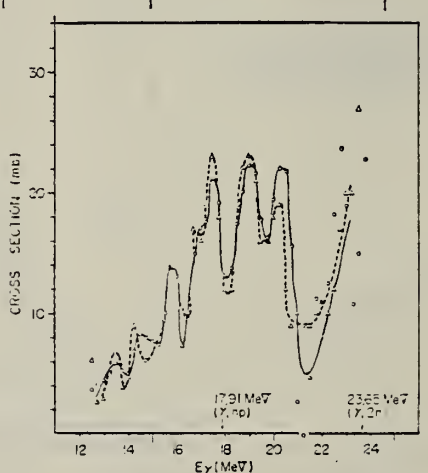

Fig. 1. Cross section for $P^{31}(\gamma, n)$ reaction, in which solid line was deduced from yield curve smoothing method and dotted line was deduced from running integral smoothing method.

Table. Characteristic constants of both reaction.

P^{31}		S^{32}	
E_{res} (Mev)	σ_{res} (mb)	E_{res} (Mev)	E_{res} (mb)
13.5	6		
14.6	8		
15.8	14	15.7	7
(17)	(17)	16.8	10
17.5	21	17.9	20
19.0	22	18.75	11
20.3	22	19.7	16
$\int_0^{22.5} \sigma(\gamma, n)dE$ = 120±10 Mev·mb		$\int_0^{22.5} \sigma(\gamma, n)dE$ = 60±5 Mev·mb	

Ref. K. Shoda, T. Ishizuka, N. Kawamura, K. Abe, M. Kimura J. Phys. Soc. 17, 401 (1962)	Elem. Sym.	A	Z
	P	31	15
Method Betatron; red P powder on gold foil target; nuclear emulsion	Ref. No. 62 Sh 12		NVB

Reaction	E or ΔE	E_o	Γ	$\int \sigma dE$	Jπ	Notes
$P^{31}(\gamma,p)$	Bremss. 19.0	9-19				

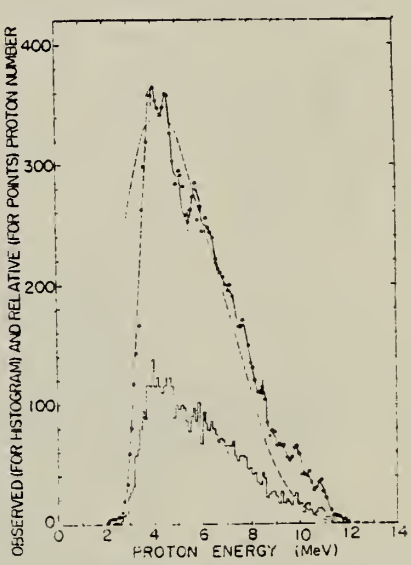

Fig. 1. The energy spectrum of photoprotons from P^{31} irradiated by 19 Mev bremsstrahlung. The solid line is a smoothed curve. The broken line is a calculated curve using the statistical model with the Weisskopf level density.

Ref.	Elem. Sym.	A	Z
P.M.Tutakin Zhur.Eksptl. i Teoret.Fiz. 43, 1140 (1962) Soviet Phys.JETP 16, 805 (1963)	P	31	15

Method	Ref. No.	
H_2^+ ion accel. (electrostatic generator) - heavy H_2O emulsion	62Tul	BG

Reaction	E or ΔE	E_o	Γ	$\int \sigma dE$	Jπ	Notes
$Si^{30}(p,\gamma)P^{31}$	keV					
	E_p = 773					Gives Jπ as determined in other experiments for 773, 939, 979.5 KeV.
	939					
	979.5					
	1393				$5/2^+$	Mixture coefficients and angular distribution determined.

Ref.	Elem. Sym.	A	Z
W.C.Barber, J.Goldemberg, G.A.Peterson, Y.Torizuka Nuclear Phys. 31, 461 (1963); erratum to be published (as of 9/3/63)	P	31	15

Method	Ref. No.	
Linac (Stanford Mark II) • counter telescope	63Bel	23

Reaction	E or ΔE	E_o	Γ	$\int \sigma dE$	Jπ	Notes
(e,e')	41.5		determined see Table II		see Table II	inelastic scattering cross section at 180° (cm^2/sr)x10^{-32}
		3.6		0.1 MeV mb		0.9±30%
		5.6		0.12		0.7±30%
		8.9		0.22		0.7±30%

Table II headings:

isotope	Energy of level (MeV)	spin and parity ground state	spin and parity excited state	Inelastic electron scat. cross section (cm^2/sr) x10^{-32}		rad. width to ground state (eV)	
				Estimated error	MeV-mb	this exp.	Weiss-kopf

TABLE 2 (Continued)

	10.6		$\{\frac{1}{2}^+, \frac{3}{2}^+, \frac{5}{2}^+$	0.6	40	0.23	{11.5, 7.7, 5.8	25
	12.8		$\{\frac{1}{2}^+, \frac{3}{2}^+, \frac{5}{2}^+$	1.4	30	0.65	{46.5, 31.2, 23.5	45
$_{16}P^{31}$	3.6	$\frac{1}{2}^+$	$\frac{1}{2}^+$	0.9	30	0.1	0.29	0.82
	5.6		$\{\frac{1}{2}^+, \frac{3}{2}^+, \frac{5}{2}^+$	0.7	30	0.12	{1.1, 0.81, 0.55	3.6
	8.9		$\frac{1}{2}^+$	0.7	30	0.22	4.0	14.5
$_{16}S^{32}$	5.7	0^+	1^+	1.3	30	0.24	0.76	3.6
	8.5		1^+	1.7	30	0.51	3.5	12.5
	11.4		1^+	2.6	30	1.11	14.2	32
$_{18}Ar^{40}$		0^+	no resonances					
$_{17}X^{35}$		$\frac{3}{2}^+$	no resonances					
$_{20}Ca^{40}$		0^+	no resonances					
$_{19}X^{39}$		$\frac{3}{2}^-$	no resonances					

*) The results in this column were derived in the "long wave approximation".

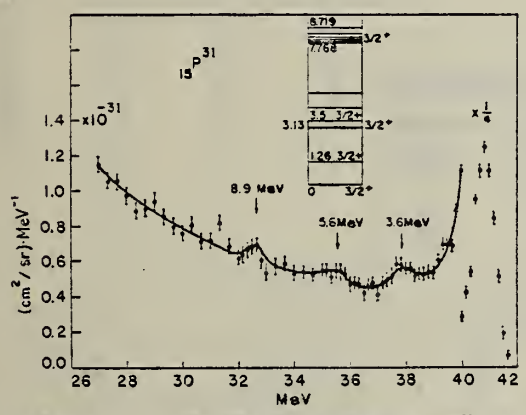

Fig. 14. Spectrum of 41.5 MeV electrons scattered from a P^{31} target at 180°.

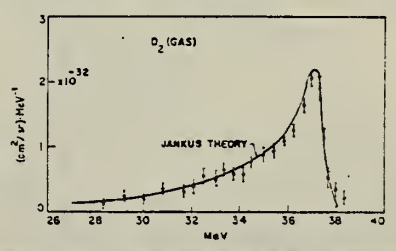

Fig. 3. Spectrum of 41.5 MeV electrons inelastically scattered from deuterium gas at 180°.

Ref. L.N. Bolen, W.D. Whitehead
Phys. Rev. 132, 2251 (1963)

Elem. Sym.	A	Z
P	31	15

Method: Synchrotron; neutron yield; BF_3 counters; NBS chamber monitor

Ref. No.: 63 Bo 1 — JHH

Reaction	E or ΔE	E_o	Γ	$\int \sigma dE$	Jπ	Notes
$P^{31}(\gamma,xn)$	Bremss. 10-30			$\int_{th}^{28}$ = 127 MeV-mb		For "E_o" and "σ(mb)", see Table III below.

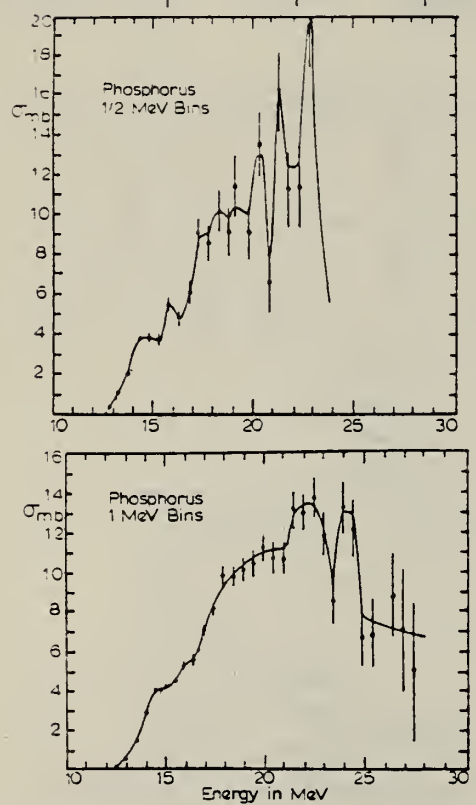

FIG. 3. P(γ,n) cross section unfolded using ½-MeV bins (top curve) and 1-MeV bins (lower curve).

TABLE III. Summary of data from this experiment, giving energy positions of levels found in our cross sections and corresponding data from other experiments.

Element	University of Virginia E(MeV)	University of Virginia σ(mb)	Gove[a] E(MeV)	Kinsey[b] E(MeV)
Si	16.0	1.2		
	18.5	8.4	18	
	19.75	14.7	18.9	18.9
	20.75	13.6	20	20.6
	22.75	9.6	21.6	21.4
	24.25	7.1		

Element	University of Virginia E(MeV)	University of Virginia σ(mb)	Mutsuro[c] E(MeV)	Mutsuro[c] σ(mb)
			13.5	6
P	14.75	3.9	14.6	8
	15.75	5.6	15.8	14
	17.25	9.2	(17)	(17)
	18.25	10.2	17.5	21
	19.25	11.5	19.0	22
	20.25	13.6	20.3	22
	21.25	16.4		
	22.75	19.5		
	24.25	13.2		

Element	University of Virginia E(MeV)	University of Virginia σ(mb)	Mutsuro[c] E(MeV)	Mutsuro[c] σ(mb)
S	16	1.7	15.7	7
	17.5	6.0	16.8	10
	18.25	9.0	17.9	20
	19.75	13.4	18.75	11
	21.25	12.5	19.7	16
	22.75	11.3		
	24.0	9.0		

[a] See Ref. 19.
[b] See Ref. 20.
[c] See Ref. 5.

TABLE II. Integrated cross-section values obtained from the (γ,n) cross sections of elements measured in this laboratory.[a]

Element	Limits of integration threshold to	$\int \sigma dE$ MeV-mb	Dipole sum rule $X=0$ MeV-mb	% of DSR exhausted by (γ,n)
O	31MeV	46	240	19
Mg	29	84	360	23
Al	28	97.5	405	24
Si	28	80	420	19
P	28	127	465	27
S	28	81	480	17
Ca	28	74	600	12
N	25	60	210	29
	50	116		55
Ar	25	392	600	65
	50	598		100
Li	25	39	105	37
	50	93		89

[a] See Refs. 1, 12, and 13.

[1] L. N. Bolen and W. D. Whitehead, Phys. Rev. Letters 9, 458 (1962).
[2] R. L. Bramblett, J. C. Coldwell, and S. C. Fultz, University of California Lawrence Radiation Laboratory Report UCRL 7156 (unpublished).
[3] F. W. K. Firk and E. R. Rae, International Symposium on Direct Interactions and Nuclear Reaction Mechanisms, Padua, 1962 (to be published).
[4] N. Mutsuro, K. Kageyama, M. Mishina, T. Nakagawa, E. Tanaka, and M. Kimura, J. Phys. Soc. Japan 17, 1672 (1962).
[5] N. Mutsuro, K. Kageyama, M. Mishina, E. Tanaka, and M. Kimura, J. Phys. Soc. Japan 17, 1673 (1962).
[12] R. W. Fast, P. A. Flournoy, R. S. Tickle, and W. D. Whitehead, Phys. Rev. 118, 535 (1960).
[13] K. Min, L. N. Bolen, and W. D. Whitehead, Phys. Rev. 132, 749 (1963).
[19] M. E. Gove, A. E. Litherland, and R. Batchelor, Nucl. Phys. 26, 480 (1961).
[20] M. Kinsey, K. Shoda, N. Mutsuro, T. Tohei, K. Sato, K. Kageyama, K. Kuriyama, and T. Akiba, J. Phys. Soc. Japan 15, 1128 (1960).

Ref.	Elem. Sym.	A	Z
S. Costa, F. Ferrero, S. Ferroni, B. Minetti, C. Milone, R. Malvano Phys. Letters 6, 226 (1963)	P	31	15

Method	Ref. No.	
100 MeV Synchrotron; 4 π neutron detector; calculated integrated cross sections - fitted with polynomial of degree η	63 Co 3	EGF

Reaction	E or ΔE	E_o	Γ	$\int \sigma dE$	Jπ	Notes
$P^{31}(\gamma, xn)$						$\sigma_b = \int \frac{\sigma(E)}{E} dE$ gets $\langle \bar{\nu}_p \cdot \bar{\nu}_n - \bar{\nu}_n \cdot \bar{\nu}_{n1} \rangle$ $= (Rc^2 - E_p^2 - \frac{3}{\pi^2} \frac{tr\ c}{e^2} \sigma_b \frac{A-1}{A^2}) \times \frac{2}{A-2}$ See "Boron" for plots of this and $\int \sigma dE/60\ NZ/A$.

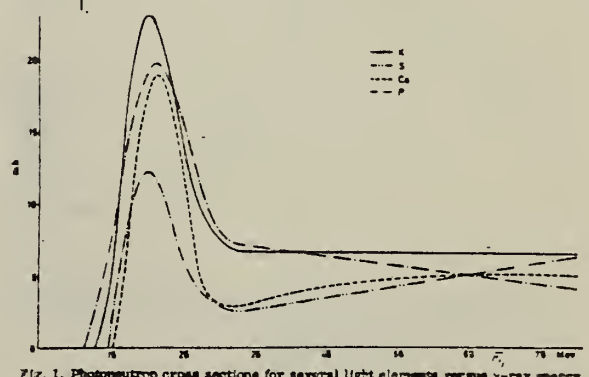

Fig. 1. Photoneutron cross sections for several light elements versus γ-ray energy.

R. Lombard, P. Kossanyi, G.R. Bishop
J. de Physique 24, 968 (1963)

P	31	15

METHOD: Linac; electron scattering; magnetic spectrometer

REF. NO.: 63 Lo 2 | NVB

REACTION	RESULT	EXCITATION ENERGY	SOURCE		DETECTOR		ANGLE
			TYPE	RANGE	TYPE	RANGE	
E,E/	FMF	1 - 6	D	130,180	MAG -D		DST

Énergie (MeV)	Spin connu	Spin prob.	$B(El)$	l	Nature trans.	$B(El)$ BW
1,26	3/2+		$(85 \pm 10)\ 10^{-52}$ cm^4	2	E	2,9
2,23	5/2+		$(114 \pm 10)\ 10^{-52}$ cm^4	2	E	4
(3,13 ± 0,1)	3/2+		$(12 \pm 6)\ 10^{-52}$ cm^4	2	E	0,4
3,5	3/2+		$(54 \pm 5)\ 10^{-52}$ cm^4	2	E	1,9
4,25				2,3		
4,63		5/2−	$(17 \pm 3)\ 10^{-76}$ cm^6	3	E	4,3
5,01 (± 0,1)		7/2+ ou 5/2+	$(8,5 \pm 1,5)\ 10^{-76}$ cm^6	3	M	70
(5,7 ± 0,1)		7/2−	$(20 \pm 3)\ 10^{-76}$ cm^6	3	E	5,1

W.J. McDonald, E. Buchholz, R.N.H. Haslam
Can. J. Phys. 41, 180 (1963)

P	31	15

METHOD: Betatron; neutron cross section; activity; $Cu^{63}(\gamma,n)$ monitor

REF. NO.: 63 Mc 3 | NVB

REACTION	RESULT	EXCITATION ENERGY	SOURCE TYPE	SOURCE RANGE	DETECTOR TYPE	DETECTOR RANGE	ANGLE
G,N	ABX	12-24	C	12-24	ACT -I		4PI
				(11.6-24.0)			

810

Peaks at: E_γ = 18.2 MeV, 19.5 MeV

σ_{max} = 19 mb, at E_γ = 19.5 MeV

Half-width of giant resonance = 7.6 MeV

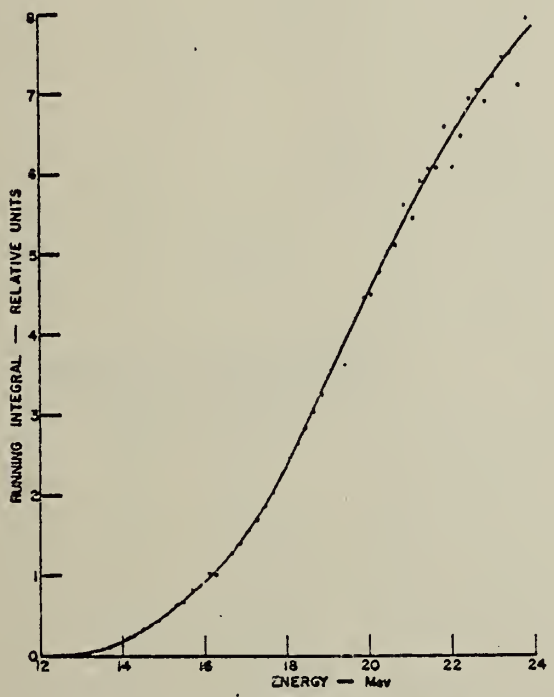

FIG. 1. Running integral curve for the reaction $P^{31}(\gamma, n)P^{30}$.

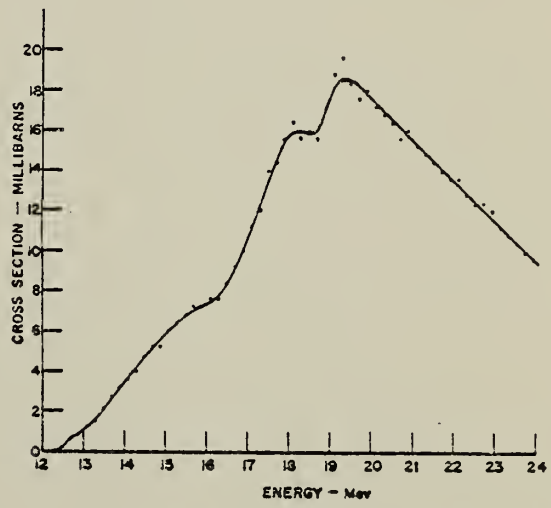

FIG. 2. Cross-section curve for the reaction $P^{31}(\gamma, n)P^{30}$.

REF. E. C. Booth, B. Chasan and K. A. Wright
Nucl. Phys. 57, 403-420 (1964)

ELEM. SYM.	A	Z
P	31	15

METHOD
Van de Graaff; resonance fluorescence

REF. NO. 64 Bo 1 NVB

REACTION	RESULT	EXCITATION ENERGY	SOURCE		DETECTOR		ANGLE
			TYPE	RANGE	TYPE	RANGE	
G,G	LFT	1-3	C	1 - 3	NAI-D		100
		(0.5 - 3.0)		(0.5 - 3.0)			

ABI

TABLE 1
Cases of observed resonance fluorescence

Nucleus multipol.	State (MeV)	Spin	Γ_0/Γ	$T(g_W\Gamma_0^2/\Gamma^2)^{-1}$ (sec).	Mean lifetime T BCW (sec)	Mean lifetime T other (sec)	Ref.	Γ_0/Γ_W BCW
P^{31}	0.00	$\frac{1}{2}^+$						
M1	1.26	$\frac{3}{2}^+$	1	$54\pm17\times10^{-14}$	$95\pm30\times10^{-14}$	$71.6^{+13}_{-10}\times10^{-14}$	14)	1.7×10^{-8}

REF.

B. S. Ishkhanov, I. M. Kapitonov, V. G. Shevchenko and B. A. Yur'ev
Phys. Letters 9, 162 (1964)

ELEM. SYM.	A	-
P	31	15

METHOD

Betatron

REF. NO.

64 Is 1 JOC

REACTION	RESULT	EXCITATION ENERGY	SOURCE		DETECTOR		ANGLE
			TYPE	RANGE	TYPE	RANGE	
G,XP	ABX	THR - 32	C	15-32	SCI-D	0-3	

809

Table 2
Measurements results

Element	Maximum cross section (b)	Peak position (MeV)	Peak half-width (MeV)	Integrated cross section $\int_0^{32} \sigma_a E$ (MeV, b)
P	0.043	21	10	0.35 ± 0.05
S	0.050	21	9	0.37 ± 0.05
Mg	0.018 0.018	22.5 26.0	11	0.18 ± 0.04

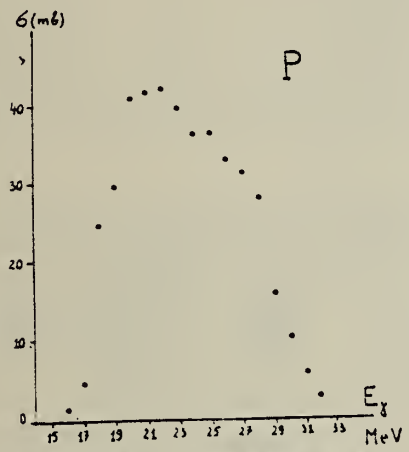

Fig. 3. The (γ,p) cross section for P.

REF.
P. M. Tutakin
Zhur. Eksp. i Teoret. Fiz. 46, 10-17 (1964)
Soviet Phys. JETP 19, 7-12 (1964)

ELEM. SYM.	A	Z
P	31	15

METHOD
Electrostatic generator; $Si^{30}(p,\gamma)P^{31}$; measured photoprotons

REF. NO. 64 Tu 1 NVB

REACTION	RESULT	EXCITATION ENERGY	SOURCE TYPE	SOURCE RANGE	DETECTOR TYPE	DETECTOR RANGE	ANGLE
$ P,G	NØX	10	D	3	EMU-D		90
		(10.492)		(3.308)			

J-PI, POL OF G

$J^{PI} = \frac{3}{2}^-$ for 10.492 level.

Table II. Numbers of photoproton tracks, observed and calculated ranges, and γ transitions for resonance at E_p = 3308 keV

Group	No. of tracks	Range, μ: Mean observed	Range, μ: Calculated	Transition
1	45	189	187	10,492 → 0 ($^1/_2^+$)
2	19	141	140	10.492 → 1.265 ($^3/_2^+$)
3	35	111	110	10.492 → 2.232 ($^5/_2^+$)

REF.

P. Kossanyi-Demay, R. M. Lombard and G. R. Bishop
Nuclear Phys. 62, 615 (1965)

P	31	15

METHOD

[Page 1 of 4]

REF. NO. 65 Ko 1

EGF

REACTION	RESULT	EXCITATION ENERGY	SOURCE TYPE	SOURCE RANGE	DETECTOR TYPE	DETECTOR RANGE	ANGLE
E,E/	FMF	1-6	D	130-180	MAG-D	120-180	DST

E_x	L	$\beta_{(10)^{-2}}$	B(↑)	Ratio to Single Particle
1.26	2	2.78 ± 0.31	73 ± 8 fm^4	2.5
2.23	2	3.72 ± 0.43	97 ±11 fm^4	3.3
3.47 ± 0.06	2	1.81 ± 0.22	47 ± 6 fm^4	1.5
	4	1.34 ± 0.16	51 ± 6 fm^3	0.95
4.20 ±.01	2	0.68 ± 0.12	17.7 ± 3 fm^2	0.6
4.56 ± 0.15	3	5.47 ± 0.7	17 ± 2(10)^2 fm^6	4.2
5 ± 0.15	2	9.2 ± 1.3	24 ± 4 fm^4	0.8
	4	6.1 ± 0.8	2.3 ± 0.3(10)^4 fm^3	4.3
5.67 ± 0.07	3	5.7 ± 0.8	18 ± 3(10)^2 fm^6	4.5
6.55 ± 0.15	2	1.8 ± 0.3	47 ± 7 fm^4	1.6

TABLE 1

Les sections efficaces mesurées pour la diffusion des électrons à différentes énergies et divers angles par le noyau de P^{31}

Énergie incidente (MeV)	Angle de diffusion θ	Transfert de quantité de mouvement q(fm^{-1})	Section efficace élastique (μb)	Sections efficaces inélastiques (mμb)							
				1.27 (MeV)	2.23 (MeV)	3.47±0.06 (MeV)	4.20±0.06 (MeV)	4.56±0.15 (MeV)	5±0.15 (MeV)	5.67±0.07 (MeV)	6.55±0.15 (MeV)
181.17	40	0.627	600±48								
128.64	65	0.699	79±5								
128.49	70	0.746	47±5	627±194	1105±148						
181.27	50	0.775	83±5								
129.38	75	0.797	28±3	431±72	571±80	322±42	112±37	252±50	225±56	235±58	229±55
179.31	60	0.907	14±0.8	604±114	953±133	430±66	140±38	490±108	252±85	405±115	476±102
180.72	65	0.983	5.25±0.32	425±105	544±80						
182.09	70	1.062	1.46±0.12	209±50	321±84	144±27					
179.44	75	1.110	0.47±0.03	141±21	153±28	87±19	28±6	152±28	95±28		
182.91	80	1.183	0.1 ±0.009	73±21	78±12	56±9	25±10	117±16	32±7	125±17	50±11
182.76	90	1.306	0.043±0.005	11±2.9	22±10	20±4	14±9	43±8	38±7	70±16	
180.09	100	1.393	0.037±0.003	6.4±2	6±1.6	8.6±1.5	3.3±1.1	28±2			
179.34	110	1.480	0.031±0.002	2.9±2.9		3.2±0.8	1.8±0.9	9.5±2.2	14.7±3.4	184±5	
180.28	120	1.575	0.015±0.002								

REACTION	RESULT	EXCITATION ENERGY	SOURCE TYPE	SOURCE RANGE	DETECTOR TYPE	DETECTOR RANGE	ANGLE

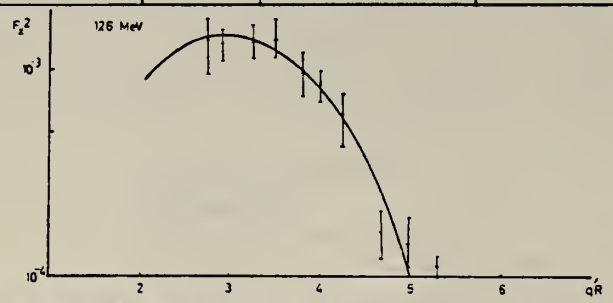

Fig. 5. Le facteur de forme expérimental du niveau à 1.26 MeV. La courbe tracée représente l'expression $F_2 = j_2^2(qR)e^{-q^2\sigma^2}$ multipliée par le facteur de normalisation $\beta_2 = 2.78 \cdot 10^{-3}$.

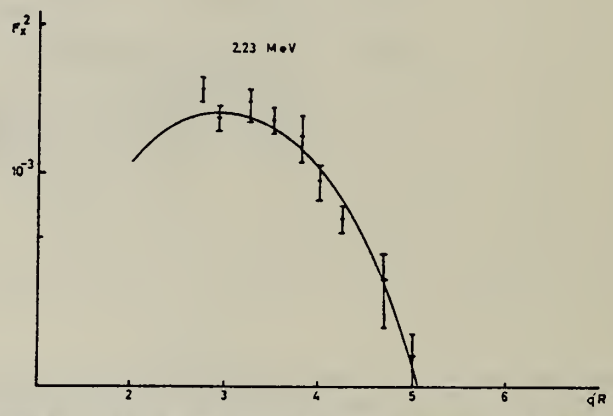

Fig. 6. Le facteur de forme expérimental du niveau à 2.234 MeV. La courbe tracée représente l'expression F_2 multipliée par $\beta_2 = 3.72 \cdot 10^{-3}$.

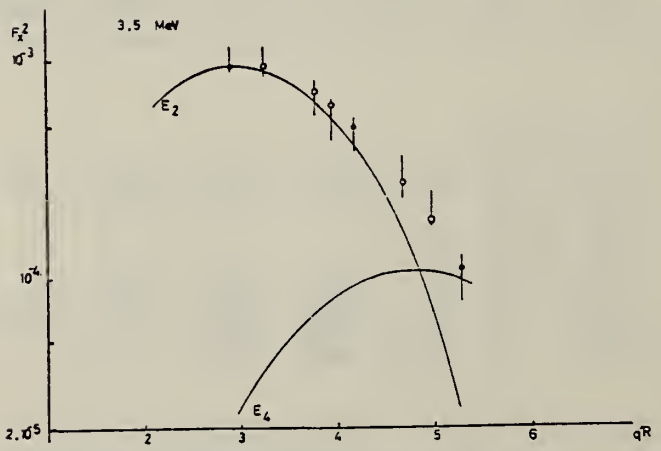

Fig. 7. Le facteur de forme expérimental du pic à 3.47±0.06 MeV. Les courbes tracées représentent F_2 et $F_4 = j_4^2(qR)e^{-q^2\sigma^2}$ multipliées par leurs facteurs de normalisation respectifs $\beta_2 = 1.81 \cdot 10^{-3}$ et $\beta_4 = 1.34 \cdot 10^{-3}$.

REACTION	RESULT	EXCITATION ENERGY	SOURCE		DETECTOR		ANGLE
			TYPE	RANGE	TYPE	RANGE	

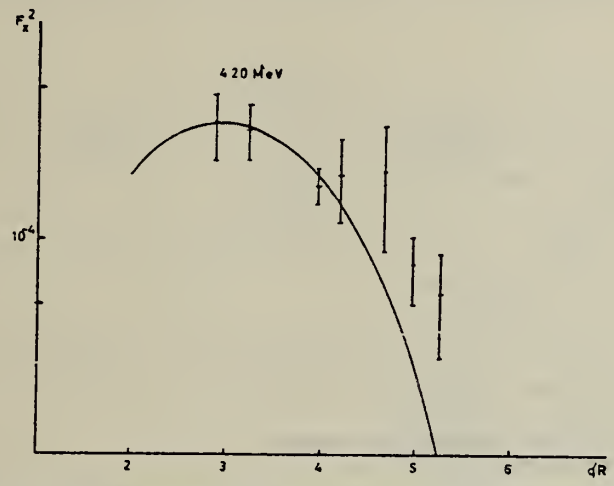

Fig. 8. Le facteur de forme expérimental du pic à 4.20±0.06 MeV. La courbe tracée représente l'expression F_2 multipliée par le facteur de normalisation $\beta_2 = 0.68 \cdot 10^{-4}$.

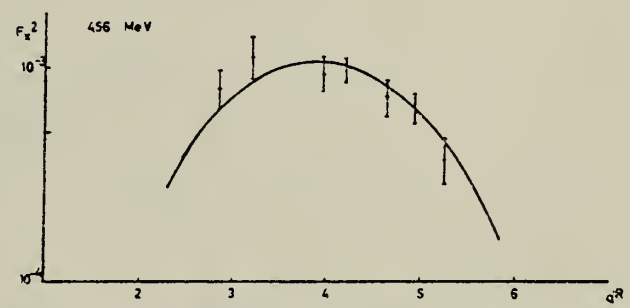

Fig. 9. Le facteur de forme expérimental du pic à 4.56±0.15 MeV. La courbe tracée représente l'expression $F_2 = j_2^2(qR)e^{-q^2a^2}$ multipliée par le facteur de normalisation $\beta_2 = 5.47 \cdot 10^{-4}$.

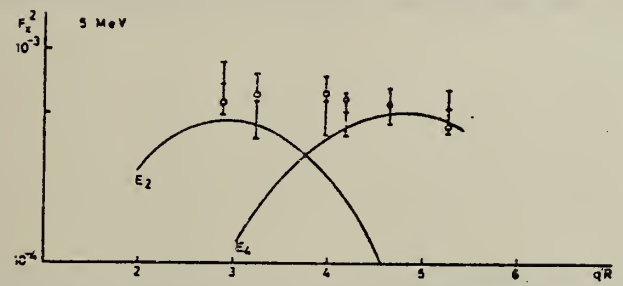

Fig. 10. Le facteur de forme expérimental du pic à 5±0.15 MeV. Les courbes tracées représentent les expressions F_2 et F_4 multipliées par leurs facteurs de normalisation respectifs $\beta_2 = 0.92 \cdot 10^{-4}$ et $\beta_4 = 6.1 \cdot 10^{-3}$.

REACTION	RESULT	EXCITATION ENERGY	SOURCE		DETECTOR		ANGLE
			TYPE	RANGE	TYPE	RANGE	

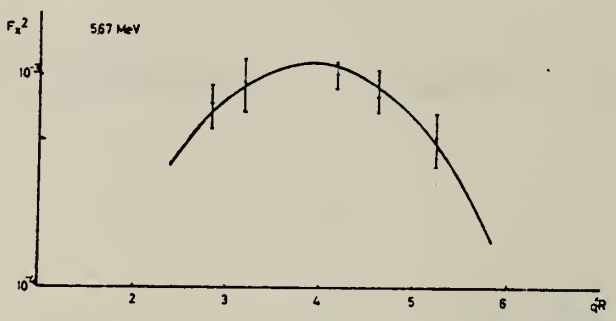

Fig. 11. Le facteur de forme expérimental du pic à 5.67±0.07 MeV. La courbe tracée représente l'expression F_2 multipliée par le facteur de normalisation $\beta_2 = 5.7 \cdot 10^{-3}$.

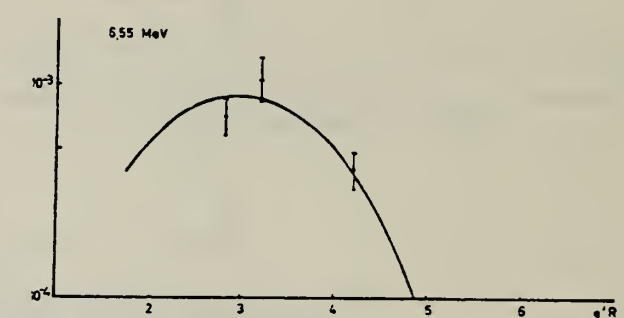

Fig. 12. Le facteur de forme expérimental du pic à 6.55±0.15 MeV. La courbe tracée représente l'expression F_2 multipliée par le facteur de normalisation $\beta_2 = 1.8 \cdot 10^{-3}$.

REF.

J.H. Hough and W.L. Mouton
Nucl. Phys. 76, 248 (1966)

ELEM. SYM.	A	Z
P	31	15

METHOD

1.4 MeV Linac; self-absorption

REF. NO.	
66 Ho 2	JDM

REACTION	RESULT	EXCITATION ENERGY	SOURCE		DETECTOR		ANGLE
			TYPE	RANGE	TYPE	RANGE	
G,G	LFT	1	C	1	NAI-D	0 - 1	117

TABLE 1
Mean lifetimes

Nucleus	State (MeV)	Spin	Mean lifetime (psec) (Hough and Mouton)	Mean lifetime (psec) (Other workers)	Ref.
^{27}Al	1.01	$\frac{1}{2}$	$0.5^{+0.5}_{-0.2}$	5.2 ± 1.7	[4]
				$0.041^{+0.029}_{-0.016}$	[3]
				$1.7^{+1.2}_{-0.5}$	[8]
^{31}P	1.26	$\frac{1}{2}$	$0.73^{+0.19}_{-0.12}$	0.46 ± 0.23	[5]
				0.22 ± 0.07	[6]
				$0.96^{+0.50}_{-0.21}$	[1]
				$0.72^{+0.13}_{-0.10}$	[7]
^{35}Cl	1.22	$\frac{1}{2}$	$0.13^{+0.03}_{-0.02}$	0.30 ± 0.10	[6]

B. S. Ishkhanov, I. M. Kapitonov, Zh. M. Seliverstova, V. G. Shevchenko and B. A. Yur'ev
Izv. Akad. Nauk SSR Fiz. 30, 1385 (1966)
Bull. Acad. Sci. USSR 30, 1446 (1966)

P	31	15

METHOD

REF. NO. 66 Is 2 egf

REACTION	RESULT	EXCITATION ENERGY	SOURCE		DETECTOR		ANGLE
			TYPE	RANGE	TYPE	RANGE	
G,P	SPC	THR-34	C	18,34	EMU-D	2-16	30

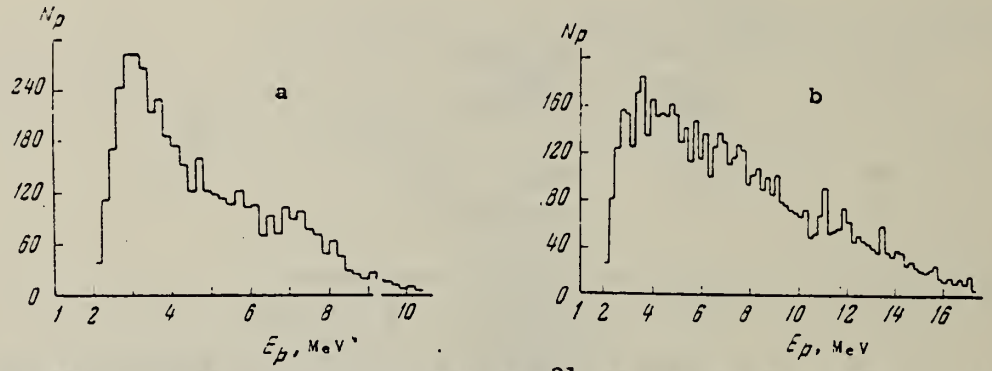

Energy distributions of photoprotons from P^{31}: a - $E_{\gamma\ max}$ = 18 MeV, b - $E_{\gamma\ max}$ = = 34 MeV.

REF.	ELEM. SYM.	A	Z
H. A. Van Rinsvelt and P. M. Endt Physica 32, 513 (1966)	P	31	15

METHOD	REF. NO.
	66 Va 2 JDM

REACTION	RESULT	EXCITATION ENERGY	SOURCE		DETECTOR		ANGLE
			TYPE	RANGE	TYPE	RANGE	
P,G	SPC	8 - 10	D	1 - 2	NAI-D	1 - 11	DST

Angular correlation data given for all resonances.

TABLE I

Resonances in $^{30}Si(p,\gamma)^{31}P$
Proton energies, excitation energies, strengths, total widths, resonance spins, decay modes.

1	2	3	4a	4b	5	6								7
E_p (keV) all ± 0.06%	E_x (MeV)	$(2J+1)\gamma$ (eV) all ± 30%	Γ(keV)		Resonance spin	Decay modes								Also reported in
			(p,γ) work	(p,p) work †		γ_0	γ_1	γ_2	γ_3	γ_4	γ_5	γ_6	Others *)	
1595.3	8.830	0.3			7/2	<2	<2	15	<3	<4	26	<3	$\gamma_{4.19} = 31$; $\gamma_{4.43} = 28$	4)5)6)
1660.4	8.893	0.6	0.11 ± 0.05	0.12 ± 0.05	1/2 +	<2	6	5	36	<3	<3	43	$\gamma_{4.63} = 10$	5)6)6)
1667.4	8.900	0.6			5/2	<1	29	9	<2	10	<2	6	$\gamma_{3.53} = 20$; $\gamma_{5.66} = 26$	5)6)
1694.4	8.926	1.7			3/2(+)	22	6	33	7	<1	<2	<2	$\gamma_{4.76} = 20$; $\gamma_{5.01} = 12$	4)5)6)6)
1746.1	8.976	0.3			3/2	100	<2	<3	<2	<2	<4	<2		
1770.1	8.999	2.0	0.10 ± 0.05	0.08 ± 0.04	5/2 +	16	2	8	<1	<2	<2	21	$\gamma_{4.19} = 35$; $\gamma_{4.26} = 6$; $\gamma_{4.63} = 12$	5)6)
1808.4	9.036	3.1	9.0 ± 1.0	9.8 ± 0.6	3/2 -	84	10	2	4	<2	<2	<2		5)6)9)
1815.2	9.043	0.7			9/2(+)	<3	<3	17	<3	<3	40	<3	$\gamma_{4.19} = 10$; $\gamma_{4.63} = 33$	5)6)
1830.1	9.057	2.4		(0.04 ± 0.02)	5/2 +	<1	5	38	<2	8	16	<2	$\gamma_{4.26} = 7$; $\gamma_{4.63} = 26$	4)5)6)
1875.6	9.101	0.9			7/2	<1	2	43	<2	2	23	5	$\gamma_{4.26} = 14$; $\gamma_{4.76} = 11$	
1878.3	9.104	4.0		(0.04 ± 0.02)	5/2 +	<2	2	48	<2	9	<2	15	$\gamma_{4.19} = 8$; $\gamma_{4.63} = 18$	5)6)5)
1891.6	9.117	0.7		(0.025 ± 0.015)	5/2 +	9	8	17	<2	9	7	4	$\gamma_{4.26} = 9$; $\gamma_{4.56} = 37$	5)
1895.2	9.121	1.1		(0.025 ± 0.015)	5/2	<1	38	2	<2	27	<2	4	$\gamma_{4.76} = 29$	5)6)
1918.2	9.142	0.7			7/2	<2	8	40	<2	<3	13	<3	$\gamma_{4.16} = 22$; $\gamma_{5.25} = 17$	
1920.4	9.144	1.9			3/2(+)	68	6	9	<1	8	<2	4	$\gamma_{5.01} = 5$	5)6)
1941.6	9.165	1.3	0.12 ± 0.05	0.20 ± 0.05	3/2 -	65	3	10	<2	8	<2	<2	$\gamma_{4.76} = 6$; $\gamma_{5.01} = 8$	5)6)
1971.7	9.194	0.5			7/2	<1	8	11	<2	67	<3	<2	$\gamma_{5.12} = 14$	6)6)
1992.8	9.215	0.8	3.1 ± 0.4	3.6 ± 0.2	1/2 -	12	61	<2	<1	<2	<2	5	$\gamma_{6.01} = 22$	5)6)6)

*) Possible transitions not reported here are weaker than 5%.
†) The bracketed widths are preliminary values.

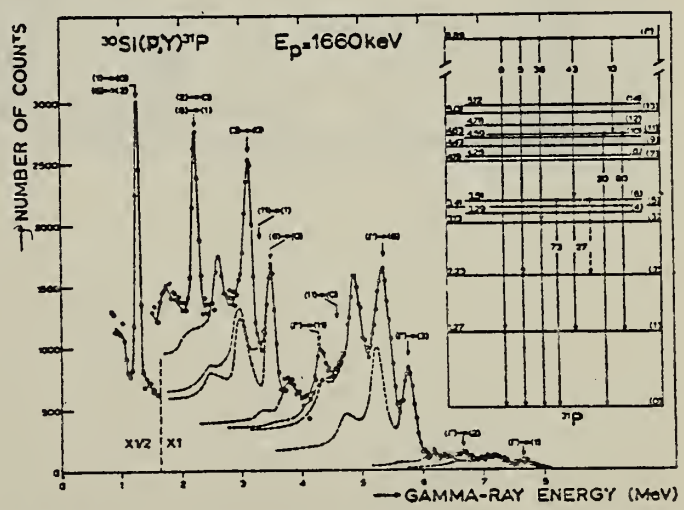

Fig. 2. Single gamma-ray spectrum at the resonance E_p = 1660 keV. The background measured just below the resonance, is subtracted. The spectrum is analysed using the "peeling" procedure. The ^{31}P level scheme can also be used as a guide in reading the rest of the text.

REF. C. H. Bornman, M. A. Meyer and D. Reitmann
Nucl. Phys. A99, 337 (1967)

ELEM. SYM.	A	Z
P	31	15

METHOD

REF. NO. 67 Bo 1 EGF

REACTION	RESULT	EXCITATION ENERGY	SOURCE		DETECTOR		ANGLE
			TYPE	RANGE	TYPE	RANGE	
P,G	NOX	9-10	D	2-3	NAI-D	1-10	55

TABLE 2

Proton energies, excitation energies and principal decay modes of resonances in $^{30}Si(p, \gamma)^{31}P$

E_p (keV)	E_x (MeV)	γ_0	γ_1	γ_2	γ_3	γ_4	γ_5	γ_6	γ_7	γ_8	Primary transitions to higher levels
1939	9.16	58	4	15	<3	9	<3	<3			$\gamma_{4.78} = 7$ $\gamma_{5.01} = 7$
2007	9.23	34		23	6					13	$\gamma_{4.78} = 15$ $\gamma_{5.63} = 9$
2021	9.24						58				$\gamma_{1.43} = 9$ $\gamma_{5.63} = 33$
2090	9.31	14	35		41					10	
2173	9.39	23	19	<5	37					21	
2186	9.40			5	5						$\gamma_{1.43} = 90$
2215	9.43	27	10	12		20				25	$\gamma_{1.63} = 6$
2223	9.44		25	13		15			15		$\gamma_{1.63} = 17$ $\gamma_{5.63} = 15$
2302	9.51	8	8	<5	<5			18	51		$\gamma_{5.77} = 15$
2315	9.53		10	75							$\gamma_{8.48} = 9$ $\gamma_{6.01} = 6$
2352	9.56	86	<4	<4	10	<4					$\gamma_{5.01} = 4$
2358	9.57	23	5	47		12			6		$\gamma_{5.01} = 7$
2375	9.58	41	59								weak
2542	9.75		65	18				10			$\gamma_{4.59} = 7$
2546	9.75	2	73	18							$\gamma_{4.63} = 7$
2551	9.76	11	57	6		11			9		$\gamma_{4.63} = 6$
2632	9.83	20	33	30							$\gamma_{4.78} = 17$
2641	9.84			56			23		21		$\gamma_{4.26} < 5$
2655	9.86	3		60	17				11		$\gamma_{5.88} = 9$
2657	9.86	64	13		23						weak
2698	9.90	50		11			30				$\gamma_{5.01} = 9$
2733	9.93			40					18		$\gamma_{4.63} = 15$ $\gamma_{5.25} = 10$ $\gamma_{5.86} = 17$
2814	10.01	4	34	34		14				7	$\gamma_{6.46} = 7$
2842	10.04	3	63	<3		19				11	$\gamma_{5.01} = 4$
2872	10.07						50				$\gamma_{5.25} = 50$
2886	10.08	6	40				9	6			$\gamma_{4.59} = 8$ $\gamma_{4.68} = 8$ $\gamma_{5.89} = 23$
2896	10.09	27	20	16	37						
2943	10.13	3	19	24			19		10		$\gamma_{4.59} < 5$ $\gamma_{6.46} = 25$
2993	10.18	7	66		13				10		$\gamma_{4.78} = 4$
3011	10.20	7		34		27			9		$\gamma_{6.01} = 23$
3027	10.22		22	28			37			13	

REF.	ELEM. SYM.	A	Z
H. M. Gerstenberg and E. G. Fuller NBS Tech. Note 416, June 1967	P	31	15

METHOD	REF. NO.
	67 Ge 2 HMG

REACTION	RESULT	EXCITATION ENERGY	SOURCE		DETECTOR		ANGLE
			TYPE	RANGE	TYPE	RANGE	
G,N	ABY	THR-27	C	22,27	BF3-I		4PI

Table 7. Comparison of neutron yields. Yields are given in units of (neutron cm^2/MeV nucleus)$\times 10^{-28}$. The estimated uncertainties in Y and Y_c are of the order of 6% and 10%, respectively.

Element	E_o	$Y(E_o)$	Y_c				Y_c/Y				Ref.
			UCRL	Saclay	Va.	NBS(Old)	UCRL Exp	Saclay Exp	Va. Exp	NBS(Old) Exp	
Pb	27	103	86				0.83				26,30
	22	111	92	116			0.83	1.05			
Au	27	89	97				1.09				24,30,
	22	92	98	88		115	1.07	0.96		1.25	38
Ta	27	81	82	77			1.01	0.95			27,30,
	22	85	79	80		113	0.93	0.94		1.33	38
Ho	27	67	75				1.12				27,31,
	22	69	77	82		103	1.12	1.19		1.49	39
Ag	27	36									
	22	34.8									
Cu	27	14.4	13.2				0.92				28,30
	22	12.6	11.5	12.4			0.91	0.98			
Co	27	12.7	12.1				0.95				29,34
	22	10.6	9.9		13.5		0.94		1.27		
Ca	27	1.69		1.13	1.01			0.67	0.60		32,35
P	27	2.35			1.76				0.75		36
Al	27	1.92	1.62		1.38		0.84		0.72		25,37
O^{16}	27	0.54	0.42	0.48	0.42		0.78	0.89			16,32, 37
C	27	0.50	0.35	0.33	0.46		0.70	0.66			25,32, 33

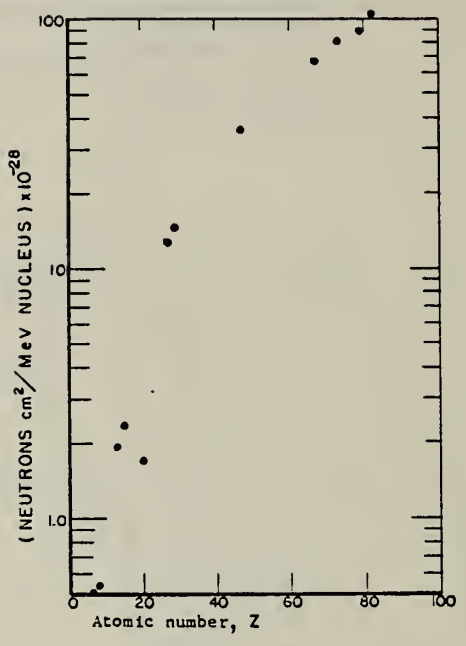

Fig. 31. Absolute neutron yield as a function of atomic number. The neutron yield from calcium (Z = 20) is particularly low in comparison with the other elements because its (γ,n) threshold is high compared to the mean energy of the giant resonance.

REF.	ELEM. SYM.	A	Z
M. Mishina, E. Tanaka, K. Kageyama, N. Mutsuro, A. Asami, Y. Kawarasaki and Y. Nakajima J. Phys. Soc. Japan 23, 919 (1967)	P	31	15

METHOD	REF. NO.	
	67 Mi 2	egf

REACTION	RESULT	EXCITATION ENERGY	SOURCE		DETECTOR		ANGLE
			TYPE	RANGE	TYPE	RANGE	
G,XN	SPC	THR-20	C	23-27	TOF-D	2-12	100

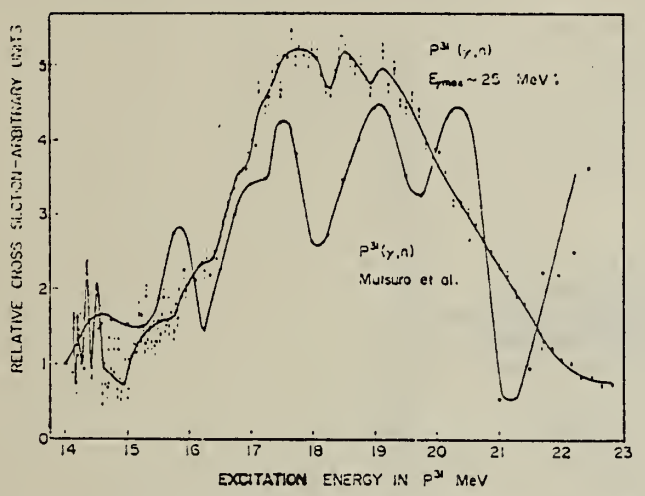

Fig. 11. Relative cross section for $P^{31}(\gamma, n)P^{30}$, deduced from the time spectrum in Fig. 9 assuming the ground state transition only.

REF.	ELEM. SYM.	A	Z
K. Abe, N. Kawamura, and N. Mutsuro J. Phys. Soc. Japan 25, 1725 (1968)	P	31	15
METHOD	REF. NO.		
	68 Ab 4		egf

REACTION	RESULT	EXCITATION ENERGY	SOURCE		DETECTOR		ANGLE
			TYPE	RANGE	TYPE	RANGE	
G,XP	SPC	THR-27	C	22,27	SCD-D	3-16	90
				(21.5)			

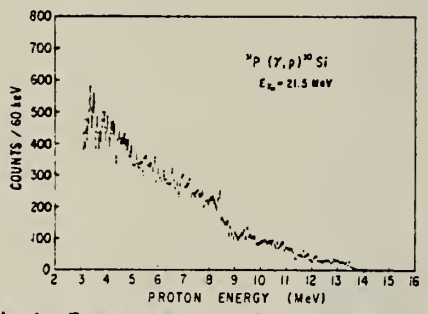

Fig. 1. Energy spectrum of photoprotons from phosphorus at 90°, with bremsstrahlung end-point energy 21.5 MeV.

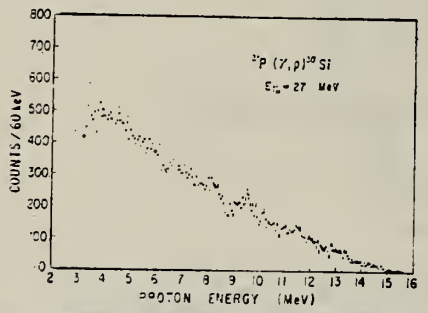

Fig. 2. Energy spectrum of photoprotons from phosphorus at 90°, with bremsstrahlung end-point energy 27 MeV.

REF.

W. L. Creten, R. J. Jacobs and H. M. Ferdinande
Nucl. Phys. A107, 347 (1968)

ELEM. SYM.	A	Z
P	31	15

METHOD

REF. NO.	
68 Cr 1	EGF

REACTION	RESULT	EXCITATION ENERGY	SOURCE		DETECTOR		ANGLE
			TYPE	RANGE	TYPE	RANGE	
G,G	LFT	3	C	3	NAI-D	0-3	135
		(3.13)					

Self-absorption measurement gives $\Gamma = 49 \pm 10$ MeV.

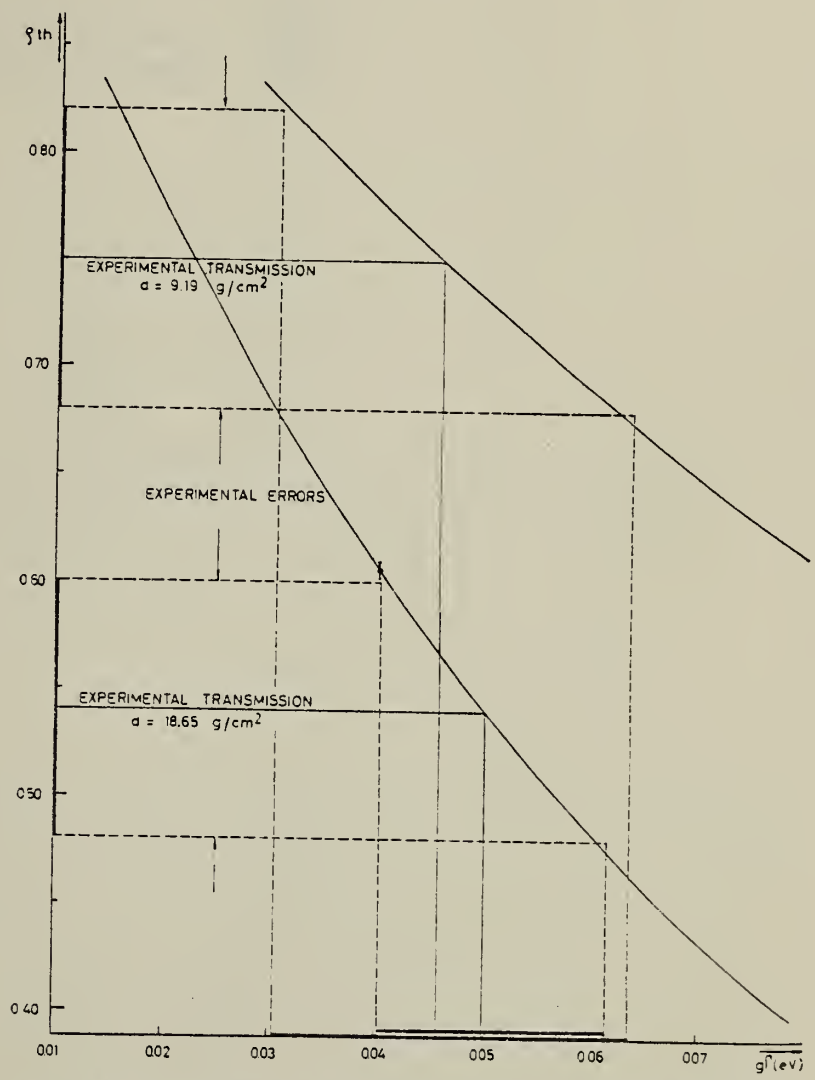

Fig. 4. Theoretical transmission versus $g\Gamma$ for both absorbers. The error flag indicates the u certainty in the theoretical transmission. The arrows indicate the experimental uncertainties.

REF.
J. H. Hough, Z. B. du Toit and W. L. Mouton
Nucl. Phys. A109, 393 (1968)

ELEM. SYM.	A	Z
P	31	15

METHOD

REF. NO.: 68 Ho 1 | EGF

REACTION	RESULT	EXCITATION ENERGY	SOURCE		DETECTOR		ANGLE
			TYPE	RANGE	TYPE	RANGE	
G,G	LFT	7-8	D	7-8	NAI-D	6-8	0

Measured self-absorption of $^{30}Si(p,\gamma)^{31}P$ radiation at E_p = 945 keV and 622 keV

E_o	Γ_t	$\Gamma_{\gamma o}$
8.201	2.6±0.2 eV	1.4±0.1 eV
7.90	68±9 eV	1.6±0.2 eV

REF. S. W. Robinson, C. P. Swann, V. K. Rasmussen
Phys. Rev. 174, 1320 (1968)

ELEM. SYM.	A	Z
P	31	15

METHOD

REF. NO. 68 Ro 1 HMG

REACTION	RESULT	EXCITATION ENERGY	SOURCE		DETECTOR		ANGLE
			TYPE	RANGE	TYPE	RANGE	
G,G	LFT	3.0	C	3	NAI-I		
		(3.13)					

E_o = 3.13 MeV Γ_o/Γ = 1 Γ = 66.3±7 MeV.

SELF-ABSORPTION

REF. K. Shoda, K. Abe, T. Ishizuka, N. Kawamura, M. Oyamada, and Baik-Nung Sung
J. Phys. Soc. Japan 25, 664 (1968)

ELEM. SYM.	A	Z
P	31	15

METHOD

REF. NO. 68 Sh 3 egf

REACTION	RESULT	EXCITATION ENERGY	SOURCE TYPE	SOURCE RANGE	DETECTOR TYPE	DETECTOR RANGE	ANGLE
G,XP	SPC	THR-19	D	19	EMU-D	2-14	DST

Table III. Anisotropic factor B/A of angular distributions estimated for the groups of strong transitions.

	Assumed residual Energy (MeV)	E_γ (MeV)	B/A	Used data[a]
^{23}Na	1.27	18.8–20.5	0.5±0.4	20.5
	3.3	20.8–22.1	∞[b]	D
		22.1–24	∞[b]	24.0
	7.0	20.7–22.7	1.5±0.3	D
^{31}P	0	15.7–21	∞[b]	24.0,19.0
	7.0	17.4–20.2	0.5±0.6	D
		20.2–22.7	1.3±1.3	D
^{32}S	0	14–20	∞[b]	(p, γ_0)
		14–14.8	2.4±0.7	17.0
		14.8–16.2	∞[b]	17.0
		16.2–17.1	∞[b]	17.0
	5.0	19.2–20.1	0.5±0.2	D
		20.1–21.3	0.4±0.2	D
^{40}Ca	0	17.1–20.5	1.5±0.2	20.5
	2.8	17.4–19.9	2.6±0.3	20.5
	6.0	17.2–18.7	0.05±0.09	20.5
		18.7–20.5	0.6±0.1	20.5

a) The numerical number indicates the maximum energy of the bremsstrahlung irradiated for the data. D shows the difference between the two distributions. (p, γ_0) shows the inverse reaction data.
b) The notation ∞ indicates that the distribution is almost $\sin^2\theta$, *i.e.*, the result has stronger maximum than $1+10\sin^2\theta$.

Table II. Anisotropic factor B/A of angular distributions determined by least-squares fits with $A+B\sin^2\theta$.

^{31}P					
($E_{\gamma max}$=19.0 MeV)		($E_{\gamma max}$=24.0 MeV)[b]		(Curve D in Fig. 2)	
E_p(MeV)	B/A	E_p(MeV)	B/A	E_p(MeV)	B/A
3.9–5.5	0.6±0.1	3.0–4.6	0.9±0.4	3.0–5.7	0.5±0.6
5.5–7.9	1.3±0.3	4.6–6.0	0.4±0.3	5.7–8.1	1.3±1.3
7.9≦	∞[a]	6.0–8.2	1.3±0.6	8.1–11.3	∞[a]
3.9≦	1.7±0.2	8.2≦	∞[a]		
		3.0≦	1.1±0.3		

a) The notation ∞ indicates that the distribution is almost $\sin^2\theta$. It is used when the result has stronger maximum than that of $1+10\sin^2\theta$.
b) The data are used from ref. 4).

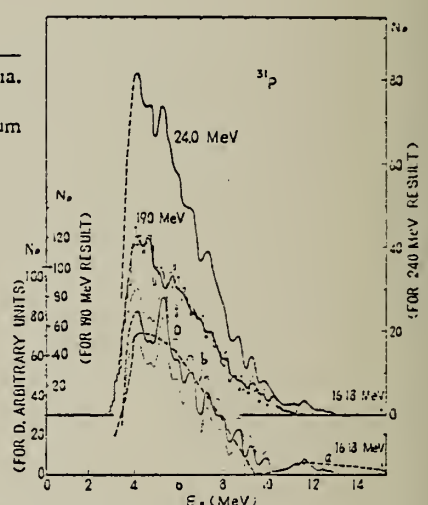

Fig. 2. Energy distributions of photoprotons from ^{31}P irradiated with 19.0 MeV bremsstrahlung. The early data on 24.0 MeV bremsstrahlung[4] is also shown. See also the caption of Fig. 1 for curves D, a and b. Here a and b correspond to the ground and 7.0 MeV state of residual nucleus respectively.

[4] K. Shoda et al.: J. Phys. Soc. Japan 16, (1961) 1807.

REF.

A. C. Wolff, M. A. Meyer and P. M. Endt
Nucl. Phys. A107, 332 (1968)

ELEM. SYM.	A	Z
P	31	15

METHOD

[Page 1 of 2]

REF. NO. 68 Wo 1

EGF

REACTION	RESULT	EXCITATION ENERGY	SOURCE		DETECTOR		ANGLE
			TYPE	RANGE	TYPE	RANGE	
P,G	SPC	0-9	D	1-2	SCD-D	0-9	90

TABLE 2

Branching ratios of bound states of ^{31}P (in percent)

Bound state		Decay to (E_x in ^{31}P in MeV)							
E_x (MeV)	J^{π} [a]	0 $\frac{1}{2}^+$	1.27 $\frac{3}{2}^+$	2.23 $\frac{5}{2}^+$	3.29 $\frac{5}{2}^+$	3.41 $\frac{7}{2}^+$	4.19 $\frac{5}{2}^+$	4.43 $\frac{7}{2}^-$	other levels
1.27	$\frac{3}{2}^+$	100							
2.23	$\frac{5}{2}^+$	100							
3.13	$\frac{1}{2}^+$	100							
3.29	$\frac{5}{2}^+$		84±2	16±2					
3.41	$\frac{7}{2}^+$		100						
3.51	$\frac{3}{2}^+$	62±4	38±4	≦ 6					
4.19	$\frac{5}{2}^+$		76±2	24±2					
4.26	$\frac{3}{2}^+$	75±3	25±3						
4.43	$\frac{7}{2}^-$			55±2	41±2	4±1			
4.59	$\frac{3}{2}^*$	24±4	54±5	22±6					
4.63	$(\frac{5}{2}, \frac{7}{2})^*$			25±3	47±5	28±3			
4.78	$\frac{5}{2}^{+*}$	42±3	12±3	15±3	31±3				
5.01	$(\frac{3}{2}, \frac{1}{2})^*$	68±3	32±3						
5.02	$(\frac{3}{2}, \frac{1}{2})^*$	40±3	60±3						
5.12	$(\frac{5}{2})^*$		40	20					unknown 40
5.25	$\frac{1}{2}^+$	100							
5.34	$(\geq\frac{5}{2})^*$			29±8	21±8	50±10			
5.53	$(\frac{5}{2})^{+*}$			30		35			unknown 35
5.56	$(\frac{3}{2})^*$	82±5		18±5					
5.67	$(\frac{5}{2})^*$		55	10		10		10	unknown 15
5.77	$(\frac{5}{2}, \frac{7}{2})^*$			15		20			4.63 25, unknown 40
5.89	$(\frac{5}{2}, \frac{7}{2})^*$			100					
5.99	$(\frac{3}{2})^*$			80±15					5.12 20±15
(6.10)		100							
(6.23)						40			unknown 60
6.38	$\frac{3}{2}^+, T=\frac{3}{2}$	18±5		82±5					
6.40	$(\frac{5}{2}, \frac{7}{2})^*$			2±1	6±2		7±3	75±4	5.12 6±2, 5.67 4±1
6.50	$(\frac{1}{2}, \frac{3}{2})^*$	60							unknown 40
6.59	$(\frac{3}{2})^*$		70						unknown 30
6.61	$(\frac{3}{2})^{-*}$	23±8							4.63 41±9, 5.01 or 5.02 36±9
6.84	$(\frac{1}{2}, \frac{5}{2})^*$						100		
(6.91)		60							unknown 40
6.93	$(\frac{5}{2}, \frac{7}{2})^*$			83±6				17±6	
7.14	$\frac{1}{2}^+, T=\frac{3}{2}$	100							

[a]) From ref. [1]) with additional information (marked with an asterisk) from the present work (see text).

TABLE 3a

Branching of $^{30}Si(p,\gamma)^{31}P$ resonances (in percent) for $E_p \leqq 1480$ keV

Resonances			Decay to (E_x in ^{31}P in MeV)															
E_p [a] (keV)	E_x (keV)	J^π [a]	0 $\frac{1}{2}^+$	1.27 $\frac{1}{2}^+$	2.23 $\frac{3}{2}^+$	3.13 $\frac{5}{2}^+$	3.29 $\frac{3}{2}^+$	3.41 $\frac{5}{2}^+$	3.51 $\frac{7}{2}^+$	4.19 $\frac{5}{2}^+$	4.26 $\frac{1}{2}^+$	4.43 $\frac{3}{2}^-$	4.59 $\frac{3}{2}$	4.63	4.78 $\frac{3}{2}^+$	5.01[b]	5.02[b]	other levels
499	7 780	$\frac{1}{2}^-$	48	29	6	11					1				3	2		
620	7 898	$\frac{1}{2}$	93	2		1			1							3		
671	7 946	$\frac{3}{2}$	13	20		4	5		16	26			2		9			
760	8 033	$\frac{3}{2}$	2	18	5		4	10	24	28		1		3	5			
777	8 050	$\frac{1}{2}$	63		2	3	2		14	5						3		5.67(3)
855	8 105	$\frac{3}{2}$		65			5		2	11	2				2			5.77(3), 5.99(2), 6.23(8)
942*	8 209	$\frac{3}{2}$	60	24	10		2		2						1			5.25(1)
959*	8 225	$(\frac{5}{2}, \frac{7}{2})^*$					50	1		3				3	11			5.12(4), 6.40(26), 6.84(2)
978*	8 244	$(\frac{7}{2})^*$		1	1			10		2	1	55					1	5.67(24), 6.84(3), 6.91(2)
983*	8 248	$\frac{5}{2}$	66	4	9	10			1								3	5.25(1), 6.50(1), 6.59(2) [c]
1 095	8 356	$\frac{5}{2}$	1	46			14	1	6		4	2	19		3			6.84(1), 6.93(3)
1 175	8 435	$\frac{7}{2}$			41		33	2		4				4				5.89(2), 6.40(10), 6.59(4)
1 203	8 462	$\frac{5}{2}^{(+)}$		4	25	2	28		13		23		1	4				
1 213	8 471	$\frac{5}{2}$		29			18	3	24	3		4					6	5.67(7), 6.59(4), 6.84(2)
1 289	8 544	$\frac{1}{2}^-$		9		54					1		2			34		
1 298	8 553	$\frac{1}{2}^+$		84	1				6		1						3	5.56(5)
1 301	8 556	$\frac{7}{2}^-$	31	14	25	12			1							12		5.25(5)
1 322	8 576	$\frac{3}{2}^+$		38	10		3	4	27	4	9			2				5.53(3)
1 331	8 585	$\frac{5}{2}$	27	14					15				24				4	6.10(8), 6.61(10)
1 348	8 602	$\frac{5}{2}$			5		10	56				4		10	2			5.89(13)
1 390	8 642	$\frac{5}{2}$		49	20		8	2	5	4		4	3	1				5.12(4)
1 398	8 650	$\frac{7}{2}^{(+)}$	3	73	1	13	3			2	3		1					5.99(1)
1 480	8 730	$\frac{5}{2}^{(+)}$	80	1	8	4	4				1				2			

[a] From ref. [1]) with additional information (marked with an asterisk) from the present work (see text).
[b] Numbers in between these two columns indicate that it is uncertain whether the $E_x = 5.01$ or 5.02 MeV level is excited.
[c] Also to 6.61(2) and 6.84(1).

TABLE 3b

Branching of $^{30}Si(p,\gamma)^{31}P$ resonances (in percent) for $E_p \geqq 1482$ keV

Resonances			Decay to (E_x in ^{31}P in MeV)															
E_p [a] (keV)	E_x (keV)	J^π [a]	0 $\frac{1}{2}^+$	1.27 $\frac{1}{2}^+$	2.23 $\frac{3}{2}^+$	3.13 $\frac{5}{2}^+$	3.29 $\frac{3}{2}^+$	3.41 $\frac{5}{2}^+$	3.51 $\frac{7}{2}^+$	4.19 $\frac{5}{2}^+$	4.26 $\frac{1}{2}^+$	4.43 $\frac{3}{2}^-$	4.59 $\frac{3}{2}$	4.63	4.78 $\frac{1}{2}^+$	5.01[b]	5.02[b]	Other levels
1 482	8 731	$\frac{5}{2}$	68	2	14	5	2		2				3			4		
1 490	8 739	$\frac{1}{2}^+$	4	8	9	8	37		2						12		13	5.25(2), 5.56(5)
1 510	8 758	$\frac{1}{2}^+$		55	7			26	1			4	3	1	3			
1 516	8 764	$\frac{1}{2}^+$	34	4		4										8		
1 595	8 841	$\frac{5}{2}$			9		3	17		4		7			6			5.67(4), 5.89(6), 6.40(32) [c]
1 660	8 904	$\frac{1}{2}^+$	2	5	1	38			47				4					5.99(3)
1 667	8 910	$\frac{3}{2}$	2	25	8		3	4	–	3		13		2				5.56(9), 5.67(24), 5.99(2) [d]
1 694	8 936	$\frac{3}{2}^{(+)}$	18	6	35	4	2		4		7				14		2	5.12(7), 7.14(1)
1 746	8 987	$\frac{5}{2}$	60															unknown 40
1 770	9 010	$\frac{1}{2}^+$	11	1	6			3	15	35		3	6	4	1			5.53(6), 5.77(6), 6.38(3)
1 808	9 047	$\frac{3}{2}^+$	90	4		6												
1 815	9 053	$(\frac{3}{2})^*$		17	10			24	8	3			9			6		5.67(13), 6.38(7), 6.93(3)
1 830	9 068	$\frac{1}{2}^+$	1	3	37		10	9	1	3		2	2	20	5			5.53(5), 5.99(2)
1 875	9 112	$\frac{3}{2}$			48		7	20		8					8			5.89(9)
1 878	9 114	$\frac{3}{2}^+$			51		5		8	8			9	3	2			5.53(6), 5.56(8)
1 891	9 127	$\frac{3}{2}^+$	7	9	26		6	12	10		4			26				
1 895	9 131	$\frac{3}{2}^+$		36			22				5	21		2	14			
1 918	9 153	$\frac{5}{2}$		7	47			13		14					1			5.34(16), 5.77(2)
1 920	9 155	$\frac{7}{2}^{(+)}$	69	5	11		12									3		
1 941	9 176	$\frac{3}{2}^-$	57	2	13		5						1			8		5.56(1), 5.67(7), 6.61(6)
1 971	9 205	$\frac{5}{2}$		6	7		81											5.12(6)
1 992	9 225	$\frac{3}{2}^-$	10	58		1			6								19	6.50(2), 6.61(2), 7.14(2)
2 187	9 413	$\frac{3}{2}^+$			3			2				88						5.12(2), 5.34(1), 5.67(3) [e]

[a] From ref. [1]) with additional information (marked with an asterisk) from the present work (see text).
[b] Numbers in between these two columns indicate that it is uncertain whether the $E_x = 5.01$ or 5.02 MeV level is excited.
[c] Also to 6.93(12). [d] Also to 6.59(3). [e] Also to 5.89(1).

REF. B.S. Ishkhanov, I.M. Kapitonov, E.V. Lazutin, I.M. Piskarev and V.G. Shevchenko
Izv. Akad. Nauk. Fiz. 33, 1742 (1969)
Bull. Acad. Sci. USSR-Phys. 33, 1594 (1969)

ELEM. SYM.	A	-
P	31	15

METHOD

REF. NO. 69 Is 3 hmg

REACTION	RESULT	EXCITATION ENERGY	SOURCE		DETECTOR		ANGLE
			TYPE	RANGE	TYPE	RANGE	
G,XN	ABX	12-30	C	5-30	BF3-I		4PI

454

$\int_{1a}^{30} \sigma dE = 211 \pm 20$ MeV mb

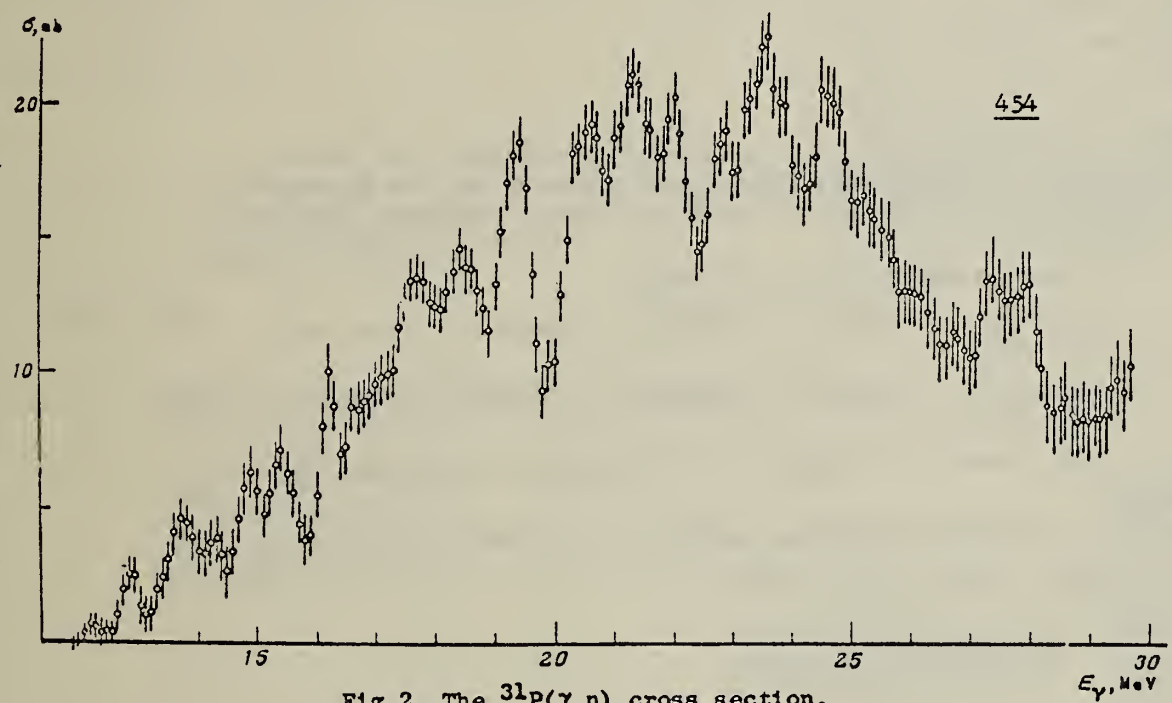

Fig.2. The $^{31}P(\gamma,n)$ cross section.

(over)

Positions (MeV) of Resonances in $^{27}Al(\gamma,n)$ and $^{31}P(\gamma,n)$

Aluminum					Phosphorous		
Our work	Ref.4	Ref.9	Ref.10	Ref.7	Our work	Ref.6	Ref.8
13,3		—	—		12,8		
	13,8			13,7	13,7		13,3
14,1		14,2					
	14,5	14,5	14,6		14,3		
14,9				14,7			
	15,4	15,2			14,8	14,75	14,6
15,6	15,7	15,6		15,75	15,4	15,75	
		16,1			16,2		15,8
16,5	16,4	16,4	16,4				17,1
	17,0	17,0		17,1	17,7	17,25	17,5
18,0	17,7	17,6					
	18,2	18,1	18,1	18,25	18,4	18,25	
19,1				19,1	19,3	19,25	19,0
		19,6					
20,0	20,0		19,8		20,5	20,25	20,3
		20,5			21,3	21,25	
21,1		21,2	21,4		22,0		
	21,5					22,75	
22,0	22,0				23,6		
		22,4			24,6	24,25	
23,0	23,1						
24,1					27,5		
25,0							
27,8	27,2						

[4] A.N. Tikhonov, V.G. Shevchenko, V.Ya. Galkin, B.I. Goryachev, P.N. Zaikin, B.S. Ishkhanov & I.M. Kapitonov, Program and Abstracts for the Eighteenth Annual Conference on Nuclear Spectroscopy and Nuclear Structure, Riga, M.-L. 1968, p. 268.

[6] L.N. Bolen & W.D. Whitehead, Ibid. 132, 5 (1965).

[7] N. Mutsuro, K. Kageyama, M. Mishina, E. Tanaka & M. Kimura, J. Phys. Soc. Japan 17, 1673 (1962).

[8] N. Mutsuro, K. Kageyama, M. Mishina, T. Nakagawa, E. Tanaka & M. Kimura, Ibid. 17, 1672 (1962).

[9] M.N. Thompson, J.M. Taylor, B.M. Spicer & J.E.E. Baglin, Nuclear Phys. 64, 486 (1965).

[10] L.N. Bolen & W.D. Whitehead, Phys. Rev. Letters 9, 458 (1962).

[13] J.E.E. Baglin, Nuclear Phys. 22, 216 (1961).

V. I. Noga, Yu. N. Ranyuk, and P. V. Sorokin
Yad. Fiz. 9, 1152 (1969)
Sov. J. Nucl. Phys. 9, 673 (1969)

P	31	15

METHOD

REF. NO. 69 No 1 egf

REACTION	RESULT	EXCITATION ENERGY	SOURCE		DETECTOR		ANGLE
			TYPE	RANGE	TYPE	RANGE	
G,NA24	ABY	69-999	C	100-999	ACT-I		4PI

999 = 1.2 GEV

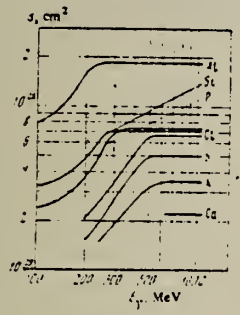

FIG. 2. Cross sections as a function of γ-ray energy.

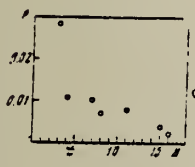

FIG. 3. Dependence of P on number of nucleons which have left the nucleus.

Table I

Reaction	Nucleons emitted	Threshold*, MeV	Target	Distribution of isotopes, %
$Al^{27} \rightarrow Na^{24}$	2p, α	31	Al	100
$Si^{29} \rightarrow Na^{24}$	3p, α	43	Si	92,27
$P^{31} \rightarrow Na^{24}$	4p, 3n	69	P	100
$S^{32} \rightarrow Na^{24}$	5p, 3n	78	S	95,02
$Cl^{35} \rightarrow Na^{24}$	6p, 5n	105	NH_4Cl	75,4
$K^{39} \rightarrow Na^{24}$	8p, 7n	140	K_2CO_3	93,08
$Ca^{40} \rightarrow Na^{24}$	9p, 7n	148	CaO	96,97

*The threshold was calculated as the binding energy of the emitted nucleons.

Table II. Cross sections for reactions in the saturation region

Reaction	σ_P, 10^{-28} cm²	Reaction	σ_P, 10^{-28} cm²
$Al^{27} \rightarrow Na^{24}$	185±20	$Cl^{35} \rightarrow Na^{24}$	69±7
$Si^{29} \rightarrow Na^{24}$	72±8	$K^{39} \rightarrow Na^{24}$	35±5
$P^{31} \rightarrow Na^{24}$	71±8	$Ca^{40} \rightarrow Na^{24}$	22±5
$S^{32} \rightarrow Na^{24}$	52±6		

FIG. 1. Cross section σ_Q per equivalent photon as a function of maximum bremsstrahlung energy. Points: ○ – Al, ● – Si, △ – P, ▲ – S, □ – Cl, ■ – K, ◇ – Ca.

According to the photomesonic mechanism, the cross section for the reaction can be written in the form

$$\sigma = \sigma_0 AP. \qquad (1)$$

Here σ_0 is the total cross section for interaction of the photon with a free nucleon with inclusion of the nucleon motion in the nucleus (σ_0, as has been shown by Roos and Peterson,[5] depends only weakly on photon energy for $E_\gamma > 300$ MeV); A is the number of nucleons in the nucleus, and P is the probability that the reaction will proceed by a given channel.

V. K. Rasmussen and C. P. Swann
Phys. Rev. 183, 918 (1969)

P	31	15

METHOD

REF. NO. 69 Ra 3 hmg

REACTION	RESULT	EXCITATION ENERGY	SOURCE TYPE	SOURCE RANGE	DETECTOR TYPE	DETECTOR RANGE	ANGLE
G,G	LFT	3	C	3	NAI-D		DST
		(3.51)		(3.66)			(96,128)

Γ = 52±8 MeV. The width of the level was determined by comparing the scattering with that by the ^{31}P and ^{6}Li 3.56 MeV levels.

3 = 3.51 MEV

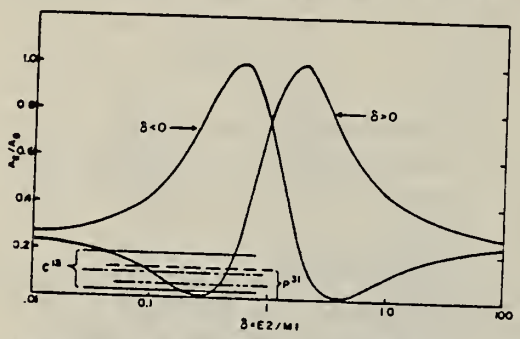

FIG. 5. Plot of the angular distribution coefficient A_2/A_0 for the spin sequence $\frac{1}{2}$-$\frac{3}{2}$-$\frac{1}{2}$. The A_4 term is identically zero for this sequence. The experimental limits for the C^{13} and P^{31} distributions are indicated.

REF. G. Wiechers, W. R. McMurray and I. J. Van Heerden
Nucl. Phys. A124, 165 (1969)

ELEM. SYM.	A	Z
P	31	15

METHOD

REF. NO. 69 Wi 1 egf

REACTION	RESULT	EXCITATION ENERGY	SOURCE		DETECTOR		ANGLE
			TYPE	RANGE	TYPE	RANGE	
P,G	LFT	10-11	D	3-4	NAI-I	0-11	55

G-G CORRELATION

TABLE 1

Properties of levels in ^{31}P

E_p (MeV) ±3 keV	^{31}P* (MeV)	J^π	$(2J+1)\Gamma_p\Gamma_\gamma/\Gamma$ (eV) ±50 %	Resonance width (keV)	Relative decay γ_0	γ_1	γ_2
2.995	10.185	$\frac{1}{2}^-$	5.0		1	5	4
3.011	10.201	$\frac{3}{2}^+$	7.0		4	4	2
3.013	10.202	$\frac{7}{2}^-$	3.0		1	1	8
3.027 a)	10.216		3.3		1	3	6
3.034	10.223	$\frac{1}{2}^-$	3.5		1	5	4
3.070	10.258	$\frac{1}{2}^-$	3.6		1	4	5
3.074	10.262	$\frac{1}{2}^-$	2.6		1	3	6
3.091	10.279	$\frac{1}{2}^-$	4.5		1	2	7
3.108	10.295	$\frac{3}{2}^+$	3.5		1	3	6
3.140	10.325	$\frac{3}{2}^+$	1.2		1	2	7
3.191	10.375	$\frac{3}{2}^+$	2.5		1	3	6
3.208	10.391	$\frac{5}{2}(^+)$	3.6		1	3	6
3.233	10.415	$(\frac{1}{2}, \frac{3}{2})$	1.0		4	3	3
3.264	10.446		0.9		0	4	6
3.293	10.473	$\frac{3}{2}^+$	1.8		0	3	7
3.295	10.476	$\frac{3}{2}^+$	3.0		2	5	3
3.297	10.478	$\frac{1}{2}^-$	2.9		4	3	3
3.313	10.494		0.8		1	3	6
3.349	10.530	$\frac{1}{2}^-$		16	5	3	2
3.377	10.555	$\frac{3}{2}^+$	1.5		3	4	3
3.422	10.599	$\frac{3}{2}^+$	9.1		1	3	6
3.435	10.612		5.0		1	4	5
3.445	10.620		3.0		1	3	6
3.461	10.636	$\frac{3}{2}^+$	3.0		2	4	4
3.466	10.641	$\frac{5}{2}(^+)$	6.0		1	6	3
3.476	10.651	$\frac{3}{2}^+$		24	2	4	4
3.489	10.664	$\frac{1}{2}^-$	3.3		1	4	5
3.516	10.689	$\frac{1}{2}^-$	11		3	5	2
3.521	10.695	$\frac{3}{2}^+$	2.9		3	5	2
3.524	10.697	$\frac{3}{2}^+$	3.2		3	4	3
3.535	10.708		0.8		1	5	4
3.578	10.750		1.3		0	4	6
3.594	10.765	$\frac{1}{2}^-$	26		3	4	3
3.613	10.784		0.8		0	0	10
3.622	10.792	$\frac{1}{2}^-$	1.8		3	3	4
3.640	10.810	$\frac{3}{2}^+$	2.7		4	4	2
3.656	10.825	$\frac{3}{2}^+$	1.5		2	4	4
3.669 a)	10.837		7.0		1	4	5
3.680	10.849		2.1		0	4	6
3.706	10.874	$\frac{3}{2}^+$	2.4		1	4	5
3.732 a)	10.898		2.0		1	4	5
3.762 a)	10.928		2.5		3	3	4
3.774	10.939	$\frac{3}{2}^+$	10		4	3	3
3.807	10.971		1.2		2	2	6
3.905	11.066	$\frac{3}{2}^+$	4.5		4	3	3
3.911	11.072		0.9		3	3	4
3.951	11.111		0.7		2	3	5
3.967	11.126	$\frac{3}{2}^+$	1.4		2	4	4
3.985	11.143		0.2		2	1	7
4.006	11.164	$\frac{5}{2}^+$	2.3		2	4	4

a) Probably doublet.

REF. D. W. Anderson and S. C. Swift
Nucl. Phys. A150, 625 (1970)

ELEM. SYM.	A	Z
P	31	15

METHOD

REF. NO. 70 An 2 egf

REACTION	RESULT	EXCITATION ENERGY	SOURCE TYPE	SOURCE RANGE	DETECTOR TYPE	DETECTOR RANGE	ANGLE
G,2P 807	ABX	23-63	C	23-63	ACT-I		4PI
G,2PN 808	ABX	23-63	C	23-63	ACT-I		4PI

10 +

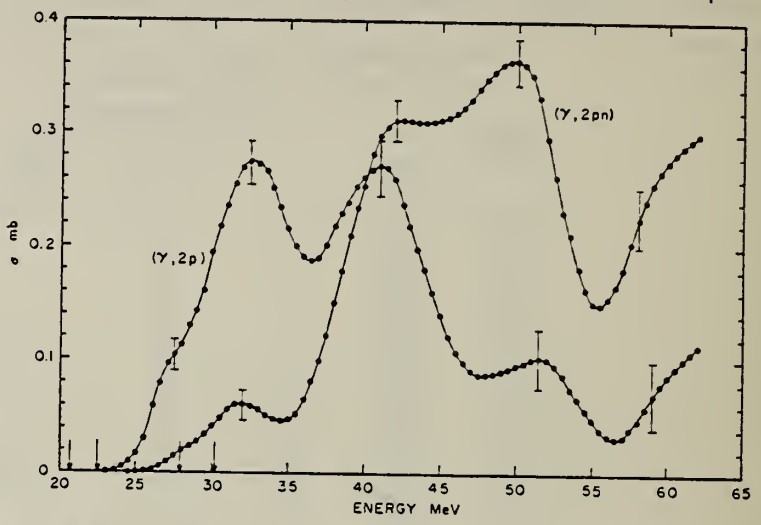

Fig. 3. The least structure cross-section solutions for the $^{31}P(\gamma, 2p)^{29}Al$ and $^{31}P(\gamma, 2pn)^{28}Al$ reactions. The flags on the points represent the estimated cross-section errors. The arrows on the energy axis indicate mass threshold energies for the $(\gamma, 2p)$, $(\gamma, {}^3He)$, (γ, dp) and $(\gamma, 2pn)$ reactions from left to right.

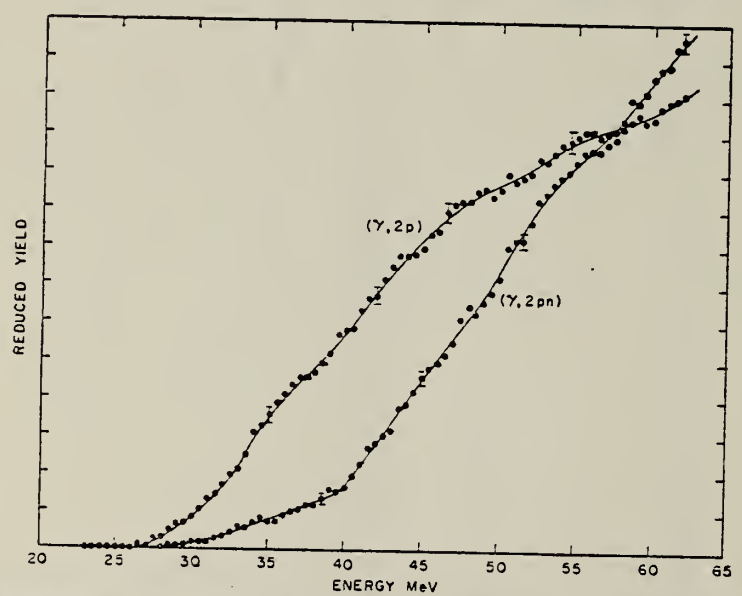

Fig. 2. The reduced yield points for the $(\gamma, 2p)$ and $(\gamma, 2pn)$ reactions in phosphorus are shown. The error bars indicate the standard deviations for the yield points. The smooth curves represent the polynomials fit to the yield points by the least structure procedure [9]).

[9] F.S. Goulding, D.A. Landis, J. Cerny and R.J. Pehl, Nucl. Instr. 31 (1964) 1.

Abstract: Bremsstrahlung activation curves were measured for the reactions $^{31}P(\gamma, 2p)^{29}Al$ and $^{31}P(\gamma, 2pn)^{28}Al$ in 0.5 MeV steps from 23.0 to 62.0 MeV. The cross sections obtained from these curves show peaks at 32.6±0.7 MeV, 41.2±0.8 MeV and 51.0±1.5 MeV for both reactions. The cross section integrated to 62 MeV for the $(\gamma, 2p)$ reaction is 5.6±0.6 MeV · mb and for the $(\gamma, 2pn)$ reaction is 7.6±0.8 MeV · mb.

REF. N. Shikazono and Y. Kawarasaki
Phys. Letters 32B, 473 (1970)

ELEM. SYM.	A	Z
P	31	15

METHOD

REF. NO. 70 Sh 2 egf

REACTION	RESULT	EXCITATION ENERGY	SOURCE		DETECTOR		ANGLE
			TYPE	RANGE	TYPE	RANGE	
G,G	LFT	6	C	14	SCD-D		

6 = 6.381 MEV

Table 1
Comparison between experimental log ft values and radiative widths: Γ_{th} represents the width estimated only from the spin part with eq. (1); R denotes the ratio of the reduced matrix element of the spin part to that of the orbital part.

	E_i (keV)	(T, J^π)	E_f (keV)	$(T, J^{\pi'})$	log ft	Γ_{th} (eV)	Γ_{obs} (eV) [a]	R
^{23}Na	7895	$(\frac{1}{2}, \frac{7}{2}^+)$	0	$(\frac{1}{2}, \frac{3}{2}^+)$	5.3	0.21	1.02 ± 0.37	5.5 ± 1.2
^{23}Na	7895	$(\frac{1}{2}, \frac{5}{2}^+)$	439	$(\frac{1}{2}, \frac{5}{2}^+)$	5.4	0.14	0.57 ± 0.21	4.8 ± 1.1
^{31}P	6381	$(\frac{1}{2}, \frac{3}{2}^+)$	0	$(\frac{1}{2}, \frac{1}{2}^+)$	5.5	0.07	≤ 0.11	≤ 1.2

a) In the estimate of Γ_{obs}, the branching ratio Γ_0/Γ for ^{23}Na and ^{31}P were assumed to be 0.64 and 0.18, respectively.

B. Friberg, G. Andersson, and B. Forkman
Nucl. Phys. A171, 551 (1971)

P	31	15

METHOD

REF. NO. 71 Fr 1 egf

REACTION	RESULT	EXCITATION ENERGY	SOURCE		DETECTOR		ANGLE
			TYPE	RANGE	TYPE	RANGE	
G,N	ABY	12-800	C	100-800	ACT-I		4PI

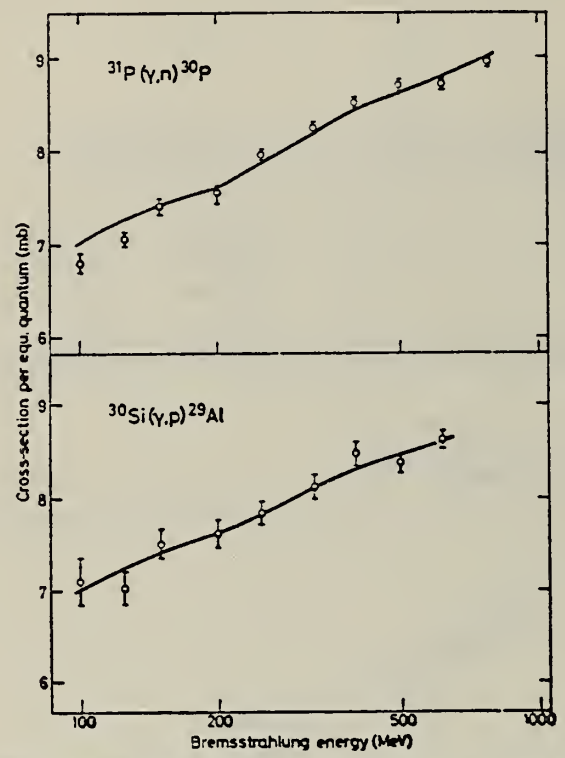

Fig. 2. Absolute yields for the reactions $^{30}Si(\gamma, p)^{29}Al$ and $^{31}P(\gamma, n)^{30}P$. Solid lines same as for fig. 1.

REF.

Tatsuya Saito
Bull. Chem. Soc. Japan 44, 1800 (1971)

ELEM. SYM.	A	Z
P	31	15

METHOD

REF. NO. 71 Sa 2 egf

REACTION	RESULT	EXCITATION ENERGY	SOURCE		DETECTOR		ANGLE
			TYPE	RANGE	TYPE	RANGE	
G,NA24	ABX	THR-250	C	20-250	ACT-I		4PI
G,3P	ABX	THR-250	C	20-250	ACT-I		4PI

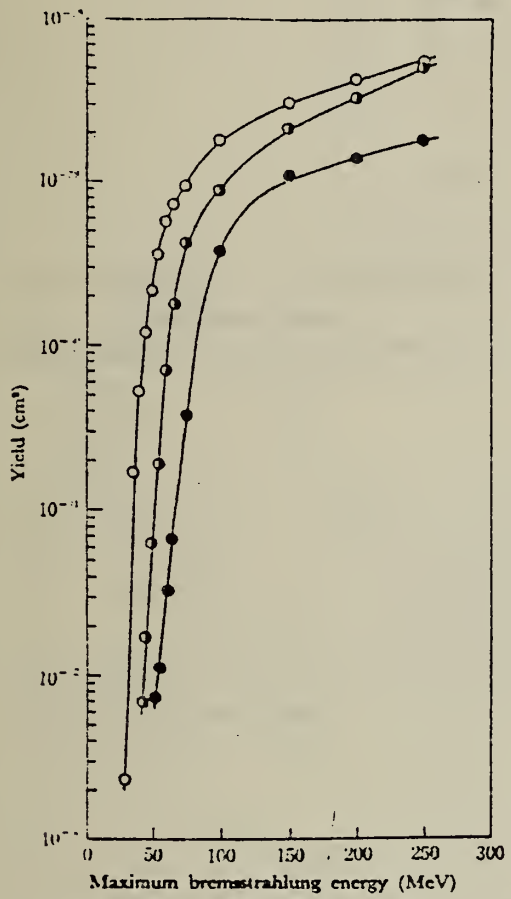

Fig. 4. The yield curves for the reactions $^{28}Si \rightarrow {}^{24}Na$, $^{31}P \rightarrow {}^{24}Na$, and $^{32}S \rightarrow {}^{24}Na$.
○: $^{28}Si \rightarrow {}^{24}Na$, ◑: $^{31}P \rightarrow {}^{24}Na$, ●: $^{32}S \rightarrow {}^{24}Na$

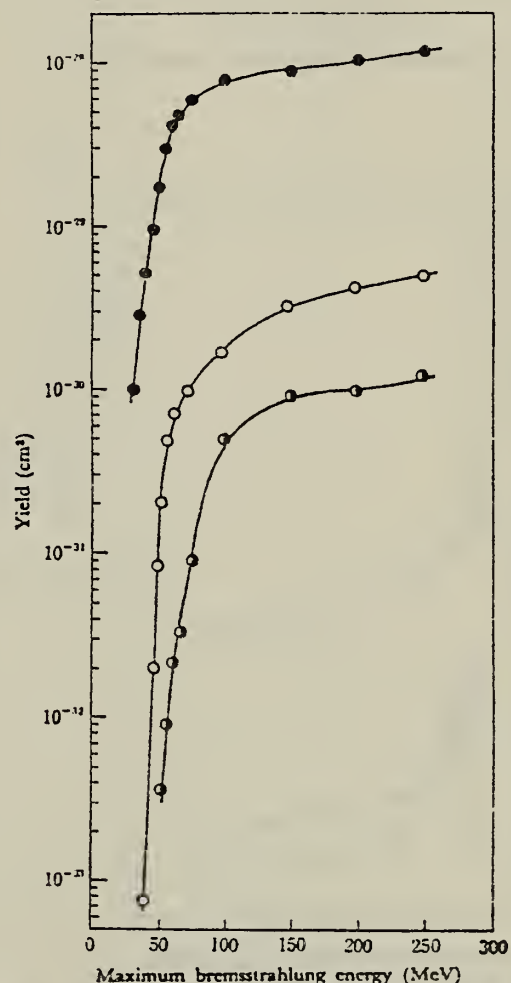

Fig. 5. The yield curves for the reactions $^{28}Si(\gamma,2p)^{28}Mg$, $^{31}P(\gamma,3p)^{28}Mg$, and $^{32}S(\gamma,4p)^{28}Mg$.
●: $^{28}Si(\gamma,2p)^{28}Mg$, ○: $^{31}P(\gamma,3p)^{28}Mg$, ◑: $^{32}S(\gamma,4p)^{28}Mg$

(over)

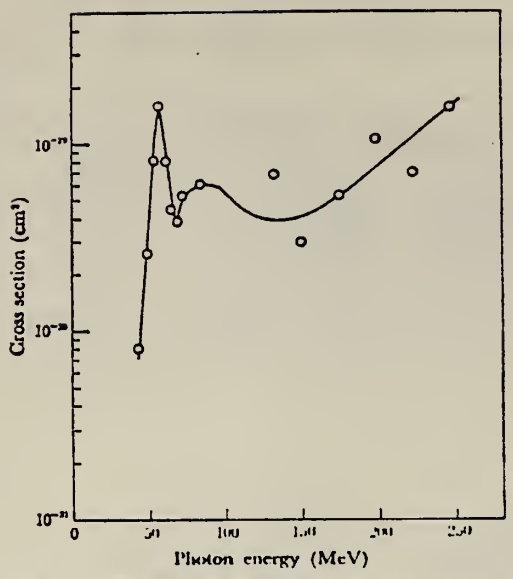

Fig. 11. The excitation function for the reaction $^{31}P(\gamma,3p)^{28}Mg$.

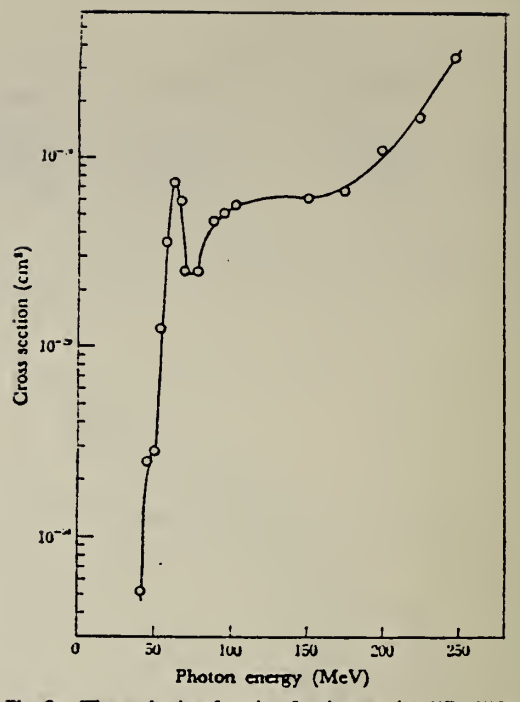

Fig. 8. The excitation function for the reaction $^{31}P \rightarrow ^{24}Na$.

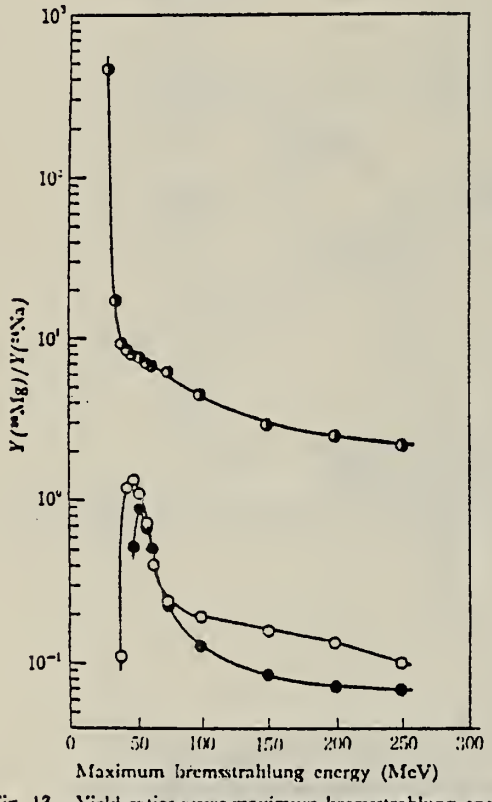

Fig. 13. Yield ratios *versus* maximum bremsstrahlung energy.
◑: $Y(^{29}Si(\gamma,2p)\ ^{28}Mg)/Y(^{29}Si \rightarrow ^{24}Na)$
○: $Y(^{31}P(\gamma,3p)\ ^{28}Mg)/Y(^{31}P \rightarrow ^{24}Na)$
●: $Y(^{32}S(\gamma,4p)\ ^{28}Mg)/Y(^{32}S \rightarrow ^{24}Na)$

REF.

D.W. Anderson, R.F. Petry and H.J. Fischbeck
Radiat. Res. 50, 33 (1972)

P	31	15

METHOD

REF. NO. 72 An 12 egf

REACTION	RESULT	EXCITATION ENERGY	SOURCE		DETECTOR		ANGLE
			TYPE	RANGE	TYPE	RANGE	
G,N	ABX	14- 60	C	14- 60	ACT-I		4PI

Least Structure Analysis 960

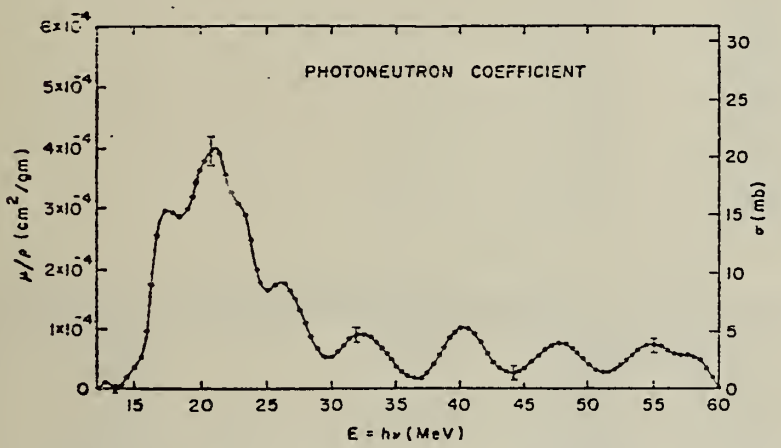

FIG. 3. The mass attenuation coefficient for the photonuclear reaction $^{31}P(\gamma, n)^{30}P$ is given as a function of photon energy.

REF.

N. Shikazono and Y. Kawarasaki
Nucl. Phys. A188, 461 (1972)

ELEM. SYM.	A	Z
P	31	15

METHOD

REF. NO.: 72 Sh 2 egf

REACTION	RESULT	EXCITATION ENERGY	SOURCE		DETECTOR		ANGLE
			TYPE	RANGE	TYPE	RANGE	
G,G/	SPC	0-14	C	14	SCD-D		87

TABLE 4

Gamma-rays resulting from the photon bombardment of a red phosphorus target

E_γ (MeV)	Observed peak	Relative intensity	Transition
3.13	F	9 ±6	3.13 → 0
5.26	D, S, F	22.0±1.7	5.26 → 0
5.56	D, (S), F	8.1±1.4	5.56 → 0
5.87	D	4.2±1.2	7.14 → 1.27
6.91	D, S	5.0±0.8	6.91 → 0
6.94	D, (S)	3.2±0.7	8.21 → 1.27
7.14	D, S, F	21.8±0.9	7.14 → 0
7.21	D, (S)	5.4±0.8	7.21 → 0
7.32	D, S, F	17.0±0.8	7.32 → 0
7.46	(D)	1.9±0.9	8.73 → 1.27
7.85	D, S, (F)	6.7±0.6	7.85 → 0
7.90	D, S	3.6±0.7	7.90 → 0
8.21	D, (S)	8.3±0.7	8.21 → 0
8.73	D, S, F	13.6±0.8	8.73 → 0
9.57	D, (S)	4.9±1.3	9.57 → 0

TABLE 8

Excitation energies and ground state transition widths obtained from the $^{31}P(\gamma,\gamma')^{31}P$ reaction

Excitation energy (keV) present work	Excitation energy (keV) previous work	$J^\pi; T$	$\Gamma_{\gamma 0}/\Gamma_\gamma$ [a]	$(2J+1)\Gamma_{\gamma 0}$ (eV) [b] present work	$(2J+1)\Gamma_{\gamma 0}$ (eV) [b] previous work
3133±5	3134.3±0.4 [c]	$\frac{1}{2}^+$ [d]	1.0	0.06±0.04	0.10±0.02 [e]
5255±4	5253 ±2 [c]	$\frac{1}{2}^+$ [f]	1.0	0.68±0.10	
5559±4	5557 ±2 [c]	$\frac{3}{2}^+$ [f]	0.82 [c]	0.37±0.08	
6909±7	6908 ±3 [c]	$\frac{3}{2}^-$ [f]	1.0	0.43±0.09	
7140±4	7139 ±3 [c]	$\frac{1}{2}^+, T=\frac{3}{2}$ [d]	0.84±0.04	3.2 ±0.4 [g]	
7214±5	7206 ±6 [f]	$(\frac{1}{2},\frac{3}{2})^-$ [d]	1.0	0.57±0.11	
7316±4	7314 ±9 [h]		1.0	2.2 ±0.3 [i]	
7850±4	7847 ±9 [h]		1.0	1.05±0.17 [i]	
7896±6	7898 [c]	$\frac{1}{2}$ [c]	0.93 [d]	3.2 ±0.7 [j]	
8209±4	8209 [c]	$\frac{3}{2}^+$ [k]	0.54±0.08 [l]	3.7 ±0.8	5.6 ±0.4 [k]
8728±4	8730 [c], 8731 [c]	$\frac{3}{2}$ [c]	0.88±0.05	7.2 ±1.1 [j]	
9565±7	9569 [m]		1.0	4.0 ±1.2 [j]	

[a]) The branchings are obtained from the relative intensities observed at the scattering angle of 87°. The effect of the angular distribution of the γ-rays is not taken into account.

[b]) The error for $(2J+1)\Gamma_{\gamma 0}$ only includes the statistical error. An estimate of the uncertainty associated with the shape of the incident bremsstrahlung is not included.

[c]) Ref. [21]).

[d]) Ref. [8]).

[e]) Ref. [56]).

[f]) Ref. [57]).

[g]) The value of $(2J+1)\Gamma_{\gamma 0}$ has been estimated by combining the value of $\Gamma_{\gamma 0}$ from ref. [23]) and the branching from the present work; this value has been used for normalization.

[h]) Ref. [22]).

[i]) The value given is not $(2J+1)\Gamma_{\gamma 0}$ but the $(2J+1)\Gamma_{\gamma 0}\Gamma_\gamma/\Gamma$ value.

[j]) The value of $(2J+1)\Gamma_\gamma\Gamma_0/\Gamma$ from ref. [8]) has been used to estimate the value of $(2J+1)\Gamma_{\gamma 0}$.

[k]) Ref. [24]).

[l]) This branching is not $\Gamma_{\gamma 0}/\Gamma_\gamma$ but $\Gamma_{\gamma 0}/\Gamma$ from ref. [24]).

[m]) Ref. [8]). The energy is corrected for the Q-value given in ref. [21]).

(over)

[8]P.M. Endt et al. Nucl.Phys. A105 (1967) 1.
[21]A.C. Wolff et al. Nucl.Phys. A107 (1968) 332.
[22]C.E. Moss, Nucl.Phys. A124 (1969) 440.
[23]P.F. Hinrichsen et al. Phys. Rev. 140 (1965) B549.
[24]J.H. Hough et al. Nucl.Phys. A109 (1967) 393.
[56]W.L. Cleeten et al. Nucl.Phys. A107 (1968) 347.
[57]A.C. Wolff et al. Nucl.Phys. A140 (1970) 319.

REF. B.J. Thomas, A. Buchnea, J.D. Irish, and K.G. McNeil
Can. J. Phys. 50, 3085 (1972)

ELEM. SYM.	A	Z
P	31	15

METHOD

REF. NO. 72 Th 5 hmg

REACTION	RESULT	EXCITATION ENERGY	SOURCE TYPE	SOURCE RANGE	DETECTOR TYPE	DETECTOR RANGE	ANGLE
G,PG	ABI	7- 22	C	19, 22	SCD-D		150
G,NG	ABI	12- 22	C	19, 22	SCD-D		150
G,AG	ABI	10- 22	C	19, 22	SCD-D		150

GAMMA DST

TABLE 3. Yields of gamma rays from the reaction $^{31}P(\gamma,x\gamma')$, $E_0 = 30$ MeV; $\theta = 150°$

Residual nucleus	State (MeV)	J^π	T	Known γ decay	Relative[a] yield	Estimate of $\int \frac{d\sigma(150)}{d\Omega} dE$ (MeV mb/sr)
^{30}P	0.678	0^+	1	GS	—	—
	0.709	1^+	0	GS	0.60	3.1 ± 0.8
	1.455	2^+	0	GS	0.19	1.0 ± 0.2
	1.976	3^+	0	35% (GS)	—	2.0 ± 0.4[c]
				50% (0.710)	0.19	
				15% (1.455)	N.O.[b]	
	3.018	(1)		10% (GS)	N.O.	0.5 ± 0.17
				90% (0.678)	0.09	
	4.181	2^+	1	10% (GS)	N.O.	0.15 ± 0.07
				60% (0.678)	0.02	
				30% (0.710)	0.01	
	5.412				0.06	0.3 ± 0.08
^{30}Si	2.233	2^+	1	GS	1.00	5.2 ± 0.2
	3.507	2^+	1	45% (GS)	0.06	0.8 ± 0.2
				55% (2.233)	0.07	
	3.767	1^+		40% (GS)	0.13	1.1 ± 0.3
				60% (2.233)	0.08	
	3.786	0^+	1	GS	0.07	0.4 ± 0.1
	6.730	1^-		80% (GS)	0.03	0.2 ± 0.5
				20% (2.233)	N.O.	
	8.930				0.03	0.2 ± 0.5
	8.950					
^{27}Al	0.843	$1/2^+$	1/2	GS	0.28	1.5 ± 0.5
	1.013	$3/2^+$	1/2	GS	1.25	6.5 ± 0.6

[a]Normalized to yield of the 2.233 MeV first excited state of ^{30}Si.
[b]N.O.—not observed.
[c]GS decay obscured by Compton edge of 2.233 MeV ^{30}Si.

REF. R. Bergere, H. Beil, P. Carlos, A. Lepretre, A. Veyssiere
PICNS-73, Vol. I, p. 525 Asilomar

ELEM. SYM.	A	Z
P	31	15

METHOD

REF. NO. 73 Be 10 hmg

REACTION	RESULT	EXCITATION ENERGY	SOURCE		DETECTOR		ANGLE
			TYPE	RANGE	TYPE	RANGE	
G,N	ABX	12- 29	D	12- 29	BF3-I		4PI
G,PN	ABX	19- 29	D	19- 29	BF3-I		4PI
G,2N	ABX	27- 29	D	27- 29	BF3-I		4PI

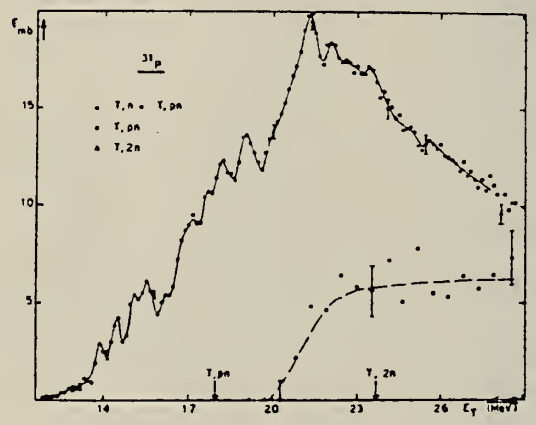

Fig. 4 Partial photoneutron cross sections $\sigma(\gamma,n)$, $\sigma(\gamma,pn)$ and $\sigma(\gamma,2n)$ of ^{31}P.

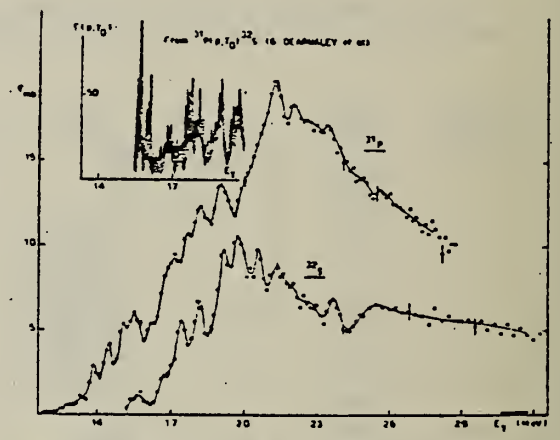

Fig. 6 Comparison of ^{31}P and ^{32}S photoneutron cross sections with $^{31}P(p,\gamma_0)^{32}S$ measured by Dearnaley.[9]

[9] G. Dearnaley et al., Nucl. Phys. 64, 177 (1965)

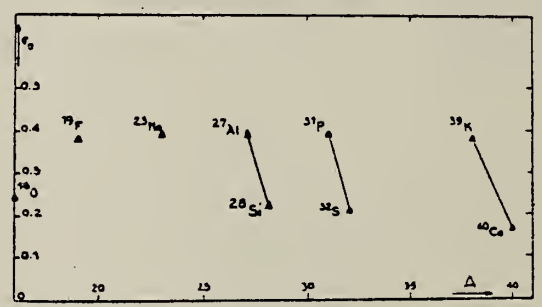

Fig. 13 Integrated photoneutron cross-sections for s-d shell nuclei.

REF. R.W. Gellie, K.H. Lokan, and N.K. Sherman
PICNS-73, Vol.I, p.171 Asilomar

ELEM. SYM.	A	Z
P	31	15

METHOD

REF. NO. 73 Ge 1 hmg

REACTION	RESULT	EXCITATION ENERGY	SOURCE		DETECTOR		ANGLE
			TYPE	RANGE	TYPE	RANGE	
G,N	ABX	13- 23	C	15- 25	TOF-D		90

GND AND EXCITED STATES

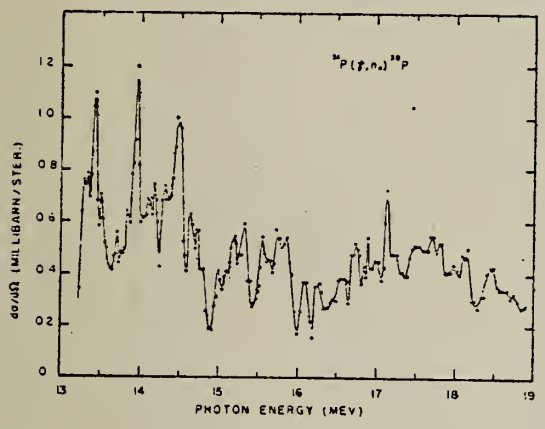

Figure 1: $^{31}P(\gamma,n_o)$ differential cross section at 90° as a function of excitation energy.

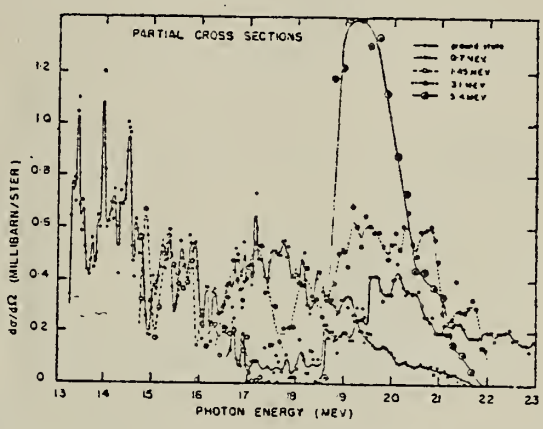

Figure 2: $^{31}P(\gamma,n)$ partial differential cross sections at 90° as a function of excitation energy.

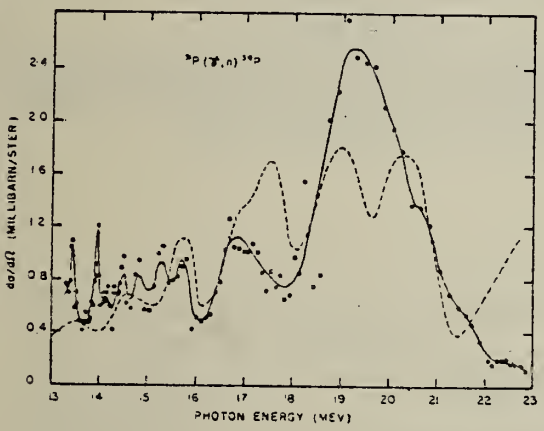

Figure 3: $^{31}P(\gamma,n)$ total differential cross section at 90° as a function of excitation energy. Dashed curve from total $^{31}P(\gamma,n)$ cross section by Mutsuro et al.[3] assuming isotropic distribution.

Table 1
Integrated $^{31}P(\gamma,n)$ cross section

Experiment	Upper limit	$\int\sigma dE$ MeV-mb
Present experiment	22 MeV	120 ± 10
Katz and Penfold[4]	26	120
Mutsuro et al.[3]	22.5	120 ± 10
Bolen and Whitehead[5]	28	127
McDonald et al.[6]	22	101

(over)

References

1. B. Weissman and H. L. Schultz, Private Communication (1969).

2. P. M. Endt and C. Van der Leun, Nucl. Phys. A105, 1 (1967).

3. N. Mutsuro, K. Kageyama, M. Mishina, E. Tanaka and M. Kimura, J. Phys. Soc. Japan, 17, 1673 (1962).

4. L. Katz and A. S. Penfold, Phys. Rev. 81, 815 (1957).

5. L. N. Bolen and W. D. Whitehead, Phys. Rev. 132, 2251 (1963).

6. W. J. McDonald, E. Buchholz and R. N. H. Haslam, Can. J. Phys. 41, 180 (1963).

REF. A. Järund, B. Friberg, and B. Forkman
Z. Physik 262, 15 (1973)

ELEM. SYM.	A	Z
P	31	15

METHOD

REF. NO. 73 Ja 3 egf

REACTION	RESULT	EXCITATION ENERGY	SOURCE		DETECTOR		ANGLE
			TYPE	RANGE	TYPE	RANGE	
G,NA24	ABY	THR-999	C	100-999	ACT-I		4PI

999=1 GEV

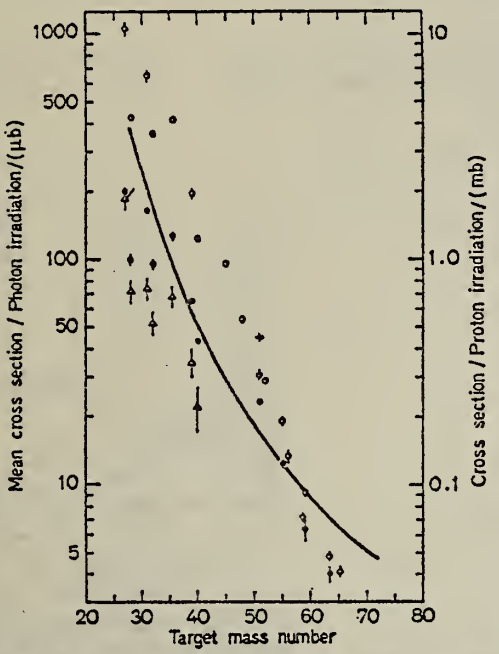

Fig. 7. Mean cross sections for ^{24}Na production as a function of target mass number. Present work filled circles. Noga *et al.* [3] open triangles, Kumbartzki *et al.* [13] cross and Korteling *et al.* [1] 400 MeV protons open circles. The solid line gives the mean cross sections calculated by Jonsson *et al.* [17]

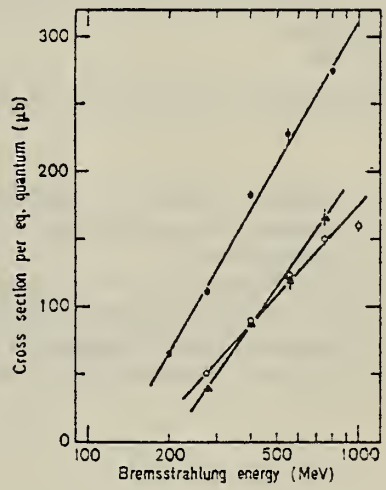

Fig. 3

Fig. 3. The determined yields for the reactions $^{31}P \rightarrow {}^{24}Na$ (filled circles), $^{32}, \cdots S \rightarrow {}^{24}Na$ (open circles) and $^{35,37}Cl \rightarrow {}^{24}Na$ (filled triangles)

[1] Korteling, R.G. et al., J. Inorg. Nucl. Chem. 29, 2863 (1967).

[3] Noga, V.I. et al., Sov. J. Nucl. Phys. 9, 637 (1969).

[13] Kumbartzki, G. et al., Nucl. Phys. A176, 23 (1971).

[17] Jonsson, G.G. et al., LUNP7212, Oct. 1972, to be published in Physica Scripta.

REF.

H. Tsubota, N. Kawamura, S. Oikawa, M. Sugawara, K. Shoda
J. Phys. Soc. Japan 35, 330 (1973)

ELEM. SYM.	A	Z
P	31	15

METHOD

REF. NO.: 73 Ts 3 egf

REACTION	RESULT	EXCITATION ENERGY	SOURCE TYPE	SOURCE RANGE	DETECTOR TYPE	DETECTOR RANGE	ANGLE
E,P	ABX	14- 26	D	16- 26	MAG-D		90

Table I. The integrated differential cross sections (mb MeV/sr) at 90°.

	$\int \frac{d\sigma(\gamma, p_0)}{d\Omega} dE$	$\int \frac{d\sigma(\gamma, p_1)}{d\Omega} dE$	$\int \frac{d\sigma(\gamma, p)}{d\Omega} dE$	R
^{31}P	1.93±0.21[c] 25.68–13.82 MeV**	0.69±0.48[a] 25.98–15.75 MeV**	27.87[b] 0–32 MeV**	0.07
^{32}S	4.7[c] 16–19 MeV**		20.71[d] 0–23 MeV**	0.23

* Deduced from the total cross section assuming an isotropic angular distributions.
** Energy region.
a) Present data.
b) ref. 17.
c) Calculated from the data of ref. 22 using a detailed balance theorem.
d) ref. 6.

6) K. Shoda, K. Abe, T. Ishizuka, N. Kawamura, M. Oyamada, Baik-N-Sung, J. Phys. Soc. Japan 25 (1968) 664.
17) B.S. Ishkhanov, L.M. Kaitonov, D.G. Shevchenko and B.A. Yur'ev, Phys. Letters 9 (1964) 162.
22) G. Dearnaly, D.S. Gemmel, B.W. Hooton and G.A. Jones; Nuclear Phys. 64 (1965) 177.

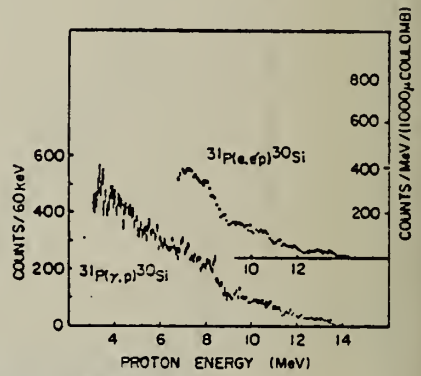

Fig. 4. The comparison of the proton energy spectra between $^{31}P(e, e'p)^{30}Si$ and $^{31}P(\gamma, p)^{30}Si$ reactions. The spectrum of $^{31}P(e, e'p)^{30}Si$ was obtained with the electron beam with 22 MeV and that of $^{31}P(\gamma, p)^{30}Si$ was obtained with the bremsstrahlung of the end point energies of which was 21.5 MeV.

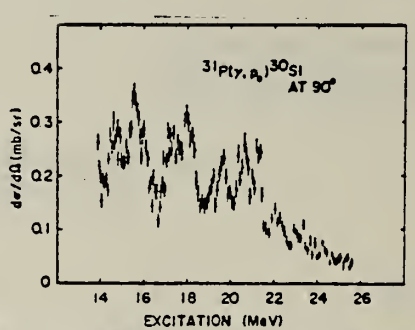

Fig. 5. The differential cross section for $^{31}P(\gamma, p_0)^{30}Si$ reaction at 90°.

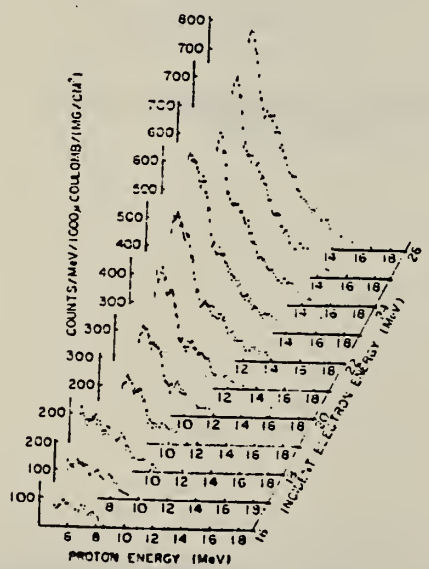

Fig. 3. The proton energy spectra for $^{31}P(e, e'p)^{30}Si$ reaction.

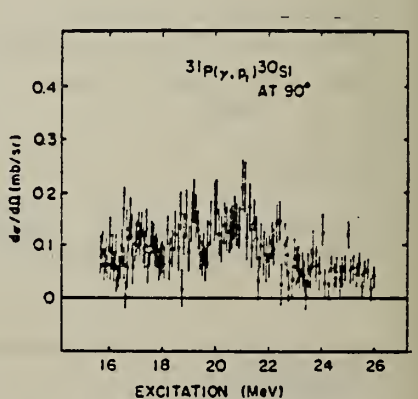

Fig. 6. The differential cross section for $^{31}P(\gamma, p_1)^{30}Si$ reaction at 90°.

USCOMM-DC 26010-P64

REF. L. Zalcman, J. E. M. Thomson and M. M. Thompson
PICNS-73, Vol. I, p. 169 Asilomar

ELEM. SYM.	A	Z
P	31	15

METHOD

REF. NO. 73 Za 1 hmg

REACTION	RESULT	EXCITATION ENERGY	SOURCE		DETECTOR		ANGLE
			TYPE	RANGE	TYPE	RANGE	
G,NG	SPC	12- 30	C	30	SCD-D		125
G,PG	SPC	7- 30	C	30	SCD-D		125

DE-EXCIT G-RAYS

Residual Level (MeV)	Known Cascade (ref. 7)	Gamma-ray Energy (MeV)	Identification (fig. 1)	Observed relative intensity	$\int_{th}^{30} \sigma\, dE$ Cascade corrected (MeV-mb/Sr)	$\int_{'}^{30} \sigma\, dE$ ref. 6. (MeV-mb/Sr)
^{30}P						
.678	100%→G.S.	.678	A	.29	2.0±.3	
.709	100%→G.S.	.709	B	.26	2.4±.6	3.1±.8
1.455	100%→G.S.	1.455	C	.18	1.3±.2	1.0±.2
1.976	35%→G.S.	1.976	D	.02	0.7±.2	2.0±.4
	50%→.709	1.267	E	.29*		
	15%→1.455	.521		N.O.		
2.539	100%→G.S.	2.539	F	.06	.8±.2	N.O.
2.725	100%→G.S.	2.725	G	.07	.7±.2	N.O.
2.937	15%→G.S.	2.937	H	.02	1.1±.4	N.O.
	40%→.678	2.259	I	.04		
	45%→1.455	1.482	J	.05		
3.018	10%→G.S.	3.018		N.O.	.7±.2	.5±.2
	90%→.678	2.340	K	.07		
5.412	100%→G.S.	5.412	-	.04	.1±.03	.3±.1
^{30}Si						
2.232	100%→G.S.	2.232	L	1.00	7.3±.9	9.2±.2
3.505	45%→G.S.	3.505	M	.22	3.8	.8±.2
	55%→2.232	1.273	N	.14		
3.767	40%→G.S.	3.767	O	.16	2.8±.6	1.1±.3
	60%→2.232	1.535	P	.11		
3.796	100%→2.232	1.564	Q	.05	.5±.15	.4±.1
6.735	80%→G.S.	6.735	-	.01	.1±.05	.2±.05
	20%→2.232	4.503	-	N.O.		

* See next

REF. J. Devos, R. Carchon, H. Ferdinande, and R. Van de Vyver
Z. Physik 271, 391 (1974)

ELEM. SYM.	A	Z
P	31	15

METHOD

REF. NO. 74 De 10 egf

REACTION	RESULT	EXCITATION ENERGY	SOURCE		DETECTOR		ANGLE
			TYPE	RANGE	TYPE	RANGE	
G,XN	ABX	12- 25	C	12- 25	BF3-I		4PI

961

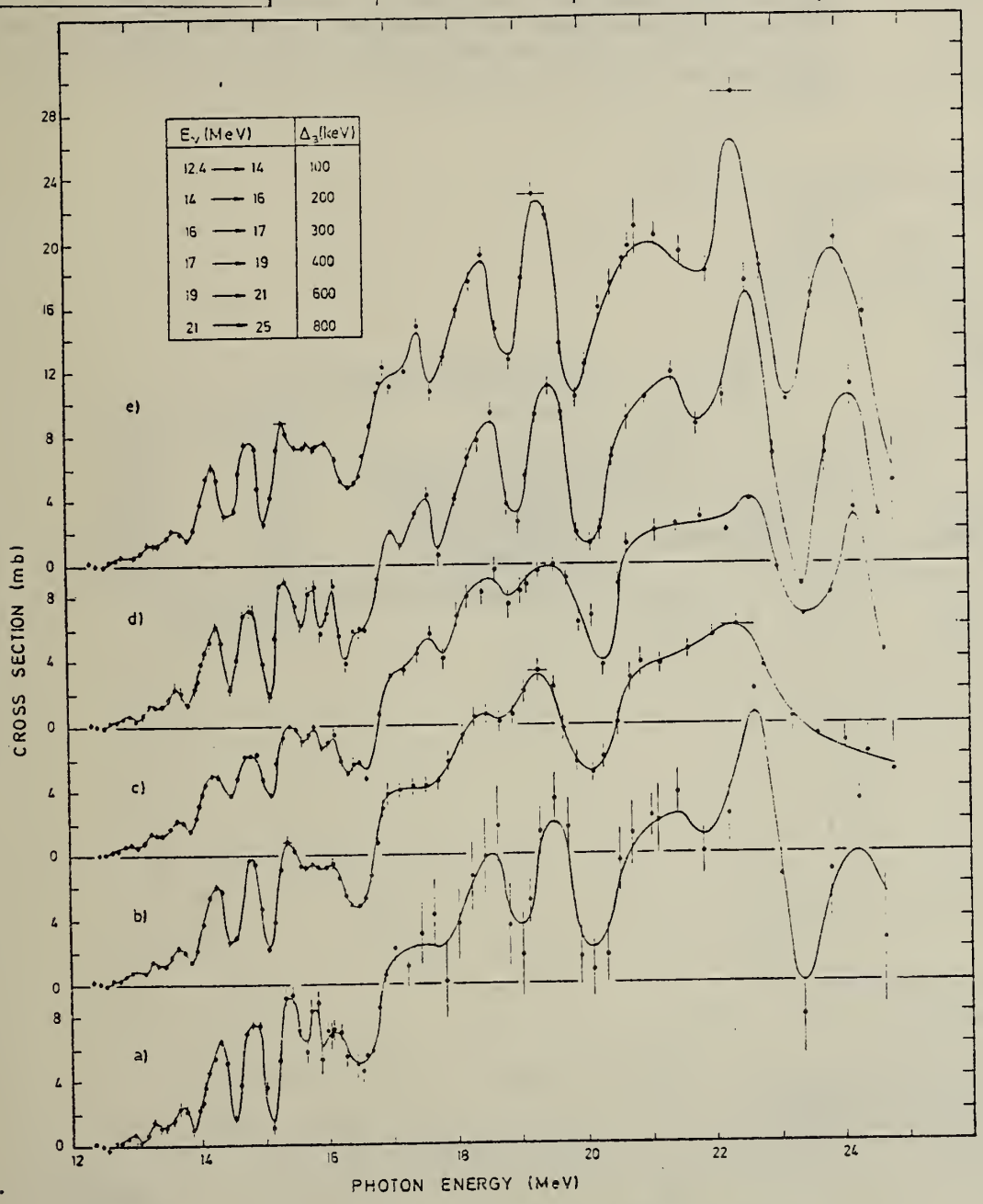

(over)

Fig. 1. The result of various analysis procedures for the $^{31}P(\gamma, x\,n)$ cross section, as explained in text: (a) VBPL method; (b) CLSM procedure; (c) VBPL including decorrelation; (d) and (e) VBPL and CLSM after smoothing of the individual yield points

[1]Ishkhanov, B.S. et al., Bull. Acad. Sci. USSSR 33, 1594 (1969).

[2]Bergere, R. et al., Proc. Int. Conf. Photonuclear Reactions & Applications (Asilomar 1973). Ed. B. Berman (1973), Vol. 1, p.525.

[9]Mutsuro, N. et al., J. Phys. Soc. Japan 17, 1673 (1962).

[12]Gellie, R.W. et al., Proc. Int. Conf. Photonuclear Reactions & Applications (Asilomar 1973). Ed. B. Berman (1973), Vol. 1, p.171.

[14]Wong, S.S.M. et al., Phys. Lett. 48B, 403 (1974).

Abstract. The $^{31}P(\gamma, x\,n)$ cross section was measured from threshold up to 25 MeV, using the bremsstrahlung photon beam from the 35 MeV linac. Several analysis procedures were used to compute the photoneutron cross section from the experimental yield curve. Our results are compared with other bremsstrahlung measurements and with the quasimonoenergetic photon work by the Saclay group. The leading edge of the giant resonance shows an extremely rich fine structure which seems to be characteristic for nuclei in the $1d-2s$ shell.

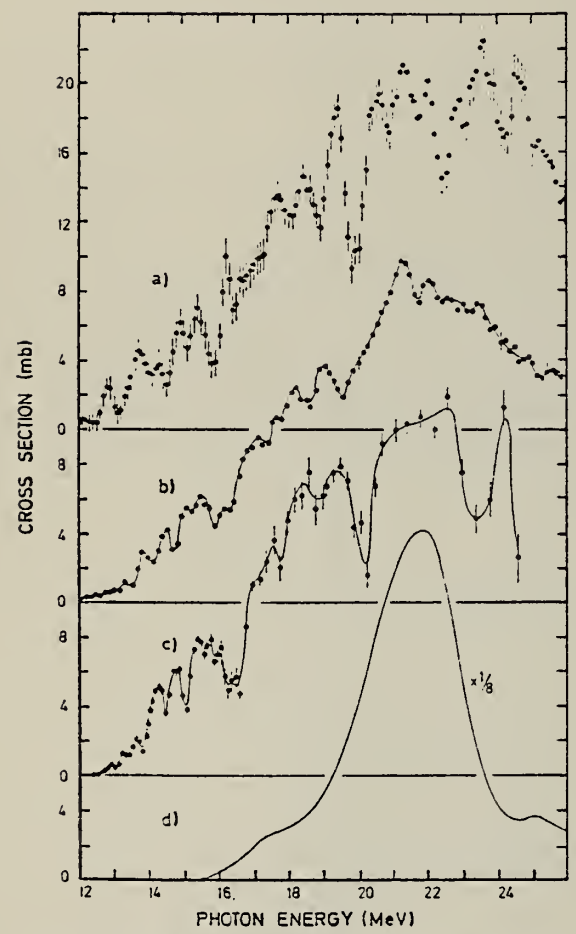

Fig. 2. Comparison of the present cross section results (c) with the data obtained by (a) Ishkhanov *et al.* [1] using bremsstrahlung, and (b) those measured by Bergère *et al.* [2] using a quasi-monoenergetic gamma-ray beam. At the bottom (d) we have plotted the total gamma absorption cross section for ^{32}S, as calculated by Wong *et al.* [14]

Table 2. Integrated $^{31}P(\gamma, x\,n)$ cross section

Experiment	Integration limit (MeV)	$\int \sigma\, dE$ (MeV. mb)
Mutsuro *et al.* [9] (1962)	22.5	120 ± 10
Ishkhanov *et al.* [1] (1969)	22.5	107 ± 10
Bergère *et al.* [2] (1973)	22.5	96 ± 10[a]
Gellie *et al.* [12] (1973)	22.0	120 ± 10
Present experiment	22.5	120 ± 6

[a] Determined from the figure in Ref. 2.

REF.

A. Veyssiere, H. Beil, R. Bergere, P. Carlos, A. Lepretre, and A. De Miniac
Nucl. Phys. A227, 513 (1974)

ELEM. SYM.	A	Z
P	31	15

METHOD

REF. NO.	
74 Ve 1	egf

REACTION	RESULT	EXCITATION ENERGY	SOURCE		DETECTOR		ANGLE
			TYPE	RANGE	TYPE	RANGE	
* G,N	ABX	12- 29	D	12- 29	BF3-I		4PI
** G,2N	ABX	24- 29	D	24- 29	BF3-I		4PI
*** G,NP	ABX	19- 29	D	19- 29	BF3-I		4PI

* 891
** 889 +
*** 890

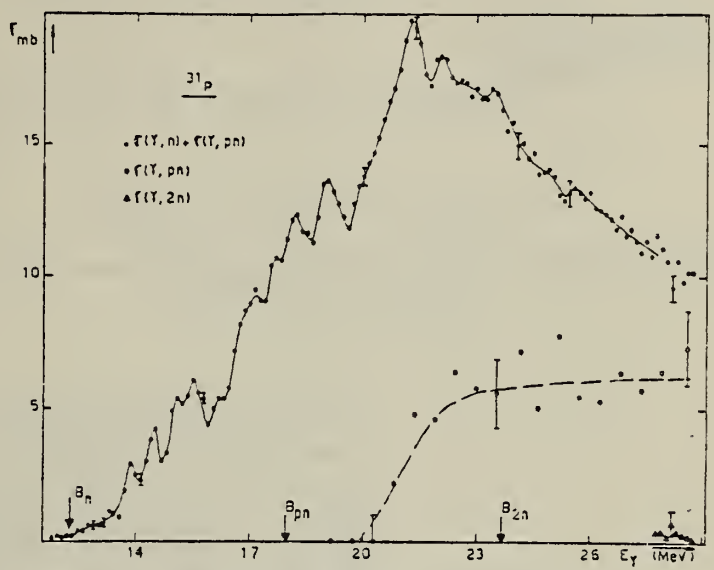

Fig. 7. Partial photoneutron cross sections $[\sigma(\gamma, n)+\sigma(\gamma, pn)]$ $\sigma(\gamma, pn)$ and $\sigma(\gamma, 2n)$ of ^{31}P.

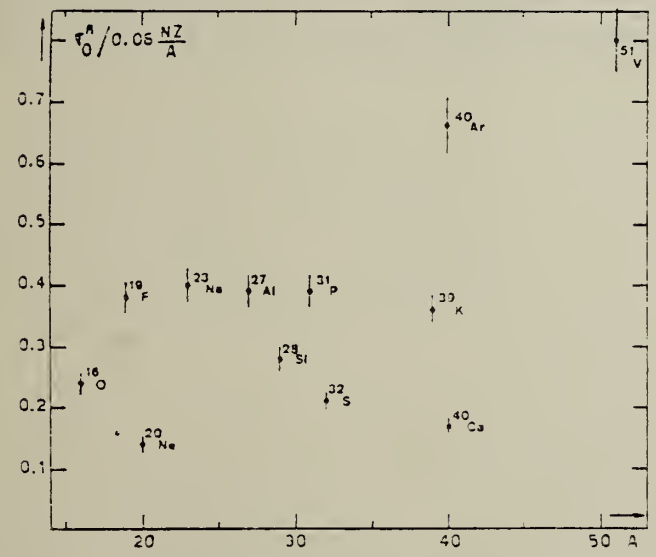

Fig. 22. Ratio of experimental integrated photoneutron cross section σ_0^n over the Thomas, Reiche and Kuhn sum rule [0.06 NZ/A]. Numerical values and upper integration limits E_{vt} are taken from table 3. Also $\Delta\sigma_0^n = \pm 7\%$ for all nuclei.

(over)

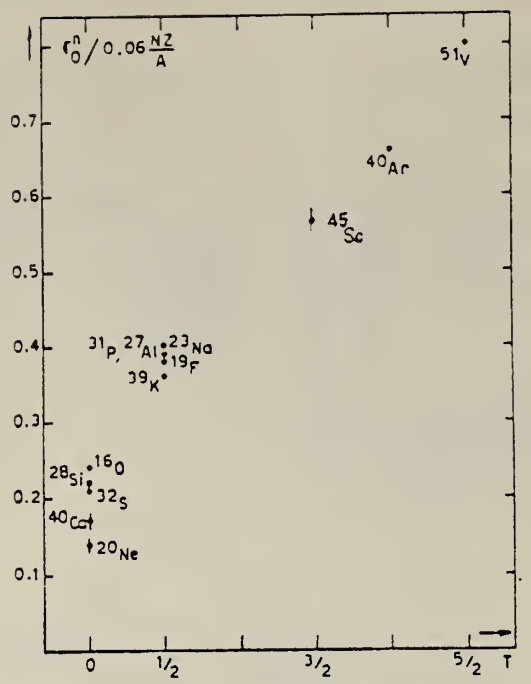

Fig. 24. The $[\sigma_0^n/(0.06\,NZ/A)]$ ratio as a function of isospin T. Possible overall errors of ± 7% are to be applied to all nuclei shown.

TABLE 3

Experimental integrated photoneutron cross sections $\sigma_0^n = \int_0^{E_M} \sigma_{Tn}(E)dE$ compared with the classical sum rule [0.06 NZ/A] of Thomas, Reich and Kuhn

	$T=0$					$T=\frac{1}{2}$					$T=\frac{3}{2}$	$T=2$	$T=\frac{5}{2}$
Nucleus	^{16}O	^{20}Ne	^{28}Si	^{32}S	^{40}Ca	^{19}F	^{23}Na	^{27}Al	^{31}P	^{39}K	^{45}Sc	^{40}Ar	^{51}V
σ_0^n (MeV · mb)	58 ±4	42 ±3	94 ±7	98 ±7	100 ±7	108 ±7	137 ±9	158 ±10	182 ±12	210 ±14	383 ±25	393 ±28	602 ±42
$\sigma_0^n/(0.06NZ/A)$	0.24	0.14	0.22	0.21	0.17	0.38	0.40	0.39	0.39	0.36	0.57	0.66	0.8
E_M (MeV)	30	26.7	30	30	29.5	29	30	30	29	30	28.1	26.7	28

REF. E. O. De Neijs, G. D. Haasbroek, M. A. Meyer, R. S. Rossouw, D. Reitmann
Nucl. Phys. A254, 45 (1975)

ELEM. SYM.	A	Z
P	31	15

METHOD

REF. NO. 75 De 3 egf

REACTION	RESULT	EXCITATION ENERGY	SOURCE		DETECTOR		ANGLE
			TYPE	RANGE	TYPE	RANGE	
P,G	LFT	9- 10	D	1- 3	SCD-D		55

30 RESONANCES

Data on strengths and branching ratios for 65 resonances tabulated.
Excitation energy 7.78-9.72 MeV.

Table 3. Cross-section per equivalent quantum $\sigma_0(\mu b)$ of photoproduction of ^{22}Na

Target nucleus	Bremsstrahlung maximum energy E_0 (GeV)				
	0·30	0·40	0·55	0·75	1·00
^{27}Al	490 ± 20	560 ± 20	667 ± 20	690 ± 20	745 ± 20
^{28}Si	290 ± 20	330 ± 20	380 ± 20	430 ± 20	470 ± 20
^{31}P	230 ± 20	250 ± 20	290 ± 20	330 ± 20	350 ± 20
^{32}S	206 ± 10	240 ± 10	280 ± 10	320 ± 10	350 ± 10
$^{35,37}Cl$	230 ± 10	260 ± 10	290 ± 10	320 ± 10	350 ± 10
^{39}K	30 ± 3	50 ± 5	65 ± 5	80 ± 5	100 ± 5
^{40}Ca	5 ± 2	20 ± 3	45 ± 5	60 ± 5	60 ± 5

Table 4. Cross-section per equivalent quantum $\sigma_0(\mu b)$ of photoproduction of ^{24}Na

Target nucleus	Bremsstrahlung maximum energy E_0 (GeV)				
	0·30	0·40	0·55	0·75	1·00
$^{27}Al^a$	370 ± 10	440 ± 10	500 ± 20	550 ± 20	660 ± 20
^{28}Si	100 ± 10	140 ± 10	160 ± 10	210 ± 10	240 ± 10
^{31}P	100 ± 20	160 ± 20	200 ± 20	270 ± 20	310 ± 20
^{32}S	120 ± 10	160 ± 10	180 ± 10	210 ± 10	240 ± 10
$^{35,37}Cl$	65 ± 10	100 ± 10	140 ± 10	190 ± 10	220 ± 10
^{39}K	20 ± 5	35 ± 5	55 ± 5	65 ± 5	80 ± 5
^{40}Ca	12 ± 3	25 ± 5	35 ± 5	50 ± 5	60 ± 5

[a]The results for ^{27}Al have already been published (see [8]) and are reported for comparison.

Table 5. Mean absolute cross-section $\bar{\sigma}_a(\mu b)$ in the energy range 0·3–1 GeV

Target nucleus	Produced radionuclide		
	^{18}F	^{22}Na	^{24}Na
^{23}Na	190 ± 30		
$^{27}Al^a$	120 ± 10	200 ± 20	220 ± 20
^{28}Si	100 ± 10	150 ± 20	120 ± 10
^{31}P	100 ± 10	100 ± 20	180 ± 20
^{32}S	110 ± 10	120 ± 10	100 ± 10
$^{35,37}Cl$	135 ± 20	100 ± 10	130 ± 10
^{39}K	45 ± 5	60 ± 5	50 ± 5
^{40}Ca	46 ± 5	60 ± 5	40 ± 5

[a]The results for the photoproduction of ^{18}F and ^{24}Na from ^{27}Al have already been published (Ref. [3] and [8], respectively).

2. V. di Napoli and M. L. Terranova, *J. inorg. nucl. Chem.* 36, 3633 (1974).
3. V. di Napoli, A. M. Lacerenza, F. Salvetti, S. M. Terenzi, H. G. de Carvalho and J. B. Martins, *J. inorg. nucl. Chem.* 35, 1419 (1973).
4. C. M. Lederer, J. M. Hollander and I. Perlman, *Table of Isotopes.* 6th Edn Wiley, New York (1967).
5. R. G. Korteling and A. A. Caretto, Jr., *J. inorg. nucl. Chem.* 29, 2863 (1967).
6. R. G. Korteling and A. A. Caretto, Jr., *Phys. Rev.* C1, 193 (1970).
7. R. G. Korteling and A. A. Caretto, Jr., *Phys. Rev.* C1, 1960 (1970).
8. V. di Napoli, A. M. Lacerenza, F. Salvetti, H. G. de Carvalho and J. B. Martins, *Lett. Nuovo Cimento* 1, 835 (1971).
9. I. Halpern, R. J. Debs, J. T. Eisinger, A. W. Fairhall and H. G. Richter, *Phys. Rev.* 97, 1327 (1955).
10. C. B. Fulmer, K. S. Toth, I. R. Williams, T. H. Handley, C. F. Dell, E. L. Callis, T. M. Jenkins and J. M. Wyckoff, *Phys. Rev.* C2, 1371 (1970).
11. G. J. Kumbartzki, U. Kim and C. K. Kwan, *Nucl Phys.* A160, 237 (1970).
12. G. J. Kumbartzki and U. Kim, *Nucl. Phys.* A176, 23 (1971).
13. K. Lindgren and G. G. Jonsson, *Nucl. Phys.* A197, 71 (1972).
14. C. E. Roos and V. Z. Peterson, *Phys. Rev.* 124, 1610 (1961).
15. T. A. Gabriel and R. G. Alsmiller, Jr., *Phys. Rev.* 182, 1035 (1969).
16. G. G. Jonsson and K. Lindgren, *Phys. Scr.* 7, 49 (1973).
17. G. Rudstam, *Z. Naturf.* 21a, 1027 (1966).
18. A. Masaike, *J. phys. Soc. Japan* 19, 427 (1964).
19. A. Järund, B. Friberg and B. Forkman, Private communication to G. G. Jonsson and K. Lindgren, quoted in Ref. [16]; see also A. Järund, B. Friberg and B. Forkman, University of Lund Report No. LUNP-7303, 1973 (unpublished).
20. V. I. Noga, Yu. N. Ranyuk and P. V. Sorokin, *Yad. Fiz.* 9, 1152 (1969) (transl.: *Sov. J. Nucl. Phys.* 9, 673 (1969)).
21. T. Methasiri and S. A. E. Johansson, *Nucl. Phys.* A167, 97 (1971).
22. J. R. Nix and E. Sassi, *Nucl. Phys.* 81, 61 (1966).
23. W. D. Myers and W. J. Swiatecki, *Nucl. Phys.* 81, 1 (1966).

REF.

V. di Napoli, G. Rosa, F. Salvetti, M. L. Terranova,
H. G. de Carvalho, J. B. Martins, O. A. P. Tavares
J. Inorg. Nucl. Chem. 37, 1101 (1975)

ELEM. SYM.	A	Z
P	31	15

METHOD

REF. NO. 75 Di 4 egf

REACTION	RESULT	EXCITATION ENERGY	SOURCE		DETECTOR		ANGLE
			TYPE	RANGE	TYPE	RANGE	
G,F18	ABY	THR-999	C	300-999	ACT-I		4PI
G,NA22	ABY	THR-999	C	300-999	ACT-I		4PI
G,NA24	ABY	THR-999	C	300-999	ACT-I		4PI

999 = 1 GEV

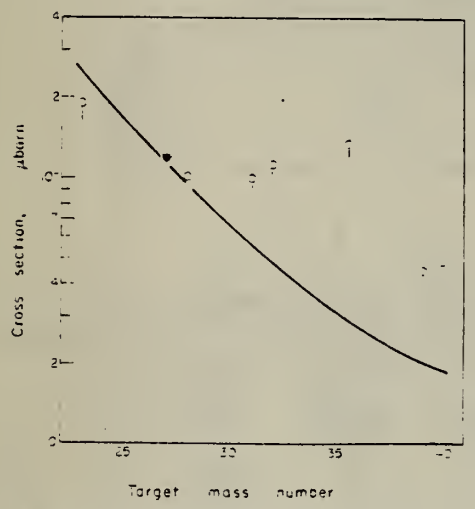

Fig. 2. Mean absolute cross section of ^{18}F photoproduction vs the target mass number. Open triangle: energy range 0·15–0·72 GeV, Ref. [18]. Filled circle: energy range 0·3–1 GeV, Ref. [3]. Open circles: present work. The curve has been calculated by means of Eqn (1).

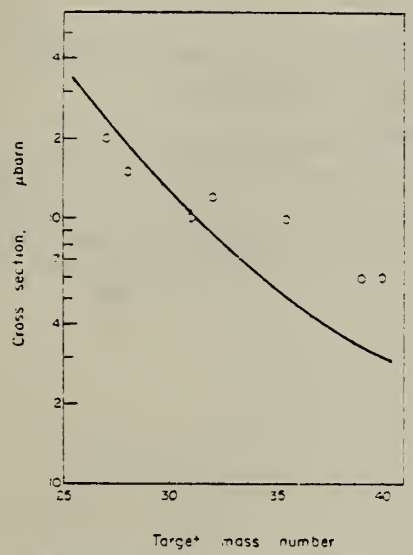

Fig. 3. Mean absolute cross section of ^{22}Na photoproduction vs the target mass number. The curve has been calculated by means of Eqn (1).

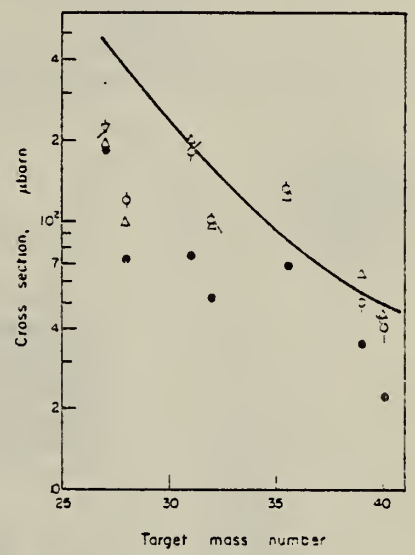

Fig. 4. Mean absolute cross section of ^{24}Na photoproduction vs the target mass number. Filled circles: energy range 0·1–1 GeV, Ref. [20]. Reversed open triangle: energy range 0·3–1 GeV, Ref. [8]. Open triangles: energy range 0·25–1 GeV, Ref. [19]. Open circles: present work. The curve has been calculated by means of Eqn (1).

Table 2. Cross-section per equivalent quantum $\sigma_2(\mu b)$ of photoproduction of ^{18}F

Target nucleus	Bremsstrahlung maximum energy E_0(GeV)				
	0·30	0·40	0·55	0·75	1·00
^{23}Na	590 ± 30	640 ± 30	720 ± 30	780 ± 30	830 ± 30
^{27}Al*	116 ± 7	172 ± 6	202 ± 6	245 ± 5	270 ± 5
^{28}Si	80 ± 10	110 ± 10	145 ± 10	170 ± 10	200 ± 10
^{31}P	60 ± 10	90 ± 10	130 ± 10	150 ± 10	180 ± 10
^{32}S	55 ± 10	90 ± 10	125 ± 10	160 ± 10	190 ± 10
^{35,37}Cl	185 ± 20	230 ± 20	270 ± 20	310 ± 20	350 ± 20
^{39}K	35 ± 5	50 ± 5	65 ± 5	75 ± 5	90 ± 5
^{40}Ca	5 ± 2	20 ± 3	35 ± 5	45 ± 5	60 ± 5

*The results for ^{27}Al have already been published (see[3]) and are reported for comparison.

(over)

TABLE 1

Fitted parameters

State	c_{tr} (fm)	t_{tr} (fm)	$B(E2, \omega)\downarrow$(s.p.u.) [d]	χ^2/f
$\frac{1}{2}^+$ 1.27 MeV	2.2 ±0.7	2.9 ±0.4	6.0±0.9	0.49
$\frac{3}{2}^+$ 2.23 MeV	3.6 ±0.8 [a]	1.5 ±1.2	6.3±0.5	0.98
	3.33±0.02 [b]	1.96±0.07	6.3±0.5	2.37
	3.31±0.02 [c]	2.03±0.05	6.9±0.3	2.24
$\frac{3}{2}^+$ 3.51 MeV	3.7 ±0.4	1.3 ±0.7	2.7±0.3	0.57

[a]) Fit to NBS data only.
[b]) Fit to Stanford data only.
[c]) Fit to NBS plus Stanford data.
[d]) Uncertainties quoted have been adjusted by $\sqrt{\chi^2/f}$.

TABLE 2

Form factor constants in the intermediate-coupling vibrational model

Excited state	A_1	A_2	A_3
$\frac{3}{2}^+$ 1.27 MeV	0.320	0.157	−0.732
$\frac{3}{2}^+$ 2.23 MeV	0.105	0.051	−1.119
$\frac{3}{2}^+$ 3.51 MeV	0.242	0.117	0.528

TABLE 3

^{31}P E2 transition strengths in Weisskopf single-particle units

	$B(E2, \omega)\downarrow$			Ref.
	1.27 MeV, $\frac{1}{2}^+$	2.23 MeV, $\frac{3}{2}^+$	3.51 MeV, $\frac{3}{2}^+$	
This experiment	6.0±0.9	6.9±0.3	2.7±0.3	
Previous experiments	4.6±0.3	6.4±0.4	1.9±0.4	[21])
Twin *et al.*, expt.	3.8±1.0	7.3±0.7	≧2.3	[22])
Glaudemans *et al.*, theory	4.7	5.1	0.01	[12])
Castel *et al.*, theory	2.8	13.5	3.5	[3])
Present calculation	3.2	8.7	6.1	

[3] B. Castel et al., Can. J. Phys. 48 (1970) 1490

[12] P.W.M. Glaudemans et al., Phys. Lett. 28B (1969) 645

[21] P.M. Endt et al., Nucl. Phys. A214 (1973) 1

[22] P.J. Twin et al. J. of Phys. A7 (1974) 1410

REF. F. J. Kline, C. L. Lin, G. A. Peterson, S. Penner
Nucl. Phys. A241, 299 (1975)

ELEM. SYM.	A	Z
P	31	15

METHOD

REF. NO. 75 Kl 3 egf

REACTION	RESULT	EXCITATION ENERGY	SOURCE TYPE	SOURCE RANGE	DETECTOR TYPE	DETECTOR RANGE	ANGLE
E,E/	LFT	1- 4	D	50-250	MAG-D		DST

1.27, 2.23, 3.51 ME

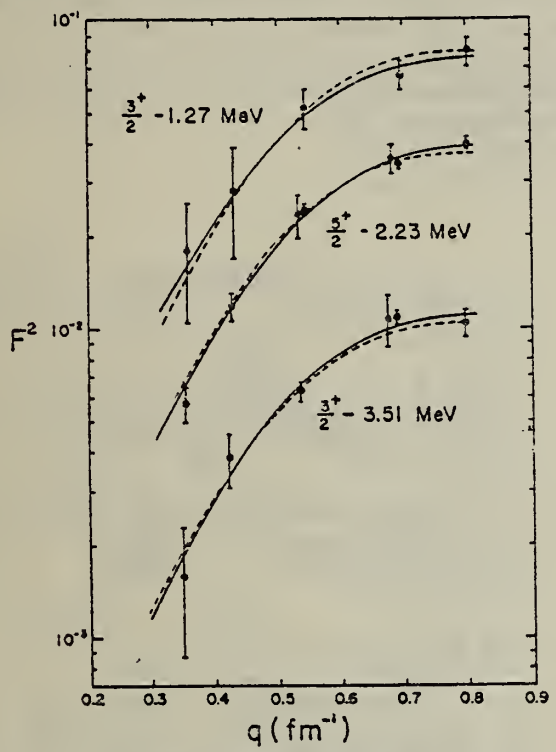

Fig. 2. Plot of converted form factors squared for the $\frac{1}{2}^+$ (1.27 MeV), $\frac{5}{2}^+$ (2.23 MeV) and $\frac{3}{2}^+$ (3.51 MeV) states in ^{31}P versus q. The data points were obtained at NBS. The solid curve is the fit using the distorted-wave code DUELS. The dashed curve is the distortion corrected and normalized (cf. text) form factors squared, calculated in the intermediate-coupling vibrational model.

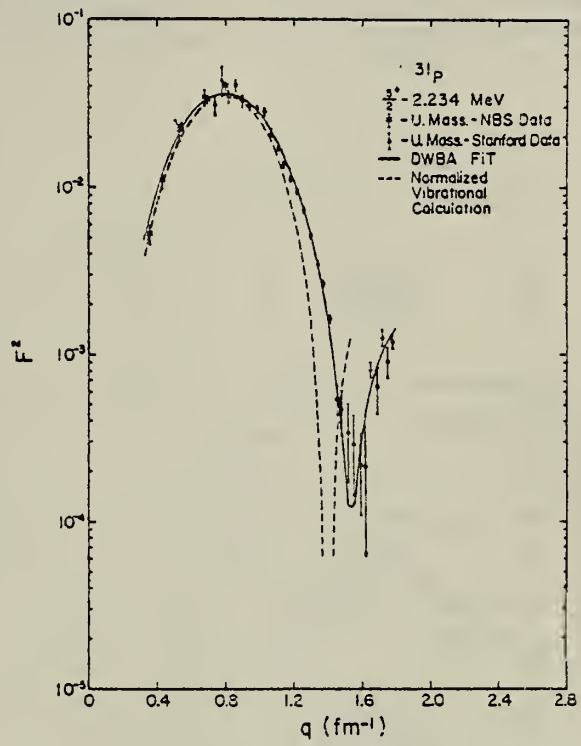

Fig. 3. Plot of converted form factors squared for combined NBS and Stanford data on the $\frac{5}{2}^+$ (2.23 MeV) state. The crosses are the U. Mass-NBS data and the circles are the U. Mass-Stanford data. The solid curve is the fit using the distorted-wave code DUELS. The dashed curve is the distortion corrected and normalized (cf. text) form factors squared calculated in the intermediate-coupling vibrational model.

(over)

REF. B. Bulow; Z. Physik A285, 323 (1978)

ELEM. SYM.	A	Z
P	31	15

METHOD

REF. NO. 78 Bu 9 RS

REACTION	RESULT	EXCITATION ENERGY	SOURCE		DETECTOR		ANGLE
			TYPE	RANGE	TYPE	RANGE	
G,2P	ABY	21-640	C	75-640	ACT-I		4PI
G,2PN	ABY	30-640	C	75-640	ACT-I		4PI
G,3P	ABY	31-640	C	75-640	ACT-I		4PI
G,3PN	ABY	40-640	C	75-640	ACT-I		4PI

The yields of the $(\gamma,2p)$ reaction on ^{30}Si and of the $(\gamma,2p)$, $(\gamma,2pn)$, $(\gamma,3p)$ and $(\gamma,3pn)$ reactions on ^{31}P have been measured as a function of the maximum bremsstrahlung energy in the range 75–640 MeV. The cross sections have been deduced and are compared to Monte-Carlo calculations. The magnitude of the cross sections in the energy range above the threshold for the photoproduction of mesons is also discussed using a simple analytical approach.

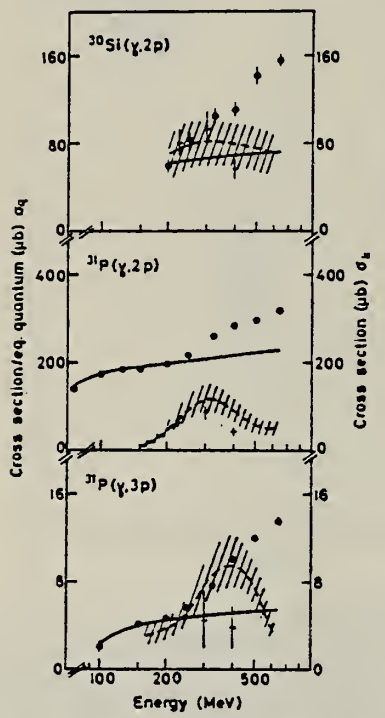

Fig. 1. The filled circles show measured yields as a function of the maximum bremsstrahlung energy. The meaning of the solid lines, the hatched areas and the plus signs is given in the text

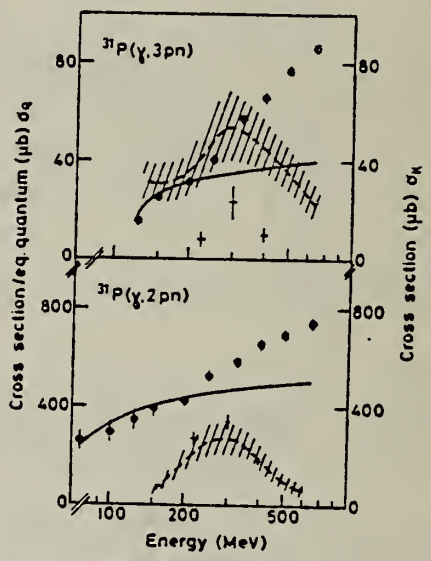

Fig. 2. The same as in Figure 1

Table 2. Reaction thresholds, *GR* and *QD* normalizationfactors and calculated mean cross sections for the different reactions

Reaction	Threshold (MeV)	Normalization-factor	$\bar{\sigma}_k$ (200–640 MeV)	*GR* and *QD* reference
^{30}Si(γ, 2p)	24.0	0.67	72.5 ± 5.9	[12]
^{31}P(γ, 2p)	20.8	0.98	88.3 ± 7.8	[11]
(γ, 2pn)	30.2	1.3	197. ±19	[11]
(γ, 3p)	31.3	1.2	5.1 ± 1.0	[12]
(γ, 3pn)	39.8	1.0	41.6 ± 1.8	–

REF. V.M. Asaturyan, E.O. Grigoryan, G.A. Vartapetyan, A.S. Danagulyan, N.A. Demëkhina & A.G. Khudaverdyan
Sov. J. Nucl. Phys. 25, 601 (1977)
Yad. Fiz. 25, 1133 (1977)

ELEM. SYM.	A	Z
P	31	15

METHOD

REF. NO. 77 As 10 hmg

REACTION	RESULT	EXCITATION ENERGY	SOURCE		DETECTOR		ANGLE
			TYPE	RANGE	TYPE	RANGE	
G,Be7 G,Na22	ABY	THR*5	C	*5	SCD-D		UKN
G,Na24				(4.5)			

Photonuclear reactions in the targets ^{27}Al, ^{28}Si, ^{31}P, ^{32}S, and ^{40}Ca have been studied for maximum bremsstrahlung energies of 2, 2.4, 3, and 4.5 GeV. The yields of the residual nuclei ^{7}Be, ^{11}C, ^{13}N, ^{18}F, ^{22}Na, and ^{24}Na were measured by means of a germanium-lithium semiconductor detector with a sensitive volume of 30 cm^3. In discussion of the results we took into account the contribution of the low energy part of the bremsstrahlung spectrum. Comparison of the measured yields with estimates calculated by Rudstam's formula permitted us to conclude that there is a difference in the mechanism of formation of the light fragments ^{7}Be, ^{11}C, and ^{13}N from that of the other residual nuclei ^{18}F, ^{22}Na, and ^{24}Na.

*GEV 5=4.5 GEV

TABLE II.

Residual nuclei	Reaction yield, mb/Q: Bremsstrahlung end-point energy (E$_{max}$), GeV	2 GeV	2.4 GeV	3 GeV	4.5 GeV	Normalized yields	$\sigma_{exp}/\sigma_{theor}$
Al target							
^{24}Na	0.46±0.02	0.81	0.81	0.87	0.87	0.98	0.55
^{22}Na	0.74±0.02		1.02±0.15		1.07±0.1	0.668	0.98
^{18}F	0.27±0.005	0.39±0.02		0.4±0.02	0.29±0.01	0.296	1.6
^{13}N		0.021±0.004		0.025±0.007	0.022±0.004	0.0127	2.54
^{11}C	0.117±0.013	0.104±0.015		0.12±0.02	0.107±0.015	0.1081	$3.3\cdot10^{5}$
^{7}Be	0.29±0.03		0.37±0.08		0.3±0.03	0.2748	$1.38\cdot10^{6}$
Si target							
^{24}Na	0.24±0.01	0.274±0.024	0.27±0.02	0.28±0.02	0.29±0.02	0.54	0.43
^{22}Na	0.67±0.02		1.22±0.2		1.22±0.1	1.17	2.38
^{18}F	0.2±0.01	0.36±0.03		0.39±0.02	0.29±0.02	0.28	2.89
^{13}N		0.033±0.01		0.007±0.01	0.039±0.04	0.0247	7.28
^{11}C		0.104±0.02		0.115±0.028	0.121±0.027	0.107	$7.2\cdot10^{5}$
^{7}Be			0.398±0.05		0.32±0.04	0.291	$8.2\cdot10^{6}$
P target							
^{24}Na	0.21±0.02				0.35±0.05	0.436	0.72
^{22}Na	0.35±0.02				0.35±0.06	0.423	2.02
^{7}Be					0.33±0.05	0.296	$8.81\cdot10^{6}$
S target							
^{24}Na	0.24±0.01	0.25±0.02	0.25±0.02	0.24±0.02	0.27±0.03	0.417	1.1
^{22}Na	0.35±0.01				0.61±0.08	0.508	3.65
^{18}F	0.19±0.01	0.28±0.01		0.25±0.01	0.27±0.01	0.284	4.73
^{13}N		0.047±0.08		0.063±0.08	0.06±0.025	0.054	$2.66\cdot10^{5}$
^{11}C	0.122±0.013	0.163±0.023		0.142±0.028	0.15±0.03	0.128	$1.23\cdot10^{6}$
^{7}Be	0.25±0.08		0.38±0.08		0.34±0.04	0.344	$1\cdot10^{7}$
Cl target							
^{24}Na	0.22±0.01	0.25±0.02		0.3±0.03	0.28±0.03	0.297	1.8
^{18}F	0.36±0.02	0.21±0.01				0.18	7.82
K target							
^{24}Na	0.08±0.005	0.1±0.01		0.125±0.012	0.15±0.015	0.16	2
^{18}F	0.09±0.005	0.11±0.02				0.1	7.58
Ca target							
^{24}Na	0.08±0.008	0.089±0.01		0.09±0.01	0.12±0.012	0.147	2.2
^{22}Na	0.06±0.005				0.21±0.02	0.21	6.37
^{7}Be					0.245±0.025	0.23	$1.5\cdot10^{7}$

Data for Cl and K targets previously published in Reference 11.

[11]G. A. Vartapetyan *et al.*, Yad. Fiz. 17, 685 (1973) [Sov. J. Nucl. Phys. 17, 350 (1973)].

[3]H. R. Weller, R. A. Blue, N. R. Roberson, D. G. Rickel, S. Maripuu, C. P. Cameron, R. D. Ledford, and D. R. Tilley, Phys. Rev. C 13, 922 (1976). (Note: an error exists in the sign of the phase in this paper. The quantity $\phi_s - \phi_d$ should be $\phi_d - \phi_s$ wherever it appears.)
[3]C. P. Cameron, N. R. Roberson, D. G. Rickel, R. D. Ledford, H. R. Weller, R. A. Blue, and D. R. Tilley, Phys. Rev. C 14, 553 (1976).
[4]C. P. Cameron, Ph.D. thesis, Duke University, 1976 (unpublished).
[5]R. D. Ledford, Ph.D. thesis, Duke University, 1976 (unpublished).
[6]J. D. Turner, C. P. Cameron, N. R. Roberson, H. R. Weller, and D. R. Tilley, Phys. Rev. C 17, 1853 (1978).

REF. H.R. Weller, N.R. Roberson & S.R. Cotanch
Phys. Rev. C18, 65 (1978)

ELEM. SYM.	A	Z
P	31	15

METHOD

REF. NO. 78 We 4 hmg

REACTION	RESULT	EXCITATION ENERGY	SOURCE		DETECTOR		ANGLE
			TYPE	RANGE	TYPE	RANGE	
$ P,G	RLX	13-22	D	6-15	UKN-D		DST

Analysis of data in reference 4.

POLARIZED PROTONS

Measurements of cross sections and analyzing powers are examined for polarized proton capture on ^{14}C, ^{30}Si, ^{54}Fe, ^{56}Fe, ^{58}Fe, ^{59}Co, and ^{88}Sr at energies which cover the giant dipole resonance region. These data are used to extract the relative amplitudes and phases of the contributing $E1$ T-matrix elements. A typical result exhibits two solutions. Calculations using the direct (or a direct-semidirect) capture model appear to provide a means for choosing the physical solution.

[NUCLEAR REACTIONS: $^{14}C(\vec{p},\gamma_0)$, $^{30}Si(\vec{p},\gamma_0)$, $^{54}Fe(\vec{p},\gamma_0)$, $^{56}Fe(\vec{p},\gamma_0)$, $^{58}Fe(\vec{p},\gamma_0)$, $^{59}Co(\vec{p},\gamma_0)$, $^{88}Sr(\vec{p},\gamma_0)$; measured $\sigma(\theta)$ and $A(\theta)$ over energy region of the giant dipole resonance. Deduced T-matrix amplitudes and phases. Compare results to direct-semidirect model calculations.]

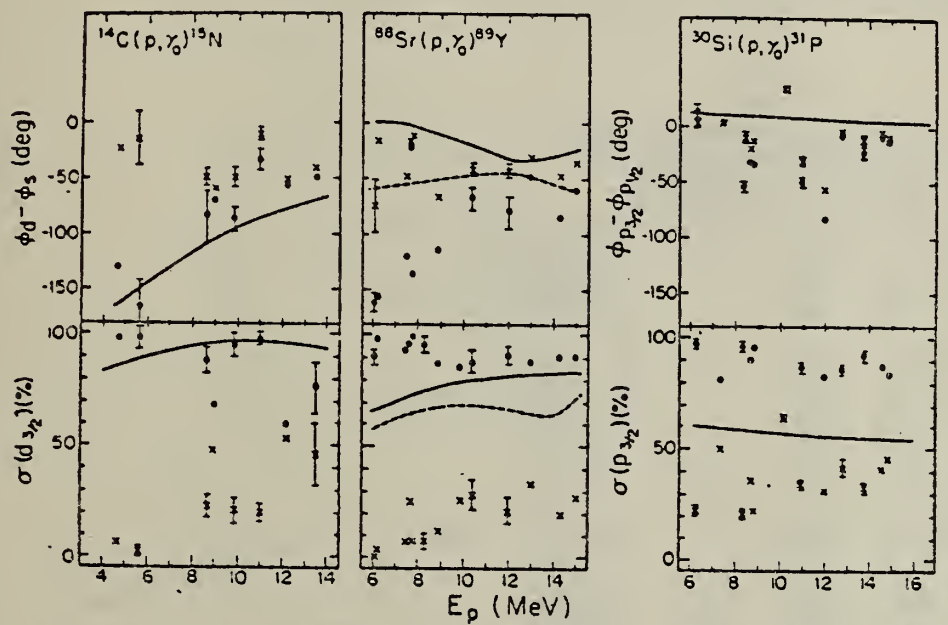

FIG. 1. The two solutions (dots and x's) resulting from a pure $E1$ analysis of the data are shown along with the results of the calculation for target nuclei of ^{14}C, ^{88}Sr, and ^{30}Si. The remaining cross section in the case of ^{14}C and ^{88}Sr is due to the $s_{1/2}$ matrix element. In the case of ^{30}Si it arises from the $p_{3/2}$ matrix element. The error bars represent typical statistical errors associated with the data points. The amplitudes are presented in terms of the percentage of the total cross section for which they are responsible. The curves represent DSD calculations as described in the text. The dashed curves in the case of ^{88}Sr were obtained using the optical model parameters of Ref. 16 while the solid lines were obtained from the parameters of Ref. 18.

TABLE 1

Summary of the angular distribution results for $^{28-30}$Si(p, γ)$^{29-31}$P resonances and comparison with previous values

Reaction	E_p (MeV)	Transition (MeV)	a_2		a_4	
			present [a])	previous	present [a])	previous
^{28}Si(p, γ)^{29}P	0.37	r → 1.95	0.52 ± 0.02	0.372 ± 0.036 [b])	−0.19 ± 0.03	0.097 ± 0.071 [b])
		r → 1.38	−0.79 ± 0.02	−0.809 ± 0.041 [b])	−0.01 ± 0.03	0.026 ± 0.074 [b])
		1.38 → 0	−0.58 ± 0.03	−0.568 ± 0.017 [b])	−0.05 ± 0.04	−0.017 ± 0.031 [b])
		1.95 → 0	0.19 ± 0.02	0.211 ± 0.039 [b])	0.13 ± 0.03	0.120 ± 0.080 [b])
	1.38	r → 1.95	−0.83 ± 0.03	−0.55 ± 0.55 [c])	0.14 ± 0.05	0.01 ± 0.07 [c])
		r → 1.38	0.67 ± 0.02	0.51 ± 0.09 [c])	−0.47 ± 0.02	−0.25 ± 0.09 [c])
		1.38 → 0	−0.61 ± 0.03	−0.59 ± 0.05 [c])	−0.03 ± 0.04	
		1.95 → 0	0.41 ± 0.02	0.44 ± 0.07 [c])	−0.34 ± 0.03	−0.30 ± 0.07 [c])
	1.65	r → 0	−0.43 ± 0.03	−0.53 ± 0.04 [c])	−0.03 ± 0.04	
^{29}Si(p, γ)^{30}P	0.42	r → 0.71	0.30 ± 0.02		0.01 ± 0.03	
		r → 0.68	−0.37 ± 0.02		0.00 ± 0.04	
^{30}Si(p, γ)^{31}P	0.50	r → 0	−0.49 ± 0.03	−0.39 ± 0.01 [d]) −0.41 ± 0.02 [e])	0.00 ± 0.02	−0.01 ± 0.01 [d])
	0.62	r → 0	0		0	
	0.78	r → 0	−0.40 ± 0.02	−0.31 ± 0.01 [e])	0.01 ± 0.04	
	0.94	r → 0	−0.83 ± 0.03	−0.72 ± 0.02 [e])	0.05 ± 0.05	
	0.98	r → 0	−0.65 ± 0.03		0.07 ± 0.04	

The E_p and E_x values are taken from ref. [25]).

[a]) The coefficients are corrected for finite solid angle of the Ge(Li) detector [30]). The correction due to the finite size of the beam spot on the target is negligible and is considered to be included in the uncertainty of the target-to-detector distance, 50 ± 2 mm.

[b]) Ref. [12]). [c]) Ref. [14]). [d]) Ref. [5]). [e]) Ref. [31]).

TABLE 2

Summary of the present strength measurements

Reaction	E_p (keV)	Transitions (MeV)	Branching [a]) (%)	$W_{exp}(55°)$ [b])	$\varepsilon(E_p)$ [c]) eV/(10^{15} at/cm^2)	$\omega\gamma$ (eV)	S_{lab} (eV)
^{28}Si(p, γ)^{29}P	370	r → 1.95	30 ± 2	1.04	14.1	(5.5 ± 0.8) × 10^{-3}	
		r → 1.38	70 ± 2	1.00		(5.4 ± 0.5) × 10^{-3}	(5.6 ± 0.4) × 10^{-3}
		1.38 → 0	70 ± 2	1.01		(5.6 ± 0.4) × 10^{-3}	
		1.95 → 0	27 ± 2	0.97		(5.7 ± 0.8) × 10^{-3}	
	1381	r → 1.95	51 ± 1	0.97	6.8	(103 ± 8) × 10^{-3}	
		r → 1.38	46 ± 1	1.09		(84 ± 8) × 10^{-3}	(92 ± 8) × 10^{-3}
		1.38 → 0	49 ± 1	1.01		(89 ± 10) × 10^{-3}	
		1.95 → 0	51 ± 1	1.07		(93 ± 9) × 10^{-3}	
	1652	r → 0	93 ± 1	1.00	6.1	9.0 ± 0.7	
	2088	r → 0	91 ± 2	1.19	5.1	0.95 ± 0.14	
^{29}Si(p, γ)^{30}P	416	r → 0.71	33 ± 1	1.00	13.3	1.09 ± 0.35	1.04 ± 0.10
		r → 0.68	57 ± 1	1.00		0.99 ± 0.15	
^{30}Si(p, γ)^{31}P	499	r → 0	52 [d])	1.00	12.1	0.33 ± 0.05	
	620	r → 0	95 ± 1	1.00	10.8	5.0 ± 0.3	
	777	r → 0	68 [d])	1.00	9.5	1.2 ± 0.2	
	942	r → 0	66 [d])	1.00	8.5	2.0 ± 0.3	
	983	r → 0	70 [d])	1.00	8.3	2.0 ± 0.3	

The E_p and E_x values are taken from ref. [25]).

[a]) All values given are relative to the value of 100 % for the total intensity for the decays of the resonance state.

[b]) As deduced from the angular distribution data obtained in the present experimental geometry. Thus the solid angle attenuation is taken into account experimentally. Error limits are within 1 %.

[c]) Ref. [24]). Error limits estimated to be ± 5 %.

[d]) Ref. [9]). Error limits estimated to be ± 2 %.

PAGE

NO(S) #536

MISSING

PAGE
NO(S) 4 5 35
MISSING

REF. M. Riihonen, J. Keinonen, A. Anttila
Nucl. Phys. A313, 251 (1979)

ELEM. SYM.	A	Z
P	31	15

METHOD

REF. NO. 79 Ri 2 hg

REACTION	RESULT	EXCITATION ENERGY	SOURCE		DETECTOR		ANGLE
			TYPE	RANGE	TYPE	RANGE	
P,G	NOX	7-9	D	0-1	SCD-D		DST
		(7.78-8.25)		(.50-.98)			

Abstract: The absolute resonance strengths of the $^{28-30}$Si(p, γ)$^{29-31}$P reactions have been studied. New values for the frequently used standard resonances at E_p = 370, 416 and 620 keV in the above reactions, respectively, have been determined. In addition, the strengths of the ^{28}Si(p, γ)^{29}P resonances at E_p = 1381, 1652 and 2088 keV and of the four dominant ^{30}Si(p, γ)^{31}P resonances at E_p = 499, 777, 942 and 983 keV have been determined. The branching ratios and angular distributions of the γ-rays used in the determinations were obtained in the same experimental set-up as the strength measurements. Using these revised resonance strengths, the astrophysical reaction rates of hydrogen burning of ^{29,30}Si in explosive carbon burning have been deduced. The reaction rates found for hydrogen burning of $^{28-30}$Si in the stellar temperature region of $T = (0.3–10) \times 10^9$ K are compared with Hauser-Feshbach calculations.

STELLAR REACTION RATE

E NUCLEAR REACTIONS ^{28}Si(p, γ), E = 0.37, 1.38, 1.65, 2.09 MeV; ^{29}Si(p, γ), MeV, ^{30}Si(p, γ), E = 0.50, 0.62, 0.78, 0.94, 0.98 MeV; measured $\sigma(E_p)$, $I_\gamma(\theta)$. ^{29,30,31}P resonances deduced γ-branchings, resonance strengths. Ge(Li) detector. Natural and enriched targets.

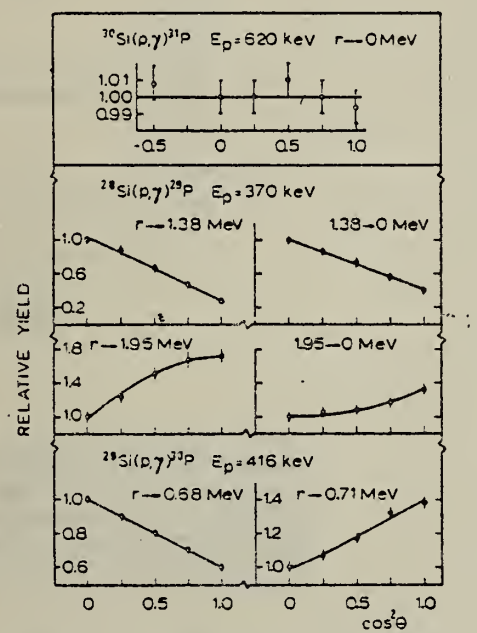

Fig. 1. The results of angular distribution measurements of the standard resonances at E_p = 370, 416 and 620 keV in the $^{28-30}$Si(p, γ)$^{29-31}$P reactions. In the case of the E_p = 620 keV resonance, the experimental points are shown without eccentricity or absorption corrections. In other cases these corrections have been made. The solid lines are the fitted curves of the form $W(\theta) = 1 + a_2 P_2(\cos\theta) + a_4 P_4(\cos\theta)$.

(over)

TABLE I. The A_0, a_k and b_k coefficients obtained from least squares fits to the $^{30}Si(p,\gamma_0)$ data with Eqs. (1) and (2), respectively. The b_k coefficients are given below the a_k coefficients at each energy. Also given in the two right-hand columns are the χ^2 values obtained when the data were fitted directly to the T-matrix element amplitudes and relative phases as described in the text. The errors given for the A_0 values are statistical.

E_p (MeV)	A_0 (μb/sr)	a_1/b_1	a_2/b_2	a_3/b_3	a_4/b_4	χ^2	χ^2(I) [a]	χ^2(II) [b]
6.36	10.6±0.2	−0.03±0.01	−0.70±0.02	−0.05±0.03	−0.10±0.04	4.0	3.4	3.4
		0.02±0.03	0.03±0.01	0.04±0.01	0.02±0.02	2.4		
7.46	19.6±0.3	0.04±0.01	−0.97±0.02	−0.05±0.03	−0.05±0.04	1.0	0.7	0.7
		−0.09±0.03	−0.02±0.01	0.05±0.02	−0.02±0.02	0.3		
8.40	14.2±0.3	0.19±0.01	−0.64±0.02	−0.00±0.02	0.02±0.03	0.9	0.6	0.6
		−0.07±0.02	−0.10±0.01	−0.02±0.01	−0.01±0.01	0.5		
8.81	13.1±0.3	0.19±0.01	−0.81±0.02	−0.09±0.03	0.06±0.03	1.5	2.2	1.8
		−0.08±0.02	−0.12±0.01	0.02±0.01	0.03±0.01	2.2		
8.85	10.0±0.3	0.24±0.02	−0.69±0.02	−0.15±0.03	−0.05±0.03	1.1	1.2	2.4
		0.01±0.03	−0.07±0.02	−0.03±0.02	−0.00±0.02	1.5		
10.23	10.3±0.2	0.18±0.01	−0.88±0.02	−0.21±0.03	−0.09±0.03	1.0	1.1	1.1
		−0.07±0.02	0.21±0.01	0.07±0.01	0.02±0.01	1.1		
11.01	7.3±0.1	0.15±0.01	−0.74±0.02	−0.04±0.03	−0.03±0.03	0.9	1.0	0.8
		−0.01±0.02	−0.18±0.01	−0.02±0.01	−0.02±0.01	0.9		
12.00	5.7±0.2	0.13±0.01	−0.48±0.02	−0.16±0.03	0.03±0.03	0.7	0.8	1.0
		−0.07±0.03	−0.27±0.02	−0.01±0.02	0.01±0.02	0.8		
12.85	6.6±0.1	0.16±0.01	−0.91±0.02	−0.12±0.03	−0.07±0.03	1.8	1.1	1.1
		0.01±0.02	−0.03±0.01	−0.02±0.01	−0.02±0.01	0.6		
13.78	6.0±0.1	0.13±0.01	−0.81±0.02	−0.16±0.03	0.04±0.03	2.7	2.2	2.7
		−0.03±0.02	−0.07±0.01	0.02±0.01	0.01±0.01	1.9		
14.63	7.3±0.2	0.17±0.01	−0.91±0.02	−0.18±0.03	−0.05±0.03	1.8	1.2	1.2
		0.01±0.02	−0.03±0.01	0.00±0.02	−0.00±0.01	0.6		
14.95	3.6±0.1	0.23±0.01	−0.93±0.02	−0.24±0.03	−0.12±0.04	0.5	0.7	0.7
		−0.03±0.02	−0.05±0.01	0.02±0.02	0.01±0.02	0.7		

[a] Set I, see text.

[b] Set II, see text.

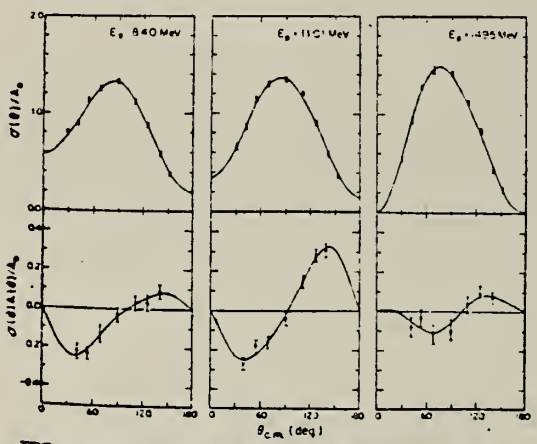

FIG. 4. Typical cross section and analyzing power angular distribution for $^{30}Si(p,\gamma_0)^{31}P$. The errors are statistical. The solid lines are fits through fourth order in Legendre and associated Legendre polynomials.

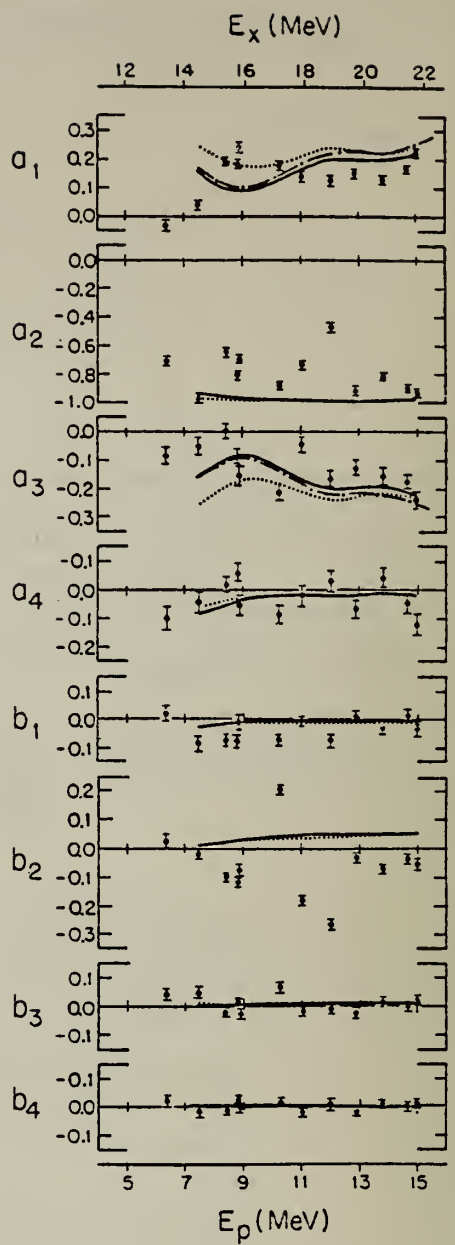

FIG. 9. The a_k and b_k coefficients for the $^{30}Si(p,\gamma_0)^{31}P$ reaction. As discussed in the text, the curves are the results of DSD model calculations with the following conditions: dotted curves—complex dipole form factor, solid curves—real dipole form factor, and dot-dashed curvee—real dipole form factor with semidirect isoscalar quadrupole form factor set to zero.

DEFINITIONS OF ABBREVIATIONS AND SYMBOLS

Note: In this list definitions are given for various photoneutron reactions in which the following symbols are used: N, NL, nN, SN and XN. Corresponding definitions apply for reactions involving other nuclear particles where the symbols N (neutron) is replaced by, e.g. P, D, T, HE, A etc. Where unknown reactions result in the production of a specific radionuclide, the chemical symbol and mass number is listed as the reaction product, e.g. a G,NA22 reaction in ^{59}Co.

A	alpha particle
ANAL	analysis
ABI	absolute integrated cross-section data
ABX	absolute cross-section data
ABY	absolute yield data. Often means cross-section per equivalent quantum is listed.
ACT	measurement of induced radioactivity of the target
ASM	asymmetric, asymmetry
AVG	average
BBL	bubble chamber
BEL B(EL)	reduced electric radiative transition probability
BF3	BF_3 neutron counter with moderator e.g., Halpern detector, long counter
BML	reduced magnetic radiative transition probability, B(ML)
BREAKS	levels located by "breaks" in the yield curve
BRKUP	breakup
BRMS	bremsstrahlung
BTW	between
C	continuous. Used to describe a photon source or a detector response function. Contrast with D = discrete.
CCH	cloud chamber
CF	compared with
CHRGD	charged
CMPT	Compton
COIN COINC	coincidence, coincide
COH	coherent
CK	Cerenkov
D	deuteron or discrete. When discrete, it is used to describe a photon source or a detector response function. Contrast with C = continuous.
DLTE	energy loss
DLTQ	momentum transfer
DST	distribution
DT BAL	detailed balance
E	electron
E/	inelastically scattered electron
E+	positron
EDST	energy distribution or spectrum
E/N	used only to indicate a coincidence experiment as in (E,E/N).

	N stands for any outgoing particle measured in coincidence with an inelastically scattered electron. Distinguish from eg., (E,N) which is used to represent an electron induced reaction when only the outgoing particle N is detected.
EMU	emulsions (photographic plates)
EXCIT	excited
F	fission
FMF	form factor
FM-1	inverse femtometers
FRAG	fragment
G	photon
G/	inelastically scattered photon
G-WIDTH	gamma-ray transition width
HAD	hadrons, hadron production
HE He3	^{3}He particle
INT	interaction, integral, intensity
INC	includes
ION	ionization chamber
ISOB	isobaric
ISM	isomer
J	multiplicity of particle defined by following symbol e.g. (G,PJN) with remark J = 2,3,5,7
JPI J-PI	spin and parity of a nuclear state
K	second multiplicity index, e.g. (G,JPKN) with both J & K positive integers greater than 1
KE	kinetic energy
L	may be an integer or zero that always follows a reaction product symbol. This is used to indicate transitions to specific states in the residual nuclide. When the letter is used as in (G,NL) the cross section given is that for the sum of transitions to two or more specific final states.
LFT	excited state lifetime
LIM	limit
LV,LVS	level, levels
LQD	liquid
MAG	magnetic spectrometer
MEAS	measurement(s)
MGC	magnetic Compton spectrometer
MGP	magnetic pair spectrometer
MOD	moderated neutron detector not employing a BF_3 counter, e.g. rhodium foil, Szilard-Chalmers reaction, ^{3}He, ^{6}Li reactions, GD loaded liquid scintillator, etc.
MSP	mass spectrometer
MULT	multiple, multipole, multiplicity
MU-T	used only in combination with G to indicate a total photon absorption cross section measurement, i.e. (G,MU-T)
N	neutron (see also XN and SN). The notation (G,N) is used to indicate a reaction in which only a single neutron is emitted, i.e. the reaction that can, in many cases, be measured by observing the radioactive decay of the residual nuclide.

nN	where n is any integer. (G,nN) indicates the sum over all reaction cross sections in which n neutrons are emitted.
NAI	NaI(Tl) spectrometer
NEUT	neutron(s)
NOX	no cross-section data
P	proton (see also XP)
PART	particle(s)
PHOT	photon(s)
PI	pion, usually written as PI+, PI-, PI0 to indicate charge
POL	polarized or polarization
Q-SQUAR	momentum transfer squared (q^2)
RCL	recoil
REL	relative
RLI	relative integrated cross-section data
RLX	relative cross-section data
RSP	reaction spectrometer
RLY	relative yield data
SCTD	scattered
SCD	semiconductor (solid state) detector
SCI	scintillator detector other than NaI, e.g., CsI, KI, organic (liquid or solid), stilbene, He
SEP	separation
SEP ISOTP	separated isotope used
SIG	SIGMA (cross section)
SN	sum of neutron producing reactions, $\sigma(\gamma,SN)=\sigma(\gamma,N) + \sigma(\gamma,NP) + \sigma(\gamma,2N) + \sigma(\gamma,3N)$ + etc.
SPC	photon or particle energy spectrum
SPK	spark chamber
SPL	spallation
STAT	statistical
SYM	symetric, symmetry
T	triton
TEL	counter telescope
THR	threshold for reaction or threshold detector, e.g., $^{29}Si(n,p)^{29}Al$.
TOF	time-of-flight detector
TRK	tracks of particles or fragments observed in solid materials (glass, mylar, etc.)
TRNS	transition
UKN UNK	unknown
VIB	vibrational
VIR PHOT	virtual photon(s)
XN	all neutrons, total neutron yield, $\sigma(\gamma,XN) = \sigma(\gamma,N) + 2\sigma(\gamma,2N) + 3\sigma(\gamma,3N) + \sigma(\gamma,NP)$ + etc.
XP	all protons, total proton yield $\sigma(\gamma,XP) = \sigma(\gamma,P) + \sigma(\gamma,NP) + 2\sigma(\gamma,2P)$ + etc.
XX XXX	reaction products defined in REMARKS
YLD	yield

PI	a 4π geometry was used or a method like radioactivity or a total absorption measurement		products was determined. The polarized particle is indicated in REMARKS.
99	energy defined in REMARKS	* or @	symbols used to indicate that the units associated with the numerals on one or both sides of the symbol in a specific column are not MeV. The units are defined in REMARKS.
S	indicates the measurement involved beams or targets that were either polarized or aligned, or that the polarization of the reaction		

NBS-114A (REV. 2-8C)

U.S. DEPT. OF COMM. BIBLIOGRAPHIC DATA SHEET (See instructions)	1. PUBLICATION OR REPORT NO. NBSIR 83-2742	2. Performing Organ. Report No.	3. Publication Date

4. TITLE AND SUBTITLE

Photonuclear Data-Abstract Sheets
1955-1982

5. AUTHOR(S)

E.G. Fuller and Henry Gerstenberg

6. PERFORMING ORGANIZATION (If joint or other than NBS, see instructions)

NATIONAL BUREAU OF STANDARDS
DEPARTMENT OF COMMERCE
WASHINGTON, D.C. 20234

7. Contract/Grant No.

8. Type of Report & Period Covered

9. SPONSORING ORGANIZATION NAME AND COMPLETE ADDRESS (Street, City, State, ZIP)

10. SUPPLEMENTARY NOTES

☐ Document describes a computer program; SF-185, FIPS Software Summary, is attached.

11. ABSTRACT (A 200-word or less factual summary of most significant information. If document includes a significant bibliography or literature survey, mention it here)

These abstract sheets cover most classes of experimental photonuclear data leading to information of the electromagnetic matrix element between the ground and excited states of a given nucleus. This fifteen volume work contains nearly 7200 abstract sheets and covers 89 chemical elements from hydrogen through americium. It represents a twenty-seven year history of the study of electromagnetic interactions. The sheets are ordered by target element, target isotope, and by an assigned bibliographic reference code. Information is given on the type of measurement, excitation energies studied, source type and energies, detector type, and angular ranges covered in the measurement. For a given reference, the relevant figures and tables are mounted on a separate sheet for each nuclide studied.

12. KEY WORDS (Six to twelve entries; alphabetical order; capitalize only proper names; and separate key words by semicolons)

data-abstract sheets, elements, experimental, isotopes, nuclear physics, photonuclear reactions

13. AVAILABILITY

☐ Unlimited

☒ For Official Distribution. Do Not Release to NTIS

☐ Order From Superintendent of Documents, U.S. Government Printing Office, Washington, D.C. 20402.

☐ Order From National Technical Information Service (NTIS), Springfield, VA. 22161

14. NO. OF PRINTED PAGES 2544

15. Price

USCOMM-DC 6043-P80